ANTIBIOTIC ALTERNATIVES AND COMBINATIONAL THERAPIES FOR BACTERIAL INFECTIONS

EDITED BY: Sanna Sillankorva, Maria Olívia Pereira and Mariana Henriques
PUBLISHED IN: Frontiers in Microbiology

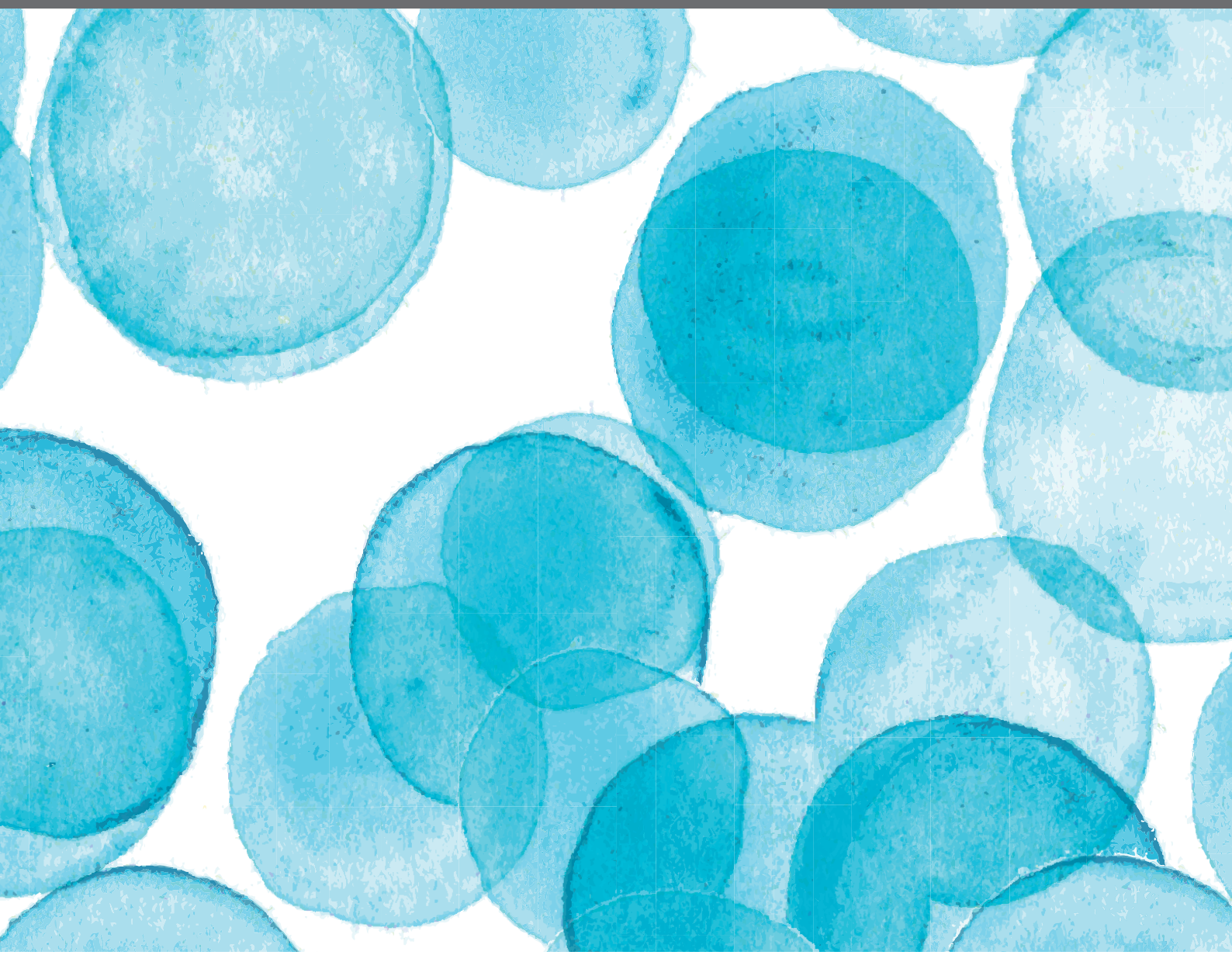

frontiers Research Topics

frontiers

ISSN 1664-8714
ISBN 978-2-88945-789-2
DOI 10.3389/978-2-88945-789-2

About Frontiers

Frontiers is more than just an open-access publisher of scholarly articles: it is a pioneering approach to the world of academia, radically improving the way scholarly research is managed. The grand vision of Frontiers is a world where all people have an equal opportunity to seek, share and generate knowledge. Frontiers provides immediate and permanent online open access to all its publications, but this alone is not enough to realize our grand goals.

Frontiers Journal Series

The Frontiers Journal Series is a multi-tier and interdisciplinary set of open-access, online journals, promising a paradigm shift from the current review, selection and dissemination processes in academic publishing. All Frontiers journals are driven by researchers for researchers; therefore, they constitute a service to the scholarly community. At the same time, the Frontiers Journal Series operates on a revolutionary invention, the tiered publishing system, initially addressing specific communities of scholars, and gradually climbing up to broader public understanding, thus serving the interests of the lay society, too.

Dedication to Quality

Each Frontiers article is a landmark of the highest quality, thanks to genuinely collaborative interactions between authors and review editors, who include some of the world's best academicians. Research must be certified by peers before entering a stream of knowledge that may eventually reach the public - and shape society; therefore, Frontiers only applies the most rigorous and unbiased reviews.
Frontiers revolutionizes research publishing by freely delivering the most outstanding research, evaluated with no bias from both the academic and social point of view. By applying the most advanced information technologies, Frontiers is catapulting scholarly publishing into a new generation.

What are Frontiers Research Topics?

Frontiers Research Topics are very popular trademarks of the Frontiers Journals Series: they are collections of at least ten articles, all centered on a particular subject. With their unique mix of varied contributions from Original Research to Review Articles, Frontiers Research Topics unify the most influential researchers, the latest key findings and historical advances in a hot research area! Find out more on how to host your own Frontiers Research Topic or contribute to one as an author by contacting the Frontiers Editorial Office: researchtopics@frontiersin.org

ANTIBIOTIC ALTERNATIVES AND COMBINATIONAL THERAPIES FOR BACTERIAL INFECTIONS

Topic Editors:
Sanna Sillankorva, International Iberian Nanotechnology Laboratory, Portugal
Maria Olívia Pereira, University of Minho, Portugal
Mariana Henriques, University of Minho, Portugal

Citation: Sillankorva, S., Pereira, M. O., Henriques, M., eds. (2019). Antibiotic Alternatives and Combinational Therapies for Bacterial Infections. Lausanne: Frontiers Media. doi: 10.3389/978-2-88945-789-2

Table of Contents

frontiers in Microbiology

EDITORIAL
published: 18 January 2019
doi: 10.3389/fmicb.2018.03359

Editorial: Antibiotic Alternatives and Combinational Therapies for Bacterial Infections

Sanna Sillankorva, Maria Olívia Pereira and Mariana Henriques*

Laboratório de Investigação em Biofilmes Rosário Oliveira, Centre of Biological Engineering, University of Minho, Braga, Portugal

Keywords: antibiotic alternatives, bacterial infection, probiotic, bacteriophage, anti-persister molecule, biofilm

Editorial on the Research Topic

Antibiotic Alternatives and Combinational Therapies for Bacterial Infections

"The thoughtless person playing with penicillin treatment is morally responsible for the death of the man who succumbs to infection with the penicillin-resistant organism." As Alexander Fleming predicted in 1945, bacteria have become increasingly resistant to antibiotics. Penicillin resistance was presumably first reported already in 1940 when Abraham and Chain reported that an enzyme from bacteria was able to destroy penicillin (Abraham and Chain, 1940). Every now and then mankind is shelled with news of infections and deaths caused by antibiotic and multiple drug resistant superbugs. This increase of resistance toward commonly in-use antibiotics, due to decades of their use, misuse and abuse, is today a global health concern. Research investments on development of new agents that can fight antimicrobial resistant microorganisms and the advent of antibiotic failure due to bacterial resistance has raised interest in other non-conventional alternative therapies.

This Research Topic gathers some of the latest science around antibiotic alternatives and the effect of combined therapies. The call was launched in July 2017, and open-call papers were submitted until May 2018. This is the editorial article introducing the 20 accepted publications addressing the antimicrobial action of varied agents representing the breadth and scope of research in this topic.

A high number of publications address the antibacterial use of bacteriophages. A mini review by Morozova et al. describes the main outcomes of English and Russian case reports regarding bacteriophage use in infected wounds, burns and trophic ulcers. The antimicrobial assessment of bacteriophage therapy include *in vitro* testing toward biofilms of *Klebsiella pneumoniae* isolated from diabetic foot patients (Taha et al.), *Staphylococcus aureus* biofilms (Kumaran et al.), and their combined use with honey to control dual species biofilms of *Pseudomonas aeruginosa* and *Escherichia coli* in an *ex vivo* wound model (Oliveira et al.). Overall, bacteriophages were able to decrease bacterial loads and destroy biofilm structures. Bacteriophage-antibiotic treatment order was investigated by Kumaran et al. and this greatly influenced the treatment outcome, and bacteriophages always augmented the activity of antibiotics. Ujmajuridze et al. screened cultures of patients planned for transurethral resection of prostate, adapted the commercial Pyo bacteriophage preparation to target the main species identified (*S. aureus*, *E. coli*, *Streptococcus* spp., *P. aeruginosa*, and *Proteus mirabilis*), administered the preparation via intravesical delivery in nine patients, and observed bacterial decrease in six of the nine patients treated. *In vivo* use of a purified bacteriophage capsule depolymerase to treat *E. coli* infections in a mouse thigh model was also studied (Lin et al.). In this work, the authors show that *E. coli* infections, usually lethal to mice, were effectively treated with an

OPEN ACCESS

Edited by:
Stephen Tobias Abedon, The Ohio State University, United States

Reviewed by:
Sarah J. Kuhl, VA Northern California Health Care System, United States
Beata Weber-Dąbrowska, Institute of Immunology and Experimental Therapy (PAN), Poland

****Correspondence:***
Sanna Sillankorva
s.sillankorva@deb.uminho.pt

Specialty section:
This article was submitted to Antimicrobials, Resistance and Chemotherapy, a section of the journal Frontiers in Microbiology

Received: *10 October 2018*
Accepted: *31 December 2018*
Published: *18 January 2019*

Citation:
Sillankorva S, Pereira MO and Henriques M (2019) Editorial: Antibiotic Alternatives and Combinational Therapies for Bacterial Infections. Front. Microbiol. 9:3359. doi: 10.3389/fmicb.2018.03359

enzyme dose of 20 μg per mouse; however this effect was enzyme and capsule type dependent.

Three original research articles assessed the use of probiotics such as *Lactobacillus plantarum* or *L. rhamnosus*. Wang et al. describe the diverse roles of *L. plantarum* from enhancing the intestinal barrier function, inducing the secretion of antimicrobial peptides that protect against pathogens, improving the gut bacterial ecology and barrier function in weaned piglets. The efficacy of *L. plantarum* in preventing enterotoxigenic *E. coli* growth and inhibiting its adhesion to a porcine intestinal epithelial cell line was also assessed (Wang et al.). *L. rhamnosus* was reported to reduce the adhesion of *E. coli* to bovine mammary epithelial cells devoid of the caspase recruitment domain by supressing the NLRP3 and NLRP4 inflammasomes and inhibiting *E. coli*-induced cell pyroptosis (Wu et al.).

Defraine and colleagues reported extensive *P. aeruginosa* membrane damage caused by a novel anti-persister molecule (Defraine et al.) and its antibacterial effect together with different classes of antibiotics toward clinically relevant ESKAPE pathogens (Defraine et al.). The molecule used (SPI009) has great potential to inhibit biofilm growth and eradicate both *P. aeruginosa* and *S. aureus* biofilms, and improved nematode survival when tested in *Caenorhabditis elegans* infected with *P. aeruginosa*. Vitamin C was shown to have antibiofilm activity against *Bacillus subtilis* by reducing the extracellular polymeric substance biosynthesis, with cells becoming more susceptible for killing (Pandit et al.).

An original article by Klitgaard et al. identified potential genes that could be suitable as targets for ciprofloxacin potentiating compounds, and found that in targeting the AcrAB-TolC efflux pump and the SOS response proteins RecA and RecC, *E. coli* resistance to ciprofloxacin was reverted in intermediate susceptible strains.

Antibiotic derivatives were reported by Ramchuran et al., who used three teixobactin derivatives to inhibit methicillin-resistant *S. aureus* (MRSA) growth, giving evidence of its dominant binding mode to lipid II. Antibiotic combinations against established *S. aureus* biofilms were also studied in a hollow fiber infection model. However, no beneficial effect of combination therapy compared to the most effective antibiotic was observed, though the addition of the second antibiotic reduced the rise of bacterial resistant to the first drug (Broussou et al.). Anti-MRSA activity using cationic nanostructured lipid carriers combined with antibiotic was evaluated in mice models of cutaneous infection resulting in infection reduction and improvement of skin barrier function and architecture (Alalaiwe et al.). The topical efficacy and safety of chitogel assembled together with an iron chelator and with a novel broad spectrum antimicrobial effectively reduced *S. aureus* biofilms in an *in vivo* sheep model without causing any topical or systemic adverse effects (Ooi et al.). The topical treatment of recalcitrant chronic rhinosinusitis using colloidal silver was assessed through a 10-day program where patients performed rinsing twice daily (Ooi et al.). Despite being safe, the group of treated patients had similar improvement in symptoms and endoscopic scores as those in the control groups and were inferior to culture-directed oral antibiotics. Tran et al. used an antineoplastic mitotane, that permeabilize the outer membrane of *P. aeruginosa*, *Acinetobacter baumannii* and *K. pneumoniae*, to exert greater effect to a novel polymyxin, and reduce the emergence of antibiotic-resistant phenotypes.

Three branched RRWQWR-based cationic peptides were designed, synthesized and evaluated revealing higher antibacterial activity against clinically relevant pathogens than the reference peptide (Vega et al.).

We hope that you enjoy reading this Research Topic and find it a useful reference for the state of the art in the emerging field of antibiotic alternatives.

AUTHOR CONTRIBUTIONS

All authors listed have made a substantial, direct and intellectual contribution to the work, and approved it for publication.

FUNDING

This study was supported by the Portuguese Foundation for Science and Technology (FCT) under the scope of the strategic funding of UID/BIO/04469 unit and COMPETE 2020 (POCI-01-0145-FEDER-006684) and BioTecNorte operation (NORTE-01-0145-FEDER-000004) funded by the European Regional Development Fund under the scope of Norte2020-Programa Operacional Regional do Norte. SS is Investigador FCT (IF/01413/2013).

REFERENCES

Abraham, E. P., and Chain, E. (1940). An Enzyme from bacteria able to destroy penicillin. *Nature* 146:837. doi: 10.1038/146837a0

Conflict of Interest Statement: The authors declare that the research was conducted in the absence of any commercial or financial relationships that could be construed as a potential conflict of interest.

frontiers in Microbiology

ORIGINAL RESEARCH
published: 07 August 2018
doi: 10.3389/fmicb.2018.01832

Adapted Bacteriophages for Treating Urinary Tract Infections

Aleksandre Ujmajuridze[1†], Nina Chanishvili[2†], Marina Goderdzishvili[2], Lorenz Leitner[3], Ulrich Mehnert[3], Archil Chkhotua[1], Thomas M. Kessler[3‡] and Wilbert Sybesma[3‡]*

[1] The Alexander Tsulukidze National Center of Urology, Tbilisi, Georgia, [2] The George Eliava Institute of Bacteriophage, Microbiology and Virology, Tbilisi, Georgia, [3] Department of Neuro-Urology, Balgrist University Hospital, University of Zurich, Zurich, Switzerland

Urinary tract infections (UTIs) are among the most widespread microbial diseases and their economic impact on the society is substantial. The continuing increase of antibiotic resistance worldwide is worrying. As a consequence, well-tolerated, highly effective therapeutic alternatives are without delay needed. Although it has been demonstrated that bacteriophage therapy may be effective and safe for treating UTIs, the number of studied patients is low and there is a lack of randomized controlled trials (RCTs). The present study has been designed as a two-phase prospective investigation: (1) bacteriophage adaptation, (2) treatment with the commercially available but adapted Pyo bacteriophage. The aim was to evaluate feasibility, tolerability, safety, and clinical/microbiological outcomes in a case series as a pilot for a double-blind RCT. In the first phase, patients planned for transurethral resection of the prostate were screened (n = 130) for UTIs and enrolled (n = 118) in the study when the titer of predefined uropathogens (*Staphylococcus aureus*, *E. coli*, *Streptococcus* spp., *Pseudomonas aeruginosa*, *Proteus mirabilis*) in the urine culture was $\geq 10^4$ colony forming units/mL. *In vitro* analysis showed a sensitivity for uropathogenic bacteria to Pyo bacteriophage of 41% (48/118) and adaptation cycles of Pyo bacteriophage enhanced its sensitivity to 75% (88/118). In the second phase, nine patients were treated with adapted Pyo bacteriophage and bacteria titer decreased (between 1 and 5 log) in six of the nine patients (67%). No bacteriophage-associated adverse events have been detected. The findings of our prospective two-phase study suggest that adapted bacteriophage therapy might be effective and safe for treating UTIs. Thus, well-designed RCTs are highly warranted to further define the role of this potentially revolutionizing treatment option.

Keywords: bacteriophage therapy, Pyo bacteriophage, adaptation, urinary tract infection, antibiotic resistance

OPEN ACCESS

Edited by:
Sanna Sillankorva, University of Minho, Portugal

Reviewed by:
Elizabeth Martin Kutter, The Evergreen State College, United States
D. Ipek Kurtböke, University of the Sunshine Coast, Australia
Konstantin Anatolievich Miroshnikov, Institute of Bioorganic Chemistry (RAS), Russia

***Correspondence:**
Thomas M. Kessler
tkessler@gmx.ch

†Shared first authorship
‡Shared last authorship

Specialty section:
This article was submitted to Antimicrobials, Resistance and Chemotherapy, a section of the journal Frontiers in Microbiology

Received: *13 April 2018*
Accepted: *23 July 2018*
Published: *07 August 2018*

Citation:
Ujmajuridze A, Chanishvili N, Goderdzishvili M, Leitner L, Mehnert U, Chkhotua A, Kessler TM and Sybesma W (2018) Adapted Bacteriophages for Treating Urinary Tract Infections. Front. Microbiol. 9:1832. doi: 10.3389/fmicb.2018.01832

INTRODUCTION

Emergence and re-emergence of multiple antibiotic resistant bacterial infections and their rapid spread in the environment has led to a new rise of scientific interest toward bacteriophage therapy as an alternative to antibiotics. Use of bacteriophages for treatment of bacterial infections has been suggested by the French-Canadian scientist Felix d'Herelle in 1917. Since then, bacteriophage therapy has been applied in different fields of medicine, for treatment of various bacterial infections (Chanishvili, 2012). However, after the discovery of penicillin in 1940s the Western scientific

societies gave the preference to antibiotic therapy, while many physicians and researchers in the former Soviet Union republics remained dedicated to bacteriophage therapy and continued to use it alone or in combination with antibiotics (Chanishvili, 2012), see also **Supplementary Material** for more references, partly in Russian.

Lower urinary tract symptoms (LUTS) are a common problem in adult men with a high impact on quality of life (Martin et al., 2011). Traditionally LUTS have been related to bladder outlet obstruction, which is often caused by prostatic enlargement (Abrams et al., 2002). Prostatic enlargement occurs in about 25% of all men in their fifties, 30% in their sixties, and in 50% of men aged 80 years or older (Kupelian et al., 2006). Transurethral resection of prostate (TURP) is regarded the cornerstone of surgical treatment of LUTS secondary to benign prostatic obstruction (Cornu et al., 2015). These patients have a relevant risk for urinary tract infections (UTIs) (Schneidewind et al., 2017). Beside the possible development of residual urine, which acts as a growth medium for bacteria (Truzzi et al., 2008), many of these patients rely on a short or long-term catheterization prior to further treatment. Single insertion of a catheter causes infection in 1–2% of cases, while catheters with open-drainage systems result in bacteriuria in almost 100% of the cases within 3–4 days (Warren, 1992; Bonkat et al., 2018).

Therefore, we decided to combine TURP with bacteriophage therapy, using bacteriophages as a replacement of perioperative antibiotics. The present study has been designed as prospective two-phase (first phase: bacteriophage adaptation, second phase: treatment with the commercially available but adapted Pyo bacteriophage) study preceding a randomized, placebo-controlled, double-blind clinical trial (Leitner et al., 2017) to assess efficacy and safety of adapted bacteriophages for treating (catheter associated) UTIs (Nicolle et al., 2005; Hooton et al., 2010; Bonkat et al., 2018) in patients undergoing TURP.

PATIENTS AND METHODS

Ethics Committee Approval

This prospective two-phase study has been approved by the local ethics committee (TNCU-02/283; Tbilisi, Georgia) and was conducted at the Alexander Tsulukidze National Center of Urology (TNCU), Tbilisi, Georgia and the Eliava Institute of Bacteriophage, Microbiology and Virology (EIBMV), Tbilisi, Georgia. The study was designed as an investigation preceding the randomized controlled trial (RCT) registered at ClinicalTrials.gov: NCT03140085 (Leitner et al., 2017).

Patients

From September 2016, 130 patients planned for TURP were screened in preparation for the RCT (Leitner et al., 2017) at the TNCU. In the first phase, urine cultures from all patients (taken by mid-stream urine, or from the existing transurethral or suprapubic catheter) were evaluated. Overall, 118 (91%) of the 130 screened patients had positive urinary cultures with predefined uropathogens (i.e., *Staphylococcus aureus*, *E. coli*, *Streptococcus* spp., *Pseudomonas aeruginosa*, *Proteus mirabilis*) and $\geq 10^4$ colony forming units (CFU)/mL. The isolated cultures were consecutively subjected to an *in vitro* bacteriophage sensitivity test to the commercially available and in Georgia registered Pyo bacteriophage solution (Eliava BioPreparations Ltd., Tbilisi, Georgia), which underwent adaptation cycles, as described in the next paragraph. In the second phase, nine patients who had scored sensitive to the cocktail were further subjected to bacteriophage treatment in a non-blinded fashion. Exclusion criteria were symptomatic UTIs, microorganisms not sensitive to Pyo bacteriophage and age under 18 years. From all patients, prostate size, prostate specific antigen (PSA), International Prostate Symptom Score (IPSS) questionnaire (Barry et al., 1992) values, maximum flow rate and post void residual were collected prior to surgery. Resected prostate volume was collected and histological results were determined. Urine culture sampling was repeated 7 days after surgery or at the time of any adverse events. Written informed consent was obtained from all included patients.

Bacteriophage Preparation and Adaptation

To cover a diversity of uropathogens a commercial preparation called Pyo bacteriophage produced by Eliava BioPreparations Ltd., Tbilisi, Georgia, was used for treating UTIs. This bacteriophage cocktail is composed of bacteriophage lines active against a broad spectrum of uropathogenic bacteria: *Staphylococcus aureus, E. coli, Streptococcus* spp. (including Streptococci group D renamed now to *Enterococcus* spp.), *Pseudomonas aeruginosa*, and *Proteus* spp. of urological infections (Chanishvili, 2012). As is common practice, commercial bacteriophage cocktails, including Pyo bacteriophage, are regularly adapted by the EIBMV with the aim to increase the efficacy of the bacteriophage cocktail toward newly emerging pathogens (Kutter et al., 2010; Villarroel et al., 2017; McCallin et al., 2018). Also in our study we applied adaptation to enhance the efficacy and coverage toward uropathogenic strains that initially scored intermediate or resistant in the *in vitro* sensitivity study, in a similar way as done in the previously conducted *in vitro* study (Sybesma et al., 2016). The method is based on Appelmans' protocol for titration of bacteriophages (Appelmans, 1921) and selects for h-mutants with a broader and stronger host–bacteriophage interaction (Merabishvili et al., 2018). Similar as for the determination of the minimal inhibitory concentration for antibiotics (Levison and Levison, 2009), Appelmans' method is based on liquid titration of bacteriophages and determines the lowest concentration of bacteriophages that show optical transparency over 24–72 h in a suspension with pre-selected bacterial strains resistant to the bacteriophage cocktail. This dilution with the lowest concentration of bacteriophages, cut-off point, is designated with negative degree values. If the initial bacteriophage titer was 10^{-1}, it may become 10^{-2} or 10^{-3} with every dilution round, which indicates that more active bacteriophage units had been able to kill bacteria and that the tested bacteria had become less resistant to the adapted bacteriophages.

The subsequent titer of the bacteriophages is determined using two methods: titration in liquid (Appelmans, 1921) and titration using a double layer agar method (Gratia, 1936). The titration is done for each component included into Pyo bacteriophages separately on a standard set of host cultures (i.e., the titer of the *E. coli* bacteriophages is determined on the set of the standard *E. coli* strains, the titer of *Staphylococcus* component is determined on the set of the standard *Staphylococcus* strains, etc.). In this way, the titer of the bacteriophages in the range of 10^7–10^9 plaque forming units per mL (pfu/mL) is estimated. However, the titer of the individual (adapted) clones included into one group of bacteriophages may vary (McCallin et al., 2018).

Microbiological Evaluation and Bacteriophage Sensitivity Test

In the first phase, urine samples were streaked in triple on the chromogenic Uriselect^{TM}4 media (Bio-Rad Laboratories, Marnes-la-Coquette, France) for quantification and qualification of uropathogenic microorganisms. Positive urinary cultures were microscopically assessed regarding Gram stains and morphology. For all bacterial strains antibiotic and phage sensitivity tests were performed. If eligible microorganisms potentially treatable with Pyo bacteriophage (*S. aureus*, *E. coli, Streptococcus* spp., *P. aeruginosa, P. mirabilis*) were found, urine cultures were sent to the EIBMV and further screened for bacteriophage sensitivity. Hereto, the urine samples were re-cultivated and their identity was re-checked. As soon as the same eligible microorganisms had been cultivated a bacterial cell lysis screening assay was performed, as described previously (Sybesma et al., 2016). If *in vitro* results showed clear confluent lyses on the petri dish with the bacterial lawn, it was classified as sensitive (**Figure 1**). Resistant and intermediate resistant strains were used in adaptation cycles. In case of sensitivity Pyo bacteriophage was sent to the hospital to start the treatment. Seven days after TURP, urine samples were again collected and cultivated in triple on the above mentioned chromogenic Uriselect^{TM}4 media and re-evaluated.

Intravesical Bacteriophage Treatment

Transurethral resection of prostate was performed according general surgical practice using a monopolar resectoscope (May and Hartung, 2006). For low pressure irrigation, a suprapubic trocar was placed in every patient. No perioperative antibiotic prophylaxis was given. After TURP a suprapubic catheter and a transurethral catheter were placed to maintain irrigation. The transurethral catheter was removed after 24–48 h. The suprapubic catheter was kept in place for 7 days to enable adapted Pyo bacteriophage instillation. Pyo bacteriophage was instilled by a health care provider two times per 24 h (i.e., 8.00 h, 20.00 h) for 7 days, starting the first day after surgery. The solution of 20 mL was retained in the bladder for approximately 30–60 min.

Assessment of Safety and Clinical/Microbiological Outcomes

All adverse events within the treatment phase were recorded as defined by the International Conference on Harmonisation (ICH) Good Clinical Practice (GCP) Guidelines (E6) (International Conference on Harmonisation, 1996) and International Organization for Standardization (ISO 14155) (International Organization for Standardization, 2011). Potential efficacy was assessed using clinical/microbiological parameters and defined as no clinical signs for infection and a reduction in CFU/mL.

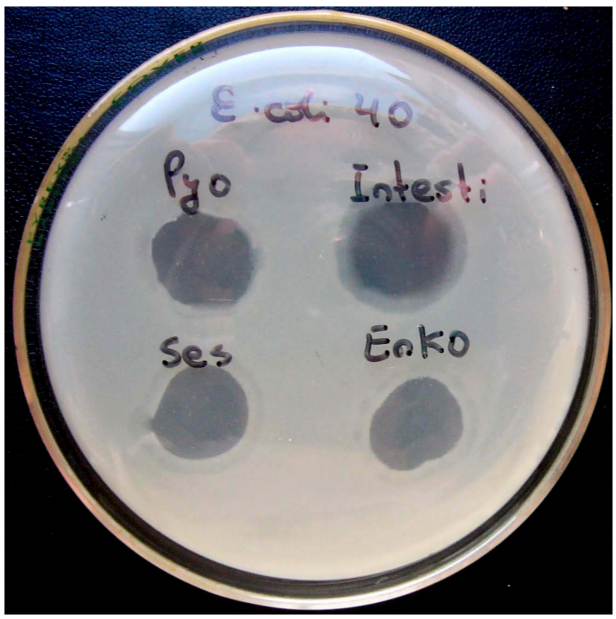

FIGURE 1 | Different degrees of lyses of bacterial culture due to bacteriophage activity. The results in upper line (for Pyo bacteriophage and Intesti bacteriophage) are considered as "S" (sensitive), while the results in the lower line (Ses bacteriophage and Enko bacteriophage) are considered as "I" (intermediate). Note: Pyo, Intesti, Ses, and Enko bacteriophage are all commercially available bacteriophage cocktails. Picture was taken during previously conducted work (Sybesma et al., 2016) where several different bacteriophage cocktails were used.

Outcome Parameters

Primary: (a) sensitivity of uropathogenic strains to the commercially available but adapted Pyo bacteriophage (first phase) and (b) effect of intravesical treatment with adapted Pyo bacteriophage (second phase).

Secondary: Occurrence/absence of adverse events, in categorization according to the National Cancer Institute Common Terminology Criteria for Adverse Events (CTCAE) version 4 in grade 1 to 5[1] during bacteriophage treatment (second phase).

Statistical Analyses

Descriptive statistics were used. Data are presented as percentages or mean ± standard deviation. Due to the limited number of subjects no further statistical analyses were performed.

[1]http://ctep.cancer.gov/protocolDevelopment/electronic_applications/ctc.htm

RESULTS

First Phase: *in vitro* Bacteriophage Sensitivity Testing and Adaptation Cycles

The distribution of bacterial strains of the 118 included patients is shown in **Figure 2**. 24% and 17% of all strains were sensitive and intermediate sensitive to the initially used Pyo bacteriophage (i.e., total sensitivity of 41%), **Figure 3A**. After four adaptation cycles the sensitivity and intermediate sensitivity increased up to 41% and 34% (i.e., total sensitivity 75%), **Figure 3B**.

Second Phase: Treatment With Adapted Pyo Bacteriophage

Patients characteristics are found in **Table 1**. The mean age was 69 ± 12 years, IPSS questionnaires revealed moderate to strong LUTS (IPSS 20 ± 2). The average prostate size was 77 ± 37 mL, all PSA values were within the non-pathological range. Maximum flow rate was 11 ± 3 mL/s with a mean post void residual of 80 ± 100 mL. Two patients relied on an indwelling catheter preoperatively. The average operation time was 48 min, no complications occurred during prostate surgery. Histological results revealed benign prostatic hyperplasia in all cases, five patients showed high grade prostatic intraepithelial neoplasia but no malignant disease was found.

Prior to treatment, urine culture revealed *E. coli* in four, *Streptococcus* spp. in two, *Enterococcus* spp. in two and *P. aeruginosa* in one of the nine patients. After treatment, four patients showed no significant bacterial growth, while *E. coli* and *Enterococcus* spp. were still isolated from the urine culture of four and one patient, respectively. In six out of nine patients (67%), bacterial titers decreased after bacteriophage treatment (**Table 1**).

No bacteriophage-associated adverse events have been detected. In one patient, an antibiotic therapy (third generation cephalosporin) was started at day 3 after development of fever (>38.0°C) and the symptoms disappeared within 48 h. Urine culture showed *P. aeruginosa*.

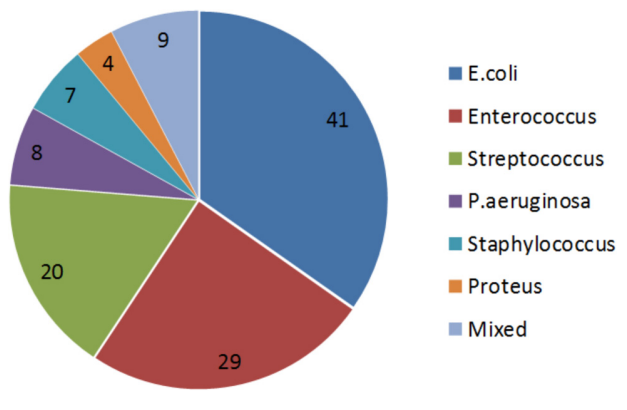

FIGURE 2 | Proportional distribution of bacterial strains. Urinary cultures of the 118 included patients showed the following distribution of bacterial strains: *E. coli* was found predominantly with 41%, followed by *Enterococcus* spp. with 29%, *Streptococcus* spp. with 20%, *Pseudomonas aeruginosa* with 8%, *Staphylococcus* spp. 7%, *Proteus* spp. 4%, and others 9%.

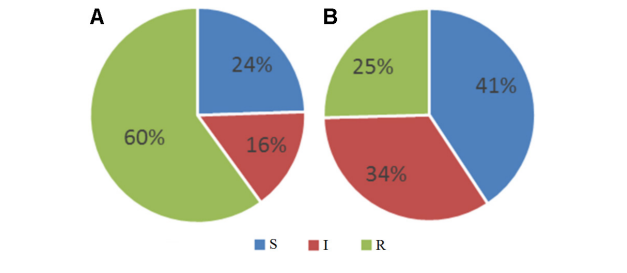

FIGURE 3 | Proportional distribution of the sensitive, intermediate, and resistant strains among 118 clinical samples before **(A)** and after **(B)** four adaptation cycles of the Pyo bacteriophage cocktail.

DISCUSSION

In vitro analysis showed a sensitivity for uropathogenic bacteria to the commercially available Pyo bacteriophage of 41%. Adaptation cycles of Pyo bacteriophage further enhanced its sensitivity to 75%. In our *in vivo* pilot series, the bacterial titers decreased after bacteriophage treatment in six out of nine patients (67%). No bacteriophage-associated adverse events have been detected but one patient developed fever due to *P. aeruginosa* infection with restitution of symptoms under antibiotic treatment.

Our study was designed as a feasibility, tolerability, and safety assessment and to evaluate clinical/microbiological outcomes of commercially available adapted Pyo bacteriophages preceding a placebo-controlled, double-blind RCT (Leitner et al., 2017). We have not investigated the composition of the continuously adapted Pyo bacteriophage cocktail by, e.g., metagenome analysis as recently described for previously used Pyo bacteriophage cocktails (Villarroel et al., 2017; McCallin et al., 2018), where it has also been reported that as a result of adaptation the titer of the individual bacteriophage clones included may vary. We expect that the detailed elucidation of the composition of bacteriophage cocktails as well as understanding the mechanisms behind the bacteriophage infection or bacterial resistance will become more relevant as soon as more conclusive outcomes about the efficacy of bacteriophage therapy has been described.

Bacteriophage therapy has already been practiced for decades in Eastern European countries (Chanishvili, 2012) and many people are aware of its existence (see also **Supplementary Material** for more references, partly in Russian). In the present open-label pioneering study for a placebo-controlled, double-blind RCT, the commercially available preparation Pyo bacteriophage was used for treating nine patients who were planned for TURP and had been diagnosed with UTI. Bacteriophage therapy only started after a positive result of an *in vitro* sensitivity analysis of the isolated uropathogen with the Pyo bacteriophage cocktail and did not cause any adverse events such as rise of body temperature, headache, hematuria, or allergic reaction in eight out of nine patients. Only in one case (# 9), on the 3rd day after prostate surgery, fever was observed. After a

TABLE 1 | Summary of results of intravesical Pyo bacteriophage treatment conducted on nine patients.

Case	Age range (years)	Pre-treatment		Post-treatment		Prostate size (g)	PSA value (μg/L)	Adverse events/remarks
		Culture ID	Titer (CFU/mL)	Culture ID	Titer (CFU/mL)			
1	61–65	*E. coli*	10^7	*E. coli*	10^5	70	1	No adverse events
2	81–85	*E. coli*	10^7	*E. coli*	10^4	140	2	No adverse events
3	56–60	*E. coli*	10^4	*E. coli*	10^4	65	0.3	No adverse events
4	81–85	*E. coli*	10^7	Non-pathogenic microflora	Not quantified	90	3.2	No adverse events
5	56–60	*Streptococcus*	10^7	*Streptococcus*	10^6	130	0.8	No adverse events
6	81–85	*Streptococcus*	10^5	No bacterial growth	Below detection limit	29	2.3	No adverse events
7	66–70	*Enterococcus*	10^6	*E. coli*	10^7	45	1	Potential secondary infection
8	66–70	*Enterococcus*	10^6	Non-pathogenic microflora	Not quantified	60	1.3	No adverse events
9	56–60	*Pseudomonas*	10^6	No data	No data	60	1.3	Sudden fever and chills started on the 3rd day

sudden onset of fever (38.5°C), the bacteriophage treatment was stopped, while a third generation cephalosporin was prescribed. In 48 h after the start of antibiotic therapy, the body temperature was normalized (24 h: 37.8°C; 48 h: <37.5°C). In this particular case the infection was caused by *P. aeruginosa*, which is known to release endotoxins during its lysis.

The secondary bacteriology testing of urine samples, taken after the bacteriophage treatment, demonstrated a positive tendency in therapy of infection, in particular a decrease of bacterial counts varying between 1 and 5 logs (cases # 1, 2, 5, 6). In one case (# 6) the secondary bacteriology analysis after bacteriophage therapy showed that urine had become below the detection limit of the Uriselect^{TM}4 media (10^4 CFU/mL for the uropathogens). In two cases (# 4, # 8) the initial infections, *E. coli* (titer 10^7 CFU/mL) and *Enterococcus* (titer 10^6 CFU/mL), respectively, had disappeared after bacteriophage therapy; however, presence of non-pathogenic micro-flora was observed which did not require any further treatment. It is notable that in these two cases the non-pathogenic flora appeared in aged patients 69–80 years old, which may be a result of urination difficulties remaining even after the operation. In one case (# 3) the titer of *E. coli* did not change after the bacteriophage treatment. In case (# 7) the initial infection caused by *Enterococcus* (titer 10^6 CFU/mL) after bacteriophage therapy was replaced by *E. coli* (titer 10^7 CFU/mL), which may be attributed to a secondary infection.

Although the design and number of cases and the diversity of the results described in this publication do not permit to draw out any statistically reliable conclusions, the trend indicated by the data from our study does not stand on its own and corresponds well with the outcome of several other recently reported cases where bacteriophage therapy was used in Western countries (Abedon et al., 2017). In terms of safety, the findings of our prospective two-phase study support earlier made conclusions that bacteriophage therapy using broad spectrum bacteriophages cocktails, including Pyo bacteriophage, is safe (McCallin et al., 2013, 2018; Sarker et al., 2016). However, for a definite conclusion about efficacy of bacteriophage treatment, well designed RCTs are urgently needed.

Due to a too high use of antibiotics in today's society, the emergence of antibiotic resistance pathogens has become a serious problem in terms of increased morbidity and mortality rates as well as the elevated healthcare costs as has been brought to the public attention by several national and international health protection agencies (CDC, 2013; European Centre for Disease et al., 2017; Leitner et al., 2017). Since the resistance mechanism of bacteria against bacteriophages differs from those against antibiotics, and since bacteriophage are self-replicating and self-evolving entities, bacteriophage therapy could be used as an alternative method to eliminate antibiotic resistant bacteria. One of the main limitations for acceptance and reimplementation of bacteriophage therapy is the lack of placebo-controlled, double-blind RCTs in agreement with Western standards (Expert round table on acceptance and re-implementation of bacteriophage therapy, 2016). We expect that the RCT we preceded with the present open-label study will contribute to conclude on the efficacy, cost and benefits of bacteriophages in case of antibiotic resistant uropathogenic bacteria.

Finally, we would like to remark that before bacteriophages can become accepted and broadly applied for treatment of certain bacterial infections, as is already practiced in several Eastern European countries, the legislative framework in the Western world needs to be adjusted. Since the intrinsic strength of bacteriophages relates to their antagonistic evolution potential with their bacterial hosts, the composition of effective bacteriophages cocktails will not be static, but adapted and adjusted over time, which assures efficacy toward evolving bacterial infections at different moments at different places for different groups of patients. However, such a dynamic approach is not compatible with today's production and admission requirements for chemical drugs. Although the use of bacteriophages is already quite old, it is remarkable to acknowledge that in fact a more tailor-made development and application of bacteriophages are in line with the increasing needs and opportunities around personalized nutrition and

personalized medicine. A recent breakthrough in this debate has been reported for Belgium, where the national authorities agreed on setting up a practical bacteriophage therapy framework that relates on the magistral preparation (compounding pharmacy in the United States) of custom-made bacteriophage medicines (Pirnay et al., 2018). This Belgian "magistral bacteriophage medicine" framework is expected to be flexible enough to exploit and further explore the specific nature of bacteriophages as co-evolving antibacterials whilst giving precedence to patients' safety.

CONCLUSION

In our prospective two-phase study preceding a placebo-controlled, double-blind RCT, adaptation cycles enhanced the *in vitro* sensitivity of 118 strains to the commercially available Pyo bacteriophage from 41% to 75%. In the *in vivo* pilot series, a promising clinical and microbiological effect and excellent tolerability of adapted Pyo bacteriophage treatment could be shown. Our findings suggest that bacteriophage therapy might be effective and safe for treating UTIs. Thus, well-designed RCTs are highly warranted to further define the role of this potentially revolutionizing treatment option.

AUTHOR CONTRIBUTIONS

All authors contributed in designing and setting up the clinical study. AU conducted the bacteriophage treatment. NC and MG conducted all work related to bacteriophages. NC and WS drafted the manuscript. AU, MG, UM, and AC critically reviewed the manuscript. LL and TK made the final editing to the manuscript. All the authors read and approved the final manuscript.

FUNDING

This study was supported by the Swiss Continence Foundation (www.swisscontinencefoundation.ch), the Swiss National Science Foundation (www.snsf.ch), and the Swiss Agency for Development and Cooperation in the framework of the programme SCOPES (Scientific co-operation between Eastern Europe and Switzerland, Grant No. 152304).

SUPPLEMENTARY MATERIAL

The Supplementary Material for this article can be found online at: https://www.frontiersin.org/articles/10.3389/fmicb.2018.01832/full#supplementary-material

REFERENCES

Abedon, S. T., García, P., Mullany, P., and Aminov, R. (2017). Editorial: phage therapy: past, present and future. *Front. Microbiol.* 8:981. doi: 10.3389/fmicb.2017.00981

Abrams, P., Cardozo, L., Fall, M., Griffiths, D., Rosier, P., Ulmsten, U., et al. (2002). The standardisation of terminology of lower urinary tract function: report from the standardisation sub-committee of the international continence society. *Neurourol. Urodyn.* 21, 167–178. doi: 10.1002/nau.10052

Appelmans, R. (1921). Le dosage des bacteriophages. *C. R. Soc. Biol.* 85, 1098–1099.

Barry, M. J., Fowler, F. J. Jr., O'leary, M. P., Bruskewitz, R. C., Holtgrewe, H. L., Mebust, W. K., et al. (1992). The american urological association symptom index for benign prostatic hyperplasia. The measurement committee of the american urological association. *J. Urol.* 148, 1549–1557; discussion 1564. doi: 10.1016/S0022-5347(17)36966-5

Bonkat, G., Pickard, R., Bartoletti, R., Cai, T., Bruyère, F., Geerlings, S. E., et al. (2018). *European Association of Urology (EAU) Guidelines on Urological Infections*. Available at: http://uroweb.org/guideline/urological-infections/ [accessed April 11, 2018].

CDC (2013). *Antibiotic Resistance Threats in the United States*. Available at: http://www.cdc.gov/drugresistance/threat-report-2013

Chanishvili, N. (2012). *A Literature Review of the Practical Application of Bacteriophage Research*. Tbilisi: George Eliava Institute of Bacteriophage, Microbiology and Virology.

Cornu, J. N., Ahyai, S., Bachmann, A., De La Rosette, J., Gilling, P., Gratzke, C., et al. (2015). A systematic review and meta-analysis of functional outcomes and complications following transurethral procedures for lower urinary tract symptoms resulting from benign prostatic obstruction: an update. *Eur. Urol.* 67, 1066–1096. doi: 10.1016/j.eururo.2014.06.017

European Centre for Disease Prevention and Control, European Food Safety Authority and European Medicines Agency (2017). ECDC/EFSA/EMA second joint report on the integrated analysis of the consumption of antimicrobial agents and occurrence of antimicrobial resistance in bacteria from humans and food-producing animals. *EFSA J.* 15:4872.

Expert round table on acceptance and re-implementation of bacteriophage therapy (2016). Silk route to the acceptance and re-implementation of bacteriophage therapy. *Biotechnol. J.* 11, 595–600. doi: 10.1002/biot.201600023

Gratia, A. (1936). The numerical relation between lysogenic bacteria and the phage particles which tey carry. *Ann. Inst. Pasteur* 57, 652–676.

Hooton, T. M., Bradley, S. F., Cardenas, D. D., Colgan, R., Geerlings, S. E., Rice, J. C., et al. (2010). Diagnosis, prevention, and treatment of catheter-associated urinary tract infection in adults: 2009 international clinical practice guidelines from the infectious diseases society of america. *Clin. Infect. Dis.* 50, 625–663. doi: 10.1086/650482

International Conference on Harmonisation. (1996). *Good Clinical Practice Guideline*. Available: http://www.ich.org/products/guidelines/efficacy/article/efficacy-guidelines.html

International Organization for Standardization (2011). *ISO 14155*. Available: http://www.iso.org/iso/catalogue_detail?csnumber=45557

Kupelian, V., Wei, J. T., O'leary, M. P., Kusek, J. W., Litman, H. J., Link, C. L., et al. (2006). Prevalence of lower urinary tract symptoms and effect on quality of life in a racially and ethnically diverse random sample: the boston area community health (BACH) survey. *Arch. Intern. Med.* 166, 2381–2387. doi: 10.1001/archinte.166.21.2381

Kutter, E., De Vos, D., Gvasalia, G., Alavidze, Z., Gogokhia, L., Kuhl, S., et al. (2010). Phage therapy in clinical practice: treatment of human infections. *Curr. Pharm. Biotechnol.* 11, 69–86. doi: 10.2174/138920110790725401

Leitner, L., Sybesma, W., Chanishvili, N., Goderdzishvili, M., Chkhotua, A., Ujmajuridze, A., et al. (2017). Bacteriophages for treating urinary tract infections in patients undergoing transurethral resection of the prostate: a randomized, placebo-controlled, double-blind clinical trial. *BMC Urol.* 17:90. doi: 10.1186/s12894-017-0283-6

Levison, M. E., and Levison, J. H. (2009). Pharmacokinetics and pharmacodynamics of antibacterial agents. *Infect. Dis. Clin. North Am.* 23, 791–815. doi: 10.1016/j.idc.2009.06.008

Martin, S. A., Haren, M. T., Marshall, V. R., Lange, K., Wittert, G. A., and Members of the Florey Adelaide Male Ageing Study (2011). Prevalence and factors associated with uncomplicated storage and voiding lower urinary tract symptoms in community-dwelling Australian men. *World J. Urol.* 29, 179–184. doi: 10.1007/s00345-010-0605-8

May, F., and Hartung, R. (2006). Surgical atlas. transurethral resection of the prostate. *BJU Int.* 98, 921–934. doi: 10.1111/j.1464-410X.2006.06474.x

McCallin, S., Alam Sarker, S., Barretto, C., Sultana, S., Berger, B., Huq, S., et al. (2013). Safety analysis of a Russian phage cocktail: from metagenomic analysis to oral application in healthy human subjects. *Virology* 443, 187–196. doi: 10.1016/j.virol.2013.05.022

McCallin, S., Sarker, S. A., Sultana, S., Oechslin, F., and Brüssow, H. (2018). Metagenome analysis of Russian and Georgian pyophage cocktails and a placebo-controlled safety trial of single phage versus phage cocktail in healthy *staphylococcus aureus* carriers. *Environ. Microbiol.* doi: 10.1111/1462-2920.14310 [Epub ahead of print].

Merabishvili, M., Pirnay, J.-P., and De Vos, D. (2018). "Guidelines to compose an ideal bacteriophage cocktail," in *Bacteriophage Therapy: From Lab to Clinical Practice*, eds J. Azeredo and S. Sillankorva (New York, NY: Springer), 99–110.

Nicolle, L. E., Bradley, S., Colgan, R., Rice, J. C., Schaeffer, A., and Hooton, T. M. (2005). Infectious diseases society of America guidelines for the diagnosis and treatment of asymptomatic bacteriuria in adults. *Clin. Infect. Dis.* 40, 643–654. doi: 10.1086/427507

Pirnay, J.-P., Verbeken, G., Ceyssens, P.-J., Huys, I., De Vos, D., Ameloot, C., et al. (2018). The magistral phage. *Viruses* 10:E64. doi: 10.3390/v10020064

Sarker, S. A., Sultana, S., Reuteler, G., Moine, D., Descombes, P., Charton, F., et al. (2016). Oral phage therapy of acute bacterial diarrhea with two coliphage preparations: a randomized trial in children from Bangladesh. *EBioMedicine* 4, 124–137. doi: 10.1016/j.ebiom.2015.12.023

Schneidewind, L., Kranz, J., Schlager, D., Barski, D., Muhlsteadt, S., Grabbert, M., et al. (2017). Mulitcenter study on antibiotic prophylaxis, infectious complications and risk assessment in TUR-P. *Cent. European J. Urol.* 70, 112–117. doi: 10.5173/ceju.2017.941

Sybesma, W., Zbinden, R., Chanishvili, N., Kutateladze, M., Chkhotua, A., Ujmajuridze, A., et al. (2016). Bacteriophages as potential treatment for urinary tract infections. *Front. Microbiol.* 7:465. doi: 10.3389/fmicb.2016.00465

Truzzi, J. C., Almeida, F. M., Nunes, E. C., and Sadi, M. V. (2008). Residual urinary volume and urinary tract infection–when are they linked? *J. Urol.* 180, 182–185. doi: 10.1016/j.juro.2008.03.044

Villarroel, J., Larsen, M. V., Kilstrup, M., and Nielsen, M. (2017). Metagenomic analysis of therapeutic PYO phage cocktails from 1997 to 2014. *Viruses* 9:E328. doi: 10.3390/v9110328

Warren, J. W. (1992). Catheter-associated bacteriuria. *Clin. Geriatr. Med.* 8, 805–819. doi: 10.1016/S0749-0690(18)30446-4

WHO (2015). *Global Action Plan on Antimicrobial Resistance*. Available at: http://www.wpro.who.int/entity/drug_resistance/resources/global_action_plan_eng.pdf. World Health Organization [accessed April 11, 2018].

Conflict of Interest Statement: The authors declare that the research was conducted in the absence of any commercial or financial relationships that could be construed as a potential conflict of interest.

frontiers in Microbiology

MINI REVIEW
published: 02 August 2018
doi: 10.3389/fmicb.2018.01696

Applications of Bacteriophages in the Treatment of Localized Infections in Humans

Vera V. Morozova, Valentin V. Vlassov and Nina V. Tikunova*

Laboratory of Molecular Microbiology, Institute of Chemical Biology and Fundamental Medicine (RAS), Novosibirsk, Russia

In the recent years, multidrug-resistant bacteria have become a global threat, and phage therapy may to be used as an alternative to antibiotics or, at least, as a supplementary approach to treatment of some bacterial infections. Here, we describe the results of bacteriophage application in clinical practice for the treatment of localized infections in wounds, burns, and trophic ulcers, including diabetic foot ulcers. This mini-review includes data from various studies available in English, as well as serial case reports published in Russian scientific literature (with, at least, abstracts accessible in English). Since, it would be impossible to describe all historical Russian publications; we focused on publications included clear data on dosage and rout of phage administration.

Keywords: phage therapy, clinical practice, wounds, burns, trophic ulcers, diabetic foot ulcers, therapeutic bacteriophage

OPEN ACCESS

Edited by:
Sanna Sillankorva, University of Minho, Portugal

Reviewed by:
Elizabeth Martin Kutter, The Evergreen State College, United States
Nina Chanishvili, George Eliava Institute of Bacteriophage, Microbiology and Virology, Georgia
Sarah J. Kuhl, VA Northern California Health Care System, United States

****Correspondence:***
Vera V. Morozova
vera_morozova@ngs.ru

Specialty section:
This article was submitted to Antimicrobials, Resistance and Chemotherapy, a section of the journal Frontiers in Microbiology

Received: *26 April 2018*
Accepted: *09 July 2018*
Published: *02 August 2018*

Citation:
Morozova VV, Vlassov VV and Tikunova NV (2018) Applications of Bacteriophages in the Treatment of Localized Infections in Humans. Front. Microbiol. 9:1696. doi: 10.3389/fmicb.2018.01696

INTRODUCTION

Since their discovery, bacteriophages have been considered to be potential antibacterial therapeutics for the treatment of various infectious diseases in humans. Initially, clinical application of bacteriophages was aimed at the treatment of acute intestinal diseases (Summers, 1999) and skin infections (Bruynoghe and Maisin, 1921). Later, bacteriophages were applied in surgical practice for treatment of purulent wounds and postoperative infectious complications, and this approach was used in the USSR in the thirties and forties of the twentieth century (Tsulukidze, 1940; Kokin, 1941; Krestovnikova, 1947). After the advent of antibiotics, phage therapy was ceased in most countries and considerably decreased in surgical practice in the USSR. However, the use of bacteriophages in the clinical treatment of infected wounds was not stopped in Eastern Europe and the former SU, as antibiotic treatment of such infections sometimes failed, even in cases of antibiotic-sensitive bacteria. Phage preparations approved for clinical application have been produced in the Russian Federation, Republic of Georgia, and Poland, and a large number of studies on phage therapy have been reported in these countries (Weber-Dabrowska et al., 2000; Sulakvelidze et al., 2001; Chanishvili, 2009, 2016; Górski et al., 2009; Miedzybrodzki et al., 2012; etc), including investigations published in Russian scientific literature (Zhukov-Verezhnikov et al., 1978; Bogovazova et al., 1991; Perepanova et al., 1995; Brusov et al., 2011; etc.).

The rapid rise of multi-drug resistant bacteria worldwide has led to a renewed interest in phage therapy as a possible alternative to antibiotics or, at least, a supplementary approach for the treatment of some bacterial infections. Recently, the results of bacteriophage and phage cocktail application for the treatment of various infections have been reported in a number of clinical cases, case series and clinical trials (Rhoads et al., 2009; Wright et al., 2009; Fish et al., 2016; Jennes et al., 2017). Despite the promising results from phage therapy, still there are no commonly approved

recommendations or therapeutic schemes for phage application. Development of these schemes is complicated by the diversity of phage preparations used (some of which are not even fully characterized), the variety of routes of administration and courses of phage treatment. Notably, the various localizations of bacterial infections require identification of the most preferable routes and therapeutic schemes of phage administration. In this mini-review, we focus on the results of phage therapy applied in the clinical treatment of localized infections in wounds, burns, and trophic ulcers, including diabetic foot ulcers.

BACTERIOPHAGE TREATMENT OF WOUND INFECTIONS AND INFECTIOUS COMPLICATIONS OF SURGICAL WOUNDS

D'Herelle's enthusiasm concerning the wide possibilities of phage therapy led to extensive attempts to isolate bacteriophages that were active against bacterial agents found in infected wounds and apply them in treatment. As a result, phage therapy was used in the USSR during the Finnish Campaign (1939–1940) and continued during the World War II (Tsulukidze, 1940, 1941; Kokin, 1941, 1946; Pokrovskaya et al., 1941; Krestovnikova, 1947). The majority of this historical data (except the study published by Pokrovskaya et al., 1941) was described in a previously published review (Chanishvili, 2012). It was reported that the mixtures of bacteriophages active against *Clostridium perfringens*, *Staphylococcus* spp., and *Streptococcus* spp. were used for the prevention and treatment of gas gangrene (Kokin, 1941). Several studies demonstrated high effectiveness of phage application in an early stage of infection (Kokin, 1941; Pokrovskaya et al., 1941; Tsulukidze, 1941). To improve the efficacy of phage therapy, "Pyophage" (a poly-specific cocktail of phages) was applied initially, and after detection of the etiologic agents, mono-specific lytic phages were used (Pokrovskaya et al., 1941; Tsulukidze, 1941; Krestovnikova, 1947). The best results were achieved in the treatment of *Staphylococcal* and *Streptococcal* infections, and phage application led to the elimination of 69 and 50% of these bacterial pathogens, respectively (Pokrovskaya et al., 1941). A course of phage treatment included washings of a wound with a phage preparation and subcutaneous injections of phages from one to four times per day. Five to eight days of therapy were sufficient for clinical improvement in the majority of cases; however, if no improvement was achieved during this period, further phage application was useless (Pokrovskaya et al., 1941; **Table 1**).

Despite the widespread introduction of antibiotics, phage preparations continued to be used in the USSR and, later, in the Russian Federation for the prevention of wound infections and treatment of infectious complications of surgical wounds (**Table 1**). Poly-specific (Pyophage, Sekstaphage) and mono-specific therapeutic phage cocktails developed in research institutes and pharmaceutical companies were used in the USSR. In the recent years, phage preparations produced in JSC Microgen (http://www.bacteriofag.ru) have been applied. Bacteriophages were administered locally, by subcutaneous injections, and orally (**Table 1**). Notably, phage therapy was carried out as a mono-therapy (Zhukov-Verezhnikov et al., 1978; Peremitina et al., 1981; Kochetkova et al., 1989; Brusov et al., 2011), or in complex treatments, which included phages and antibiotics administration (Kochetkova et al., 1989; Khairullin et al., 2002). The investigations revealed that complex treatments decreased the healing time by 1.2–2.5 times compared to an antibiotic treatment (Kochetkova et al., 1989; Khairullin et al., 2002; **Table 1**). Even application of bacteriophages specific to one of the infectious agents in a wound improved healing and stimulated faster purification (Ponomareva et al., 1985; Khairullin et al., 2002). This positive effect was, probably, due to the partial destruction of biofilms, influence of bacteriophages on the regenerative processes in a wound and on the immune system of a patient (Miedzybrodzki et al., 2009; Górski et al., 2017; Van Belleghem et al., 2017). Importantly, it has been shown that a single application of a bacteriophage could not be enough to prevent infectious complications of wounds (Brusov et al., 2011; **Table 1**).

Phage therapy was applied for the treatment of infected post-operative wounds in cancer patients (Ponomareva et al., 1985; Kochetkova et al., 1989). It resulted in faster cleaning of wounds from purulent masses, granulation, and healing without deforming scars compared to a group of cancer patients which were treated with antibiotics (**Table 1**). In one of these studies, the fastest wound healing was observed in patients treated only by bacteriophages (Kochetkova et al., 1989; **Table 1**). However, it would not be correct to conclude that application of bacteriophages without antibiotics is preferable, as investigators have used complex treatments in patients with more severe infections, previously unsuccessfully treated with antibiotics. Based on the obtained data, the authors have suggested that application of phage preparations provided positive effect in mono-infection, while complex therapy, including bacteriophages and antibiotics, was required in mixed bacterial infection (Kochetkova et al., 1989). One of the reasons for using complex treatments may be the inability of quick selection of lytic bacteriophages active against all pathogens in a wound.

Another important issue of phage therapy is the question of which is better to use: one specific bacteriophage or a poly-specific phage cocktail. Application of highly specific bacteriophages (adapted by cultivation on a bacterial strain isolated from a patient) was more effective than treatment with poly-specific phage cocktails (Zhukov-Verezhnikov et al., 1978; **Table 1**). The significantly higher efficiency of this type of personalized phage therapy can be explained by the improvement of the specificity and virulence of phages to host strains. However, the adapted phage preparations require detailed characterization because they may contain temperate bacteriophages produced by the clinical bacterial strain, which was used for adaptation.

PHAGE TREATMENT OF INFECTED BURNS

Burn surfaces are rapidly colonized by bacteria, which are capable of producing biofilms and are often resistant to multiple

TABLE 1 | Case series and reports of phage therapy of infected wounds in humans.

References	Patients, n (PT, CT, AT)[a]	Phage prophylaxis/ Phage therapy	Type of lesion	Pathogens	Applied phages, titer, pfu/ml[b]	Route of administration (dosage)	Course of phage treatment, days	Characteristics of outcomes
Pokrovskaya et al., 1941	16^{PT}	3/16	Infected wounds	Staphylococci, Streptococci	Pyophage, Streptococcus phage cocktail, Staphylococcus phage cocktail	Washing of the wound (up to 40 ml once a day) Subcutaneous injection (2–10 ml once a day)	2–8	Wound healing in 16/16 patients
Zhukov-Verezhnikov et al., 1978	60 (30^{Pyo}, 30^{APT})[c]	0/60	Infected surgical wounds	*E. coli*, Enterococci, Staphylococci, *P. aeruginosa*	Pyophage, Adapted phage preparations, 10^4-10^6	Topical application once a day	7–10	**Pyo:** Wound healing in 19/30 patients **APT:** Wound healing in 28/30 patients
Ponomareva et al., 1985	77 (19^{PT}, 58^{CT})	0/77	Infected surgical wounds	*E. coli*, Enterococci, *P. aeruginosa*, Staphylococci	Pyophage	Washing of the wound and topical application once a day	5	**PT:** positive responses in 13/19 patients (68%) **CT:** positive responses in 41/58 patients (70.6%)
Kochetkova et al., 1989	78 (7^{PT}, 32^{CT}, 39^{AT})	0/39	Infected surgical wounds	Enterococci, *P. aeruginosa*, Staphylococci	Pyophage, Staphylococcus phage cocktail, Pseudomonas phage cocktails	Washing of the wound (up to 40 ml) and topical application (2–10 ml) once a day	7–10	**PT:** wound healing in 7/7 patients within 17.2 ± 2 days **CT:** Wound healing in 29/32 patients within 26.8 ± 2 days[e] **AT:** Wound healing in 32/39 patients within 32.2 ± 3 days
Khairullin et al., 2002	37 (27^{CT}, 10^{AT})	0/27	Infected surgical wounds	*E. coli, P. aeruginosa*, *Proteus* spp, *S. aureus, S. pyogenes*	Pyophage	Topical application once a day	4–8	**CT:** Wound healing in 27/27 patients within 4–8 days **AT:** Wound healing in 10/10 patients within 10–14 days
Brusov et al., 2011	120[d] (90^{PT})	90/0	Non-infected surgical wounds	No	Sekstaphage	Washing of the wound (up to 40 ml)	Once, at the end of surgical intervention	2 cases of infection in a group of 30 patients
						Per os (20 ml)	Twice, before surgery and 5 days later	No infectious complications in a group of 30 patients
						Subcutaneous injection (2 ml)		
						No phage application	—	3 cases of infection in a group of 30 patients

[a] *PT, phage treatment without antibiotics; CT, complex treatments, including phages and antibiotics; AT, antibiotics treatment.*

[b] *Russian manufactured phage cocktails must contain at least 10^6 pfu/ml of each phage component according to instruction of manufacturer.*

[c] *Pyo, phage treatment with therapeutic phage cocktails; APT, phage treatment with adapted phage preparations.*

[d] *All patients were treated by Cefazolin intramuscularly once before surgery.*

[e] *Previous unsuccessful antibiotic treatment.*

antibiotics (Erol et al., 2004; Church et al., 2006; Asati and Chaudhary, 2017). Additionally, patients with burns frequently suffer from lymphopenia, sepsis, intoxication, and changes in the microbiota (Erol et al., 2004). Phage therapy could potentially be used to treat burns and prevent sepsis. Several case series have been reported (Gomareli et al., 1976; Abul-Hassan et al., 1990; Lazareva et al., 2001; Sivera Marza et al., 2006; Rose et al., 2014), and promising results have been demonstrated in some reports (**Table 2**). Topical application of phages led to the elimination of multiple drug resistant (MDR) *P. aeruginosa* or successful skin graft take in 18 of 30 patients with burns, but the method was time-consuming, and the authors recommended this therapy only for infections resistant to available antibiotics (Abul-Hassan et al., 1990). In other investigation, it was revealed that bacteriophage application in complex therapy (bacteriophages *per os* and antibiotics) provided better clinical dynamics in patients with infected burns compared to a group of antibiotic-treated patients (Lazareva et al., 2001; **Table 2**). Notably, the first group included a higher number (29%) of initially complicated cases (intoxication, sepsis, purulent discharge of wounds), in contrast to 12.6% of such cases in the antibiotic-treated group (Lazareva et al., 2001).

The dosage of phage preparation is believed to be very important in phage therapy, and the therapeutic titer should be higher than 10^6 pfu/ml. Much more concentrated phage suspensions are applied in the majority of reported cases (**Table 2**). However, phage BS24 (Soothill, 1994), which was used at a low titer (10^3 pfu/ml, single application), provided a positive effect (Sivera Marza et al., 2006). In another investigation (Rose et al., 2014), no positive response was recorded when the phage cocktail BFC-1 (Merabishvili et al., 2009) was applied at a high titer (10^9 pfu/ml, single application). The investigators explained this insufficient result by several possible reasons, such as a delay in phage application, previously initiated systemic and topical antimicrobial treatment, and unsuitable pharmaceutical form of BFC-1 (Rose et al., 2014). It is possible that the result of phage therapy depends on both phage titer and a number of other reasons, including sensitivity and accessibility of bacterial host to the phage, routes of phage administration, duration of phage treatment course, and so on.

Recently, a phase I/II clinical trial was dedicated to the study of safety, effectiveness, and pharmacodynamics of two phage cocktails to treat *E. coli*, and *P. aeruginosa* burn wound infections (http://www.phagoburn.eu). The results of this study, which was conducted for 3 years in France, Switzerland, and Belgium, may help the development of dose and treatment scheme recommendations for phage therapy of infected burns.

PHAGE THERAPY OF PATIENTS WITH INFECTED ULCERS

Chronic trophic ulcers occur as a complication of some disorders, such as chronic insufficiency of blood circulation (atherosclerosis, varicosity), diabetes, peripheral polyneuropathy of the limbs, and so on. It is believed that the rate of healing of ulcers depends on the concurrent infection; meanwhile, the spectrum of aerobic and anaerobic microorganisms inhabiting chronic wounds is very diverse (Rhoads et al., 2012; Wolcott et al., 2016). Microbiomes of chronic ulcers and, particularly, of diabetic foot ulcers (DFU) are associated with clinical factors: superficial ulcers and those with a shorter duration are usually infected with *Staphylococcus* spp., mainly *S. aureus*, in a relatively high titer; deep ulcers and those with a longer duration are colonized with the diverse microbiota that contains Proteobacteria and anaerobes, including *Anaerococcus*, *Peptonihilus*, *Bacteroides*, and *Clostridium* genera (Gardner et al., 2013; Spichler et al., 2015). According to 16S rDNA pyrosequence analyses of microbiomes from ∼3,000 ulcers, only one infectious agent was found in 7% of infected ulcers (Wolcott et al., 2016). *S. aureus* and *P. aeruginosa* were found to be predominant and the most pathogenic species commonly persisting in chronic wounds (Wolcott et al., 2016), and their elimination would lead to improvement and wound healing in the majority of cases. However, antibacterial treatment of ulcers infected with diverse microbial agents is usually complicated, primarily by microbial biofilm formation and high level of antibiotic resistance (Malik et al., 2013; Rahim et al., 2016; Di Domenico et al, 2017). Long-term administration of antibiotics is sometimes ineffective; especially in diabetes mellitus patients, long-term administration of antibiotics is often unsafe, because they may suffer from diabetic nephropathy and hepatic insufficiency.

Phage therapy could be an alternative to antibiotics or, at least, a supplementary approach to the treatment of infected ulcers. Currently, several studies (**Table 2**) have reported the efficiency and safety of phage treatment of infected trophic ulcers in humans (Markoishvili et al., 2002; Rhoads et al., 2009; Fish et al., 2016, 2018; Vlassov et al., 2016; Morozova et al., 2018). A large case series (96 patients) demonstrated a positive effect of PhagoBioDerm (a biodegradable wound dressing impregnated with the phage cocktail Pyophage) on the healing of venous leg ulcers (Markoishvili et al., 2002; **Table 2**). These biodegradable polymers contain different antimicrobial substances and are of particular interest because of their ability to degrade slowly and release active antimicrobials, including phage particles, for a long time. The use of PhagoBioDerm reduced the number of treatments and hence, injuring of wounds; therefore, this type of material is promising for both therapy and prevention of microbial infections in wounds (Markoishvili et al., 2002; Jikia et al., 2005).

Later, a phase I safety trial of a cocktail of bacteriophages WPP-201 was performed (Rhoads et al., 2009). WPP-201 was applied topically to venous leg ulcers, and its safety was confirmed as it did not lead to an increase in the number of side effects compared to the standard therapy. Meanwhile, the rate of wound healing was the same in both the experimental and control groups (Rhoads et al., 2009). Since the aim of the trial was to demonstrate the safety of the phage cocktail rather than its effectiveness, the study did not provide information on the composition and number of infectious microorganisms, which might not be sensitive to phages from the WPP-201 cocktail.

TABLE 2 | Case series and reports of phage therapy of burns and trophic ulcers in humans.

References	Patients, n (PT, CT, AT)[a]	Phage prophylactic/ Phage therapy	Type of lesion	Pathogen	Applied phages, titer, pfu/ml[b]	Route of administration of phages (dosage)	Course of phage treatment	Characteristics of outcomes
Abul-Hassan et al., 1990	30^{PT}	0/30	Infected burns	MDR *P. aeruginosa*	Pseudomonas phages, 10^{10}	Dressing with gauze soaked with phage preparation 3 times a day	5–17 days	Elimination of P. aeruginosa in 12/30 patients. Significant improvement in wound healing in15/30 patients. Skin grafts take: good results in 18/30 patients
Lazareva et al., 2001	94 (9^{PT} 45^{CT} 40^{AT})	$9^{PT}/45^{CT}$	Infected burns	Enterococci, *E. coli, P. aeruginosa,* Staphylococci	Pyophage	Per os (2 tablets 3 times a day in 1–1.5 h before meals)	7 days	**PT:** Wound healing in 9/9 patients. **CT:** Decrease of a number of microbial isolates in wounds in 2.2 times and number of positive hemocultures from 55 to 36.8%. Mortality rate: 2 fatal outcomes. **AT:** A number of microbial isolates in wounds remained, number of positive hemocultures go up from 33.3 to 75%. Mortality rate: 6 fatal outcomes
Jikia et al., 2005	2^{CT}	0/2	Infected radiation burns	MDR *S. aureus*	PhagoBioDerm impregnated with Pyophage, 1×10^6	Topical application of PhagoBioDerm	Single application	Purulent drainage stopped in 2–3 days *S. aureus* elimination in 7 days in 2/2 patients[c]
Sivera Marza et al., 2006	1^{CT}	0/1	Infected burns	*P. aeruginosa*	Pseudomonas phage BS24, 5×10^3	Topical application	Single application	No infection after 3 days of CT[c]
Rose et al., 2014	9^{CT}	0/9	Infected burns	MDR *P. aeruginosa*, MDR *S. aureus*	Phage cocktail BFC-1, 10^9	Topical application	Single application	No positive response
Markoishvili et al., 2002	96^{CT}	0/96	Infected venous stasis ulcers	*E. coli, P. aeruginosa, Proteus* spp., Staphylococci, Streptococci	PhagoBioDerm impregnated with Pyophage, 1×10^6	Topical application of PhagoBioDerm every 3–5 days	From single to multiple applications	Wound healing in 67/96 patients, Ulcers reduced in size, elimination of purulent drainage in 24/96 patients No improvement in 5/96 patients with diabetes mellitus
Fish et al., 2016	6^{PT}	0/6	Infected diabetic toe ulcers	*S. aureus*	Phage Sb-1, (Kvachadze et al., 2011), 10^7-10^8	Dressing with gauze soaked with phage preparation once in a week,	4–18 weeks	Wound healing in 6/6 patients after PT[c]
Vlassov et al., 2016	23^{CT}	0/23	Infected diabetic foot ulcers	Enterococci, *E. coli, Klebsiella* spp., *P. aeruginosa*, *Proteus* spp, Staphylococci	Staphylococcus phages, Pseudomonas phages, *E. coli* phages, Enterococcus phages; 10^8-10^{10}	Washing of the wound, topical application, 1–4 times a day	5–14 days	Elimination of *S. aureus* and *E. coli*, the titer of *P. aeruginosa* decreased in 3–4 orders in 13/13 patients with mono-infections. Elimination or decrease in the titers of all bacterial isolates in 4/10 patients with poly-microbial infections

[a] *PT, phage treatment without antibiotics; CT, complex treatments, including phages and antibiotics; AT, antibiotics treatment.*

[b] *Russian manufactured phage cocktails must contain at least 10^6 pfu/ml of each phage component according to instruction of manufacturer.*

[c] *Previous unsuccessful antibiotic treatment.*

The use of bacteriophages that were specific to infectious agents demonstrated clear positive results (**Table 2**). Staphylococcus phage Sb-1 (Kvachadze et al., 2011) was successfully used in the treatment of patients with DFU infected with methicillin-resistant and methicillin-sensitive *S. aureus* strains, as it has been described in a case series report (Fish et al., 2016). Phage therapy without antibiotics resulted in subsequent wound healing in all treated patients (Fish et al., 2016, 2018; **Table 2**). Another investigation reported phage treatment of patients with various infections of DFU, in whom previous antibiotic treatment was not successful (Vlassov et al., 2016; Morozova et al., 2018; **Table 2**). Importantly, commercially available phage cocktails were selected in each case individually according to their specificity to particular infectious agents in an ulcer. When no specific phage cocktail was found, a custom-made phage preparation was prepared. Phage treatment was most effective in ulcers with one bacterial agent (100%), but a personalized approach led to the elimination of pathogens, even in several cases with mixed infections. The main difficulty in treating of wounds infected with several pathogenic bacteria was the inability to quickly select phages against all identified bacterial agents (Vlassov et al., 2016; Morozova et al., 2018; **Table 2**).

CONCLUSION

Extensive empirical experience of phage therapy of localized infections has been accumulated over 100 years of bacteriophage application in treatment of infectious diseases (Weber-Dabrowska et al., 2000; Sulakvelidze et al., 2001; Miedzybrodzki et al., 2012; Chanishvili, 2016; Górski et al., 2017), and the safety of bacteriophages for use in humans has been repeatedly demonstrated (Bruttin and Brüssow, 2005; Rhoads et al., 2009; Wright et al., 2009; Rose et al., 2014). Different schemes and routes of phage administration have been applied, varying from single oral or intravenous applications to multiple topical treatments per day for 12–15 weeks (Arsentieva, 1941; Meladze et al., 1982; Weber-Dabrowska et al., 2000; Brusov et al., 2011; Miedzybrodzki et al., 2012; Fish et al., 2016; Jennes et al., 2017; Chan et al., 2018; etc). Analysis of reported results of phage therapy of localized infections allowed us to draw several conclusions.

Phage application was more effective in an early stage of acute wound infection and 5–10 days of phage therapy provided positive clinical results in the majority of cases (Kokin, 1941; Pokrovskaya et al., 1941; Tsulukidze, 1941). The results of phage treatment depended on the pathogen species, and the best results were achieved in the treatment of infections caused by *Staphylococcus* spp. and *Streptococcus* spp. (Kokin, 1941; Pokrovskaya et al., 1941; Miedzybrodzki et al., 2012).

In the treatment of infected chronic ulcers, mostly long-term application of phage preparations (up to several weeks) provided positive clinical effect (Weber-Dabrowska et al., 2000; Markoishvili et al., 2002; Miedzybrodzki et al., 2012; Fish et al., 2016). Importantly, multiple changes of dominant pathogens may occur in infected chronic ulcers during phage treatment (Morozova et al., 2018). This situation requires timely replacement of ineffective bacteriophages. Therefore, large collections of therapeutic phage preparations would be useful, because diverse bacterial communities have been recorded in most chronic wounds and ulcers. Even when only part of the infectious agents are susceptible to therapeutic phages, phage therapy might be a reasonable supplementary approach providing the elimination of dominant pathogens. Moreover, different bacteria in the ulcer's microbiota may be resistant to various antibiotics, leading to the inability to choose one appropriate antibiotic for therapy. So, complex treatments, including antibiotics and bacteriophages, may be the optimal solution in this case.

It is possible that phage therapy should be personalized, which means individual selection and custom-made phage preparation, and in some cases, an adaptation of bacteriophage to infectious agent isolated from a patient (Zhukov-Verezhnikov et al., 1978; Pirnay et al., 2011, 2018; Schooley et al., 2017; Rohde et al., 2018). Poly-specific cocktails of bacteriophages might be applied preventively or at the beginning of treatment before identification of etiologic agents.

Phages were applied topically in the majority of studies (**Tables 1**, **2**); though the early Soviet investigations reported subcutaneous, intramuscular, and intravenous administration of phages in successful treatment of wound infection (Arsentieva, 1941; Kokin, 1941; Krestovnikova, 1947, etc). It should be noted, that Staphylococcus phage developed by the Eliava Institute of Bacteriophage (Tbilisi, Republic of Georgia) was successfully applied intravenously for treatment of infections in children and adults in the late soviet times (Meladze et al., 1982; Samsygina and Boni, 1984). A range of doses of phage preparations provided positive results, presumably reflecting their ability to replicate where the target pathogen is present. Further accumulation of data in the field of phage therapy of localized infections should help to develop optimal dosage and routes of administration of phage preparation.

AUTHOR CONTRIBUTIONS

All co-authors have made equal contribution to the writing and editing of the article. All authors read and approved the final version of the manuscript.

FUNDING

This study was supported by the Program of Fundamental Scientific Research of Russian Academy of Sciences Project ST No 0309-2018-0011, and Russian Federal Agency for Science and Innovation project VI.55.1.1, No 0309-201 6-0002.

REFERENCES

Abul-Hassan, H. S., El-Tahan, K., Massoud, B., and Gomaa, R. (1990). Bacteriophage therapy of *Pseudomonas* burn wound sepsis. *Ann. Mediterr. Burn Club* 3, 262–264.

Arsentieva, A. V. (1941). Intravenous use of high doses of bacteriophages in surgery. *Sov Med.* 9, 18–20. [Article in Russian].

Asati, S., and Chaudhary, U. (2017). Prevalence of biofilm producing aerobic bacterial isolates in burn wound infections at a tertiary care hospital in northern India. *Ann. Burns Fire Disasters* 30, 39–42.

Bogovazova, G. G., Voroshilova, N. N., and Bondarenko, V. M. (1991). The efficacy of *Klebsiella pneumoniae* bacteriophage in the therapy of experimental Klebsiella infection. *Zh. Mikrobiol. Epidemiol. Immunobiol.* 4, 5–8. [Article in Russian].

Brusov, P. G., Zubritsky, V. F., Nizovoy, A. V., and Fominykh, E. M. (2011). Phagoprophylaxis and bacteriophage treatment of surgical infections. *Mil. Med. J.* 4, 34–39. [Article in Russian].

Bruttin, A., and Brüssow, H. (2005). Human volunteers receiving Escherichia coli phage T4 orally: a safety test of phage therapy. *Antimicrob. Agents Chemother.* 49, 2874–2878. doi: 10.1128/AAC.49.7.2874-2878.2005

Bruynoghe, R., and Maisin, J. (1921). Essais de the'rapeutique au moyen du bacteriophage. *C. R. Soc. Biol.* 85, 1120–1121.

Chan, B. K., Turner, P. E., Kim, S., Mojibian, H. R., Elefteriades, J. A., and Narayan, D. (2018). Phage treatment of an aortic graft infected with *Pseudomonas aeruginosa*. *Evol Med Public Health*. 2018. 60–66. doi: 10.1093/emph/eoy005

Chanishvili, N. (2009). *A Literature Review of the Practical Application of Bacteriophage Research*. New York, NY: Nova Science Publishers.

Chanishvili, N. (2012). Phage therapy—history from twort and d'herelle through soviet experience to current approaches. *Adv. Virus Res.* 83, 4–40. doi: 10.1016/B978-0-12-394438-2.00001-3

Chanishvili, N. (2016). Bacteriophages as therapeutic and prophylactic means: summary of the Soviet and Post-Soviet Experiences. *Curr. Drug Deliv.* 13, 309–323. doi: 10.2174/1567201813031605201939 46

Church, D., Elsayed, S., Reid, O., Winston, B., and Lindsay, R. (2006). Burn wound infections. *Clin. Microbiol. Rev.* 19, 403–434. doi: 10.1128/CMR.19.2.403-434.2006

Di Domenico, E. G., Farulla, I., Prignano, G., Gallo, M. T., Vespaziani, M., Cavallo, I., et al.(2017). Biofilm is a major virulence determinant in bacterial colonization of chronic skin ulcers independently from the multidrug resistant phenotype. *Int. J. Mol. Sci.* 18:E1077. doi: 10.3390/ijms18051077

Erol, S., Altoparlak, U., Akcay, M. N., Celebi, F., and Parlak, M. (2004). Changes of microbial flora and wound colonization in burned patients. *Burns* 4, 357–361. doi: 10.1016/j.burns.2003.12.013

Fish, R., Kutter, E., Wheat, G., Blasdel, B., Kutateladze, M., and Kuhl, S. (2016). Bacteriophage treatment of intransigent diabetic toe ulcers: a case series. *J. Wound Care* 25, S27–S33. doi: 10.12968/jowc.2016.25.7.S27

Fish, R., Kutter, E., Wheat, G., Blasdel, B., Kutateladze, M., and Kuhl, S. (2018). Compassionate use of bacteriophage therapy for foot ulcer treatment as an effective step for moving towards clinical trials. *Methods Mol. Biol.* 1693, 159–170. doi: 10.1007/978-1-4939-7395-8_14

Gardner, S. E., Hillis, S. L., Heilmann, K., Segre, J. A., and Grice, E. A. (2013). The neuropathic diabetic foot ulcer microbiome is associated with clinical factors. *Diabetes* 62, 923–930. doi: 10.2337/db12-0771

Gomareli, G. G., Iasvili, B. P., Chanisvvili, T. G., Sharashidze, T. G., and Katsitadze, G. L. (1976). Experience of using bacteriophages passaged on auto cultures in the treatment of burn wounds. *Proc. Res. Inst. Emerg. Care*. 25, 96–98.

Górski, A., Dabrowska, K., Miedzybrodzki, R., Weber-Dabrowska, B., Łusiak-Szelachowska, M., Jonczyk-Matysiak, E., et al. (2017). Phages and immunomodulation. *Future Microbiol.* 12, 905–914. doi: 10.2217/fmb-2017-0049

Górski, A., Miedzybrodzki, R., Borysowski, J., Weber-Dabrowska, B., Lobocka, M., Fortuna, W., et al. (2009). Bacteriophage therapy for the treatment of infections. *Curr Opin Investig Drugs*. 10, 766–774.

Jennes, S., Merabishvili, M., Soentjens, P., Pang, K. W., Rose, T., Keersebilck, E., et al. (2017). Use of bacteriophages in the treatment of colistin-only-sensitive *Pseudomonas aeruginosa* septicaemia in a patient with acute kidney injury-a case report. *Crit. Care* 21:129. doi: 10.1186/s13054-017-1709-y

Jikia, D., Chkhaidze, N., Imedashvili, E., Mgaloblishvili, I., Tsitlanadze, G., Katsarava, R., et al. (2005). The use of a novel biodegradable preparation capable of the sustained release of bacteriophages and ciprofloxacin, in the complex treatment of multidrug-resistant Staphylococcus aureus-infected local radiation injuries caused by exposure to Sr90. *Clin. Exp. Dermatol.* 30, 23–26. doi: 10.1111/j.1365-2230.2004.01600.x

Khairullin, I. N., Pozdeev, O. K., and Shaimordanov, R. (2002). Efficiency of using specific bacteriophages in the treatment and prophylaxis of surgical postoperative infections. *Kazan Med. J.* 83, 258–261. [Article in Russian].

Kochetkova, V. A., Mamontov, A. S., Moskovtseva, R. L., Erastova, E. I., Trofimov, E. I., Popov, M. I., et al. (1989). Phagotherapy of postoperative suppurative-inflammatory complications in patients with neoplasms. *Sov. Med.* 6, 23–26. [Article in Russian].

Kokin, G. A. (1941). Use of bacteriophages in surgery. *Sov. Med*. 9, 15–18. [Article in Russian].

Kokin, G. A. (1946). "Phage therapy and phage prophylaxis of gas gangrene," *in The Experience of the Soviet Military Medicine during the Great Patriotic War 1941–1945*, (Moscow: Medgiz), Vol. 3, 56–63.

Krestovnikova, V. A. (1947). Phage treatment and phage prophylactics and their approval in the works of the Soviet researchers. *J. Microb. Epidemiol. Immunol.* 3, 56–65. [Article in Russian].

Kvachadze, L., Balarjishvili, N., Meskhi, T., Tevdoradze, E., Skhirtladze, N., and Pataridze, T. (2011). Evaluation of lytic activity of staphylococcal bacteriophage Sb-1 against freshly isolated clinical pathogens. *Microb. Biotechnol.* 4, 643–650. doi: 10.1111/j.1751-7915.2011.00259.x

Lazareva, E. B., Smirnov, S. V., Khvatov, V. B., Spiridonova, T. G., Bitkova, E. E., Darbeeva, O. S., et al. (2001). Efficacy of bacteriophages in complex treatment of patients with burn wounds. *Antibiot. Khimioter.* 46, 10–14. [Article in Russian].

Malik, A., Mohammad, Z., and Ahmad, J. (2013). The diabetic foot infections: biofilms and antimicrobial resistance. *Diabetes Metab. Syndr.* 7, 101–107. doi: 10.1016/j.dsx.2013.02.006

Markoishvili, K., Tsitlanadze, G., Katsarava, R., Morris, J. G., and Sulakvelidze, A. (2002). A novel sustained-release matrix based on biodegradable poly(ester amide)s and impregnated with bacteriophages and an antibiotic shows promise in management of infected venous stasis ulcers and other poorly healing wounds. *Int. J. Dermatol.* 41, 453–458. doi: 10.1046/j.1365-4362.2002.01451.x

Meladze, G. D., Mebuke, M. G., Chkhetia, N.,Sh., Kiknadze, N.,Ya., Koguashvili, G. G., Timoshuk, I. I., et al. (1982). The efficacy of staphylococcal bacteriophage in the treatment of purulent diseases of the lungs and pleura. *Grudnaya Khirurgiya* 24, 53–56. [Article in Russian].

Merabishvili, M., Pirnay, J.-P., and Verbeken, G. (2009). Quality-controlled small-scale production of a well-defined bacteriophage cocktail for use in human clinical trials. *PLoS ONE* 4:e4944. doi: 10.1371/journal.pone.0004944

Miedzybrodzki, R., Borysowski, J., Weber-Dabrowska, B., Fortuna, W., Letkiewicz, S., Szufnarowski, K., et al. (2012). Clinical aspects of phage therapy. *Adv. Virus Res.* 83, 73–121. doi: 10.1016/B978-0-12-394438-2.00003-7

Miedzybrodzki, R., Fortuna, W., Weber-Dabrowska, B., and Górski, A. (2009). A retrospective analysis of changes in inflammatory markers in patients treated with bacterial viruses. *Clin. Exp. Med.* 9, 303–312. doi: 10.1007/s10238-009-0044-2

Morozova, V. V., Kozlova, Y.u., Ganichev, D., and Tikunova, N. (2018). Bacteriophage treatment of infected diabetic foot ulcers. *Methods Mol. Biol.* 1693, 151–158. doi: 10.1007/978-1-4939-7395-8_13

Peremitina, L. D., Berillo, E. A., and Khvoles, A. G. (1981). Experience in the therapeutic use of bacteriophage preparations in suppurative surgical infections. *Z. Mikrobiol. Epidemiol. Immunobiol.* 9, 109–110. [Article in Russian].

Perepanova, T. S., Darbeeva, O. S., Kotliarova, G. A., Kondrat'eva, E. M., Maiskaia, L. M., Malysheva, V. F., et al. (1995). The efficacy of bacteriophage preparations in treating inflammatory urologic diseases. *Urol. Nefrol.* 5, 14–17. [Article in Russian].

Pirnay, J. P., De Vos, D., Verbeken, G., Merabishvili, M., Chanishvili, N., Vaneechoutte, M., et al. (2011). The phage therapy paradigm: prêt-à-porter or sur-mesure? *Pharm. Res.* 28, 934–937. doi: 10.1007/s11095-010-0313-5

Pirnay, J. P., Verbeken, G., Ceyssens, P. J., Huys, I., De Vos, D., Ameloot, C., et al. (2018). The magistral phage. *Viruses*. 10:e64. doi: 10.3390/v10020064

Pokrovskaya, M. P., Kaganova, L. C., Morosenko, M. A., Bulgakova, A. G., and Skatsenko, E. E. (1941). *Treatment of Wounds with Bacteriophages.* Moscow: Narkomzdrav.

Ponomareva, T. R., Smolianskaia, A. Z., Sokolova, E. N., Sokolova, V. I., and Garnova, N. A. (1985). Bacteriophages in the treatment of postoperative complications in cancer patients. *Sov. Med.* 4, 89–92. [Article in Russian].

Rahim, K., Qasim, M., Rahman, H., Khan, T. A., Ahmad, I., Khan, N., et al. (2016). Antimicrobial resistance among aerobic biofilm producing bacteria isolated from chronic wounds in the tertiary care hospitals of Peshawar, Pakistan. *J. Wound Care* 25, 480–486. doi: 10.12968/jowc.2016.25.8.480

Rhoads, D. D., Wolcott, R. D., Kuskowski, M. A., Wolcott, B. M., Ward, L. S., and Sulakvelidze, A. (2009). Bacteriophage therapy of venous leg ulcers in humans: results of a phase I safety trial. *J. Wound Care* 18, 240–243. doi: 10.12968/jowc.2009.18.6.42801

Rhoads, D. D., Wolcott, R. D., Sun, Y., and Dowd, S. E. (2012). Comparison of culture and molecular identification of bacteria in chronic wounds. *Int. J. Mol. Sci.* 13, 2535–2550. doi: 10.3390/ijms13032535

Rohde, C., Resch, G., Pirnay, J. P., Blasdel, B. G., Debarbieux, L., Gelman, D., et al. (2018). Expert opinion on three phage therapy related topics: bacterial phage resistance, phage training and prophages in bacterial production strains. *Viruses* 10: E178. doi: 10.3390/v10040178

Rose, T., Verbeken, G., Vos, D. D., Merabishvili, M., Vaneechoutte, M., and Lavigne, R., et. al. (2014). Experimental phage therapy of burn wound infection: difficult first steps. *Int. J. Burns Trauma* 4, 66–73.

Samsygina, G. A., and Boni, E. G. (1984). Bacteriophages and phage therapy in pediatric practice. *Pediatrics* 4, 67–70. [Article in Russian].

Schooley, R. T., Biswas, B., Gill, J. J., Hernandez-Morales, A., Lancaster, J., Lessor, L., et al. (2017). Development and use of personalized bacteriophage-based therapeutic cocktails to treat a patient with a disseminated resistant acinetobacter baumannii infection. *Antimicrob. Agents Chemother.* 61, e00954–e00917. doi: 10.1128/AAC.00954-17

Sivera Marza, J. A., Soothill, J. S., and Boydell, P. (2006). Multiplication of therapeutically administered bacteriophages in *Pseudomonas aeruginosa* infected patients. *Burns* 32, 644–646. doi: 10.1016/j.burns.2006.02.012

Soothill, J. S. (1994). Bacteriophage prevents destruction of skin grafts by *Pseudomonas aeruginosa*. *Burns* 20, 209–211. doi: 10.1016/0305-4179(94)90184-8

Spichler, A., Hurwitz, B. L., Armstrong, D. G., and Lipsky, B. A. (2015). Microbiology of diabetic foot infections: from Louis Pasteur to 'crime scene investigation'. *BMC Med.* 13:2. doi: 10.1186/s12916-014-0232-0

Sulakvelidze, A., Alavidze, Z., and Morris, J. G. (2001). Bacteriophage therapy antimicrob agents chemother. 45, 649–659. doi: 10.1128/AAC.45.3.649-659.2001

Summers, W. C. (1999). *Felix d'Herelle and the Origins of Molecular Biology*. New Haven, CT: Yale University Press.

Tsulukidze, A. P. (1940). Phage treatment in surgery. *Surgery ("Khirurgia")* 12, 132–133. [Article in Russian].

Tsulukidze, A. P. (1941). *Experience of Use of Bacteriophages in the Conditions of War Traumatism*. Tbilisi: Gruzmedgiz. [Article in Russian].

Van Belleghem, J. D., Clement, F., Merabishvili, M., Lavigne, R., and Vaneechoutte, M. (2017). Pro- and anti-inflammatory responses of peripheral blood mononuclear cells induced by Staphylococcus aureus and *Pseudomonas aeruginosa* phages. *Sci. Rep.* 7:8004. doi: 10.1038/s41598-017-08336-9

Vlassov, V. V., Ganichev, D. A., Kozlova, J. N., Morozova, V. V., Saranina, I. V., and Tikunova, N. V. (2016). "Personalised phage therapy of infected trophic ulcers on the background of diabetis," in *Abstract Retrieved from Book of Abstracts of 3-rd International Scientific Conference Bacteriophages: Theoretical and Practical Aspects of Their Application in Medicine, Veterinary and Food.* Available online at: http://www.congress-phages.ru/_pictures/tezis_bf-2016_block.pdf

Weber-Dabrowska, B., Mulczyk, M., and Górski, A. (2000). Bacteriophage therapy of bacterial infections: an update of our institute's experience. *Arch. Immunol. Ther. Exp.* 48, 547–551.

Wolcott, R. D., Hanson, J. D., Rees, E. J., Koenig, L. D., Phillips, C. D., Wolcott, R. A., et al. (2016). Analysis of the chronic wound microbiota of 2,963 patients by 16S rDNA pyrosequencing. *Wound Repair Regen.* 24, 163–174. doi: 10.1111/wrr.12370

Wright, A., Hawkins, C. H., Anggård, E. E., and Harper, D. R. (2009). A controlled clinical trial of a therapeutic bacteriophage preparation in chronic otitis due to antibiotic-resistant *Pseudomonas aeruginosa*; a preliminary report of efficacy. *Clin. Otolaryngol.* 34, 349–357. doi: 10.1111/j.1749-4486.2009.01973.x

Zhukov-Verezhnikov, N. N., Peremitina, L. D., Berillo, E. A., Komissarov, V. P., and Bardymov, V. M. (1978). Therapeutic effect of bacteriophage preparations in the complex treatments of suppurative surgical diseases. *Sov. Med.* 12, 64–66. [Article in Russian].

Conflict of Interest Statement: The authors declare that the research was conducted in the absence of any commercial or financial relationships that could be construed as a potential conflict of interest.

frontiers in Microbiology

ORIGINAL RESEARCH
published: 11 September 2018
doi: 10.3389/fmicb.2018.02127

Bacteriophage ZCKP1: A Potential Treatment for *Klebsiella pneumoniae* Isolated From Diabetic Foot Patients

Omar A. Taha[1], *Phillippa L. Connerton*[2], *Ian F. Connerton*[2] *and Ayman El-Shibiny*[1,3]*

[1] *Biomedical Sciences, University of Science and Technology, Zewail City of Science and Technology, Giza, Egypt,* [2] *Division of Food Sciences, School of Biosciences, University of Nottingham, Loughborough, United Kingdom,* [3] *Faculty of Environmental Agricultural Sciences, Arish University, Arish, Egypt*

The recorded growth in infection by multidrug resistant bacteria necessitates prompt efforts toward developing alternatives to antibiotics, such as bacteriophage therapy. Immuno-compromised patients with diabetes mellitus are particularly prone to foot infections by multidrug resistant *Klebsiella pneumoniae*, which may be compounded by chronic osteomyelitis. Bacteriophage ZCKP1, isolated from freshwater in Giza, Egypt, was tested *in vitro* to evaluate its lytic activity against a multidrug resistant *K. pneumoniae* KP/01, isolated from foot wound of a diabetic patient in Egypt. Characterization of ZCKP1 phage indicated that it belonged to the *Myoviridae* family of bacteriophages with a ds-DNA genome size of 150.9 kb. Bacteriophage ZCKP1 lysed a range of osteomyelitis pathogenic agents including *Klebsiella* spp., *Proteus* spp. and *E. coli* isolates. The bacteriophage reduced the bacterial counts of host bacteria by $\geq$2 $\log_{10}$ CFU/ml at 25°C, and demonstrated the ability to reduce bacterial counts and biofilm biomass (>50%) when applied at high multiplicity of infection (50 PFU/CFU). These characteristics make ZCKP1 phage of potential therapeutic value to treat *K. pneumoniae* and associated bacteria present in diabetic foot patients.

Keywords: *Klebsiella*, bacteriophage, ulcer, diabetes, biofilm, osteomyelitis

OPEN ACCESS

Edited by:
Sanna Sillankorva,
University of Minho, Portugal

Reviewed by:
Pilar García,
Consejo Superior de Investigaciones Científicas (CSIC), Spain
Adelaide Almeida,
University of Aveiro, Portugal

***Correspondence:**
Ayman El-Shibiny
aelshibiny@zewailcity.edu.eg

Specialty section:
This article was submitted to Antimicrobials, Resistance and Chemotherapy, a section of the journal Frontiers in Microbiology

Received: *03 October 2017*
Accepted: *20 August 2018*
Published: *11 September 2018*

Citation:
Taha OA, Connerton PL, Connerton IF and El-Shibiny A (2018) Bacteriophage ZCKP1: A Potential Treatment for Klebsiella pneumoniae Isolated From Diabetic Foot Patients. Front. Microbiol. 9:2127. doi: 10.3389/fmicb.2018.02127

INTRODUCTION

Klebsiella pneumoniae belongs to the *Enterobacteriaceae* family. It primarily affects patients with compromised defenses to cause severe complications. It is a particular problem for patients with diabetes mellitus leading to "diabetic foot" infections and osteomyelitis (Podschun and Ullmann, 1998). Once infection is established *K. pneumoniae* forms a biofilm that enables evasion of the host's defenses (Akers et al., 2014; Gupta et al., 2016). Moreover, phagocytosis by polymorphonuclear granulocytes is dramatically hindered, as *K. pneumoniae* possesses an outer protective polysaccharide capsule, a key determinant of their subsequent pathogenicity. The capsule suppresses complement components, particularly C3b (Domenico et al., 1994; Diago-Navarro et al., 2014). Among many other pathogenicity factors, bone adherence is attributed to adhesin production that may be fimbrial, or non-fimbrial (Malhotra et al., 2014). *Staphylococcus aureus* is considered the most frequently implicated bacterium in cases of diabetic foot infection (Richard, 2011) but recent data indicate that *K. pneumoniae* is responsible for approximately 21.7% of cases (Mukkunnath et al., 2015. With rising numbers of diabetes patients and the severity of foot osteomyelitis complications, this represents a considerable economic burden on health providers,

notwithstanding the suffering of the individuals affected. In the past, *K. pneumoniae* was primarily associated with pulmonary and urinary infections, and was only relatively recently recognized as a significant cause of foot osteomyelitis (Dourakis et al., 2006; Prokesch et al., 2016).

Foot osteomyelitis is a common and serious problem in diabetic patients resulting chiefly from peripheral neuropathy or, less commonly, by vasculopathy and wound healing impediments (Grayson et al., 1995). It occurs in approximately two thirds of cases of diabetic foot patients (Grayson et al., 1995). *K. pneumoniae* is able to migrate to bone tissues haematogeneously (derived from or transported by blood) or contiguously from areas of local infections in the feet of diabetic patients (Mathews et al., 2010; Rana et al., 2013). If not effectively treated, viable cells of the infectious agent can be trapped in the devitalized bone and thus evade host defenses, and eventually cause chronic osteomyelitis (NADE, 1975; Ross et al., 2003; Calhoun and Manring, 2005).

In addition to the virulence characteristics described, the emergence of MDR *K. pneumoniae* strains, resistant to the last-line antibiotic treatment colistin, is a major concern (Kidd et al., 2017). Resistance arises from mutations of the *mgr*B gene, which are stably maintained in *Klebsiella* populations, from which resistance can be disseminated, in addition to plasmid mediated resistance due to mcr-1 and mcr-2 genes (Cannatelli et al., 2015). With the advent of the post-antibiotic era, severe cases of osteomyelitis may require more frequent surgical intervention in the form of resection of the infected and necrotic bone (Sanchez et al., 2013). It is therefore vital to seek alternative therapies to treat *K. pneumoniae* and other bacterial infections especially in developing countries (Nagel et al., 2016). Bacteriophage therapy is a good candidate and has been shown, using mice as animal models, to provide significant protection against respiratory and other infections caused by *K. pneumoniae* such as liver abscesses and bacteremia (Chhibber et al., 2008; Hung et al., 2011). Bacteriophage therapy has also been used to treat *K. pneumoniae* infected burn wound infections, in mice (Malik and Chhibber, 2009). Intranasal administration of lytic bacteriophage reduced the bacterial burden of *K. pneumoniae* in the lungs of mice (Cao et al., 2015). Other studies have characterized a number of diverse lytic bacteriophages to *K. pneumoniae* belonging to different families and demonstrated their potential *in vitro* (Bogovazova et al., 1991; Kesik-Szeloch et al., 2013; Hoyles et al., 2015). Bacteriophage therapy is regarded as a simple, safe and highly effective alternative to counter the rising problems associated with multidrug resistant bacteria (Qadir, 2015; El-Shibiny et al., 2017). Here we evaluate the lytic activity of bacteriophage ZCKP1 isolated from an environmental freshwater source in Egypt against a MDR *K. pneumoniae* KP/01 isolated from the foot of a diabetic patient.

Abbreviations: BIMs, bacteriophage insensitive mutants; IC, phage infective centers; MOI, multiplicity of infection; MTT, 3-(4,5-dimethylthiazol-2-yl)-2,5-diphenyltetrazolium bromide.

MATERIALS AND METHODS

Bacterial Strains and Growth Media

K. pneumoniae KP/01, used as a host for bacteriophage infection, was isolated from a human clinical diabetic-foot sample from a male patient in May 2016 and identified by National Institute of Diabetes using the VITEK method for identification (Cairo, Egypt). Other clinical isolates of *K. pneumoniae* ($n = 21$), *Proteus mirabilis* ($n = 18$) and *E. coli* ($n = 15$) were also isolated by National Institute of Diabetes, for bacteriophage host-range analysis, from wound infection samples and provided to the microbiology research lab at Zewail City. Isolates were kept in tryptone soy broth (TSB; Oxoid, England) containing (w/v) 20% of glycerol, at −80°C. In the following experiments, bacterial strains were grown on tryptic soy agar (TSA; Oxoid, England) overnight, and isolated colonies of bacteria were grown at 37°C, in TSB, to reach OD_{600} approximately 0.3.

Bacterial Identification Using PCR Specific Primers and Gel Electrophoresis

PCR amplification was performed to confirm the identity of the *K. pneumoniae* isolate (KP/01) using specific primers for 16s RNA gene (forward primer: 5′-ATTTGAAGAGGTTGCAAA CGAT-3′ and reverse primer: 5′-TTCACTCTGAAGTTTTCT TGTGTTC-3′; Woese and Fox, 1977; Woese et al., 1990). Thirty cycles were performed at denaturation temperature of 95°C for 30 s; annealing at 58°C for 60 s and extension at 72°C for 1 min looking for a PCR product of 133 bp length using an Applied Biosystems thermal cycler (Cady et al., 2012). The PCR product was run on a 1% (w/v) agarose gel to identify its size.

Antibiotic Sensitivity Test

K. pneumoniae KP/01 strain was subjected to antibiotic resistance evaluation against a set of antibiotic discs including: tigecycline (TGC; 15 μg), imipenem (IPM; 10 μg), piperacillin-tazobactam (TZP; 100/10 μg), levofloxacin (LEV; 5 μg), linezolid (LZD; 30 μg), ceftazidime (CAZ; 30 μg), and cefepime (FEP; 30 μg) all from Oxoid (England). Antimicrobial sensitivity testing was performed for strains of *K. pneumoniae, E. coli* and *P. mirabilis*by using the disk diffusion methods in accordance with National Committee for Clinical Standards guidelines (Clinical and Laboratory Standards Institute, 1999). The antibiotics chosen are usually used for the treatment of diabetic foot infections in National Institute of Diabetes, due to their efficacy against members of the *Enterobacteriaceae*.

Bacteriophage Isolation, Amplification and Purification

Bacteriophages were isolated from environmental water samples from freshwater in El- Maryoteyya-Haram area, Giza, Egypt. *K. pneumoniae* (KP/01) used as a bacterial host upon which the clear plaquing phage were selected for further characterization. The bacteriophage plaques were purified by repeated single plaque isolation using sterile micropipette tips (Adams, 1959). All isolated bacteriophages were amplified in liquid culture (TSB) and the lysates were centrifuged at 6,400 × *g* for 15 min at 4°C to remove remaining bacterial cells and debris (Marcó et al., 2012).

The supernatant containing phages was then centrifuged for 1 h 15,300 × *g* at 4°C. The pellet was resuspended in SM buffer (100 mM $MgSO_4$.7 H_2O; 10 mM NaCl; 50 mM TrisHCl; pH 7.5) and filtered using 0.22 μm syringe filters (Chromtech, Taiwan). Bacteriophage titers were determined using double-agar overlay plaque assays (Mazzocco et al., 2009).

Examination of Bacteriophage Morphology by Electron Microscopy

The morphology of bacteriophage ZCKP1 was investigated using transmission electron microscopy at the National Research Center (Cairo, Egypt). Formvar carbon coated copper grids (Pelco International) were immersed into phage suspension, the phage were fixed using glutaraldehyde (2.5% v/v), washed and stained using 2% phosphotungstic acid (pH 7.0). After drying, grids were examined using a transmission electron microscope (JEOL 1230).

Pulsed Field Gel Electrophoresis (PFGE)

DNA was prepared from bacteriophage ZCKP1 (10^{10} PFU/ml) to determine the genome size by pulsed field gel electrophoresis (PFGE; Senczek et al., 2000). Briefly, bacteriophage suspended in agarose plugs were digested with lysis buffer (0.2% w/v SDS [Sigma]; 1% w/v N-Lauryl sarcosine [Sigma]; 100 mM EDTA; 1 mg/ml Proteinase K [Fischer Scientific]), overnight at 55°C. Following washing 2 mm slices of agaraose containing DNA were inserted into the wells of a 1% w/v agarose gel. The gel was run by using a Bio-Rad CHEF DRII system, in 0.5 X Tris-borate-EDTA, for 18 h at 6 V/cm with a switch time of 30 to 60 s. The size of the genome was determined by comparison to standard concatenated lambda DNA markers (Sigma Aldrich, Gillingham, UK).

Phage DNA Sequencing

Genomic DNA was prepared from phage ZCKP1 (10^{10} PFU/ml) lysates by proteinase K treatment (100 μg/ml in 10 mM EDTA pH 8) followed by resin purification using the Wizard DNA kit (Promega, UK) following the manufacturer's instructions. DNA sequencing was performed using the Illumina MiSeq platform. The data consisted of 3.1 million paired-end sequence reads of 250 bp in length. Initial processing of the raw data and *de novo* assembly was performed using CLC Genomics Workbench version 11.0.1 (Qiagen, Aarhus, Denmark). ORFs were predicted from PHASTER and manually curated (Arndt et al., 2016). Nucleotide sequences appear under the GenBank accession number MH252123.

Lytic Profiles of Isolated Bacteriophages

Using double-agar overlay plaque assays (Mazzocco et al., 2009), the lytic profile of phage ZCKP1 and other isolated phages was determined against a clinical isolate panel when spotted phage concentrations were not $<10^9$ PFU/ml [34]. The experiment was performed using log phase bacteria. The panel included bacteria that cause osteomyelitis, including *K. pneumoniae*, *P. mirabilis* and *E. coli*. The lytic activity of bacteriophages was determined based on plaques of clear lysis. If ≥20 plaques were produced, the tested bacteria were regarded as being sensitive to the phages.

Efficiency of Plating

Bacteriophage ZCKP1 was tested in triplicate over eight decimal dilutions against all the susceptible bacterial strains lysed in the spot assays as previously described (Viazis et al., 2011). Conditions of these experiments were the same as spot test using log-phase bacteria. Thus, 200 μl of all bacterial isolates were added to top agar, and different dilutions of phages were spotted on petri dishes. The plates were incubated overnight at 37°C. Next day, EOP was estimated as the average PFU on target bacteria/average PFU on host bacteria.

Determination of the Frequency of Bacteriophage Insensitive Mutants

The frequency of the emergence of bacteriophage insensitive mutants (BIMs) was estimated as previously described (O'Flynn et al., 2004). Phage ZCKP1 was mixed with bacterial host strains confirmed to be susceptible to the bacteriophage including strains of *K. pneumoniae*, *P. mirabilis*, and *E. coli* at an MOI of 100. After 10 min of incubation at 37°C, the suspension was serial diluted and spotted using double-agar overlay plaque assays. Plates were incubated overnight and BIM was calculated correspondingly by dividing bacterial viable counts remained after phage infection by initial viable counts. Experiments were conducted in triplicate.

One Step Growth Curve

One step growth curves were performed as previously described (Hyman and Abedon, 2009). Briefly, KP/01 strain was grown at concentration of 10^8 and mixed with bacteriophage at multiplicity of infection of 1 and incubated at 37°C for 2 h. Directly after infection and every 10 min, aliquots of 200 μl were withdrawn and divided into two volumes of 100 μl. Chloroform was added to one of two volumes with a concentration of 1% (v/v); to set intracellular phages free while other 100 μl was left with no chloroform addition. After serial dilution, phage titer was estimated by spotting on top agar using double-layer method. Three replicates were conducted for each time interval.

Bacteriophage Potency Against Planktonic Cells

The survival lysis characteristics of phage ZCKP1 were estimated KP/01 in the presence of ZCKP1 phage at multiplicities of infection of 0.1, 10 and 100 PFU/CFU was estimated in comparison to bacterial control at a temperature of 37°C (phage-free samples; Armon and Kott, 1993). Phage infective centers (IC) and plaque forming units (PFU) were also estimated, at different time intervals (0, 5, 10, 20, 30, 40, 60, 90, 120, and 180 min). IC is the amount of free phage particles released from the bacterial cells, without the need to add chloroform, while PFU refers to the number of nascent phage both inside and outside the bacterial cell. Briefly, two flasks were filled with either bacterial culture at a given concentration (control) or with bacterial culture at the same concentration and bacteriophage matching the desired MOI (Test). At every time interval, the concentration of bacterial control (B), bacterial survival (BS) IC, and PFU were simultaneously estimated. Bacterial concentration were determined using the Miles and Misra method (Miles et al.,

1938), while phage concentration was estimated using double-agar overlay plaque assays by adding chloroform to the aliquot to be estimated in case of PFU determination, or not adding chloroform to calculate the IC.

Bacteriophage ZCKP1 was added to *K. pneumoniae* KP/01 in log-phase of growth, at 25°C, at an MOI of 1. Bacterial survival, number of infective centers, and number of plaque forming units were estimated periodically at different time intervals (0, 8, 24, 32, and 48 h).

Bacteriophage Activity Against Established Biofilms of *K. pneumoniae*

The activity of ZCKP1 against established biofilms of KP1/01 was examined using a modification of previously described protocols (Cerca et al., 2005; Pettit et al., 2005). One hundred microliter aliquots of *K. pneumoniae* KP/01 (5×10^6 CFU/ml) in 96-well flat-bottomed polystyrene microtitre plate (Sigma Aldrich) were incubated for 24 h at 37°C. Unattached planktonic cells were carefully removed. The number of bacterial cells in a biofilm per well were estimated to be 10^7 CFU after 24 h (Mottola et al., 2013). Using different MOIs (5, 10, and 50), 100 μl aliquots of phage ZCKP1 diluted in TSB were added to each well, 1 day after biofilm establishment. Other wells received an equivalent amount of TSB as positive controls. In a parallel experiment, phage was introduced to wells every 4 h carefully replacing the previous suspension (containing TSB, planktonic cells and released phages) without disturbing the established biofilms. The biomass of preformed biofilms was quantified by staining with crystal violet (0.2% w/v). Following washing to remove excess dye with PBS, the crystal violet was solubilized in ethanol (95%). The absorbance was measured using a microplate reader at OD_{600} (Biotek, USA). The bacterial counts in biofilms were estimated using an MTT [3-(4,5-dimethylthiazol-2-yl)-2,5-diphenyltetrazolium bromide] assay (Serva Electrophores, Germany) as described by Cady et al. (2012). The absorbance was then measured at 570 nm at 4, 12, and 24 h, using a microplate reader (BioTek, USA). Control and test samples were assayed in triplicate.

Bacteriophage pH and Temperature Stability

The temperature stability of phage ZCKP1 (10^{10} PFU/ml) was evaluated at 45, 55, 65, 75, 85, and 95°C, at 10 min intervals, over 1 h in adjusted water bath incubator. Immediately after incubation, serial dilutions of phage were spotted in triplicate, using standard double layer technique; on a lawn of host strain (KP/01) to estimate phage titers as previously described (Capra et al., 2004; Hammerl et al., 2014).

The bacterial counts of ZCKP1 at different pH values (5, 6, 7, 8, and 9) was determined after 1 h incubation, followed by determining the phage titer as previously described (Hammerl et al., 2014). Different pH values were achieved in SM phage buffer to maintain comparative conditions.

Statistical Analysis

In all data sets, test and control sets were compared using Student's *t*-test. A significance level of 0.05 was applied in all cases. Analytical statistics were undertaken using GraphPad PRISM version 7.00 for Windows (GraphPad Software, La Jolla, USA).

RESULTS

Klebsiella Identification and Sensitivity to Antibiotics

The identity of the KP/01 strain was confirmed to be *K. pneumoniae* by PCR, by the presence of 133 bp band corresponding to conserved region in 16s RNA gene of *K. pneumoniae*, following amplification with the specific primers. The antibiotic sensitivity of *K. pneumoniae* isolate KP/01 was tested using the disc diffusion method and the results showed that *K. pneumoniae* isolate KP/01 was sensitive to tigecycline (TGC), imipenem (IPM) and piperacillin-tazobactam (TZP) but resistant to levofloxacin (LEV), linezolid (LZD), ceftazidime (CAZ) and cefepime (FEP).

Bacteriophage Isolation

Bacteriophages were isolated from freshwater near the pyramids of Egypt in Giza. Selection of the bacteriophage was undertaken upon serial passage according to their ability to lyse a broad range of *K. pneumoniae* isolates and other pathogens causing osteomyelitis, generate reproducible clear zones of lysis, produce hallow zones around lysis zones indicative of exopolysaccharide depolymerase activity and capable of replication to produce high titers on the selected host with respect to time. Bacteriophage ZCKP1 fulfilled these criteria.

Morphology of Lytic ZCKP1 Phage

Electron microscopy revealed that ZCKP1 had an icosahedral head and contractile tail with collar, and base plate, and therefore typical of phages belonging to the family of *Myoviridae* (**Figure 1**). The proportions of the phage head and tail length were also typical of the *Myoviridae* with the head size being 80 ± 0.7 nm while tail length was calculated to be 138.5 ± 2.5 nm.

Phage Genome

Bacteriophage ZCKP1 contains a double-stranded DNA genome estimated to be 160 kbp by PFGE, which is comparable to values indicated by International Committee on Taxonomy of Viruses (ICTV) for bacteriophages belonging to the *Myoviridae* family. DNA sequencing of the phage DNA enabled *de novo* assembly and accurate size determination of a circular permuted genome of 150,925 bp with a G + C content of 39.1%. The genome contained 267 open reading frames, the majority of which are hypothetical proteins or recognized in BLASTP database searches as phage proteins without any ascribed function. Reading frames for which putative functional information could be ascribed to the products appear in **Supplementary Table 1**. Notably these include the phage structural proteins, nucleotide metabolism and components of the replication machinery that are conserved amongst *Myoviridae* infecting hosts within the *Enterobacteriaceae*. Of interest are enzymes that have the potential to modify infected cell surface polysaccharides that may impede superinfection. These include an O-antigen biosynthesis

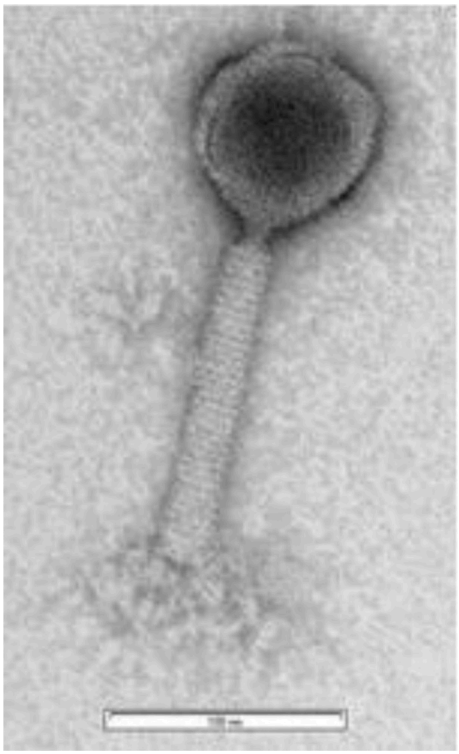

FIGURE 1 | Transmission electronmicroscopic image of phage ZCKP1.

TABLE 1 | Lytic activity of isolated phages against *K. pneumoniae* and other selected members of the *Enterobacteriaceae*.

Bacteriophage name	Bacteriophage activity				
	ZCKP1	**P2**	**K4**	**EC4**	**P9**
K. pneumonia (21 isolates)	15	3	5	1	2
P. mirabilis (18 isolates)	5	5	0	0	8
E. coli (30 isolates)	9	0	0	2	0

TABLE 2 | Efficiency of plating of phage ZCKP1 against different species of *Enterobacteriacae*.

Bacterial species	*K. pneumoniae* ($n = 5$)	*P. mirabilis* ($n = 5$)	*E. coli* ($n = 9$)
EOP >0.5	7	–	6
EOP >0.1 < 0.5	6	–	2
EOP >0.001 < 0.1	1	5	1

protein, a glycosyltransferase and a wcaM superfamily protein associated with colonic acid biosynthesis clusters present in *Enterobacteriaceae* that feature exopolysaccharide production. Four genes encoding proteins related to tellurite resistance are present. Tellurite resistance is frequently used for selection in culture isolation media but is not used for antimicrobial therapy. The genes are thought to contribute to colicin and phage resistance (Taylor and Summers, 1979), which may provide reasons for their presence in phage ZCKP1 in that colicin resistance will provide a selective advantage to the phage infected cell and phage resistance to prevent superinfection. Also of note the phage encodes a member of the hydrolase 2 superfamily implicated in bacterial cell wall hydrolysis. The nearest database phage sequence was PHAGE_Escher_phAPEC8 that infects avian pathogenic *E. coli* and is also a member of the *Myoviridae* (Tsonos et al., 2012).

Bacteriophage Host Range and Efficiency of Plating

The host range of five different phages isolated from freshwater, including phage ZCKP1 were tested on bacteria that were isolated from diabetic patients suffering from osteomyelitis. The ZCKP1 phage was capable of producing lysis zones ($\geq$20 plaques) on 15 out of 21 *K. pneumoniae* isolates, 5 out of 18 *P. mirabilis* isolates and 9 out of 30 *E. coli* isolates, while other phages did not display a comparable spectrum of activity against the *K. pneumoniae* isolates (**Table 1**). A range of EOP for ZCKP1 phage was observed against different species of *Enterobacteriacae* (**Supplementary Table 2**). For *K. pneumoniae* seven phages demonstrated EOPs similar to the multidrug resistant host strain. For *P. mirabilis*, all susceptible strains showed EOP <0.1, whereas for *E. coli six* strains supported replication with EOPs approaching that of the permissive *K. pneumoniae* hosts (**Table 2**).

Frequency of BIMS

BIMs were recovered following high multiplicity infections (100) of host bacteria *K. pneumoniae, P. mirabilis* and *E. coli* with bacteriophage ZCKP1 at 37°C. Mutational frequencies of $7.5 \times 10^{-5} \pm 1.7 \times 10^{-4}$ and $3.7 \times 10^{-5} \pm 6.8 \times 10^{-5}$ were determined for *Klebsiella* and *E. coli*, respectively where *K. pneumoniae* KP1 alone exhibited a lower frequency of $5 \times 10^{-6} \pm 4.04 \times 10^{-6}$.

In vitro Characterization of Phage ZCKP1

A single-step growth curved demonstrated bacteriophage virions were naturally released from bacterial cells after 30 min: the latent period which is the time taken for phages to be assembled and released after infection. However, viruses were assembled 10 min before. This was indicated by eclipse period that was estimated to be 20 min, as chloroform aids new phage particles to free from bacterial cell wall (**Figure 2**). Burst size was estimated to be ~110 virions per single bacterium.

The infection and lysis characteristics of phage ZCKP1 were estimated at different MOIs, over a period of 3 h (**Figures 3A–C**) in a growing culture of *K. pneumoniae* KP/01 (**Figures 3A–C**). *K. pneumoniae* KP/01 was lysed by phage ZCKP1 at each MOI tested but the MOI of 100 reduced the viable bacteria from 9.0 $\log_{10}$ CFU/ml to below the limit of detection at 37°C by 2 h

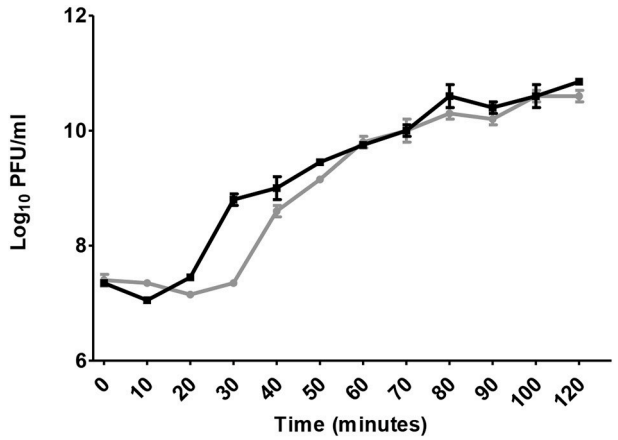

FIGURE 2 | Single step growth curve. Gray dashed line represents nascent phage without chloroform addition (PFU/ml), while the black line represents phages released after chloroform addition (PFU/ml).

(**Figures 3A–C**). Under these circumstances the reductions in bacterial count were not accompanied by a measurable rise in phage titer (**Figure 3C**). Phage replication was observed at lower MOI, which coincided with the commencement of the fall in viable count.

Bacteriophage Activity Against *K. pneumoniae* Established in Biofilms

A single application of ZCKP1 to established biofilms of *K. pneumoniae* KP/01 resulted in a reduction crystal violet stainable biofilm content ($P < 0.01$; **Figure 4A**) and the percentage of viable cells observed by MTT staining ($P < 0.01$; **Figure 4C**) after 4 h. The most effective treat represented the highest MOI (50 PFU/CFU). However, following this disruption there was recovery in biofilm estimates accompanied by a recovery in cell viability. Multiple treatments of phage ZCKP1 on established *K. pneumoniae* KP/01 biofilms at 4 h intervals resulted in significant reductions in biofilm content and prevented the recovery of cell viability throughout the 24 h period of the experiment ($P < 0.01$; **Figures 4B,D**).

Bacteriophage Temperature and pH Stability

The stability of phage ZCKP1 at different temperatures and pH values was investigated (**Figures 5A,B**). Phage titers were stable, at approximately 10^9 PFU/ml, for 1 h at temperatures of 45 and 55°C. The phage titer decreased after 40 min at 65°C to 10^8 PFU/ml, and continued to decline below 10^7 PFU/ml after 1 h. A significant decline ($P < 0.005$) was observed when phages were incubated at 75 and 85°C. However, phage could still be recovered after 1 h at 75°C at a titer of 10^3 PFU/ml. Phage could not be recovered after 40 min at 85°C. Acidic pH of <6 significantly ($P < 0.005$) reduced the phage stability after 1 h. The optimum stability was observed to be pH 6 but persisted at alkaline pH values to pH 9 (**Figure 5B**).

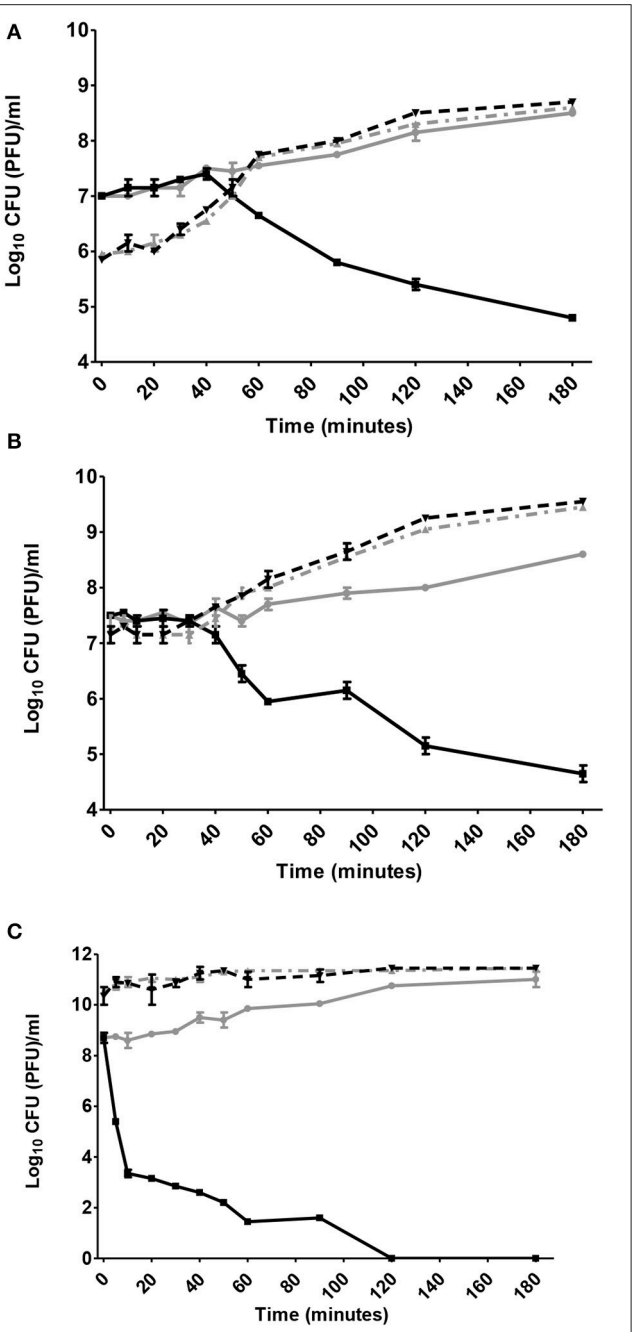

FIGURE 3 | *In vitro* activity of phage ZCKP1 at 37°C. Panels show bacterial counts and phage titers of *K. pneumoniae* KP/01 infected with ZCKP1 at: **(A)** MOI 0.1; **(B)** MOI 1; **(C)** MOI 100. Black solid line represents viable count of *K. pneumoniae* KP/01 infected with phage (CFU/ml); Gray solid line represents *K. pneumoniae* KP/01 uninfected control (CFU/ml); black dashed line represents phage infective centers (PFU/ml) and gray dashed line represents nascent phage (PFU/ml).

DISCUSSION

K. pneumoniae is an enteric pathogen that causes pneumonia and wound infections (Podschun and Ullmann, 1998). The

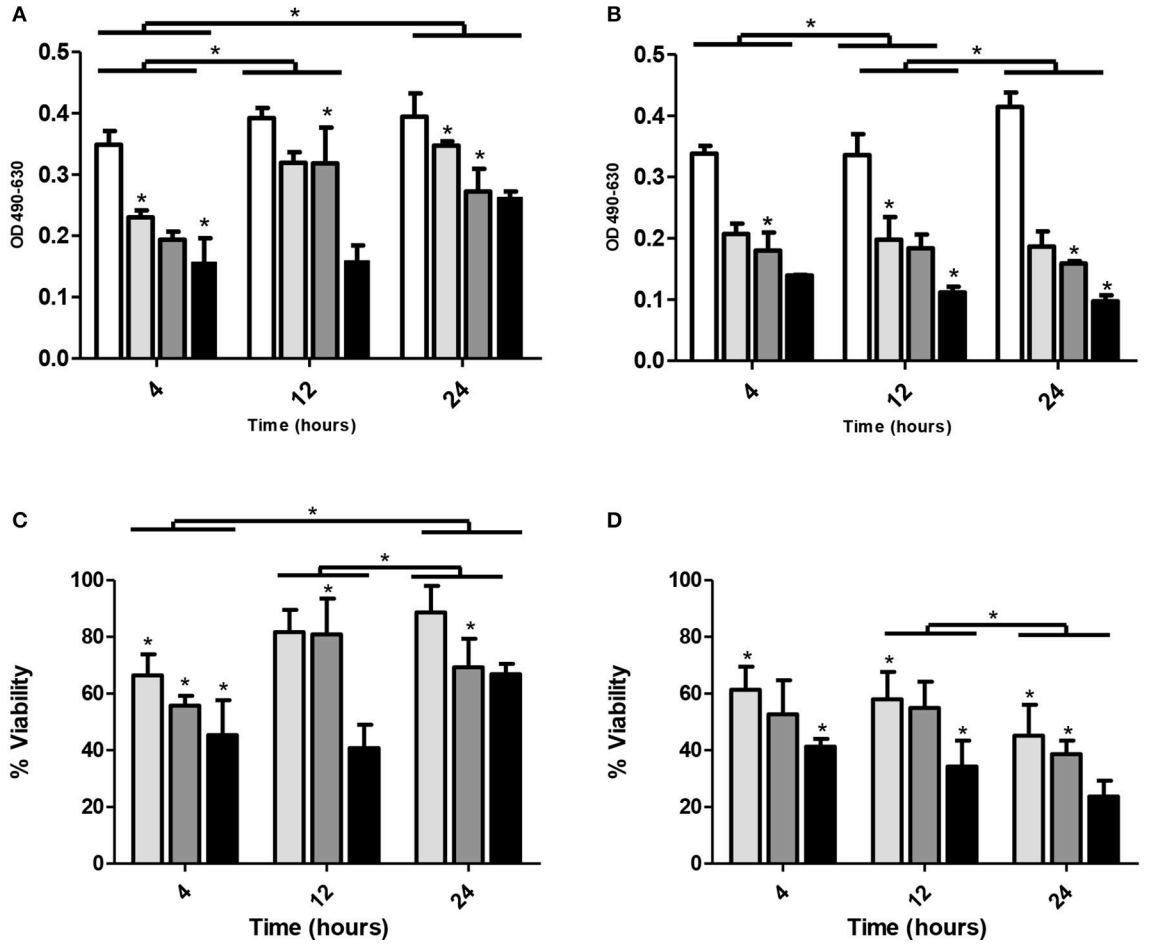

FIGURE 4 | Phage treatments of *K. pneumoniae* KP/01 biofilms. Panels **(A)** and **(B)** show the effect of phage treatment on preformed biofilms determined by crystal violet staining and solubilization estimates of biomass: **(A)** single treatment with phage ZCKP1; **(B)** with multiple treatments with phage ZCKP1 using different MOIs. White columns represent untreated control; light gray columns represent a starting MOI of 5; dark gray columns represent a starting MOI of 10 and solid black columns represent a starting MOI of 50. Panels **(C)** and **(D)** show bacterial counts in biofilms determined using an MTT assay, **(C)** single treatment with phage ZCKP1 bacteriophage or **(D)** with multiple treatments with phage ZCKP1 bacteriophage using different MOIs: Light gray columns represent a starting MOI of 50; dark gray columns represent a starting MOI of 10 and solid black columns represent a starting MOI of 5. $^*P < 0.01$ (brackets specify comparisons between groups).

effectiveness of antibiotics to treat such infections has been reduced significantly in recent years due to the increasing numbers of antibiotic-resistant bacteria, and as a result morbidity and mortality remain high. Antibiotic resistance is a growing public health threat for which the use of bacteriophage as an alternative to antibiotics may be considered to combat MDR infections. In particular phage therapy has also been considered a promising approach to eliminate diabetic foot ulcer after infection by MRSA in human subjects (Fish et al., 2016). In order to get the maximum benefits of bacteriophage based therapies, it is important to determine the characteristics of individual bacteriophages so that treatments can be tailored for the situation where treatment is to be applied. Moreover, it is crucial to ensure that phages selected do not have the capacity to transfer resistance or pathogenic traits to the resident microbiota (Abedon and Thomas-Abedon, 2010).

Antibiotics that were previously effective in the elimination of diabetic foot infections are now less effective. The *K. pneumoniae* KP/01 isolate recorded here shows resistance to levofloxacin, fluoroquinolone and was identified as a ceftazidime-resistant *K. pneumoniae* (CSKP). Ceftazidime is a cephalosporin antibiotic that can be degraded by extended spectrum beta lactamases (ESBL) that include SHV, TEM, CTX and YOU types (Sougakoff et al., 1988; Urban et al., 1994). *K. pneumoniae* KP/01 also showed resistance to the cephalosporin cefepime. As a clinical multiple drug resistant bacteria the KP/01 isolate was an ideal host for this study (Sougakoff et al., 1988).

Both morphological analysis and genome size confirmed that bacteriophage ZCKP1 belonged to the *Caudovirales* order with typical features of *Myoviridae*. It had an icosahedral head, a contractile tail with base plates showing tail fibers and spikes in addition to a collar. The genome of 151 kb,

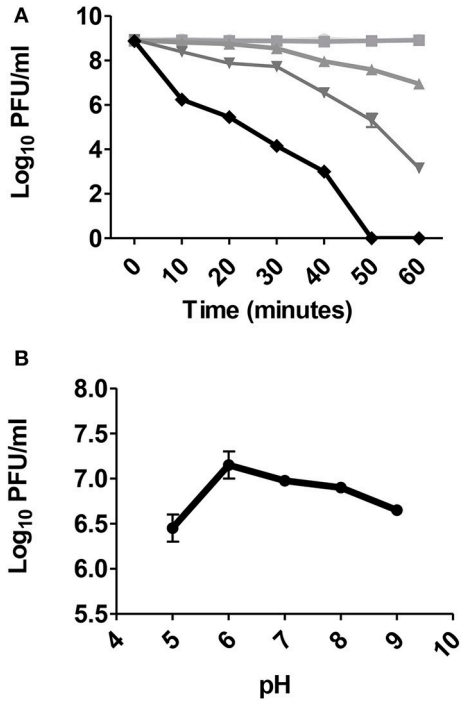

FIGURE 5 | The stability of phage ZCKP1 at **(A)** different temperatures (45°C: circle, 55°C: square, 65°C: triangle, 75°C: inverted triangle and 85°C: diamond) and **(B)** pH values. Results are shown as means ± Standard error.

differs in size to the 45 kbp of KLPN1 phage previously reported as isolated against *K. pneumoniae* (Hoyles et al., 2015). Bacteriophage ZCKP1 demonstrated a broad lytic profile covering a variety of bacterial pathogens including *K. pneumoniae*, *Proteus* and *E. coli* that all contribute to osteomyelitis cases and were isolated from patients with "diabetic foot."

In vitro studies of potential therapeutic bacteriophages ensures only the most effective phages progress to clinical trials based on their capability to lyse pathogens in planktonic and biofilm formations with wide host range coverage. Phage ZCKP1 was shown to be highly effective at reducing *K. pneumoniae* counts *in vitro* and proved to be stable at high temperatures and over a wide pH range. Phage ZCKP1 was also effective against other members of *Enterobacteriacae* that cause osteomyelitis, which contributes to the therapeutic potential. With the application of high concentrations of bacteriophages (MOI of 100), ZCKP1 was demonstrated to reduce *K. pneumoniae* without producing new phages. This is an established phenomenon called "lysis from without," where many phages become absorbed to bacterial cells causing lysis without release of new phage (Abedon, 2011). In addition, a single high dose applied in a clinical situation may enable the human immune system to overcome reduced numbers of pathogens by working synergistically with the phage. Even with lower doses of phage, the rate of development of resistance to bacteriophages is approximately 10-fold lower than the rate of the development of antibiotic resistance (Carlton, 1999). The conditions of application and the influence of immune system can vary so the action of a particular phage must be considered before therapeutic use (O'Flynn et al., 2004; Lu and Koeris, 2011). In this context the mutation frequencies determined at high MOI applications would dictate the use of phage cocktails, and possibly the availability of reserve phage. Developing a cocktail of isolated lytic phages may increase the efficacy of bacteriophages to lyse multiple hosts and reduce the frequency that resistant strains may emerge.

Klebsiella are able to form thick biofilms on tissues and on medical implants making them more resistant than free-living planktonic cells to antibacterial agents and have reduced susceptibility to antibiotics (Calhoun and Manring, 2005). Phage ZCKP1 treatment of *K. pneumoniae* KP/01 biofilms was shown to be an effective method for biofilm reduction, although repeated treatments were required to prevent regrowth. Reductions in biofilm biomass have been attributed to the action of a soluble exopolysaccharide depolymerase (Cornelissen et al., 2011). These enzymes have the ability to disrupt the capsule of *Klebsiella* making it more susceptible to antibacterial agents (Hughes et al., 1998; Kesik-Szeloch et al., 2013). The nucleotide sequence of phage ZCKP1 revealed enzyme activities consistent with polysaccharide modification, However, the presence of wcaM could influence exopolysaccharide structure to adversely affect biofilm integrity when embedded bacteria become phage infected.

Previously reported phage treatments of *K. pneumoniae* biofilms include: a phage belonging to the *Podoviridae* family (Chhibber et al., 2013); a *Siphoviridae* named bacteriophage Z (Jamal et al., 2015) and *Myoviridae* phages (Kesik-Szeloch et al., 2013). Of these, the Myoviridae are likely the most promising as they represent virulent bacteriophage that do not mobilize and transfer genetic information. The gene sequence of phage ZCKP1 suggests that it does indeed fall into this category. Four genes associated with tellurite resistance were observed but are not used for antimicrobial therapy. Tellurite resistance is often associated with colicin and phage resistance phenotypes (Taylor and Summers, 1979), and likely extends this advantage to the virus infected cell as insurance against superinfection.

CONCLUSION

Phage ZCKP1 has been fully characterized *in vitro* and shows excellent potential to be used as a therapeutic agent against *K. pneumoniae* infections of diabetic foot. It can reduce the bacterial pathogen in both planktonic and biofilms and is extremely stable over a range of pH and temperatures. Therapeutic trials are needed to confirm its potential *in vivo*.

DATA AVAILABILITY

All data generated or analyzed during this study are included in this published article and are available from

the corresponding author. Nucleotide sequences appear in the NCBI public database under the GenBank accession number MH252123.

AUTHOR CONTRIBUTIONS

AE-S: primary responsibility for design of the work. OT and AE-S: substantial contributions to the design of the work and analysis and interpretation of the data. OT, PC, IC, and AE-S: drafting the work and revising it critically for important intellectual content. OT, PC, IC, and AE-S: final approval of the version to be published.

ACKNOWLEDGMENTS

This research was supported by Zewail City of Science and Technology. This work was also supported by the Biotechnology and Biological Sciences Research Council (grant number BB/GCRF-IAA/15).

SUPPLEMENTARY MATERIAL

The Supplementary Material for this article can be found online at: https://www.frontiersin.org/articles/10.3389/fmicb.2018.02127/full#supplementary-material

REFERENCES

Abedon, S. T. (2011). Lysis from without. *Bacteriophage* 1, 46–49. doi: 10.4161/bact.1.1.13980

Abedon, S. T., and Thomas-Abedon, C. (2010). Phage therapy pharmacology. *Curr. Pharm. Biotechnol.* 11, 28–47. doi: 10.1016/B978-0-12-387044-5.00001-7

Adams, H. (1959). "Methods of study of bacterial viruses," in *Bacteriophages* (London: Interscience Publishers), 447–448.

Akers, K. S., Mende, K., Cheatle, K. A., Zera, W. C., Yu, X., Beckius, M. L., et al. (2014). Biofilms and persistent wound infections in United States military trauma patients: a case–control analysis. *BMC Infect. Dis.* 14:190. doi: 10.1186/1471-2334-14-190

Armon, R., and Kott, Y. (1993). A simple, rapid and sensitive presence/absence detection test for bacteriophage in drinking water. *J. Appl. Bacteriol.* 74, 490–496. doi: 10.1111/j.1365-2672.1993.tb05159.x

Arndt, D., Grant, J., Marcu, A., Sajed, T., Pon, A., Liang, Y., et al. (2016). PHASTER: a better, faster version of the PHAST phage search tool. *Nucleic Acids Res.* 44, W16–W21. doi: 10.1093/nar/gkw387

Bogovazova, G. G., Voroshilova, N. N., and Bondarenko, V. M. (1991). The efficacy of *Klebsiella pneumoniae* bacteriophage in the therapy of experimental *Klebsiella* infection. *Zh. Mikrobiol. Epidemiol. Immunobiol.* 5–8.

Cady, N. C., McKean, K. A., Behnke, J., Kubec, R., Mosier, A. P., Kasper, S. H., et al. (2012). Inhibition of biofilm formation, quorum sensing and infection in *Pseudomonas aeruginosa* by natural products-inspired organosulfur compounds. *PLoS ONE* 7:e38492. doi: 10.1371/journal.pone.0038492

Calhoun, J. H., and Manring, M. M. (2005). Adult osteomyelitis. *Infect. Dis. Clin. North Am.* 19, 765–786. doi: 10.1016/j.idc.2005.07.009

Cannatelli, A., Santos-Lopez, A., Giani, T., Gonzalez-Zorn, B., and Rossolini, G. M. (2015). Polymyxin resistance caused by mgrB inactivation is not associated with significant biological cost in *Klebsiella pneumoniae*. *Antimicrob. Agents Chemother.* 59, 2898–2900. doi: 10.1128/AAC.04998-14

Cao, F., Wang, X., Wang, L., Li, Z., Che, J., Wang, L., et al. (2015). Evaluation of the efficacy of a bacteriophage in the treatment of pneumonia induced by multidrug resistance *Klebsiella pneumoniae* in mice. *Biomed Res. Int.* 2015:752930. doi: 10.1155/2015/752930

Capra, M. L., Quiberoni, A., and Reinheimer, J. A. (2004). Thermal and chemical resistance of *Lactobacillus casei* and *Lactobacillus paracasei* bacteriophages. *Lett. Appl. Microbiol.* 38, 499–504. doi: 10.1111/j.1472-765X.2004.01525.x

Carlton, R. M. (1999). Phage therapy: past history and future prospects. *Arch. Immunol. Ther. Exp. (Warsz)* 47, 267–274. doi: 10.2217/fvl.15.3

Cerca, N., Martins, S., Pier, G. B., Oliveira, R., and Azeredo, J. (2005). The relationship between inhibition of bacterial adhesion to a solid surface by sub-MICs of antibiotics and subsequent development of a biofilm. *Res. Microbiol.* 156, 650–655. doi: 10.1016/j.resmic.2005.02.004

Chhibber, S., Kaur, S., and Kumari, S. (2008). Therapeutic potential of bacteriophage in treating *Klebsiella pneumoniae* B5055-mediated lobar pneumonia in mice. *J. Med. Microbiol.* 57, 1508–1513. doi: 10.1099/jmm.0.2008/002873-0

Chhibber, S., Nag, D., and Bansal, S. (2013). Inhibiting biofilm formation by *Klebsiella pneumoniae* B5055 using an iron antagonizing molecule and a bacteriophage. *BMC Microbiol.* 13:174. doi: 10.1186/1471-2180-13-174

Clinical and Laboratory Standards Institute (1999). Methods for determining bactericidal activity of antimicrobial agents; approved guideline M26-A. *Clin. Lab. Stand. Inst.* 19, 7.

Cornelissen, A., Ceyssens, P. J., T'Syen, J., van Praet, H., Noben, J. P., Shaburova, O. V., et al. (2011). The T7-related *Pseudomonas putida* phage ϕ15 displays virion-associated biofilm degradation properties. *PLoS ONE* 6:e18597. doi: 10.1371/journal.pone.0018597

Diago-Navarro, E., Chen, L., Passet, V., Burack, S., Ulacia-Hernando, A., Kodiyanplakkal, R. P., et al. (2014). Carbapenem-resistant *Klebsiella pneumoniae* exhibit variability in capsular polysaccharide and capsule associated virulence traits. *J. Infect. Dis.* 210, 803–813. doi: 10.1093/infdis/jiu157

Domenico, P., Salo, R. J., Cross, A. S., and Cunha, B. A. (1994). Polysaccharide capsule-mediated resistance to opsonophagocytosis in *Klebsiella pneumoniae*. *Infect. Immun.* 62, 4495–4499.

Dourakis, S. P., Alexopoulou, A., Metallinos, G., Thanos, L., and Archimandritis, A. J. (2006). Pubic osteomyelitis due to *Klebsiella pneumoniae* in a patient with diabetes mellitus. *Am. J. Med. Sci.* 331, 322–324. doi: 10.1097/00000441-200606000-00006

El-Shibiny, A., El-Sahhar, S., and Adel, M. (2017). Phage applications for improving food safety and infection control in Egypt. *J. Appl. Microbiol.* 123, 556–567. doi: 10.1111/jam.13500

Fish, R., Kutter, E., Wheat, G., Blasdel, B., Kutateladze, M., and Kuhl, S. (2016). Bacteriophage treatment of intransigent diabetic toe ulcers: a case series. *J. Wound Care* 25, S27–33. doi: 10.12968/jowc.2016.25.7.S27

Grayson, M. L., Gibbons, G. W., Balogh, K., Levin, E., and Karchmer, A. W. (1995). Probing to bone in infected pedal ulcers. A clinical sign of underlying osteomyelitis in diabetic patients. *JAMA* 273, 721–723. doi: 10.1001/jama.1995.03520330051036

Gupta, P., Sarkar, S., Das, B., Bhattacharjee, S., and Tribedi, P. (2016). Biofilm, pathogenesis and prevention–a journey to break the wall: a review. *Arch. Microbiol.* 198, 1–15. doi: 10.1007/s00203-015-1148-6

Hammerl, J. A., Jäckel, C., Alter T, Janzcyk, P., Stingl, K., Knüver MT, et al. (2014). Reduction of campylobacter jejuni in broiler chicken by successive application of Group II and Group III phages. *PLoS ONE* 9:e114785. doi: 10.1371/journal.pone.0114785.eCollection2014

Hoyles, L., Murphy, J., Neve, H., Heller, K. J., Turton, J. F., Mahony, J., et al. (2015). *Klebsiella pneumoniae* subsp. Pneumoniae-bacteriophage combination from the caecal effluent of a healthy woman. *PeerJ* 3:e1061. doi: 10.7717/peerj.1061

Hughes, K. A., Sutherland, I. W., Clark, J., and Jones, M. V. (1998). Bacteriophage and associated polysaccharide depolymerases–novel tools for study of bacterial biofilms. *J. Appl. Microbiol.* 85, 583–590. doi: 10.1046/j.1365-2672.1998.853541.x

Hung, C. H., Kuo, C. F., Wang, C. H., Wu, C. M., and Tsao, N. (2011). Experimental phage therapy in treating *Klebsiella pneumoniae*-mediated liver abscesses

and bacteremia in mice. *Antimicrob. Agents Chemother.* 55, 1358–1365. doi: 10.1128/AAC.01123-10

Hyman, P., and Abedon, S. T. (2009). Practical methods for determining phage growth parameters. *Methods Mol. Biol.* 501, 175–202. doi: 10.1007/978-1-60327-164-6_18

Jamal, M., Hussain, T., Rajanna Das, C., and Andleeb, S. (2015). Characterization of siphoviridae phage Z and studying its efficacy against multidrug-resistant *Klebsiella pneumoniae* planktonic cells and biofilm. *J. Med. Microbiol.* 64, 454–462. doi: 10.1099/jmm.0.000040

Kesik-Szeloch, A., Drulis-Kawa, Z., Weber-Dabrowska, B., Kassner, J., Majkowska-Skrobek, G., Augustyniak, D., et al. (2013). Characterising the biology of novel lytic bacteriophages infecting multidrug resistant *Klebsiella pneumoniae*. *Virol. J.* 10:100. doi: 10.1186/1743-422X-10-100

Kidd, T. J., Mills, G., Sá-Pessoa, J., Dumigan, A., Frank, C. G., Insua, J. L., et al. (2017). A *Klebsiella pneumoniae* antibiotic resistance mechanism that subdues host defences and promotes virulence. *EMBO Mol. Med.* 9, 430–447. doi: 10.15252/emmm.201607336

Lu, T. K., and Koeris, M. S. (2011). The next generation of bacteriophage therapy. *Curr. Opin. Microbiol.* 14, 524–531. doi: 10.1016/j.mib.2011.07.028

Malhotra, R., Shu-Yi Chan, C., and Nather, A. (2014). Osteomyelitis in the diabetic foot. *Diabet. Foot Ankle* 5, 1–8. doi: 10.3402/dfa.v5.24445

Malik, R., and Chhibber, S. (2009). Protection with bacteriophage KØ1 against fatal *Klebsiella pneumoniae*-induced burn wound infection in mice. *J.Microbiol. Immunol. Infect.* 42, 134–140.

Marcó, M. B., Garneau, J. E., Tremblay, D., Quiberoni, A., and Moineau, S. (2012). Characterization of two virulent phages of *Lactobacillus plantarum*. *Appl. Environ. Microbiol.* 78, 8719–8734. doi: 10.1128/AEM.02565-12

Mathews, C. J., Weston, V. C., Jones, A., Field, M., and Coakley, G. (2010). Bacterial septic arthritis in adults. *Lancet* 375, 846–855. doi: 10.1016/S0140-6736(09)61595-6

Mazzocco, A., Waddell, T. E., Lingohr, E., and Johnson, R. P. (2009). Enumeration of bacteriophages by the direct plating plaque assay. *Methods Mol. Biol.* 501, 77–80. doi: 10.1007/978-1-60327-164-6_8

Miles, A. A., Misra, S. S., and Irwin, J. O. (1938). The estimation of the bactericidal power of the blood. *J. Hyg. (Lond).* 38, 732–749. doi: 10.1017/S002217240001158X

Mottola, C., Mendes, J., Cavaco-Silva, P., and Melo-Cristino, J. O. M. (2013). Relevance of inoculum size on biofilm formation by diabetic foot bacterial isolates. *Port. Congr. Microbiol. Biotechnol.*

Mukkunnath, S., Manjunath, R., and Desai, M. (2015). A study of the bacteriological profile of diabetic foot ulcer and antibiotic sensitivity pattern. *J. Evol. Med. Dental Sci.* 4, 6832–6840. doi: 10.14260/jemds/2015/991

NADE, S. (1975). Acute septic arthritis in infancy and childhood. *J. Paediatr. Child Health* 11, 145–153. doi: 10.1111/j.1440-1754.1975.tb02302.x

Nagel, T. E., Chan, B. K., De Vos, D., and El-Shibiny, A. K. E. (2016). The developing world urgently needs phages to combat pathogenic bacteria. *Front. Microbiol.* 7:882. doi: 10.3389/fmicb.2016.00882

O'Flynn, G., Ross, R. P., Fitzgerald, G. F., and Coffey, A. (2004). Evaluation of a cocktail of three bacteriophages for biocontrol of *Escherichia coli* O157:H7. *Appl. Environ. Microbiol.* 70, 3417–3424. doi: 10.1128/AEM.70.6.3417-3424.2004

Pettit, R. K., Weber, C. A., Kean, M. J., Hoffmann, H., Pettit, G. R., Tan, R., et al. (2005). Microplate alamar blue assay for *Staphylococcus epidermidis* biofilm susceptibility testing. *Antimicrob. Agents Chemother.* 49, 2612–2617. doi: 10.1128/AAC.49.7.2612-2617.2005

Podschun, R., and Ullmann, U. (1998). Klebsiella spp. as nosocomial pathogens: Epidemiology, taxonomy, typing methods, and pathogenicity factors. *Clin. Microbiol. Rev.* 11, 589–603.

Prokesch, B. C., TeKippe, M., Kim, J., Raj, P., TeKippe, E. M. E., and Greenberg, D. E. (2016). Primary osteomyelitis caused by hypervirulent *Klebsiella pneumoniae*. *Lancet Infect. Dis.* 16, e190–e195. doi: 10.1016/S1473-3099(16)30021-4

Qadir, M. I. (2015). Review: phage therapy: a modern tool to control bacterial infections. *Pak. J. Pharm. Sci.* 28, 265–70. Available online at: http://www.ncbi.nlm.nih.gov/pubmed/25553704

Rana, M. M., Sturdevant, M., Patel, G., and Huprikar, S. (2013). *Klebsiella* necrotizing soft tissue infections in liver transplant recipients: a case series. *Transpl. Infect. Dis.* 15, E157–E163. doi: 10.1111/tid.12103

Richard, J.-L. (2011). New insights in diabetic foot infection. *World J. Diabetes* 2:24. doi: 10.4239/wjd.v2.i2.24

Ross, J. J., Saltzman, C. L., Carling, P., and Shapiro, D. S. (2003). Pneumococcal septic arthritis: review of 190 cases. *Clin. Infect. Dis.* 36, 319–27. doi: 10.1086/345954

Sanchez, M. C., Sebti, R., Hassoun, P., Mannion, C., Goy, A. H., Feldman, T., et al. (2013). Osteomyelitis of the patella caused by *Legionella anisa*. *J. Clin. Microbiol.* 51, 2791–2793. doi: 10.1128/JCM.03190-12

Senczek, D., Stephan, R., and Untermann, F. (2000). Pulsed-field gel electrophoresis (PFGE) typing of *Listeria* strains isolated from a meat processing plant over a 2-year period. *Int. J. Food Microbiol.* 62, 155–159. doi: 10.1016/S0168-1605(00)00395-0

Sougakoff, W., Goussard, S., Gerbaud, G., and Courvalin, P. (1988). Plasmid-mediated resistance to third-generation cephalosporins caused by point mutations in tem-type penicillinase genes. *Clin. Infect. Dis.* 10, 879–884. doi: 10.1093/clinids/10.4.879

Taylor, D. E., and Summers, A. O. (1979). Association of tellurium resistance and bacteriophage inhibition conferred by R plasmids. *J. Bacteriol.* 137, 1430–1433.

Tsonos, J., Adriaenssens, E. M., Klumpp, J., Hernalsteens, J. P., Lavigne, R., De Greve, H. (2012). Complete genome sequence of the novel *Escherichia coli* phage phAPEC8. *J. Virol.* 86, 13117–13118. doi: 10.1128/JVI.02374-12

Urban, C., Meyer, K. S., Mariano, N., Rahal, J. J., Flamm, R., Rasmussen, B. A., et al. (1994). Identification of TEM-26 β-lactamase responsible for a major outbreak of ceftazidime-resistant *Klebsiella pneumoniae*. *Antimicrob. Agents Chemother.* 38, 392–395. doi: 10.1128/AAC.38.2.392

Viazis, S., Akhtar, M., Feirtag, J., Brabban, A. D., and F. Diez-Gonzalez, F. (2011). Isolation and characterization of lytic bacteriophages against enterohaemorrhagic *Escherichia coli*. *J. Appl. Microbiol.* 110, 1323–1331. doi: 10.1111/j.1365-2672.2011.04989.x

Woese, C. R., and Fox, G. E. (1977). Phylogenetic structure of the prokaryotic domain: the primary kingdoms. *Proc. Natl. Acad. Sci. U.S.A.* 74, 5088–5090. doi: 10.1073/pnas.74.11.5088

Woese, C. R., Kandler, O., and Wheelis, M. L. (1990). Towards a natural system of organisms: proposal for the domains Archaea, Bacteria, and Eucarya. *Proc. Natl. Acad. Sci. U.S.A.* 87, 4576–4579. doi: 10.1073/pnas.87.12.4576

Conflict of Interest Statement: The authors declare that the research was conducted in the absence of any commercial or financial relationships that could be construed as a potential conflict of interest.

frontiers in Microbiology

ORIGINAL RESEARCH
published: 31 July 2018
doi: 10.3389/fmicb.2018.01725

Chestnut Honey and Bacteriophage Application to Control *Pseudomonas aeruginosa and Escherichia coli* Biofilms: Evaluation in an *ex vivo* Wound Model

*Ana Oliveira, Jéssica C. Sousa, Ana C. Silva, Luís D. R. Melo and Sanna Sillankorva**

Centre of Biological Engineering, Laboratório de Investigação em Biofilmes Rosário Oliveira, University of Minho, Braga, Portugal

OPEN ACCESS

Edited by:
Pilar García, Consejo Superior de Investigaciones Científicas (CSIC), Spain

Reviewed by:
Mariusz Stanislaw Grinholc, Intercollegiate Faculty of Biotechnology of University of Gdansk and Medical University of Gdansk, Poland
Victor Krylov, I. I. Mechnikov Research Institute of Vaccines and Sera (RAS), Russia

***Correspondence:**
Sanna Sillankorva
s.sillankorva@deb.uminho.pt

Specialty section:
This article was submitted to Antimicrobials, Resistance and Chemotherapy, a section of the journal Frontiers in Microbiology

Received: *01 May 2018*
Accepted: *11 July 2018*
Published: *31 July 2018*

Citation:
Oliveira A, Sousa JC, Silva AC, Melo LDR and Sillankorva S (2018) Chestnut Honey and Bacteriophage Application to Control Pseudomonas aeruginosa and Escherichia coli Biofilms: Evaluation in an ex vivo Wound Model. Front. Microbiol. 9:1725. doi: 10.3389/fmicb.2018.01725

Chronic skin wounds represent a major burn both economically and socially. *Pseudomonas aeruginosa* and *Escherichia coli* are among the most common colonizers of infected wounds and are prolific biofilm formers. Biofilms are a major problem in infections due to their increasingly difficult control and eradication, and tolerance to multiple prescribed drugs. As so, alternative methods are necessary. Bacteriophages (phages) and honey are both seen as a promising approach for biofilm related infections. Phages have specificity toward a bacterial genus, species or even strain, self-replicating nature, and avoid dysbiosis. Honey has gained acknowledgment due to its antibacterial, antioxidant and anti-inflammatory and wound healing properties. In this work, the effect of *E. coli* and *P. aeruginosa* phages vB_EcoS_CEB_EC3a and vB_PaeP_PAO1-D and chestnut honey, alone and combined, were tested using *in vitro* (polystyrene) and *ex vivo* (porcine skin) models and against mono and dual-species biofilms of these bacteria. In general, colonization was higher in the porcine skins and the presence of a second microorganism in a consortium of species did not affect the effectiveness of the treatments. The antibacterial effect of combined therapy against dual-species biofilms led to bacterial reductions that were greater for biofilms formed on polystyrene than on skin. Monospecies biofilms of *E. coli* were better destroyed with phages and honey than *P. aeruginosa* monospecies biofilms. Overall, the combined phage-honey formulations resulted in higher efficacies possibly due to honey's capacity to damage the bacterial cell membrane and also to its ability to penetrate the biofilm matrix, promoting and enhancing the subsequent phage infection.

Keywords: *ex vivo*, *in vitro*, biofilms, dual-species, *P. aeruginosa*, *E. coli*

INTRODUCTION

Chronic wounds are defined as wounds which failed the sequential reparative process responsible to repair the anatomic and functional integrity of the damaged tissue in a period of 4-8 weeks (Lazarus et al., 1994; Mustoe et al., 2006). These wounds lead to considerable morbidity and high costs associated with treatment, which represents an increasing burden on public and health systems worldwide.

In a chronic wound, bacterial growth occurs in biofilms, sessile communities organized in a three-dimensional structure, embedded in a self-produced matrix containing extracellular polymeric substances (EPS) such as polysaccharides, proteins, extracellular DNA, membrane vesicles, and other polymers. Biofilms are a protected mode of growth that allows bacteria to survive in hostile environments, presenting an altered growth rate (Baillie and Douglas, 1998) and gene expression (Whiteley et al., 2001), and an increased tolerance to antimicrobials (Fux et al., 2005), when comparing to their planktonic equivalents. Within a chronic wound, the biofilm tolerance to several antibiotics and host defenses (Flemming and Wingender, 2010) is promoted by numerous factors. The biofilm matrix offers structural stability, acting as a diffusional barrier both to antibiotics (Billings et al., 2013) and to host defenses (Jensen et al., 2007). Besides, extracellular DNA can be easily exchanged among bacteria allowing the transference of genes responsible by protective behaviors against external molecules (Chiang et al., 2013). For example, efflux pumps have been identified in several biofilm forming pathogens, such as *E. coli* (Ito et al., 2009), *P. aeruginosa* (Zhang and Mah, 2008) and *S. aureus* (Ding et al., 2008) and the production of antibiotic degrading-enzymes, such as β-lactamase, was identified in biofilm forming strains (Hengzhuang et al., 2013).

Bacteriophages (phages) are highly specific viruses that infect and replicate within bacteria. Phage attachment to a host cell occurs after specific recognition of complementary receptors on the bacterial cell surface (Weinbauer, 2004). The great increase of multi-drug resistant microorganisms has revitalized the interest in using phages as an effective alternative to antimicrobial therapy, including for wound healing (Pirnay et al., 2011).

Honey is a viscous solution derived from nectar gathered and modified by honeybee. It is composed by ∼31.3% glucose, 38.2% fructose, 1% sucrose and 17% water, and in minor quantity by organic acids, proteins, amino acids, vitamins, minerals and enzymes (Bogdanov et al., 2008). The use of honey in wounds was firstly documented by the ancient Egyptians 4,000 years ago and it has been used for this purpose since ancient times, by Romans, Greeks, and Chinese (Sato and Miyata, 2000). Antimicrobial properties of honey are associated with a combination of factors as high osmolarity, low availability of water (Molan, 1992), production of hydrogen peroxide [product of the enzyme glucose oxidase activity while degrading glucose (Molan and Betts, 2004; Brudzynski, 2006)], acidic pH levels (Gethin et al., 2008), presence of methylglyoxal (MGO) [reacting with macromolecules such as DNA, RNA, and proteins (Adams et al., 2008; Majtan et al., 2014)], among others.

In this work, the antibacterial effect of two lytic bacteriophages vB_EcoS_CEB_EC3a and vB_PaeP_PAO1-D were evaluated either alone or combined with a Portuguese honey, C1, in 24 h biofilms formed in porcine skin explants.

MATERIALS AND METHODS

Bacterial Strains and Growth Conditions

Two *Escherichia coli* strains were used in this study: the clinical isolate EC3a that was kindly provided by the Hospital Escala Braga (Portugal) for phage vB_EcoS_CEB_EC3a (EC3a) propagation and the *E. coli* reference strain CECT 434 (purchased from the Spanish Type Culture Collection) for biofilm experiments.

Pseudomonas aeruginosa reference strain PA01 (DSM22644), purchased from the German Collection of Microorganisms and Cell Cultures, was used for isolation and propagation of phage vB_PaeP_PAO1-D (PAO1-D) and for biofilm experiments. Other 36 strains of *P. aeruginosa*, were used for PAO1-D host range evaluation that included 3 culture collection strains—ATCC 10145, CECT 111, PAO1—and 33 clinical isolates [Hospital Escala Braga (Portugal)].

Bacteria were cultured at 37°C for ∼18 h in Tryptic Soy Broth (TSB, VWR) or Tryptic Soy Agar medium (TSA; TSB containing 1.2% (w/v) agar, NZYTech). MacConkey Agar (Merck®) and Pseudomonas isolation agar (PIA, Sigma-Aldrich) with 5% (w/v) glycerol (Sigma-Aldrich), were used as selective media for *E. coli* and *P. aeruginosa*, respectively, for viable cell counts.

C1 Honey Origin, Minimum Inhibitory Concentration and Physicochemical Characterization

The honey C1 is a single-flower honey from chestnut (92% *Castanea sativa*) collected from the Minho region in Portugal that has a conductivity of 1534 $\mu S.cm^{-1}$. The minimum inhibitory concentration (MIC) values for *E. coli* and *P. aeruginosa* were determined as described in the guidelines of the Clinical and Laboratory Standards Institute (Andrews and Andrews, 2001; Ferraro et al., 2003) using a honey concentration range from 50% (w/v) to 3,125% (w/v). C1 was physicochemical characterized as previously described (Nishio et al., 2016): the pH was performed as described by the International Honey Commission (Bogdanov, 2002), the color was determined according to the standards already established by the United States Department of Agriculture (USDA) (United States Deparment of Agriculture, 1985), the MGO concentration was obtained by RP-HPLC as described previously (Adams et al., 2008), the protein content was determined using the BCA Protein Assay Kit (Thermo Scientific™ Pierce™) according to manufacturer instructions, and the Hydroxymethylfurfural (HMF) content was determined by White's method (White, 1979).

Bacteriophage Origin and Production

The phages used in this work were EC3a for *E. coli*, isolated from raw sewage (Nishio et al., 2016), and PAO1-D, for *P. aeruginosa*, isolated from the Sextaphage commercial cocktail (Microgen, ImBio Nizhny Novgorod, Russia). Each phage was produced in the respective isolation host: EC3a in EC3a strain and PAO1-D in PAO1 strain, using the plate lysis and elution method (Sambrook and Russell, 2001). Briefly, 5 μL of phage suspension were spread evenly on host bacterial lawns using a paper strip and incubated overnight (O/N) at 37°C. Then, 3 mL of SM Buffer (5.8 $g.L^{-1}$ NaCl, 2 132 $g.L^{-1}$ $MgSO_4.7H_2O$, 50 $mL.L^{-1}$ 1 M Tris-HCl pH 7.5, VWR) were added to each plate and re-incubated O/N at 4°C with gentle stirring (50 rpm on a PSU-10i Orbital Shaker 134 (BIOSAN)). The floating liquid was collected and

centrifuged (10 min, 9,000 × g, 4°C), and afterwards, phages were concentrated by incubating the lysate with 58.4 g.L^{-1} NaCl for 1 h at 4°C under slow agitation, and the resultant supernatant with 100 g.L^{-1} PEG 8000 (ThermoFisher Scientific) at 37°C O/N. The subsequent suspension was centrifuged, purified with 1:4 (v/v) chloroform, filter sterilized (PES, GE Healthcare, 0.2 μm) and stored at 4 °C until use.

Phage Growth Parameters

One-step growth curves of the two phages in the two different strains were performed as described previously (Sillankorva et al., 2008). Briefly, 10 mL of a mid-exponential-phase culture was harvested by centrifugation (7,000 × *g*, 5 min, 4°C) and resuspended in 5 mL fresh TSB medium in order to obtain an OD_{600} of 1.0. To this suspension, 5 mL of phage solution were added in order to have a MOI of 0.001 and phages were allowed to adsorb for 5 min at room temperature. The mixture was than centrifuged as described above and the pellet was resuspended in 10 mL of fresh TSB medium. Samples were taken every 5 min over a period of 1 h and immediately plated.

Transmission Electron Microscopy Analysis

Phage PAO1-D particles were sedimented by centrifugation (25,000 × g, 60 min, 4°C) and washed twice in tap water by repeating the centrifugation step. Subsequently, the suspension was deposited on copper grids with carbon-coated Formvar films, stained with 2% (w/v) uranyl acetate (pH 4.0) (Agar Scientific), and examined using a Jeol JEM 1400 (Tokyo, Japan) transmission electron microscope (TEM). Images were digitally recorded using a CCD digital camera Orious 1,100 W, Tokyo, Japan.

Assessment of Phage Viability in C1 Honey

Phage PAO1-D and EC3a viability was tested in C1 honey. For that, 2 × 10^9 PFU.mL^{-1} were incubated at 37°C with 25% (w/v) and 50% (w/v) C1 honey, mentioned hereafter as $C1_{25\%}$ and $C1_{50\%}$, respectively. Samples were taken every hour until 6 h, and then after 24 h.

Controls were performed in sterile deionized water instead of honey. For each time point, phages were serial-diluted and quantified by mixing 100 μL of diluted solution with 100 μL of host bacteria culture and with 3 mL of TSA top agar (TSB supplemented with 0.6% (w/v) agar). The mixture was poured onto a layer of TSA (Adams, 1959). After an O/N incubation at 37°C, the plaque forming units (PFU) were determined. Three independent experiments were performed.

In Vitro Biofilm Formation and Treatment

The turbidimetry (620 nm) of a 16 h-grown EC3a or PAO1 inoculum was adjusted to 0.13 (corresponding between 2-3 × 10^{-8} CFU.mL^{-1}), and 10-fold diluted in TSB in order to have an initial inoculum concentration of 10^{-7} CFU.mL^{-1} (Crouzet et al., 2014; Pires et al., 2017). For biofilm formation, 200 μL of the bacterial suspension were added to wells of a 96-well plate that was subsequently incubated for 24 h at 37°C and 120 rpm [orbital shaker ES-20/60 214 (BIOSAN)]. For the formation of dual-species biofilms, the turbidimetry of both bacteria was adjusted to 0.13 and 5-fold diluted in TSB. After, 100 μL of each suspension were added to the wells and biofilm formation allowed to proceed as described above.

Phage treatments were performed with 1×10^9 PFU.mL^{-1} and honey challenge was done with $C1_{25\%}$ and $C1_{50\%}$. Monospecies biofilms formed during 24 h, were washed twice with saline [0.9% (w/v) NaCl, VWR] to remove non-adhered cells. After, 200 μL of phage, honey or 100 μL of phage 2 × concentrated and 100 μL of honey 2 × concentrated were added to each well and plates were incubated at 37°C, 120 rpm [orbital shaker ES-20/60 (BIOSAN)]. Dual-species biofilms were treated with 100 μL of the *P. aeruginosa* phage and 100 μL of *E. coli* phage, 200 μL of honey or with 50 μL of the *P. aeruginosa* phage and 50 μL of the *E. coli* phage both 4 × concentrated and 100 μL of honey 2 × concentrated. The control samples were performed with 100 μL of 2 × TSB, and 100 μL of SM buffer. Samples were analyzed at 0, 6, 12, and 24 h for viable cell quantification. At each sampling time point, biofilms were washed twice with saline [0.9% (w/v) NaCl, VWR], 200 μL saline added to each well and all biomass detached from the polystyrene bottom and side wall, by scraping, before CFU analysis. Three independent experiments were performed in triplicate.

Preparation of Porcine Skin Explants

Fresh porcine skin explants were generously supplied by ICVS - Life and Health Sciences Research Institute (Braga, Portugal), immediately stored in vacuum at −20 °C and thawed only before use.

Explants were cut into 2 × 2 cm pieces and disinfected as described previously (da Costa et al., 2015). After disinfection, each skin piece was placed between two sterile stainless steel plates with an o-ring in the center, to delimit the infection region. The skin was immobilized by fixing the upper metal plate with wing nuts (da Costa et al., 2015).

Ex Vivo Biofilm Formation and Treatment

Three different biofilm treatments were evaluated: phage, honey and the combination of both agents. Similar to *in vitro* treatments, 1 × 10^9 PFU.mL^{-1} of phages EC3a and PAO1-D, and $C1_{25\%}$ and $C1_{50\%}$ were used. The combinatorial effect of phage-honey was accomplished using the concentrations used in the single-agent experiments.

For monospecies biofilm formation, 80 μL of the bacterial suspension prepared as described above were placed in direct contact with the skin inside of the O-ring, and for dual-species biofilms 40 μL of both bacterial suspensions were used. The stainless steel plates holding the skins were placed in previously disinfected desiccators and incubated for 24 h at 37°C.

The infected area was washed twice with saline and after, in monospecies biofilms 80 μL of phage, honey or both agents were placed in the O-ring area, and incubated at 37°C. In dual-species biofilms the volumes of each agent were: 40 μL of each phage 2 × concentrated; 80 μL of honey; or 20 μL of each phage 4 × concentrated and honey 2 × concentrated. Biofilm cells were collected with the aid of a cotton swab that was then immersed in 1 mL saline. The suspension was centrifuged (8,000 × g, 10 min, 4°C) and the pellet resuspended in 1 mL saline. Samples were

analyzed at 0, 6, 12 and 24 h, for viable cell quantification. Three independent experiments were performed in triplicate.

Quantification of Viable Cells From Biofilms

Viable cells in biofilms were quantified by adapting a previously described method (Pires et al., 2017). Serial dilutions were performed in saline containing 1 mM ferrous ammonium sulfate (FAS, Applichem Panreac) to assure that all non-infecting phages were destroyed (Park et al., 2003). Samples (10 μL) were plated on MacConkey Agar or PIA plates, for *E. coli* or *P. aeruginosa* cell counts, respectively, using the microdrop technique (Naghili et al., 2013). Plates were incubated 16 h at 37°C, and colony forming units (CFU) were determined.

Interpretation of the Results

For each combined therapy (phage EC3a, phage PAO1-D, honey $C1_{25\%}$, honey $C1_{50\%}$) we determined if the outcome of the combination was synergistic according to the methodology described by Chaudhry et al. (2017). In brief, an outcome was regarded as synergistic when the equation $\text{Log}(C)-\log(S_P)-\log(S_H)+\log(S_{PH})<0$ was valid. In the equation, C refers to the cell density obtained in the control (no treatment), and S_P, S_H, and S_{PH} are the surviving cell densities after treatment with phage (P), honey (H), or both combined (PH), respectively (Chaudhry et al., 2017). The calculations are presented only for monospecies biofilms formed on porcine skin, and dual-species biofilms formed on polystyrene and porcine skin (Table S3).

Statistical Analysis

Statistical analysis of the results was performed using GraphPad Prism 6. Mean and standard deviations (SD) were determined for the independent experiments and the results were presented as mean ± SD. Results were compared using Two-way ANOVA, with Tukey's multiple comparison statistical test. Differences were considered statistically different if $p \leq 0.05$ (95% confidence interval).

RESULTS

C1 Honey Physicochemical Characterization and MIC Determination

C1 honey is a white honey with a pH of 5.4. The total protein content is 81.7 $mg.kg^{-1}$, the MGO concentration 1000.2 $mg.kg^{-1}$ and the HMF is $< 4\ mg.kg^{-1}$. The MIC experiments of C1 on *E. coli* and *P. aeruginosa* was 12.5% (w/v) and 25% (w/v), respectively.

Phage Growth Parameters and Morphology

Phage EC3a is a strictly virulent *Siphovirus* that has already been partly characterized (Nishio et al., 2016). EC3a has a latent period of ∼15 min giving rise to ∼53 progeny per infected cell.

PAO1-D, isolated from the Sextaphage preparation, is a *Podovirus* showing a 56 nm × 64 nm icosahedral capsid, and a 12 nm non-contractile tail (**Figure 1**). This phage was selected for all further experiments based on its lytic spectra toward the clinical isolates (Table S1) and also on the dimension of its large halo (Table S2, Figure S1) that may suggest the presence of enzymes with higher efficiency to degrade the EPS matrix of biofilms. PAO1-D has a short latent period (5 min) and a burst size of ∼61 phages per infected cell (**Figure 2**).

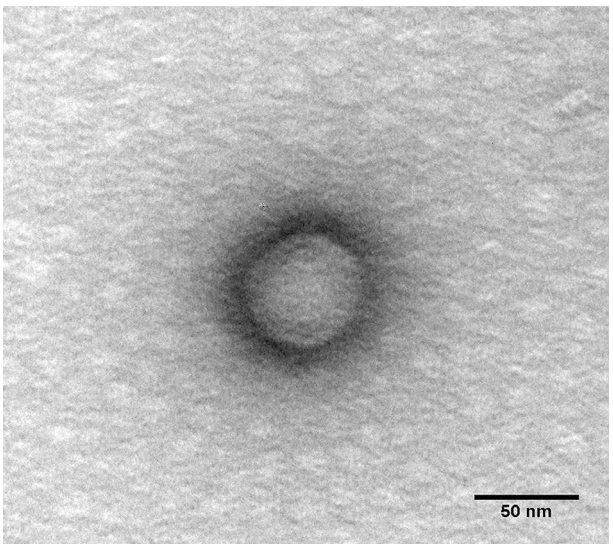

FIGURE 1 | TEM micrograph of PAO1-D bacteriophage particle (scale bar 50 nm).

Phage Viability in C1 Honey

Viability of both phages, EC3a and PAO1-D, was assessed on $C1_{25\%}$ and $C1_{50\%}$ (**Figure 3**). Until 9 h, there was no evident effect on EC3a viability in $C1_{25\%}$ and $C1_{50\%}$. However, no infective EC3a were recorded after 24 h of contact with both concentrations of C1 ($p < 0.05$). Furthermore, although PAO1-D showed to be slightly more sensible to honey until 9 h of contact, $C1_{25\%}$ did not cause complete inactivation of this phage at 24 h.

E. Coli and *P. aeruginosa* Colonization of Surfaces

E. coli CECT434 and *P. aeruginosa* PAO1 colonization was assessed in 24 h mono- and dual-species biofilms formed *in vitro* and in porcine skin explants (**Figure 4**). Although, monospecies biofilms of *E. coli* colonized better the skin surfaces than polystyrene, no significant differences in colonization were observed for monospecies *P. aeruginosa* biofilms ($p < 0.05$). Dual-species biofilms of both bacteria on polystyrene presented statistically more cells than monospecies biofilms formed in this material. The colonization of porcine skins by *E. coli* and *P. aeruginosa* alone and when mixed was also analyzed. In general, the level of colonization by *P. aeruginosa* was similar in both experiments, however the colonization by *E. coli* was highly influenced by the presence of *P. aeruginosa* resulting in less 2.6-Log cells than in monospecies *E. coli* biofilms ($p < 0.05$).

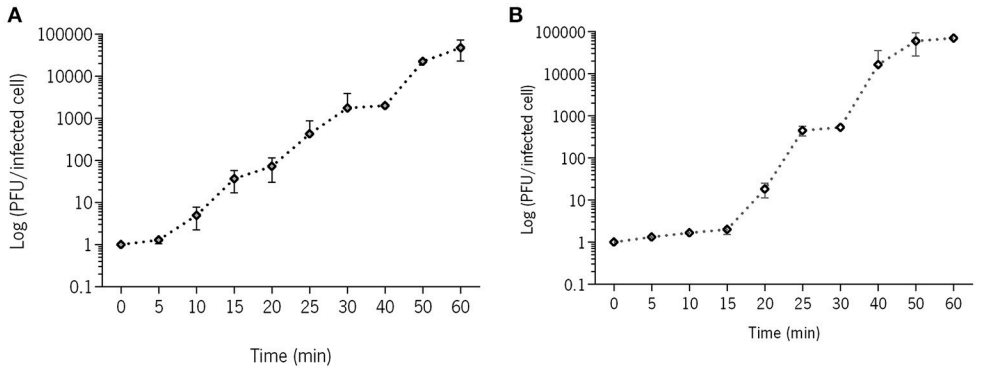

FIGURE 2 | One-step growth curve of phages **(A)** PAO1-D and **(B)** EC3a in their respective hosts. Error bars represent standard deviations from 2 independent experiments performed in duplicate.

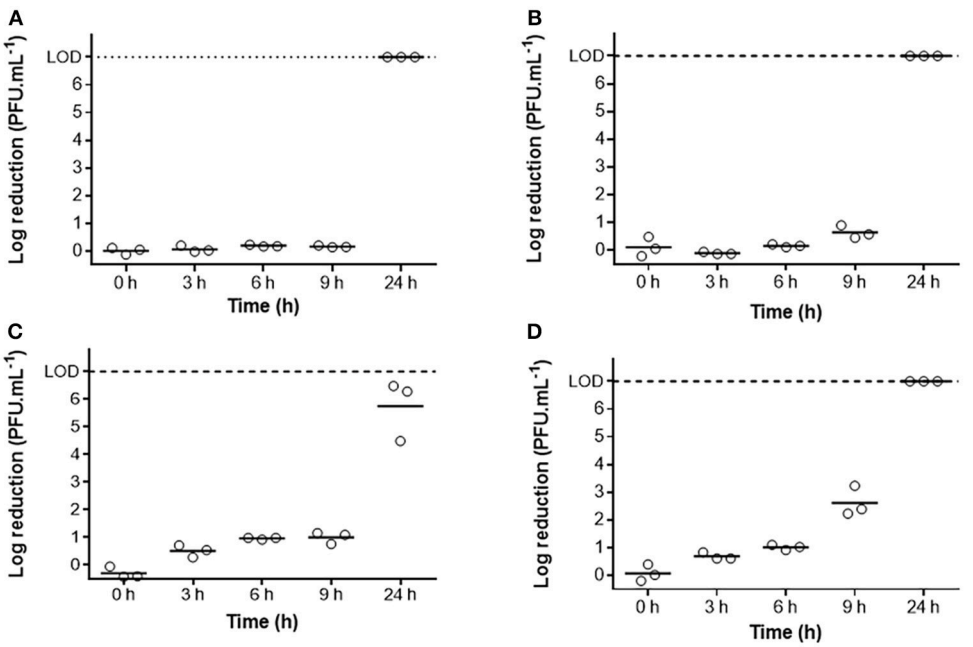

FIGURE 3 | Viability (PFU.mL^{-1}) of phage EC3A and PAO1-D over 24 h in C1 honey: **(A)** EC3a in C1 25%, **(B)** EC3a in C1 50%, **(C)** PAO1-D in C1 25%, and **(D)** PAO1-D in C1 50%. Each independent assay (o) and the mean (–) are represented. LOD (Limit of Detection) = 7-Log.

Antibiofilm Effect of Honey and Phage on Polystyrene–Formed Biofilms

The effect of phage and honey was evaluated in 24 h-old biofilms formed in 96-well polystyrene plates (**Figure 5**).

Phages EC3a and PAO1-D were used against *E. coli* and *P. aeruginosa* biofilms, respectively. EC3a antibiofilm activity was highest after 6 h of infection, reducing about 2.7-Log *E. coli* viable cells. However, no effect of EC3a was noticed after 24 h. Contrarily to EC3a, phage PAO1-D caused a uniform cell reduction throughout the 24 h experiment that was always higher compared to the reductions caused by $C1_{25\%}$.

The effect of $C1_{25\%}$ on cell count reductions was always less evident (varied form a 1.2 to a 1.6-Log reduction) than the effect of $C1_{50\%}$ that varied from 4.0-Log to a 4.7-Log reduction in the time-points assessed.

$C1_{50\%}$ showed always superior antibiofilm activity compared to the lower honey concentration and also significantly higher killing capacity than both tested phages at 24 h of treatment ($p < 0.05$).

Antibiofilm Effect of Phage, Honey, and Phage-Honey Combination on Dual-Species Biofilms Formed on Polystyrene

Dual-species biofilms formed on polystyrene were challenged with a cocktail of both phages, honey or all combined (**Figure 6**).

E. coli cell reductions observed at 6 h of combined honey-phage treatment were in great part due to phage EC3a resulting in similar values to those obtained when applying phage alone. Honey alone resulted in a gradual increase of the number of *E. coli* cells killed from less than 1-Log at 6 h to 1.8–1.9-Log at 24 h with $C1_{25\%}$ and $C1_{50\%}$, respectively. At 12 h, honey at 50% combined with phage was significantly better ($p < 0.05$) than honey alone. By 24 h of treatment, the decrease of cells obtained when a combined therapy was used was, contrarily to the initial 6 h time point, greatly due to the action of C1 honey. Nonetheless, honey alone was never as efficient in killing *E. coli* living in dual-species biofilms compared to its effect on monospecies *E. coli* biofilms (compare **Figures 5**, **6**).

In terms of treatment effects on *P. aeruginosa* present in the dual-species biofilms, overall the numbers of cells killed gradually increased with phage and both honey concentrations alone. The combined treatment using phage and honey $C1_{25\%}$ was statistically higher ($p < 0.05$) than the action of phage alone at 6 h than honey alone at 12 and 24 h ($p < 0.05$). Phage combination with honey $C1_{50\%}$ was not significantly different from the action exerted by honey alone ($p > 0.05$).

Even though statistically significant differences where observed after the different combinations, overall the antibacterial action of EC3a phage until 12 h was better than honey, at both concentrations, in killing *E. coli* from dual-species biofilms. Phage PAO1-D had a similar or slightly better effect than honey at 25%. Combined treatment resulted in a slightly better antibacterial outcome than phage and honey alone however without resulting in a synergy effect (see Table S3).

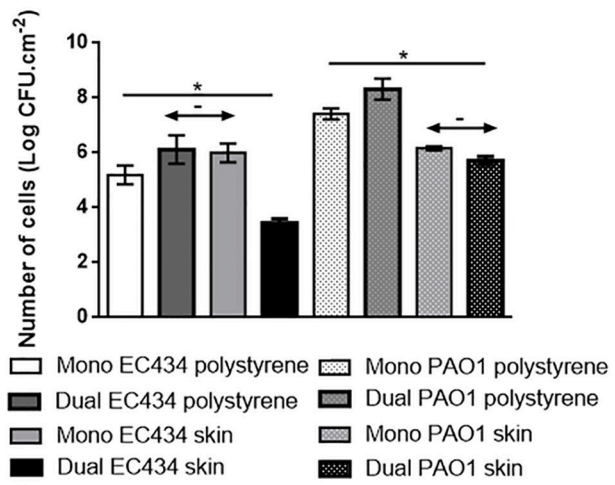

FIGURE 4 | Bacterial colonization (CFU.cm^{-2}) of 24 h-old biofilms of *E. coli* 434 and *P. aeruginosa* PAO1 formed individually (Mono) or combined (Dual). Number of cells in dual species biofilms were counted separately on MacConkey for *E. coli* or PIA for *P. aeruginosa*. Data are shown as mean ± SD and results. With the exception of the two arrowheads with "-" all other values were considered statistically different (*$p \leq 0.05$).

Antibiofilm Effect of Phage, Honey, and the Phage-Honey Combination on 24 h-Old Porcine Skin-Formed Biofilms

The effect of phage, honey and also the combination of both antimicrobial agents was evaluated in *E. coli* and *P. aeruginosa* monospecies biofilms formed in porcine skin explants (**Figure 7**).

Considering *E. coli* biofilms, the effect of phage EC3a in the *ex vivo* model was constant ($p > 0.05$) (∼1-Log reduction in average) from 6 to 24 h (contrarily to the 6 h reduction observed over time in the *in vitro* assay). A similar consistency was observed with the $C1_{25\%}$ or $C1_{50\%}$ effect in the porcine skin, ∼1-Log viable cell reduction over 24 h.

Throughout the experiment, the combination of EC3a and $C1_{25\%}$ or $C1_{50\%}$ were statistically similar to, at least, one of the antimicrobial agents used separately ($p > 0.05$). The exception was observed 6 h after treatment with EC3a and $C1_{25\%}$ when the reduction of viable cells was higher with the combination (1.6-Log) comparatively to phage (0.9- Log) or honey (0.9-Log) ($p < 0.05$).

Regarding *P. aeruginosa* biofilms, $C1_{25\%}$ had no effect on cell reduction (there was even an increase in CFU count at 6 and 12 h after treatment), while $C1_{50\%}$ reduced cell concentration in no more than 0.6-Log during the 24 h treatment.

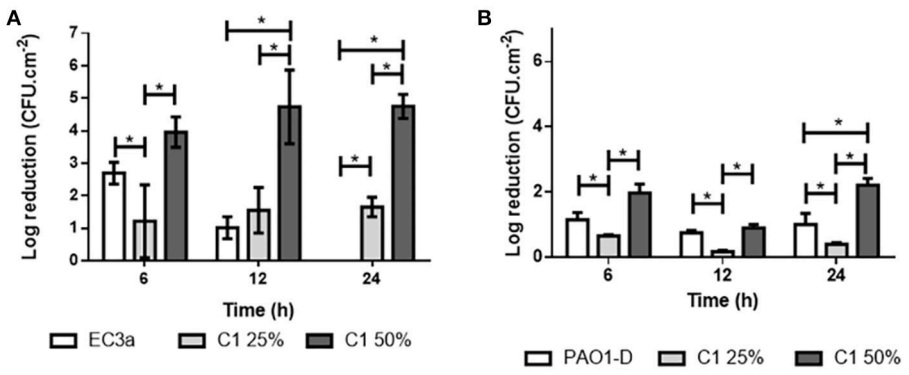

FIGURE 5 | Antibiofilm effect of phage and honey against monospecies biofilms formed in polystyrene surfaces: **(A)** EC3a, $C1_{25\%}$ and $C1_{50\%}$ on *E. coli* biofilms and **(B)** PAO-D, $C1_{25\%}$ and $C1_{50\%}$ in *P. aeruginosa* biofilms. Data are shown as mean ± SD and results were considered statistically different if *$p \leq 0.05$.

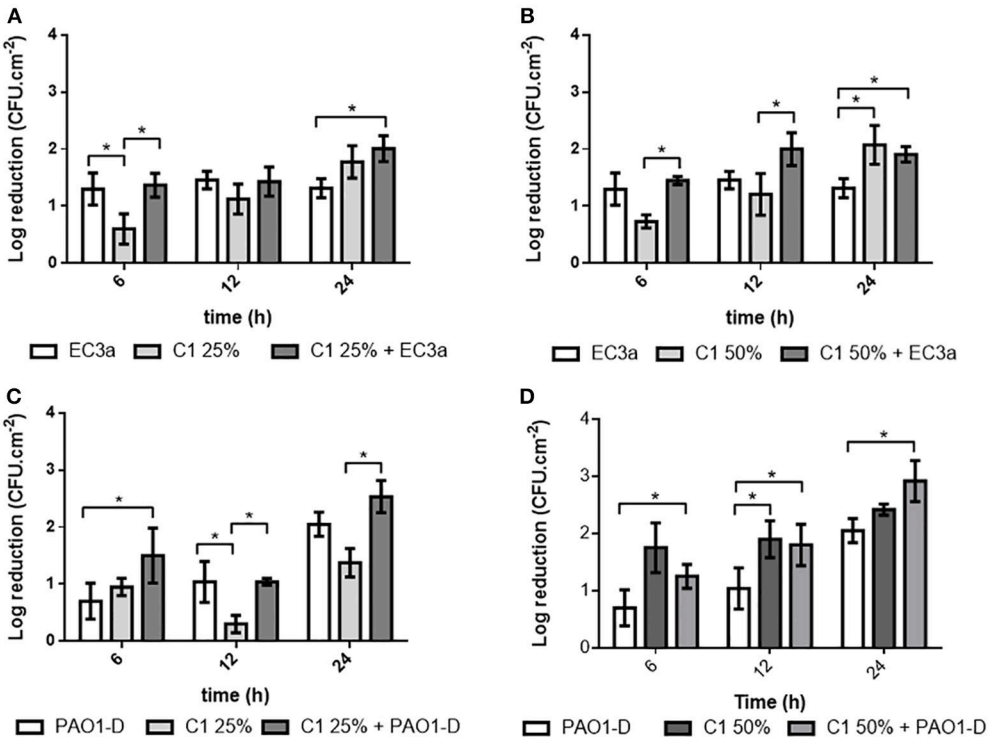

FIGURE 6 | Antibiofilm effect of phage, honey and combined therapy against dual-species biofilms formed in polystyrene surfaces: **(A)** EC3a and $C1_{25\%}$ on *E. coli*; **(B)** EC3a and $C1_{50\%}$ on *E. coli*; **(C)** PAO1-D and $C1_{25\%}$ on *P. aeruginosa*; **(D)** PAO1-D and $C1_{50\%}$ on *P. aeruginosa*. Data are shown as mean ± SD and results were considered statistically different if $^*p \leq 0.05$.

The antibiofilm effect of PAO1-D increased over time ($p < 0.05$) leading to 1.6-Log cell reduction after 24 h of treatment.

The combination of PAO1-D with $C1_{25\%}$ led to a constant effect along the 24 h experiment ($p > 0.05$) with a maximum viable cell reduction at 12 h (1.3-Log reduction). PAO1-D combined with $C1_{50\%}$, also displayed highest reduction of viable cells at 12 h (1.8-Log cell reduction).

Antibiofilm Effect of Phage, Honey, and Phage-Honey Combination on Dual Species Biofilms Formed in Porcine Skin

The antibiofilm effect of phage, honey, and their combination was tested against dual-species biofilms of *E. coli* and *P. aeruginosa* formed on porcine skin and the effect reported per bacterial species, respectively (**Figure 8**).

The antibiofilm effect of EC3a against *E. coli* in dual-species biofilms was similar among time points showing a 0.6-Log reduction, in average, at 12 h post-infection. Similarly, $C1_{25\%}$ alone maintained a cell reduction below 0.5-Log in all analyzed samples, and $C1_{50\%}$ alone below 1.0-Log. The combination of phage EC3a with $C1_{25\%}$ didn't vary considerably throughout time resulting in ∼0.5 to 0.8-Log reductions of *E. coli* viable cells from dual-species biofilms, while the combination of EC3a + $C1_{50\%}$ varied from no cell reductions up to 1.4-Log reduction, at 24 h post-treatment, of *E. coli* from dual-species biofilms.

Concerning *P. aeruginosa* reductions in dual-species biofilms, $C1_{25\%}$ alone contributed with no more than 0.9-Log observed at 12 h, while $C1_{50\%}$ displayed a 1.8-Log reduction in the same period. On the other hand, the effect of PAO1-D on *P. aeruginosa* increased significantly from 6 to 24 h ($p \leq 0.05$).

The combination of PAO1-D and $C1_{25\%}$ revealed a synergistic effect 24 h after treatment (**Figure 8** and Table S3), causing an average cell reduction of 2.2-Log, higher than the sum of phage and honey alone [1.0-Log (PAO1-D) + 0.6-Log ($C1_{25\%}$)]. Synergism was also observed for $C1_{50\%}$ combined with phage, at 12 h: 2.3-Log > 0.1-Log (PAO1-D) + 1.4-Log ($C1_{50\%}$) (see also result in Table S3).

Overall, honey and phage were more effective in controlling *P. aeruginosa* in dual-species biofilms formed in porcine skin than in monospecies *P. aeruginosa* biofilms.

DISCUSSION

The reduction of bacterial wound bioburden to host-manageable levels, as well as the elimination of certain virulent forms of wound pathogens has become a goal of the wound care professionals. In fact, a direct link between bacterial load and subsequent healing has been demonstrated (Bendy et al., 1964) being the successful closure of wounds apparently dependent on maintaining a bacterial level below 10^5 CFU.g^{-1} of tissue (Robson, 1997; Bowler, 2003). In the wound-healing scheme,

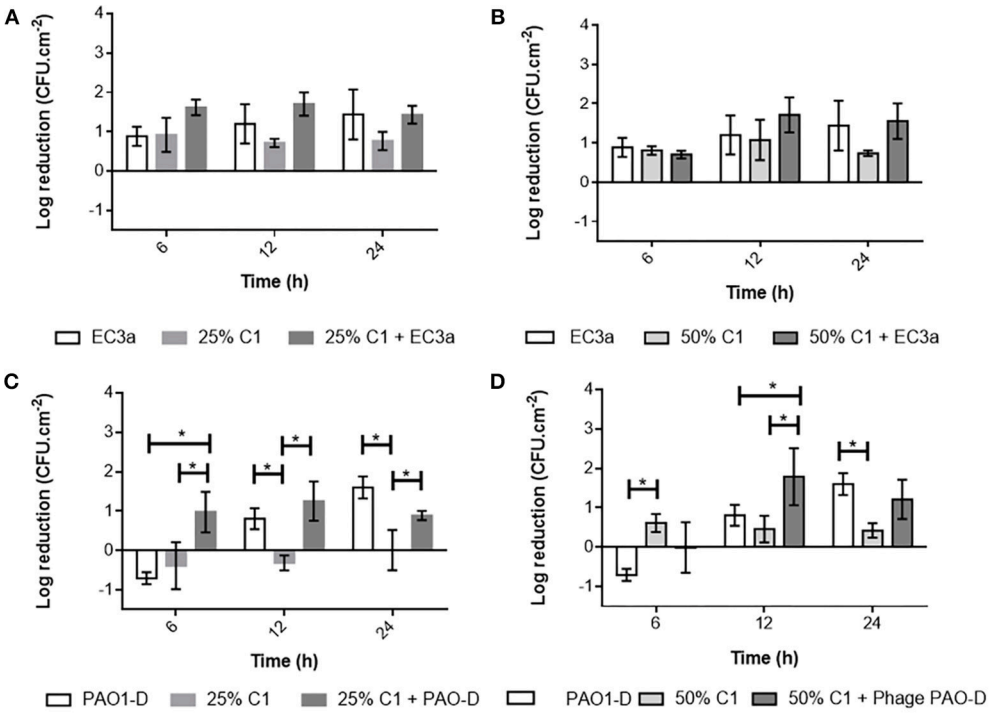

FIGURE 7 | Antibiofilm effect of phage and honey against monospecies biofilms formed in pig skin: **(A)** EC3a and $C1_{25\%}$ on *E. coli*; **(B)** EC3a and $C1_{50\%}$ on *E. coli*; **(C)** PAO1-D and $C1_{25\%}$ on *P. aeruginosa*; **(D)** PAO1-D and $C1_{50\%}$ on *P. aeruginosa*. Data are shown as mean ± SD and results were considered statistically different if $*p \leq 0.05$.

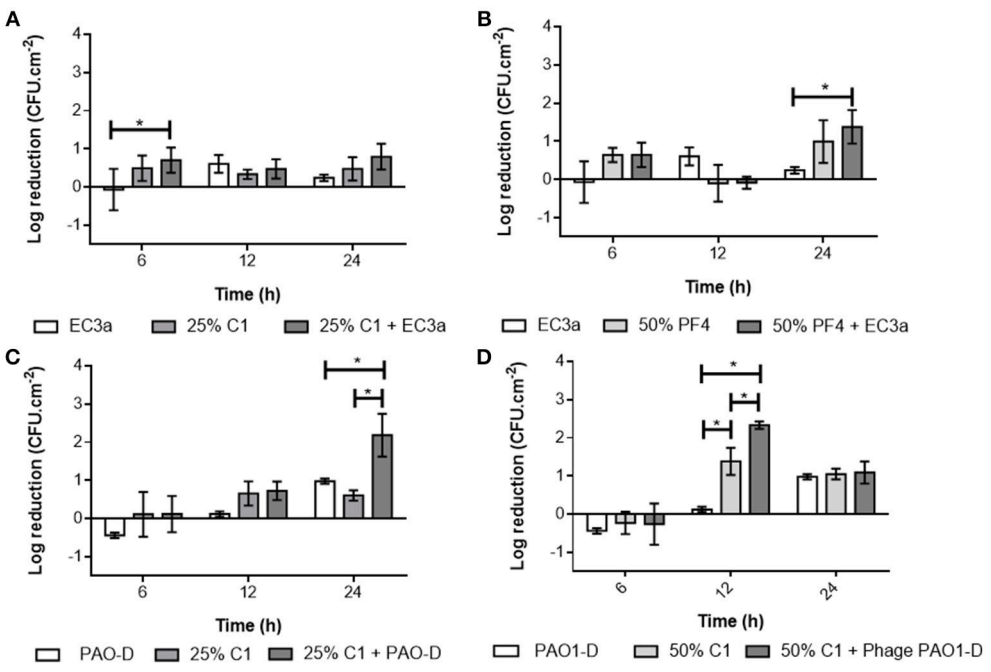

FIGURE 8 | Antibiofilm effect of phage, honey, and honey-phage combinations against dual-species biofilms formed in pig skin: **(A)** EC3a and $C1_{25\%}$ on *E. coli*; **(B)** EC3a and $C1_{50\%}$ on *E. coli*; **(C)** PAO1-D and $C1_{25\%}$ on *P. aeruginosa*; **(D)** PAO1-D and $C1_{50\%}$ on *P. aeruginosa*. Data are shown as mean ± SD and results were considered statistically different if $*p \leq 0.05$.

the use of alternative antimicrobial agents is considered when other approaches as the use of moisture-retentive dressings (that assist the hosts' phagocytic defense mechanisms by creating a moist wound environment) have been unsuccessful. These alternative antimicrobial agents are expected to supplement the host immune activity in reducing wound bioburden until a balance in favor of the host is restored. The antimicrobial potential of honey and phage to control biofilm-related infections can be a potentially good alternative for topical applications, particularly for treatment of chronic wounds. Phage therapy effectiveness (orally and locally administered) in chronic suppurative infections of the skin caused by *Pseudomonas*, *Staphylococcus*, *Klebsiella*, *Proteus* and *Escherichia* was described over 30 years ago with ∼50% of the 31 studied patients resulting in an "outstanding" improvement (Cislo et al., 1987). In 2002, a phage impregnated polymer used to treat infected venous stasis skin ulcers achieved complete healing in 70% of the 107 patients (Markoishvili et al., 2002). Research using animal models has also supporting evidences of phage safety and efficacy in treating chronic wounds infected by *S. aureus*, *P. aeruginosa* and *Acinetobacter baumannii* (Mendes et al., 2013; Seth et al., 2013). Recent works also have shown superior chronic wound healing rates and a lower healing time of honey when compared to commonly used products (Sharp, 2009; Imran et al., 2015). For example, Medihoney dressing used in non-healing venous leg ulcers during 12 weeks revealed a decrease in ulcer pain, size and odor (Dunford and Hanano, 2004). Bacteriological changes in venous leg ulcers treated with Manuka honey or hydrogel were evaluated in 108 patients (Gethin and Cowman, 2008), and after 4 weeks, Manuka honey was able to eradicate MRSA in 70% of treated wounds.

Chronic wounds are usually polymicrobial in nature and therefore, this work focused on evaluating the interaction of honey and phages, alone and both combined, with dual-species biofilms of *P. aeruginosa* and *E. coli*.

One essential step before carrying the combined antimicrobial therapy was to assess the viability of phages in honey. Although our phage collection comprises some fully characterized *P. aeruginosa* phages (Pires et al., 2011, 2014, 2015, 2017), all showed to be highly sensitive to this chestnut honey. Therefore, isolation of phages from the Sextaphage and also from Intestiphage preparations (both from Microgen, Russia) using PAO1 as host strain allowed the isolation of phages presenting an increased insensitivity to the chestnut honey used. Different phages were isolated, however PAO1-D showed the best features (Table S1, Figure S1) and was therefore chosen for the antimicrobial experiments. The *E. coli* phage on the other hand was chosen taking advantage of its known morphologic and genomic characteristics, and also due to its known survival on two polyflora honeys (Oliveira et al., 2017) during the first 6 h. In this work, chestnut honey partially or completely destroyed both phages after 24 h of exposure resulting in phage concentrations below the limit of detection. The main characteristics of honey that seem to cause loss in phage viability are its low pH (between 3.2 and 4.5), high sugar content (about 80%) that can cause an osmotic shock, possible presence of proteases, and the slow release of hydrogen peroxide when dissolved in water (about 1 $mmol.L^{-1}$) (Rossano et al., 2012; Agún et al., 2018). Nevertheless, this late destruction of phage particles, only at 24 h, grants them capacity to complete several infection cycles before destruction since both phages have relatively short latent and burst periods (**Figure 2**).

The antimicrobial actions of each of these agents have distinct mechanisms in biofilms. While phages specifically destroy bacteria through host-receptor recognition and infection, honey reaches the same destruction by oxidative stress, osmotic pressure, acidity, hydrogen peroxide release, presence of methylglyoxal (MGO) among other mechanisms. We recently observed an enhanced antibacterial effect of phage and other two Portuguese honeys in monospecies biofilms of *E. coli* formed *in vitro*, and these results led us to pursue research with other honey types, and other bacteria, this time using a more complex and already validated model—the porcine skin explant model (da Costa et al., 2015). The results obtained where nonetheless compared with those obtained using the easiest and most commonly used high-throughput biofilm model—the polystyrene microplate biofilm model.

Analyzing the effect of the phages alone, the two lytic phages tested, EC3a and PAO1-D, decreased *E. coli* and *P. aeruginosa* cells from biofilms formed in polystyrene and porcine skin, respectively. The phages action against biofilms formed in porcine skin explants increased with time when compared with *in vitro*-formed biofilms (compare **Figures 5**, **7**). Furthermore, between 6 and 24 h no bacterial regrowth on porcine skins experiments challenged with phage was observed, suggesting a reduced emergence of phage-resistant phenotypes. This phenomenon might be due to the lower cell reductions achieved by EC3a in the later model (1.9-Log) compared to the reductions observed in the polystyrene experiments (2.7-Log) which minimizes the adaptation of *E. coli* to evade EC3a infection.

The honey used in the experiments is a monofloral honey (92% *Castanea sativa*). Regarding the feasibility of safeguarding the inter-lot reproducibility of a honey-based product, the use of honey with a single floral source, as happens with manuka honey (at least 70% of its pollen content should come from *Leptospermum scoparium*) seems to be more convenient. Besides, the chestnut honey has already been reported to have high antimicrobial effect against *E. coli* (Coniglio et al., 2013) and, together with Manuka honey, against *P. aeruginosa* including PAO1 (Hao et al., 2012; Voncina et al., 2015; Bolognese et al., 2016). The tissue of chestnut plants contains compounds such as tannins and antioxidants (Hao et al., 2012), which have inhibitory effects on microorganisms, and 3-aminoacetophenone is the main volatile compound occurring specially in this floral source, known as having antibacterial properties (Bonaga and Giumanini, 1986). Contrarily to phages, the antimicrobial effect of chestnut honey was evident *in vitro*, when the polystyrene-formed monospecies biofilms were treated with a 50% (w/v) honey preparation resulting in a maximum of 5.6-Log and 2.8-Log reductions from *E. coli* and *P. aeruginosa* biofilms, respectively. This is in accordance with the obtained MIC results showing that a lower concentration of C1 honey is needed in order to eradicate *E. coli* in the suspension form, compared

with *P. aeruginosa*. However, in an *ex vivo* context, honey was less effective toward *P. aeruginosa*. The lower sensitivity of *P. aeruginosa* to honey might be due to the lower permeability of its cell wall to antimicrobial compounds and its ability to grow in an environment with higher MGO levels. A study led by Kilty in 2011 tested the effect of different MGO concentrations on different strains of *P. aeruginosa* biofilms, within a range of 1800–7300 $mg.kg^{-1}$. According to these tests, MGO concentrations from 3600 to 7300 $mg.kg^{-1}$ were required to reduce the biofilm biomass of different *P. aeruginosa* strains (Kilty et al., 2011). A study led by Lu in 2013 supports this hypothesis, where *P. aeruginosa* was shown to have a higher tolerance to MGO than *Bacillus subtilis, E. coli,* and *S. aureus* (Lu et al., 2013). On the other hand, the active compounds of C1 seemed to be able to diffuse through the EPS matrix of established *E. coli* biofilms reaching and causing damage to the bacterial cells as reported previously (Oliveira et al., 2017). For instance, Lee et al. (2011) demonstrated that even at low concentrations, honey was able to reduce the colonization and subsequent biofilm formation, and virulence of a pathogenic *E. coli* strain assessed by crystal violet staining of the total biofilm biomass, and analysis of expression of quorum sensing and virulence genes. Furthermore, these authors observed that curli fibers, a common factor controlling biofilm formation in *E. coli* 0157:H7, were repressed by acacia honey.

Although honey was not nearly as effective against biofilms formed in porcine skin explants compared to those formed on polystyrene, it can be highlighted that honey provides other properties that may be interesting for wound treatment purposes, such as its role in tissue regeneration (Majtan, 2014; Oryan et al., 2016; Mohamed, 2017).

In this work, we aimed to determine whether the combined treatments with phage and honey exerted an enhanced antibacterial outcome and synergy testing was not the main interest of this study. There is an extensive literature regarding terminology of combined treatment outcomes and how these are described (Greco et al., 1992; Piggott et al., 2015). We use the term "synergy" when the combined phage-honey treatment kills a greater fraction than the effect of the two agents independently and for the interpretation of the results we adopted the approach described by Chaudhry et al. (2017).

The combined treatment using phage and honey against dual-species biofilms formed on polystyrene (**Figure 6**) caused a slightly improved killing activity compared to the addition of phage or honey alone however, never resulting in a synergistic effect (Table S3). Comparing the efficacy of both phages against mono and dual-species biofilms, while in monospecies biofilms the ability of phages to infect decreased over time, possibly due to the emergence of phage resistant phenotypes, the same was not observed in the presence of another bacterial species where phages continued to be able to reduce cells over the 24 h-period assessed (compare **Figures 5**, **6**).

Monospecies biofilms of *E. coli* and *P. aeruginosa* formed on porcine skins were also targeted using combined therapy. *E. coli* cell numbers started being reduced upon application of EC3a or both honey concentrations and resulted, overall, in slightly more cells killed using the combined therapy approach. On the other hand, *P. aeruginosa* biofilms increased in numbers after 6 h of application of both phage and honey at 25% but surprisingly the combined treatment exerted antibacterial effect. As already described above for the treatment of biofilms formed on polystyrene, honey alone presented lower efficacy against *P. aeruginosa* biofilms formed on porcine skins than *E. coli*.

In dual-species biofilms of *E. coli and P. aeruginosa* only *P. aeruginosa* had a real benefit in dual-species biofilms, clearly outnumbering *E. coli*. This has already been described before and by Cerqueira et al. (2013) whom also analyzed the biofilm structure by confocal laser scanning microscopy and found that these species colonize surfaces forming co-aggregated biofilm organization (Cerqueira et al., 2013). Dual-species biofilms formed on porcine skin explants were not as easily reduced by phage and honey as monospecies biofilms.

However, their removal using the combinatorial phage-honey approach was beneficial at 24 h with $C1_{25\%}$ and phage PAO1-D and at 12 h with $C1_{50\%}$ also with phage PAO1-D resulting in a synergy outcome. *P. aeruginosa* control on porcine skin explants was more efficient when this bacterium was in the presence of *E. coli*. Moreover, synergistic effects on dual-species biofilm control were observed for both honey concentrations combined with phage although at different time points. These results suggest that in this context honey and phage are enhancing each other's antimicrobial properties. Even though we use the "synergy" terminology, we are aware that this does not give evolutionary dynamics during treatment since these results are limited to the time points assessed (6, 12, 24 h). The validation of the synergy outcome should also be further confirmed employing approved standard methodology for synergy testing (Breitinger, 2012).

Possibly, this is due to honeys penetration through the biofilm EPS as demonstrated with *S. aureus* biofilms (Lu et al., 2014) that will then allow that the phages used can more easily access the target host cells. Taking into account the direct link between bacterial load and subsequent wound healing described above (bacterial levels $< 10^5$ $CFU.g^{-1}$ of tissue), in our work we observed a cell load below the 10^5 $CFU.cm^{-2}$ for *E. coli* 434 and *P. aeruginosa* PAO1 under certain treatment conditions such as using phage and honey at 50% (w/v) after different time points (see **Figure 8**). Based on this threshold and based on previous works reporting healing in ulcers only when the bacterial load was below 10^6 CFU/ml (Bendy et al., 1964) and successful skin grafting in patients with wound contamination under 5×10^4 CFU/cm^2 (Majewski et al., 1995), it might be inferred that this combined treatment presents potential to effectively reduce viable bacterial levels. Moreover, the recognized anti-inflammatory activity of honey that stimulate immune responses by increasing the release of citokines supports this assumption (Visavadia et al., 2008).

In general, clear differences between the results obtained *in vitro* and *ex vivo* were observed. These include variations of viable cell reductions that can be mainly explained by the possible different biofilm architectures due to differences in the surfaces where the biofilms were formed, namely in roughness, and hydrophobicity, by the conditions adopted in each case that varied in terms of humidity and nutrient supply when biofilms were formed on polystyrene and porcine skin. Rougher materials

tend, indeed, to promote bacterial adhesion due to microbial adherence to irregularities (Alnnasouri et al., 2011). In this work, *E. coli* showed 10-fold better ability to colonize the porcine skins than the polystyrene surfaces. Hydrophobicity can have an influence higher than roughness in surface colonization. In general, hydrophilic materials are favorable for cell attachment when bacteria have larger surface energy than the liquid in which they are suspended. However, the contrary is more common to happen, as bacterial surface energy is normally inferior to the surface energy of the liquids. This mismatch leads to cell adhesion preferentially to hydrophobic materials (Tuson and Weibel, 2013). According to Elkhyat et al. (2004) human skin contact angle is hydrophobic (91°) and therefore it is expected that porcine skins will also be hydrophobic. Polystyrene, on the other hand, is generally more hydrophilic than skin having a contact angle between 73° and 90° (Baier and Meyer, 1996; Cho et al., 2005; Kondyurin et al., 2006). The 10-fold higher colonization of porcine skin by *E. coli* suggests that the difference in surface roughness and hydrophobicity might be sufficient to interfere with the mechanisms of gene expression (including motility and attachment gene expression) (Tuson and Weibel, 2013), secretion of EPS, among other factors. These, particularly the secretion of EPS can have a great influence in the action of phages and honey, and even in the antimicrobial action of the individual components that are present in honeys.

Overall, this work provides novel insights into alternative strategies to control biofilm-related infections caused by *E. coli* and *P. aeruginosa* using phage-honey formulations. This work indicates that EC3a and PAO1-D may effectively be combined with chestnut honey to treat wound beds with *P. aeruginosa* and *E. coli* microbial biofilms. This formulation can potentially be used for topical applications due to the known advantages of phages in the control of antibiotic-resistant bacteria and of honeys ability to accelerate wound healing. Further improvements are required to obtain greater microbial reductions, which may include testing other phages and honey types as well as producing encapsulated particles where for instance phages are entrapped in the core and honey in the shell layer in order to preserve phage viability.

AUTHOR CONTRIBUTIONS

AO and SS conceived the study. AS, JS, and LM performed the experiments. AO and SS wrote the paper. All authors critically analyzed and revised the manuscript.

FUNDING

This study was supported by the Portuguese Foundation for Science and Technology (FCT) under the scope of the strategic funding of UID/BIO/04469/2013 unit and COMPETE 2020 (POCI-01-0145-FEDER-006684) and BioTecNorte operation (NORTE-01-0145-FEDER-000004) funded by the European Regional Development Fund under the scope of Norte2020—Programa Operacional Regional do Norte and the Project RECI/BBB-EBI/0179/2012 (FCOMP-01-0124-FEDER-027462). AO acknowledge financial support from the Portuguese Foundation for Science and Technology (FCT) through the project PTDC/CVT-EPI/4008/2014 (POCI-01-0145-FEDER-016598). SS is an Investigador FCT (IF/01413/2013).

SUPPLEMENTARY MATERIAL

The Supplementary Material for this article can be found online at: https://www.frontiersin.org/articles/10.3389/fmicb.2018.01725/full#supplementary-material

REFERENCES

Adams, C. J., Boult, C. H., Deadman, B. J., Farr, J. M., Grainger, M. N. C., Manley-Harris, M., et al. (2008). Isolation by HPLC and characterisation of the bioactive fraction of New Zealand manuka (Leptospermum scoparium) honey. *Carbohydr. Res.* 343, 651–659. doi: 10.1016/j.carres.2007.12.011

Adams, M. (1959). *Bacteriophages*. New York, NY: Interscience Publishers, Inc.

Agún, S., Fernández, L., González-Menéndez, E., Martínez, B., Rodríguez, A., and García, P. (2018). Study of the interactions between bacteriophage phiIPLA-RODI and four chemical disinfectants for the elimination of *Staphylococcus aureus* contamination. *Viruses* 10:E103. doi: 10.3390/v10030103

Alnnasouri, M., Lemaitrea, C., Gentric, C., Dagot, C., and Pon, M.-N. (2011). Influence of surface topography on biofilm development: experiment and modeling. *Biochem. Eng. J.* 57, 38–45. doi: 10.1016/j.bej.2011.08.005

Andrews, J. M., and Andrews, J. M. (2001). Determination of minimum inhibitory concentrations. *J. Antimicrob Chemother* 48 (Suppl. 1), 5–16. doi: 10.1093/jac/48.suppl_1.5

Baier, R. E., and Meyer, A. E. (1996). *Interfacial Phenomena and Bioproducts*. New York, NY:Marcel Dekker.

Baillie, G. S., and Douglas, L. J. (1998). Effect of growth rate on resistance of candida albicans biofilms to antifungal agents. *Antimicrob. Agents Chemother.* 42, 1900–1905.

Bendy, R. H., Nuccio, P. A., Wolfe, E., Collins, B., Tamburro, C., Glass, W., et al. (1964). Counts to healing of decubiti: effect of topical gentamicin relationship of quantitative wound bacterial. *Antimicrob. Agents Chemother.* 10, 147–155.

Billings, N., Ramirez Millan, M., Caldara, M., Rusconi, R., Tarasova, Y., Stocker, R., et al. (2013). The extracellular matrix component Psl provides fast-acting antibiotic defense in *Pseudomonas aeruginosa* biofilms. *PLoS Pathog.* 9:e1003526. doi: 10.1371/journal.ppat.1003526

Bogdanov, S. (2002). *Harmonized Methods of the European Honey Commission*. Swiss Bee Research Centre, FAM, Liebefeld.

Bogdanov, S., Jurendic, T., Sieber, R., and Gallmann, P. (2008). Honey for nutrition and health: a review. *J. Am. Coll. Nutr.* 27, 677–689. doi: 10.1080/07315724.2008.10719745

Bolognese, F., Bistoletti, M., Barbieri, P., and Orlandi, V. T. (2016). Honey-sensitive *Pseudomonas aeruginosa* mutants are impaired in catalase A. *Microbiol* 162, 1554–1562. doi: 10.1099/mic.0.000351

Bonaga, G., and Giumanini, A. G. (1986). The volatile fraction of chestnut honey. *J. Apic Res.* 25, 113–120. doi: 10.1080/00218839.1986.11100703

Bowler, G. B. (2003). Bacterial growth guideline: reassessing its clinical relevance in wound healing. *Ostomy Wound Manag.* 49, 1–10.

Breitinger, 2012∼Breitinger, H.-G. (2012). Drug synergy – mechanisms and methods of analysis. *Toxic Drug Test* 143–166.

Brudzynski, K. (2006). Effect of hydrogen peroxide on antibacterial activities of Canadian honeys. *Can. J. Microbiol.* 52, 1228–1237. doi: 10.1139/w06-086

Cerqueira, L., Oliveira, J. A., Nicolau, A., Azevedo, N. F., and Vieira, M. J. (2013). Biofilm formation with mixed cultures of *Pseudomonas aeruginosa*/*Escherichia coli* on silicone using artificial urine to mimic urinary catheters. *Biofouling* 29, 829–840. doi: 10.1080/08927014.2013.807913

Chaudhry, W. N., Concepción-Acevedo, J., Park, T., Andleeb, S., Bull, J. J., Levin, B. R., et al. (2017). Synergy and Order Effects of Antibiotics and Phages in Killing *Pseudomonas aeruginosa* Biofilms. *PLoS ONE* 12:e0168615. doi: 10.1371/journal.pone.0168615

Chiang, W.-C., Nilsson, M., Jensen, P. O., Hoiby, N., Nielsen, T. E., Givskov, M., et al. (2013). Extracellular DNA shields against aminoglycosides in *Pseudomonas aeruginosa* biofilms. *Antimicrob. Agents Chemother.* 57, 2352–2361. doi: 10.1128/AAC.00001-13

Cho, J. S., Han, S., Kim, K. H., Han, Y. G., Lee, J. H., Lee, C. S., et al. (2005). *Adhesion Aspects of Thin Films*. Utrecht:VSP.

Cislo, M., Dabrowski, M., Weber-Dabrowska, B., and Woyton, A. (1987). Bacteriophage treatment of suppurative skin infections. *Arch. Immunol. Ther. Exp.* 35, 175–183.

Coniglio, M. A., Faro, G., Giammanco, G., Pignato, S., and Marranzano, M. (2013). Antimicrobial potential of sicilian honeys against commensal *Escherichia coli* and pathogenic *Salmonella* serovar infantis. *J. Prev. Med. Hyg.* 54, 223–226.

Crouzet, M., Le Senechal, C., Brözel, V. S., Costaglioli, P., Barthe, C., Bonneu, M., et al. (2014). Exploring early steps in biofilm formation: set-up of an experimental system for molecular studies. *BMC Microbiol.* 14:253. doi: 10.1186/s12866-014-0253-z

da Costa, A. M. A., Machado, R., Ribeiro, A., Collins, T., Thiagarajan, V., Neves Petersen, M. T., et al. (2015). Development of elastin like recombinamer films with antimicrobial activity. *Biomacromolecules*. 16, 625–635. doi: 10.1021/bm5016706

Ding, Y., Onodera, Y., Lee, J. C., and Hooper, D. C. (2008). NorB, an efflux pump in *Staphylococcus aureus* strain MW2, contributes to bacterial fitness in abscesses. *J. Bacteriol.* 190, 7123–7129. doi: 10.1128/JB.00655-08

Dunford, C. E., and Hanano, R. (2004). Acceptability to patients of a honey dressing for non-healing venous leg ulcers. *J. Wound Care* 13, 193–197. doi: 10.12968/jowc.2004.13.5.26614

Elkhyat, A., Courderot-Masuyer, C., Gharbi, T., and Humbert, P. (2004). Influence of the hydrophobic and hydrophilic characteristics of sliding and slider surfaces on friction coefficient: *in vivo* human skin friction comparison. *Ski Res. Technol.* 10, 215–221. doi: 10.1111/j.1600-0846.2004.00085.x

Ferraro, M. J., Wikler, M. A., Craig, W. A., Dudley, M. N., Eliopoulos, G. M., Hecht, D. W., et al. (2003). *Methods for Dilution Antimicrobial Susceptibility Tests for Bacteria That Grow Aerobically; Approved Standard, 6th Edn*. Wayne, PA: Clinical and Laboratory Standards Institute.

Flemming, H., and Wingender, J. (2010). The biofilm matrix. *Nat. Rev. Microbiol.* 8, 623–633. doi: 10.1038/nrmicro2415

Fux, C. A., Costerton, J. W., Stewart, P. S., and Stoodley, P. (2005). Survival strategies of infectious biofilms. *Trends Microbiol.* 13, 34–40. doi: 10.1016/j.tim.2004.11.010

Gethin, G. T., Cowman, S., and Conroy, R. M. (2008). The impact of Manuka honey dressings on the surface pH of chronic wounds. *Int. Wound J.* 5, 185–194. doi: 10.1111/j.1742-481X.2007.00424.x

Gethin, G., and Cowman, S. (2008). Bacteriological changes in sloughy venous leg ulcers treated with manuka honey or hydrogel: an RCT. *J. Wound Care* 17, 241–247. doi: 10.12968/jowc.2008.17.6.29583

Greco, W., Unkelbach, H.-D., Pöch, G., Sühnel, J., and Kundi, M., W B. (1992). Consensus on concepts and terminology for combined-action assessment: the Saariselkä Agreement. *Arch. Complex Environ. Stud.* 4, 65–69.

Hao, J. J., Liu, H., Donis-Gonzalez, I. R., Lu, X. H., Jones, A. D., and Fulbright, D. W. (2012). Antimicrobial activity of chestnut extracts for potential use in managing soilborne plant pathogens. *Plant Dis.* 96, 354–360. doi: 10.1094/PDIS-03-11-0169

Hengzhuang, W., Ciofu, O., Yang, L., Wu, H., Song, Z., Oliver, A., et al. (2013). High beta-lactamase levels change the pharmacodynamics of beta-lactam antibiotics in *Pseudomonas aeruginosa* biofilms. *Antimicrob. Agents Chemother.* 57, 196–204. doi: 10.1128/AAC.01393-12

Imran, M., Hussain, M. B., and Baig, M. (2015). A randomized, controlled clinical trial of honey-impregnated dressing for treating diabetic foot ulcer. *J. Coll. Physicians Surg. Pak.* 25, 721–725. doi: 10.2015/JCPSP.721725

Ito, A., Taniuchi, A., May, T., Kawata, K., and Okabe, S. (2009). Increased antibiotic resistance of Escherichia coli in mature biofilms. *Appl. Environ. Microbiol.* 75, 4093–4100. doi: 10.1128/AEM.02949-08

Jensen, P. O., Bjarnsholt, T., Phipps, R., Rasmussen, T. B., Calum, H., Christoffersen, L., et al. (2007). Rapid necrotic killing of polymorphonuclear leukocytes is caused by quorum-sensing-controlled production of rhamnolipid by *Pseudomonas aeruginosa*. *Microbiology* 153, 1329–1338. doi: 10.1099/mic.0.2006/003863-0

Kilty, S. J., Duval, M., Chan, F. T., Ferris, W., and Slinger, R. (2011). Methylglyoxal: (Active agent of manuka honey) in vitro activity against bacterial biofilms. *Int. Forum Allergy Rhinol.* 1, 348–350. doi: 10.1002/alr.20073

Kondyurin, A., Gan, B. K., Bile, M. M. M., Mizuno, K., and McKenzie, D. R. (2006). Etching and structural changes of polystyrene films during plasma immersion ion implantation from argon plasma. *Nucl Instrum. Methods Phys Res Sect B* 251, 413–418. doi: 10.1016/j.nimb.2006.06.027

Lazarus, G. S., Cooper, D. M., Knighton, D. R., Percoraro, R. E., Rodeheaver, G., and Robson, M. C. (1994). Definitions and guidelines for assessment of wounds and evaluation of healing. *Wound Repair Regen.* 2, 165–170. doi: 10.1046/j.1524-475X.1994.20305.x

Lee, J. H., Park, J. H., Kim, J. A., Neupane, G. P., Cho, M. H., Lee, C. S., et al. (2011). Low concentrations of honey reduce biofilm formation, quorum sensing, and virulence in *Escherichia coli* O157:H7. *Biofouling* 27, 1095–1104. doi: 10.1080/08927014.2011.633704

Lu, J., Carter, D. A., Turnbull, L., Rosendale, D., Hedderley, D., Stephens, J., et al. (2013). The effect of new zealand kanuka, manuka and clover honeys on bacterial growth dynamics and cellular morphology varies according to the species. *PLoS ONE* 8:e0055898. doi: 10.1371/journal.pone.0055898

Lu, J., Turnbull, L., Burke, C. M., Liu, M., Carter, D., a, Schlothauer, R. C., et al. (2014). Manuka-type honeys can eradicate biofilms produced by *Staphylococcus aureus* strains with different biofilm-forming abilities. *PeerJ* 2:e326. doi: 10.7717/peerj.326

Majewski, W., Cybulski, Z., Napierala, M., Pukacki, F., Staniszewski, R., Pietkiewicz, K., et al. (1995). The value of quantitative bacteriological investigations in the monitoring of treatment of ischaemic ulcerations of lower legs. *Int. Angiol.* 14, 381–384.

Majtan, J. (2014). Honey: an immunomodulator in wound healing. *Wound Repair Regen.* 22, 187–192. doi: 10.1111/wrr.12117

Majtan, J., Bohova, J., Prochazka, E., and Klaudiny, J. (2014). Methylglyoxal may affect hydrogen peroxide accumulation in manuka honey through the inhibition of glucose oxidase. *J. Med. Food* 17, 290–293. doi: 10.1089/jmf.2012.0201

Markoishvili, K., Tsitlanadze, G., Katsarava, R., Morris, J. G. J., and Sulakvelidze, A. (2002). A novel sustained-release matrix based on biodegradable poly(ester amide)s and impregnated with bacteriophages and an antibiotic shows promise in management of infected venous stasis ulcers and other poorly healing wounds. *Int. J. Dermatol.* 41, 453–458. doi: 10.1046/j.1365-4362.2002.01451.x

Mendes, J. J., Leandro, C., Corte-Real, S., Barbosa, R., Cavaco-Silva, P., Melo-Cristino, J., et al. (2013). Wound healing potential of topical bacteriophage therapy on diabetic cutaneous wounds. *Wound Repair Regen.* 21, 595–603. doi: 10.1111/wrr.12056

Mohamed, H. (2017). Healing of chronic diabetic foot ulcers with natural honey: an alternative paradigm in wound healing. *Wound Repair Regen.* 25:A18. doi: 10.1111/wrr.12573

Molan, P. C. (1992). The Anitbacterial Activity of Honey: 1. The nature of the antibacterial activity. *Bee World* 73, 5–28.

Molan, P. C., and Betts, J. A. (2004). Clinical usage of honey as a wound dressing: an update. *J. Wound Care* 13, 353–356. doi: 10.12968/jowc.2004.13.9.26708

Mustoe, T. A., O'Shaughnessy, K., and Kloeters, O. (2006). Chronic wound pathogenesis and current treatment strategies: a unifying hypothesis. *Plast Reconstr. Surg.* 117, 35S—41S. doi: 10.1097/01.prs.0000225431.63010.1b

Naghili, H., Tajik, H., Mardani, K., Razavi Rouhani, S. M., Ehsani, A., and Zare, P. (2013). Validation of drop plate technique for bacterial enumeration by parametric and nonparametric tests. *Vet Res forum an Int Q J* 4, 179–183.

Nishio, E. K., Ribeiro, J. M., Oliveira, A. G., Andrade, C. G. T. J., Proni, E. A., Kobayashi, R. K. T., et al. (2016). Antibacterial synergic effect of honey from two stingless bees: *Scaptotrigona bipunctata* Lepeletier, 1836, and S. postica Latreille, (1807). *Sci. Rep.* 6:21641. doi: 10.1038/srep21641

Oryan, A.,Alemzadeh,E., and Moshiri, A. (2016). Biological properties and therapeutic activities of honey in wound healing: a narrative review and meta-analysis. *J. Tissue Viability* 25, 98–118. doi: 10.1016/j.jtv.2015.12.002

Oliveira, A., Ribeiro, H. G., Silva, A. C., Silva, M. D., Sousa, J. C., Rodrigues, C. F., et al. (2017). Synergistic antimicrobial interaction between honey and phage against *Escherichia coli* biofilms. *Front. Microbiol.* 8:2407. doi: 10.3389/fmicb.2017.02407

Park, D. J., Drobniewski, F. A., Meyer, A., and Wilson, S. M. (2003). Use of a phage-based assay for phenotypic detection of mycobacteria directly from sputum. *J. Clin. Microbiol.* 41, 680–688. doi: 10.1128/JCM.41.2.680-688.2003

Piggott, J. J., Townsend, C. R., and Matthaei, C. D. (2015). Reconceptualizing synergism and antagonism among multiple stressors. *Ecol. Evol.* 5, 1538–1547. doi: 10.1002/ece3.1465

Pires, D. P., Dötsch, A., Anderson, E. M., Hao, Y., Khursigara, C. M., Lam, J. S., et al. (2017). A genotypic analysis of five *P. aeruginosa* strains after biofilm infection by phages targeting different cell surface receptors. *Front. Microbiol.* 8:1229. doi: 10.3389/fmicb.2017.01229

Pires, D. P., Kropinski, A. M., Azeredo, J., and Sillankorva, S. (2014). Complete genome sequence of the *Pseudomonas aeruginosa* Bacteriophage phiIBB-PAA2. *Genome Announc.* 2, e01102–e01113. doi: 10.1128/genomeA.01102-13

Pires, D.P., Sillankorva, S., Faustino, A., and Azeredo, J. (2011). Use of newly isolated phages for the control of *Pseudomonas aeruginosa* PAO1 and ATCC 10145 biofilms. *Res. Microbiol*. 162, 798–806. doi: 10.1016/j.resmic.2011.06.010

Pires, D. P., Sillankorva, S., Kropinski, A. M., Lu, T. K., and Azeredo, J. (2015). Complete Genome Sequence of *Pseudomonas aeruginosa* Phage vB_PaeM_CEB_DP1. *Genome Announc.* 3:e00918. doi: 10.1128/genomeA.00918-15

Pirnay, J. P., De Vos, D., Verbeken, G., Merabishvili, M., Chanishvili, N., Vaneechoutte, M., et al. (2011). The phage therapy paradigm: Prêt-à-porter or sur-mesure? *Pharm. Res.* 28, 934–937. doi: 10.1007/s11095-010-0313-5

Robson, M. C. (1997). Wound infection: a failure of wound healing caused by an imbalance of bacteria. *Surg. Clin. North Am.* 77, 637–650. doi: 10.1016/S0039-6109(05)70572-7

Rossano, R., Larocca, M., Polito, T., Perna, A. M., Padula, M. C., Martelli, G., et al. (2012). What are the proteolytic enzymes of honey and what they do tell us? a fingerprint analysis by 2-D Zymography of Unifloral Honeys. *PLoS ONE* 7:e0049164. doi: 10.1371/journal.pone.0049164

Sambrook, J. W., and Russell, D. (2001). *Molecular Cloning: A Laboratory Manual*. New York, NY: Cold Spring Harb Lab Press.

Sato, T., and Miyata, G. (2000). The nutraceutical benefit, Part III: Honey. *Nutrition* 16, 468–469. doi: 10.1016/S0899-9007(00)00271-9

Seth, A. K., Geringer, M. R., Nguyen, K. T., Agnew, S. P., Dumanian, Z., Galiano, R. D., et al. (2013). Bacteriophage therapy for *Staphylococcus aureus* biofilm-infected wounds: a new approach to chronic wound care. *Plast. Reconstr. Surg.* 131, 225–234. doi: 10.1097/PRS.0b013e31827e47cd

Sharp, A. (2009). Beneficial effects of honey dressings in wound management. *Nurs Stand.* 24, 66–68. doi: 10.7748/ns.24.7.66.s54

Sillankorva, S., Neubauer, P., and Azeredo, J. (2008). Isolation and characterization of a T7-like lytic phage for *Pseudomonas fluorescens*. *BMC Biotechnol.* 8:80. doi: 10.1186/1472-6750-8-80

Tuson, H. H., and Weibel, D. B. (2013). Bacteria-surface interactions. *Soft. Matter.* 9, 4368–4380. doi: 10.1039/c3sm27705d

United States Deparment of Agriculture (1985). United States Standards for Grades of Extracted Honey. *Fed. Regist.* 50FR15861:R15812.

Visavadia, B. G., Honeysett, J., and Danford, M. H. (2008). Manuka honey dressing: an effective treatment for chronic wound infections. *Br. J. Oral Maxillofac. Surg.* 46, 55–56. doi: 10.1016/j.bjoms.2006.09.013

Voncina, B., Zemljič Fras, L., and Ristic, T. (2015). Active Textile Dressings for Wound Healing." in *Advances in Smart Medical Textiles: Treatments and Health Monitoring*, ed L. Langenhove (Swaston; Cambridge, MA; Woodhead Publishing), 73–92.

Weinbauer, M. G. (2004). Ecology of prokaryotic viruses. *FEMS Microbiol. Rev.* 28, 127–181. doi: 10.1016/j.femsre.2003.08.001

White, J. W. (1979). Spectrophotometric method for hydroxymethylfurfural in honey. *J. Assoc.* 62, 509–514.

Whiteley, M., Bangera, M. G., Bumgarner, R. E., Parsek, M. R., Teitzel, G. M., Lory, S., et al. (2001). Gene expression in *Pseudomonas aeruginosa* biofilms. *Nature* 413, 860–864. doi: 10.1038/35101627

Zhang, L., and Mah, T.-F. (2008). Involvement of a novel efflux system in biofilm-specific resistance to antibiotics. *J. Bacteriol.* 190, 4447–4452. doi: 10.1128/JB.01655-07

Conflict of Interest Statement: The authors declare that the research was conducted in the absence of any commercial or financial relationships that could be construed as a potential conflict of interest.

frontiers in Microbiology

ORIGINAL RESEARCH
published: 05 February 2018
doi: 10.3389/fmicb.2018.00127

Does Treatment Order Matter? Investigating the Ability of Bacteriophage to Augment Antibiotic Activity against *Staphylococcus aureus* Biofilms

*Dilini Kumaran[1], Mariam Taha[1], QiLong Yi[2], Sandra Ramirez-Arcos[2], Jean-Simon Diallo[1], Alberto Carli[3] and Hesham Abdelbary[1,3]**

[1] Center for Innovative Cancer Therapeutics, Ottawa Hospital Research Institute, Ottawa, ON, Canada, [2] Centre for Innovation, Canadian Blood Services, Ottawa, ON, Canada, [3] Division of Orthopedic Surgery, The Ottawa Hospital, Ottawa, ON, Canada

The inability to effectively treat biofilm-related infections is a major clinical challenge. This has been attributed to the heightened antibiotic tolerance conferred to bacterial cells embedded within biofilms. Lytic bacteriophages (phages) have evolved to effectively infect and eradicate biofilm-associated cells. The current study was designed to investigate the ability of phage treatment to enhance the activity of antibiotics against biofilm-forming *Staphylococcus aureus*. The biofilm positive *S. aureus* strain ATCC 35556, the lytic *S. aureus* phage SATA-8505, and five antibiotics (cefazolin, vancomycin, dicloxacillin, tetracycline, and linezolid), used to treat *S. aureus* infections, were tested in this study. The ability of the SATA-8505 phage to augment the effect of these antibiotics against biofilm-associated *S. aureus* cells was assessed by exposing them to one of the five following treatment strategies: (i) antibiotics alone, (ii) phage alone, (iii) a combination of the two treatments simultaneously, (iv) staggered exposure to the phage followed by antibiotics, and (v) staggered exposure to antibiotics followed by exposure to phage. The effect of each treatment strategy on biofilm cells was assessed by enumerating viable bacterial cells. The results demonstrate that the treatment of biofilms with either SATA-8505, antibiotics, or both simultaneously resulted in minimal reduction of viable biofilm-associated cells. However, a significant reduction [up to 3 log colony forming unit (CFU)/mL] was observed when the phage treatment preceded antibiotics. This effect was most pronounced with vancomycin and cefazolin which exhibited synergistic interactions with SATA-8505, particularly at lower antibiotic concentrations. This *in vitro* study provides proof of principle for the ability of phages to augment the activity of antibiotics against *S. aureus* biofilms. Our results also demonstrate that therapeutic outcomes can be influenced by the sequence in which these therapeutic agents are administered, and the nature of their interactions. Further investigation into the interactions between lytic phages and antibiotics against various biofilm-forming organisms is important to direct future clinical translation of efficacious antibiotic–phage combination therapeutic strategies.

Keywords: bacteriophage, *Staphylococcus aureus*, biofilm, antibiotics, synergy

OPEN ACCESS

Edited by:
Maria Olivia Pereira, University of Minho, Portugal

Reviewed by:
Ananda Shankar Bhattacharjee, Bigelow Laboratory for Ocean Sciences, United States
Ruchi Tiwari, Veterinary University (DUVASU), India

***Correspondence:**
Hesham Abdelbary
habdelbary@toh.ca

Specialty section:
This article was submitted to Antimicrobials, Resistance and Chemotherapy, a section of the journal Frontiers in Microbiology

Received: *24 August 2017*
Accepted: *18 January 2018*
Published: *05 February 2018*

Citation:
Kumaran D, Taha M, Yi Q, Ramirez-Arcos S, Diallo J-S, Carli A and Abdelbary H (2018) Does Treatment Order Matter? Investigating the Ability of Bacteriophage to Augment Antibiotic Activity against Staphylococcus aureus Biofilms. Front. Microbiol. 9:127. doi: 10.3389/fmicb.2018.00127

INTRODUCTION

The majority of human bacterial infections are thought to involve biofilm-associated bacterial pathogens (Römling and Balsalobre, 2012). Broadly defined, biofilms are communities of microbial cells adhered to biotic or abiotic surfaces encased in a self-produced matrix (Costerton et al., 1999). The ability to form biofilms has been shown to provide associated bacterial cells with heightened tolerance to antibiotics when compared to their planktonic counterparts. Biofilms account for the observed recalcitrance of biofilm-associated chronic bacterial infections (Mah and O'Toole, 2001). The heightened resistance displayed by biofilms is thought to be multifaceted, with the matrix serving as the first line of defense. The physical and biochemical properties of the matrix have been reported to impede the diffusion of antimicrobial agents into the biofilm which leads to suboptimal concentrations of these agents within the biofilm thereby reducing their efficacy (Gordon et al., 1988). Additionally, mature biofilms display physiochemical stratification caused by the varying availability of nutrients and waste products within the biofilm. As a result, cells found in the deeper layers of biofilms are generally less metabolically active than those found in the periphery, and are consequently less susceptible to antimicrobials that rely on active replication for their activity (Fauvart et al., 2011). The differential expression of genes within biofilms has also been shown to contribute to heightened antibacterial tolerance. This was observed in *Escherichia coli* and *Pseudomonas aeruginosa* biofilms, where efflux pumps and periplasmic glucans were upregulated, respectively (Mah et al., 2003; Lynch et al., 2007). Finally, the presence of a subset of isogenic cells called persister cells and naturally occurring antibiotic-resistant cells play a key role in the persistence of biofilms following antibiotic treatment. Persister cells become metabolically dormant and exhibit tolerance in the presence of antimicrobials; however, they are able revert to an active metabolic state in its absence (Lebeaux et al., 2014). These factors together with the ever-mounting threat of antibiotic resistance have made the search for alternative treatments of biofilm-related infections a high priority in several clinical disciplines including orthopedic surgery and cardiac surgery (Archer et al., 2011; Tande and Patel, 2014).

Bacteriophages (phages) are viruses that are highly specific to their bacterial hosts. They were discovered in the early 1900s (Salmond and Fineran, 2015) and were quickly shown to be effective in treating bacterial infections (Schultz, 1929; MacNeal and Frisbee, 1936). However, with the introduction of antibiotics, the appeal of phage therapy rapidly diminished. Due to the emergence of multi-drug-resistant bacterial pathogens in recent years, there has been renewed interest in phage therapy as an alternative antimicrobial strategy (Doss et al., 2017). Phages co-evolve with bacteria in nature; consequently, phages have developed mechanisms to overcome the obstacles posed by the biofilm state. Some of these mechanisms include exploiting water channels within the biofilm to penetrate into the deeper layers of the biofilm (Doolittle et al., 1996), or the expression of depolymerases that can disrupt the extracellular matrix allowing phage to penetrate and spread within the biofilm (Parasion et al., 2014). Biofilms also provide an excellent niche for phage replication since bacteria are found at high densities. Therefore, phages can self-amplify and reach high concentrations at the site of infection with a low initial dose (Burrowes et al., 2011). Phages have also been shown to infect antibiotic-resistant bacterial cells, since the evolved resistance mechanisms against antibiotics do not affect phage infection. As a result, the utilization of phage to treat infections caused by these resistant bacterial cells can help eliminate the selection of these cells and consequently minimizes persistence (Loc-Carrillo and Abedon, 2011). Additionally, Pearl et al. (2008) demonstrated that though phages require metabolically active hosts to replicate, they can infect persister host cells where they remain dormant. However, the phage lytic cycle is activated upon reversion to an active metabolic state, thereby abrogating the risk of reseeding.

A notable example of a human pathogen that is able to cause biofilm-related chronic infections is the commensal opportunistic bacterium *Staphylococcus aureus*. This bacterium is the leading cause of biofilm-related infections associated with implanted medical devices, such as heart valves, catheters, and prosthetic joints (Archer et al., 2011; Tande and Patel, 2014). In an effort to combat these recalcitrant infections, studies have investigated the potential of using matrix dispersal agents in conjunction with antibiotics (Lauderdale et al., 2010; Reffuveille et al., 2014). However, several shortcomings of this approach include the presentation of suboptimal levels of antibiotics within the biofilm, which lead to either acute infections or inadvertent upregulation of biofilm-forming genes (Lister and Horswill, 2014). Encouragingly, studies have demonstrated that a *S. aureus*-specific phage can successfully treat *S. aureus* infections when used in conjunction with antibiotics (Chhibber et al., 2013; Yilmaz et al., 2013). However, the effect of staggering the administration of these therapeutic agents on *S. aureus* biofilms has not been investigated.

The main aim of the current study is to investigate the ability of phage to enhance antibiotic activity against biofilm-forming *S. aureus*. Furthermore, the study aimed to elucidate whether the order in which treatment was administered had an impact on biofilm eradication outcomes.

MATERIALS AND METHODS

Bacterial Strain and Phage

The *S. aureus* biofilm-forming strain ATCC 35556 and the lytic phage SATA-8505 were obtained from the American Type Culture Collection (ATCC). This *S. aureus* isolate served as the host strain for phage propagation. All bacterial cultures were incubated at 37°C unless otherwise stated.

Antibiotics

Five antibiotics clinically used to treat *S. aureus* infections were assessed. These antibiotics were divided into two groups based on their mode of action. The first group consisted of vancomycin, dicloxacillin sodium salt, and cefazolin sodium salt which inhibit bacterial cell wall synthesis, while the second group consisted of linezolid and tetracycline hydrochloride which inhibit protein synthesis. All antibiotics tested in this study were

obtained from Sigma–Aldrich (Canada). Stock solutions of the antibiotics were prepared in sterile double distilled water to a final concentration of 10 mg/mL, with the exception of linezolid which was prepared in dimethyl sulfoxide (Sigma–Aldrich) according to manufacturers' recommendations. Working stocks of these antibiotics were prepared in Mueller Hinton II cation-adjusted (MH-CA).

Minimal Inhibitory Concentration (MIC)

Minimal inhibitory concentration values were determined according to the Clinical Laboratory Standards Institute [CLSI] (2015) M107-A10 guidelines. Briefly, overnight liquid cultures of *S. aureus* were adjusted to $OD_{600} = 0.1$ in MH-CA media (BD Biosciences, Sparks Glencoe, MD, United States), and was further diluted in a 1:1 ratio in MH-CA. Fifty microliters of the adjusted bacterial culture was added to the wells of a 96-well plate (tissue culture treated; Falcon, Corning Inc., Durham, NC, United states) (approximately 10^5 CFU/well). A twofold serial dilution of the antibiotics was prepared from stock solutions in MH-CA to obtain concentrations of 1024–0.125 μg/mL. The antibiotics were then added to the bacterial cell suspension (50 μL/ well) to obtain an antibiotic concentration gradient across the plate. The plates were statically incubated for 24 h at 37°C. Visible growth was monitored and MIC values were assigned.

Establishing Biofilms

Overnight liquid bacterial cultures were adjusted to $OD_{600} = 0.1$ (10^7 CFU/mL) in tryptic soy broth media supplemented with 0.5% glucose (TSBg). A 500 μL aliquot of the bacterial suspension was added to each well of 48-well polystyrene tissue culture plates (Falcon, Corning Inc., Durham, NC, United States) and incubated at 37°C statically for 24 h to allow for the formation of mature biofilms.

Minimal Biofilm Eradication Concentration (MBEC)

Minimal Biofilm Eradication Concentration values were determined following the method described by Cui et al. (2016) with some modifications. Briefly, following mature biofilm formation (described above), planktonic cells were aspirated and 500 μL of increasing concentrations of antibiotics (32–1024 μg/mL) prepared in MH-CA was added to the biofilms and allowed to incubate at 37°C, for 24 h statically. The planktonic cells were aspirated, and the residual biofilm cells were mechanically dislodged into phosphate-buffered saline (pH 7.4), and homogenized by vigorous pipetting. The bacterial suspension was serially diluted, plated on tryptic soy broth agar (TSA), and incubated overnight at 37°C. Following incubation MBEC values were assigned. MBEC values were determined using the 48-well format since this format was used to assess antibiotic and phage interactions against biofilms.

Assessment of Antibiotic and Phage Interactions

This assay was performed to evaluate the nature of the interactions between the tested antibiotics and the SATA-8505 phage against pre-formed biofilms of *S. aureus* ATCC 35556. The concentration of phage used for all the experiments was 10^6 plaque forming unit (PFU)/mL [it was determined that a concentration of 10^5 PFU/well in a total volume of 500 μL was sufficient for successful infection in this assay format (data not shown)]. The antibiotics were tested at six concentrations: 1024, 512, 256, 128, 64, and 32 μg/mL. The highest concentration of tetracycline used was 256 μg/mL, and this was due to difficulties associated with accurately quantifying viable biofilm cells caused by the bacteriostatic nature of the antibiotic. All treatments were prepared in MH-CA. Biofilms treated with MH-CA alone served as the cell control. The experiments were repeated at least three independent times.

Following the formation of mature biofilms the supernatant was aspirated to remove planktonic cells and the biofilm cells were treated with 500 μL of either the "individual" or "combination (simultaneous or staggered)" treatments (**Figure 1**).

In the individual format, biofilms were treated with either the phage alone ($\sim 10^5$ PFU/well) or with the concentration gradient (described above) of antibiotics alone and incubated at 37°C for 24 or 48 h statically (**Figure 1**). Following the treatment regimen, the supernatant was removed and the biofilms were mechanically dislodged and homogenized by vigorous pipetting. The residual viable biofilm cells were enumerated by plating 10-fold serial dilutions of the bacterial cell suspensions on TSA.

In the simultaneous combined treatment format, the pre-formed biofilms were treated with 500 μL/well of the concentration gradient of antibiotics described above with the exception that the suspension contained a total phage content of $\sim 10^5$ PFU/500 μL. The plates were then allowed to incubate at 37°C for either 24 or 48 h.

In the staggered format, the pre-formed biofilms were first exposed to one of the treatments (phage alone or antibiotic alone) at the concentrations described above and allowed to incubate at 37°C for 24 h after which the supernatant was removed and the biofilm was then exposed to the second treatment for an additional 24 h at 37°C. The residual viable biofilm cells were enumerated as described previously.

Statistical Analysis

Bacterial CFU counts were $\log_{10}$ transformed. Mixed model analysis was performed to determine the nature of the interaction (synergistic, additive, or antagonistic) of the combined treatment of phage and antibiotics against *S. aureus* biofilms. A p-value of <0.05 was considered significant. Reduction in viable bacteria counts was calculated as the difference between viable counts of the untreated biofilms (control) and the treated biofilms. An interaction was defined as being synergistic when the combination of the treatments led to greater reduction of bacteria than the sum of the individual effects. An interaction was defined as being additive in nature if the combination of the treatments resulted in bacterial reductions equal to the sum of the individual effects. While an antagonistic interaction was one that resulted in bacterial reductions that were lower than the sum of the

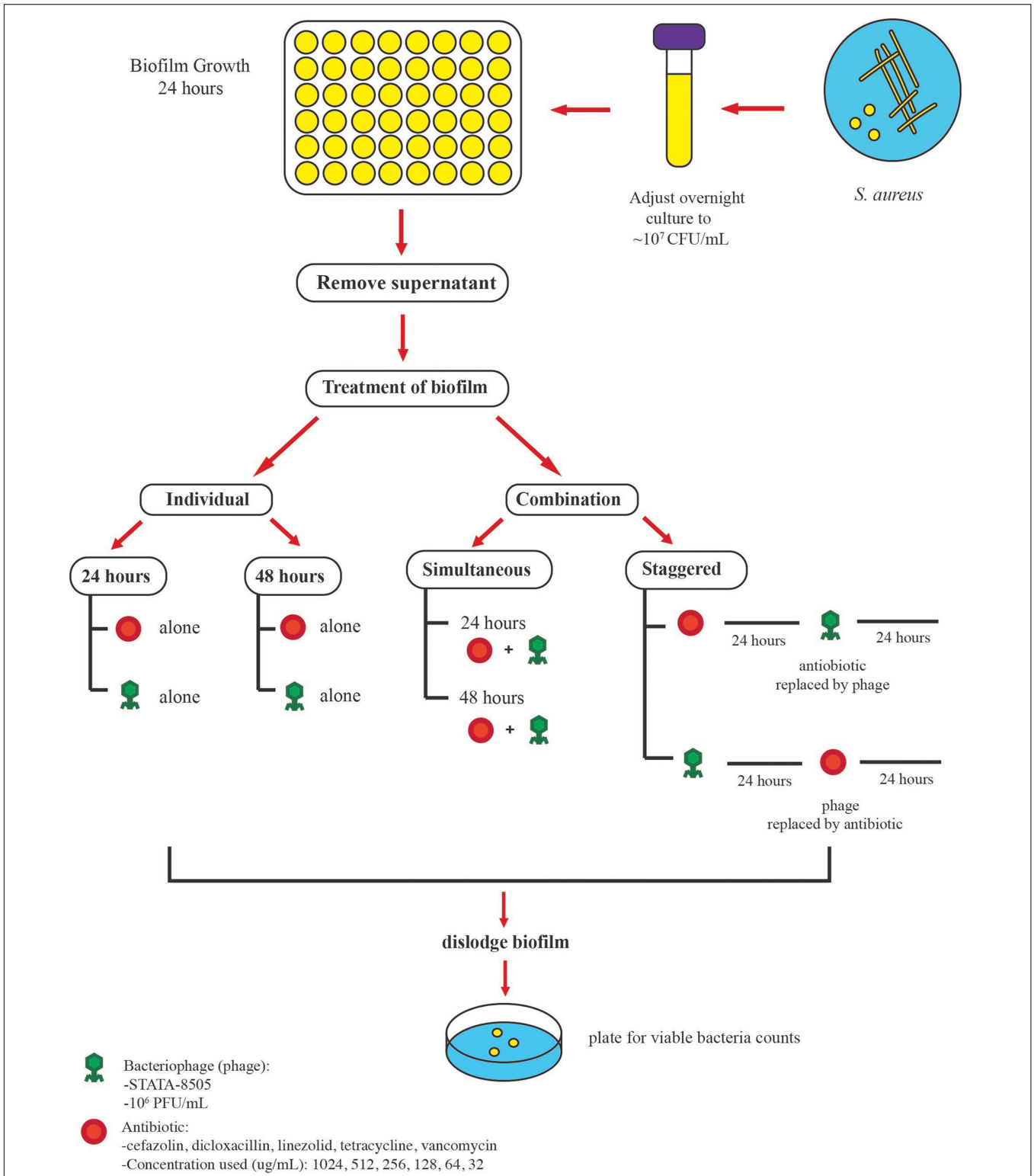

FIGURE 1 | Protocol used to examine the antimicrobial activities of phage SATA-8505 and five different antibiotics against *S. aureus* ATCC 35556 biofilms. Mature biofilms were obtained after 24 h of incubation, planktonic cells were removed, and the biofilms were exposed to different treatments. The biofilm was exposed to either (a) individual treatment (phage or antibiotic alone) for 24 or 48 h or (b) a combination of phage and antibiotics. Two approaches were employed for the combination treatment, the first was to expose the biofilm to antibiotics and phage simultaneously (24 or 48 h) and the second was to stagger the exposure to phage and antibiotics over 48 h. Phage was used at a concentration of 10^6 PFU/mL and different antibiotic concentrations were used.

individual effects. This could be described by the following equations:

Coefficient of interaction is equal to $\log(AB^R) - ((\log(A^R) + (\log(B^R))$,

where

A^R, reduction in bacteria counts treatment A;
B^R, reduction in bacteria counts treatment B;
AB^R, reduction in bacterial counts following the combined treatment (AB) (staggered or simultaneous).

If the coefficient is:

$$= 0, \text{additive interaction}, \quad (1)$$

$$> 0, \text{Synergistic interaction}, \quad (2)$$

$$< 0, \text{Antagonistic interaction}. \quad (3)$$

From the mixed model analysis, if the interaction was significant (p-value < 0.05), with a positive coefficient, it was concluded that combining the treatments resulted in a synergistic interaction (Equation 2). However, a significant interaction with a negative coefficient (Equation 3) was an indicator of an antagonistic effect. If the interaction was not significant (p-value > 0.05), then the combined treatment was considered to act in an additive (independent) manner against the biofilm (Equation 1).

To evaluate the possible effect of antibiotic concentrations on the efficiency of the treatment, the antibiotic concentrations were $\log_2$ transformed and linear regression analysis was performed. Data analyses were performed with computer software [Statistical Analysis System (SAS) 2002–2010, SAS Institute, Inc., Cary, NC, United States].

TABLE 1 | MIC and MBEC values (μg/mL) of different antibiotics against *S. aureus* ATCC 35556.

Vancomycin		Cefazolin		Tetracycline		Linezolid		Dicloxacillin	
MIC	**MBEC**	**MIC**	**MBEC**	**MIC**	**MBEC**	**MIC**	**MBEC**	**MIC**	**MBEC**
4	>1024	0.5	>1024	0.5	>1024	4	>1024	0.125	>1024

TABLE 2 | Interactions between SATA-8505 and different antibiotics exhibited when *S. aureus* biofilms were exposed to the simultaneous treatment of these two agents over 24 h.

Concentration (μg/mL)	Antibiotic				
	Vancomycin	**Dicloxacillin**	**Cefazolin**	**Tetracycline**	**Linezolid**
	Interaction				
32	A	G	G	A	A
64	A	G	G	A	A
128	G	G	G	A	A
258	G	G	G	A	A
512	G	G	G	n/a	A
1024	A	G	G	n/a	A

A, additive interaction; G, antagonistic interaction; n/a, not applicable.

RESULTS

Anti-biofilm Activity of the Simultaneous Treatment of Antibiotics and Phage

Pre-formed biofilms were simultaneously treated with antibiotics and SATA 8505 over 24 and 48 h. The MIC and MBEC values of the five tested antibiotics were determined (**Table 1**), and it was found that the MBEC of all the antibiotics were >1024 μg/mL.

The antibiotic concentrations used in the successive experiments which evaluated antibiotic and phage interactions were the same range utilized for MBEC determination. Following the 24 h incubation period, the combination treatment of SATA-8505 with linezolid or tetracycline demonstrated an additive effect at all concentration of antibiotics tested ($p > 0.05$, **Table 2**). Vancomycin showed a similar pattern at lower concentrations ($p > 0.05$), however at concentrations higher than 64 μg/mL, the interaction with the phage was mostly antagonistic in nature ($p < 0.05$, **Table 2**). An antagonistic interaction was observed at all concentrations of cefazolin and dicloxacillin tested as well ($p < 0.05$, **Table 2**).

The exposure of biofilms to cefazolin, linezolid, or tetracycline in combination with the phage over 48 h resulted mostly in an antagonistic effect (**Figures 2C**, **3A,B**) ($p < 0.05$) with no major reductions of bacterial viable counts being observed. In the case of vancomycin, an additive interaction was observed when the antibiotic was used in conjunction with the phage up to a concentration of 128 μg/mL ($p > 0.05$). At concentrations of 256 μg/mL and higher, an antagonistic interaction was observed (**Figure 2A**) ($p < 0.05$). Of the antibiotics tested, dicloxacillin alone exhibited additive interactions at all concentrations tested (**Figure 2B**) ($p > 0.05$). Therefore, results indicate that simultaneous phage and antibiotic treatments for either 24 or 48 h have limited antibacterial activity against *S. aureus* biofilms.

Staggered Treatment of the Phage and the Antibiotic

A strategy to stagger the phage and antibiotic treatments against biofilms was employed to assess the effect that the order of treatment may have on biofilm viability. Exposing pre-formed biofilms to antibiotics (vancomycin, cefazolin, tetracycline, or linezolid) prior to phage treatment resulted in antagonistic interactions between the two agents at all concentrations tested (**Figures 2A,C**, **3A,B**) ($p < 0.05$). On the other hand, when the phage treatment preceded exposure to either vancomycin or cefazolin, significant anti-biofilm activities were observed corresponding to a synergistic interaction between the antibiotics and the phage (**Figures 2A,C**) ($p < 0.05$). The exposure of biofilms to phage prior to either linezolid or tetracycline gave rise to levels of biofilm reduction indicative of an additive interaction (**Figures 3A,B**) ($p > 0.05$). The data suggest that biofilm exposure to phage prior to antibiotics is more effective at eliminating biofilm-associated cells. Interestingly, dicloxacillin and the phage interacted in an additive manner regardless of whether they were exposed to the biofilm simultaneously or in a staggered fashion (**Figure 2B**) ($p > 0.05$).

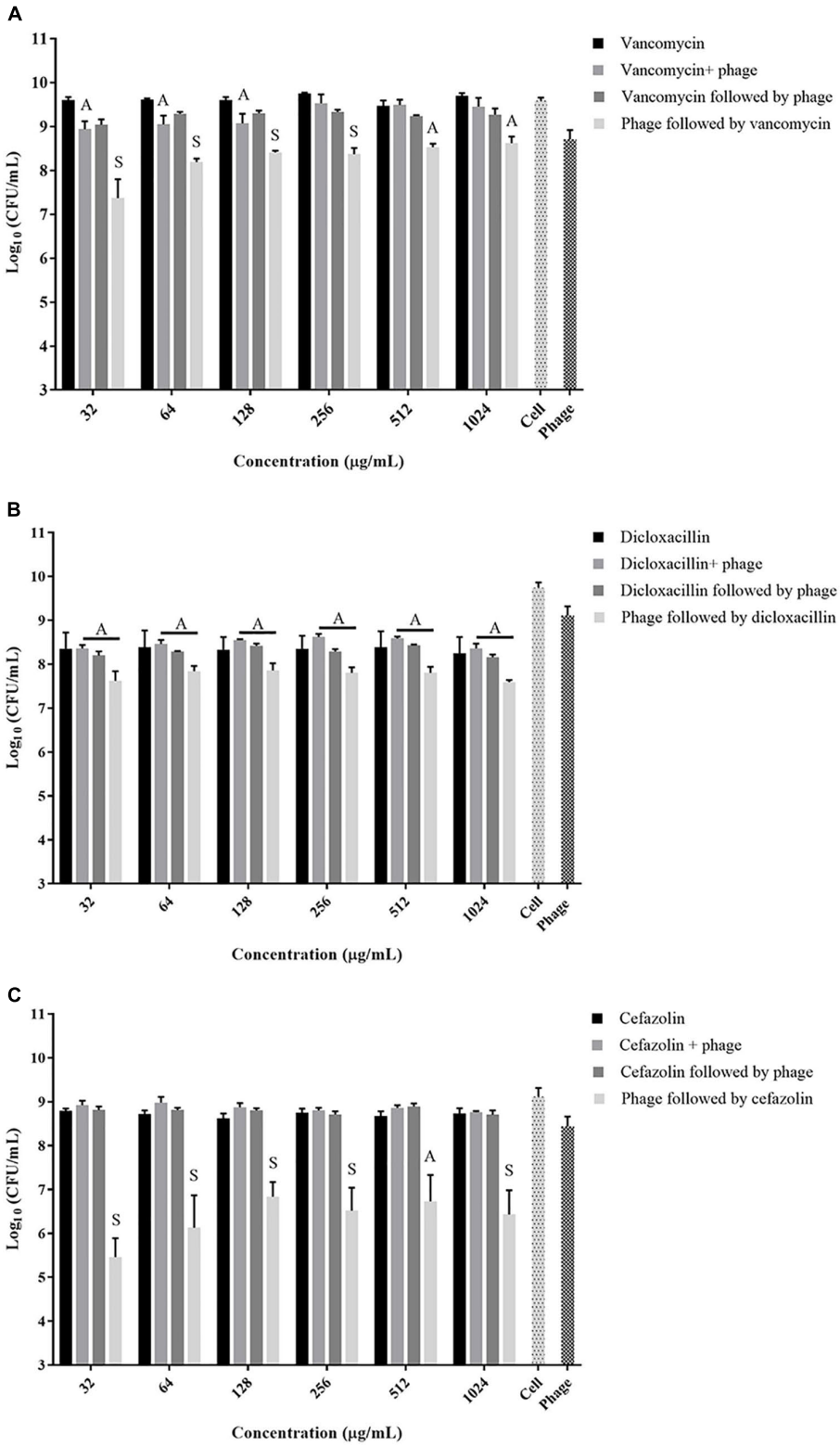

FIGURE 2 | Viable *S. aureus* ATCC 35556 counts following 48 h exposure to phage SATA-8505 and different concentrations of the cell wall synthesis inhibitor antibiotics; **(A)** vancomycin, **(B)** dicloxacillin, or **(C)** cefazolin. The treatment strategies employed were: antibiotic alone, phage alone, phage and antibiotic simultaneously, phage first followed by antibiotic, or antibiotic first followed by phage. Synergistic (S) and additive (A) interactions have been indicated. Bacterial cells treated with Mueller Hinton cation-adjusted (MH-CA) alone served as a control (cell). $N = 3–4 \pm SD$.

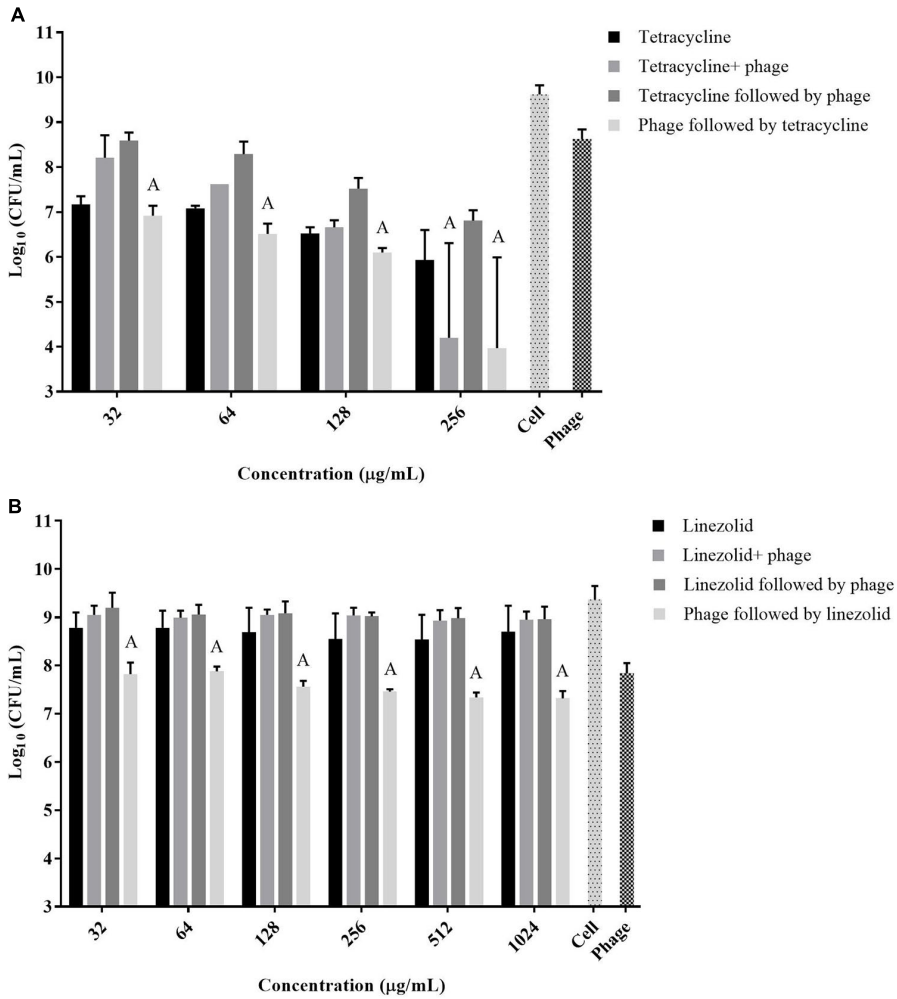

FIGURE 3 | Viable *S. aureus* ATCC 35556 counts 48 h following exposure to phage SATA-8505 and different concentrations of antibiotics that inhibit translation; **(A)** tetracycline and **(B)** linezolid. The treatment scenarios: antibiotic alone, phage alone, phage and antibiotic simultaneously, phage first then followed by antibiotic, or antibiotic first followed by phage. Synergistic (S) and additive (A) interactions have been indicated. Bacterial cells treated with MH-CA alone served as a control (cell). $N = 3 \pm SD$.

Antibiotic Concentration and Staggered Treatment Efficiency

Since our data indicated that better biofilm reduction outcomes can be achieved when phage is administered prior to antibiotics, we investigated the effect of the antibiotic concentrations on enhancing the staggered treatment efficiency. Linear regression analysis of the data demonstrated that there was linear relationship between the concentration of most antibiotics and biofilm reduction (**Figure 4**). The biofilm reduction observed was directly proportional to the concentration of linezolid and tetracycline used ($p = 0.0019$). However, the biofilm reduction observed for vancomycin was enhanced when lower concentrations were used ($p = 0.0014$). In the case of cefazolin, an inversely proportional relationship between antibiotic concentration and anti-biofilm effect was observed up to a concentration of 128 µg/mL. No linear correlation was observed between the concentration of dicloxacillin and tetracycline employed and biofilm elimination ($p = 0.6791$ and $p = 0.0654$, respectively).

DISCUSSION

The emergence of multi-drug-resistant bacteria has been on the rise over the past decade; a problem that has been compounded by a significant decline in the discovery of novel antibiotics. Consequently, there has been a resurgent interest in harnessing the antimicrobial properties of phages as a therapeutic platform.

Staphylococcus aureus biofilms are the leading cause of clinical infections such as osteomyelitis and infections associated with artificial implants (Archer et al., 2011; Tande and Patel, 2014). The successful treatment of biofilm-related infections using current antibiotic therapy continues to be a major challenge. Therefore, alternative therapeutic platforms that utilize phage to overcome the biofilm state offer a promising alternative to traditional

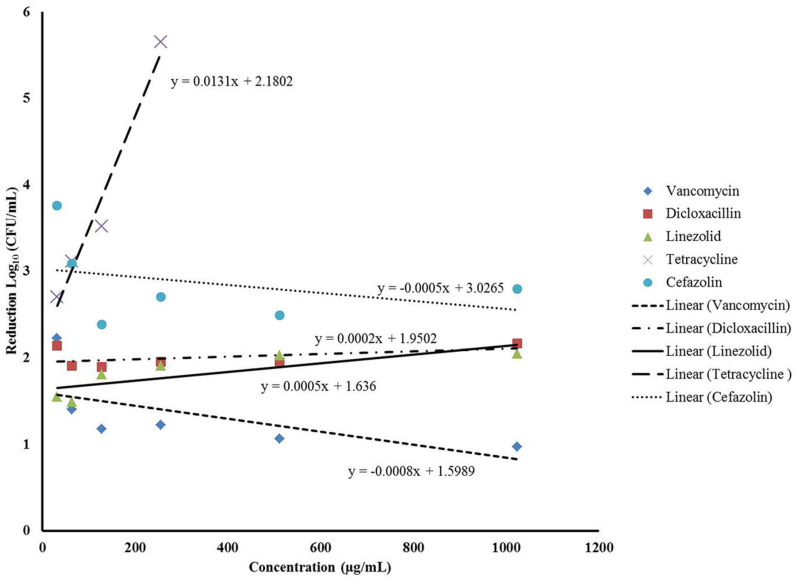

FIGURE 4 | Linear regression analysis assessing the correlation between the different concentrations of the antibiotics and the average biofilm reduction observed during the staggered treatment where the phage preceded antibiotics.

antibiotic treatments (Cornelissen et al., 2011; Gutiérrez et al., 2012).

Different groups have investigated the effectiveness of combining antibiotics with phage to eradicate bacterial populations existing in both planktonic and biofilm states. Zhang and Buckling (2012) demonstrated that when planktonic cultures of *Pseudomonas fluorescens* had been exposed to a combination of lytic phage and antibiotics, it resulted in a higher reduction in viable cells when compared with cultures treated with antibiotics alone. The simultaneous addition of phage to antibiotic regimens has also been reported to have a fascinating outcome of enhancing the sensitivity of multi-drug-resistant bacteria to antibiotics (Chan et al., 2016). Studies have also assessed how planktonic cultures are affected when these agents are added sequentially. Of note, groups led by Escobar-Paramo and Torres-Barcelo reported that the order in which the treatment was administered impacted bacterial reduction outcomes and antibiotic resistance profiles in the planktonic populations of *Pseudomonas* spp. studied (Escobar-Páramo et al., 2012; Torres-Barceló et al., 2014). Torres-Barceló et al. (2014) also claimed that the order in which the treatment was administered affected resistance profiles to a greater extent than the antibiotic dose employed.

According to the National Institute of Health, up to 80% of chronic infections are biofilm related (National Institute of Health [NIH], 2007). Consequently, strategies aimed at eradicating biofilms are of clinical significance. A majority of the studies that have investigated the effects of antibiotic and phage treatment on biofilm eradication have administered the two antibacterial agents simultaneously (Bedi et al., 2009; Verma et al., 2009, 2010). These studies have demonstrated that the efficacy of such treatments vary, and is dependent on the antibiotic, bacteria, and the phage employed. However, the value of utilizing phage to augment antibiotic effects cannot be underestimated. Bedi et al. (2009) demonstrated that a significant reduction in biofilm mass could be achieved *in vitro* following combined therapy as a result of phage-mediated biofilm disruption. Additionally, successful *in vivo* studies and clinical data in human subjects highlight the promise of using phage in conjunction with antibiotics to treat recalcitrant infections such as *Staphylococcus* sepsis, lung infection, and osteomyelitis (Chhibber et al., 2013; Yilmaz et al., 2013; Kaur et al., 2016). A key study by Chaudhry et al. (2017) investigated different strategies of administrating phage and antibiotics to treat *P. aeruginosa* biofilms. They were able to demonstrate that the order in which the two treatments were administered greatly affected biofilm eradication outcomes (Chaudhry et al., 2017). This, to our knowledge, is the only study that has investigated the effect that an order of treatment has on biofilm eradication.

In the current study, we assessed whether phage can augment the activity of five antibiotics against *S. aureus* biofilms *in vitro*. In addition, the effectiveness of sequential or simultaneous administration of the treatments was compared. Our data demonstrated that the order in which *S. aureus* biofilms were exposed to the treatments was a key determinant of biofilm reduction outcomes. An analysis of the interplay between the antibiotics and the phage during simultaneous treatment demonstrated that of the five antibiotics tested, only dicloxacillin displayed additive interactions with the phage, while the other four antibiotics displayed predominantly antagonistic interactions at the different concentrations tested. This suggested that the interaction between phage and antibiotics was dependent on the antibiotic being studied. This observation is in line

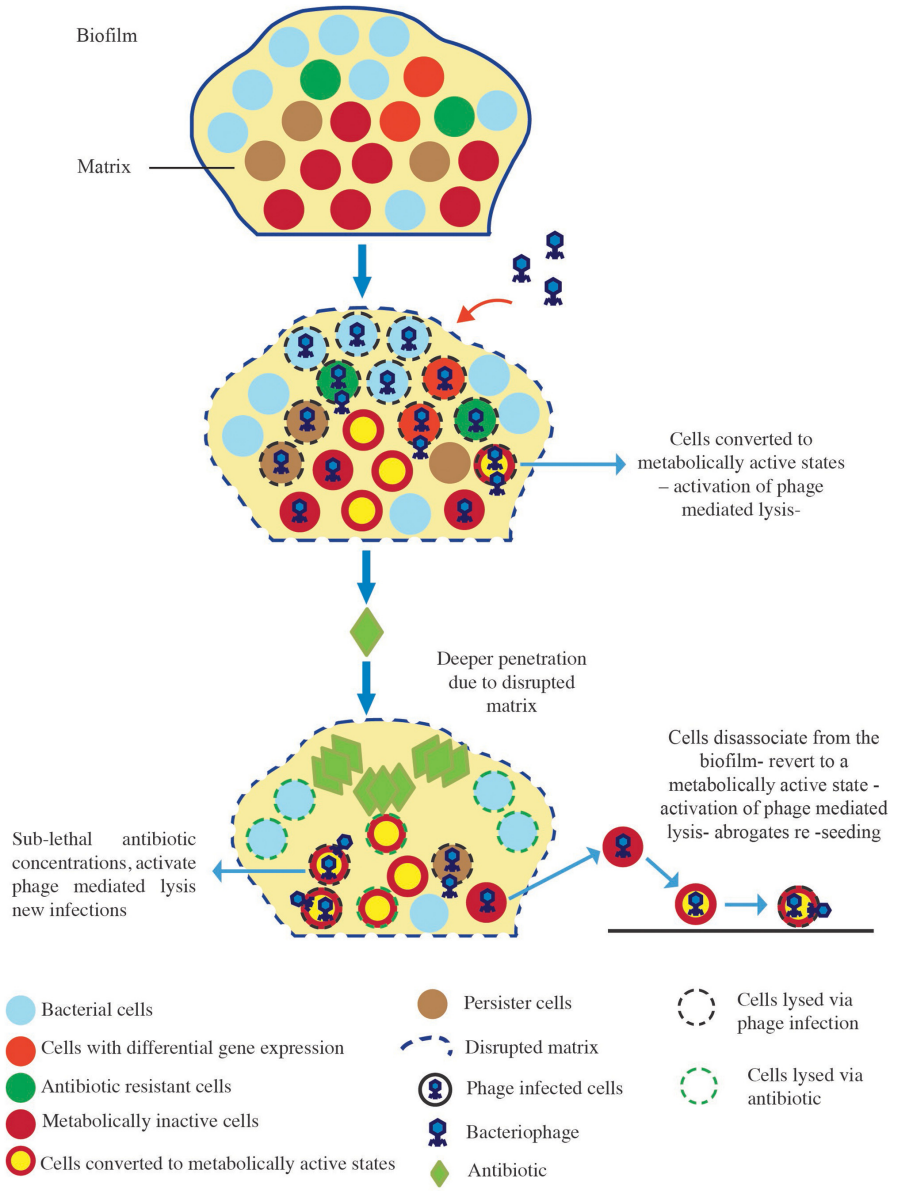

FIGURE 5 | Proposed model of biofilm reduction by the "phage first" staggered treatment. Exposure of the biofilm to phage first results in the disruption of the matrix, and the phage mediated lysis of biofilm-associated cells including antibiotic-resistant cells, differentially regulated cells, metabolically inactive cells, and persister cells. The addition of antibiotics to such a system leads to enhanced antibacterial effects due to higher local concentrations resulting from deeper penetration of these agents. Sub-lethal concentrations experienced by phage-infected cells in deeper layers of the biofilm elicit the activation of phage-mediated lysis resulting in further bacterial reductions.

with other *in vitro* studies that showed varying degrees of biofilm reduction when biofilms were treated simultaneously with antibiotics and phage (Verma et al., 2009, 2010; Chaudhry et al., 2017). Our findings gave credence to investigating other strategies that could be used to bolster the effects of phage and antibiotics. Consequently, we demonstrated that establishing a phage infection in the biofilm prior to antibiotic exposure led to the highest *S. aureus* biofilm reductions. Our results also highlighted that biofilm reduction after phage treatment was dependent on the type and concentration of antibiotics utilized. Furthermore, we were able to demonstrate that this strategy paved the way for synergistic interactions to occur between the phage and two antibiotics (vancomycin and cefazolin), leading to the highest biofilm reductions observed. Our results were comparable to those reported by Chaudhry et al. (2017) who observed enhanced eradication of *P. aeruginosa* biofilms that were pre-exposed to phage prior to gentamycin or tobramycin. Their group was also able to recover high phage titers when biofilms were treated with phage prior to antibiotic exposure, which translated to enhanced anti-biofilm activity. However,

much lower phage titers were obtained when other treatment strategies were employed, and were accompanied with lower anti-biofilm efficiencies. The treatment of biofilms with phage prior to antibiotics allows phages to rapidly replicate in the bacterially dense environment of the biofilm leading to high phage densities and the disruption of the biofilm matrix (Chaudhry et al., 2017). The addition of antibiotics to such a system leads to more robust bacterial reduction owing to the deeper penetration of these agents. However, when biofilms are exposed to antibiotics first followed by phage, the bacterial populations available for phage infection are reduced which can negatively affect infection kinetics and ultimately affect eradication outcomes (Payne and Jansen, 2000; Escobar-Páramo et al., 2012). Taken together, these factors can account for the heightened anti-biofilm activity observed in our study when a sequential (phage first) treatment approach was employed (**Figure 5**). Further investigation is needed to determine the precise mechanisms involved in the observed biofilm reduction.

The mode of action of the antibiotics being used in conjunction with phage may have contributed to the outcomes observed in our study. Cefazolin and vancomycin are both cell wall synthesis inhibitors, and when they were administered to biofilms following phage treatment it resulted in markedly higher biofilm eradication outcomes, especially at the lower concentrations tested. This can be explained by the fact that sub-lethal concentrations of antibiotics that affect cell wall integrity have been reported to activate the bacterial stress response resulting in an up-regulation of phage replication and cell lysis (Comeau et al., 2007; Chaudhry et al., 2017). The reduction in anti-biofilm activity observed at higher concentrations can be caused by diminished bacterial densities which curtail new phage infections, thereby diminishing the overall anti-biofilm effect. Interestingly, although dicloxacillin also affects cell wall integrity, a robust anti-biofilm reduction was not achieved when used in conjunction with phage. This observation suggested that other factors may play a role in biofilm elimination in combination therapy.

In this study, we have demonstrated that the antibiotic-mediated eradication of *S. aureus* biofilms can be augmented if a bacteriophage infection is established prior to antibiotic treatment. These results are the first to document the impact that an order of treatment has on *S. aureus* biofilm eradication. Our study shed light on the importance of investigating the effect treatment order can have in optimizing phage–antibiotic treatment efficacy against biofilms. Furthermore, results from the current study suggested that the success of such a treatment regimen depends on numerous factors including: the nature of the interaction between the phage and antibiotic, the type of antibiotic, and the concentration of antibiotic employed. Our findings provide a basis for parameters to be considered while assessing phage antibiotic pairings for the treatment of biofilm-related infections. Our work, as well as other *in vitro* studies, highlights the potential clinical benefit of combination therapies using libraries of lytic phages and antibiotics to treat biofilm-related infections.

AUTHOR CONTRIBUTIONS

DK and MT designed and conducted the experiments, analyzed the data, and drafted the manuscript. HA, QY, SR-A, J-SD, and AC contributed to the conception and design of the work and revised the manuscript critically.

FUNDING

This work was funded by The Ottawa Hospital Academic Medical Organization (TOHAMO) innovation fund.

ACKNOWLEDGMENTS

The authors would like to thank Zarique Akanda for preparing the schematics. They are grateful to Dr. Thien-Fah Mah for her conceptual advice. They would also like to especially thank the staff of the Centre for Innovation, Canadian Blood Services (Ottawa, ON, Canada) for their invaluable logistical and technical support.

REFERENCES

Archer, N. K., Mazaitis, M. J., Costerton, J. W., Leid, J. G., Powers, M. E., and Shirtliff, M. E. (2011). *Staphylococcus aureus* biofilms: properties, regulation, and roles in human disease. *Virulence* 2, 445–459. doi: 10.4161/viru.2.5.17724

Bedi, M. S., Verma, V., and Chhibber, S. (2009). Amoxicillin and specific bacteriophage can be used together for eradication of biofilm of *Klebsiella pneumoniae* B5055. *World J. Microbiol. Biotechnol.* 25, 1145–1151. doi: 10.1007/s11274-009-9991-8

Burrowes, B., Harper, D. R., Anderson, J., McConville, M., and Enright, M. C. (2011). Bacteriophage therapy: potential uses in the control of antibiotic-resistant pathogens. *Expert Rev. Anti Infect. Ther.* 9, 775–785. doi: 10.1586/eri.11.90

Chan, B. K., Sistrom, M., Wertz, J. E., Kortright, K. E., Narayan, D., and Turner, P. E. (2016). Phage selection restores antibiotic sensitivity in MDR *Pseudomonas aeruginosa*. *Sci. Rep.* 6:26717. doi: 10.1038/srep26717

Chaudhry, W. N., Concepción-Acevedo, J., Park, T., Andleeb, S., Bull, J. J., and Levin, B. R. (2017). Synergy and order effects of antibiotics and phages in killing *Pseudomonas aeruginosa* biofilms. *PLOS ONE* 12:e0168615. doi: 10.1371/journal.pone.0168615

Chhibber, S., Kaur, T., and Kaur, S. (2013). Co-therapy using lytic bacteriophage and linezolid: effective treatment in eliminating methicillin resistant *Staphylococcus aureus* (MRSA) from diabetic foot infections. *PLOS ONE* 8:e56022. doi: 10.1371/journal.pone.0056022

Clinical Laboratory Standards Institute [Clsi]. (2015). *M07-A10 Methods for Dilution Antimicrobial Susceptibility Tests for Bacteria That Grow Aerobically*, 10th Edn. Wayne, PA: Clinical Laboratory Standards Institute.

Comeau, A. M., Tétart, F., Trojet, S. N., Prere, M. F., and Krisch, H. M. (2007). Phage-antibiotic synergy (PAS): β-lactam and quinolone antibiotics stimulate virulent phage growth. *PLOS ONE* 2:e799. doi: 10.1371/journal.pone.0000799

Cornelissen, A., Ceyssens, P. J., T'syen, J., Van Praet, H., Noben, J. P., Shaburova, O. V., et al. (2011). The T7-related *Pseudomonas putida* phage φ15 displays virion-associated biofilm degradation properties. *PLOS ONE* 6:e18597. doi: 10.1371/journal.pone.0018597

Costerton, J. W., Stewart, P. S., and Greenberg, E. P. (1999). Bacterial biofilms: a common cause of persistent infections. *Science* 284, 1318–1322. doi: 10.1126/science.284.5418.1318

Cui, H., Ma, C., and Lin, L. (2016). Co-loaded proteinase K/thyme oil liposomes for inactivation of *Escherichia coli* O157: H7 biofilms on cucumber. *Food Funct.* 7, 4030–4040. doi: 10.1039/C6FO01201A

Doolittle, M. M., Cooney, J. J., and Caldwell, D. E. (1996). Tracing the interaction of bacteriophage with bacterial biofilms using fluorescent and chromogenic probes. *J. Ind. Microbiol.* 16, 331–341. doi: 10.1007/BF01570111

Doss, J., Culbertson, K., Hahn, D., Camacho, J., and Barekzi, N. (2017). A review of phage therapy against bacterial pathogens of aquatic and terrestrial organisms. *Viruses* 9:E50. doi: 10.3390/v9030050

Escobar-Páramo, P., Gougat-Barbera, C., and Hochberg, M. E. (2012). Evolutionary dynamics of separate and combined exposure of *Pseudomonas fluorescens* SBW25 to antibiotics and bacteriophage. *Evol. Appl.* 5, 583–592. doi: 10.1111/j.1752-4571.2012.00248.x

Fauvart, M., De Groote, V. N., and Michiels, J. (2011). Role of persister cells in chronic infections: clinical relevance and perspectives on anti-persister therapies. *J. Med. Microbiol.* 60, 699–709. doi: 10.1099/jmm.0.030932-0

Gordon, C. A., Hodges, N. A., and Marriott, C. (1988). Antibiotic interaction and diffusion through alginate and exopolysaccharide of cystic fibrosis-derived *Pseudomonas aeruginosa*. *J. Antimicrob. Chemother.* 22, 667–674. doi: 10.1093/jac/22.5.667

Gutiérrez, D., Martínez, B., Rodríguez, A., and García, P. (2012). Genomic characterization of two *Staphylococcus epidermidis* bacteriophages with anti-biofilm potential. *BMC Genomics* 13:228. doi: 10.1186/1471-2164-13-228

Kaur, S., Harjai, K., and Chhibber, S. (2016). *In Vivo* assessment of phage and linezolid based implant coatings for treatment of methicillin resistant *Staphylococcus aureus* (MRSA) mediated orthopaedic device related infections. *PLOS ONE* 11:e0157626. doi: 10.1371/journal.pone.0157626

Lauderdale, K. J., Malone, C. L., Boles, B. R., Morcuende, J., and Horswill, A. R. (2010). Biofilm dispersal of community-associated methicillin-resistant *Staphylococcus aureus* on orthopedic implant material. *J. Orthop. Res.* 28, 55–61. doi: 10.1002/jor.20943

Lebeaux, D., Ghigo, J. M., and Beloin, C. (2014). Biofilm-related infections: bridging the gap between clinical management and fundamental aspects of recalcitrance toward antibiotics. *Microbiol. Mol. Biol. Rev.* 78, 510–543. doi: 10.1128/MMBR.00013-14

Lister, J. L., and Horswill, A. R. (2014). *Staphylococcus aureus* biofilms: recent developments in biofilm dispersal. *Front. Cell. Infect. Microbiol.* 4:178. doi: 10.3389/fcimb.2014.00178

Loc-Carrillo, C., and Abedon, S. T. (2011). Pros and cons of phage therapy. *Bacteriophage* 1, 111–114. doi: 10.4161/bact.1.2.14590

Lynch, S. V., Dixon, L., Benoit, M. R., Brodie, E. L., Keyhan, M., Hu, P., et al. (2007). Role of the *rapA* gene in controlling antibiotic resistance of *Escherichia coli* biofilms. *Antimicrob. Agents Chemother.* 51, 3650–3658. doi: 10.1128/AAC.00601-07

MacNeal, W. J., and Frisbee, F. C. (1936). One hundred patients with Staphylococcus septicemia receiving bacteriophage service. *Am. J. Med. Sci.* 191, 179–195. doi: 10.1097/00000441-193602000-00004

Mah, T. F., Pitts, B., Pellock, B., Walker, G. C., Stewart, P. S., and O'toole, G. A. (2003). A genetic basis for *Pseudomonas aeruginosa* biofilm antibiotic resistance. *Nature* 426, 306–310. doi: 10.1038/nature02122

Mah, T. F. C., and O'Toole, G. A. (2001). Mechanisms of biofilm resistance to antimicrobial agents. *Trends Microbiol.* 9, 34–39. doi: 10.1016/S0966-842X(00)01913-2

National Institute of Health [NIH]. (2007). *Department of Health and Human Services. Immunology of Biofilms*. Available at: http://grants.nih.gov/grants/guide/pa-files/PA-07-288.html [accessed November 08, 2017].

Parasion, S., Kwiatek, M., Gryko, R., Mizak, L., and Malm, A. (2014). Bacteriophages as an alternative strategy for fighting biofilm development. *Pol. J. Microbiol.* 63, 137–145.

Payne, R. J., and Jansen, V. A. (2000). Phage therapy: the peculiar kinetics of self-replicating pharmaceuticals. *Clin. Pharmacol. Ther.* 68, 225–230. doi: 10.1067/mcp.2000.109520

Pearl, S., Gabay, C., Kishony, R., Oppenheim, A., and Balaban, N. Q. (2008). Nongenetic individuality in the host–phage interaction. *PLOS Biol.* 6:e120. doi: 10.1371/journal.pbio.0060120

Reffuveille, F., de la Fuente-Núñez, C., Mansour, S., and Hancock, R. E. (2014). A broad-spectrum antibiofilm peptide enhances antibiotic action against bacterial biofilms. *Antimicrob. Agents Chemother.* 58, 5363–5371. doi: 10.1128/AAC.03163-14

Römling, U., and Balsalobre, C. (2012). Biofilm infections, their resilience to therapy and innovative treatment strategies. *J. Intern. Med.* 272, 541–561. doi: 10.1111/joim.12004

Salmond, G. P., and Fineran, P. C. (2015). A century of the phage: past, present and future. *Nat. Rev. Microbiol.* 3, 777–786. doi: 10.1038/nrmicro3564

Schultz, E. W. (1929). The bacteriophage as a therapeutic agent. *Cal. West. Med.* 31, 5–10.

Tande, A. J., and Patel, R. (2014). Prosthetic joint infection. *Clin. Microbiol. Rev.* 27, 302–345. doi: 10.1128/CMR.00111-13

Torres-Barceló, C., Arias-Sánchez, F. I., Vasse, M., Ramsayer, J., Kaltz, O., and Hochberg, M. E. (2014). A window of opportunity to control the bacterial pathogen *Pseudomonas aeruginosa* combining antibiotics and phages. *PLOS ONE* 9:e106628. doi: 10.1371/journal.pone.0106628

Verma, V., Harjai, K., and Chhibber, S. (2009). Restricting ciprofloxacin-induced resistant variant formation in biofilm of *Klebsiella pneumoniae* B5055 by complementary bacteriophage treatment. *J. Antimicrob. Chemother.* 64, 1212–1218. doi: 10.1093/jac/dkp360

Verma, V., Harjai, K., and Chhibber, S. (2010). Structural changes induced by a lytic bacteriophage make ciprofloxacin effective against older biofilm of *Klebsiella pneumoniae*. *Biofouling* 26, 729–737. doi: 10.1080/08927014.2010.511196

Yilmaz, C., Colak, M., Yilmaz, B. C., Ersoz, G., Kutateladze, M., and Gozlugol, M. (2013). Bacteriophage Therapy in Implant-Related Infections: an experimental study. *J. Bone. Joint. Surg. Am.* 95, 117–125. doi: 10.2106/JBJS.K.01135

Zhang, Q. G., and Buckling, A. (2012). Phages limit the evolution of bacterial antibiotic resistance in experimental microcosms. *Evol. Appl.* 5, 575–582. doi: 10.1111/j.1752-4571.2011.00236.x

Conflict of Interest Statement: The authors declare that the research was conducted in the absence of any commercial or financial relationships that could be construed as a potential conflict of interest.

frontiers in Microbiology

ORIGINAL RESEARCH
published: 16 November 2017
doi: 10.3389/fmicb.2017.02257

Therapeutic Application of Phage Capsule Depolymerases against K1, K5, and K30 Capsulated *E. coli* in Mice

Han Lin[1], *Matthew L. Paff*[1,2], *Ian J. Molineux*[2,3]* *and James J. Bull*[1,2,4]*

[1] Department of Integrative Biology, The University of Texas at Austin, Austin, TX, United States, [2] Institute for Cellular and Molecular Biology, The University of Texas at Austin, Austin, TX, United States, [3] Department of Molecular Biosciences, The University of Texas at Austin, Austin, TX, United States, [4] Center for Computational Biology and Bioinformatics, The University of Texas at Austin, Austin, TX, United States

Capsule depolymerase enzymes offer a promising class of new antibiotics. *In vivo* studies are encouraging but it is unclear how well this type of phage product will generalize in therapeutics, or whether different depolymerases against the same capsule function similarly. Here, *in vivo* efficacy was tested using cloned bacteriophage depolymerases against *Escherichia coli* strains with three different capsule types: K1, K5, and K30. When treating infections with the cognate capsule type in a mouse thigh model, the previously studied K1E depolymerase rescued poorly, whereas K1F, K1H, K5, and K30 depolymerases rescued well. K30 gp41 was identified as the catalytically active protein. In contrast to the *in vivo* studies, K1E enzyme actively degraded K1 capsule polysaccharide *in vitro* and sensitized K1 bacteria to serum killing. The only *in vitro* correlate of poor K1E performance *in vivo* was that the purified enzyme did not form the expected trimer. K1E appeared as an 18-mer which might limit its *in vivo* distribution. Overall, depolymerases were easily identified, cloned from phage genomes, and as purified proteins they proved generally effective.

Keywords: bacterial capsule, phage, capsule depolymerase, infection, antibiotic

OPEN ACCESS

Edited by:
Sanna Sillankorva, University of Minho, Portugal

Reviewed by:
Zuzanna Drulis-Kawa, University of Wrocław, Poland
Diana Gutiérrez, Instituto de Productos Lácteos de Asturias (CSIC), Spain

***Correspondence:**
Ian J. Molineux
molineux@austin.utexas.edu
James J. Bull
bull@utexas.edu

Specialty section:
This article was submitted to Antimicrobials, Resistance and Chemotherapy, a section of the journal Frontiers in Microbiology

Received: *19 July 2017*
Accepted: *31 October 2017*
Published: *16 November 2017*

Citation:
Lin H, Paff ML, Molineux IJ and Bull JJ (2017) Therapeutic Application of Phage Capsule Depolymerases against K1, K5, and K30 Capsulated E. coli in Mice. Front. Microbiol. 8:2257. doi: 10.3389/fmicb.2017.02257

INTRODUCTION

Both intact phages and their proteins are promising therapies for antibiotic resistant bacteria (Lewis, 2013; Drulis-Kawa et al., 2015; Abedon et al., 2017) especially given the current slow pace of new antibiotic discovery (Silver, 2011). Phage therapy's advantages include high host specificity, amplification where bacteria are dense, an abundance and diversity of wild phages, and evolution in response to bacterial resistance (Weber-Dabrowska et al., 2016). Yet there are also drawbacks, such as the need to match phages to the infecting strain and the simple fact that bacteria have many mechanisms of escape.

The use of intact phages to treat infections is an old concept; the first phage therapy in humans was attempted in 1919 (D'Herelle and Smith, 1926; Sulakvelidze et al., 2001) and the first report of clinical phage therapy was published in 1921 (Bruynoghe and Maisin, 1921). More recently, it has been realized that therapy may utilize phage proteins instead of intact phages. These alternative technologies have many advantages of phages – an abundant and diverse collection of phage proteins occur in nature, evolved specifically to act against bacteria, and they potentially overcome

one of the main drawbacks of traditional phage therapy, namely the narrow specificity of phages. Thus, Gram-positive phage endolysins also lyse Gram-positive bacteria from the outside and have far broader host ranges than do individual phages (Fischetti, 2011; Pastagia et al., 2013; Nakonieczna et al., 2015; Pires et al., 2016). Mycobacterial phage endolysins have activity against mycobacteria when added to cells (Payne and Hatfull, 2012; Grover et al., 2014), and combining an endolysin with a cell-permeating peptide (Artilysin®) also shows promise for disrupting the complex cell envelope of Gram-negative bacteria (Briers et al., 2014; Gerstmans et al., 2016; Pires et al., 2016). Phage-encoded polysaccharide depolymerases, which potentially also have a broad host range, can degrade carbohydrate barriers on bacterial cell surfaces such as capsule, lipopolysaccharide and biofilm matrix to compromise bacterial virulence (Latka et al., 2017). Capsule depolymerases are one class of polysaccharide depolymerases that can strip capsules and thereby expose bacteria to immune attack, with the further advantage that the bacteria are not lysed and thus do not release endotoxins (Azeredo and Sutherland, 2008).

A bacterial capsule is a thick polysaccharide layer found on many bacteria. Over 80 different types of *Escherichia coli* capsules have been identified and classified into four groups, based on their varied serological, biochemical and genetic properties (Orskov et al., 1977; Whitfield, 2006). Our work involves K1 and K5 capsules in Group 2, two types highly frequently found in extra-intestinal infection (Orskov et al., 1977), and the K30 capsule in Group 1, a type found in intestinal infection and well-studied for capsule biosynthesis (Whitfield, 2006). Characterization of capsules surrounding other bacteria has revealed both the same and novel structures but nomenclature is often specific for a particular genus (Orskov et al., 1977; Roberts, 1996). Possible functions of capsules include protecting bacteria from desiccation, bacterial adherence to surfaces and to each other, helping bacteria escape complement-mediated killing or phagocytosis, and resisting immune response (Roberts, 1996).

Phages that grow on capsulated strains commonly encode tailspike enzymes that degrade the capsule, providing a ready source of enzymes. Some capsule depolymerases assemble as trimers with the help of a C-terminal domain that functions as a chaperone, which is then autoproteolytically cleaved (Gerardy-Schahn et al., 1995; Muhlenhoff et al., 2003; Schwarzer et al., 2007, 2012; Leiman and Molineux, 2008). One of the depolymerases used in this work, K1E, assembles on the phage virion using an adaptor protein, which in addition likely contributes to accurate trimerization (Tomlinson and Taylor, 1985; Gerardy-Schahn et al., 1995; Stummeyer et al., 2006). However, other tailspike enzymes, e.g., P22 gp9, autonomously fold as a trimer and spontaneously assemble correctly on a mature phage head, although a cellular chaperone may improve efficiency (Brunschier et al., 1993).

This study tests capsule depolymerases as therapeutic agents against capsulated bacteria. The few experimental studies of phage depolymerase treatments in rodents, including those with the K1E depolymerase in a neonatal rat infection model, have met with apparent success (Mushtaq et al., 2004, 2005; Lin et al., 2014; Pan et al., 2015), but the generality and wide-scale technical feasibility of the approach remains unclear because few types of capsules and depolymerases have been tested. Further, different infection models have been used, and different enzymes degrading the same capsule have not been compared side-by-side. Further evidence of depolymerase efficacy is offered here for five different phage depolymerases against three capsule types in a mouse infection model.

MATERIALS AND METHODS

Strains and Culture Conditions

The *E. coli* strains RS218 (O18:K1:H7) (Achtman et al., 1983), ATCC 23506 (O10:K5(L):H4), and E69 (O9:K30) (Orskov et al., 1977) were used for mouse infection, capsule isolation and serum sensitivity assays. *E. coli* BL21(DE3) was used for protein expression and purification. Bacteria were grown in LB (10 g tryptone, 5 g yeast extract, 10 g NaCl per liter) broth in 37°C shakers unless otherwise noted. The concentration of viable bacteria was determined by colony counts using LB agar (1.3% w/v) plates.

The *E. coli* strain EV36 (Vimr and Troy, 1985) was used to propagate the coliphages K1E, K1F, and K1H (Bull et al., 2010). *E. coli* ATCC 23506 and E69 were used for propagation, respectively, of the coliphages K1-5 (Scholl et al., 2001, 2004) and K30 (Whitfield and Lam, 1986). Phages were grown and purified as previously described (Scholl et al., 2001; Leiman et al., 2007). Briefly, the coliphages were added to bacterial cultures at an $OD_{600} = 0.25–0.4$ at a multiplicity of infection of 4, followed by incubation at 37°C with aeration until the culture cleared. Phages were precipitated with 0.5 M NaCl and 10% PEG 8000, and then purified by equilibrium CsCl gradient centrifugation in SM buffer (50 mM Tris–HCl, 100 mM NaCl, 8 mM $MgSO_4$, pH 7.5) supplemented with CsCl to a density of 1.5 g/ml. After dialysis into SM buffer using 12–14 kDa MWCO dialysis membranes (Spectrum), phage titers were determined by plaque counts using a LB soft agar (0.65%) overlay.

Cloning of Phage Capsule Depolymerase Genes

Phage genomic DNA was extracted as described for phage λ (Sambrook et al., 1989), and then was used as template to amplify the depolymerase genes K1E, K1F, K1H, K5 or those for the putative enzymes K30 gp41 and K30 gp42. Gene information and the PCR primers are listed in Supplementary Table S1. PCR products were then assembled into NdeI- and EcoRI-digested pET28b (EMD Biosciences Inc.) using the Gibson Assembly Master Mix (NEB Inc.).

Protein Expression and Purification

After overexpression of their genes, capsule depolymerases were purified essentially as previously described (Leggate et al., 2002). Briefly, the pET28b derivatives were transformed into *E. coli* BL21(DE3). Expression of the recombinant His-tagged depolymerase genes was induced at $A_{600} = 0.6$ with

0.5 mM isopropyl-β-D-thiogalactopyranoside (IPTG) followed by overnight growth at 20°C. Cells were lysed by sonication in lysis buffer (50 mM Na_2HPO_4, 300 mM NaCl, 10 mM imidazole, pH 7.5) and the depolymerases were purified using HisPur Ni-NTA resin (Thermo Fisher Scientific Inc.) according to the user guide. After dialysis into phosphate-buffered saline (PBS) buffer (137 mM NaCl, 2.7 mM KCl, 10 mM Na_2HPO_4, 1.8 mM KH_2PO_4, pH 7.5) using 3.5 kDa MWCO dialysis membranes (Spectrum), the depolymerases were used directly in all experiments. Protein concentrations were estimated by A_{280}, using a Nanodrop ND-1000.

Purified proteins were analyzed by SDS-PAGE and size exclusion chromatography. SDS-PAGE was performed using a 10% resolving gel with a 4% stacking gel. Proteins were denatured at 100°C for 5 min. After electrophoresis, proteins were stained with Coomassie brilliant blue. Size exclusion chromatography was performed on an AKTA FPLC (GE Healthcare) at 4°C. Depolymerases, in 25 mM sodium phosphate, 150 mM NaCl, pH 7.5, were applied to a Superose 6 10/300 GL column (GE Healthcare). Elution was at a flow rate of 0.4 ml/min and proteins were detected at A_{280}. Molecular weights were estimated using the high molecular weight gel filtration calibration kit (GE Healthcare).

Mouse Infections and Depolymerase Treatment

Mouse work conformed to NIH guidelines and the University of Texas IACUC protocol approval (AUP-2015-00035). 4–6 weeks old female NIH Swiss outbred mice (Envigo Inc.) weighing 20–25 g were used. For infections, $1 - 4 \times 10^8$ CFU (colony forming units) of bacteria in up to 100 µl were injected into the left thigh (Smith and Huggins, 1982; Bull et al., 2012; Ponnusamy et al., 2016). Doses ranged from 1.2 to 3.5×10^8 CFU for *E. coli* RS218, $1.7 - 3.7 \times 10^8$ CFU for *E. coli* ATCC 23506, and $1.0–3.7 \times 10^8$ CFU for *E. coli* E69. The lower end of the dose range may be near a threshold that enables viability, e.g., infection by 1.2×10^8 CFU of *E. coli* ATCC 23506 allowed 2 of 3 control mice to survive, whereas doses above 1.7×10^8 CFU were routinely inimical to survival.

Treatment was performed by injecting a depolymerase appropriate for the capsule type into the right thigh within 0.5 h after the bacterial injection, i.e., K1E, K1F, or K1H depolymerase with *E. coli* RS218, K5 depolymerase with *E. coli* ATCC 23506, K30 gp41 or K30 gp42 with *E. coli* E69. Different doses were obtained by dilution of the stock depolymerase into PBS to yield 100 µl for an injection. The effective doses were first determined by giving 3 mice each dose (0, 2, 5, or 20 µg). Optimal doses were then used with more mice to allow statistical analysis of therapeutic efficacy. Mice were monitored at least twice daily for 5 days, and moribund mice were euthanized. The numbers of surviving mice at Day 5 were plotted, and Fisher's Exact Test was used to evaluate the therapeutic efficacy of a depolymerase. Using SPSS software, Kaplan–Meier survival curves (Rich et al., 2010) were plotted to show the cumulative probability of survival over the 5-day period, using the Log Rank test or generalized Wilcoxon test for statistics.

To assess potential acute toxicity from the depolymerase, 3–5 mice were injected with 100 µg of depolymerase (in 100 µl PBS) or 100 µl PBS alone in the right thigh, in the absence of bacterial infection. Mice were monitored for 5 days for survival; behavior and daily body weights were measured. Statistics of the body weight gains over 5 days were performed by mixed ANOVA with repeated measures using SPSS software.

Capsule Polysaccharide Isolation and Assay

Escherichia coli RS218, ATCC 23506 and E69 were grown overnight at 37°C in defined medium (10 g Casamino Acids, 10 g glucose, 12.5 g $Na_2HPO_4 \cdot 2H_20$, 0.9 g KCl, and 0.6 g $MgSO_4 \cdot 7H_20$ per liter). Isolation of K1, K5, or K30 type capsule used extraction with pyridine acetate as previously described (Pelkonen et al., 1988). Capsules were dissolved in sterile water and stored at 4°C. The capsule concentrations were quantified by the phenol-sulfuric acid method (Dubois et al., 1956), using glucose to generate standard curves.

Degradation of capsules was monitored by gel electrophoresis followed by alcian blue staining (Møller et al., 1993; Pan et al., 2013). 10–20 µg of capsule was mixed with serial dilutions of corresponding depolymerase and incubated at 37°C for 1 h (K1E, K1F, or K1H depolymerase with K1 capsule; K5 depolymerase with K5 capsule; K30 gp41 or K30 gp42 with K30 capsule). Reactions were loaded on 12% TBE-PAGE (Tris-Boric acid-EDTA polyacrylamide gel electrophoresis) essentially as previously described (Pelkonen et al., 1988). XC (xylene cyanol), BPB (bromophenol blue) and PR (phenol red) were used together with all blue protein standards (Bio-Rad Inc.) as tracking dyes and molecular weight markers.

Quantitative analyses of depolymerase activity were performed by incubating 30–45 µg of capsule with serial dilutions of depolymerase, or by incubating 10 µg/ml depolymerase with serial dilutions of capsule, both for 30 min at 37°C, followed by determination of reducing sugar using the modified dinitrosalicylic acid (DNSA) reagent (Miller, 1959). Glucose served as the standard. The quantity of reducing sugar released against enzyme concentration was plotted, and enzyme specific activity is expressed as nmol glucose equivalents released per min per mg protein (McCallum et al., 1989). Hanes–Woolf plots (a/v against a, where a is the capsule concentration and v is the reaction velocity) allowed the determination of kinetic parameters, assuming K1 capsule at a molecular weight of 54 kDa (Hallenbeck et al., 1987; Leggate et al., 2002).

Serum Sensitivity Assay

The assay was adapted from previous work (Podschun et al., 1993; Fang et al., 2004; Mushtaq et al., 2004). Briefly, $4–6 \times 10^7$ CFU/ml of log phase bacteria were incubated with or without depolymerase (100 µg/ml) for 1.5 (K1, K5) or 2 h (K30) at 37°C. Mixtures were diluted and $4–6 \times 10^4$ cells were incubated with 75% of human serum (Sigma–Aldrich Inc.), heat inactivated serum (56°C, 30 min) or PBS for 1.5

(K5) or 2 h (K1, K30) at 37°C and then plated to determine CFU. Assays were repeated at least three times, and Student's *t*-test with an appropriately adjusted degree of freedom was used to evaluate the enzyme's effect in sensitizing cells to serum killing by the survival ratio X(serum)/X(PBS), where *X* is CFU/ml. The null hypothesis is that one treatment is the same as the other, or X1(serum)/X1(PBS) = X2(serum)/X2(PBS), i.e., log [X1(serum)] – log[X1(PBS)] – {log [X2(serum)] – log[X2(PBS)]} = 0.

RESULTS

Expression and Purification of Recombinant Depolymerases

Depolymerases from phages K1E, K1F, K1H, and K5 were purified from expression plasmids of previously identified genes (Petter and Vimr, 1993; Long et al., 1995; Clarke et al., 2000; Machida et al., 2000; Muhlenhoff et al., 2003; Scholl et al., 2004). K30 depolymerase was described as a trimer of a heterodimer of 90 and 52 kDa proteins (McCallum et al., 1989). Inspection of the subsequently deposited and annotated K30 genome sequence (Genbank NC_015719), which is largely syntenic with the well-characterized T7 genome, revealed only two likely candidate genes for the proteins: the K30 gene *42* product is a putative lipase/acylhydrolase, and gene *41* is a putative tailspike. Expected sizes of both proteins correspond to subunits of the depolymerase originally characterized biochemically. Both genes were therefore cloned into expression plasmids and all the His-tagged proteins were purified, yielding approximately 10 mg of K5 or K30 gp41 per liter culture, 20 – 30 mg per liter of K1E, K1F, or K1H, and 40 mg per liter of K30 gp42. We therefore expressed and tested a total of six proteins, including four depolymerases and two putative depolymerases.

The affinity-purified K1 and K5 depolymerases migrated on SDS-PAGE in accordance with their expected sizes after proteolysis (K1E 76 kDa, K1F 103 kDa, K1H 93 kDa and K5 52 kDa) (**Figure 1**). Sizes of the two K30 proteins were estimated to be 97 and 57 kDa, suggesting that they are not post-translationally cleaved. By densitometry analysis all purified proteins appeared >90% pure in SDS-PAGE.

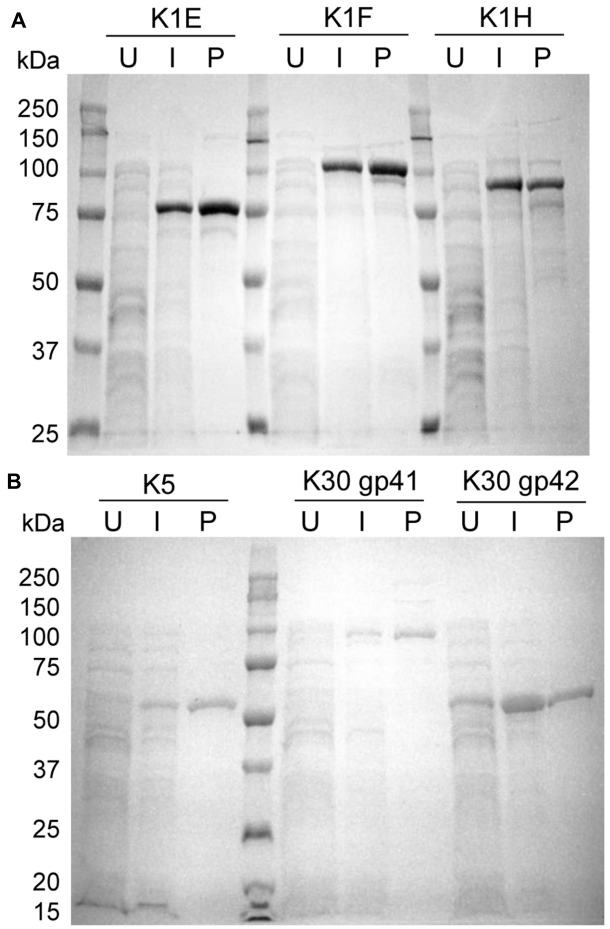

FIGURE 1 | Expression and purification of recombinant K1, K5, and K30 depolymerases. **(A)** SDS-PAGE showing induced expression and purification of K1E, K1F, and K1H depolymerases. 50 μg of uninduced or induced whole cell lysate obtained after sonication, or 2 μg of enzyme purified was fractionated by SDS-PAGE followed by Coomassie Blue staining. U, uninduced whole cell lysate; I, induced whole cell lysate; P, purified enzyme. **(B)** SDS-PAGE of K5 and putative K30 depolymerases after a similar induction and protein purification.

Capsule Depolymerases Can Be Effective Therapeutics

Capsule depolymerases were tested in a mouse thigh model of infection. Without treatment, infection was usually lethal, whereas most mice were rescued by treatment when the enzyme dose was 20 μg per mouse, i.e., 0.8–1 mg/kg weight (**Figures 2**, **3**). The exception was the K1E enzyme, which rescued only 3 of 32 mice at a dose of 20 μg per mouse (**Figures 2A**, **3A**). Preliminary trials of the three K1 enzymes at lower doses suggested the effective doses of K1F and K1H were between 2 μg (both partially rescuing) and 5 μg (both rescuing 3 of 3 mice) per mouse (**Figure 2A**).

For K5, the effective dose was between 2 and 20 μg per mouse (**Figures 2B**, **3B**). Of the two putative K30 depolymerases, only K30 gp41 rescued mice and then only at the higher dose tested (20 μg per mouse) (**Figures 2C**, **3C**). A mixture of both K30 gp41 and K30 gp42 yielded the same survival outcome as K30 gp41 alone (**Figure 2C**), although the small sample size limits a statistical resolution. K30 gp41 appears somewhat less effective than K5 and two of the K1 enzymes.

To evaluate potential acute toxicity from enzyme injection, mice received 100 μg of depolymerase in the right thigh and were monitored for survival, behavior and body weight gains for 5 days. All the mice survived and appeared healthy without any behavior change observed. Statistics by ANOVA indicates no significant difference in body weight gains of the treated mice compared to that of the control mice receiving PBS injection (Supplementary Figure S1). These indicate no or little toxicity from enzyme injection.

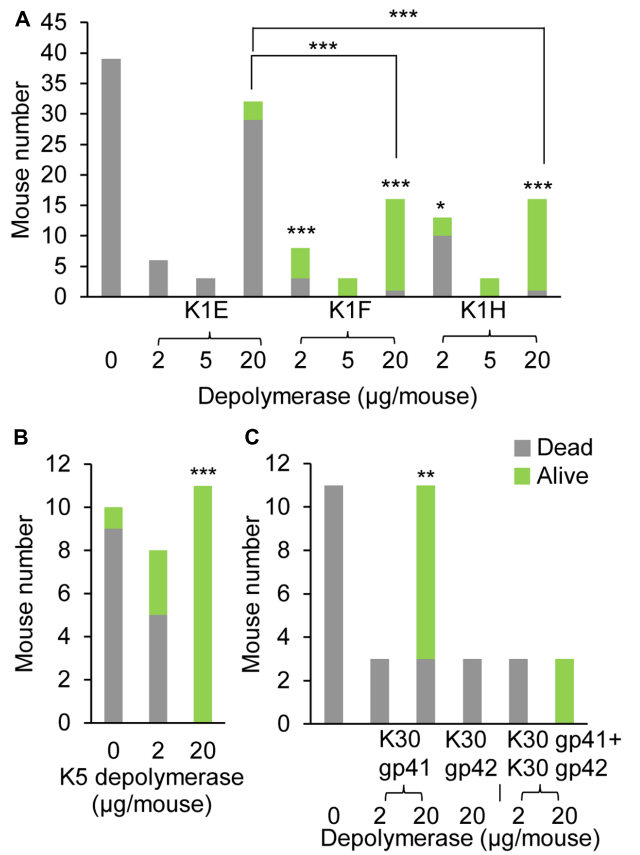

FIGURE 2 | Mouse survival at Day 5 post infection and depolymerase treatment. 1.2–3.5 × 10^8 CFU of *Escherichia coli* RS218 **(A)**, 1.7–3.7 × 10^8 of *E. coli* ATCC 23506 **(B)**, or 1.0–3.7 × 10^8 of *E. coli* E69 **(C)** were injected to the left thigh, followed by corresponding depolymerase injection in the right thigh at various doses. Three mice each dose were preliminarily tested for dose titration, then more mice were repeated at select doses to validate the treatment efficacy. Mouse survival was monitored for 5 days. The numbers of surviving and dead mice at day 5 were evaluated by Fisher's Exact Test for treatments with $n >= 8$: $^*p < 0.05$, $^{**}p < 0.01$, $^{***}p < 0.001$ compared to control or as noted.

In Vitro Depolymerase Assays

The depolymerases were generally effective for the *in vivo* treatment, but different enzymes also showed differences in efficacy, especially K1E, which was a relatively poor therapeutic agent. K30 gp42 had no effect and likely lacks depolymerase activity. Therefore, *in vitro* assays were conducted to directly assess enzyme activities.

Activities of the different K1 enzymes were compared using a gel assay to monitor capsule degradation. Apparent complete degradation (by visual inspection) of 10–20 μg of K1 capsule in 1 h was achieved by 4–8 μg/ml of K1E or K1F depolymerase, and by 8–16 μg/ml of the K1H enzyme (**Figure 4A**). Two μg/ml of K1E or K1F enzyme completely degraded the capsule within 3 h, but K1H was again significantly less effective (data not shown). Thus, both K1E and K1F perform better than K1H during *in vitro* capsule degradation, in contrast to *in vivo* therapeutic efficiencies.

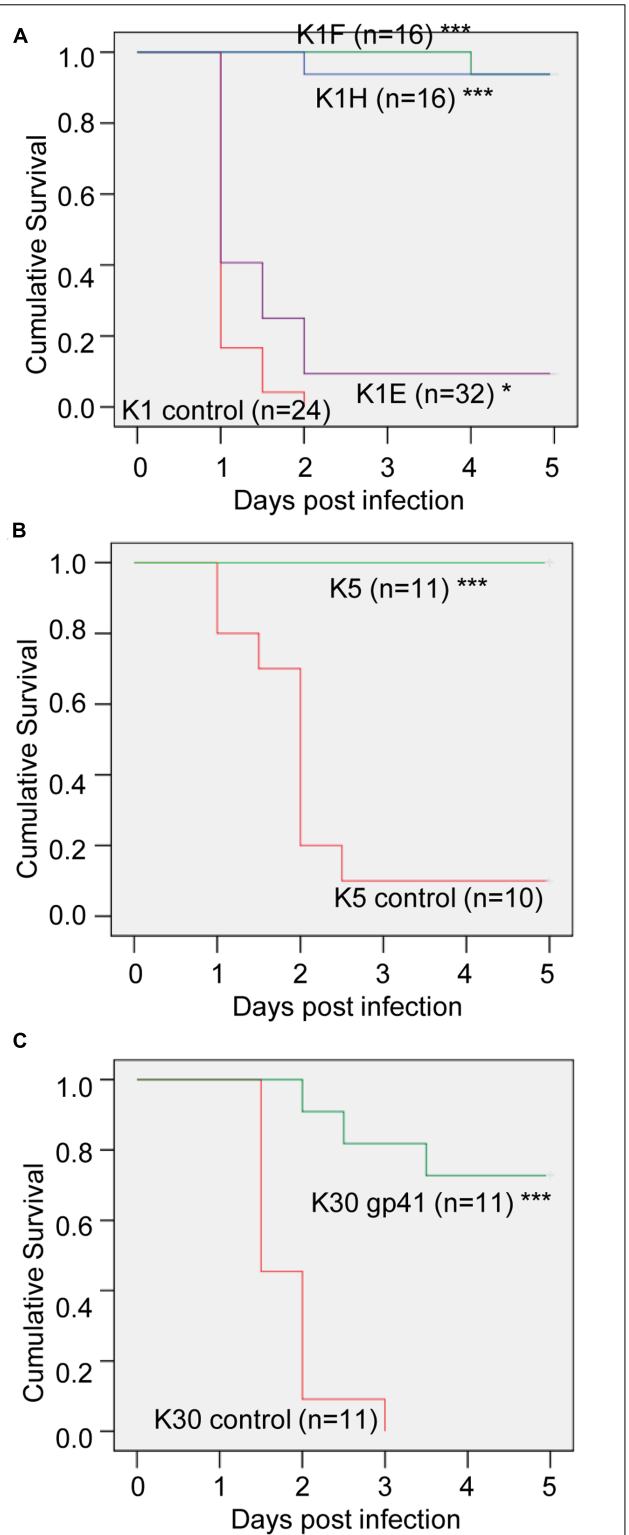

FIGURE 3 | Mouse survival curves of depolymerase treatment. Kaplan–Meier survival curves of the 20 μg-K1 **(A)**, K5 **(B)**, or K30 **(C)** depolymerase treated mice and control mice in **Figure 2** were plotted with the cumulative probability of survival over 5 days. The total mouse number n of each treatment is labeled by each curve. Log Rank test or generalized Wilcoxon test: $^*p < 0.05$, $^{***}p < 0.001$ compared to control.

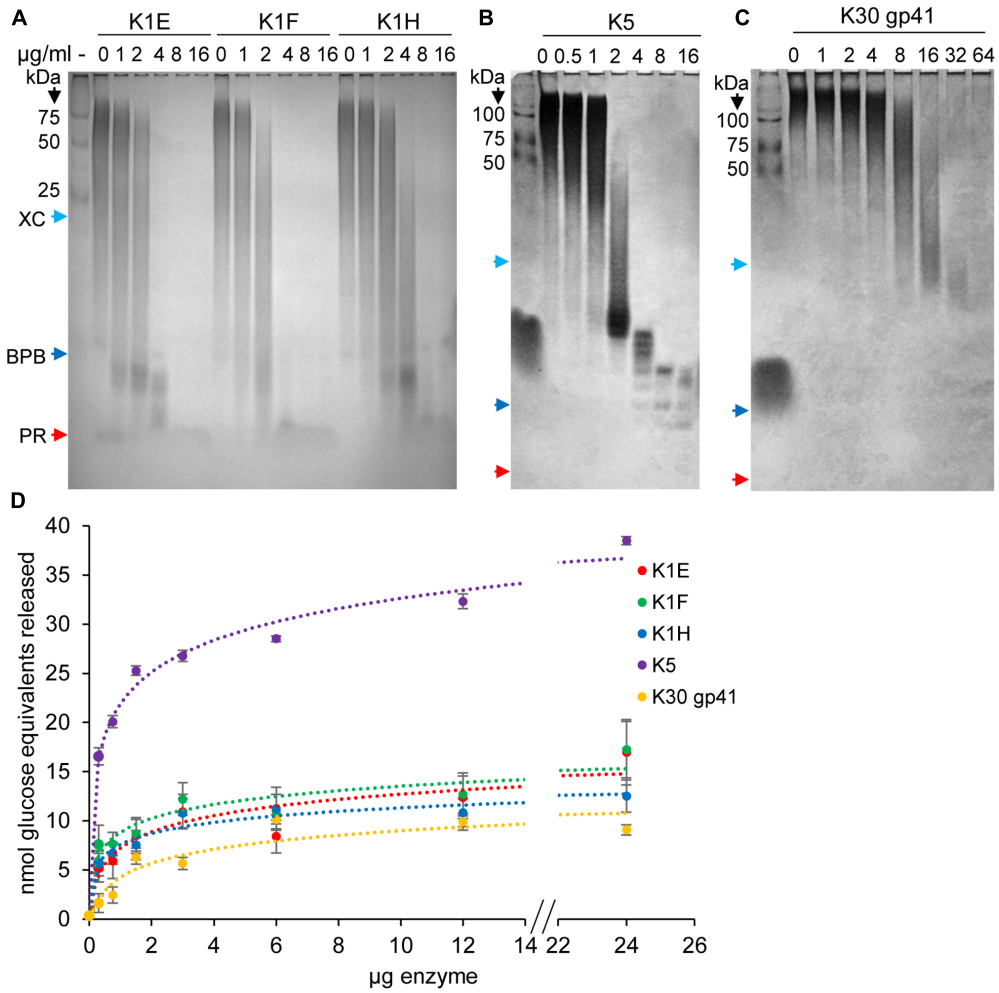

FIGURE 4 | Capsule degradation by depolymerases. **(A)** 10–20 µg of K1 capsule was incubated with serial dilutions of K1E, K1F, or K1H depolymerase at 37°C for 1 h, and then fractionated using 12% TBE-PAGE gel followed by Alcian Blue staining. Protein standards and dyes (XC, xylene cyanol FF; BPB, bromophenol blue; PR, phenol red) were loaded as molecular weight markers. Similar assays were performed using K5 **(B)** or putative K30 **(C)** depolymerase and their respective capsules. **(D)** Quantitative assay of capsule degradation by depolymerases. 30–45 µg of capsule was incubated with ranged doses of depolymerase for 30 min at 37°C. The product of reducing sugar was quantified by dinitrosalicylic acid (DNSA), with glucose as standard. The calculated amount of reducing sugar (nmol glucose equivalents) was plotted against enzyme doses.

K1E depolymerase activity was quantified by assaying reducing sugar release from capsule (**Figure 4D** and Supplementary Table S2). Assays with 30 µg of K1 capsule and varying K1 enzyme doses showed similar kinetics of the three K1 enzymes, with similar specific activities at lower enzyme doses (K1E 80 – 240, K1F 80 – 360, K1H 70 – 260 nmol glucose equivalents released per min per mg protein) (**Figure 4D**). Assays with 10 µg/ml of depolymerase and varying K1 capsule concentrations showed slightly better binding affinity for K1E [K_M = 4.16 µM, similar to previous reports (Long et al., 1995; Leggate et al., 2002)] than K1F and K1H, and higher catalytic efficiency than K1H (Supplementary Table S2).

Similar assays were performed with K5 and K30. 10–20 µg of K5 capsule was degraded in 1 h by 4–8 µg/ml K5 depolymerase (**Figure 4B**). Of the two putative K30 depolymerases, 64 µg/ml K30 gp41 was required to degrade 20 µg K30 capsule in 1 h (**Figure 4C**). K30 gp42 did not detectably degrade capsule, and combining K30 gp42 with K30 gp41 in different molar ratios provided no increase in reactivity (data not shown) though the two proteins appeared to bind when mixed (Supplementary Figure S2). Quantitative assays confirmed the high activity of K5 depolymerase (260–850 nmol glucose equivalents released per min per mg protein), low activity of K30 gp41 (35–60 nmol per min per mg protein) (**Figure 4D**), and no activity of K30 gp42 (not shown).

Depolymerase Sensitization of Bacteria to Serum Killing

Depolymerases can strip capsules and expose the underlying bacterium to immune attack such as complement-mediated killing (Roberts, 1996; Finlay and McFadden, 2006). We therefore

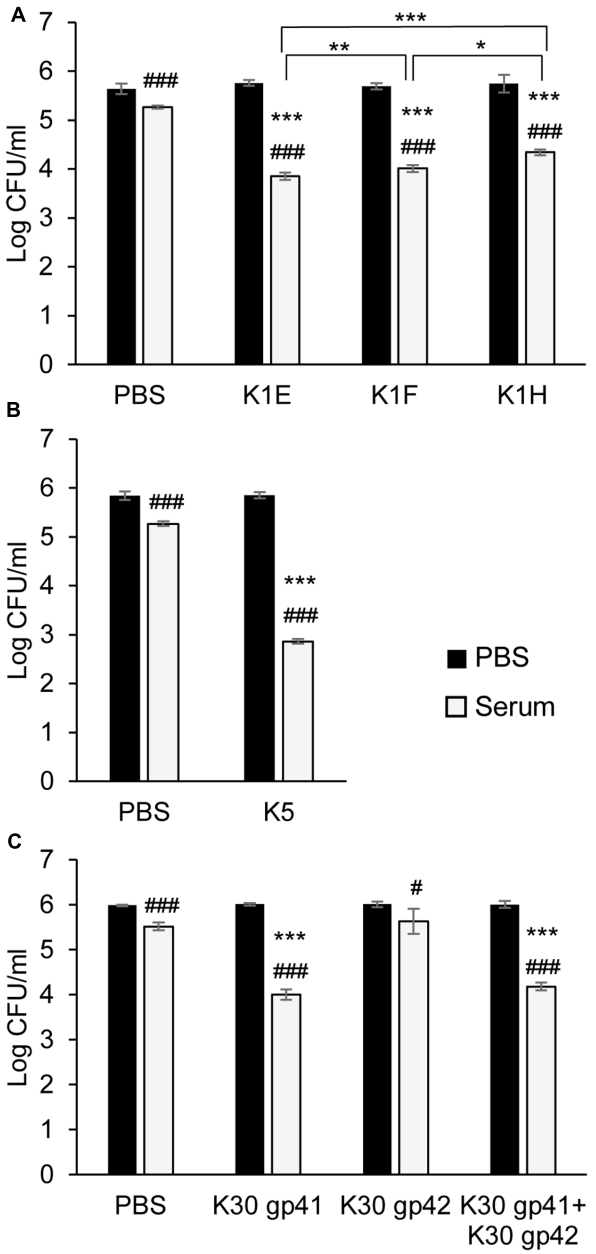

FIGURE 5 | Serum sensitivity assay. 4×10^7 CFU of *E. coli* RS218 **(A)**, ATCC 23506 **(B)**, or 6×10^7 of *E. coli* E69 **(C)** were incubated with or without their respective depolymerases (100 μg/ml) for 1.5–2 h at 37°C. The mixtures were diluted and 4–6 $\times 10^4$ cells were treated with 75% serum for 1.5–2 h at 37°C before plating to determine CFU. Assays were repeated at least three times. The serum's bactericidal effect was analyzed by Student's *t*-test to compare cell survival in serum to that in PBS within each treatment: $^{\#}p < 0.05$, $^{\#\#\#}p < 0.001$. The enzyme's effect on serum sensitivity of the bacteria was analyzed by Student's *t*-test to compare the ratio of cell survival in serum over survival in PBS between different enzyme treatments or the control (PBS): $^{*}p < 0.05$, $^{**}p < 0.01$, $^{***}p < 0.001$ compared to control or as noted.

tested our purified proteins using *in vitro* serum sensitivity assays. In the absence of serum, none of the depolymerases affected bacterial survival. Serum alone had a small effect in killing (**Figure 5**), while heat-inactivated serum slightly increased bacterial numbers (Supplementary Figure S3). For K1 bacteria, enzyme plus serum decreased bacterial survival by at least an order of magnitude (**Figure 5A**), with $>10^4$ killing if the incubation time was extended to 3 h (not shown). As in the capsule degradation assays, K1E exhibited similar activity to K1F depolymerase, and both were superior to K1H in sensitizing bacteria to serum (**Figure 5A**).

K30 gp41 depolymerase, and especially K5 depolymerase, also sensitized bacteria to serum (**Figures 5B,C**). K30 gp42 alone had no significant effect on bacterial survival (with or without serum), and failed to provide any synergistic effect when combined with K30 gp41 (**Figure 5C**).

Oligomerization of Purified Depolymerases

Most depolymerases are homotrimers, and one possible explanation for the discrepancy between the poor therapeutic performance of K1E in mice but good *in vitro* activity is that the purified proteins did not correctly trimerize. Analytical size exclusion chromatography of the depolymerases indicated that the K1E enzyme was mostly present as an ∼18-mer with only a trace of an apparent trimer (**Figure 6A**), while the K1F and K1H enzymes, and those from K5 and K30, were mostly trimeric (**Figures 6B–F**). Multimerization of K1E may limit its *in vivo* distribution following intramuscular injection, as further discussed below.

DISCUSSION

Capsule depolymerases are a promising class of new and non-traditional antibiotics. They have potential advantages over phage therapy: a broader host range than the phages that encode them, and an avoidance of bacterial lysis with concomitant endotoxin release. One downside is that they are active only on specific capsules. To our knowledge, seven phage-encoded depolymerases have now been shown to rescue laboratory rodents from bacterial infections (Mushtaq et al., 2004, 2005; Lin et al., 2014; Pan et al., 2015; and this work). These studies should motivate further investigations: (i) Does the approach generalize to any phage-derived capsular depolymerase? (ii) Can effective depolymerases be isolated from other environmental microorganisms? (iii) Can *in vitro* assays be developed that would serve as a predictor of *in vivo* activity?

This study addressed the general efficacy of phage-derived depolymerases as potential therapeutics by testing three distinct K1 depolymerases, plus similar enzymes from phages K5 and K30. We have shown that using depolymerases for treating bacterial infections is likely a generalizable and feasible therapeutic option, at least in the context of some infection models. Although we have not carefully optimized concentrations, 20 μg K1 or K5 depolymerase delivered intramuscularly into mice (∼1 mg/kg body weight) was sufficient to rescue mice from an otherwise lethal infection. This concentration is well within the range necessary for a practical human or other mammalian therapeutic. The K30 enzyme was

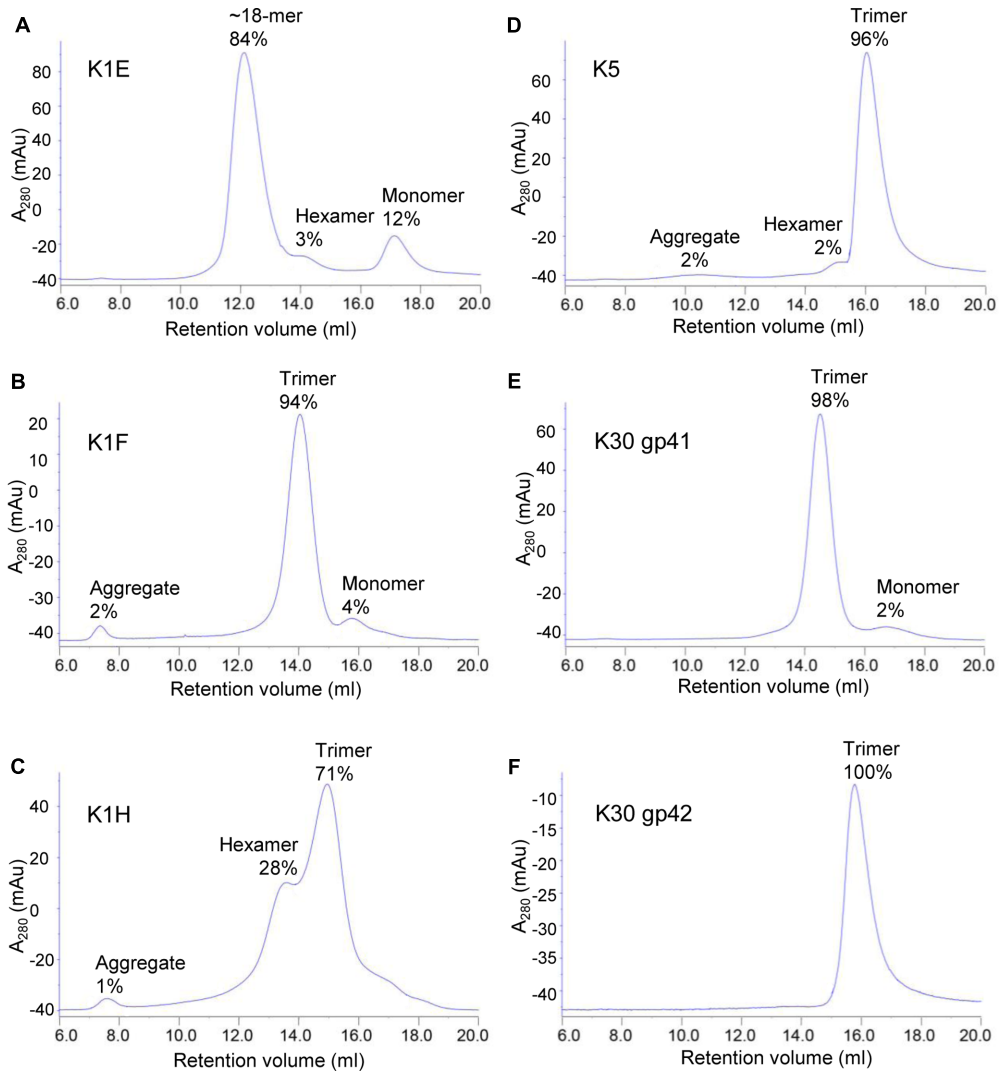

FIGURE 6 | Size exclusion chromatography of purified depolymerases. 1 mg K1E **(A)**, 200 μg K1F **(B)**, 500 μg K1H **(C)**, 500 μg K5 **(D)**, 200 μg K30 gp41 **(E)** or 200 μg K30 gp42 **(F)** was loaded to a Superose 6 10/300 GL column for chromatographic analysis. mAu, micro absorbance unit. Molecular weight of each peak was estimated using calibration standards (GE Healthcare). The estimated multimeric status and percentage are indicated.

first purified from K30 lysates as a complex of two proteins at 90 and 52 kD (McCallum et al., 1989). K30 gp41 and K30 gp42 appear to be the only two logical candidates at these sizes. However, K30 gp41 was sufficient and experienced no increased activity by the presence of K30 gp42, although the two proteins were purified separately. It is possible that co-expression, as occurs during phage infection, would yield improved activity. However, the N-terminal domain of K30 gp41 is homologous to that of the tail-binding domain of the T7 tail fiber, and it is possible that the interaction with K30 gp42 is more for binding the latter protein to the K30 virion rather than for improved enzymatic efficiency.

Besides testing the general therapeutic efficacy of capsule depolymerases, this study is also the first one to compare depolymerases of different origin against the same capsule type or bacterial strain *in vivo*. An unexpected result was that only two of the three K1 depolymerases, provided by intramuscular delivery, performed well in rescuing mice from a lethal bacterial infection. K1E did not, which was surprising for several reasons: (i) the enzyme worked well in previous work where a different, neonatal rat, model was used with gastrointestinal administration of bacteria (Mushtaq et al., 2004, 2005), (ii) K1E phage worked well *in vivo* using the same infection protocol (Bull et al., 2012), and (iii) K1F and K1H enzymes both worked well. To identify the basis of K1E depolymerase inferiority in the mouse infection model, *in vitro* activity assays were conducted, which showed that K1E depolymerase is at least equally efficient as the other K1 enzymes. Thus the *in vitro* assays failed to explain the *in vivo* inferiority of K1E.

Size exclusion chromatography may have revealed the cause of the discrepancy. The purified K1E depolymerase appeared as an 18mer, unlike other enzymes, which were mostly trimers.

This observation is consistent with other reports that K1E depolymerase tends to aggregate (Hallenbeck et al., 1987; Gerardy-Schahn et al., 1995) although our preparation remains a soluble species. Phage tailspikes often require chaperones to fold correctly (Muhlenhoff et al., 2003; Schwarzer et al., 2007; Leiman and Molineux, 2008). The 38 kDa phage adaptor protein K1E gp37, which attaches the K1E depolymerase to the phage virion (Tomlinson and Taylor, 1985; Gerardy-Schahn et al., 1995; Stummeyer et al., 2006), may contribute to forming a specific trimeric species. It seems possible that multimers of a trimeric K1E depolymerase, although retaining activity *in vitro*, are unable to be efficiently disseminated *in vivo* following intramuscular injection. A preliminary test using intraperitoneal injection of 20 μg depolymerase following thigh injection of *E. coli* RS218 showed that K1E enzyme had good efficacy in treatment (data not shown). This observation together with the size exclusion chromatography suggests that poor dissemination of the K1E enzyme when administered intramuscularly may be the cause of the discrepancy. These variations highlight the difficulty of predicting therapeutic efficacy in humans from *in vitro* studies or from different rodent models, especially when using different routes of administration.

This study, like many others with a similar goal of treating an acute and lethal infection, administered the therapeutic agent at the same time as the pathogenic bacteria. Even though the depolymerases were injected into the opposite thigh of the mouse and thus had to diffuse or be transported to where the bacteria were growing, this "simultaneous" treatment is clearly not representative of natural therapeutic interventions. Treatment success with simultaneous administration is an important first step, but may not be a sufficient criterion for successful therapy in a natural setting. Our current investigations are testing the therapeutic efficacy of depolymerases after a designed delay in initiating treatment, which would better reflect actual clinical therapeutics. Tests of depolymerases in other infection environments, i.e., using additional model systems, are also now warranted.

Nonetheless, this study shows general efficacy of capsule depolymerases. These enzymes may thus provide an alternative to phage therapy *sensu stricto*, one with a broader host range than the source phages themselves. For instance, phage K1F does not grow on *E. coli* RS218; however, K1F depolymerase worked well in rescuing mice from a lethal dose of the bacterium. This study also shows that different depolymerases for the same capsule type may perform differently in certain settings. It may therefore be useful to have multiple sources of enzymes, which although structurally similar have different amino acid sequences, for the same capsule type. This would be particularly valuable in the event that patients develop immune responses to one. Environmental bacteria and other types of microbes can provide additional sources of depolymerases (Avery and Dubos, 1931; Dubos and Avery, 1931; Negus and Taylor, 2014). At a minimum, non-phage sources of depolymerases would further expand the possible sources of such enzymes, but they also offer the possibility of broader host range depolymerases and of evolving better activities (Bull and Gill, 2014).

ETHICS STATEMENT

This study was carried out in accordance with the recommendations of NIH (National Institutes of Health) guidelines. The protocol (AUP-2015-00035) was approved by the University of Texas IACUC (Institutional Animal Care and Use Committee).

AUTHOR CONTRIBUTIONS

HL, JB, and IM designed the experiments. HL, MP, and JB carried out the animal experiments, and HL carried out all the other experiments. All authors analyzed data and wrote the manuscript.

FUNDING

This work was supported by the NIH AI 121685-02 to JB and IM. JB is also supported as the University of Texas Miescher Regents Professor.

ACKNOWLEDGMENTS

We thank Eric Vimr for plasmids, consultation and advice on protocols, Ashima Sharma for constructing plasmids pET28b-K1E and pET28b-K5, and Arlen Johnson and Sharmishtha Musalgaonkar for their help with FPLC.

SUPPLEMENTARY MATERIAL

The Supplementary Material for this article can be found online at: https://www.frontiersin.org/articles/10.3389/fmicb.2017.02257/full#supplementary-material

REFERENCES

Abedon, S. T., García, P., Mullany, P., and Aminov, R. (2017). Editorial: phage therapy: past, present and future. *Front. Microbiol.* 8:981. doi: 10.3389/fmicb.2017.00981

Achtman, M., Mercer, A., Kusecek, B., Pohl, A., Heuzenroeder, M., Aaronson, W., et al. (1983). Six widespread bacterial clones among *Escherichia coli* K1 isolates. *Infect. Immun.* 39, 315–335.

Avery, O. T., and Dubos, R. (1931). The protective action of a specific enzyme against type III *Pneumococcus* infection in mice. *J. Exp. Med.* 54, 73–89. doi: 10.1084/jem.54.1.73

Azeredo, J., and Sutherland, I. W. (2008). The use of phages for the removal of infectious biofilms. *Curr. Pharm. Biotechnol.* 9, 261–266. doi: 10.2174/138920108785161604

Briers, Y., Walmagh, M., Van Puyenbroeck, V., Cornelissen, A., Cenens, W., Aertsen, A., et al. (2014). Engineered endolysin-based "Artilysins" to combat

multidrug-resistant gram-negative pathogens. *MBio* 5:e01379-14. doi: 10.1128/mBio.01379-14

Brunschier, R., Danner, M., and Seckler, R. (1993). Interactions of phage P22 tailspike protein with GroE molecular chaperones during refolding in vitro. *J. Biol. Chem.* 268, 2767–2772.

Bruynoghe, R., and Maisin, J. (1921). Essais de thérapeutique au moyen du bacteriophage. *C. R. Soc. Biol.* 85, 1120–1121.

Bull, J. J., and Gill, J. J. (2014). The habits of highly effective phages: population dynamics as a framework for identifying therapeutic phages. *Front. Microbiol.* 5:618. doi: 10.3389/fmicb.2014.00618

Bull, J. J., Otto, G., and Molineux, I. J. (2012). In vivo growth rates are poorly correlated with phage therapy success in a mouse infection model. *Antimicrob. Agents Chemother.* 56, 949–954. doi: 10.1128/AAC.05842-11

Bull, J. J., Vimr, E. R., and Molineux, I. J. (2010). A tale of tails: sialidase is key to success in a model of phage therapy against K1-capsulated *Escherichia coli*. *Virology* 398, 79–86. doi: 10.1016/j.virol.2009.11.040

Clarke, B. R., Esumeh, F., and Roberts, I. S. (2000). Cloning, expression, and purification of the K5 capsular polysaccharide lyase (KflA) from coliphage K5A: evidence for two distinct K5 lyase enzymes. *J. Bacteriol.* 182, 3761–3766. doi: 10.1128/JB.182.13.3761-3766.2000

D'Herelle, F., and Smith, G. H. (1926). *The Bacteriophage and its Behavior*. Baltimore, MD: Williams & Wilkins Co.

Drulis-Kawa, Z., Majkowska-Skrobek, G., and Maciejewska, B. (2015). Bacteriophages and phage-derived proteins–application approaches. *Curr. Med. Chem.* 22, 1757–1773. doi: 10.2174/0929867322666150209152851

Dubois, M., Gilles, K. A., Hamilton, J. K., Rebers, P. A., and Smith, F. (1956). Colorimetric method for determination of sugars and related substances. *Anal. Chem.* 28, 350–356. doi: 10.1021/ac60111a017

Dubos, R., and Avery, O. T. (1931). Decomposition of the capsular polysaccharide of *Pneumococcus* Type III by a bacterial enzyme. *J. Exp. Med.* 54, 51–71. doi: 10.1084/jem.54.1.51

Fang, C. T., Chuang, Y. P., Shun, C. T., Chang, S. C., and Wang, J. T. (2004). A novel virulence gene in *Klebsiella pneumoniae* strains causing primary liver abscess and septic metastatic complications. *J. Exp. Med.* 199, 697–705. doi: 10.1084/jem.20030857

Finlay, B. B., and McFadden, G. (2006). Anti-immunology: evasion of the host immune system by bacterial and viral pathogens. *Cell* 124, 767–782. doi: 10.1016/j.cell.2006.01.034

Fischetti, V. A. (2011). Exploiting what phage have evolved to control gram-positive pathogens. *Bacteriophage* 1, 188–194. doi: 10.4161/bact.1.4.17747

Gerardy-Schahn, R., Bethe, A., Brennecke, T., Mühlenhoff, M., Eckhardt, M., Ziesing, S., et al. (1995). Molecular cloning and functional expression of bacteriophage PK1E-encoded endoneuraminidase Endo NE. *Mol. Microbiol.* 16, 441–450. doi: 10.1111/j.1365-2958.1995.tb02409.x

Gerstmans, H., Rodriguez-Rubio, L., Lavigne, R., and Briers, Y. (2016). From endolysins to Artilysin(R)s: novel enzyme-based approaches to kill drug-resistant bacteria. *Biochem. Soc. Trans.* 44, 123–128. doi: 10.1042/BST20150192

Grover, N., Paskaleva, E. E., Mehta, K. K., Dordick, J. S., and Kane, R. S. (2014). Growth inhibition of *Mycobacterium smegmatis* by mycobacteriophage-derived enzymes. *Enzyme Microb. Technol.* 63, 1–6. doi: 10.1016/j.enzmictec.2014.04.018

Hallenbeck, P. C., Vimr, E. R., Yu, F., Bassler, B., and Troy, F. A. (1987). Purification and properties of a bacteriophage-induced endo-N-acetylneuraminidase specific for poly-alpha-2,8-sialosyl carbohydrate units. *J. Biol. Chem.* 262, 3553–3561.

Latka, A., Maciejewska, B., Majkowska-Skrobek, G., Briers, Y., and Drulis-Kawa, Z. (2017). Bacteriophage-encoded virion-associated enzymes to overcome the carbohydrate barriers during the infection process. *Appl. Microbiol. Biotechnol.* 101, 3103–3119. doi: 10.1007/s00253-017-8224-6

Leggate, D. R., Bryant, J. M., Redpath, M. B., Head, D., Taylor, P. W., and Luzio, J. P. (2002). Expression, mutagenesis and kinetic analysis of recombinant K1E endosialidase to define the site of proteolytic processing and requirements for catalysis. *Mol. Microbiol.* 44, 749–760. doi: 10.1046/j.1365-2958.2002.02908.x

Leiman, P. G., Battisti, A. J., Bowman, V. D., Stummeyer, K., Muhlenhoff, M., Gerardy-Schahn, R., et al. (2007). The structures of bacteriophages K1E and K1-5 explain processive degradation of polysaccharide capsules and evolution of new host specificities. *J. Mol. Biol.* 371, 836–849. doi: 10.1016/j.jmb.2007.05.083

Leiman, P. G., and Molineux, I. J. (2008). Evolution of a new enzyme activity from the same motif fold. *Mol. Microbiol.* 69, 287–290. doi: 10.1111/j.1365-2958.2008.06241.x

Lewis, K. (2013). Platforms for antibiotic discovery. *Nat. Rev. Drug Discov.* 12, 371–387. doi: 10.1038/nrd3975

Lin, T. L., Hsieh, P. F., Huang, Y. T., Lee, W. C., Tsai, Y. T., Su, P. A., et al. (2014). Isolation of a bacteriophage and its depolymerase specific for K1 capsule of *Klebsiella pneumoniae*: implication in typing and treatment. *J. Infect. Dis.* 210, 1734–1744. doi: 10.1093/infdis/jiu332

Long, G. S., Bryant, J. M., Taylor, P. W., and Luzio, J. P. (1995). Complete nucleotide sequence of the gene encoding bacteriophage E endosialidase: implications for K1E endosialidase structure and function. *Biochem. J.* 309(Pt 2), 543–550. doi: 10.1042/bj3090543

Machida, Y., Miyake, K., Hattori, K., Yamamoto, S., Kawase, M., and Iijima, S. (2000). Structure and function of a novel coliphage-associated sialidase. *FEMS Microbiol. Lett.* 182, 333–337. doi: 10.1111/j.1574-6968.2000.tb08917.x

McCallum, K. L., Laakso, D. H., and Whitfield, C. (1989). Use of a bacteriophage-encoded glycanase enzyme in the generation of lipopolysaccharide O side chain deficient mutants of *Escherichia coli* O9:K30 and *Klebsiella* O1:K20: role of O and K antigens in resistance to complement-mediated serum killing. *Can. J. Microbiol.* 35, 994–999. doi: 10.1139/m89-166

Miller, G. L. (1959). Use of dinitrosalicylic acid reagent for determination of reducing sugar. *Anal. Chem.* 31, 426–428. doi: 10.1021/ac60147a030

Møller, H. J., Heinegård, D., and Poulsen, J. H. (1993). Combined alcian blue and silver staining of subnanogram quantities of proteoglycans and glycosaminoglycans in sodium dodecyl sulfate-polyacrylamide gels. *Anal. Biochem.* 209, 169–175. doi: 10.1006/abio.1993.1098

Muhlenhoff, M., Stummeyer, K., Grove, M., Sauerborn, M., and Gerardy-Schahn, R. (2003). Proteolytic processing and oligomerization of bacteriophage-derived endosialidases. *J. Biol. Chem.* 278, 12634–12644. doi: 10.1074/jbc.M212048200

Mushtaq, N., Redpath, M. B., Luzio, J. P., and Taylor, P. W. (2004). Prevention and cure of systemic *Escherichia coli* K1 infection by modification of the bacterial phenotype. *Antimicrob. Agents Chemother.* 48, 1503–1508. doi: 10.1128/aac.48.5.1503-1508.2004

Mushtaq, N., Redpath, M. B., Luzio, J. P., and Taylor, P. W. (2005). Treatment of experimental *Escherichia coli* infection with recombinant bacteriophage-derived capsule depolymerase. *J. Antimicrob. Chemother.* 56, 160–165. doi: 10.1093/jac/dki177

Nakonieczna, A., Cooper, C. J., and Gryko, R. (2015). Bacteriophages and bacteriophage-derived endolysins as potential therapeutics to combat Gram-positive spore forming bacteria. *J. Appl. Microbiol.* 119, 620–631. doi: 10.1111/jam.12881

Negus, D., and Taylor, P. W. (2014). A poly-gamma-(D)-glutamic acid depolymerase that degrades the protective capsule of *Bacillus anthracis*. *Mol. Microbiol.* 91, 1136–1147. doi: 10.1111/mmi.12523

Orskov, I., Orskov, F., Jann, B., and Jann, K. (1977). Serology, chemistry, and genetics of O and K antigens of *Escherichia coli*. *Bacteriol. Rev.* 41, 667–710.

Pan, Y. J., Lin, T. L., Chen, Y. H., Hsu, C. R., Hsieh, P. F., Wu, M. C., et al. (2013). Capsular types of *Klebsiella pneumoniae* revisited by wzc sequencing. *PLOS ONE* 8:e80670. doi: 10.1371/journal.pone.0080670.t001

Pan, Y. J., Lin, T. L., Lin, Y. T., Su, P. A., Chen, C. T., Hsieh, P. F., et al. (2015). Identification of capsular types in carbapenem-resistant *Klebsiella pneumoniae* strains by wzc sequencing and implications for capsule depolymerase treatment. *Antimicrob. Agents Chemother.* 59, 1038–1047. doi: 10.1128/AAC.03560-14

Pastagia, M., Schuch, R., Fischetti, V. A., and Huang, D. B. (2013). Lysins: the arrival of pathogen-directed anti-infectives. *J. Med. Microbiol.* 62(Pt 10), 1506–1516. doi: 10.1099/jmm.0.061028-0

Payne, K. M., and Hatfull, G. F. (2012). Mycobacteriophage endolysins: diverse and modular enzymes with multiple catalytic activities. *PLOS ONE* 7:e34052. doi: 10.1371/journal.pone.0034052

Pelkonen, S., Häyrinen, J., and Finne, J. (1988). Polyacrylamide gel electrophoresis of the capsular polysaccharides of *Escherichia coli* K1 and other bacteria. *J. Bacteriol.* 170, 2646–2653. doi: 10.1128/jb.170.6.2646-2653.1988

Petter, J. G., and Vimr, E. R. (1993). Complete nucleotide sequence of the bacteriophage K1F tail gene encoding endo-*N*-acylneuraminidase (endo-*N*) and comparison to an endo-*N* homolog in bacteriophage PK1E. *J. Bacteriol.* 175, 4354–4363. doi: 10.1128/jb.175.14.4354-4363.1993

Pires, D. P., Cleto, S., Sillankorva, S., Azeredo, J., and Lu, T. K. (2016). Genetically engineered phages: a review of advances over the last decade. *Microbiol. Mol. Biol. Rev.* 80, 523–543. doi: 10.1128/MMBR.00069-15

Podschun, R., Sievers, D., Fischer, A., and Ullmann, U. (1993). Serotypes, hemagglutinins, siderophore synthesis, and serum resistance of *Klebsiella* isolates causing human urinary tract infections. *J. Infect. Dis.* 168, 1415–1421. doi: 10.1093/infdis/168.6.1415

Ponnusamy, D., Kozlova, E. V., Sha, J., Erova, T. E., Azar, S. R., Fitts, E. C., et al. (2016). Cross-talk among flesh-eating *Aeromonas hydrophila* strains in mixed infection leading to necrotizing fasciitis. *Proc. Natl. Acad. Sci. U.S.A.* 113, 722–727. doi: 10.1073/pnas.1523817113

Rich, J. T., Neely, J. G., Paniello, R. C., Voelker, C. C., Nussenbaum, B., and Wang, E. W. (2010). A practical guide to understanding Kaplan-Meier curves. *Otolaryngol. Head Neck Surg.* 143, 331–336. doi: 10.1016/j.otohns.2010.05.007

Roberts, I. S. (1996). The biochemistry and genetics of capsular polysaccharide production in bacteria. *Annu. Rev. Microbiol.* 50, 285–315. doi: 10.1146/annurev.micro.50.1.285

Sambrook, J., Fritsch, E. F., and Maniatis, T. (1989). *Molecular Cloning: a Laboratory Manual*, 2nd Edn. New York N.Y: Cold Spring Harbor Laboratory Press.

Scholl, D., Kieleczawa, J., Kemp, P., Rush, J., Richardson, C. C., Merril, C., et al. (2004). Genomic analysis of bacteriophages SP6 and K1-5, an estranged subgroup of the T7 supergroup. *J. Mol. Biol.* 335, 1151–1171. doi: 10.1016/j.jmb.2003.11.035

Scholl, D., Rogers, S., Adhya, S., and Merril, C. R. (2001). Bacteriophage K1-5 encodes two different tail fiber proteins, allowing it to infect and replicate on both K1 and K5 strains of *Escherichia coli*. *J. Virol.* 75, 2509–2515. doi: 10.1128/JVI.75.6.2509-2515.2001

Schwarzer, D., Buettner, F. F., Browning, C., Nazarov, S., Rabsch, W., Bethe, A., et al. (2012). A multivalent adsorption apparatus explains the broad host range of phage phi92: a comprehensive genomic and structural analysis. *J. Virol.* 86, 10384–10398. doi: 10.1128/JVI.00801-12

Schwarzer, D., Stummeyer, K., Gerardy-Schahn, R., and Muhlenhoff, M. (2007). Characterization of a novel intramolecular chaperone domain conserved in endosialidases and other bacteriophage tail spike and fiber proteins. *J. Biol. Chem.* 282, 2821–2831. doi: 10.1074/jbc.M609543200

Silver, L. L. (2011). Challenges of antibacterial discovery. *Clin. Microbiol. Rev.* 24, 71–109. doi: 10.1128/CMR.00030-10

Smith, H. W., and Huggins, M. B. (1982). Successful treatment of experimental *Escherichia coli* infections in mice using phage: its general superiority over antibiotics. *J. Gen. Microbiol.* 128, 307–318. doi: 10.1099/00221287-128-2-307

Stummeyer, K., Schwarzer, D., Claus, H., Vogel, U., Gerardy-Schahn, R., and Muhlenhoff, M. (2006). Evolution of bacteriophages infecting encapsulated bacteria: lessons from *Escherichia coli* K1-specific phages. *Mol. Microbiol.* 60, 1123–1135. doi: 10.1111/j.1365-2958.2006.05173.x

Sulakvelidze, A., Alavidze, Z., and Morris, J. G. Jr. (2001). Bacteriophage therapy. *Antimicrob. Agents Chemother.* 45, 649–659. doi: 10.1128/AAC.45.3.649-659.2001

Tomlinson, S., and Taylor, P. W. (1985). Neuraminidase associated with coliphage E that specifically depolymerizes the *Escherichia coli* K1 capsular polysaccharide. *J. Virol.* 55, 374–378.

Vimr, E. R., and Troy, F. A. (1985). Regulation of sialic acid metabolism in *Escherichia coli*: role of N-acylneuraminate pyruvate-lyase. *J. Bacteriol.* 164, 854–860.

Weber-Dabrowska, B., Jonczyk-Matysiak, E., Zaczek, M., Lobocka, M., Lusiak-Szelachowska, M., and Gorski, A. (2016). Bacteriophage procurement for therapeutic purposes. *Front. Microbiol.* 7:1177. doi: 10.3389/fmicb.2016.01177

Whitfield, C. (2006). Biosynthesis and assembly of capsular polysaccharides in *Escherichia coli*. *Annu. Rev. Biochem.* 75, 39–68. doi: 10.1146/annurev.biochem.75.103004.142545

Whitfield, C., and Lam, M. (1986). Characterisation of coliphage K30, a bacteriophage specific for *Escherichia coli* capsular serotype K30. *FEMS Microbiol. Lett.* 37, 351–355. doi: 10.1111/j.1574-6968.1986.tb01823.x

Conflict of Interest Statement: The authors declare that the research was conducted in the absence of any commercial or financial relationships that could be construed as a potential conflict of interest.

frontiers in Microbiology

ORIGINAL RESEARCH
published: 08 February 2018
doi: 10.3389/fmicb.2018.00129

1-((2,4-Dichlorophenethyl)Amino)-3-Phenoxypropan-2-ol Kills *Pseudomonas aeruginosa* through Extensive Membrane Damage

Valerie Defraine[1,2‡], Veerle Liebens[1‡], Evelien Loos[1], Toon Swings[1,2], Bram Weytjens[1], Carolina Fierro[1], Kathleen Marchal[3], Liam Sharkey[4], Alex J. O'Neill[4], Romu Corbau[5†], Arnaud Marchand[5], Patrick Chaltin[5,6], Maarten Fauvart[1,7§] and Jan Michiels[1,2§]*

[1] Centre of Microbial and Plant Genetics, KU Leuven, Leuven, Belgium, [2] Center for Microbiology, Vlaams Instituut voor Biotechnologie, Leuven, Belgium, [3] Data Integration and Biological Networks, Ghent University, Ghent, Belgium, [4] School of Molecular and Cellular Biology, University of Leeds, Leeds, United Kingdom, [5] CISTIM Leuven vzw, Leuven, Belgium, [6] Centre for Drug Design and Discovery, Leuven, Belgium, [7] Smart Electronics Unit, Department of Life Sciences and Imaging, imec, Leuven, Belgium

The ever increasing multidrug-resistance of clinically important pathogens and the lack of novel antibiotics have resulted in a true antibiotic crisis where many antibiotics are no longer effective. Further complicating the treatment of bacterial infections are antibiotic-tolerant persister cells. Besides being responsible for the recalcitrant nature of chronic infections, persister cells greatly contribute to the observed antibiotic tolerance in biofilms and even facilitate the emergence of antibiotic resistance. Evidently, eradication of these persister cells could greatly improve patient outcomes and targeting persistence may provide an alternative approach in combatting chronic infections. We recently characterized 1-((2,4-dichlorophenethyl)amino)-3-phenoxypropan-2-ol (SPI009), a novel anti-persister molecule capable of directly killing persisters from both Gram-negative and Gram-positive pathogens. SPI009 potentiates antibiotic activity in several *in vitro* and *in vivo* infection models and possesses promising anti-biofilm activity. Strikingly, SPI009 restores antibiotic sensitivity even in resistant strains. In this study, we investigated the mode of action of this novel compound using several parallel approaches. Genetic analyses and a macromolecular synthesis assays suggest that SPI009 acts by causing extensive membrane damage. This hypothesis was confirmed by liposome leakage assay and membrane permeability studies, demonstrating that SPI009 rapidly impairs the bacterial outer and inner membranes. Evaluation of SPI009-resistant mutants, which only could be generated under severe selection pressure, suggested a possible role for the MexCD-OprJ efflux pump. Overall, our results demonstrate the extensive membrane-damaging activity of SPI009 and confirm its clinical potential in the development of novel anti-persister therapies.

Keywords: *Pseudomonas aeruginosa*, mechanism of action studies, membrane damage, antibiotic tolerance, anti-persister therapies

OPEN ACCESS

Edited by:
Maria Olivia Pereira, University of Minho, Portugal

Reviewed by:
William Farias Porto, Universidade Católica de Brasília, Brazil
Rodolfo García-Contreras, Universidad Nacional Autónoma de México, Mexico

***Correspondence:**
Jan Michiels
jan.michiels@kuleuven.vib.be

†Present address:
Romu Corbau, Freeline Therapeutics, UCL Royal Free Medical School, London, United Kingdom

‡These authors have contributed equally to this work as first authors.

§These authors have contributed equally to this work as senior authors.

Specialty section:
This article was submitted to Antimicrobials, Resistance and Chemotherapy, a section of the journal Frontiers in Microbiology

Received: *15 September 2017*
Accepted: *18 January 2018*
Published: *08 February 2018*

Citation:
Defraine V, Liebens V, Loos E, Swings T, Weytjens B, Fierro C, Marchal K, Sharkey L, O'Neill AJ, Corbau R, Marchand A, Chaltin P, Fauvart M and Michiels J (2018) 1-((2,4-Dichlorophenethyl)Amino)-3-Phenoxypropan-2-ol Kills Pseudomonas aeruginosa through Extensive Membrane Damage. Front. Microbiol. 9:129. doi: 10.3389/fmicb.2018.00129

INTRODUCTION

Modifying existing antibiotic scaffolds upon emergence of resistance has proven a successful strategy to extend a drug class' utility in the past. However, recent data suggest that multidrug-resistance increases at an alarming rate while few novel antibacterials reach the market (Wright, 2014; O'Neill, 2015). A particular issue are multidrug-resistant Gram-negative pathogens such as *Pseudomonas aeruginosa*, posing additional challenges to antibiotic discovery due to their highly impermeable outer membrane (Livermore, 2002; Breidenstein et al., 2011), and the so-called ESKAPE pathogens (*Enterococcus faecium*, *Staphylococcus aureus*, *Klebsiella pneumoniae*, *Acinetobacter baumannii*, *P. aeruginosa*, and *Enterobacter* spp.), efficiently evading antibiotic treatment and responsible for the majority of bacterial infections (Rice, 2008; Delcour, 2009; Poole, 2011). Since no new antibiotic scaffolds active against Gram-negative pathogens have been identified in the last decades, physicians are reverting to the use of polymyxins, once avoided due to toxic effects, as a last-resort treatment for these strains. Therefore, new antibacterial scaffolds are desperately needed (Falagas and Kasiakou, 2005; Walsh and Wencewicz, 2014).

Contributing to the difficult treatment of bacterial infections is the presence of persister cells which constitute a small but important fraction of phenotypic variants tolerant to treatment with high doses of antibiotics (Lewis, 2010). Their occurrence in many bacterial pathogens combined with a demonstrated link between persistence and the recalcitrant nature of chronic bacterial infections renders persisters a serious threat to immunocompromised patients and effective anti-persister treatments are much needed (Fauvart et al., 2011; Zhang, 2014; Fisher et al., 2017). Previous research revealed the strong antibacterial effect of the novel anti-persister molecule SPI009 (Liebens et al., 2017; **Figure 1**) as an adjuvant in combination therapies against different bacterial pathogens. In addition, the compound proved highly successful in the treatment of intracellular and *in vivo P. aeruginosa* infections when combined with the fluoroquinolone ciprofloxacin. SPI009 sensitizes bacteria to antibiotic activity and, strikingly, restores antibiotic sensitivity even in resistant strains. In addition, SPI009 monotherapy exhibited extensive inhibition and eradication activity in biofilms of *P. aeruginosa* and *S. aureus* (Defraine et al., 2017). The current need for novel antibacterials active against Gram-negative species, together with the unique characteristic of SPI009 to kill both normal and persister cells, prompted us to further investigate the mode of action of this compound.

Current approaches to identify the next generation of antibacterials involve high-throughput screenings of natural and chemical products, the characterization and adaptation of new antibacterial structures (Samanta et al., 2013; Mandal et al., 2017), genome hunting, whole-cell-based assays and the targeting of non-multiplying bacteria (Coates et al., 2002). As these options offer interesting alternatives that can bypass the identification of novel antibiotic targets, mechanism of action studies become increasingly important to characterize and select interesting candidates after initial discovery (Terstappen et al., 2007).

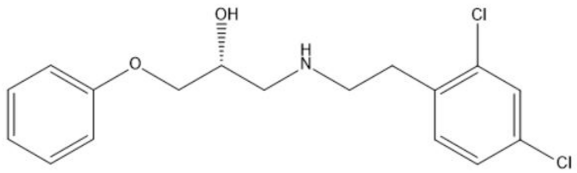

FIGURE 1 | Chemical structure of the propanol-amine derivative 1-((2,4-dichlorophenethyl)amino)-3-phenoxypropan-2-ol (SPI009).

In this study, we set out to determine the mode of action of a recently discovered antibacterial compound, SPI009, showing a broad spectrum antibacterial effect and capable of killing both dividing cells and non-dividing or dormant persister cells (Liebens et al., 2017). While generating useful information for the further development of this compound as an antibacterial therapy, determination of the mode of action could also greatly assist in the development of future anti-persister therapies. A combination of genetic and cellular approaches was employed, revealing the membrane damaging activity of SPI009 and suggesting the ability of SPI009 to attack the bacterial membrane(s) both from the cytoplasm and extracellular environment.

MATERIALS AND METHODS

Bacterial Strains, Media, and Growth Conditions

Bacterial strains were cultured in 1:20 diluted trypticase soy broth (1:20 TSB) at 37°C, shaking at 200 rpm. For solid medium, TSB was supplemented with 1.5% agar. The following antibacterials were used: ofloxacin, ciprofloxacin, erythromycin, polymyxin B, rifampicin (Sigma – Aldrich), fosfomycin, meropenem (TCI Europe), triclosan (Merck Chemicals), melittin (Bachem), and SPI009 (**Figure 1**). Concentrations are indicated throughout the text. Bacterial strains used in this study are listed in **Table 1**.

Screening of a *P. aeruginosa* Mutant Library

A genetic screen of the *P. aeruginosa* PA14 transposon mutant library (Liberati et al., 2006) was performed to identify single gene knockouts sensitive or resistant for SPI009. Stationary phase mutant cultures were split in two and treated for 5 h with either 10 μg/mL ofloxacin or the combination of ofloxacin and 51 μg/mL of SPI009. Treated cultures were diluted 1:100 in fresh TSB medium and incubated at 37°C, shaking at 200 rpm. Growth was monitored over a total period of 40 h by means of periodic OD595 measurements. Average OD595 was calculated for each 96-well plate and used to correct mutant OD595 values. Mutants were identified as sensitive if the OD595 after 24 h of growth was $\leq 0.3\times$ average OD595 after 24 h. Alternatively, mutants having an OD595 $>3\times$ average were defined as resistant. The screening was performed twice to prevent false-positive hits and, to allow identification of SPI009

TABLE 1 | Strains used in this study.

Strain	Description	Source or reference
Pseudomonas aeruginosa		
PA14 WT	Wild type UCBPP–PA14	Pierre Cornelis; Lee et al., 2006
YM WT	PAO1 WT, K767	De Kievit et al., 2001
YM64	*mexAB-oprM::FRT*, *mexXY::FRT*, *mexCD-oprJ::FRT*, *mexEF-oprN::FRT*	Morita et al., 2001
K1521	K767 Δ*mexCD-oprJ*	De Kievit et al., 2001
K1525	K767 Δ*mexXY*	De Kievit et al., 2001
Liberati WT	Wild type UCBPP-PA14 (Lib WT)	Liberati et al., 2006
Δ*galU*	PA14_38350::Mar2xT7 (52640)	Liberati et al., 2006
Δ*nfxB*	PA14_60860::Mar2xT7 (55219)	Liberati et al., 2006
ΔPA14_0812	PA14_08120::Mar2xT7 (47659)	Liberati et al., 2006
Acinetobacter baumannii		
Ab-84	MDR clinical isolate	García-Quintanilla et al., 2014
Ab-84R	Ab-84::40nt insertion at nt 321 of *lpxC*	García-Quintanilla et al., 2014

specific effects, selected mutants showing a clear sensitivity or resistance for ofloxacin were excluded. Resistant hits were additionally confirmed via detailed monitoring of growth in the presence of 51 μg/mL SPI009, using an automated OD reader (Bioscreen C). Functional enrichment analysis was performed based on PseudoCAP classifications and using Fisher's exact test. A schematic overview of the described workflow can be found in Supplementary Figure S1.

RNA Sequencing and Data Analysis

Overnight cultures of *P. aeruginosa* were diluted 1:100 in fresh 1/20 TSB medium and allowed to grow until late-exponential phase (OD595 = 0.2). Cells were treated for 15 min with 50 μM SPI009, 50 μM of the inactive analog SPI014 or 1% DMSO. Total RNA isolation was performed in triplicate for each sample, as previously described (Liebens et al., 2014). The Ribo-Zero^{TM} rRNA Removal Kit for Gram-negative bacteria (Epicentre) was used to deplete ribosomal RNA and RNA samples were sent to the Genomics Core facility of EMBL (Heidelberg, Germany). The quality of the raw sequencing reads was verified using FastQC after which genomic alignments of the reads were performed with Bowtie2, using the *P. aeruginosa* UCBPP-PA14 genome as a reference (NC_008463.1). Differential expression analysis between treated and control samples was done using the DESeq2 package with a False Discovery Rate threshold of 5% (Love et al., 2014). Genes with a $\log_2$ fold-change above 1 and no differential expression under the inactive compound treatment were selected, allowing the detection of SPI009 specific effects on gene expression. Functional annotation of the obtained results was performed using PseudoCAP functional classes obtained from www.pseudomonas.com (Winsor et al., 2016) and functional enrichment was assessed using Fisher's exact test. A UCBPP-PA14 interaction network was created using the STRING database (Szklarczyk et al., 2011) where only reactions with a minimum reliability score of 0.8 were retained. PheNetic was run using both this network and the obtained omics data to generate a downstream interaction network, using the standard parameters and a cost of 0.25 (De Maeyer et al., 2013). Obtained networks containing more than two genes were visualized using Cytoscape (Shannon et al., 2003).

Macromolecular Synthesis Assay

An overnight culture of *P. aeruginosa* PA14 wild type (WT) was diluted 1:10 in 1/20 TSB and grown to an OD600 of 0.3 at 37°C (late exponential phase). Radiolabeled precursors for DNA (1 μCi/mL [methyl-3H]-thymidine), RNA (2.5 μCi/mL [5,6-3H]-uridine), protein (2.5 μCi/mL L-[4,5-3H]-leucine), peptidoglycan (2.5 μCi/mL D-[6-3H(N)]-glucosamine hydrochloride), and fatty acids (1 μCi/mL [2-3H]-glycerol) were added after which cultures were treated with 17 μg/mL SPI009 or 8× MIC concentrations of relevant control antibiotics. Thirty minutes after onset of treatment, 100 μL samples were added to 3.5 mL of ice-cold 10% TCA and precipitates were collected under vacuum on 25 mm glass microfiber filters (Whatman® Grade GF/C). Filters were washed twice with 4 mL ice-cold distilled water and added to 3.5 mL scintillation liquid (Ultima-Flo M, PerkinElmer). Incorporation of the different radiolabels was assessed using a Hidex 300SL scintillation counter. Counts per minute at different treatment conditions were used to evaluate the incorporation of radiolabeled precursors relative to the untreated control, as previously described (Cotsonas King and Wu, 2009; Grzegorzewicz et al., 2012; Nowakowska et al., 2013; Ling et al., 2015).

Fluorescein Leakage Assay

Small unilamellar vesicles (SUVs) representing the Gram-negative membrane and loaded with carboxyfluorescein (CF) were produced as described previously (Randall et al., 2013; Gerits et al., 2016). The total phospholipid concentration was kept at 25 μM, containing a mixture of 1,2-dioleoyl-sn-glycero-3-phosphoethanolamine (DOPE)/1,2-dioleoyl-sn-glycero-3-phospho-(1′-rac-glycerol) (DOPG) (4:1) (Avanti Polar Lipids, Inc). Liposomes were treated with increasing concentrations of SPI009 and an inactive chemical analog, SPI023, keeping the final DMSO concentration at 1% (v:v). Release of CF (λex = 485 nm, λem = 520 nm) was measured in function of time. The percentage of CF leakage was determined relative to the treatment with 0.5% Triton X-100.

Assessment of Inner and Outer Membrane Permeabilization

Inner membrane permeabilization was examined using a SYTOX Green uptake assay, as previously described (Gerits et al., 2016). A PA14 WT culture was grown until late exponential phase and corrected to a final OD595 of 0.5 in 1× phosphate-buffered saline supplemented with 1 μM SYTOX Green. Cultures were treated with Milli-Q (MQ; untreated control), DMSO (1%;

carrier control), 10 μg/mL melittin (1× MIC) and increasing concentrations of SPI009 and transferred to the wells of a black microtiter plate (clear bottom). Fluorescence (λex = 504 nm, λem = 523) and absorbance (OD595) were measured every minute, using a Synergy MX multimode reader (BioTek) at 37°C.

Pseudomonas aeruginosa outer membrane permeabilization by SPI009 was measured using a 1-*N*-phenylnaphthylamine (NPN, Sigma, United States) uptake assay (Gerits et al., 2016). Briefly, a *P. aeruginosa* PA14 WT culture was grown until late exponential phase, after which the OD595 was corrected to 0.5 in 5 mM HEPES (pH = 7.2). A total of 150 μL volumes of culture were treated with MQ (untreated control), DMSO (1%; carrier control), 0.625 μg/mL polymyxin B (1× MIC) and different concentrations of SPI009 (4.25–34 μg/mL) and transferred to the wells of a black microtiter plate (clear bottom). Fifty microliters of a 40 μM NPN solution in 5 mM HEPES (pH = 7.2) was added and fluorescence was measured immediately using a Synergy MX multimode reader (BioTek) at 37°C.

Independent assays for outer and inner membrane permeabilization assessment were performed three times. Measured fluorescence signals were divided by well-specific OD595 to correct for cell density after which the values of the respective untreated controls were subtracted. Results are expressed in relative fluorescence units.

Microscopic Confirmation of Membrane Damage

Overnight cultures of *P. aeruginosa* and *S. aureus* were treated for 20 min with 0.5% DMSO (carrier control) or 34 μg/mL SPI009, centrifuged and stained with 10 μg/mL *N*-(3-triethylammoniumpropyl)-4-(6-(4-(diethyl amino)phenyl)hexatrienyl)pyridinium dibromide (FM®4-64, Molecular Probes). Samples were spotted on 2% agarose pads for imaging with Zeiss Axio imager Z1 fluorescence microscope, using an EC Plan-NEOFLUAR 100× objective (λex = 540–580 nm; λem = 593–668 nm).

Interaction of SPI009 with LPS

To assess possible interaction between SPI009 and the lipid A compound of Gram-negative LPS layers, a whole-cell BODIPY™ TR Cadaverine displacement assay was performed. Briefly, a late-exponential PA14 WT culture was corrected to an OD595 of 0.3 in 50 mM Tris–HCl and added to the BODIPY™ TR Cadaverine conjugate (BC, 5 μM; Life Technologies) in the wells of a black microtiter plate (clear bottom). Cultures were incubated for 2 h to allow BC binding after which equimolar amounts of Tris–HCl (negative control), meropenem, polymyxin B and SPI009 were added and fluorescence (λex = 580 nm, λem = 620 nm) was measured continuously for 1 h. Fluorescence values from the negative control (Tris–HCl) were used to correct for background fluorescence.

Antibacterial Assay

The effect of SPI009 on different bacterial cultures was assessed as described previously (Liebens et al., 2017). Briefly, stationary phase cultures were treated for 5 h with DMSO (carrier control) and different concentrations of SPI009. After treatment, cultures were washed twice in 10 mM $MgSO_4$ and appropriate dilutions were plated onto solid agar plates to assess the number of colony forming units.

Generation and Whole Genome Sequencing of SPI009-Resistant Mutants

In an attempt to generate resistant mutants, *P. aeruginosa* was plated out on solid TSB agar plates containing high concentrations of SPI009. The plates were incubated at 37°C for a total of 10 days but no colonies were able to grow, proving the absence of any resistance development under the specific conditions (our own, unpublished data). Alternatively, resistance development was assessed using a MIC-based protocol as previously described, with minor modifications (Briers et al., 2014; Ling et al., 2015). An initial MIC test was performed in three independent *P. aeruginosa* PA14 WT cultures with ofloxacin and SPI009, according to EUCAST standards (EUCAST, 2003). After 24 h of growth at 37°C, shaking, the MIC value was determined as the minimal concentration that completely inhibited bacterial growth. A new MIC assay was prepared using 1:100 diluted cells at MIC/4 as a starting condition. The assay was repeated for 10 passages with daily assessment and, if necessary, adjustment of antibiotic and compound concentrations. Intermediate and endpoint cultures were stored at −80°C in glycerol (25% v/v) for further analysis. Genomic DNA of the *P. aeruginosa* PA14 WT strain and the three evolved resistant mutants was isolated from overnight cultures grown in 1/20 TSB using the DNeasy Blood & Tissue Kit (Qiagen) following the manufacturer's instructions. DNA quantity and purity were verified using a NanoDrop ND-1000, after which samples were sent to the Genomics Core Facility of EMBL (Heidelberg, Germany) for whole genome sequencing on the Illumina HiSeq 2500 platform. Assembly of the 125 bp paired-end reads and further analysis was performed using CLC Genomics Workbench v8.0. Genome sequences of the resistant mutants were aligned with the genome of the PA14 WT strain in order to detect genetic differences, taking into account a coverage above 10× and cutoff frequency of 75%. Identified non-synonymous mutations were confirmed via PCR amplification and Sanger sequencing (GATC Biotech).

RESULTS

Genetic Analysis of the SPI009 Mode of Action

To gain more information about the mode of action of SPI009 and allow the detection of possible persister-specific effects, individual single-gene knockouts from a *P. aeruginosa* mutant library were treated with ofloxacin alone or in combination with SPI009 and screened for altered sensitivity to SPI009 (see overview in Supplementary Figure S1). Analysis of the obtained screening results revealed a total of 118 and 37 different mutants that showed an increased or decreased sensitivity for SPI009, respectively. Functional enrichment analysis of the sensitive mutants based on their PseudoCAP functions (Winsor

et al., 2016), revealed an over-representation for genes involved in "adaptation and protection" and "cell wall/LPS/capsule" (**Figure 2A** and Supplementary Table S1). The relatively low levels of resistance, combined with the functional enrichment analysis (**Figure 2A**) suggest that single-gene knockouts are not sufficient to obtain significant resistance toward the anti-persister effects of SPI009 and point to a more general effect of the compound.

Next, we compared genome-wide gene expression levels of *P. aeruginosa* PA14 WT following treatment with either SPI009 or an inactive analog. RNA sequencing analysis generated a list of 297 genes that were specifically differentially expressed ($\log_2$-fold change >1) upon treatment with SPI009 (Supplementary Table S2). Functional enrichment analysis of up- and downregulated genes (**Figure 2B**), combined with network analysis (Supplementary Figure S2) revealed a first group of SPI009 upregulated genes to be involved in antibacterial efflux and multidrug resistance, suggesting the increased efforts of the cell to protect itself against SPI009. Another group of mostly upregulated genes are involved in fatty acid metabolism and degradation, suggesting altered amounts of available fatty acids upon treatment of the cell with SPI009. Furthermore, there is a downregulation of multiple genes involved in virulence; including phenazine biosynthesis, pilus assembly and protein secretion and the bacterial Type VI secretion system and biofilm formation (Imperi et al., 2013).

Taking both genetic analyses into account, there does not appear to be a single process or pathway that emerges as the target for SPI009. Instead, membrane-related functions are perturbed, supplemented with more general effects in different regulatory and metabolic pathways. This could point to SPI009 causing membrane damage.

SPI009 Inhibits Macromolecular Biosynthesis in a Non-specific Manner

To further explore the hypothesis of SPI009-induced membrane damage and rule out other bacterial mechanisms targeted by the compound, a macromolecular synthesis assay was performed (Cotsonas King and Wu, 2009). Addition of 17 μg/mL of SPI009 strongly reduced incorporation of radio-labeled precursors for

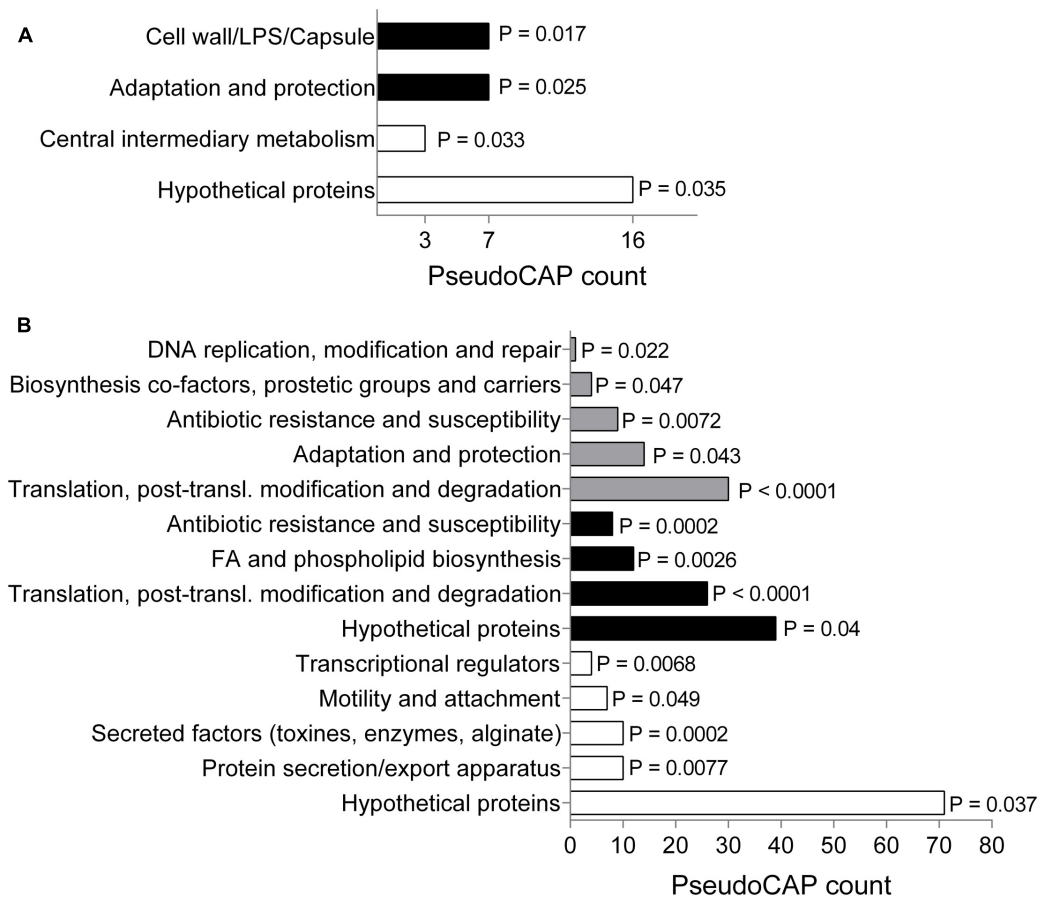

FIGURE 2 | Genetic analysis of SPI009 mode of action. **(A)** Functional enrichment of the obtained set of sensitive (black bars) and resistant (white bars) mutants using PseudoCAP classifications. *P*-values were determined using a two-tailed Fisher's exact test ($\alpha = 0.05$). PseudoCAP counts represent the number of mutants in the respective classes. **(B)** Functional enrichment analysis of the up- and downregulated differentially expressed genes ($\log_2$ fold change >1) as determined after RNA sequencing upon treatment with SPI009. A two-tailed Fisher's exact test was used to determine *P*-values for the classes of downregulated genes (white bars), upregulated genes (black bars), and the total set (gray bars).

DNA, RNA, proteins, fatty acids, and peptidoglycan, resulting in a more than 50% decrease in synthesis for all macromolecules tested (**Figure 3**). When compared to different antibiotics, known to inhibit incorporation of precursors, 1/3× MIC concentrations of SPI009 show a generally stronger inhibitory effect, a pattern previously reported for membrane-damaging compounds (Hobbs et al., 2008; Nowakowska et al., 2013; Masschelein et al., 2015; Gerits et al., 2016).

SPI009 Is Capable of Disrupting Artificial Bacterial Bilayers

To further confirm the suggested membrane damaging effect of SPI009, its capacity to disrupt lipid bilayers that mimic the Gram-negative inner membrane was tested. Increasing concentrations of SPI009 clearly induced CF leakage in a concentration-dependent manner, while the inactive analog SPI005, displaying no antibacterial or anti-persister effect, and the conventional antibiotic ofloxacin, did not cause any significant leakage (**Figure 4**). When comparing SPI009 with the membrane damaging antibiotic polymyxin B, 50% CF leakage was obtained at concentrations of 11.92 ± 0.07 and 1.16 ± 0.04 μg/mL, representing 0.185× MIC and 1.85× MIC concentrations of SPI009 and polymyxin B (Supplementary Figure S3), respectively. These results indicate that SPI009 is indeed capable of effectively disturbing an artificial lipid bilayer and further support the membrane-damaging hypothesis.

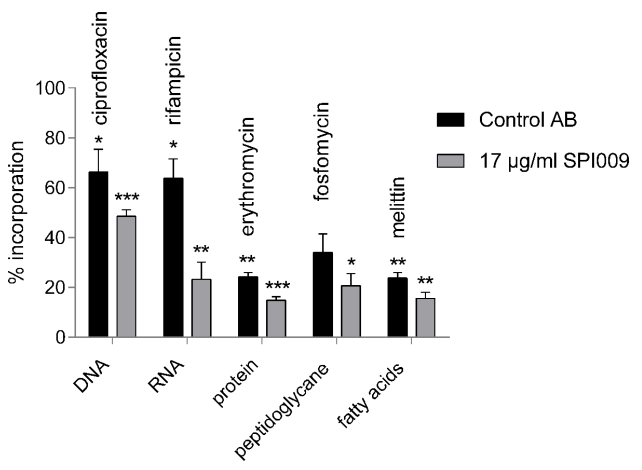

FIGURE 3 | SPI009 inhibits macromolecular synthesis. Incorporation of [methyl-^{3}H]-thymidine (DNA), [5,6-^{3}H]-uridine (RNA), L-(4,5-^{3}H)-leucine (protein), D-[6-^{3}H(N)]-glucosamine (peptidoglycan), 2-^{3}H-glycerol (fatty acids) by *P. aeruginosa* PA14 WT after treatment with relevant control antibiotics at 8× MIC concentrations or 17 μg/mL of SPI009. Incorporation was measured after 30 min and expressed relative to an untreated control. Bars represent the average of at least three independent repeats ± SEM. Statistical analysis was performed on "counts per minute" obtained upon radioactivity detection after treatment of the bacterial cells with MQ (untreated control), the control antibiotic or 17 μg/mL SPI009. One-way ANOVA ($\alpha = 0.05$) with appropriate correction for multiple testing was used to determine statistically relevant differences between the untreated control and antibiotic or untreated control and SPI009 treatment. *$P < 0.05$; **$P < 0.01$; ***$P < 0.001$.

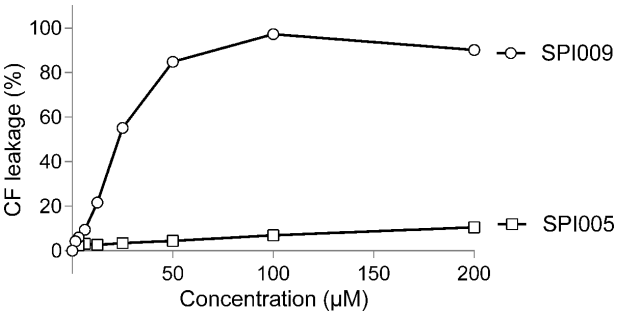

FIGURE 4 | SPI009 causes extensive CF leakage. SUVs were treated for 15 min with increasing concentrations (*x*-axis) of SPI009 (open circles) or the inactive analog SPI005 (open squares). Increasing concentrations of ofloxacin, used as a negative control, did not result in any CF leakage (data not shown). % CF leakage was determined by fluorescence measurements, corrected for background fluorescence and expressed relative to the positive control (0.5% Triton X-100). Data points represent the mean of three independent repeats ± SEM.

Membrane Permeabilization Studies

To evaluate membrane disruption activity of SPI009 on whole *P. aeruginosa* cells, NPN and SYTOX Green assays were carried out, allowing the investigation of respectively outer and inner membrane permeabilization. SYTOX Green shows a strong increase in fluorescence upon binding to DNA. This is, however, only possible when the inner membrane of the cell is compromised, thus correlating the observed fluorescence with the amount of inner membrane damage (Roth et al., 1997). Thirty-minute treatment of *P. aeruginosa* with increasing concentrations of SPI009 caused a strong increase in fluorescence as compared to the untreated control (**Figure 5A** and Supplementary Figure S4A). At concentrations of 17 μg/mL (= 0.33× MIC), the observed membrane damage was comparable to the effect of treatment with 1× MIC concentrations of melittin, the active compound in bee venom known to induce inner membrane damage (Raghuraman and Chattopadhyay, 2007).

Next, permeabilization of the outer membrane was assessed by means of the hydrophobic fluorescent probe NPN. Bacterial cells normally exclude NPN. Consequently, increasing fluorescence caused by the insertion of the probe in the phospholipid bilayer is indicative of damage to the bacterial outer membrane (Helander and Mattila-Sandholm, 2000). Fluorescence measurements revealed a rapid outer membrane permeabilization by SPI009 in a clear concentration-dependent manner (**Figure 5B** and Supplementary Figure S4B). In comparison, treatment with 1× MIC concentration of polymyxin B resulted in a comparable fluorescence level at 1/6× MIC concentrations of SPI009. These results strongly support the hypothesis that SPI009 is capable of disrupting the bacterial membrane, and this for both the inner and outer membrane of *P. aeruginosa*.

Microscopic Confirmation of Membrane Damage

Since the bacterial membrane is such a critical part of the cell's architecture, membrane stains are commonly used

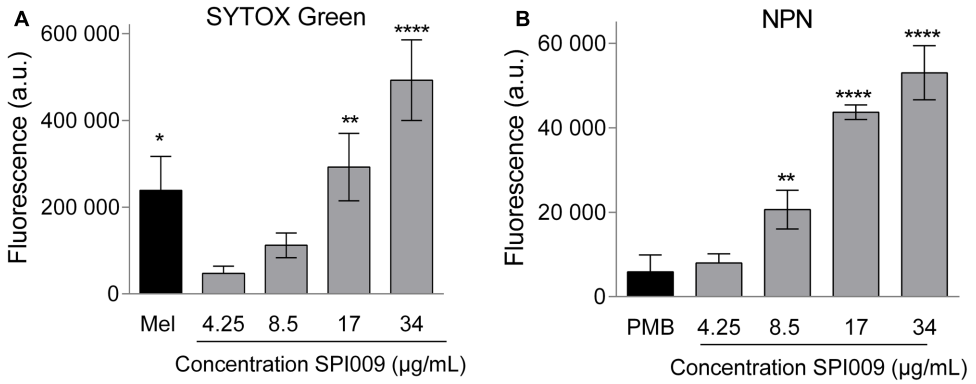

FIGURE 5 | SPI009 extensively permeabilizes both inner and outer membrane of *P. aeruginosa.* **(A)** Effect of increasing concentrations of SPI009 on the inner membrane permeability, as measured by the SYTOX Green uptake assay. Cells were treated for 30 min using melittin (Mel; 1× MIC) as a positive control. **(B)** Outer membrane permeability after treatment with increasing concentrations of SPI009, using polymyxin B (PMB, 1× MIC) as a positive control. Data for both assays represent the mean of at least three independent repeats ± SEM. Statistical comparisons with the untreated control were performed using a one-way ANOVA ($\alpha = 0.05$) with Dunnett's correction for multiple comparison (*$P < 0.05$, **$P < 0.01$, ****$P < 0.0001$).

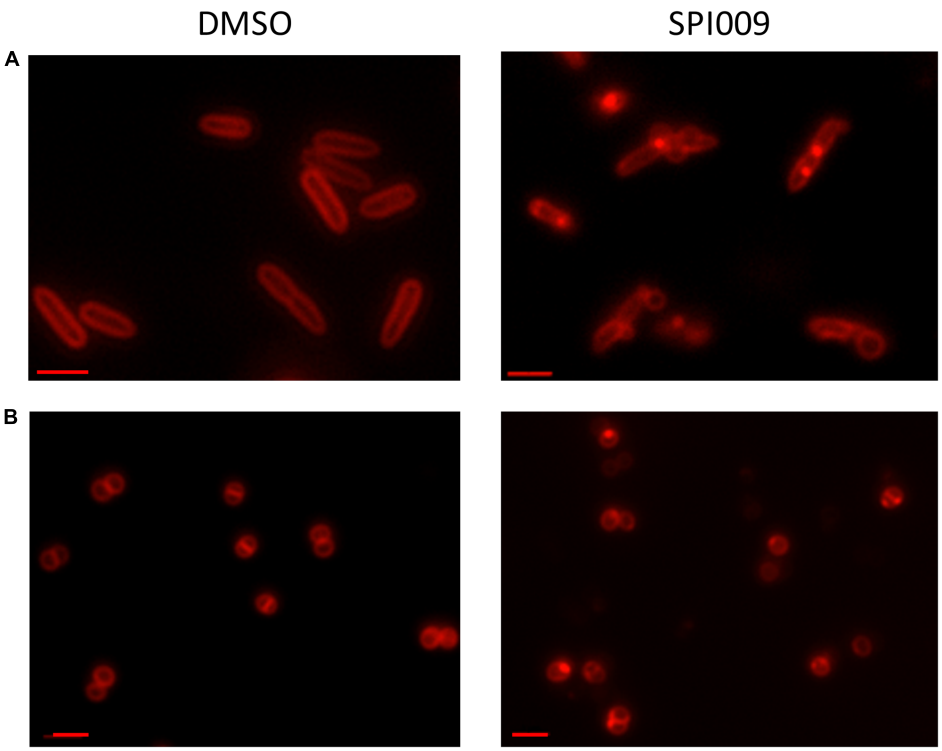

FIGURE 6 | Microscopic confirmation of SPI009 induced membrane damage. Overnight cultures of **(A)** *P. aeruginosa* and **(B)** *S. aureus* cultures were treated for 20 min with 1% DMSO (carrier control) or 34 µg/mL of SPI009. Treated cells were stained with 10 µg/mL of FM® 4-64 and visualized using a Zeiss Axio imager Z1 fluorescence microscope equipped with an EC Plan-NEOFLUAR 100× objective (λ_{ex} = 540–580 nm; λ_{em} = 593–668 nm). Scale bars correspond to 2 µM. Pictures are representatives of repeated experiments.

for microscopic visualization of cell integrity. Treatment of *P. aeruginosa* and *S. aureus* with DMSO (1%, carrier control) resulted in uniformly stained membranes while addition of 34 µg/mL SPI009 induced brightly fluorescent membrane accumulations (**Figure 6**). In the Gram-negative *P. aeruginosa*, a second phenotype was visible: stained membrane blebs, possibly originating from severe outer membrane deformations (Kulp and Kuehn, 2010). The observed membrane accumulations after treatment with SPI009 confirm a direct effect of the compound on the bacterial membrane for both Gram-negative and Gram-positive species.

SPI009 Interacts with the Lipid A Compound of the Bacterial LPS Layer

The BODIPY^{TM}-TR-cadaverine probe (BC) was used to reveal possible interactions of SPI009 with the bacterial LPS layer. If compounds are added that have the ability to bind lipid A, BODIPY^{TM}-TR Cadaverine will be displaced, resulting in a strong increase in fluorescence (Torrent et al., 2008; Gerits et al., 2016). Positive and negative controls consisted of, respectively, polymyxin B, known to use the interaction with lipid A for self-promoted uptake and resulting in cell lysis (Yu et al., 2015), and meropenem, not capable of interacting with LPS. Comparison of the effects of equimolar amounts of SPI009 and these controls demonstrated a clear time and concentration-dependent interaction between SPI009 and lipid A (**Figure 7**). However, since it was previously shown that SPI009 maintains its antibacterial and anti-persister activity in Gram-positive bacteria, the interaction with lipid A in the bacterial LPS layer cannot be the sole mechanism of SPI009-induced membrane damage.

The Role of Efflux Pumps in SPI009 Activity

The SPI009-induced inner membrane damage, as indicated by the SYTOX Green uptake assay, could be a secondary effect resulting from extensive outer membrane damage caused by SPI009. Alternatively, the compound may enter the bacterial cell and cause membrane damage from within. To explore these possibilities, different efflux mutants were evaluated for their sensitivity toward SPI009 (**Figure 8** and Supplementary Figure S5). Upon treatment with SPI009, the PAO1-derived YM64 mutant, lacking the four major mex operons of *P. aeruginosa*; *mexAB-oprM*, *mexCD-oprJ*, *mexEF-oprN*, and *mexXY-oprM* (Morita et al., 2001), showed a significantly decreased survival for all concentrations tested. Treatment with 8.5, 17, and 34 μg/mL SPI009 caused significant 2.0 ± 0.3, 4.5 ± 0.9, and 3.7 ± 0.4 log unit decreases in survival as compared to the YM WT, respectively, while 68 μg/mL of SPI009 was capable of completely eradicating the efflux mutant. To further explore the role of the different efflux pumps missing in YM64, separate Δ*mexCD-oprJ* and Δ*mexXY* mutants were also analyzed. For these, only the Δ*mexCD-oprJ* strain showed decreased survival compared to the YM WT after treatment with 34 μg/mL SPI009. The obtained results clearly show that some *P. aeruginosa* efflux pumps, including MexCD-OprJ, are capable of actively removing SPI009 from the bacterial cell and suggest the involvement of other Mex pumps, most likely not MexXY-OprM. These experiments confirm the inner membrane as an important target of SPI009, in addition to the observed outer membrane permeabilization.

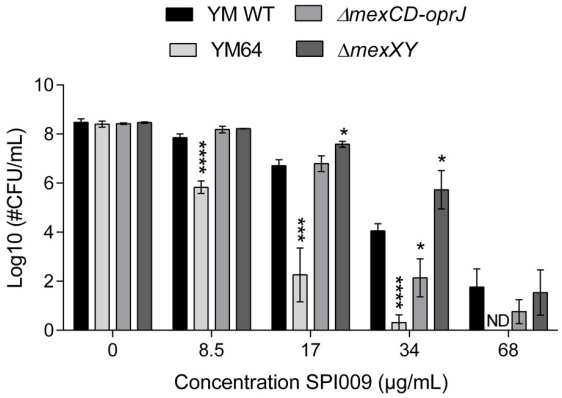

FIGURE 8 | Activity of SPI009 in efflux mutants. *P. aeruginosa* efflux mutants YM64, Δ*mexCD-oprJ* and Δ*mexXY*, together with their WT strain YM, were treated for 5 h with increasing concentrations of SPI009. Significant differences in sensitivity toward SPI009 between the WT and different mutants were detected using multiple *t*-tests ($\alpha = 0.05$) with Holm–Sidak correction for multiple comparisons and represented by $^{*}P < 0.05$; $^{***}P \leq 0.001$; and $^{****}P < 0.0001$. Values represent the average of at least three independent repeats with error bars depicting SEM values. ND, not detected.

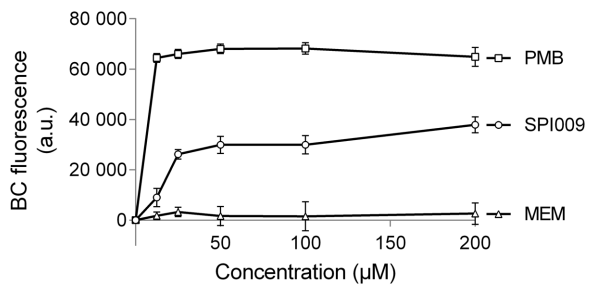

FIGURE 7 | SPI009 interacts with the LPS layer. BC bound *P. aeruginosa* cultures were treated with equimolar amounts of SPI009, polymyxin B (positive control; PMB) and meropenem (negative control; MEM). Fluorescence was measured continuously, using λ_{ex} = 580 nm and λ_{em} = 620 nm, and corrected for background fluorescence. Results represent the average of four independent repeats ± SEM with BC fluorescence values obtained after 1 h.

Role of Natural Membrane Permeability in SPI009 Sensitivity

Since the natural membrane permeability of different bacterial species contributes to their intrinsic antibiotic resistance (Breidenstein et al., 2011), we investigated whether this also affected the activity of SPI009. *P. aeruginosa* Δ*galU*, is no longer capable of synthesizing UDP-glucose, a precursor required for the formation of the glycosyl residues found in the bacterial LPS layer (Choudhury et al., 2005). Natural membrane permeability was assessed by measuring NPN fluorescence of MQ-treated samples and revealed a significantly higher permeability for Δ*galU* (**Figure 9A**). Treatment with 17 or 34 μg/mL SPI009 revealed respective 1.4 ± 0.3 log and 2.9 ± 0.7 log unit decreases in survival as compared to the WT strain.

We next wanted to evaluate the effect of SPI009 in the complete absence of LPS. However, no *P. aeruginosa* strain lacking LPS has been described to date. In contrast, a 40 nt insertion in *A. baumannii lpxC* results in the complete loss of the bacterial LPS layer without affecting viability (García-Quintanilla et al., 2014). Moreover, like *P. aeruginosa*, *A. baumannii* is also a member of the Pseudomonadales and an important contributor to the spread of antibiotic resistance. As compared to the WT

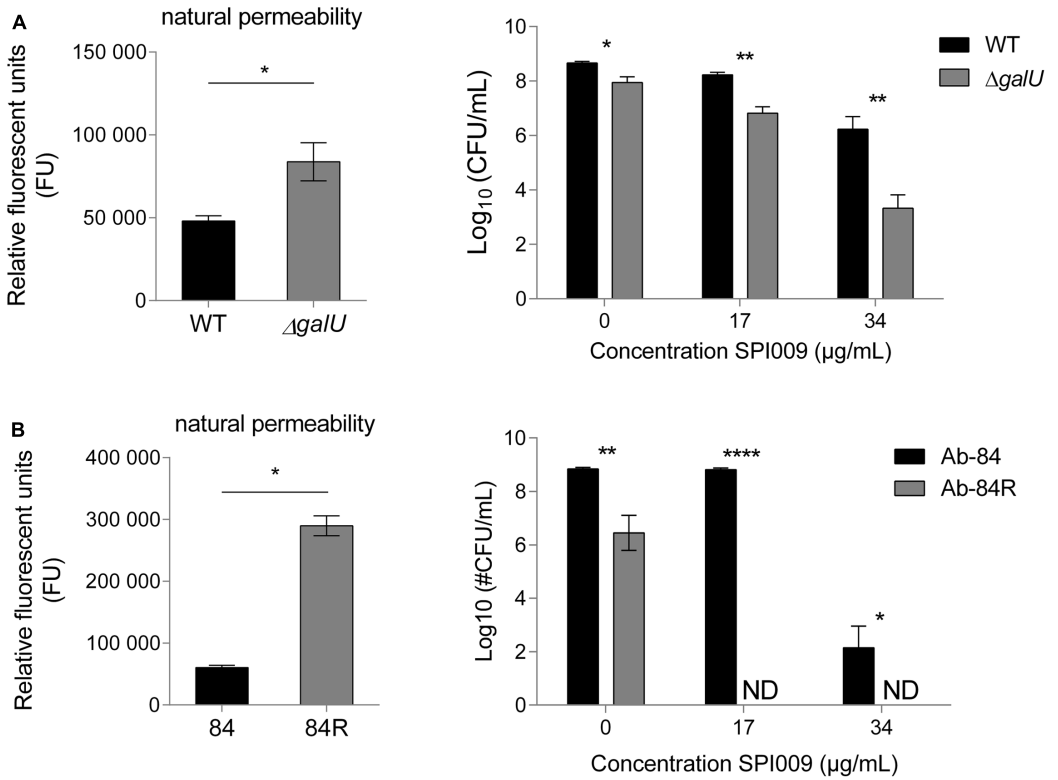

FIGURE 9 | Cells displaying increased membrane permeability show higher sensitivity toward SPI009. Mutants resulting in LPS biosynthesis malfunction or complete loss of the LPS layer were selected for **(A)** *P. aeruginosa* and **(B)** *Acinetobacter baumannii*, respectively. Natural membrane permeability was assessed by means of NPN assays of untreated cultures (left panel). Statistical analysis was done by means of a single unpaired, two-tailed *t*-test ($\alpha = 0.05$). Next, stationary phase cultures of WT and mutant strains were treated for 5 h with increasing concentrations of SPI009 (right panel). Statistical analysis was done by means of multiple *t*-tests ($\alpha = 0.05$) to compare the antibacterial effect of SPI009 between the WT and mutant strain, with Holm–Sidak correction for multiple testing. Displayed data points show the average of at least three independent repeats ± SEM. $^{*}P < 0.05$; $^{**}P < 0.01$; $^{***}P < 0.001$; and $^{****}P \leq 0.0001$; ND, not detected.

strain Ab-84, the absence of the LPS layer greatly increased the observed natural membrane permeability (**Figure 9B**). The differential sensitivity of these strains for SPI009 shows a more pronounced character than for *P. aeruginosa* since treatment with 17 μg/mL of SPI009 already completely eradicated the LPS-deficient Ab-84R strain. Together, these results indicate that the structure of the bacterial LPS layer, which partly determines membrane integrity and strength, strongly influences the susceptibility of the cell toward SPI009.

Generation and Analysis of SPI009-Resistant Mutants

Being so far unable to generate spontaneous SPI009-resistant mutants on solid growth medium (our own, unpublished data), an evolution experiment using the MIC broth dilution method was used to generate mutants showing a 10-fold increase in the SPI009 MIC. MIC values slowly increased for the strains grown in the presence of SPI009 while resistance to the conventional antibiotic ofloxacin showed a more abrupt transition with a first plateau of 16-fold increase in MIC being reached after just 2 days (Supplementary Figure S6A). The results obtained for ofloxacin are in agreement with previous fluoroquinolone resistance evolution experiments (Wong et al., 2012; Briers et al., 2014; Ling et al., 2015). Decreased sensitivity for SPI009 of the evolved strains was confirmed via MIC and plate assays, where treatment with 68 μg/mL of SPI009 caused a maximal 1.46 log decrease in the number of surviving cells (Supplementary Figure S6B). Whole genome sequencing and analysis of the evolved strains revealed two identical non-synonymous SNPs in each of the parallel lines. A first mutation involved a 47A > C change in PA14_08120 (PA0625), a phage tail length determination protein located in the outer membrane or outer membrane vesicles (Choi et al., 2011; Winsor et al., 2016). PA0625 is part of a 16-ORF gene cluster coding for R-type phage tail-like pyocins in *P. aeruginosa*, bacteria-produced bacteriocins that are capable of depolarizing the cytoplasmic membrane in sensitive cells and inhibiting active transport (Nakayama et al., 2000; Ghequire and De Mot, 2014; Choudhary et al., 2015). A second SNP, 88G > A, was identified in nfxB, the negative regulator of the MexCD-OprJ efflux system. Interestingly, this SNP is located in a predicted helix-turn-helix region responsible for DNA-binding. Other similar mutations in this region have been shown to disturb the binding to the MexCD-OprJ promotor and thus cause overexpression of this efflux pump and active expulsion of SPI009 from the cell (Okazaki and Hirai, 1992; Purssell and Poole, 2013).

A transposon mutant of nfxB showed a significant decrease in sensitivity toward SPI009 resulting in 1.7 ± 0.4 and 3.1 ± 0.9 log unit increases in survival as compared to the WT after treatment with 17 and 34 μg/mL of SPI009, respectively (Supplementary Figure S6B). In contrast to the whole genome sequencing results, full gene knockout of PA14_08120 did not cause a significant increase in survival. Taken together, these results confirm the hypothesis that the MexCD-OprJ efflux is capable of protecting the cell against SPI009-mediated membrane damage. Further research will, however, be necessary to unravel the exact role of PA14_08120 in this mechanism.

DISCUSSION

Increased understanding of persister formation mechanisms and the general acknowledgment of their clinical importance has resulted in a growing number of reports on anti-persister molecules, contributing to potential future treatment options in the fight against bacterial infections (Wood, 2015; Van den Bergh et al., 2017). Targeting persisters is likely to greatly improve patient outcomes but unfortunately the rational target-based design of anti-persister therapies remains a great challenge. Contributing to this are the limited numbers of persister cells, the incomplete knowledge and redundancy in mechanisms controlling persister formation and the observation that these processes are often species-specific (Harms et al., 2016; Michiels et al., 2016; Van den Bergh et al., 2017). A possible way of bypassing these issues is the use of well-designed whole-cell screenings that can identify novel compounds based on anti-persister activity rather than target (Coates et al., 2002). We recently reported the use of such a screening in the identification of SPI009 (1-((2,4-dichlorophenethyl)amino)-3-phenoxypropan-2-ol) (Liebens et al., 2017), a small molecule capable of directly killing persister cells of clinically relevant Gram-negative and Gram-positive pathogens in different *in vitro* and *in vivo* set-ups. Other anti-persister compounds reported to directly kill bacterial persister cells use varying strategies such as depolarization and destruction of the cell membrane, DNA cross-linking, inhibition of essential enzymes, and generation of reactive oxygen species (Helaine and Kugelberg, 2014; Wood, 2015; Van den Bergh et al., 2017). Several characteristics of SPI009, such as its broad-spectrum activity, ability to tackle both dividing and non-dividing cells and the potentiation of mechanistically different antibiotics presented a first indication of a non-specific target. Identifying the mechanism of action for this novel anti-persister and antibacterial compound is not only important for the further development of possible therapies but also increases our knowledge about persister cells and contributes to the identification of possible targets for future anti-persister therapies (Terstappen et al., 2007).

In this study, we present the detailed exploration of the mode of action of SPI009, combining complementary genetic and cellular approaches. Several lines of evidence support that SPI009 kills persister and non-persister cells by causing extensive membrane damage. The overall inhibition of macromolecular synthesis at relatively low concentrations of SPI009, together with the obtained genetic data, provided us with the indication that SPI009 induced membrane damage (Hobbs et al., 2008; Nowakowska et al., 2013; Masschelein et al., 2015; Gerits et al., 2016). Several membrane and whole-cell-based assays confirmed this hypothesis and revealed the possibility of SPI009 to efficiently and extensively damage both the outer and inner bacterial membrane. Furthermore, microscopic analysis revealed membrane damage and severe outer membrane deformations and blebs in *P. aeruginosa*. The observed changes upon treatment of the Gram-positive *S. aureus* suggest a similar mechanism of membrane damage, but further research will be necessary to confirm this. Since the integrity of the bacterial membrane remains crucial for the viability of persister cells, membranes have previously been suggested as potential targets for anti-persister strategies (Hurdle et al., 2011). Several anti-persister compounds described in literature, such as the Artilysin® Art-175 (Briers et al., 2014; Defraine et al., 2016), membrane-acting peptides (Chen et al., 2011), HT61 (Hu et al., 2010; Hubbard et al., 2017), and AM-0016 (Zou et al., 2013) use this strategy to efficiently tackle antibiotic-tolerant persister cells of both Gram-negative and Gram-positive species.

Although SPI009 proved capable of interacting with the lipid A moiety of the bacterial LPS layer, the demonstrated activity in Gram-positive species and LPS-deficient strains exclude LPS as the primary binding target of SPI009. However, the architecture of the LPS layer and resulting membrane permeability do have a strong influence on SPI009 activity. Possible explanations include the physical barrier formed by the LPS sugars, its influence on overall membrane strength or the changes in membrane charge due to the absence or presence of sugars and phosphate groups (Rana et al., 1991; Papo and Shai, 2005). Additionally, the increased SPI009 sensitivity of the *P. aeruginosa* YM64 mutant, lacking the four major Mex efflux pumps (Morita et al., 2001) and resulting in increased intracellular concentrations of the compound, provided evidence that SPI009 can cause cytoplasmic membrane damage and suggests the possible use of efflux pump inhibitors to further increase SPI009 activity.

Additional experiments revealed a possible role for MexCD-OprJ in the efflux of SPI009, but the substantial difference in sensitivity between YM64 and Δ*mexCD-oprJ* suggests that additional efflux mechanisms are involved. Interestingly, both the genetic screen and RNA sequencing revealed genes belonging to the *mexCD-oprJ* system and its regulator *nfxB*, previously reported to be inducible by membrane-damaging agents and best known for its role in fluoroquinolone resistance (Morita, 2003; Fraud et al., 2008; Purssell and Poole, 2013). Besides increasing the efflux of antibacterial compounds through MexCD-OprJ, Δ*nfxB* also influences cell membrane permeability (Okazaki and Hirai, 1992), thus suggesting an alternative role for *nfxB* in SPI009 resistance. The involvement of this bacterial efflux pump was corroborated through genetic analysis of the evolved SPI009-resistant strains, where all three independent mutants showed SNPs in *nfxB* and PA14_08120. While inactivation of *nfxB* strongly decreased sensitivity toward SPI009, this was not the case for PA14_08120. The R2 region of *P. aeruginosa* has previously been linked with antibiotic resistance. Fluoroquinolone induced production and release of pyocins was shown to cause cell lysis,

while deletion of several R2 genes induced significant resistance to ciprofloxacin (Brazas and Hancock, 2005; Breidenstein et al., 2008). However, the lack of upregulation of any of the R2 genes in response to SPI009 (see Supplementary Table S2), suggests a different role for PA14_08120 in SPI009 susceptibility. Differences in survival between the *nfxB* knockout mutant and the SPI009-resistant strains could suggest the enhancement of the observed SPI009 resistance after accumulation of both mutations. The absence of SPI009 resistant mutants in earlier attempts, combined with the lack of any clear resistance phenotypes after single-gene knockout, predicted fitness defects of Δ*nfxB* (Stickland et al., 2010) and possibility of using efflux pump inhibitors (Lomovskaya and Watkins, 2001) all decrease the chances of SPI009 resistance emerging in *in vivo* situations.

Overall, the use of different combined approaches resulted in compelling evidence that the novel antibacterial compound SPI009 is capable of directly killing *P. aeruginosa* cells as a consequence of severe membrane damage. Further experiments revealed the ability of the compound to impair both the outer and inner membrane of *P. aeruginosa*, the latter being a direct consequence of SPI009 entry into the cell. The crucial importance of membrane integrity for survival of both active and metabolically inactive bacterial cells combined with the suggested limited resistance potential of membrane-damaging compounds (Hurdle et al., 2011) and the previously reported limited cytotoxicity (Liebens et al., 2017), further support the clinical potential of SPI009 and its role as a scaffold in the development of future anti-persister therapies.

AUTHOR CONTRIBUTIONS

Conceptualization: VD, VL, RC, AM, PC, MF, and JM; Methodology: VD, VL, MF, and JM; Formal analysis: VD and VL; Investigation: VD, VL, EL, TS, LS, BW, CF, and KM; Writing-original draft: VD; Writing- Review and Editing: VD, VL, AO, MF, and JM; Visualization: VD; Supervision: MF and JM.

FUNDING

This work was supported by Ph.D. grants of the Agency for Innovation through Science and Technology (IWT) to VD; the KU Leuven Excellence Center (grant number PF/2010/07), the KU Leuven Research Council (grant number PF/10/010, "NATAR"); the Belgian Science Policy Office (BELSPO) (IAP P7/28), and the Fund for Scientific Research, Flanders (FWO) (grant numbers G047112N; G0B2515N; G055517N).

ACKNOWLEDGMENTS

We would like to thank Sanne Schrevens and Prof. Patrick Van Dijck (Molecular Biotechnology of Plants and Micro-organisms, Department of Biology, KU Leuven) for their practical and logistic help with the macromolecular synthesis experiments. We would also like to thank Prof. Wim De Borggraeve, Koen Nuyts, and Brecht Egle (KU Leuven) for their expertise and technical assistance with the preparation of the small unilamellar vesicles.

SUPPLEMENTARY MATERIAL

The Supplementary Material for this article can be found online at: https://www.frontiersin.org/articles/10.3389/fmicb.2018.00129/full#supplementary-material

REFERENCES

Brazas, M. D., and Hancock, R. E. W. (2005). Ciprofloxacin induction of a susceptibility determinant in *Pseudomonas aeruginosa*. *Antimicrob. Agents Chemother.* 49, 3222–3227. doi: 10.1128/AAC.49.8.3222-3227.2005

Breidenstein, E. B., de la Fuente-Núñez, C., and Hancock, R. E. (2011). *Pseudomonas aeruginosa*: all roads lead to resistance. *Trends Microbiol.* 19, 419–426. doi: 10.1016/j.tim.2011.04.005

Breidenstein, E. B., Khaira, B. K., Wiegand, I., Overhage, J., and Hancock, R. E. W. (2008). Complex ciprofloxacin resistome revealed by screening a *Pseudomonas aeruginosa* mutant library for altered susceptibility. *Antimicrob. Agents Chemother.* 52, 4486–4491. doi: 10.1128/AAC.00222-08

Briers, Y., Walmagh, M., Grymonprez, B., Biebl, M., Pirnay, J.-P., Defraine, V., et al. (2014). Art-175 is a highly efficient antibacterial against multidrug-resistant strains and persisters of *Pseudomonas aeruginosa*. *Antimicrob. Agents Chemother.* 58, 3774–3784. doi: 10.1128/AAC.02668-14

Chen, X., Zhang, M., Zhou, C., Kallenbach, N. R., and Ren, D. (2011). Control of bacterial persister cells by Trp/Arg-containing antimicrobial peptides. *Appl. Environ. Microbiol.* 77, 4878–4885. doi: 10.1128/AEM.02440-10

Choi, D.-S., Kim, D.-K., Choi, S. J., Lee, J., Choi, J., Rho, S., et al. (2011). Proteomic analysis of outer membrane vesicles derived from *Pseudomonas aeruginosa*. *Proteomics* 11, 3424–3429. doi: 10.1002/pmic.201000212

Choudhary, G. S., Yao, X., Wang, J., Peng, B., Bader, R. A., and Ren, D. (2015). Human granulocyte macrophage colony-stimulating factor enhances antibiotic susceptibility of *Pseudomonas aeruginosa* persister cells. *Sci. Rep.* 5:17315. doi: 10.1038/srep17315

Choudhury, B., Carlson, R. W., and Goldberg, J. B. (2005). The structure of the lipopolysaccharide from a *galU* mutant of *Pseudomonas aeruginosa* serogroup-O11. *Carbohydr. Res.* 340, 2761–2772. doi: 10.1016/j.carres.2005.09.017

Coates, A., Hu, Y., Bax, R., and Page, C. (2002). The future challenges facing the development of new antimicrobial drugs. *Nat. Rev. Drug Discov.* 1, 895–910. doi: 10.1038/nrd940

Cotsonas King, A., and Wu, L. (2009). Macromolecular synthesis and membrane perturbation assays for mechanisms of action studies of antimicrobial agents. *Curr. Protoc. Pharmacol* 47, 13A.7.1–13A.7.23. doi: 10.1002/0471141755.ph13a07s47

Defraine, V., Schuermans, J., Grymonprez, B., Govers, S. K., Aertsen, A., Fauvart, M., et al. (2016). Efficacy of Artilysin Art-175 against resistant and persistent *Acinetobacter baumannii*. *Antimicrob. Agents Chemother.* 60, 3480–3488. doi: 10.1128/AAC.00285-16

Defraine, V., Verstraete, L., Van Bambeke, F., Anantharajah, A., Townsend, E. M., Ramage, G., et al. (2017). Antibacterial activity of 1-[(2,4-Dichlorophenethyl)amino]-3-Phenoxypropan-2-ol against antibiotic-resistant strains of diverse bacterial pathogens, biofilms and in pre-clinical infection models. *Front. Microbiol.* 8:2585. doi: 10.3389/fmicb.2017.02585

De Kievit, T. R., Parkins, M. D., Gillis, R. J., Srikumar, R., Ceri, H., Poole, K., et al. (2001). Multidrug efflux pumps: expression patterns and contribution to antibiotic resistance in *Pseudomonas aeruginosa* biofilms. *Antimicrob. Agents Chemother.* 45, 1761–1770. doi: 10.1128/AAC.45.6.1761-1770.2001

De Maeyer, D., Renkens, J., Cloots, L., De Raedt, L., and Marchal, K. (2013). PheNetic: network-based interpretation of unstructured gene lists in *E. coli*. *Mol. Biosyst.* 9, 1594–1603. doi: 10.1039/c3mb25551d

Delcour, A. H. (2009). Outer membrane permeability and antibiotic resistance. *Biochim. Biophys. Acta* 1794, 808–816. doi: 10.1016/j.bbapap.2008.11.005

EUCAST. (2003). Determination of minimum inhibitory concentrations (MICs) of antibacterial agents by broth dilution. *Clin. Microbiol. Infect.* 8, 9–15.

Falagas, M. E., and Kasiakou, S. K. (2005). Colistin: the revival of polymyxins for the management of multidrug-resistant Gram-negative bacterial infections. *Pediatr. Infect. Dis. J.* 24:945. doi: 10.1097/01.inf.0000174577.97635.7b

Fauvart, M., De Groote, V. N., and Michiels, J. (2011). Role of persister cells in chronic infections: clinical relevance and perspectives on anti-persister therapies. *J. Med. Microbiol.* 60, 699–709. doi: 10.1099/jmm.0.030932-0

Fisher, R. A., Gollan, B., and Helaine, S. (2017). Persistent bacterial infections and persister cells. *Nat. Rev. Microbiol.* 15, 453–464. doi: 10.1038/nrmicro.2017.42

Fraud, S., Campigotto, A. J., Chen, Z., and Poole, K. (2008). MexCD-OprJ multidrug efflux system of *Pseudomonas aeruginosa*: involvement in chlorhexidine resistance and induction by membrane-damaging agents dependent upon the AlgU stress response sigma factor. *Antimicrob. Agents Chemother.* 52, 4478–4482. doi: 10.1128/AAC.01072-08

García-Quintanilla, M., Pulido, M. R., Moreno-Martínez, P., Martín-Peña, R., López-Rojas, R., Pachón, J., et al. (2014). Activity of host antimicrobials against multidrug-resistant *Acinetobacter baumannii* acquiring colistin resistance through loss of lipopolysaccharide. *Antimicrob. Agents Chemother.* 58, 2972–2975. doi: 10.1128/AAC.02642-13

Gerits, E., Blommaert, E., Lippell, A., O'Neill, A. J., Weytjens, B., De Maeyer, D., et al. (2016). Elucidation of the mode of action of a new antibacterial compound active against *Staphylococcus aureus* and *Pseudomonas aeruginosa*. *PLOS ONE* 11:e0155139. doi: 10.1371/journal.pone.0155139

Ghequire, M., and De Mot, R. (2014). Ribosomally encoded antibacterial proteins and peptides from *Pseudomonas*. *FEMS Microbiol. Rev.* 38, 523–568. doi: 10.1111/1574-6976.12079

Grzegorzewicz, A. E., Hess, T., Jones, V., Gruppo, V., Born, S. E. M., Chavadi, S. S., et al. (2012). Inhibition of mycolic acid transport across the *Mycobacterium tuberculosis* plasma membrane. *Nat. Chem.* 8, 334–341. doi: 10.1038/nchembio.794.INHIBITION

Harms, A., Maisonneuve, E., and Gerdes, K. (2016). Mechanisms of bacterial persistence during stress and antibiotic exposure. *Science* 354:aaf4268. doi: 10.1126/science.aaf4268

Helaine, S., and Kugelberg, E. (2014). Bacterial persisters: formation, eradication, and experimental systems. *Trends Microbiol.* 22, 417–424. doi: 10.1016/j.tim.2014.03.008

Helander, I. M., and Mattila-Sandholm, T. (2000). Fluorometric assessment of gram-negative bacterial permeabilization. *J. Appl. Microbiol.* 88, 213–219. doi: 10.1046/j.1365-2672.2000.00971.x

Hobbs, J. K., Miller, K., O'Neill, A. J., and Chopra, I. (2008). Consequences of daptomycin-mediated membrane damage in *Staphylococcus aureus*. *J. Antimicrob. Chemother.* 62, 1003–1008. doi: 10.1093/jac/dkn321

Hu, Y., Shamaei-Tousi, A., Liu, Y., and Coates, A. R. M. (2010). A new approach for the discovery of antibiotics by targeting non-multiplying bacteria: a novel topical antibiotic for staphylococcal infections. *PLOS ONE* 5:e11818. doi: 10.1371/journal.pone.0011818

Hubbard, A. T., Barker, R., Rehal, R., Vandera, K. A., Harvey, R. D., and Coates, A. R. M. (2017). Mechanism of action of a membrane-active quinoline-based antimicrobial on natural and model bacterial membranes. *Biochemistry* 56, 1163–1174. doi: 10.1021/acs.biochem.6b01135

Hurdle, J. G., O'Neill, A. J., Chopra, I., and Lee, R. E. (2011). Targeting bacterial membrane function: an underexploited mechanism for treating persistent infections. *Nat. Rev. Microbiol.* 9, 62–75. doi: 10.1038/nrmicro2474

Imperi, F., Massai, F., Ramachandran Pillai, C., Longo, F., Zennaro, E., Rampioni, G., et al. (2013). New life for an old drug: the anthelmintic drug niclosamide inhibits *Pseudomonas aeruginosa* quorum sensing. *Antimicrob. Agents Chemother.* 57, 996–1005. doi: 10.1128/AAC.01952-12

Kulp, A., and Kuehn, M. J. (2010). Biological functions and biogenesis of secreted bacterial outer membrane vesicles. *Annu. Rev. Microbiol.* 64, 163–184. doi: 10.1146/annurev.micro.091208.073413

Lee, D. G., Urbach, J. M., Wu, G., Liberati, N. T., Feinbaum, R. L., Miyata, S., et al. (2006). Genomic analysis reveals that *Pseudomonas aeruginosa* virulence is combinatorial. *Genome Biol.* 7:R90. doi: 10.1186/gb-2006-7-10-r90

Lewis, K. (2010). Persister cells. *Annu. Rev. Microbiol.* 64, 357–372. doi: 10.1146/annurev.micro.112408.134306

Liberati, N. T., Urbach, J. M., Miyata, S., Lee, D. G., Drenkard, E., Wu, G., et al. (2006). An ordered, nonredundant library of *Pseudomonas aeruginosa* strain PA14 transposon insertion mutants. *Proc. Natl. Acad. Sci. U.S.A.* 103, 2833–2838. doi: 10.1073/pnas.0511100103

Liebens, V., Defraine, V., Knapen, W., Swings, T., Beullens, S., Corbau, R., et al. (2017). Identification of 1-((2,4-Dichlorophenethyl)Amino)-3-Phenoxypropan-2-ol, a novel antibacterial compound active against persisters of *Pseudomonas aeruginosa*. *Antimicrob. Agents Chemother.* 61:e00836-17. doi: 10.1128/AAC.00836-17

Liebens, V., Defraine, V., Van der Leyden, A., De Groote, V. N., Fierro, C., Beullens, S., et al. (2014). A putative de-N-acetylase of the PIG-L superfamily affects fluoroquinolone tolerance in *Pseudomonas aeruginosa*. *Pathog. Dis.* 71, 39–54. doi: 10.1111/2049-632X.12174

Ling, L. L., Schneider, T., Peoples, A. J., Spoering, A. L., Engels, I., Conlon, B. P., et al. (2015). A new antibiotic kills pathogens without detectable resistance. *Nature* 517, 455–459. doi: 10.1038/nature14098

Livermore, D. M. (2002). Multiple mechanisms of antimicrobial resistance in *Pseudomonas aeruginosa*: our worst nightmare? *Clin. Infect. Dis.* 34, 634–640. doi: 10.1086/338782

Lomovskaya, O., and Watkins, W. J. (2001). Efflux pumps: their role in antibacterial drug discovery. *Curr. Med. Chem.* 8, 1699–1711. doi: 10.2174/0929867013371743

Love, M. I., Huber, W., and Anders, S. (2014). Moderated estimation of fold change and dispersion for RNA-seq data with DESeq2. *Genome Biol.* 15:550. doi: 10.1186/s13059-014-0550-8

Mandal, S. M., Pegu, R., Porto, W. F., Franco, O. L., and Pratihar, S. (2017). Novel boronic acid derivatives of bis(indolyl) methane as anti-MRSA agents. *Bioorganic Med. Chem. Lett.* 27, 2135–2138. doi: 10.1016/j.bmcl.2017.03.070

Masschelein, J., Clauwers, C., Stalmans, K., Nuyts, K., De Borggraeve, W., Briers, Y., et al. (2015). The zeamine antibiotics affect the integrity of bacterial membranes. *Appl. Environ. Microbiol.* 81, 1139–1146. doi: 10.1128/AEM.03146-14

Michiels, J. E., Van den Bergh, B., Verstraeten, N., and Michiels, J. (2016). Molecular mechanisms and clinical implications of bacterial persistence. *Drug Resist. Updat.* 29, 76–89. doi: 10.1016/j.drup.2016.10.002

Morita, Y. (2003). Induction of *mexCD-oprJ* operon for a multidrug efflux pump by disinfectants in wild-type *Pseudomonas aeruginosa* PAO1. *J. Antimicrob. Chemother.* 51, 991–994. doi: 10.1093/jac/dkg173

Morita, Y., Komori, Y., Mima, T., Kuroda, T., Mizushima, T., and Tsuchiya, T. (2001). Construction of a series of mutants lacking all of the four major *mex* operons for multidrug efflux pumps or possessing each one of the operons from *Pseudomonas aeruginosa* PAO1: MexCD-OprJ is an inducible pump. *FEMS Microbiol. Lett.* 202, 139–143. doi: 10.1016/S0378-1097(01)00314-7

Nakayama, K., Takashima, K., Ishihara, H., Shinomiya, T., Kageyama, M., Kanaya, S., et al. (2000). The R-type pyocin of *Pseudomonas aeruginosa* is related to P2 phage, and the F-type is related to lambda phage. *Mol. Microbiol.* 38, 213–231. doi: 10.1046/j.1365-2958.2000.02135.x

Nowakowska, J., Griesser, H. J., Textor, M., Landmann, R., and Khanna, N. (2013). Antimicrobial properties of 8-hydroxyserrulat-14-en-19-oic acid for treatment of implant-associated infections. *Antimicrob. Agents Chemother.* 57, 333–342. doi: 10.1128/AAC.01735-12

Okazaki, T., and Hirai, K. (1992). Cloning and nucleotide sequence of the *Pseudomonas aeruginosa nfxB* gene, conferring resistance to new quinolones. *FEMS Microbiol. Lett.* 97, 197–202. doi: 10.1111/j.1574-6968.1992.tb05462.x

O'Neill, J. (2015). "Securing new drugs for future generations: the pipeline of antibiotics," in *The Review on Antimicrobial Resistance*. Available at: https://amr-review.org/sites/default/files/SECURING%20NEW%20DRUGS%20FOR%20FUTURE%20GENERATIONS%20FINAL%20WEB_0.pdf

Papo, N., and Shai, Y. (2005). A molecular mechanism for lipopolysaccharide protection of Gram-negative bacteria from antimicrobial peptides. *J. Biol. Chem.* 280, 10378–10387. doi: 10.1074/jbc.M412865200

Poole, K. (2011). *Pseudomonas aeruginosa*: resistance to the max. *Front. Microbiol.* 2:65. doi: 10.3389/fmicb.2011.00065

Purssell, A., and Poole, K. (2013). Functional characterization of the NfxB repressor of the mexCD-oprJ multidrug efflux operon of *Pseudomonas aeruginosa*. *Microbiology* 159, 2058–2073. doi: 10.1099/mic.0.069286-0

Raghuraman, H., and Chattopadhyay, A. (2007). Melittin: a membrane-active peptide with diverse functions. *Biosci. Rep.* 27, 189–223. doi: 10.1007/s10540-006-9030-z

Rana, F. R., Macias, E. A., Sultany, C. M., Modzrakowski, M. C., and Blazyk, J. (1991). Interactions between magainin 2 and *Salmonella typhimurium* outer membranes: effect of lipopolysaccharide structure. *Biochemistry* 30, 5858–5866. doi: 10.1021/bi00238a008

Randall, C. P., Mariner, K. R., Chopra, I., and O'Neill, A. J. (2013). The target of daptomycin is absent from *Escherichia coli* and other gram-negative pathogens. *Antimicrob. Agents Chemother.* 57, 637–639. doi: 10.1128/AAC.02005-12

Rice, L. B. (2008). Federal funding for the study of antimicrobial resistance in nosocomial pathogens: no ESKAPE. *J. Infect. Dis.* 197, 1079–1081. doi: 10.1086/533452

Roth, B. L., Poot, M., Yue, S. T., and Millard, P. J. (1997). Bacterial viability and antibiotic susceptibility testing with SYTOX green nucleic acid stain. *Appl. Environ. Microbiol.* 63, 2421–2431.

Samanta, T., Roymahapatra, G., Porto, W. F., Seth, S., Ghorai, S., Saha, S., et al. (2013).). N, N'-Olefin functionalized bis-imidazolium gold(I) salt is an efficient candidate to control keratitis-associated eye infection. *PLOS ONE* 8:e58346. doi: 10.1371/journal.pone.0058346

Shannon, P., Markiel, A., Ozier, O., Baliga, N. S., Wang, J. T., Ramage, D., et al. (2003). Cytoscape: a software environment for integrated models of biomolecular interaction networks. *Genome Res.* 13, 2498–2504. doi: 10.1101/gr.1239303

Stickland, H. G., Davenport, P. W., Lilley, K. S., Griffin, J. L., and Welch, M. (2010). Mutation of *nfxB* causes global changes in the physiology and metabolism of *Pseudomonas aeruginosa*. *J. Proteome Res.* 9, 2957–2967. doi: 10.1021/pr9011415

Szklarczyk, D., Franceschini, A., Kuhn, M., Simonovic, M., Roth, A., Minguez, P., et al. (2011). The STRING database in 2011: functional interaction networks of proteins, globally integrated and scored. *Nucleic Acids Res.* 39, D561–D568. doi: 10.1093/nar/gkq973

Terstappen, G. C., Schlüpen, C., Raggiaschi, R., and Gaviraghi, G. (2007). Target deconvolution strategies in drug discovery. *Nat. Rev. Drug Discov.* 6, 891–903. doi: 10.1038/nrd2410

Torrent, M., Navarro, S., Moussaoui, M., Nogués, M. V., and Boix, E. (2008). Eosinophil cationic protein high-affinity binding to bacteria-wall lipopolysaccharides and peptidoglycans. *Biochemistry* 47, 3544–3555. doi: 10.1021/bi702065b

Van den Bergh, B., Fauvart, M., and Michiels, J. (2017). Formation, physiology, ecology, evolution and clinical importance of bacterial persisters. *FEMS Microbiol. Rev.* 41, 219–251. doi: 10.1093/femsre/fux001

Walsh, C. T., and Wencewicz, T. A. (2014). Prospects for new antibiotics: a molecule-centered perspective. *J. Antibiot.* 67, 7–22. doi: 10.1038/ja.2013.49

Winsor, G. L., Griffiths, E. J., Lo, R., Dhillon, B. K., Shay, J. A., and Brinkman, F. S. L. (2016). Enhanced annotations and features for comparing thousands of *Pseudomonas* genomes in the Pseudomonas genome database. *Nucleic Acids Res.* 44, D646–D653. doi: 10.1093/nar/gkv1227

Wong, A., Rodrigue, N., and Kassen, R. (2012). Genomics of adaptation during experimental evolution of the opportunistic pathogen *Pseudomonas aeruginosa*. *PLOS Genet.* 8:e1002928. doi: 10.1371/journal.pgen.1002928

Wood, T. K. (2015). Combatting bacterial persister cells. *Biotechnol. Bioeng.* 113, 476–483. doi: 10.1002/bit.25721

Wright, G. D. (2014). Something old, something new: revisiting natural products in antibiotic drug discovery. *Can. J. Microbiol.* 60, 147–154. doi: 10.1139/cjm-2014-0063

Yu, Z., Qin, W., Lin, J., Fang, S., and Qiu, J. (2015). Antibacterial mechanisms of polymyxin and bacterial resistance. *Biomed Res. Int* 2015:679109. doi: 10.1155/2015/679109

Zhang, Y. (2014). Persisters, persistent infections and the Yin–Yang model. *Emerg. Microbes Infect* 3:e3. doi: 10.1038/emi.2014.3

Zou, H., Koh, J. J., Li, J., Qiu, S., Aung, T. T., Lin, H., et al. (2013). Design and synthesis of amphiphilic xanthone-based, membrane-targeting antimicrobials with improved membrane selectivity. *J. Med. Chem.* 56, 2359–2373. doi: 10.1021/jm301683j

Conflict of Interest Statement: The authors declare that the research was conducted in the absence of any commercial or financial relationships that could be construed as a potential conflict of interest.

frontiers in Microbiology

ORIGINAL RESEARCH
published: 22 December 2017
doi: 10.3389/fmicb.2017.02585

Antibacterial Activity of 1-[(2,4-Dichlorophenethyl)amino]-3-Phenoxypropan-2-ol against Antibiotic-Resistant Strains of Diverse Bacterial Pathogens, Biofilms and in Pre-clinical Infection Models

Valerie Defraine[1,2], Laure Verstraete[1,2], Françoise Van Bambeke[3], Ahalieyah Anantharajah[3], Eleanor M. Townsend[4,5], Gordon Ramage[4], Romu Corbau[6†], Arnaud Marchand[6], Patrick Chaltin[6,7], Maarten Fauvart[1,8‡] and Jan Michiels[1,2‡]*

[1] Centre of Microbial and Plant Genetics, University of Leuven, Leuven, Belgium, [2] Center for Microbiology, Vlaams Instituut voor Biotechnologie, Leuven, Belgium, [3] Pharmacologie Cellulaire et Moléculaire, Louvain Drug Research Institute, Université catholique de Louvain, Brussels, Belgium, [4] Oral Science Research Group, Glasgow Dental School, University of Glasgow, Glasgow, United Kingdom, [5] Institute of Healthcare Policy and Practice, University of West of Scotland, Paisley, United Kingdom, [6] CISTIM Leuven vzw, Leuven, Belgium, [7] Centre for Drug Design and Discovery, Leuven, Belgium, [8] Department of Life Sciences and Imaging, Smart Electronics Unit, imec, Leuven, Belgium

We recently described the novel anti-persister compound 1-[(2,4-dichlorophenethyl)amino]-3-phenoxypropan-2-ol (SPI009), capable of directly killing persister cells of the Gram-negative pathogen *Pseudomonas aeruginosa*. This compound also shows antibacterial effects against non-persister cells, suggesting that SPI009 could be used as an adjuvant for antibacterial combination therapy. Here, we demonstrate the broad-spectrum activity of SPI009, combined with different classes of antibiotics, against the clinically relevant ESKAPE pathogens *Enterobacter aerogenes, Staphylococcus aureus, Klebsiella pneumoniae, Acinetobacter baumannii, P. aeruginosa, Enterococcus faecium* and *Burkholderia cenocepacia* and *Escherichia coli*. Importantly, SPI009 re-enabled killing of antibiotic-resistant strains and effectively lowered the required antibiotic concentrations. The clinical potential was further confirmed in biofilm models of *P. aeruginosa* and *S. aureus* where SPI009 exhibited effective biofilm inhibition and eradication. *Caenorhabditis elegans* infected with *P. aeruginosa* also showed a significant improvement in survival when SPI009 was added to conventional antibiotic treatment. Overall, we demonstrate that SPI009, initially discovered as an anti-persister molecule in *P. aeruginosa*, possesses broad-spectrum activity and is highly suitable for the development of antibacterial combination therapies in the fight against chronic infections.

Keywords: antibacterials, *P. aeruginosa*, ESKAPE pathogens, anti-persister therapies, antibiotic resistance

OPEN ACCESS

Edited by:
Maria Olivia Pereira, University of Minho, Portugal

Reviewed by:
Rodolfo García-Contreras, Universidad Nacional Autónoma de México, Mexico
Vishvanath Tiwari, Central University of Rajasthan, India
Paul Cos, University of Antwerp, Belgium

***Correspondence:**
Jan Michiels
jan.michiels@kuleuven.vib.be

†Present address:
Romu Corbau, Freeline Therapeutics, UCL Royal Free Medical School, London, United Kingdom

‡ *These authors are joint senior authors.*

Specialty section:
This article was submitted to Antimicrobials, Resistance and Chemotherapy, a section of the journal Frontiers in Microbiology

Received: *07 August 2017*
Accepted: *12 December 2017*
Published: *22 December 2017*

Citation:
Defraine V, Verstraete L, Van Bambeke F, Anantharajah A, Townsend EM, Ramage G, Corbau R, Marchand A, Chaltin P, Fauvart M and Michiels J (2017) Antibacterial Activity of 1-[(2,4-Dichlorophenethyl)amino]-3-Phenoxypropan-2-ol against Antibiotic-Resistant Strains of Diverse Bacterial Pathogens, Biofilms and in Pre-clinical Infection Models. Front. Microbiol. 8:2585. doi: 10.3389/fmicb.2017.02585

INTRODUCTION

Antibiotic resistance is rapidly increasing in the majority of nosocomial pathogens, complicating the effective treatment of bacterial infections and transforming once easily cured diseases into serious human health threats (European Centre for Disease Prevention and Control, 2013; O'Neill, 2016). Although selection for resistance in microorganisms is inevitable, the widespread and excessive use of antibiotics allowed pathogens to efficiently adapt to these stressful conditions, resulting in the occurrence of extensively drug-resistant and pan-drug resistant strains (Livermore, 2004; Fischbach and Walsh, 2009). In an attempt to guide research and development toward the most critical pathogens, the World Health Organization (WHO) recently published their 'global priority list,' containing 12 bacterial pathogens that raise particular concern (WHO, 2017). Among these are the so-called ESKAPE pathogens, *Enterococcus faecium, Staphylococcus aureus, Klebsiella pneumoniae, Acinetobacter baumannii, P. aeruginosa,* and *Enterobacter* spp., which efficiently evade antibiotic treatment and represent new paradigms in pathogenesis, transmission, and resistance (Rice, 2008). Together, this select group of bacteria is responsible for most of the hospital-acquired infections and, despite increasing research efforts, therapeutic options remain scarce (Bassetti et al., 2013; Pendleton et al., 2013). Greatly contributing to the difficult treatment of these bacterial infections is the presence of non-growing persister cells. These phenotypic variants show a reduced metabolic activity, are able to withstand intensive antibiotic treatment, and when antibiotic pressure drops, are capable of restoring the bacterial population, causing recurrence of infection (Fauvart et al., 2011; Van den Bergh et al., 2017). Persistence is widely acknowledged as a major culprit of treatment failure in chronic and biofilm infections and recent research has identified the persister fraction as a possible reservoir for the development of resistance (Lewis, 2007; Cohen et al., 2013). Effective elimination of persister cells could significantly improve patient outcomes, but their small numbers and the apparent redundancy in persister mechanisms greatly hampers the development of targeted anti-persister therapies.

We recently reported the identification of a novel anti-persister molecule capable of directly killing persister cells of *P. aeruginosa* (Liebens et al., 2017). SPI009 was identified in a screening of 23,909 small molecules for compounds that decrease the persister fraction of *P. aeruginosa* in combination with the conventional antibiotic ofloxacin. In the present study, we explore the activity of SPI009 in several additional pathogens and demonstrate broad spectrum activity and the ability to sensitize resistant strains. Furthermore, SPI009 was shown to retain activity in different biofilm models and is capable of significantly improving antibiotic efficacy both in *in vitro* and *in vivo* infection models. Overall, these results further increase the clinical potential of SPI009 and offer compelling perspectives for the use of SPI009 as an adjuvant in effective antimicrobial therapies.

MATERIALS AND METHODS

Bacterial Strains, Human Cell Lines, *C. elegans*, and Culture Conditions

Bacterial strains used in this study are listed in **Table 1**. All strains were cultured in 1:20 diluted Trypticase Soy Broth (1/20 TSB) at 37°C shaking at 200 rpm. For solid medium, TSB was supplemented with 1.5% agar. Human THP-1 cell lines were cultivated in RPMI-1640 medium containing 10% fetal calf serum at 37°C with 5% CO_2. The *C. elegans* AU37 strain [*glp-4(bn2); sek-1(km4)*] was obtained from the Caenorhabditis Genetics Center (CGC) and maintained according to standards (Stiernagle, 2006). The following antibacterials were used: ofloxacin, ciprofloxacin, rifampicin, polymyxin B, vancomycin (Sigma–Aldrich), and 1-[(2,4-dichlorophenethyl)amino]-3-phenoxypropan-2-ol (SPI009; CD3) with concentrations indicated throughout the text.

Antibacterial Assays

Antibacterial assays were performed on different clinically relevant pathogens as previously described (Liebens et al., 2017). Briefly, stationary phase cultures were treated for 5 h with 17 or 34 μg/mL of SPI009 alone or in combination with an appropriate antibiotic to assess anti-bacterial and anti-persister effects, respectively. To evaluate activity against resistant strains, stationary phase cultures were treated for 5 h with 1x, 4x, and 8x MIC concentrations of the respective antibiotic; 17 or 34 μg/mL SPI009 or the combination of both. After treatment, cells were washed and viability was assessed via plating.

Quantification of Biofilm Formation and Eradication after Treatment with SPI009

Overnight cultures of *P. aeruginosa* PA14 WT or *S. aureus* ATCC 33591 were diluted 1:100 in 1/20 TSB medium supplemented with 2% DMSO (carrier control) or increasing concentrations of SPI009 (4.25–68 μg/mL). Biofilms were grown for 24 h at 37°C on the bottom of a polystyrene 96-well plate, non-shaking. Medium and free-living cells were removed and the biofilms were washed, scraped off and passed five times through a syringe (0.5 mm × 1.6 mm) to disrupt any cell clumps and obtain single cells (Hermans et al., 2011). Appropriate dilutions made in 1x PBS were plated on solid TSB agar plates to assess biofilm growth under different conditions.

To explore the biofilm eradicating effects of SPI009, overnight cultures of *P. aeruginosa* PA14 WT or *S. aureus* ATCC 33591 were diluted 1:100 in 1/20 TSB medium and incubated for 24 h at 37°C (non-shaking). Mature biofilms were treated for 5 h with 2% DMSO and increasing concentrations of SPI009 (8.5–136 μg/mL) at 37°C, non-shaking, after which the remaining biofilms were processed as described above.

Chronic Wound Model

A three-dimensional wound biofilm model was used, as previously described (Townsend et al., 2016). *P. aeruginosa* coated cellulose matrices, obtained after 2 h of adhesion (1×10^6

TABLE 1 | Strains used in this study.

Strain	Description	Source or reference
P. aeruginosa PA14	Wild type; UBCPP-PA14	Pierre Cornelis; Lee et al., 2006
P. aeruginosa PAO1	Wild type	Dieter Haas (ETH)
P. aeruginosa PA62	Broncho-pulmonary clinical isolate OFX^R, CIP^R, GEN^R, AMK^R, ATM^R, TIC^R, PIP^R, TZP^R, CAZ^R, FEP^R	Françoise van Bambeke (UCL)
P. aeruginosa 9BR	Clinical isolate, PBM^R, MEM^R, CIP^R, and FEP^R, CAZ^R, or TZP^R	Bob Hancock; Boyle et al., 2012
E. aerogenes	ATCC 13048 (KCTC 2190)	Shin et al., 2012
S. aureus Rosenbach 1844	Wild type, methicillin resistant, ATCC 33591	BCCM/LGM bacterial collection; Conlon et al., 2013
K. pneumoniae	ATCC 13883	Arivett et al., 2015
A. baumannii	RUH134	Jean-Paul Pirnay; Merabishvili et al., 2014
E. faecium	LMG 8148	Descheemaeker et al., 1997
B. cenocepacia K56-2	LMG 18863	Van Acker et al., 2013
E. coli BW25113	F^-, Δ(araD-araB)567, ΔlacZ4787(::rrnB-3), λ^-, rph-1, Δ(rhaD-rhaB)568, *hsd*R514	Baba et al., 2006

Resistance profiles determined according to EUCAST MIC breakpoints (European Committee on Antimicrobial Susceptibility Testing, 2017). OFX, ofloxacin; CIP, ciprofloxacin; GEN, gentamicin; AMK, amikacin; ATM, aztreonam; TIC, ticarcillin; PIP, piperacillin; TZP, piperacillin-tazobactam; CAZ, ceftazidime; FEP, cefepime; PBM, polymyxin B; MEM, meropenem.

cells/mL), were placed onto the hydrogels after which 3D biofilm development was allowed for 24 h at 37°C. Mature biofilms were treated for 24 h with DMSO (1%), 10 μg/mL ofloxacin, 34 and 69 μg/mL of SPI009 or the combination of ofloxacin and SPI009. Any non-adherent cells were removed by rinsing after which biomass was removed by sonication at 35 kHz for 10 min and DNA was extracted. Samples were prepared as previously described and viability-based qPCR using *P. aeruginosa* specific primers F- GGGCGAAGAAGGAAATGGTC and R- CAGGTGGCGTAGGTGGAGAA was used to determine live and total fractions of biofilm cells under different treatment conditions (Smith et al., 2016). Standard curves were used to convert the obtained qPCR values to colony forming estimates (CFEs), after which $\log_{10}$-transformed values were used for statistical analysis, as described below. All experiments were carried out in triplicate, each containing three technical repeats.

Intracellular Infection Model

Infection of human THP-1 cells was performed as described previously, with minor modifications (Buyck et al., 2013). Since a newly synthesized batch of SPI009 was used for this experiment, cytotoxicity assessment via an LDH enzyme assay was repeated for the THP-1 cell line, as previously described (Liebens et al., 2017). After THP-1 infection with *P. aeruginosa* PAO1 and subsequent removal of any non-phagocytozed or adherent bacteria, ciprofloxacin and SPI009 were added in final concentrations of, respectively, 0–20 μg/mL and 6.8 or 10.2 μg/mL. After 5 h of treatment, eukaryotic cells were collected in three consecutive centrifugation steps and complete cell lysis was obtained by sonication (10 s). Lysates were used for bacterial CFU counting and determination of protein content by Lowry's assay (Bio-Rad DC protein assay kit; Bio-Rad laboratories, Hercules, CA, United States). For analysis of surviving bacterial cells, CFU data were divided by corresponding protein content for normalization.

C. elegans Toxicity Testing and Survival Assay

AU37 nematodes were synchronized as previously described (Porta-de-la-Riva et al., 2012) to obtain L4 worms suitable for toxicity and infection assays (Briers et al., 2014). Larvae obtained after bleaching were plated onto solid NGM-OP50 agar plates and incubated at 25°C during 2 days to allow development of the worms to the L4 stage. Worms were transferred to fresh NGM agar plates containing OP50 (toxicity testing and uninfected control) or PA14 (infection) for an additional 24 h at 25°C.

To evaluate toxicity of SPI009 L4 nematodes grown on OP50 were transferred to 12-well plates (20–30 worms/well) containing different concentrations of SPI009 (8.5–136 μg/mL) in 1.5 mL NGM:M9 (1:4). Controls consisted of untreated worms and DMSO (2% and 20%). For the infection assay, adult worms were allowed to feed on NGM-PA14 plates for 24 h, after which residual bacteria were removed and nematodes were divided over a 12-well plate (20–30 worms/well). Different treatments were prepared in 1.5 mL NGM:M9 (1:4) and consisted of an untreated control, 1.56 μg/mL ciprofloxacin (5x MIC), 8.5 μg/mL of SPI009 and the combination of ciprofloxacin and SPI009. As an additional control, uninfected worms were included. For both assays, worms were incubated at 25°C and survival was scored visually for 6 days.

Statistical Analysis

Unless mentioned otherwise, all statistical analyses were performed on $\log_{10}$-transformed data using GraphPad Prism software (version 6.01). Bacterial survival after different treatments was compared to the untreated or antibiotic control using a one-way ANOVA ($\alpha = 0.05$), with Dunnett's correction for multiple comparisons. Statistical comparison of mono- and combination treatment in resistant strains was done using a two-way ANOVA ($\alpha = 0.05$) with Tukey correction for multiple comparisons. Statistical analysis of the *in vivo C. elegans* data was done by means of a log-rank test using GraphPad Prism.

RESULTS

SPI009 Shows Broad-Spectrum Activity against Different Clinically Relevant Bacterial Species

The activity of SPI009 was previously assessed in *P. aeruginosa* PA14 and several clinical isolates where combination with ofloxacin significantly decreased the persister fraction in all strains tested (Liebens et al., 2017). In the present study, we challenged a panel of clinically relevant species, including the ESKAPE pathogens (**Figure 1A**), *B. cenocepacia* and *E. coli* (**Figure 1B**). For each species appropriate concentrations of a conventional antibiotic used in the clinic were selected to allow only persister cells to survive (Supplementary Figure S1). Combination of the antibiotic with 17 μg/mL SPI009 significantly decreased the number of surviving bacteria for five of the eight species with reductions in CFU ranging between 1.5 ± 0.1 and 6.0 ± 0.2 log units and complete eradication of *K. pneumoniae*. Addition of 34 μg/mL completely eradicated the bacterial cultures of five of the eight species tested and resulted in significant 6.6 ± 0.5 log, 6.2 ± 1.3 log, and 5.4 ± 0.5 log reductions in bacterial survival for *S. aureus*, *E. faecium*, and *B. cenocepacia*, respectively. No reduction in survival is observed after treatment with 17 μg/mL for either of the Gram-positive species, *E. faecium* and *S. aureus*. These results suggest that the latter two species, and the Gram-negative *B. cenocepacia*, are slightly less sensitive toward the combination therapy. *K. pneumoniae* proved the most susceptible species toward SPI009. Overall, the obtained results further support the antibacterial effect of SPI009 and reveal a broad-spectrum activity.

SPI009 Sensitizes Antibiotic-Resistant Strains

To investigate the possible use of SPI009 as an adjuvant in antibacterial combination therapies, several (multi)drug-resistant strains were treated with 1x, 4x, and 8x MIC concentrations of the antibiotic, alone and in combination with SPI009. While SPI009 alone did not cause a significant decrease in survival of the ofloxacin resistant *P. aeruginosa* PA62, addition of 17 or 34 μg/mL of SPI009 significantly reduced the number of surviving cells by 5.3 ± 0.9 and 7.8 ± 0.9 log units at 4x MIC of ofloxacin while combination with 8x MIC completely eradicated the bacterial culture (**Figure 2A**). In comparison, treatment with ofloxacin alone caused 0.8 ± 0.9 log and 2.8 ± 0.9 log decreases in surviving cells at concentrations of 4x MIC and 8x MIC, respectively.

A similar trend was observed in the polymyxin B resistant *P. aeruginosa* 9BR (**Figure 2B**). Here, addition of the antibiotic alone had a slightly greater effect but combination with SPI009 still significantly improved the treatment and 17 μg/mL of SPI009 successfully eradicated the entire bacterial culture in combination with 4x MIC of polymyxin B. A somewhat smaller effect was observed in the polymyxin B resistant *B. cenocepacia* strain K56-2, for which addition of 17 μg/mL and 34 μg/mL SPI009 to 4x MIC polymyxin B resulted in significant 4.9 ± 0.5 and

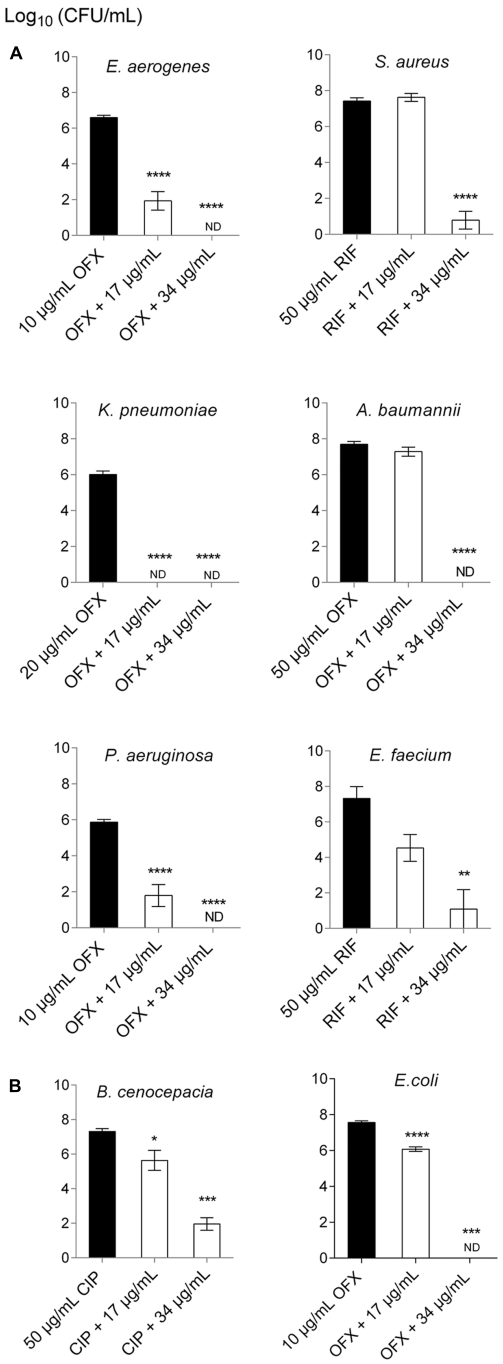

FIGURE 1 | SPI009 possesses broad-spectrum activity against different clinically important pathogens. 200 μL volumes of stationary phase cultures of **(A)** ESKAPE pathogens *E. aerogenes, S. aureus, K. pneumoniae, A. baumannii, P. aeruginosa,* and *E. faecium* and **(B)** *B. cenocepacia* and *E. coli* were treated for 5 h with the combination of a conventional antibiotic; ofloxacin (OFX), ciprofloxacin (CIP), or rifampicin (RIF) and 17 or 34 μg/mL SPI009. Black bars represent the antibiotic and white bars the combination of antibiotic with SPI009. Results are the mean of at least three independent experiments with error bars depicting SEM values. One-way ANOVA with Dunnett's correction for multiple comparisons was used to detect significant differences to the antibiotic control with $^{*}P \leq 0.05$, $^{**}P \leq 0.01$, $^{***}P \leq 0.001$, $^{****}P \leq 0.0001$. ND, not detected.

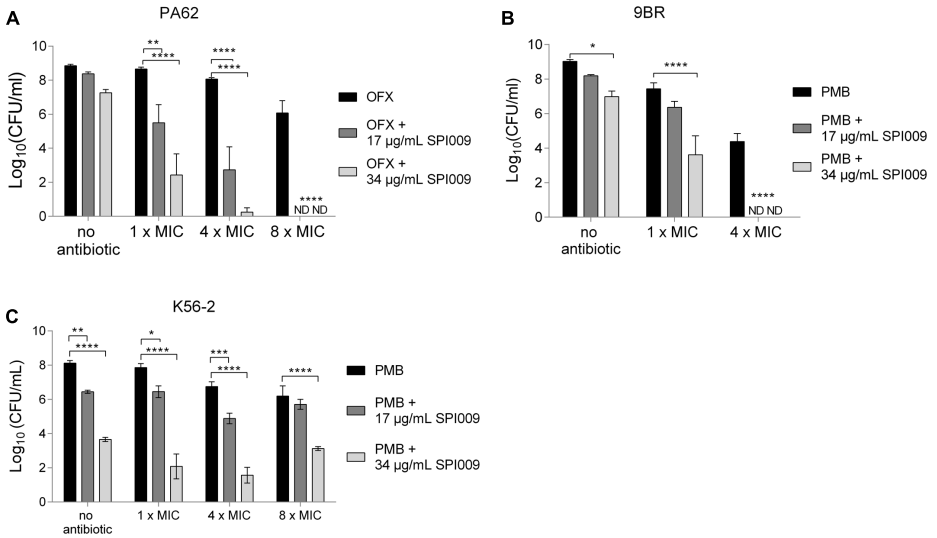

FIGURE 2 | SPI009 re-enables the treatment of (multi)drug-resistant strains. Stationary phase cultures of **(A)** *P. aeruginosa* PA62 (OFX^R), **(B)** *P. aeruginosa* 9BR (PMB^R) and **(C)** *B. cenocepacia* K56-2 (PMB^R) were treated for 5 h with 1x MIC, 4x MIC, and 8x MIC concentrations of the respective antibiotic alone and in combination with 17 or 34 μg/mL of SPI009. Data points represent the average of at least three biological repeats. SEM values are shown as error bars. Statistical analysis was done by means of two-way ANOVA ($\alpha = 0.05$) with Tukey correction for multiple comparisons and $^*P \leq 0.05$, $^{**}P \leq 0.01$, $^{***}P \leq 0.001$, $^{****}P \leq 0.0001$; ND, not detected.

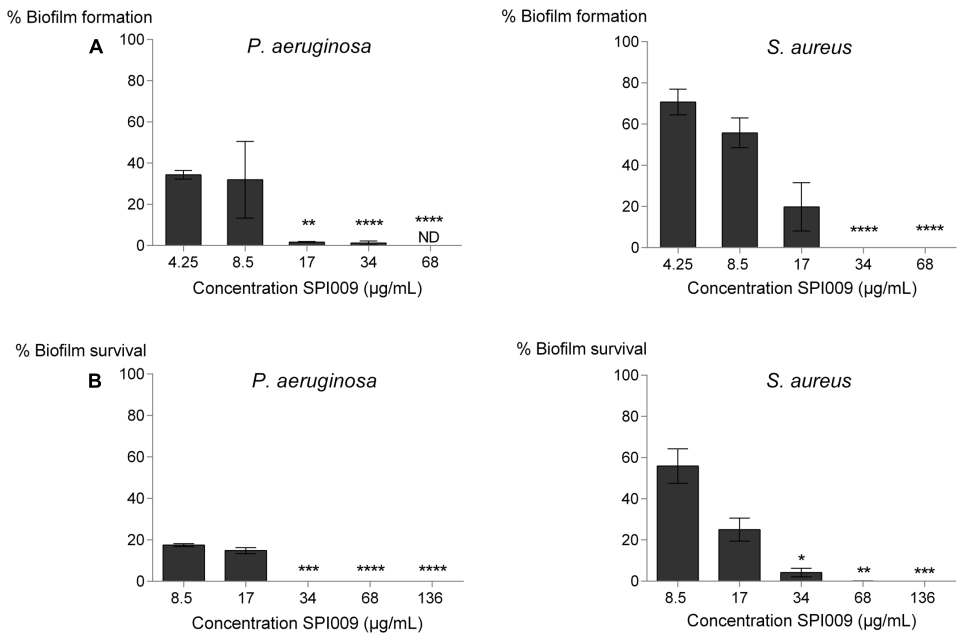

FIGURE 3 | Anti-biofilm effects of SPI009 in *P. aeruginosa* and *S. aureus.* Increasing concentrations of SPI009 (4.25–136 μg/mL) and a DMSO control were added for **(A)** 24 h to 1:100 diluted cultures or **(B)** 5 h to 24-h-old biofilms in 96-well microtiter plates to assess biofilm inhibition and eradication, respectively. After treatment, biofilms were washed, disturbed and plated out to calculate the number of surviving cells. Data points represent the percentage of surviving cells relative to the untreated control as an average of at least three biological repeats, each containing three technical repeats. Error bars depict SEM values. Statistical significance was calculated on $\log_{10}$ transformed CFU counts using a one-way ANOVA with Dunnett's correction for multiple comparisons. $^*P \leq 0.05$, $^{**}P \leq 0.01$, $^{***}P \leq 0.001$, $^{****}P \leq 0.0001$. ND, not detectable.

5.2 ± 0.5 log decreases in survival. Combinations with higher concentrations of polymyxin B (8x MIC) did not further decrease the number of surviving cells (**Figure 2C**). The obtained results clearly demonstrate the effective use of SPI009 as an adjuvant for antibacterial therapy thereby facilitating the treatment of different antibiotic-resistant strains. Furthermore, SPI009 retains

activity in multidrug-resistant strains, revealing the lack of cross-resistance. Importantly, resensitization of resistant strains could restore the effectiveness of established antibiotics.

Biofilm Inhibition and Eradication Effects of SPI009

To assess biofilm inhibiting properties of SPI009 in *P. aeruginosa* and *S. aureus*, biofilm growth was allowed in the presence of increasing concentrations of SPI009 (**Figure 3A**). Analysis of the obtained results clearly show an effective inhibition of biofilm growth in both *P. aeruginosa* and *S. aureus.* For *P. aeruginosa,* a steep increase in inhibitory activity was observed at concentrations above 8.5 μg/mL, resulting in 1.8 ± 0.5 log and 2.4 ± 0.4 log decreases at 17 or 34 μg/mL SPI009, respectively, and complete inhibition of biofilm growth at 68 μg/mL. *S. aureus* showed a more gradual decrease in biofilm formation with 34 μg/mL and 68 μg/mL resulting in significant 6.2 ± 0.6 log and 6.4 ± 0.6 log decreases in biofilm formation, respectively. These results clearly demonstrate the potent biofilm inhibiting activity of SPI009 for both Gram-negative and Gram-positive model pathogens.

To explore biofilm eradication, SPI009 was added to mature biofilms and survival was assessed after 5 h of treatment. For *P. aeruginosa* the lower concentrations (8.5 and 17 μg/mL) caused a decrease in biofilm survival of about 0.8 log units (**Figure 3B**). Doses of 34 μg/mL or higher significantly decreased the number of surviving biofilms cells, resulting in 4.2 ± 0.6; 6.2 ± 0.6; and 6.6 ± 0.6 log reductions. In comparison, 10 μg/mL of the conventional antibiotic ofloxacin caused a significant 4.5 ± 1 log decrease in the number of surviving biofilm cells (Supplementary Figure S2A). For *S. aureus*, the treatment of mature biofilms with lower concentrations of SPI009 proved slightly less effective than for *P. aeruginosa*. Treatment with higher concentrations did cause extensive damage, resulting in significant decreases in biofilm survival ranging between 2.5 ± 0.7 and 5.4 ± 0.6 log. For the 96-well biofilm models used in this study, the combination of SPI009 with a conventional antibiotic did not further decrease the number of surviving cells as compared to mono-treatment with SPI009 (Supplementary Figure S2). Overall, SPI009 shows potent activity in biofilms of both Gram-negative and Gram-positive species and is capable of significantly inhibiting biofilm formation and decreasing survival of mature biofilms.

SPI009 Reduces Bacterial Load in a Chronic Wound Model

After confirming the biofilm eradication capacity of SPI009 in a standard biofilm set-up, a more clinically relevant model was used to assess the clinical potential of SPI009 as a topical antibacterial treatment. Using a porous cellulose matrix placed upon a moist hydrogel allowed the growth of a complex, three-dimensional hydrated structure, effectively mimicking biofilms in a chronic wound environment (Townsend et al., 2016; Kean et al., 2017). Assessment of viability was performed by means of live/dead quantitative PCR (**Figure 4**). For the viable cells, treatment with increasing concentrations of SPI009

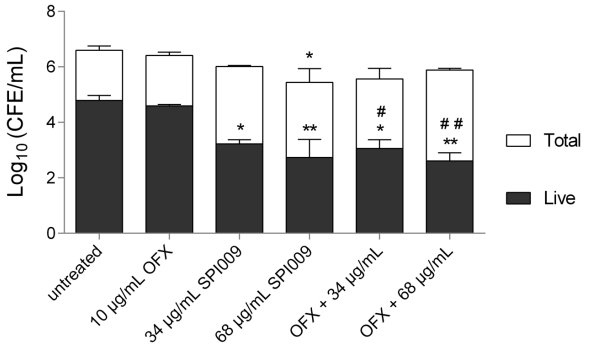

FIGURE 4 | Effect of SPI009 in a chronic wound model. Mature biofilms, grown on hydrogels supporting a cellulose matrix, were treated for 24 h with 10 μg/mL ofloxacin, 34 or 68 μg/mL of SPI009 alone or in combination with ofloxacin. Washed biofilms were removed by sonication and viability was assessed by means of Live/Dead PCR. Values are shown as the $\log_{10}$ transformation of colony forming estimates (CFEs), as determined for three biological repeats each containing three technical repeats. Error bars represent SEM values. Significant differences relative to untreated control are depicted by *, # represent significant differences relative to ofloxacin treatment with */# $P \leq 0.05$, **/## $P \leq 0.01$, as determined by means of one-way ANOVA with Dunnett's correction.

alone resulted in significant 1.6 ± 0.5 log (34 μg/mL) and 2.0 ± 0.5 log (68 μg/mL) decreases in the number of surviving cells. The obtained results confirm the biofilm eradication capacity of SPI009, both as an antimicrobial and as part of a combination therapy, and this in a more complex, realistic biofilm environment.

SPI009 Potentiates Antibiotic Activity in an Intracellular Infection Model

Next, the anti-persister and antibacterial activities of SPI009 were verified in a recently developed *P. aeruginosa* intracellular infection model (Buyck et al., 2013). Human THP-1 cells were infected with PAO1 cells (MOI 10) and treated for 5 h with different concentrations of ciprofloxacin, alone or in combination with 6.8 or 10.2 μg/mL of SPI009. Concentrations of SPI009 were chosen to be well below the determined IC_{50} value of 24.5 ± 1.36 μg/mL. After treatment, both the number of surviving PAO1 cells and the amount of eukaryotic proteins present was assessed, as this can provide information about the possible toxic effect of the different treatments and the infecting bacteria. While treatment with SPI009 alone caused non-significant decreases of 0.78 ± 0.7 and 0.89 ± 0.7 log units in surviving bacteria, addition of SPI009 to ciprofloxacin greatly improved the antibacterial effect for all concentrations tested and this in a dose-dependent manner (**Figure 5**). Maximal antibacterial activity for the combination therapy with 10.2 μg/mL of SPI009 occurs at ciprofloxacin concentrations of 10 μg/mL, resulting in complete eradication of the bacterial culture. Moreover, all combinations tested significantly reduced the bacterial load as compared to ciprofloxacin alone. Combination treatment with 6.8 μg/mL SPI009 showed a maximal 0.78 ± 0.6 log decrease as compared

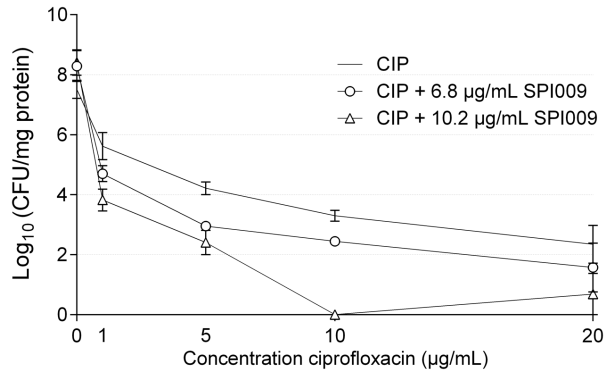

FIGURE 5 | Addition of SPI009 enhances antibiotic treatment of intracellular infections. Human THP-1 cells were infected for 5 h with *P. aeruginosa* PAO1 (MOI 1:10) after which extracellular bacteria were removed and cells were treated with increasing concentrations of ciprofloxacin, alone or in combination with 6.8 µg/mL or 10 µg/mL of SPI009. Data points represent the average of at least two biological repeats, each containing three technical repeats. Error bars depict SEM values. Statistical comparison between ciprofloxacin treatment and the different combination treatments was done by means of one-way ANOVA testing with correction for multiple comparisons (Dunnett) ($\alpha = 0.05$).

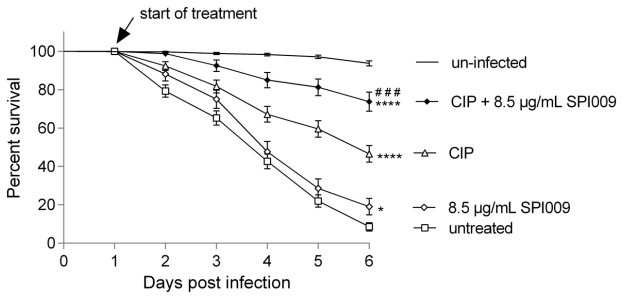

FIGURE 6 | SPI009 combination therapy enhances *C. elegans* survival in a PA14 WT infection assay. Δ*glp-4(bn2)/* Δ*sek-1(km4) C. elegans* worms were infected with *P. aeruginosa* by feeding them on NGM-PA14 WT plates for 24 h. Worms were treated with 8.5 µg/mL SPI009 (open diamonds), 1.56 µg/mL ciprofloxacin (5x MIC; open triangles) or the combination of SPI009 with ciprofloxacin (filled circles). Untreated worms (open squares) and uninfected worms (solid line) served as controls. Worms were counted daily for 6 days with nematode survival expressed as a percentage relative to the viability on day 1. Data points represent the mean of at least three independent repeats ± SEM. Statistical analysis was performed on Kaplan–Meier plots by means of the log-rank test ($\alpha = 0.05$). Significant differences to the untreated control are represented by *, # represent significant differences to the ciprfloxacin control. $^{*}P \leq 0.05$, $^{\#\#\#}P \leq 0.001$ and $^{****}P \leq 0.0001$.

to antibiotic alone at a ciprofloxacin concentration of 20 µg/mL. These results clearly show that SPI009 can effectively penetrate the eukaryotic cell membrane, without causing extensive damage, to eradicate the intracellular *P. aeruginosa* infection.

SPI009 Combination Therapy Significantly Improves *in Vivo* Survival

Since the antibacterial effect of SPI009 was demonstrated extensively *in vitro*, a next step was to assess the effect of this new compound in an *in vivo C. elegans* gut infection model. Toxicity testing of SPI009 in *C. elegans* revealed minor levels of toxicity at 68 µg/mL and >80% killing at 136 µg/mL (Supplementary Figure S3), excluding these concentrations from further experiments. Analysis of the different DMSO concentrations suggests that the observed toxicity is mainly caused by increasing concentrations of the solvent.

Infection of nematodes with PA14 resulted in 91.5% killing within 6 days after the start of infection, confirming the highly virulent nature of the PA14 strain in this model (**Figure 6**). Addition of 8.5 µg/mL of SPI009 alone slightly improved survival but not as good as 5x MIC of ciprofloxacin, resulting in survival rates of 19.0% ($P = 0.045$) and 46.6% ($P < 0.0001$), respectively. However, addition of 8.5 µg/mL of SPI009 to ciprofloxacin greatly increased survival, resulting in 73.8% nematode survival after 6 days. These results show a significant improvement in antibacterial effect of the combination therapy compared to the untreated ($P < 0.0001$) and ciprofloxacin-treated ($P = 0.0001$) controls (Supplementary Table S1). Since low doses of SPI009 can greatly enhance the effect of conventional antibiotic treatment, resulting in more than 73% survival, these results indicate the highly efficient antibacterial and potentiating effect of SPI009 as part of a combination therapy.

DISCUSSION

Decades of excessive drug prescription, misuse of antimicrobials and extensive agricultural applications have caused a massive increase in drug resistance. Conventional antibiotic therapies are losing the battle against emerging extensively drug-resistant strains, resulting in 25,000 annual deaths in the European Union (European Centre for Disease Prevention and Control, 2009). A group of pathogens raising particular concern are the so-called ESKAPE pathogens, *E. faecium, S. aureus, K. pneumoniae*, *A. baumannii*, *P. aeruginosa*, and *Enterobacter* spp. Responsible for the majority of nosocomial infections, these pathogens show significant rises in resistance rates and are becoming increasingly difficult to treat with currently available antibiotics (Boucher et al., 2009; Pendleton et al., 2013). Since it is becoming alarmingly difficult to identify novel antibiotic targets, combination therapies could provide an alternative strategy for the effective treatment of bacterial infections. When different mode of actions are combined, they can lower the risk of resistance development and extend the life span of currently available antibiotics (Tamma et al., 2012; Gill et al., 2015). However, additional research is needed to assess possible negative effects associated with combination therapies and to determine an optimal combination *in vivo* (Tamma et al., 2012; Pena-Miller et al., 2013). An additional advantage of combination therapies is their potential use in the treatment of persister cells (Cui et al., 2016; Feng et al., 2016; Yang et al., 2016; Gallo et al., 2017; Koeva et al., 2017), a small reservoir of phenotypical variants that tolerate antibiotic treatment and reinitiate bacterial infection when the antibiotic pressure drops. The antibiotic-tolerant phenotype of persister cells contributes to the recalcitrant nature of chronic infections,

greatly complicates treatment and increases the chances of resistance development (Lewis, 2007; Fauvart et al., 2011; Michiels et al., 2016).

We recently described the discovery of the propanol-amine derivative SPI009, a novel anti-persister molecule capable of directly killing persister cells of *P. aeruginosa* (Liebens et al., 2017). Most anti-persister molecules described in literature are only active against one or a very limited number of bacterial species, which can be explained by a very specific mode of action or the sensitizing of persister cells to a specific class of antibiotics (Wood, 2015; Van den Bergh et al., 2017). Other examples of small organic compounds capable of directly killing persister cells include the recently described α-bromocinnamaldehyde (Shen et al., 2017), 5-iodoindole (Lee et al., 2016), halogenated phenazines (Garrison et al., 2015) and the nitroimidazole prodrug PA-284 (Singh et al., 2008). In this study, we showed that SPI009 possesses broad-spectrum activity and is capable of significantly decreasing or even eradicating the bacterial culture for all pathogens tested, including the notorious ESKAPE pathogens. In addition, combination therapy of conventional antibiotics with SPI009 allowed the efficient treatment of polymyxin B and ofloxacin resistant strains and could lower the required concentration of antibiotics, thereby enabling their use in resistant strains.

The close relationship between persisters and chronic infections (LaFleur et al., 2006; Mulcahy et al., 2010) is partly caused by their presence in biofilms. The presence of the biofilm matrix is capable of physically protecting the persister cells against the human immune system, thereby enabling the persister cells to resume growth when antibiotic pressure drops and cause recurrence of infection. When compared to other anti-biofilm compounds or conventional antibiotics, SPI009 monotherapy shows a promising anti-biofilm effect, both decreasing biofilm formation and causing a strong reduction in the number of surviving biofilm cells, for both Gram-negative and Gram-positive species. A more clinically relevant biofilm model was obtained by *P. aeruginosa* growth on cellulose matrices and hydrogels, providing a three-dimensional structure and moist environment closely mimicking the environment of a chronically infected wound. In this 3D model, clinical treatments have been shown to have less impact on the viability of biofilms in comparison to traditional 2D models, which are more susceptible to eradication (Townsend et al., 2016; Kean et al., 2017). Therefore this further supports the ability of SPI009 mono-treatment to eradicate cells in a more complex biofilm model and suggests the possible use of SPI009 in the topical treatment of chronically infected wounds. For all biofilm experiments executed, the addition of SPI009 to a conventional antibiotic did not further decrease the biofilm population as compared to SPI009 alone. In comparison to planktonic cultures, where combination therapy with antibiotics strongly enhances the antibacterial effect, the specific lay-out and environment of the bacterial biofilm, including a possibly reduced penetration of antibacterials, could impair the cooperation between both antibacterials.

Besides the biofilm matrix, persister cells have also been shown to use eukaryotic cells to shield themselves from the human immune system. The presence of intracellular persister reservoirs has been confirmed *in vivo* and can be associated with the chronic nature of infections (Buyck et al., 2013; Helaine et al., 2014). The ability of SPI009 to effectively reduce the intracellular bacteria further confirms the potential of SPI009 as an adjuvant in combination therapies. Capable of increasing nematode survival to more than 70% when combined with ciprofloxacin, the *in vivo* *C. elegans* model further contributes to the clinical potential of SPI009. The *C. elegans* model has been extensively used in the identification and clinical assessment of novel antibacterials and antifungals with ample studies confirming the consistent correlation between toxic effects in *C. elegans* and mammalian models (Hunt, 2017).

CONCLUSION

We demonstrated that the anti-persister molecule SPI009 possesses a broad-spectrum antibacterial activity and, taken into account that it can be combined with different classes of antibiotics, shows great potential for the development of case-specific antibacterial combination therapies. The clinical potential of SPI009 was further confirmed by the observation of an excellent anti-biofilm activity, successful eradication of an intracellular infection in human eukaryotes and the significant increase in *C. elegans* survival after treatment with the combination of SPI009 and ciprofloxacin. Additional *in vivo* experiments will be required to assess the future applicability of SPI009 but its excellent activity in antibacterial combination therapies holds great promise.

AUTHOR CONTRIBUTIONS

Conceptualization, VD, RC, AM, PC, MF, and JM. Methodology, VD, FVB, GR, MF, and JM. Formal analysis, VD. Investigation, VD, LV, AA, and EMT. Wrote the original draft, VD. Contributed in writing review and editing, VD, FVB, GR, MF, and JM. Visualization, VD. Supervision, MF and JM.

FUNDING

This work was supported by Ph.D. grants of the Agency for Innovation through Science and Technology (IWT) to VD; the KU Leuven Excellence Center (grant number PF/2010/07), the KU Leuven Research Council (grant number PF/10/010, 'NATAR'); the Belgian Science Policy Office (BELSPO) (IAP P7/28) and the Fund for Scientific Research, Flanders (FWO) (grant numbers G047112N; G0B2515N; G055517N).

ACKNOWLEDGMENTS

The authors thank Pierre Cornelis and Bob Hancock for providing us with the *P. aeruginosa* PA14 wild type

strain and *P. aeruginosa* clinical isolate 9BR. They would like to thank Prof. Liesbet Temmerman (Animal Physiology and Neurobiology, KU Leuven, Leuven, Belgium) and Francisco José Naranjo Galindo for introducing us to the *C. elegans* model.

SUPPLEMENTARY MATERIAL

The Supplementary Material for this article can be found online at: https://www.frontiersin.org/articles/10.3389/fmicb.2017.02585/full#supplementary-material

REFERENCES

Arivett, B. A., Ream, D. C., Fiester, S. E., Mende, K., Murray, C. K., Thompson, M. G., et al. (2015). Draft genome sequences of *Klebsiella pneumoniae* clinical type strain ATCC 13883 and three multidrug-resistant clinical isolates. *Genome Announc.* 3:e01385-14. doi: 10.1128/genomeA.01385-14

Baba, T., Ara, T., Hasegawa, M., Takai, Y., Okumura, Y., Baba, M., et al. (2006). Construction of *Escherichia coli* K-12 in-frame, single-gene knockout mutants: the Keio collection. *Mol. Syst. Biol.* 2:2006.0008. doi: 10.1038/msb4100050

Bassetti, M., Merelli, M., Temperoni, C., and Astilean, A. (2013). New antibiotics for bad bugs: where are we? *Ann. Clin. Microbiol. Antimicrob.* 12:22. doi: 10.1186/1476-0711-12-22

Boucher, H. W., Talbot, G. H., Bradley, J. S., Edwards, J. E., Gilbert, D., Rice, L. B., et al. (2009). Bad bugs, no drugs: no ESKAPE! An update from the Infectious Diseases Society of America. *Clin. Infect. Dis.* 48, 1–12. doi: 10.1086/595011

Boyle, B., Fernandez, L., Laroche, J., Kukavica-Ibrulj, I., Mendes, C. M. F., Hancock, R. E. W., et al. (2012). Complete genome sequences of three *Pseudomonas aeruginosa* isolates with phenotypes of polymyxin B adaptation and inducible resistance. *J. Bacteriol.* 194, 529–530. doi: 10.1128/JB.06246-11

Briers, Y., Walmagh, M., Van Puyenbroeck, V., Cornelissen, A., Cenens, W., Aertsen, A., et al. (2014). Engineered endolysin-based "Artilysins" to combat multidrug-resistant Gram-negative pathogens. *mBio* 5:e1379-14. doi: 10.1128/mBio.01379-14

Buyck, J. M., Tulkens, P. M., and Van Bambeke, F. (2013). Pharmacodynamic evaluation of the intracellular activity of antibiotics towards *Pseudomonas aeruginosa* PAO1 in a model of THP-1 human monocytes. *Antimicrob. Agents Chemother.* 57, 2310–2318. doi: 10.1128/AAC.02609-12

Cohen, N. R., Lobritz, M. A., and Collins, J. J. (2013). Microbial persistence and the road to drug resistance. *Cell Host Microbe* 13, 632–642. doi: 10.1016/j.chom.2013.05.009

Conlon, B. P., Nakayasu, E. S., Fleck, L. E., LaFleur, M. D., Isabella, V. M., Coleman, K., et al. (2013). Activated ClpP kills persisters and eradicates a chronic biofilm infection. *Nature* 503, 365–370. doi: 10.1038/nature12790

Cui, P., Niu, H., Shi, W., Zhang, S., Zhang, H., Margolick, J., et al. (2016). Disruption of membrane by colistin kills uropathogenic *Escherichia coli* persisters and enhances killing of other antibiotics. *Antimicrob. Agents Chemother.* 60, 6867–6871. doi: 10.1128/AAC.01481-16

Descheemaeker, P., Lammens, C., Pot, B., Vandamme, P., and Goossens, H. (1997). Evaluation of arbitrarily primed PCR analysis and pulsed-field gel electrophoresis of large genomic DNA fragments for identification of enterococci important in human medicine. *Int. J. Syst. Bacteriol.* 47, 555–561. doi: 10.1099/00207713-47-2-555

European Centre for Disease Prevention and Control (2009). *The Bacterial Challenge: Time to React*. Stockholm: ECDC. doi: 10.2900/2518

European Centre for Disease Prevention and Control (2013). *Point Prevalence Survey of Healthcare-associated Infections and Antimicrobial Use in European Acute Care Hospitals 2011–2012*. Stockholm: ECDC.

European Committee on Antimicrobial Susceptibility Testing (2017). *Breakpoint Tables for Interpretation of MICs and Zone Diameters. Version 7.1, 2017*. Available at: http://www.eucast.org

Fauvart, M., De Groote, V. N., and Michiels, J. (2011). Role of persister cells in chronic infections: clinical relevance and perspectives on anti-persister therapies. *J. Med. Microbiol.* 60, 699–709. doi: 10.1099/jmm.0.030932-0

Feng, J., Shi, W., Zhang, S., Sullivan, D., Auwaerter, P. G., and Zhang, Y. (2016). A drug combination screen identifies drugs active against amoxicillin-induced round bodies of *in vitro Borrelia burgdorferi* persisters from an FDA drug library. *Front. Microbiol.* 7:743. doi: 10.3389/fmicb.2016.00743

Fischbach, M. A., and Walsh, C. T. (2009). Antibiotics for emerging pathogens. *Science* 325, 1089–1093. doi: 10.1126/science.1176667

Gallo, S. W., Ferreira, C. A. S., and de Oliveira, S. D. (2017). Combination of polymyxin B and meropenem eradicates persister cells from *Acinetobacter baumannii* strains in exponential growth. *J. Med. Microbiol.* 66, 57–60. doi: 10.1099/jmm.0.000542

Garrison, A. T., Abouelhassan, Y., Kallifidas, D., Bai, F., Ukhanova, M., Mai, V., et al. (2015). Halogenated phenazines that potently eradicate biofilms, MRSA persister cells in non-biofilm cultures, and *Mycobacterium tuberculosis*. *Angew. Chem. Int. Ed.* 54, 14819–14823. doi: 10.1002/anie.201508155

Gill, E. E., Franco, O. L., and Hancock, R. E. W. (2015). Antibiotic adjuvants: diverse strategies for controlling drug-resistant pathogens. *Chem. Biol. Drug Des.* 85, 56–78. doi: 10.1111/cbdd.12478

Helaine, S., Cheverton, A. M., Watson, K. G., Faure, L. M., Matthews, S., and Holden, D. W. (2014). Internalization of *Salmonella* by macrophages induces formation of nonreplicating persisters. *Science* 343, 204–208. doi: 10.1126/science.1244705

Hermans, K., Nguyen, T. L. A., Roberfroid, S., Schoofs, G., Verhoeven, T., De Coster, D., et al. (2011). Gene expression analysis of monospecies *Salmonella* Typhimurium biofilms using differential fluorescence induction. *J. Microbiol. Methods* 84, 467–478. doi: 10.1016/j.mimet.2011.01.012

Hunt, P. R. (2017). The *C. elegans* model in toxicity testing. *J. Appl. Toxicol.* 37, 50–59. doi: 10.1002/jat.3357

Kean, R., Rajendran, R., Haggarty, J., Townsend, E. M., Short, B., Burgess, K. E., et al. (2017). *Candida albicans* mycofilms support *Staphylococcus aureus* colonization and enhances miconazole resistance in dual-species interactions. *Front. Microbiol.* 8:258. doi: 10.3389/fmicb.2017.00258

Koeva, M., Gutu, A. D., Hebert, W., Wager, J. D., Yonker, L. M., O'Toole, G. A., et al. (2017). An anti-persister strategy for the treatment of chronic *Pseudomonas aeruginosa* infections. *Antimicrob. Agents Chemother.* 16:S12. doi: 10.1128/AAC.00987-17

LaFleur, M. D., Kumamoto, C. A., and Lewis, K. (2006). *Candida albicans* biofilms produce antifungal-tolerant persister cells. *Antimicrob. Agents Chemother.* 50, 3839–3846. doi: 10.1128/AAC.00684-06

Lee, D. G., Urbach, J. M., Wu, G., Liberati, N. T., Feinbaum, R. L., Miyata, S., et al. (2006). Genomic analysis reveals that *Pseudomonas aeruginosa* virulence is combinatorial. *Genome Biol.* 7:R90. doi: 10.1186/gb-2006-7-10-r90

Lee, J.-H., Kim, Y.-G., Gwon, G., Wood, T. K., and Lee, J. (2016). Halogenated indoles eradicate bacterial persister cells and biofilms. *AMB Express* 6:123. doi: 10.1186/s13568-016-0297-6

Lewis, K. (2007). Persister cells, dormancy and infectious disease. *Nat. Rev. Microbiol.* 5, 48–56. doi: 10.1038/nrmicro1557

Liebens, V., Defraine, V., Knapen, W., Swings, T., Beullens, S., Corbau, R., et al. (2017). Identification of 1-((2,4-Dichlorophenethyl)Amino)-3-Phenoxypropan-2-ol, a novel antibacterial compound active against persisters of *Pseudomonas aeruginosa*. *Antimicrob. Agents Chemother.* 61:e00836-17. doi: 10.1128/AAC.00836-17

Livermore, D. M. (2004). The need for new antibiotics. *Clin. Microbiol. Infect.* 10, 1–9. doi: 10.1111/j.1465-0691.2004.1004.x

Merabishvili, M., Vandenheuvel, D., Kropinski, A. M., Mast, J., De Vos, D., Verbeken, G., et al. (2014). Characterization of newly isolated lytic bacteriophages active against *Acinetobacter baumannii*. *PLOS ONE* 9:e104853. doi: 10.1371/journal.pone.0104853

Michiels, J. E., Van den Bergh, B., Verstraeten, N., and Michiels, J. (2016). Molecular mechanisms and clinical implications of bacterial persistence. *Drug Resist. Updat.* 29, 76–89. doi: 10.1016/j.drup.2016.10.002

Mulcahy, L. R., Burns, J. L., Lory, S., and Lewis, K. (2010). Emergence of *Pseudomonas aeruginosa* strains producing high levels of persister cells in patients with cystic fibrosis. *J. Bacteriol.* 192, 6191–6199. doi: 10.1128/JB.01651-09

O'Neill, J. (2016). *Tackling Drug-resistant Infections Globally: Final Report and Recommendations. The Review on Antimicrobial Resistance*. London: HM Government.

Pena-Miller, R., Laehnemann, D., Jansen, G., Fuentes-Hernandez, A., Rosenstiel, P., Schulenburg, H., et al. (2013). When the most potent combination of antibiotics selects for the greatest bacterial load: the smile-frown transition. *PLOS Biol.* 11:e1001540. doi: 10.1371/journal.pbio.1001540

Pendleton, J. N., Gorman, S. P., and Gilmore, B. F. (2013). Clinical relevance of the ESKAPE pathogens. *Expert Rev. Anti Infect. Ther.* 11, 297–308. doi: 10.1586/eri.13.12

Porta-de-la-Riva, M., Fontrodona, L., Villanueva, A., and Cerón, J. (2012). Basic *Caenorhabditis elegans* methods: synchronization and observation. *J. Vis. Exp.* 64:e4019. doi: 10.3791/4019

Rice, L. B. (2008). Federal funding for the study of antimicrobial resistance in nosocomial pathogens: no ESKAPE. *J. Infect. Dis.* 197, 1079–1081. doi: 10.1086/533452

Shen, Q., Zhou, W., Hu, L., Qi, Y., Ning, H., Chen, J., et al. (2017). Bactericidal activity of alpha-bromocinnamaldehyde against persisters in *Escherichia coli*. *PLOS ONE* 12:e0182122. doi: 10.1371/journal.pone.0182122

Shin, S. H., Kim, S., Kim, J. Y., Lee, S., Um, Y., Oh, M.-K., et al. (2012). Complete genome sequence of *Enterobacter aerogenes* KCTC 2190. *J. Bacteriol.* 194, 2373–2374. doi: 10.1128/JB.00028-12

Singh, R., Manjunatha, U., Boshoff, H. I. M., Ha, Y. H., Niyomrattanakit, P., Ledwidge, R., et al. (2008). PA-824 kills nonreplicating *Mycobacterium tuberculosis* by intracellular NO release. *Science* 322, 1392–1395. doi: 10.1126/science.1164571

Smith, K., Collier, A., Townsend, E. M., O'Donnell, L. E., Bal, A. M., Butcher, J., et al. (2016). One step closer to understanding the role of bacteria in diabetic foot ulcers: characterising the microbiome of ulcers. *BMC Microbiol.* 16:54. doi: 10.1186/s12866-016-0665-z

Stiernagle, T. (2006). *Maintenance of C. elegans*. Available at: http://www.wormbook.org

Tamma, P. D., Cosgrove, S. E., and Maragakis, L. L. (2012). Combination therapy for treatment of infections with Gram-negative bacteria. *Clin. Microbiol. Rev.* 25, 450–470. doi: 10.1128/CMR.05041-11

Townsend, E. M., Sherry, L., Rajendran, R., Hansom, D., Butcher, J., Mackay, W. G., et al. (2016). Development and characterisation of a novel three-dimensional inter-kingdom wound biofilm model. *Biofouling* 32, 1259–1270. doi: 10.1080/08927014.2016.1252337

Van Acker, H., Sass, A., Bazzini, S., De Roy, K., Udine, C., Messiaen, T., et al. (2013). Biofilm-grown *Burkholderia cepacia* complex cells survive antibiotic treatment by avoiding production of reactive oxygen species. *PLOS ONE* 8:e58943. doi: 10.1371/journal.pone.0058943

Van den Bergh, B., Fauvart, M., and Michiels, J. (2017). Formation, physiology, ecology, evolution and clinical importance of bacterial persisters. *FEMS Microbiol. Rev.* 41, 219–251. doi: 10.1093/femsre/fux001

WHO (2017). *Global Priority List of Antibiotic-resistant Bacteria to Guide Research, Discovery, and Development of New Antibiotics*. Geneva: WHO.

Wood, T. K. (2015). Combatting bacterial persister cells. *Biotechnol. Bioeng.* 113, 476–483. doi: 10.1002/bit.25721

Yang, S., Hay, I. D., Cameron, D. R., Speir, M., Cui, B., Su, F., et al. (2016). Antibiotic regimen based on population analysis of residing persister cells eradicates *Staphylococcus epidermidis* biofilms. *Sci. Rep.* 5:18578. doi: 10.1038/srep18578

Conflict of Interest Statement: The authors declare that the research was conducted in the absence of any commercial or financial relationships that could be construed as a potential conflict of interest.

frontiers in Microbiology

ORIGINAL RESEARCH
published: 02 March 2018
doi: 10.3389/fmicb.2018.00329

Design, Synthesis and Evaluation of Branched RRWQWR-Based Peptides as Antibacterial Agents Against Clinically Relevant Gram-Positive and Gram-Negative Pathogens

Sandra C. Vega[1], Diana A. Martínez[1], María del S. Chalá[2], Hernán A. Vargas[2] and Jaiver E. Rosas[1]*

[1] Department of Pharmacy, Faculty of Science, Universidad Nacional de Colombia, Bogotá, Colombia, [2] Laboratory of Public Health, Secretaria Distrital de Salud, Bogotá, Colombia

OPEN ACCESS

Edited by:
Sanna Sillankorva, University of Minho, Portugal

Reviewed by:
César de la Fuente, Massachusetts Institute of Technology, United States
Osmar Nascimento Silva, Universidade Católica Dom Bosco, Brazil

***Correspondence:**
Sandra C. Vega
sacvegach@unal.edu.co

Specialty section:
This article was submitted to Antimicrobials, Resistance and Chemotherapy, a section of the journal Frontiers in Microbiology

Received: *30 November 2017*
Accepted: *12 February 2018*
Published: *02 March 2018*

Citation:
Vega SC, Martínez DA, Chalá MS, Vargas HA and Rosas JE (2018) Design, Synthesis and Evaluation of Branched RRWQWR-Based Peptides as Antibacterial Agents Against Clinically Relevant Gram-Positive and Gram-Negative Pathogens. Front. Microbiol. 9:329. doi: 10.3389/fmicb.2018.00329

Multidrug resistance of pathogenic bacteria has become a public health crisis that requires the urgent design of new antibacterial drugs such as antimicrobial peptides (AMPs). Seeking to obtain new, lactoferricin B (LfcinB)-based synthetic peptides as viable early-stage candidates for future development as AMPs against clinically relevant bacteria, we designed, synthesized and screened three new cationic peptides derived from bovine LfcinB. These peptides contain at least one RRWQWR motif and differ by the copy number (monomeric, dimeric or tetrameric) and structure (linear or branched) of this motif. They comprise a linear palindromic peptide (RWQWRWQWR), a dimeric peptide $(RRWQWR)_2KAhx$ and a tetrameric peptide $(RRWQWR)_4K_2Ahx_2C_2$. They were screened for antibacterial activity against *Enterococcus faecalis* (ATCC 29212 and ATCC 51575 strains), *Pseudomonas aeruginosa* (ATCC 10145 and ATCC 27853 strains) and clinical isolates of two Gram-positive bacteria (*Enterococcus faecium* and *Staphylococcus aureus*) and two Gram-negative bacteria (*Klebsiella pneumoniae* and *Pseudomonas aeruginosa*). All three peptides exhibited greater activity than did the reference peptide, LfcinB (17–31), which contains a single linear RRWQWR motif. Against the ATCC reference strains, the three new peptides exhibited minimum inhibitory concentration (MIC_{50}) values of 3.1–198.0 μM and minimum bactericidal concentration (MBC) values of 25–200 μM, and against the clinical isolates, MIC_{50} values of 1.6–75.0 μM and MBC values of 12.5–100 μM. However, the tetrameric peptide was also found to be strongly hemolytic (49.1% at 100 μM). Scanning Electron Microscopy (SEM) demonstrated that in the dimeric and tetrameric peptides, the RRWQWR motif is exposed to the pathogen surface. Our results may inform the design of new, RRWQWR-based AMPs.

Keywords: antibacterial activity, antimicrobial peptide, cationic peptide, lactoferrin, lactoferricin, multidrug resistance

INTRODUCTION

The emergence of multidrug-resistant (MDR) bacterial pathogens is a clinically urgent phenomenon that demands the development of new antibiotics (Draenert et al., 2015; Brunetti et al., 2016; da Cunha et al., 2017). Moreover, the incidence of bacteria in healthcare-associated infections (HAIs) is a constantly evolving public health threat that varies geographically (Prakash, 2014). Pathogens currently implicated in HAIs include bacteria such as *S. aureus*, *K. pneumoniae*, *P. aeruginosa*, *E. coli*, and *E. faecalis*, which have widely become multidrug resistant (MDR) (Percival et al., 2015; Brunetti et al., 2016; da Cunha et al., 2017).

Antimicrobial peptides (AMPs) have garnered interest as potential therapeutic agents for MDR infections (Brunetti et al., 2016), especially as they exhibit broad-spectrum activities against diverse strains of Gram-positive and Gram-negative bacteria, including resistant ones, and against fungi (Chung and Khanum, 2017). The rational design of new AMPs offers hope for enhanced biological activity and cheaper, more-efficient production. Rational design methodologies include *in silico* methodologies. Large-scale, high-quality recombinant production can be done using tobacco mosaic virus and gene-editing techniques such as CRISPR (Clustered Regularly Interspaced Short Palindromic Repeats) recombinant peptide biosynthesis (da Cunha et al., 2017).

Evaluation of AMPs usually involves ascertaining how their bioactivity is influenced by physicochemical properties such as the presence of conserved domains; their length, hydrophobicity or hydrophilicity; their structural form (e.g., linear, branched, or cyclic); and their net charges (Shang et al., 2012; de la Fuente-Nunez et al., 2017; Mishra et al., 2017). Previous work has shown that how structural changes to the RRWQWR motif can influence the antimicrobial activity of the resulting peptides (Tam, 1988). Moreover, use of engineered prodrugs and peptide conjugates can improve the specificity of the therapeutic peptide for its intended target.

AMPs with reported antimicrobial activity include peptides derived from the protein bovine lactoferricin B (LfcinB) (Leon-Calvijo et al., 2015). Interestingly, this activity has been attributed to the RRWQWR motif within LfcinB, which is considered to be the smallest known motif with antibacterial (Richardson et al., 2009; Leon-Calvijo et al., 2015; Huertas et al., 2017) or anticarcinogenic (Solarte et al., 2015) activity.

In the present work, we sought to better understand the contribution of the RRWQWR motif to the antimicrobial activity of LfcinB-derived AMPs, so that we could obtain new, lactoferricin B (LfcinB)-based synthetic peptides as viable early-stage candidates for future development as AMPs against clinically relevant bacteria. To this end, we designed, synthesized and screened a set of cationic LfcinB-based peptides that contain at least one motif RRWQWR and that vary by the copy number and structure of this motif. After preparing these peptides by solid-phase peptide synthesis, we screened them against various bacterial cell lines from ATCC and against clinical bacterial isolates relevant to HAIs. This enabled us to identify two peptides with attractive biological and physicochemical profiles that could ultimately inform a new generation of antibiotics.

MATERIALS AND METHODS

Microorganisms

We sought to assess antibiotic-sensitive and antibiotic-resistant strains of representative Gram-positive and Gram-negative bacteria from the American Type Culture Collection (ATCC). Accordingly, we chose *E. faecalis* as the Gram-positive species (lines ATCC 29212 and ATCC 51575 as sensitive and resistant, respectively) and *P. aeruginosa* as the Gram-negative species (lines ATCC 10145 and ATCC 27853 as sensitive and resistant, respectively). All strains were purchased from ATCC.

For the clinical isolates, we used 20 different isolates from the Public Health Reference Laboratory collection of the Secretaría de Salud del Distrito (SdSD; Bogotá, Colombia). The samples were collected from June to December 2016. For each isolate, the patient parameters (age, gender and location) and the culture site were recorded for epidemiologic monitoring (**Table 1**). All isolates had been previously tested for antibiotic sensitivity at the Public Health Microbiology Laboratory using either the Phoenix™ system (Gram-positive) or the VITEK 2 system (Gram-negative).

Antibacterial Peptides

We designed and synthesized three new cationic peptides based on the RRWQWR motif and prepared two other peptides for comparison (hy): LfcinB (20–25) (RRWQWR) and LfcinB (17–31) (FKCRRWQWRMKKLGA), the latter as reference peptide or antibacterial activity, based on results previously reported by Leon-Calvijo et al. (2015). All peptides were synthesized on solid phase using the Fmoc/tBu methodology, as previously reported (Solarte et al., 2015; Huertas et al., 2017). The sequences described in **Table 2** were synthesized by Fmoc/tBu solid-phase peptide synthesis, as previously reported (Shang et al., 2012; Percival et al., 2015; de la Fuente-Nunez et al., 2017; Mishra et al., 2017). The steps are listed below. Firstly, the solid support, Rink-amide resin (0.66 meq/g substitution), was swelled with dimethylformamide (DMF) for 2 h at room temperature with constant stirring. Next, the resin was treated with a 20% solution of 4-methylpiperidine in DMF to remove the Fmoc group, to enable coupling of the first amino acid. For all coupling steps, the desired Fmoc-protected amino acid was first pre-activated with DCC/HOBt (0.20 mmol/0.21 mmol) in DMF, and then added to the deprotected resin. Each coupling reaction was monitored using the ninhydrin test. Once coupling was complete, the terminal Fmoc-group of the newly added amino acid was removed as above. Iterative coupling and deprotection was performed until the desired peptide sequence was obtained. Finally, the side chains were deprotected as follows: firstly, the peptide was cleaved from the solid support using "cleavage" cocktail containing (TFA/water/ Triisopropyl silane (TIS)/EDT (93/2/2.5/2.5% v/v). The reaction was stirred for 6 h (for some sequences up to 12 h) at RT, and then the mixture was filtered and the solution was collected. Next, the peptide was precipitated out with cold ethyl ether, and finally, it was purified by extraction in solid phase. All peptides were characterized by reverse-phase, high-performance liquid chromatography (RP-HPLC) and mass spectrometry. To obtain

TABLE 1 | The clinical isolates of HCAI-relevant bacteria used in this study.

Gram classification	Species	Isolate	Age (years) /sex	Clinical service	Origin
Gram-positive	*E. faecium*	550	1 (M)	ICU	Blood
		1,040	39 (F)	Surgical unit	Brain tumor
		1,225	58 (F)	Medical unit	Urine
		1,461	26 (M)	Observation	Skin
		1,462	80 (M)	ICU	Peritoneal liquid
	S. aureus	52,013	63 (F)	Medical unit	Body fluids
		43,062	69 (F)	ICU	Trachea
		43,337	22 days (F)	Emergency unit	Eye
		48,575	41 (M)	Hematology	Blood
		48,577	42 (F)	Medical unit	Secretion ulcer
Gram-negative	*K. pneumoniae*	49,644	69 (M)	Medical unit	Blood
		50,181	59 (M)	ICU	Bronchoalveolar lavage
		50,424	32 (F)	ICU	Abdominal wall secretion
		51,048	72 (M)	ICU	Blood
		51,009	47 (M)	Medical unit	Urine
	P. aeruginosa	47,661	65 (F)	Medical unit	Catheter
		48,220	81 (M)	Medical unit	Urine
		48,221	76 (M)	Medical unit	Urine
		48,458	94 (M)	ICU	Urine
		48,526	55 (F)	Medical unit	Urine

From the Public Health Reference Laboratory collection of the Secretaría de Salud del Distrito (SdSD; Bogotá, Colombia). Samples gathered from July to December 2016.

TABLE 2 | Structure and physicochemical properties of the cationic peptides used in this study.

Alternate name	Sequence	RP-HPLC	MALDI-TOF (M/Z) $[M+H]^+$		[b]Net charge	Residues	Hydro-phobic amino acids (%)	[b]GRAVY
		[a]t_R(Min)	Theor.	Exper.				
Motif	^{20}**R R W Q W R**^{25}	4.33	985.55	986.66	+3	6	33.3	−3.133
Lineal/palindromic	**R W Q W R** W Q W R	5.95	1,485.75	1,488.58	+3	9	44.4	−2.678
Lfc B reference Peptide	^{17}F K C **R R W Q W R** M K K L G A^{31}	5.25	1,992.09	1,994.71	+6	15	33.3	−1.207
Dimeric	**(R R W Q W R)**$_2$ K Ahx	5.21	2,195.24	2,198.51	+6	15	26.7	–
Tetrameric	**(R R W Q W R)**$_4$ K_2 Ahx_2 C_2	19.11	2,298.32[c]	2,302.96[c]	+12	30	26.7	–

[a]*tR: Retention time of the main product (in minutes).*
[b]*Net charge values and Grand Average of Hydropathy (GRAVY) values were calculated using the Antimicrobial Peptide Calculator and Predictor (http://aps.unmc.edu/AP/prediction/prediction_main.php). However, this was not possible for the branched peptides.*
[c]*Experimental molecular weight that correspond to dimeric molecule before oxidation.*

the dimeric peptide, di-FMOC-protected lysine was used, which enabled simultaneous synthesis of the two peptide chains (one from the α-amino group and the other, from the ε-amino group of this amino acid). The tetrameric peptide was obtained via oxidation of the dimeric peptide, $(RRWQWR)_2$-K-Ahx-C, with 10% DMSO % in PBS buffer (pH 7.5), as described by Leon-Calvijo et al. (2015), which led to formation of a disulfide bond between the side chains of the cysteine residues at the carboxyl terminus (**Figure 1**). All peptides were >90% pure (as determined by RP-HPLC) and had the expected molecular weight (determined by MALDI-TOF MS). The peptides were synthesized by the SAMP research group of the Faculty of Science of the Universidad Nacional de Colombia and stored in lyophilized form.

Screening for Antibacterial Activity

We screened all five peptides against the ATCC reference strains and the clinical isolates according to Method M7-A7 of the National Committee for Clinical Laboratory Standards (CLSI, 2007). The MIC_{50} and MBC values were determined using a broth microdilution and growth inhibition method previously reported by Leon-Calvijo et al. (2015), with some modifications (Wiegand et al., 2008). Briefly, the MIC_{50} experiments comprised a liquid-inhibition growth assay in a sterile, untreated, 96-well flat-bottom tissue culture plate. The bacteria were cultured overnight n Mueller Hinton agar; three colonies were transferred to 8 mL of Mueller Hilton broth and incubated at 37°C until the mid-exponential phase of growth. The turbidity of the cultures was measured and adjusted spectrophotometrically to

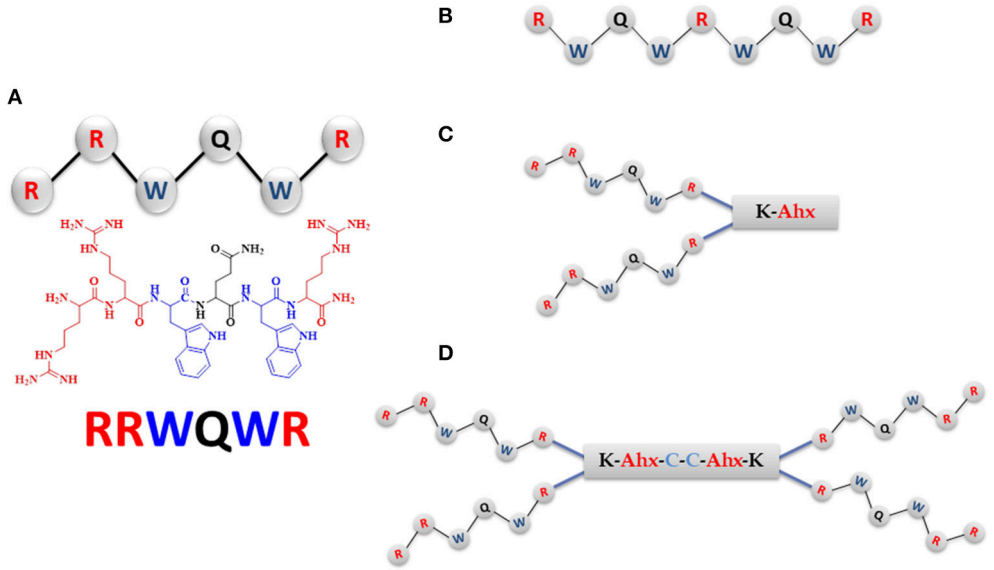

FIGURE 1 | The RRWQWR-based peptides designed, synthesized, and screened for antibacterial activity**.** In blue: hydrophobic amino acids; in red: cationic amino acids. **(A)** Linear monomer. **(B)** Linear palindromic peptide. **(C)** Branched dimeric peptide, in which the two monomers are linked to a tripeptide comprising Lys, Ahx (in red) and terminating in Cys (in blue). **(D)** Branched tetrameric peptide, comprising two of the peptides shown in **(C)** linked by a cysteine disulfide bridge (in blue).

a McFarland standard of 0.5, and then diluted to a final concentration of 5×10^7 colony forming units (CFU) per well. Stock solutions (2,000 μM) of each test peptide were serially diluted to final concentrations (per well) of 200, 100, 50, 25, 12.5, and 6.25 μM. Each concentration was evaluated in duplicate and each assay was performed in triplicate.

Wells containing Mueller Hilton broth with bacterial inoculum only served as bacterial-growth controls. Additional controls included Mueller Hilton broth alone (as blank) and Mueller Hilton broth with ciprofloxacin (2 μg/mL; as positive control). The microplate was incubated for 24 h at 37°C, and growth inhibition was measured by monitoring the optical density at 620 nm (OD_{620}). The MIC_{50} was defined as the peptide concentration at which bacterial growth was inhibited by 50%.

To determine the MBC, an aliquot from each well of the MIC_{50} assay was spread onto Mueller Hilton agar. After 18 h at 37°C, the concentration that inhibited bacterial growth was determined. Each of these tests was performed four times. MBC was defined as the lowest concentration of peptide at which the number of bacteria was reduced by 99.9% *in vitro* (European Committee for Antimicrobial Susceptibility Testing, 2000).

Scanning Electron Microscopy

We observed bacterial morphology by SEM. The *E. faecalis* and *P. aeruginosa* strains were grown to mid-logarithmic phase, and adjusted spectrophotometrically to a McFarland standard of 0.5 (corresponding to $\sim 1 \times 10^8$ CFU/mL). Subsequently, 1 mL of bacterial suspension was distributed into three tubes: one tube was treated with $(RRWQWR)_2KAhx$ at 3× the MIC_{50}; another tube, with $(RRWQWR)_4K_2Ahx_2C_2$ at the same concentration; and the third tube was left untreated, as a control. The samples were incubated aerobically at 37°C for 2 h, and the bacterial suspensions were centrifuged at 1,459 × g for 3 min and then, washed twice with Millonig's Phosphate Buffer (0.10 M, pH 7.4). For SEM, each sample was fixed with 1 mL of 2.5% glutaraldehyde at 4°C for 2 h. The fixed samples were dehydrated in an ethanol gradient (50, 70, 80, 90, and 100%) for 20 min and then, centrifuged at 1,459 × g for 10 min. The bacterial pellet was resuspended in 100% ethyl alcohol and air-dried. Finally, the slides were taped onto stubs, coated with gold using a Quorum Q150R sputter coater, and observed with an FEI Quanta 200-r microscope.

Hemolytic Activity

Human erythrocytes collected from the blood samples of healthy humans were harvested by centrifugation for 7 min at 162 × g and washed three times in phosphate-buffered saline (PBS). The erythrocytes (2% hematocrit in PBS) were incubated with peptide molecules at several concentrations (6.25, 12.5, 25, 50, and 100 μM) for 2 h at 37°C. PBS was used as negative control for hemolysis, and sterile distilled water was used as positive control (100% hemolysis). The plate was subsequently centrifuged at 1,459 × g for 10 min at 4°C. Aliquots of the supernatant from each well (75 μL) were carefully transferred to a new sterile 96-well plate, and hemolytic activity was evaluated by measuring the OD_{492} using an Asys Expert Plus Microplate reader. The experiments were performed in duplicate, and hemolytic activity was calculated for each peptide.

Therapeutic Index

We determined the therapeutic index of each peptide, which we defined as the ratio of Maximum Hemolytic Activity (H_{max}) to MIC_{50} (H_{max}/MIC_{50}).

Statistical Analysis

We analyzed all the data using SPSS 11.0 software. The results are presented here as the mean ± standard deviation. MIC_{50} values were determined by interpolation on a four-parametric curve of pharmacology functions.

RESULTS

Antibacterial Peptides

The crude products were characterized using RP-HPLC and then purified. The chromatogram of each purified product exhibited a primary peak corresponding to the desired peptide (purity: > 90%). The molecular weight of each peptide was confirmed by MALDI-TOF-MS (**Table 2**). Stock solutions of each peptide were prepared in water (2,000 μM), sterilized by 0.22 μm filtration, and stored at −20°C until used in the subsequent experiments.

Antibacterial Assay: ATCC Strains

The screening results for each peptide against the sensitive and resistant strains of *E. faecalis* are shown in **Figure 2**, which shows that the activities varied by peptide and by strain. Activity was assessed in terms of bacterial viability, whereby the control (untreated) samples showed a viability of 100%. As shown in **Figure 2A**, against the sensitive strain, the highest activity (lowest viability value) observed for each peptide was: for the RRWQWR monomer, 72.8% at 200 μM; for the palindromic peptide, 33.3% at 50 μM; for the dimeric peptide, 40.9% at 25 μM; for the tetrameric peptide, 48.9% at 6.2 μM; and for the reference peptide (LfcinB), 25.6% at 100 μM. Overall, the RRWQWR monomer appeared to be the weakest antibacterial agent. However, and rather curiously, for the samples treated with LfcinB at 6.25, 13.0, and 25.0 μM, the bacterial viability was actually higher than for the untreated sample. As shown in **Figure 2B**, against the resistant strain of *E. faecalis*, the highest activity (lowest viability value) observed for each peptide was: for the RRWQWR monomer, 48.4% at 200 μM; for the palindromic peptide, 61% at 12.5 μM; for the dimeric peptide, 65.3% at 25.0 μM; for the tetrameric peptide, 62.4% at 12.5 μM; and for the reference peptide (LfcinB), 8.3% at 200 μM. Overall, the most active peptide appeared to be the tetramer. Studying the dose-response plot of 1B from another perspective (**Figure 1B**, inset), reveals two important findings: firstly, that these peptides are generally inactive against the resistant strain of *E. faecalis*; and secondly, that at the highest concentration, all of them except for the monomer induced strong bacterial proliferation.

The experiments on *E. faecalis*, **Figure 2** revealed three major findings: firstly, that the most active peptides were the tetrameric peptide and the dimeric peptide; secondly, that at most concentrations, the monomer was inactive against both strains; and lastly, that at some concentrations, some of these peptides actually induced proliferation of either strain. Overall, the palindromic and Lfc B peptides exhibited significant antimicrobial activity with the higher concentration evaluated in this study (200 μM). The dimeric peptide and the tetrameric peptide exhibited the strongest antimicrobial activity on each strain at the lowest concentrations (50 and 25 μM, respectively).

The screening results for each peptide against the sensitive and resistant strains of *P. aeruginosa* are shown in **Figure 3**.

We calculated the MIC_{50} values for each peptide against the sensitive and resistant strains of *E. faecalis* and of *P. aeruginosa*, using a broth microdilution assay. The values are shown in **Table 3**. In terms of activity against all four bacterial strains, the peptides ranked, from most active to least active, as follows: tetrameric > dimeric > palindromic > reference > monomer.

Importantly, the RRWQWR monomer was generally inactive against all *E. faecalis* and *P. aeruginosa* strains (MIC_{50} > 200 μM); moreover, it exhibited a MIC_{50} of 198 μM against the resistant strain of *E. faecalis*. Importantly, against the resistant strain of *E. faecalis*, none of the other peptides exhibited any activity (MIC_{50} > 200 μM). The reference peptide (LfcinB) exhibited a similar profile to that of the monomer, except against the sensitive strain of *E. faecalis*, against which it was moderately active (MIC_{50} < 50 μM). Intriguingly, the palindromic, dimeric and tetrameric peptides were each more active against the Gram-positive bacteria than against the Gram-negative bacteria. These experiments demonstrated that in the range of concentrations tested, all of the peptides showed at least some activity against at least one of the bacterial lines, with the palindromic, dimeric and tetrameric peptides generally the most active.

We calculated the MBC values for each peptide, which showed the activity against the sensitive *E. faecalis* strain (or both strains) relative to the corresponding value(s) for the tetrameric peptide (MBC_{tet}), as it was the most active one (e.g., MBC_{tet} against the sensitive *E. faecalis* strain: 25.0 μM). Thus, the activity ranking for the three active peptides is: tetramer (MBC_{tet}) > dimer (4× MBC_{tet}) = palindromic (4× MBC_{tet}). The MBC of this peptide against the sensitive *P. aeruginosa* strain was 25.0 μM. Therefore, the activity ranking for the two active peptides is: tetramer (MBC_{tet}) > dimer (4× MBC_{tet}). Finally, the MBC of the tetrameric peptide against the resistant *P. aeruginosa* strain and 4× MBC for the resistant strain, which gives an activity ranking of: tetramer (MBC_{tet}) > dimer (4× MBC_{tet}).

Scanning Electron Microscopy (SEM)

We used SEM to study the morphology of bacterial cells before and after treatment with either branched peptide (dimeric and tetrameric). To this end, each strain of *E. faecalis* and *P. aeruginosa* was first studied by SEM; then, independently treated in the exponential phase with either peptide at 3× the corresponding MIC_{50} value for 2 h (except for the resistant *E. faecalis* strain, for which a peptide concentration of 200 μM was used); and finally, studied by SEM again.

E. faecalis

Before treatment, the antibiotic-sensitive *E. faecalis* cells were spherical or ovoid, had a smooth surface and exhibited a primarily diplococcic structure; the untreated antibiotic-resistant *E. faecalis* cells had a similar appearance but exhibited little surface mucus (**Figure S1**). After treatment with the dimeric peptide, the sensitive *E. faecalis* cells exhibited a random organization with morphological alterations (e.g., pitted and wrinkled surface) and alterations to cell-membrane surface morphology and agglutination, which might have caused leakage

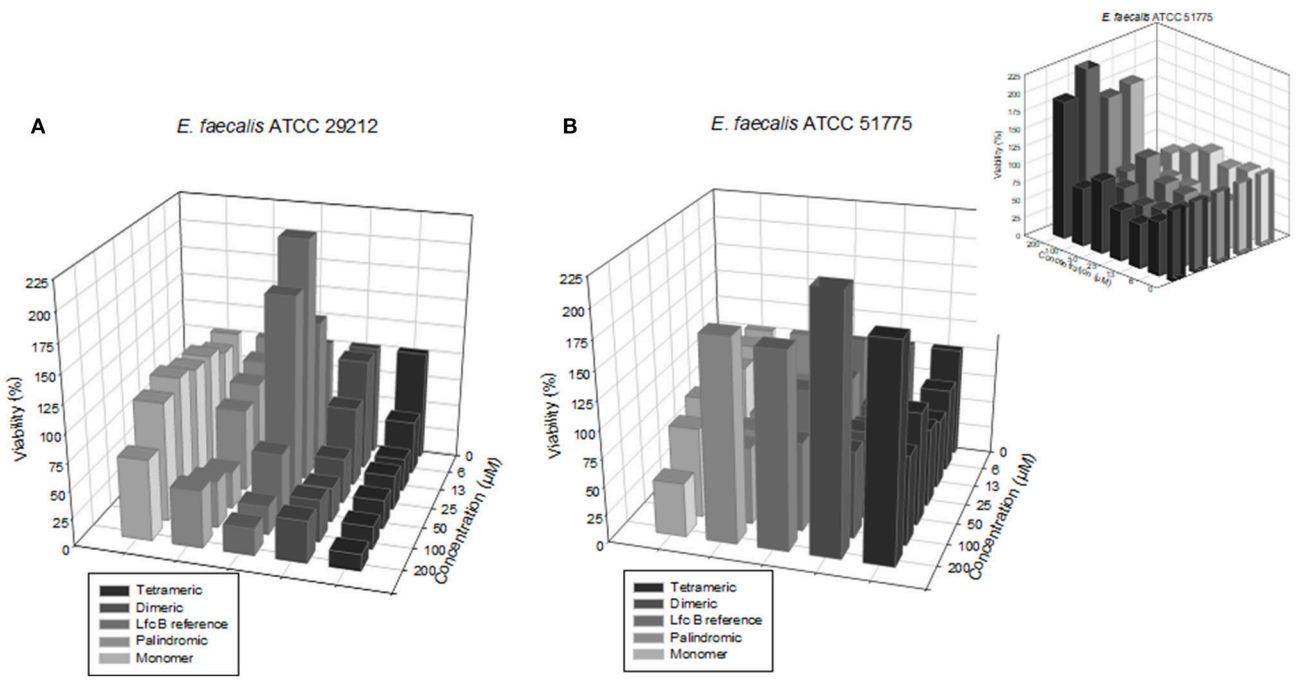

FIGURE 2 | Dose-response plots of the antibacterial activity of the test peptides against the two *E. faecalis* strains. **(A)** Sensitive strain. **(B)** Resistant strain. (**B**: inset) Plot seen from a different perspective, revealing that at higher concentrations, all of the peptides except the monomer induced strong bacterial proliferation.

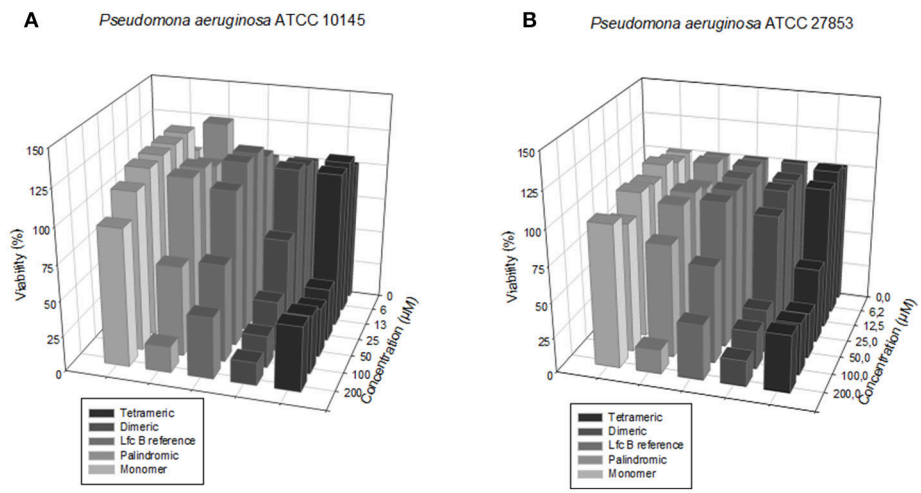

FIGURE 3 | Dose-response plots of the antibacterial activity of the test peptides against the two *P. aeruginosa* strains. **(A)** Sensitive strain. **(B)** Resistant strain.

of cellular contents. In contrast, treatment of sensitive *E. faecalis* cells with the tetrameric peptide induced population decline, cell-size heterogeneity and cell-surface alterations in the form of protrusions. Treatment of the resistant *E. faecalis* cells with either of these peptides induced alterations in the surface mucus levels and, in some cases, morphologic alterations (e.g., amorphous cells or surface changes, in the case of the tetrameric peptide); however, there were no changes in population.

P. aeruginosa

Before treatment, the untreated antibiotic-sensitive *P. aeruginosa* cells were uniformly rod-shaped and exhibited intact cell membranes (**Figure S1**). However, treatment with the dimeric peptide induced a clear reduction in population and caused morphological alterations (e.g., wrinkling and surface shrinkage). Treatment of this strain with the tetrameric peptide led to a very heterogeneous population and to alterations in the cell surface, namely in the form of protrusions, pores and

TABLE 3 | Antibacterial activity of the RRWQWR-based peptides against the ATCC strains of HCAI-relevant bacteria.

Bacterium		*Enterococcus faecalis*				*Pseudomonas aeruginosa*			
Strain		Sensitive		Resistant		Sensitive		Resistant	
ATCC#		29212		51575		10145		27853	
Peptide	**Alternate name**	**MIC_{50} (μM)**	**MBC (μM)**	**MIC_{50} (μM)**	**MBC (μM)**	**MIC_{50} (μM)**	**MBC (μM)**	**MIC_{50} (μM)**	**MBC (μM)**
LfcinB (20–25)	Monomer	> 200.0	> 200.0	198.0	> 200.0	> 200.0	> 200.0	> 200.0	> 200.0
PLS	Palindromic	25.6	100.0	> 200.0	> 200.0	99.7	> 200.0	107.2	> 200.0
LfcinB (17–31)	Reference	34.3	> 200.0	> 200.0	> 200.0	111.7	> 200.0	99.6	> 200.0
$LfcinB\ (20–25)_2$	Dimeric	13.1	100.0	> 200.0	> 200.0	29.1	100.0	34.8	200.0
$LfcinB\ (20–25)_4$	Tetrameric	3.1	25.0	> 200.0	> 200.0	18.1	50.0	21.7	50.0

disrupted membranes. Moreover, the tetrameric peptide induced a total transformation of cell morphology, from rod-shaped to spherical, and led to aggregation of diversely sized spheres. Before treatment, the antibiotic-resistant *P. aeruginosa* cells resembled those of the sensitive strain, but were slightly longer and exhibited surface mucus. Treatment with the dimeric peptide caused a marked drop in population and severe morphological alterations (e.g., cell elongation and cell-membrane porosity). Treatment with the tetrameric peptide was even more dramatic, leading to disintegrated and irregularly-shaped mucoid cells that exhibited surface changes and to heterogeneous aggregates. Importantly, in both strains of *P. aeruginosa*, both treatments appeared to induce leakage of cellular contents that may have contributed to the observed aggregation.

Hemolytic Activity

To evaluate the effects of all five test peptides on normal human erythrocytes, we independently treated erythrocytes with each of the five test peptides, using the standard microtiter dilution method (**Table 4**). For all peptides, the H_{50} was > 100 μM. However, the H_{max} values demonstrated a clear ranking of hemolytic activity for the peptides, from strongest to weakest: tetrameric > palindromic > monomer > Lfcin-B (reference peptide) > dimeric. This demonstrated that the dimeric was the least pernicious to human erythrocytes.

TABLE 4 | Hemolytic activity of the tested peptides.

Peptide	Alternate name	[a]H_{max}		[b]H_{50} (μM)
		(%)	Peptide Concentration (μM)	
LfcinB (20–25)	Monomer	7.1	25	>100
PLS	Palindromic	24.8	100	>100
LfcinB (17–31)	Reference Peptide	6.6	25	>100
$LfcinB\ (20–25)_2$	Dimeric	5.6	100	>100
$LfcinB\ (20–25)_4$	Tetrameric	49.1	100	>100

[a] *H_{max}.: Maximum hemolytic activity attained of human red blood cells after 2 h of treatment at 37°C with each peptide molecule.*
Peptide concentration: concentration (μM) of peptide corresponding to H_{max}.
[b] *H_{50}: concentration of peptide (μM) leading to 50% hemolysis of human red blood cells after 2 h of treatment at 37°C.*

Antimicrobial Activity on Clinical Isolates of HCAI Pathogens

Having investigated the antibacterial activity of the peptides on diverse bacterial cell lines, we next sought to assess their activity against Gram-positive and Gram-negative bacteria from the 20 HCAI clinical isolates. We tested four species in total: *E. faecium* and *S. aureus* (Gram-positive) and *K. pneumoniae* and *P. aeruginosa* (Gram-negative) (**Table 5**). We did not test *E. faecalis* here because currently, it is relatively rare among the patient population (Bogotá hospital network). Thus, we replaced it with vancomycin-resistant *E. faecium*, a Gram-positive species frequently encountered in the clinic.

According to the MIC_{50} and MBC values, the monomer RRWQWR was active primarily against *S. aureus*; the palindromic peptide, predominantly against *S. aureus* and *K. pneumoniae*; and the dimeric and tetrameric peptides had the widest antibacterial spectra and strongest activities, inhibiting *S. aureus*, *K. pneumonia*, and *P. aeruginosa*. Thus, based on MIC_{50} values, the overall activity ranking for these peptides against all clinical isolates was, from strongest to weakest: tetrameric > dimeric > palindromic > monomer. However, the MBC values give a different picture. Firstly, the monomer was not effective against any of the bacteria. Secondly, the palindromic peptide was active against all four species, as follows (from highest inhibition to lowest): *S. aureus* > *K. pneumoniae* > *E. faecium* = *P. aeruginosa*. The dimeric peptide was active against all the isolates except for one *E. faecium* sample. And, again, the tetrameric peptide was strongly active against all the isolates (from highest inhibition to lowest): *S. aureus* > *K. pneumoniae* > *E. faecium* > *P. aeruginosa*. Interestingly, the tetrameric peptide was highly specific for the Gram-positive isolates.

Therapeutic Index

The therapeutic index (TI) is a ratio of the toxic dose of a substance to its therapeutically-active dose and can be calculated different ways (e.g., LD_{50}/ED_{50}). Here, we calculated a TI value for each peptide against all the Gram-positive or the Gram-negative ATCC strains, by dividing its H_{max} by its MIC_{50} for the given group of strains. Since the tetrameric peptide was consistently the most active, here we report the TI values

TABLE 5 | Antibacterial activity of the RRWQWR-based peptides against the clinical isolates of HCAI-relevant bacteria.

Gram classification	Bacteria	Isolates	MIC_{50} (μM)				MBC (μM)				Resistant phenotype
			LfcinB (20–25)	PLS	LfcinB $(20–25)_2$	LfcinB $(20–25)_4$	LfcinB (20–25)	PLS	LfcinB $(20–25)_2$	LfcinB $(20–25)_4$	
			Monomer	Palindromic	Dimeric	Tetrameric	Monomer	Palindromic	Dimeric	Tetrameric	
Gram-positive	*Enterococcus faecium*	550	>100	>100	>100	>100	>100	100.0	>100	12.5	STR, CIP, LVX, ERY, TEC, VAN, TET, SXT
		1,040	>100	>100	>100	>100	>100	>100	>100	>100	STR, CIP, LVX, ERY, TEC, VAN, TET, TMS
		1,225	>100	>100	>100	>100	>100	100.0	>100	12.5	STR, CIP, LVX, ERY, TEC, VAN, TET, TMS
		1,461	>100	>100	>100	>100	>100	100.0	>100	12.5	STR, CIP, LVX, ERY, TEC, VAN, TET, TMS
		1,462	>100	5.7	49.8	>100	>100	100.0	>100	12.5	STR, CIP, LVX, ERY, TEC, VAN, TET y TMS
	Staphylococcus aureus	52,013	5.1	8.3	12.6	6.7	>100	100.0	25.0	12.5	Sensitive
		43,062	5.1	50.4	13.5	6.7	>100	100.0	50.0	12.5	OXA
		43,337	3.7	13.0	13.5	6.3	>100	50.0	25.0	12.5	OXA
		48,575	3.7	36.5	13.4	9.2	>100	100.0	25.0	12.5	CLI
		48,577	3.7	5.7	12.9	6.3	>100	100.0	50.0	100.0	OXA
Gram-negative	*Klebsiella pneumoniae*	49,644	>100	12.5	12.3	ND	>100	100.0	50.0	ND	IPM, MEM, ETP, DOR, FEP, CAZ, CRO, TZP, CIP
		50,181	>100	>100	6.6	5.5	>100	>100	100.0	100.0	IPM, MEM, ETP, DOR, FEP, CAZ, CRO, TZP
		50,424	11.3	5.6	5.8	7.8	>100	>100	>100	100.0	IPM, MEM, ETP, DOR, FEP, CAZ, CRO, TZP, GEN, CIP
		51,048	>100	11.7	5.7	5.2	>100	>100	100.0	50.0	IPM, MEM, ETP, DOR, FEP, CAZ, CRO, TZP
		51,009	>100	25.6	5.6	1.6	>100	100.0	25.0	25.0	MEM, ETP, CTX, CRO, AMK, GEN, SXT, FEP, CAZ y CIP, NOR, NIT
	Pseudomonasss aeruginosa	47,661	>100	75.0	13.4	7.5	>100	>100	>100	25.0	MEM, IPM, FEP, CAZ, CIP, AMK, GEN, TGC
		48,220	>100	>100	50.0	12.6	>100	>100	50.0	25.0	Sensitive
		48,221	>100	>100	64.2	11.9	>100	>100	>100	50.0	MEM, FEP, CAZ, AMK, CIP
		48,458	>100	>100	75.0	72.8	>100	>100	>100	>100	MEM, GEN, CAZ, FEP, AMK
		48,526	>100	>100	36.3	24.9	>100	100.0	>100	>100	Sensitive

Amikacin (AMK), cefepime (FEP), cefotaxime (CTX), ceftriaxone (CRO), ceftazidime (CAZ), ciprofloxacin (CIP), clindamycin (CLI), doripenem (DOR), ertapenem (ETP), erythromycin (ERY), gentamicin (GEN), imipenem (IPM), levofloxacin (LVX), meropenem (MEM), oxacillin (OXA), piperacillin-tazobactam (TZP), streptomycin (STR), teicoplanin (TEC), tetracycline (TET), tigecycline (TGC), trimethoprim-sulfamethoxazole (SXT), vancomycin (VAN).
ND: Not determined.

for the other peptides relative to its value, using fold values. Additionally, to make our quantitative analysis more robust [geometric mean (Khachatryan et al., 2017) and fold values], we have included MIC_{50} values for these peptides against *S. aureus* and *K. pneumoniae* that we previously obtained using the same assay, the M7-A7 method of the National Committee for Clinical Laboratory Standards (Leon-Calvijo et al., 2015).

Firstly, we calculated separate TI values for each peptide against all the Gram-positive or all the Gram-negative ATCC strains (**Table 6**). The tetrameric peptide had the highest TI value, suggesting that it may have a wide therapeutic window for antibacterial use, particularly against Gram-positive bacteria.

Finally, we determined the TI values of the three most active peptides from the previous experiments against four of the clinical isolates (two Gram-positive bacteria and two Gram-negative bacteria). We did not calculate values for the monomer, as it was generally inactive against the ATCC strains and the isolates. The results are shown in **Table 7** (Gram-positive) and **Table 8** (Gram-negative). Regarding the Gram-positive bacteria, the palindromic, dimeric and tetrameric peptides were active chiefly against *S. aureus*. This trend was consistent with results of the experiments on the ATCC strains, in which these peptides were only active against the sensitive strain of the *Enterococcus* bacteria. The GM values demonstrate that the tetrameric peptide was active at lower doses than were the palindromic or dimeric peptides, which had similar potencies. Calculating the fold-MIC_{50} values relative to the MIC_{50} value for the tetrameric peptide gave values of 2.4 for the dimeric peptide and 2.0 for the palindromic peptide. Taken together, the observed values for GM, MIC_{50}, and TIC against the clinical isolates suggest that the tetrameric peptide has the strongest antibacterial activity.

Regarding the Gram-negative bacteria, the palindromic, dimeric, and tetrameric peptides were all active *K. pneumoniae* and *P. aeruginosa* (**Table 8**). As indicated by the GM values, the tetramermic peptide was the most active and the palindromic peptide, the least. Calculating the fold-MIC_{50} relative to the MIC_{50} for the tetrameric peptide gave values of 1.7 for the dimeric peptide and 1.8 for the palindromic peptide. The tetrameric peptide again had the highest TI value, which was even higher than its TI value against Gram-positive bacteria. All together, these values suggest that the tetrameric peptide is the most active of the peptides against Gram-negative bacteria.

TABLE 6 | Therapeutic Index values for the RRWQWR-based peptides against the ATCC strains of HCAI-relevant bacteria.

Peptide	Attribute	[a]H_{max}		Gram positive						Gram negative						
				MIC (μM)			[g]Gm	[h]Fold	[i]Therapeutic index	MIC (μM)			[g]Gm	[h]Fold	[i]Therapeutic index	
		(%)	(μM)	[b]29212-[c]S	[d]25923-[c]S	[e]33591-[f]R			MHC/MIC	[j]Fold	[k]13883-[c]S	[l]700603-[f]R	[m]10145-[c]S	[n]27853-[f]R			MHC/MIC	[j]Fold
LfcinB (20–25)	Monomer	7.1	25.0	> 200.0	> 200.0	> 200.0					> 200.0	> 200.0	> 200.0	> 200.0				
PLS	Palindromic	24.8	100.0	25.6	34.9	25.0	28.2	9.0	3.6	0.1	30.7	26.2	99.7	107.2	54.1	4.1	1.8	0.2
LfcinB (17–31)	Lfc B reference peptide	6.6	25.0	34.3	> 200.0	50.0	414.4	13.2	0.6	0.0	> 200.0	> 200.0	111.7	99.6	105.5	8.1	0.2	0.0
LfcinB $(20–25)_2$	Dimeric	5.6	100.0	13.1	3.0	24.1	9.8	3.1	10.2	0.3	9.0	7.3	29.1	34.8	16.1	1.2	6.2	0.8
LfcinB $(20–25)_4$	Tetrameric	49.1	100.0	3.1	1.7	5.9	3.1	1.0	31.8	1.0	12.0	6.2	18.1	21.7	13.1	1.0	7.6	1.0

[a]H_{max}: *Maximum Hemolytic Activity of the indicated peptide against human erythrocytes after 2 h of treatment at 37°C.*

[b]*29212: Enterococcus faecalis.*

[c]*S: sensitive strain.*

[d]*25923: Staphylococcus aureus.*

[e]*33591: Staphylococcus aureus.*

[f]*R: resistant strain.*

[g]*GM: geometric mean of MIC_{50} values from all three Gram-positive or Gram-negative bacterial ATCC strains in the table.*

[h]*Fold: Calculated as (GM for the indicated peptide)/(GM for the tetrameric peptide).*

[i]*Therapeutic Index: H_{max}/GM for the peptides against the Gram-positive or Gram-negative bacteria studied here. A larger value correlates to greater antimicrobial specificity.*

[j]*Fold: Calculated as (TI for the indicated peptide)/(TI for the tetrameric peptide).*

[k]*13883: Klebsiella pneumonia.*

[l]*700603: Klebsiella pneumoniae.*

[m]*10145: Pseudomonass aeruginosa.*

[n]*27853: Pseudomonass aeruginosa.*

DISCUSSION

The antibacterial activity of AMPs has been correlated to physicochemical properties such as net charge and hydrophobicity. For instance, the cationic segments of AMPs are known to favor electrostatic attraction, thereby driving the peptides toward negatively-charged components on bacterial membrane surface (Shang et al., 2012; Ma et al., 2014; Chen et al., 2015). However, the relationship between charge and antibacterial activity is not linear: above a certain threshold (usually, +6), increasing the positive charge does not improve activity (Dathe et al., 2001; Park and Hahm, 2012; Yin et al., 2012). Given that in our five peptides, net charge

TABLE 7 | Therapeutic Index values for the RRWQWR-based peptides against the clinical isolates of HCAI-relevant, Gram- positive bacteria.

Peptide	Attribute	[a]H_{max}		MIC_{50} (μM)										bGm	[c]Fold	Therapeutic index	
		(%)	(μM)	*Enterococcus faecium*					*Staphylococcus aureus*							MHC/MIC_{50}	[d]Fold
				550	1040	1225	1461	1462	52013	43062	43337	48575	48577				
PLS	Palindromic	24.8	100.0					5.7	8.3	50.4	13	36.5	5.74	13.7	2.0	7.3	0.5
LfcinB $(20–25)_2$	Dimeric	5.6	100.0					49.8	12.6	13.5	13.5	13.4	12.9	16.4	2.4	6.1	0.4
LfcinB $(20–25)_4$	Tetrameric	49.1	100.0						6.7	6.7	6.3	9.2	6.3	7.0	1.0	14.4	1.0

[a]H_{max}: *Maximum Hemolytic Activity of the indicated peptide against human erythrocytes after 2 h of treatment at 37°C.*
[b]*GM: geometric mean of the* MIC_{50} *values for the indicated peptide against the indicated bacterial strains.*
[c]*Fold: Calculated as (GM for the indicated peptide)/(GM for the tetrameric peptide).*
[d]*Fold: Calculated as (TI for the indicated peptide)/(TI for the tetrameric peptide).*

TABLE 8 | Therapeutic Index values for the RRWQWR-based peptides against the clinical isolates of HCAI-relevant, Gram- negative bacteria.

Peptide	Attribute	[a]H_{max}		MIC_{50} (μM)										[b]Gm	[c]Fold	Therapeutic index	
		(%)	(μM)	*Klebsiella pneumoniae*					*Pseudomonas aeruginosas*							MHC/MIC_{50}	[d]Fold
				49644	50181	50424	51048	51009	47661	48220	48221	48458	48526				
PLS	Palindromic	24.8	100.0	12.5		5.6	11.7	25.6	75.0					17.4	1.8	5.8	0.6
LfcinB $(20–25)_2$	Dimeric	5.6	100.0	12.3	6.6	5.8	5.7	5.6	13.4	50.0	64.2	75.0	36.3	16.8	1.7	6.0	0.6
LfcinB $(20–25)_4$	Tetrameric	49.1	100.0		5.5	7.8	5.2	1.6	7.5	12.6	11.9	72.8	24.9	9.7	1.0	10.4	1.0

[a]H_{max}: *Maximum Hemolytic Activity of the indicated peptide against human erythrocytes after 2 h of treatment at 37°C.*
[b]*GM: geometric mean of the* MIC_{50} *values for the indicated peptide against the indicated bacterial strains.*
[c]*Fold: Calculated as (GM for the indicated peptide)/(GM for the tetrameric peptide).*
[d]*Fold: Calculated as (TI for the indicated peptide)/(TI for the tetrameric peptide).*

was directly proportional to the number of RRWQWR motifs (tetrameric > dimeric > reference > palindromic = monomer), then by extension, higher net charge appeared to correlate to stronger bacterial activity (tetrameric > dimeric > monomer). Indeed, our two most active AMPs, with net charges of +12 (tetrameric) and +6 (dimeric), exhibited strong activity against seven of the eight ATCC bacterial strains (MIC_{50}: 1.7–21.7 μM) and against 17 of the 20 clinical isolates (1.6–73.8 μM for clinical isolates).

The hydrophobicity of our peptides might also have influenced their activity. We designed the two branched RRWQWR-based peptides by linking each pair of monomers to a shared Lys residue in the linker, which also included one or two residues of Ahx, a common hydrophobic spacer that prevents steric hindrance (Leon-Calvijo et al., 2015). The short sequence RRWQWR contains an interesting combination of hydrophobic (W, tryptophan) and cationic (R, arginine) amino acids (**Table 2**). Our results corroborated a direct link between the proportion of hydrophobic residues and the activity. Thus, among the linear peptides, the palindromic peptide (44.4% hydrophobic residues) was more active against the ATCC strains (seven of eight; **Table 3**) and the clinical isolates (fourteen of 20; **Table 5**) than was the reference peptide (33.3% hydrophobic residues) or the monomer (33.3% hydrophobic residues).

Finally, from a synthetic perspective, among the three most active peptides (tetrameric > dimeric > palindromic), the two branched peptides were easier to prepare, as they implied fewer coupling steps (9 for the tetrameric and 8 for the dimeric, compared to 9 for the palindromic). This practical advantage, combined with their superior activity, contributes to their attractiveness as starting points for possible antibacterial agents. Our results are consistent with those of previous reports that branched short peptides are more active than linear ones (Lopez-Garcia et al., 2002; Park and Hahm, 2012; Pires et al., 2015).

Although we did not screen the five peptides against many bacterial species, our objective was merely to establish a preliminary assessment of their antibacterial activities against a small variety of antibiotic-sensitive and antibiotic-resistant Gram-positive and Gram-negative bacteria relevant to HAIs.

Among the most surprising results that we observed with the ATCC lines was that at certain concentrations, some of the peptides induced growth of certain strains (**Figure 2**). This might simply reflect the diverse effects that AMPs and bacteria can have on each other, including proteolytic degradation of peptides by bacterial enzymes (peptidases and proteases) (Schmidtchen et al., 2002), as has been reported by other authors studying LfcinB-derived peptides in *E. faecalis* and other bacteria (Schmidtchen et al., 2001). Thus, such peptides must be studied carefully to determine their proper therapeutic window, which may be rather narrow. This might simply reflect an inherent lack of activity of LfcinB-derived peptides against the entire *Enterococcus* genus. Curiously, in our study, the monomer was inactive against the ATCC strains (**Table 3**); however, in previous reports, it was shown to be active against the same sensitive strain of *E. faecalis*

that we tested (ATCC 29212; MIC_{50}: 101.5 μM) (Leon-Calvijo et al., 2015). This discrepancy underscores that, while ATCC lines can be useful tools for assaying antimicrobial activity, they are not definitive indicators of activity, which must be assessed using clinical isolates.

Our SEM analysis revealed that the dimeric and tetrameric peptides induced changes in the sensitive strain of *E. faecalis* (**Figure 3**) only, and in both the sensitive and resistant strains of *P. aeruginosa* (**Figure S1**). These results agree with those obtained for other cationic peptides studied at the surface of these bacteria (Winfred et al., 2014; Spitzer et al., 2016), which suggest that the mechanism of action of each peptide involves the membrane. Interestingly, our observations that each peptide induced damage and porosity in the membrane of *P. aeruginosa* (**Figure S1**), mirror literature reports on other AMPs (Benli and Yigit, 2008; Cao et al., 2017). Also the SEM microphotographys display how *P. aeruginosa* has not surface biofilm As others authors has been demonstrate that Lactoferrin has anti-biofilm activity interfering with its formation and promoting the formation of thin, flat biofilm, allowing *P. aeruginosa* be more susceptible (Chung and Khanum, 2017).

Our results on the clinical isolates confirmed some of the results that we observed with the ATCC reference strains. Among the most important results was that against the clinical isolates of *E. faecium*, the peptides were either inactive or had MIC_{50} values of at least 100 μM (**Table 5**), similarly to their activity against the ATCC reference strain of antibiotic-sensitive *E. faecalis*. It was interesting to find again that in terms of activity against *Enterococcus*, the palindromic molecule was more active than the dimer (**Table 5**). This result open new overview because it could indicate that lineal and palindromic repetition of the short motif may useful design as antibacterial molecules for this gender of bacteria. A recent World Health Organization study has underscored the challenge of developing of antibacterials active against *P. aeruginosa* (WHO, 2014). Thus, among our most encouraging findings, was that the dimeric peptide and the tetrameric peptide were each active against *P. aeruginosa*. These results gave further evidence of the therapeutic potential of these two branched peptides and suggest that might exhibit specificity against Gram-positive species.

Considering our all our findings, we propose here that our dimeric and tetrameric have the following mode of action to inhibit bacterial growth: their large net cationic charge enables them to attach to the bacterial membrane surface, where they create small, permeable holes that disrupt the membrane and provoke cell permeation. The superior activity of these branched peptides relative to the three other RRWQWR-based peptides is consistent with previous reports that branched peptides are more active than linear ones (Tam, 1988; Pires et al., 2015), including a study on antigenic peptides derived from human Lfcin (Azuma et al., 1999).

Although the tetrameric peptide was nearly always the most active in all the assays, it also exhibited the highest hemolytic activity (Hmax: 49.1% = 8x that of the dimer). Hemolytic activity is directly related to the net positive charge of the molecule, which for the tetrameric peptide was +12. Interestingly, we attributed the antibacterial activity of this peptide to this very charge. Our first attempt to reduce the hemolytic activity was to synthesize the dimeric peptide, whose net charge (+6) is half that of the tetrameric peptide. Encouragingly, the dimeric peptide exhibited similar antibacterial and lower hemolytic activity relative to the tetrameric peptide. In terms of future work, one strategy to reduce hemolytic effects would be to explore controlled-release systems for the tetrameric, dimeric or other peptide, whereby the concentration of the released peptide could be controlled temporally to maximize therapeutic efficacy while minimizing hemolytic effects. Another option would be to explore the use of prodrugs and/or peptide conjugates, to improve specific targeting. Examples of such prodrugs include a bioactive peptide linked to delivery peptides or cell-penetrating peptides (Mishra et al., 2017).

Intriguingly, during our experiments using Muller Hinton Broth and the tetrameric peptide at concentrations of 100 and 200 μM, the peptide appeared somewhat unstable: upon addition of the peptide solution, the culture developed turbidity, which disappeared with time. This effect may be down to the salt content in Muller Hinton Broth, as various AMPs have been reported to lose activity in physiological salt solutions and in sera (Goldman et al., 1997; Lee et al., 1997; Wu et al., 1999; Rothstein et al., 2001). Further studies salt interactions and serum binding will be required to determine the utility of the tetrameric peptide, whose use as antimicrobial agent may currently be limited to lower concentrations (hemolytic activity at 12.5 μM: 11.2%).

CONCLUSION

We have reported the design, synthesis and screening of a set of short, cationic, LfcinB-derived peptides containing at least one RRWQWR motif, as antibacterial agents against ATCC reference strains and clinical isolates of Gram-positive and Gram-negative bacteria associated with HAIs. Our findings suggest that the branched dimeric peptide is the most attractive candidate for further development: although it was generally less active than the branched tetrameric peptide, it was far less hemolytic and did not suffer from the stability problems that the latter peptide showed in culture. We are currently performing detailed membrane, cellular and systemic toxicity studies on both peptides.

ETHICS STATEMENT

This study was approved by the Ethics Committees of the Universidad Nacional de Colombia and the Secretaría de Salud de Bogotá. All patient records were anonymized prior to analysis.

AUTHOR CONTRIBUTIONS

SV and JR contributed conception and design of the study; DM synthesized the peptides molecules; SV performed *in vitro* assays and SEM microscopy of ATCC strains. SV, JR, and HV contributed conception and design of the clinical isolates test. MC and SV performed the *in vitro* assay with clinical isolates;

SV wrote the first draft of the manuscript; DM, MC, HV, SV, and JR wrote sections of the manuscript. All authors contributed to manuscript revision, read and approved the submitted version.

ACKNOWLEDGMENTS

The authors wish to thank the Departamento Administrativo de Ciencia y Tecnología, COLCIENCIAS (FP44842-154-2015), for its financial support under Convocatoria 656-2014 "Es Tiempo de Volver." We also thank the Department of Pharmacy the Universidad Nacional de Colombia in Bogotá for the hospitality. Lastly, we are grateful to Claudia L. Avendaño, of the SEM Laboratory at the Universidad Nacional de Colombia, for her technical advice on SEM.

SUPPLEMENTARY MATERIAL

The Supplementary Material for this article can be found online at: https://www.frontiersin.org/articles/10.3389/fmicb.2018.00329/full#supplementary-material

Figure S1 | Scanning electron microscopy (SEM) images of Gram-positive (*E. faecalis*: Sensitive ATCC-29212; Resistance ATCC-51575) and Gram-negative (*P. aeruginosa:* Sensitive ATCC-10145; Resistance ATCC-27853) strains before and after treatment with the dimeric or tetrameric peptides. **(Top)** The sensitive strain, untreated (left), and after treatment with either the dimeric (middle) or tetrameric (right) peptide at 3× MIC_{50} for 2h. **(Top)** *E. faecalis*: ATCC-29212 (300.0 and 75.0 μM, dimeric or tetrameric peptides respectively); Resistance ATCC-51575 (200 μM was used because those peptides have not induced MIC_{50} on this strain). **(Bottom)** *P. aeruginosa*: Sensitive ATCC-10145 (87.3 and 54.3 μM, dimeric or tetrameric peptides respectively) and for the Resistance ATCC-27853 (104.4 and 63.3 μM respectively).

REFERENCES

Azuma, M., Kojima, T., Yokoyama, I., Tajiri, H., Yoshikawa, K., Saga, S., et al. (1999). Antibacterial activity of multiple antigen peptides homologous to a loop region in human lactoferrin. *J. Pept. Res.* 54, 237–241. doi: 10.1034/j.1399-3011.1999.00090.x

Benli, M., and Yigit, N. (2008). Antibacterial activity of venom from funnel web spider *Agelena labyrinthica* (Araneae: Agelenidae). *J. Venom Anim. Toxins Incl. Trop. Dis.* 14, 641–650. doi: 10.1590/S1678-91992008000400007

Brunetti, J., Falciani, C., Roscia, G., Pollini, S., Bindi, S., Scali, S., et al. (2016). *In vitro* and *in vivo* efficacy, toxicity, bio-distribution and resistance selection of a novel antibacterial drug candidate. *Sci. Rep.* 6:26077. doi: 10.1038/srep26077

Cao, X., Meng, L., Zhang, N., and Zhou, Z. (2017). Microscopic examination of polymeric monoguanidine, hydrochloride-induced cell membrane damage in multidrug-resistant *Pseudomonas aeruginosa*. *Polymers* 9:398. doi: 10.3390/polym9090398

Chen, L., Li, X., Gao, L., and Fang, W. (2015). Theoretical insight into the relationship between the structures of antimicrobial peptides and their actions on bacterial membranes. *J. Phys. Chem. B* 119, 850–860. doi: 10.1021/jp505497k

Chung, P. Y., and Khanum, R. (2017). Antimicrobial peptides as potential anti-biofilm agents against multidrug-resistant bacteria. *J. Microbiol. Immunol. Infect.* 50, 405–410. doi: 10.1016/j.jmii.2016.12.005

CLSI (2007). *Methods for Dilution Antimicrobial Susceptibility Tests for Bacteria that Grow Aerobically; Approved Standard M7-A7*, Wayne, PA: CLSI.

da Cunha, N. B., Cobacho, N. B., Viana, J. F. C., Lima, L. A., Sampaio, K. B. O., Dohms, S. S. M., et al. (2017). The next generation of antimicrobial peptides (AMPs) as molecular therapeutic tools for the treatment of diseases with social and economic impacts. *Drug Discov. Today* 22, 234–248. doi: 10.1016/j.drudis.2016.10.017

Dathe, M., Nikolenko, H., Meyer, J., Beyermann, M., and Bienert, M. (2001). Optimization of the antimicrobial activity of magainin peptides by modification of charge. *FEBS Lett.* 501, 146–150. doi: 10.1016/S0014-5793(01)02648-5

de la Fuente-Nunez, C., Torres, M. D., Mojica, F. J., and Lu, T. K. (2017). Next-generation precision antimicrobials: towards personalized treatment of infectious diseases. *Curr. Opin. Microbiol.* 37, 95–102. doi: 10.1016/j.mib.2017.05.014

Draenert, R., Seybold, U., Grutzner, E., and Bogner, J. R. (2015). Novel antibiotics: are we still in the pre-post-antibiotic era? *Infection* 43, 145–151. doi: 10.1007/s15010-015-0749-y

European Committee for Antimicrobial Susceptibility Testing (2000). EUCAST definitive document E DEF 3.1, June 2000: determination of minimum inhibitory concentrations (MICs) of antibacterial agents by agar dilution. *Clin. Microbiol. Infect.* 6, 509–515. doi: 10.1046/j.1469-0691.2000.00142.x

Goldman, M. J., Anderson, G. M., Stolzenberg, E. D., Kari, U. P., Zasloff, M., and Wilson, J. M. (1997). Human beta-defensin-1 is a salt-sensitive antibiotic in lung that is inactivated in cystic fibrosis. *Cell* 88, 553–560. doi: 10.1016/S0092-8674(00)81895-4

Huertas, N. J., Monroy, Z. J. R., Medina, R. F., and Castaneda, J. E. G. (2017). Antimicrobial activity of truncated and polyvalent peptides derived from the FKCRRQWQWRMKKGLA sequence against *Escherichia coli* ATCC 25922 and *Staphylococcus aureus* ATCC 25923. *Molecules* 22:987. doi: 10.3390/molecules22060987

Khachatryan, V., Sirunyan, A. M., Tumasyan, A., Adam, W., Asilar, E., Bergauer, T., et al. (2017). Measurement of the WZ production cross section in pp collisions at [Formula: see text] and 8[Formula: see text] and search for anomalous triple gauge couplings at [Formula: see text]. *Eur. Phys. J. C. Part Fields* 77:236. doi: 10.1140/epjc/s10052-017-4730-z

Lee, I. H., Cho, Y., and Lehrer, R. I. (1997). Effects of pH and salinity on the antimicrobial properties of clavanins. *Infect. Immun.* 65, 2898–2903.

Leon-Calvijo, M. A., Leal-Castro, A. L., Almanzar-Reina, G. A., Rosas-Perez, J. E., Garcia-Castaneda, J. E., and Rivera-Monroy, Z. J. (2015). Antibacterial activity of synthetic peptides derived from lactoferricin against *Escherichia coli* ATCC 25922 and *Enterococcus faecalis* ATCC 29212. *Biomed Res. Int.* 2015:453826. doi: 10.1155/2015/453826

Lopez-Garcia, B., Perez-Paya, E., and Marcos, J. F. (2002). Identification of novel hexapeptides bioactive against phytopathogenic fungi through screening of a synthetic peptide combinatorial library. *Appl. Environ. Microbiol.* 68, 2453–2460. doi: 10.1128/AEM.68.5.2453-2460.2002

Ma, Q., Jiao, W., Lv, Y., Dong, N., Zhu, X., and Shan, A. (2014). Structure-function relationship of Val/Arg-rich peptides: effects of net charge and pro on activity. *Chem. Biol. Drug Des.* 84, 348–353. doi: 10.1111/cbdd.12325

Mishra, B., Reiling, S., Zarena, D., and Wang, G. (2017). Host defense antimicrobial peptides as antibiotics: design and application strategies. *Curr. Opin. Chem. Biol.* 38, 87–96. doi: 10.1016/j.cbpa.2017.03.014

Park, Y., and Hahm, K. S. (2012). Novel short AMP: design and activity study. *Protein Pept. Lett.* 19, 652–656. doi: 10.2174/092986612800494093

Percival, S. L., Suleman, L., Vuotto, C., and Donelli, G. (2015). Healthcare-associated infections, medical devices and biofilms: risk, tolerance and control. *J. Med. Microbiol.* 64, 323–334. doi: 10.1099/jmm.0.000032

Pires, J., Siriwardena, T. N., Stach, M., Tinguely, R., Kasraian, S., Luzzaro, F., et al. (2015). *In Vitro* activity of the novel antimicrobial peptide dendrimer G3KL against multidrug-resistant *Acinetobacter baumannii* and *Pseudomonas aeruginosa*. *Antimicrob. Agents Chemother.* 59, 7915–7918. doi: 10.1128/AAC.01853-15

Prakash, S. K. (2014). *Nosocomial Infection-an Overview* [Online]. Available online at: http://citeseerx.ist.psu.edu/viewdoc/download?doi=10.1.1.512.439&rep=rep1&type=pdf (Accessed October 10, 2014).

Richardson, A., de Antueno, R., Duncan, R., and Hoskin, D. W. (2009). Intracellular delivery of bovine lactoferricin's antimicrobial core (RRWQWR) kills T-leukemia cells. *Biochem. Biophys. Res. Commun.* 388, 736–741. doi: 10.1016/j.bbrc.2009.08.083

Rothstein, D. M., Spacciapoli, P., Tran, L. T., Xu, T., Roberts, F. D., Dalla Serra, M., et al. (2001). Anticandida activity is retained in P-113, a 12-amino-acid fragment of histatin 5. *Antimicrob. Agents Chemother.* 45, 1367–1373. doi: 10.1128/AAC.45.5.1367-1373.2001

Schmidtchen, A., Frick, I. M., Andersson, E., Tapper, H., and Bjorck, L. (2002). Proteinases of common pathogenic bacteria degrade and inactivate the antibacterial peptide LL-37. *Mol. Microbiol.* 46, 157–168. doi: 10.1046/j.1365-2958.2002.03146.x

Schmidtchen, A., Frick, I. M., and Bjorck, L. (2001). Dermatan sulphate is released by proteinases of common pathogenic bacteria and inactivates antibacterial alpha-defensin. *Mol. Microbiol.* 39, 708–713. doi: 10.1046/j.1365-2958.2001.02251.x

Shang, D., Li, X., Sun, Y., Wang, C., Sun, L., Wei, S., et al. (2012). Design of potent, non-toxic antimicrobial agents based upon the structure of the frog skin peptide, temporin-1CEb from Chinese brown frog, *Rana chensinensis*. *Chem. Biol. Drug Des.* 79, 653–662. doi: 10.1111/j.1747-0285.2012.01363.x

Solarte, V. A., Rosas, J. E., Rivera, Z. J., Arango-Rodriguez, M. L., Garcia, J. E., and Vernot, J. P. (2015). A tetrameric peptide derived from bovine lactoferricin exhibits specific cytotoxic effects against oral squamous-cell carcinoma cell lines. *Biomed Res. Int.* 2015:630179. doi: 10.1155/2015/630179

Spitzer, P., Condic, M., Herrmann, M., Oberstein, T. J., Scharin-Mehlmann, M., Gilbert, D. F., et al. (2016). Amyloidogenic amyloid-beta-peptide variants induce microbial agglutination and exert antimicrobial activity. *Sci. Rep.* 6:32228. doi: 10.1038/srep32228

Tam, J. P. (1988). Synthetic peptide vaccine design: synthesis and properties of a high-density multiple antigenic peptide system. *Proc. Natl. Acad. Sci. U.S.A.* 85, 5409–5413. doi: 10.1073/pnas.85.15.5409

WHO (2014). *World Health Organization. Antimicrobial Resistance: Global Report on Surveillance*. Available online at: http://www.who.int/drugresistance/documents/surveillancereport/en/ (Accessed July 5, 2015).

Wiegand, I., Hilpert, K., and Hancock, R. E. (2008). Agar and broth dilution methods to determine the minimal inhibitory concentration (MIC) of antimicrobial substances. *Nat. Protoc.* 3, 163–175. doi: 10.1038/nprot.2007.521

Winfred, S. B., Meiyazagan, G., Panda, J. J., Nagendrababu, V., Deivanayagam, K., Chauhan, V. S., et al. (2014). Antimicrobial activity of cationic peptides in endodontic procedures. *Eur. J. Dent.* 8, 254–260. doi: 10.4103/1305-7456.130626

Wu, M., Maier, E., Benz, R., and Hancock, R. E. (1999). Mechanism of interaction of different classes of cationic antimicrobial peptides with planar bilayers and with the cytoplasmic membrane of *Escherichia coli*. *Biochemistry* 38, 7235–7242. doi: 10.1021/bi9826299

Yin, L. M., Edwards, M. A., Li, J., Yip, C. M., and Deber, C. M. (2012). Roles of hydrophobicity and charge distribution of cationic antimicrobial peptides in peptide-membrane interactions. *J. Biol. Chem.* 287, 7738–7745. doi: 10.1074/jbc.M111.303602

Conflict of Interest Statement: The authors declare that the research was conducted in the absence of any commercial or financial relationships that could be construed as a potential conflict of interest.

frontiers in Microbiology

ORIGINAL RESEARCH
published: 27 March 2018
doi: 10.3389/fmicb.2018.00572

Differential Activity of the Combination of Vancomycin and Amikacin on Planktonic vs. Biofilm-Growing *Staphylococcus aureus* Bacteria in a Hollow Fiber Infection Model

*Diane C. Broussou[1,2], Marlène Z. Lacroix[1], Pierre-Louis Toutain[3], Frédérique Woehrlé[2], Farid El Garch[2], Alain Bousquet-Melou[1] and Aude A. Ferran[1]**

[1] INTHERES, INRA, ENVT, Université de Toulouse, Toulouse, France, [2] Vétoquinol, Global Drug Development, Lure, France, [3] Department of Veterinary Basic Sciences, Royal Veterinary College, London, United Kingdom

OPEN ACCESS

Edited by:
Mariana Henriques, University of Minho, Portugal

Reviewed by:
Fintan Thomas Moriarty, AO Research Institute, Switzerland
Anabela Portela Borges, Faculdade de Engenharia da Universidade do Porto, Portugal

***Correspondence:**
Aude A. Ferran
a.ferran@envt.fr

Specialty section:
This article was submitted to Antimicrobials, Resistance and Chemotherapy, a section of the journal Frontiers in Microbiology

Received: *15 September 2017*
Accepted: *13 March 2018*
Published: *27 March 2018*

Citation:
Broussou DC, Lacroix MZ, Toutain P-L, Woehrlé F, El Garch F, Bousquet-Melou A and Ferran AA (2018) Differential Activity of the Combination of Vancomycin and Amikacin on Planktonic vs. Biofilm-Growing Staphylococcus aureus Bacteria in a Hollow Fiber Infection Model. Front. Microbiol. 9:572. doi: 10.3389/fmicb.2018.00572

Combining currently available antibiotics to optimize their use is a promising strategy to reduce treatment failures against biofilm-associated infections. Nevertheless, most assays of such combinations have been performed *in vitro* on planktonic bacteria exposed to constant concentrations of antibiotics over only 24 h and the synergistic effects obtained under these conditions do not necessarily predict the behavior of chronic clinical infections associated with biofilms. To improve the predictivity of *in vitro* combination assays for bacterial biofilms, we first adapted a previously described Hollow-fiber (HF) infection model by allowing a *Staphylococcus aureus* biofilm to form before drug exposure. We then mimicked different concentration profiles of amikacin and vancomycin, similar to the free plasma concentration profiles that would be observed in patients treated daily over 5 days. We assessed the ability of the two drugs, alone or in combination, to reduce planktonic and biofilm-embedded bacterial populations, and to prevent the selection of resistance within these populations. Although neither amikacin nor vancomycin exhibited any bactericidal activity on *S. aureus* in monotherapy, the combination had a synergistic effect and significantly reduced the planktonic bacterial population by −3.0 to −6.0 $\log_{10}$ CFU/mL. In parallel, no obvious advantage of the combination, as compared to amikacin alone, was demonstrated on biofilm-embedded bacteria for which the addition of vancomycin to amikacin only conferred a further maximum reduction of 0.3 $\log_{10}$ CFU/mL. No resistance to vancomycin was ever found whereas a few bacteria less-susceptible to amikacin were systematically detected before treatment. These resistant bacteria, which were rapidly amplified by exposure to amikacin alone, could be maintained at a low level in the biofilm population and even suppressed in the planktonic population by adding vancomycin. In conclusion, by adapting the HF model, we were able to demonstrate the different bactericidal activities of the vancomycin and amikacin combination on planktonic and biofilm-embedded bacterial populations, suggesting that, for

biofilm-associated infections, the efficacy of this combination would not be much greater than with amikacin monotherapy. However, adding vancomycin could reduce possible resistance to amikacin and provide a relevant strategy to prevent the selection of antibiotic-resistant bacteria during treatments.

Keywords: hollow-fiber infection model, antibiotic combination, amikacin, vancomycin, biofilm, antimicrobial resistance, *Staphylococcus aureus*

INTRODUCTION

Staphylococcus aureus possesses the ability to form biofilms and is responsible for chronic infections which are hard to treat and cause significant morbidity and mortality.

Biofilms are communities of bacteria which adhere to surfaces and are encapsulated in a self-produced extracellular polysaccharide matrix. They constitute an important strategy implemented by microorganisms to survive in harsh environmental conditions (Donlan and Costerton, 2002). Biofilms are responsible for chronic, recurrent infections and are known to survive very high concentrations of antibiotics (Lewis, 2008; Lebeaux et al., 2014). One hypothesis to explain the lower activity of antimicrobial drugs on biofilms is the high prevalence of persister cells in biofilms (Lewis, 2008; Singh et al., 2009). These persisters, unlike resistant bacteria which are genetically modified, consist of clones of bacteria expressing a different but reversible phenotype which allows them to transiently escape the effects of antibiotics (Lewis, 2008).

The antibiotic therapies currently used against biofilm infections are often associated with poor clinical responses and frequent relapses (Davies, 2003). For several years, different solutions have been proposed to eradicate biofilm bacteria such as phages, quorum sensing inhibitors or physical methods (Ivanova et al., 2017). However, although highly innovative strategies still need to be developed to deal with severe infections by both tolerant and multi-resistant bacteria, the method which can most rapidly and easily be implemented in patients at present is to combine existing drugs or to modify their therapeutic regimen (dose, frequency, and mode of administration).

In the case of suspected *S. aureus* infection, vancomycin therapy is often initiated in patients to provide antibacterial activity against both Methicillin-Sensitive *S. aureus* (MSSA) and Methicillin-Resistant *S. aureus* (MRSA) (Deresinski, 2009). However, although vancomycin can kill planktonic bacteria, its activity against Biofilm-Embedded Bacteria (BEB) is quite low. Lebeaux et al. (2015) showed that after exposure to a very high, constant concentration of vancomycin (5000 mg/L) for 24 h, the percentage of bacteria surviving in a 24 h-old *S. aureus* biofilm exceeded 20% and was even close to 100% for 2 of the 4 tested strains. Singh et al. (2009) reported similar results and found no statistically significant difference between the bacteria remaining in a non-treated *S. aureus* biofilm or in a biofilm exposed for 24 h to vancomycin concentrations equal to or higher than those clinically achievable. Post et al. (2017) demonstrated that vancomycin is able to eradicate a mature biofilm of *S. aureus* from metal implants by using a static concentration of 200 mg/L over 28 days. Nevertheless, such a concentration profile cannot be achieved by systemic administration or local delivery vehicles currently available. To overcome this poor activity on biofilms, an aminoglycoside is often combined with vancomycin. Synergistic activity between vancomycin and aminoglycosides had already been demonstrated on *S. aureus* (Watanakunakorn and Glotzbecker, 1974; Cokça et al., 1998) but these studies were performed by exposing planktonic bacteria for no more than 24 h to constant antibiotic concentrations whereas in the *in vivo* situation, antibiotic concentrations continuously fluctuate over several days. The effects of a combination of gentamicin and vancomycin on *S. aureus* were more rarely tested under dynamic *in vitro* conditions with varying antibiotic concentrations or in animal models of infection. No significant synergy was observed in two studies where low inocula of *S. aureus* were exposed to the two drugs (Backo et al., 1999; Aeschlimann et al., 2000). Another study on large inocula of MRSA and MSSA, representative of a biofilm-associated infection, was performed in an *in vitro* simulated endocardial vegetation model. The effect of vancomycin alone was statistically significant compared to the control after 3 days but the activity of vancomycin on MSSA or MRSA was not improved by adding gentamicin (LaPlante and Woodmansee, 2009). However, in this study, the vancomycin concentrations tested were almost two times higher than the free and active concentrations routinely obtained in patients because no correction was performed for the 45% plasma protein binding of vancomycin (Liu et al., 2002; Butterfield et al., 2011).

To propose new treatment optimizations, the predictivity of *in vitro* experiments needs to be improved, for example by exposing both planktonic and BEB in parallel over the complete duration of treatment (several days), to drug concentrations identical to those that would be encountered under clinical conditions in patients.

In this study, we studied the effects of amikacin, an aminoglycoside, and vancomycin on planktonic and biofilm-embedded *S. aureus* by using an *in vitro* dynamic model, the Hollow-Fiber (HF) infection model, which mimics the fluctuations of antibiotic concentrations over time, as would occur in the plasma of patients during a 5-day treatment. The HF model was recently labeled by the European Medicines Agency (European Medicines Agency, 2015; Gumbo et al., 2015) for drug dosage optimization in the treatment of tuberculosis. We have further adapted this model to explore drug activity not only on planktonic but also on biofilm-embedded *S. aureus*. Indeed, in previous studies conducted in HF (Nicasio et al., 2012; Ferro et al., 2015), the bacteria were systematically

exposed to drugs during the exponential phase of growth, when there was no time for biofilm development, whereas in this study, the biofilm was allowed to form for 3 days before drug exposure. The killing effects of drugs and the potential selection of resistance were assessed both on planktonic bacteria over time and on BEB at the end of exposure. We first compared monotherapy and combinations of amikacin and vancomycin at the currently recommended dosing regimens, i.e., 1g vancomycin twice a day and 15 mg/kg amikacin once a day for 5 days. Such therapeutic regimens are considered sufficient to achieve the PK/PD indices classically expected to obtain drug efficacy. For aminoglycosides, the most predictive PK/PD index is the Maximal Concentration (C_{max}) divided by the Minimal Inhibitory Concentration (MIC) ratio (Moore et al., 1987) and a value from 8 to 10 is usually recommended to ensure efficacy against the pathogen (Toutain et al., 2002). For vancomycin, the best predictive index is the AUC over 24 h divided by the MIC (AUC_{24h}/MIC) (Nielsen et al., 2011), and value of 400 is recommended to achieve clinical effectiveness (Rybak et al., 2009; Jung et al., 2014; Song et al., 2015).

We then explored the effects of a slight deviation from these standard dosages by simulating an increased dose of amikacin, which is a concentration-dependent antibiotic, (Frimodt-Møller, 2002) and by modifying the mode of administration (infusion vs. bolus) of vancomycin, which is a time-dependent antibiotic (Waineo et al., 2015).

MATERIALS AND METHODS

Bacterial Strain

The Methicillin-sensitive *S. aureus* strain HG 001, derived from NCTC 8325, was used for all experiments.

Antimicrobial Agents

Amikacin sulfate powder (Amikacine Mylan®) and vancomycin chlorhydrate powder (Vancomycine Sandoz®) were used to prepare antibiotic stock solutions with water. Vials were stored at −20°C for less than 1 month and were thawed and diluted to the desired concentrations for the assay just before each antibiotic administration.

Minimal Inhibitory Concentration (MIC) Determination

Minimal inhibitory concentrations of vancomycin and amikacin on the MSSA strain were performed in triplicate by broth microdilution in cation-adjusted Mueller Hinton broth (Ca-MH, Mueller-Hinton II, Sigma Aldrich, Saint Quentin-Fallavier, France) according to the CLSI reference methods (Clinical and Laboratory Standards Institute [CLSI], 2012), and also in Roswell Park Medium Institute 1640 Medium (RPMI, Gibco, Thermo Fischer Scientific, MA, United States). Briefly, a bacterial suspension, diluted in Mueller-Hinton Broth or RPMI to give a final organism density of 5.7 $\log_{10}$ CFU/mL, was added to wells of a microtiter plate containing serial twofold dilutions of vancomycin or amikacin. Growth was recorded after incubation for 18 h at 35°C.

PK/PD Study

Hollow-Fiber Infection Model

A HF infection model was used to assess the antibacterial activity of the combination of amikacin and vancomycin on planktonic and biofilm-embedded *S. aureus* during exposure to fluctuating clinically relevant antibiotic concentrations. A diagrammatic representation of the Hollow Fiber Infection Model was kindly provided by FiberCell Systems® (**Figure 1**). Basically, the HF model includes a cartridge with capillaries composed of a semipermeable polysulfone membrane. The pore size of the capillaries (42 kDa) allows equilibration of the concentrations of chemicals which circulate through the central and peripheral compartments by means of a peristaltic pump (Duet pump, FiberCell Systems, Inc., Frederick, MD, United States) while the bacteria stay confined to the extracapillary space in the peripheral compartment.

In this study, twenty milliliters of a suspension containing 5.7 $\log_{10}$ CFU/mL of *S. aureus* were inoculated into the extracapillary space of each hollow-fiber cartridge (C2011 polysulfone cartridge, FiberCell Systems, Inc., Frederick, MD, United States) and incubated at 37°C in RPMI from Day 0 (D0) to Day 2 (D2) without any drug, to allow biofilm formation.

From D3 to D7, the bacteria were then subjected to amikacin and/or vancomycin. The drugs were added to the central compartment to obtain the maximum concentration (C_{max}) and were continuously diluted with RPMI by means of a peristaltic pump (Mini Rythmic PN+, SMD, Fleury-sur-Orne, France) to mimic the human terminal half-life of each antibiotic. The antibiotics also constantly circulated through the central and peripheral compartments by means of a second peristaltic pump (Duet pump, FiberCell Systems, Inc., Frederick, MD, United States).

The first antibiotic exposure tested in the HF model simulated the plasma concentrations of patients receiving 15 mg/kg amikacin once a day (Kato et al., 2017) and/or 1 g vancomycin every 12 h (Nicasio et al., 2012). Since the free plasma drug concentration is known to be one of the best surrogates of the concentration at the site of infection (Liu et al., 2002), we exposed the bacteria in the HF model to concentrations similar to the free plasma concentrations obtained in patients after administration of the above dosing regimens. For amikacin, plasma protein binding was considered negligible and a plasma C_{max} of treated patients ranging from 60 to 80 mg/L (A70 treatment) was reproduced in the HF model (Gálvez et al., 2011). For vancomycin, plasma protein binding is around 45% (Butterfield et al., 2011) so the total plasma concentrations obtained from patients described in the literature were corrected to calculate the free C_{max} of 18 μg/mL, which was then simulated in the HF model (V18 treatment) (Mandell et al., 2007). The simulated elimination half-life for both drugs in the HF model (4 h) was similar to the plasma elimination half-lives of amikacin and vancomycin in patients (Matzke et al., 1986; Adamis et al., 2004).

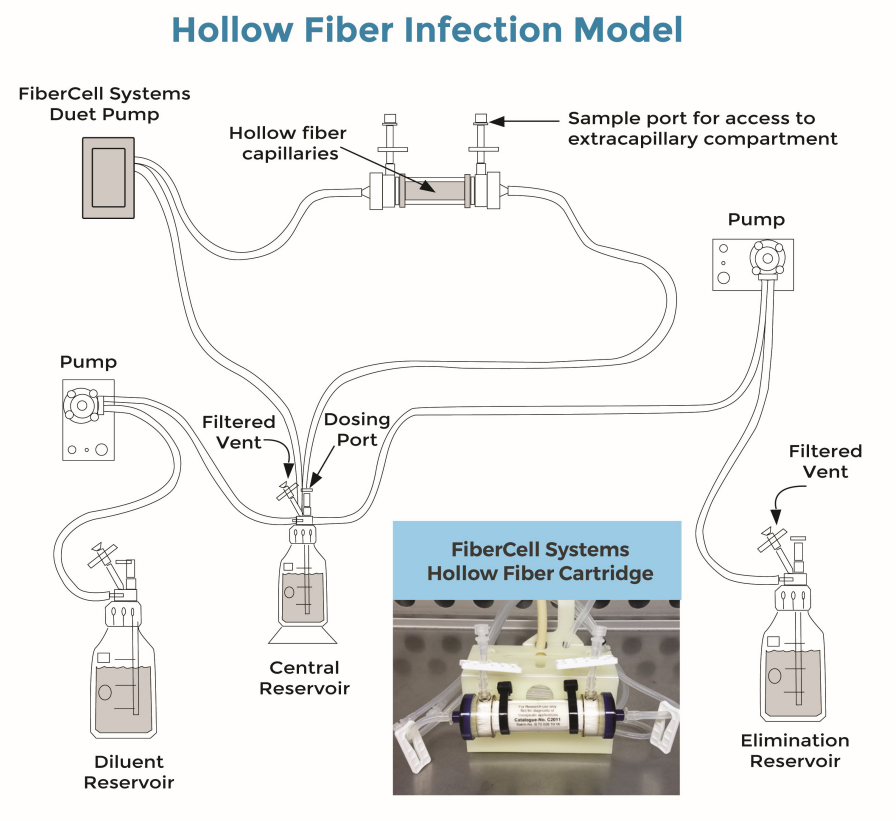

FIGURE 1 | Diagrammatic representation of the Hollow Fiber Infection Model kindly provided by FiberCell Systems® (Cadwell, 2015). Bacteria were trapped by the hollow fiber capillaries in the cartridge (see also embedded photo). Drugs were added to the central reservoir and freely circulated through the cartridge and bacteria by means of the Fibercell Systems Duet pump® (FiberCell Systems, Inc., Frederick, MD, United States). Drug concentrations decreased over time after drug administrations, due to the continuous addition of a diluent (RPMI) by means of another set of pumps (here, Mini Rythmic® PN+, SMD, Fleury-sur-Orne, France).

For the combinations, we first tested both drugs at the current dosing regimens for amikacin and vancomycin (A70 V18 treatment) and then simulated different pharmacokinetic profiles. We then tested two higher peak concentrations of 90 μg/mL (A90 V18 treatment) and 130 μg/mL (A130 V18 treatment) of amikacin, that could theoretically be attained in patients with a dose of 2500 mg (Álvarez et al., 2016), to investigate the relation between amikacin concentration and activity. For vancomycin, a dosage of 2 g a day has been recently recommended (Patel et al., 2011; Waineo et al., 2015), so a Continuous Rate Infusion (CRI) of 2 g a day of vancomycin was simulated by directly adding the drug to the fresh diluting medium to obtain a constant vancomycin concentration of 9 μg/mL (A70 CRIV9 treatment) (Hanrahan et al., 2015). All the experiments, including control and exposure to amikacin and vancomycin in monotherapy or in combination, were performed in duplicate to check reproducibility.

Planktonic Bacteria Quantification

One milliliter samples were collected from the extracapillary space in the HF cartridge to count the planktonic bacteria at 0 h (baseline), 2, 4, 6, 8, and 10 h after the morning antibiotic administration each day for 5 days (D3 to D7). The samples were centrifuged at 3000 *g* for 10 min. The supernatant was removed and the pellet resuspended in 1 mL of NaCl 0.9%. The suspension was then serially diluted and the bacteria counted in triplicate after an overnight incubation at 37°C on tryptic soy agar supplemented with magnesium sulfate and activated charcoal to prevent any carry-over effect of the antibiotic. The counts were verified again 8 h after to include colonies that could have slower grown. The limit of detection was 2.5 $\log_{10}$ CFU/mL.

After two washes to remove the antibiotic contained in the suspension, the less-susceptible planktonic bacteria were counted once a day prior to morning antibiotic administrations from D3 to D7 on agars containing threefold (3 μg/mL) and sixfold MIC (6 μg/mL) of amikacin or vancomycin. The plates were incubated for 3 days at 37°C before the bacteria were counted. The proportion of less-susceptible bacteria in the total bacterial population was calculated as the ratio of the colony counts on drug-supplemented agar divided by the colony counts on drug-free agar at the same sampling time.

Biofilm Bacteria Quantification

At the end of the experiment (D7), the extracapillary space in the cartridge containing the bacteria was washed four times

with 50 mL of sterile NaCl 0.9% to remove the planktonic bacteria. The biofilm was then disrupted by sonication of the cartridge for 15 min at 42 kHz (Bransonic 5800, Branson Ultrasonics Corporation, Emerson, Angoulême, France) which suspended the BEB in the 20 ml of NaCl 0.9% remaining in the cartridge after the washes. These bacteria were collected for quantification with the same technic as for planktonic bacteria. The colonies were plated on the drug-free and drug-supplemented agar and were counted, before and after ultrasound treatment. After an overnight incubation at 37°C, or more if needed, the size of the biofilm was calculated in $\log_{10}$ CFU/mL from the difference between the bacterial counts in the extracapillary space before and after ultrasound treatment. For each combination, the MIC of amikacin or vancomycin was also determined on a single bacterial colony growing on the drug-containing agar plates to accurately quantify the loss of susceptibility.

Drug Assay

Samples for antibiotic quantification were withdrawn from the central reservoir and from the extracapillary space of the cartridge before and after each antibiotic administration and at 2, 4, 6, and 8 h on the 1st day and twice a day thereafter. Samples were centrifuged at 3000 *g* for 10 min and stored at −20°C for less than 2 months before dosing.

Samples were prepared in 1.5 mL tubes. Two hundred µL of 15% of trichloroacetic acid containing the vancomycin d12 and amikacin d5 internal standards at 10 µg/mL were added to 100 µL of calibrators, quality controls, or samples. Antibiotics were quantified on an Acquity ultra performance liquid chromatography (UPLC) coupled to a Xevo triple quadrupole mass spectrometer (Waters, Milford, MA, United States). Chromatographic data were monitored by Targetlynx software (Waters, Milford, MA, United States). The method was validated in terms of linearity, sensitivity and repeatability. Accuracies ranged from 84 to 94% and from 99 to 107% with CV intra-day precisions below 9 and 10% for amikacin and vancomycin, respectively. The limit of quantification was set at 0.5 µg/mL for both antibiotics.

The concentration of antibiotic in the system was calculated according to equation 1.

Statistics

The planktonic bacterial inoculum sizes before (D3) and after (D7) in the 5-day combined treatments were compared by applying a paired T-test with the R® software (R Development Core Team, 2014).

The sizes of the planktonic bacteria and BEB populations after treatment with the amikacin and vancomycin combination for 5 days (D7) were also compared by paired T-test with R®.

RESULTS

Minimal Inhibitory Concentration (MIC)

The MIC of vancomycin, for the *S. aureus* strain tested, was 1 µg/mL both in Ca-MH and in RPMI and the MIC of amikacin was 1 µg/mL in Ca-MH and 0.5 µg/mL in RPMI. Based on the EUCAST breakpoints, the tested strain was therefore considered as susceptible to vancomycin and amikacin.

PK Analysis

The concentrations in the central compartment and in the extra capillary space of the cartridge (containing bacteria) attained equilibrium within 15 min after adding the antibiotic to the central compartment (data not shown). The predicted vs. observed free concentration-time profiles of amikacin and vancomycin in the HF model, corresponding to the dosing regimen of 15 mg/kg of amikacin once a day (A70) and 1 g of vancomycin every 12 h (V18), are provided in **Figure 2**.

For vancomycin, the targeted $AUC_{24\ h}$ was 400 µg.h.mL^{-1}, i.e., 16.6 times the MIC over 24 h (Toutain et al., 2007), and $AUC_{24\ h}$ ranging from 372 to 417 µg.h.mL^{-1}, i.e., deviations ranging from −7.0 to +4.3% from the targeted $AUC_{24\ h}$, were obtained. For amikacin, the targeted C_{max} was 70 µg/mL and, at steady-state, a C_{max} of 59.3 ± 25.8 µg/mL (mean ± SD) i.e., a mean deviation of 15.3% from the expected C_{max}, was obtained.

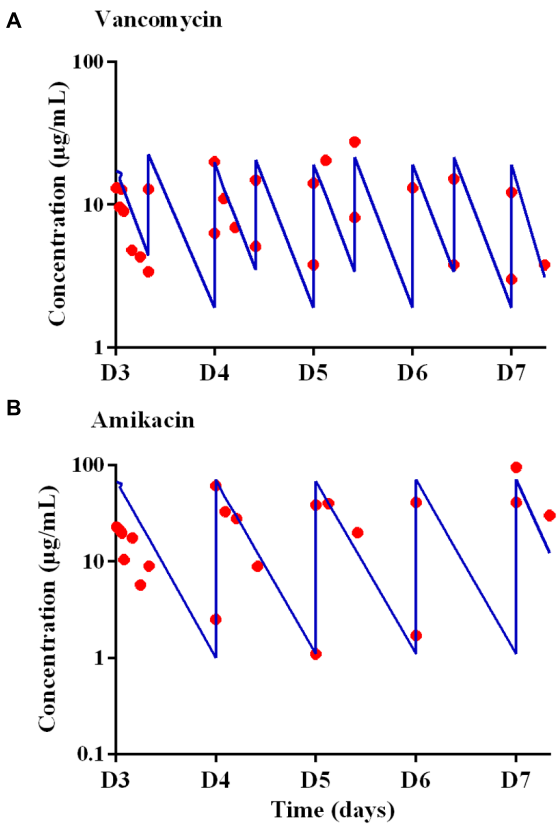

FIGURE 2 | Expected (blue lines) and observed (red circles) concentration-time profiles in the Hollow Fiber system from D3 to D7 for **(A)** vancomycin after administrations twice a day with peak concentrations of 18 µg/mL (V18 treatment) and for **(B)** amikacin after administrations once a day with peak concentrations of 70 µg/mL.

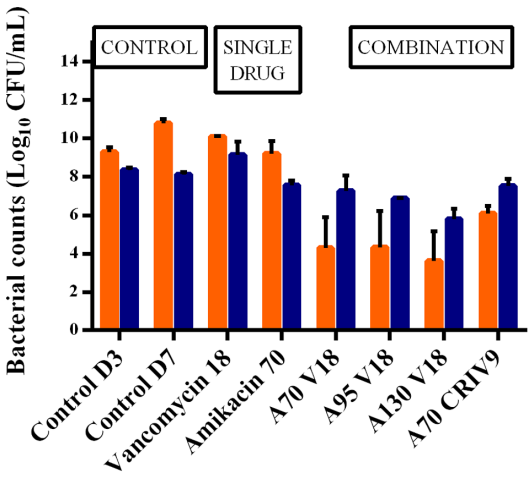

FIGURE 3 | Mean ± SD of the bacterial counts (log_{10} CFU/mL) for planktonic (in orange) and biofilm-embedded bacteria (in blue) at the end of the experiments (D7) for control assays and the different treatments (n = 2 for each antibiotic combination). The BEB population was smaller than the planktonic population in the control experiments, and also after monotherapy with amikacin or vancomycin. In contrast, the BEB populations were 1.2–2.0 log_{10} CFU/mL higher than the planktonic populations ($p < 0.001$).

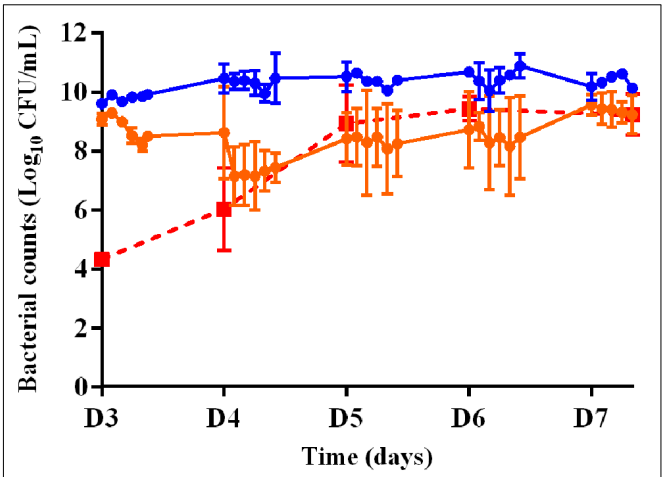

FIGURE 4 | Changes in the planktonic bacterial populations (log_{10} CFU/mL) after exposure to amikacin or vancomycin in monotherapy from D3 to D7. Full circles represent the bacterial counts in the HF model during 5 days of treatment with vancomycin twice a day (V18 treatment, in blue) or amikacin once a day (A70 treatment, in orange). Full red squares represent the bacterial counts of planktonic bacteria growing on agar supplemented with threefold MIC of amikacin over time during A70 treatment. Mean ± SD of the bacterial counts are shown (n = 2 for each treatment).

PK/PD Study

Killing Activity on Planktonic Bacterial Populations

After incubation for 3 days in the HF cartridge (D3), the planktonic and biofilm populations of *S. aureus* were 9.3 ± 0.3 log_{10} CFU/mL and 8.4 ± 0.1 log_{10} CFU/mL, respectively.

In the absence of antibiotic (control experiments), the planktonic and biofilm populations remained quite stable for a further 5 days with bacterial counts of 10.8 ± 0.2 log_{10} CFU/mL and 8.1 ± 0.1 log_{10} CFU/mL, respectively, at the end of the experiments (D7) (**Figure 3**).

The time-kill curves for the planktonic bacteria associated with the 3-days old biofilm and exposed to amikacin or vancomycin alone and the bacterial counts of planktonic bacteria growing on agar supplemented with threefold MIC of amikacin over time during A70 treatment for 5 days (from D3 to D7) are shown in **Figure 4**. After 5 days of exposure to vancomycin (from D3 to D7) administered twice a day with a peak concentration of 18 μg/mL (V18 treatment), the planktonic population never decreased below the initial population size. After exposure to amikacin administered once a day with a peak concentration of 70 μg/mL (A70 treatment), a mean reduction of 0.9 log_{10} was observed over the 1st day of treatment (D3) but after 5 days (D7), the size of the planktonic population, 9.2 ± 0.7 log_{10} CFU/mL, was very similar to that of the population before exposure to amikacin and not much lower than in the control experiments.

We then assessed the killing activity of the amikacin and vancomycin combinations over 5 days (from D3 to D7). For amikacin, three peak concentrations of 70 (A70 V18 treatment), 95 (A95 V18 treatment), or 130 (A130 V18 treatment) μg/mL were tested and for vancomycin, a single peak concentration of 18 μg/mL (A70 V18 treatment) twice a day was compared

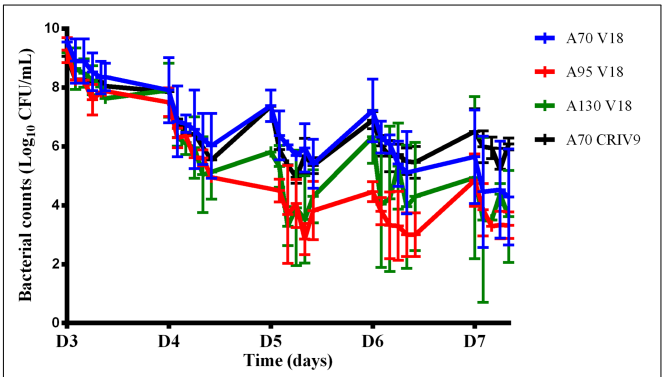

FIGURE 5 | Changes in the planktonic bacterial population (log_{10} CFU/mL) after exposure to combinations of amikacin and vancomycin from D3 to D7. The marks represent the mean ± SD of the bacterial counts for the different tested treatments [blue: A70 V18 treatment, red: A95 V18 treatment, green: A130 V18 treatment and black: A70 CRIV9 treatment (n = 2 for each antibiotic combination)]. The reduction of the planktonic bacterial population between the 1st day (D3) and the last day (D7) of treatments with combinations of amikacin and vancomycin was significant ($p < 0.001$).

to a steady concentration of 9 μg/mL (A70 CRIV9 treatment). The time-kill curves of planktonic bacteria exposed to the drug combinations from D3 to D7 are shown in **Figure 5**. Similar time-kill profiles were observed for the planktonic bacteria, whatever the drug concentration profiles tested. The mean decrease of the bacterial population during the 1st day of treatment (D3) with the different drug combination regimens was very similar and ranged from −0.9 to −1.4 log_{10} CFU/mL, followed by stabilization or a slight increase overnight. The killing activity of the drugs during the following days (D4–D7) ranged from

a decrease of 3.0 $\log_{10}$ to an increase of 0.5 $\log_{10}$ of the planktonic population between two successive administrations of amikacin.

After exposure to combinations for 5 days (D7), no eradication of planktonic bacteria was observed but the overall reduction ranged from −3.0 $\log_{10}$ to −6.0 $\log_{10}$ compared to the population before drug exposure. This reduction of the planktonic bacterial population between the 1st day (D3) and the last day (D7) of treatments with combinations of amikacin and vancomycin was significant ($p < 0.001$) whereas amikacin or vancomycin alone failed to reduce the planktonic population over 5 days (the planktonic bacterial populations were equal to or higher after monotherapy than before monotherapy, **Figure 4**).

Killing Activity on BEB

The counts of biofilm-embedded bacteria recovered at the end of each experiment (D7) and the planktonic bacterial counts at the same time point are compared in **Figure 3**.

After exposure to vancomycin alone, the BEB count was 9.2 ± 0.7 $\log_{10}$ CFU/mL, i.e., approximately one $\log_{10}$ higher than the biofilm without treatment, while amikacin alone (A70) decreased the size of the biofilm by 0.6 $\log_{10}$ CFU/mL. The addition of vancomycin (V18 or CRI V9) to amikacin (A70) did not increase BEB reduction and showed that the combination did not exhibit any synergy on these bacteria.

In parallel, we observed that the BEB population was smaller than the planktonic population in the control experiments, and also after monotherapy with amikacin or vancomycin. In contrast, the BEB populations were 1.2 to 2.0 $\log_{10}$ CFU/mL higher than the planktonic populations ($p < 0.001$) in all the combination experiments.

Prevention of the Selection of Resistance

No bacterial growth was observed on vancomycin-supplemented agar, whatever the experiment.

The counts of planktonic bacteria and BEB growing on agar supplemented with 3-MIC and 6-MIC-amikacin, after exposure to the drugs for 5 days (D7), are compared to the total counts in **Figures 6**, **7**. Less-susceptible bacteria were systematically observed on the amikacin- supplemented agar plates before any drug exposure (D3) at a proportion of about 10^{-6} of the total bacterial population for planktonic bacteria (assessed in all the experiments) and BEB (assessed in control experiments). Similar proportions (around 10^{-6}) were also found at the end of the control experiments (D7).

After 5 days of exposure to amikacin alone (D7), all the planktonic bacteria and BEB (proportion around 1) were able to grow on 6MIC-amikacin agar (**Figure 6**), which implied that the less-susceptible bacterial population, rather than fully susceptible bacteria, was selected by the drug. The time-development of the less-susceptible planktonic population, represented in **Figure 4**, showed that the fully susceptible population was drastically reduced from the 3rd day of treatment (D5). The addition of vancomycin to amikacin reduced the counts of planktonic bacteria growing on 3-MIC-amikacin and 6-MIC-amikacin, which were only detected in 4 on 1 out of 8 assays, respectively. Exposure of biofilm to the drug combinations, rather than to amikacin alone, also reduced the populations of less-susceptible bacteria (**Figure 7**).

The highest MIC of amikacin for the sampled biofilm bacteria was 16 μg/mL (a 16-fold increase), corresponding to bacteria with intermediate amikacin-susceptibility with regard to the EUCAST breakpoints.

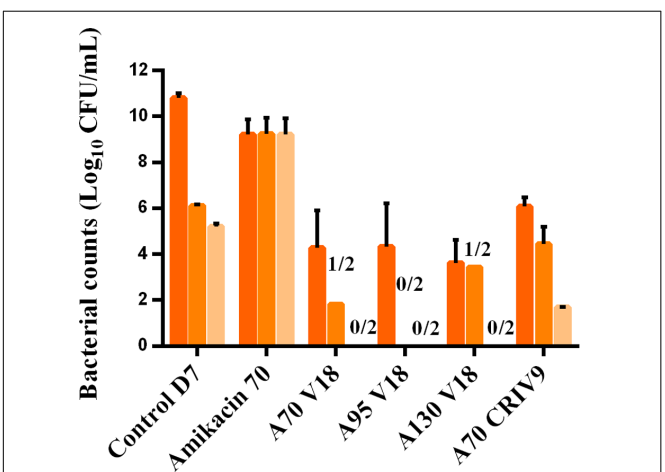

FIGURE 6 | Mean ± SD of the bacterial counts ($\log_{10}$ CFU/mL) of total planktonic bacteria (dark orange) and bacteria growing on agar supplemented with three-times the MIC of amikacin (medium orange) and six-times the MIC of amikacin (light orange) in the control experiment or after 5 days of exposure to different treatments (D7) ($n = 2$ for each condition).

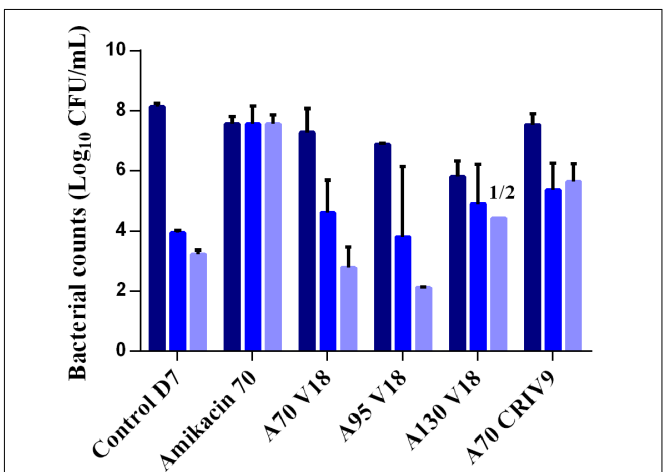

FIGURE 7 | Mean ± SD of the bacterial counts ($\log_{10}$ CFU/mL) of total biofilm-embedded bacteria (dark blue) and of biofilm-embedded bacteria growing on agar supplemented with three-times the MIC of amikacin (blue) and six-times the MIC of amikacin (light blue) in the control experiment or after 5 days of exposure to different treatments (D7) ($n = 2$ for each condition).

DISCUSSION

Due to the refractoriness of *S. aureus* biofilm infections to antibiotic treatments, there is an urgent need to optimize the use of currently available drugs to ensure bacterial killing and the prevention of resistance. In this study, we developed an innovative use of the HF model by delaying exposure to the antibiotics and studied the effects of a combination of vancomycin and amikacin both on planktonic bacteria and on BEB in conditions representative of clinical situations. Different concentration profiles of the drugs were tested, and bacteria were subjected to the fluctuating concentrations that might be encountered in patients during a complete treatment. These experimental conditions should have greater predictive value than simple static assays in which bacteria are exposed to a fixed concentration over time. Moreover, due to the lack of medium renewal in static assays, such experiments are often conducted over 24 h whereas longer periods are needed to assess the selection of resistance by antibiotics (Drusano, 2017). Compared to animal models, which may exhibit very different pharmacokinetics to humans and in which some human pathogens cannot develop, all bacteria can be cultured in the HF model and exposed to drug concentration profiles that mimic the range of human profiles (Toutain et al., 2010). For example, as vancomycin is eliminated much faster in mice (half-life = 32 min) than in humans (Knudsen et al., 2000), dosage regimens tested in mice can hardly be extrapolated to humans. Obviously, the main weakness of static or dynamic *in vitro* assays is the absence of the immune system which can cooperate with antibiotics to clear an infection.

Several *in vitro* studies in dynamic systems including the HF model (Nicasio et al., 2012; Lenhard et al., 2016) have investigated the antibacterial activity of drugs combined with vancomycin against planktonic *S. aureus*. However, the use of dynamic *in vitro* systems, such as the CDC biofilm device or others, to study the effects of combinations on biofilm is rarely reported. To our knowledge, the present study is the first to use a HF model to conduct experiments on a 3-day old biofilm of a single *S. aureus* strain to assess the activity of drugs combination, over 5 days, on both planktonic bacteria and BEB. The HF model had already been used to simulate in two distinct studies the free concentration-time profiles of amikacin or vancomycin that can be achieved in patients receiving the recommended doses (Nicasio et al., 2012; Ferro et al., 2015). In our study, exposure to different dosage regimens of a susceptible strain of *S. aureus* with MICs of 1 μg/mL for amikacin and vancomycin led to equal or higher values of the PK/PD indices than those classically expected to obtain drug efficacy (Zelenitsky et al., 2003; Rybak et al., 2009; Song et al., 2015). For aminoglycosides, for which the most predictive PK/PD index is the C_{max}/MIC ratio (Moore et al., 1987), we targeted C_{max}/MIC values from 70 to 130 in the HF model whereas a value from 8 to 10 is usually recommended to ensure efficacy against the pathogen (Toutain et al., 2002). For vancomycin, for which the best predictive index is the AUC over 24 h divided by the MIC ($AUC_{24\ h}$/MIC) (Nielsen et al., 2011), we targeted the value of 400 recommended to achieve clinical effectiveness (Rybak et al., 2009; Jung et al., 2014; Song et al., 2015) and obtained $AUC_{24\ h}$/MIC values ranging from 372 to 417 for the bolus of vancomycin in the HFIM and 480 for the constant infusion. Even though these targeted values of the PK/PD indices were attained for both drugs, almost no bactericidal activity was observed on the 3-day old biofilm or on the co-existing planktonic bacteria when amikacin or vancomycin were administered alone for 5 days. These results are in agreement with previous studies which demonstrated the low activity of vancomycin on large bacterial inocula (LaPlante and Rybak, 2004; LaPlante and Woodmansee, 2009) and on biofilms (Hogan et al., 2016). One study involving a HF model showed that a peak concentration as high as 80 mg/L was needed to achieve bactericidal activity against a large inoculum of a MRSA strain with a MIC of 1 μg/mL for vancomycin (Lenhard et al., 2016). One proposed explanation for the inoculum effect and reduced efficacy of vancomycin is that bacteria at high density are in a stationary growth phase with low dividing rate and low cell wall synthesis (Brown et al., 1988; Lamp et al., 1992). Another explanation is that vancomycin may be sequestrated by *S. aureus* on peptidoglycan layers, thus reducing the free vancomycin concentrations surrounding the bacteria (Srinivasan et al., 2002; Ekdahl et al., 2005; Yanagisawa et al., 2009). Finally, a reduced penetration of vancomycin through *S. aureus* and *S. epidermidis* biofilms has also been described (Doroshenko et al., 2014; Singh et al., 2016) and, even worse than the lack of efficacy, low concentrations of vancomycin were reported to stimulate biofilm formation in some clinical isolates of *S. epidermidis* (Cargill and Upton, 2009). In this study on *S. aureus*, our results were concordant as the biofilm which was exposed to vancomycin alone contained 10 times more bacteria than the control.

The lack of efficacy of the drugs used in monotherapy in this study supports the clinical recommendation to associate an aminoglycoside with vancomycin for the treatment of *S. aureus* biofilm infection (Deresinski, 2009). Compared with the absence of activity of amikacin or vancomycin alone, exposure to combinations of vancomycin and amikacin for 5 days in the HF model had a synergistic bactericidal effect on the planktonic bacterial populations. However, despite this synergy, the planktonic bacteria remaining after 5 days of exposure to the combination (D7) still exceeded 2.5 $\log_{10}$ CFU/mL. We therefore investigated the ability of other dosage regimens of amikacin and vancomycin to improve the antibacterial efficacy against this planktonic population. Contrary to our expectations, given the concentration-dependent activity of aminoglycosides, increasing the C_{max} of amikacin 1.8-fold (from 70 to 130 μg/mL) did not increase the efficacy on planktonic bacteria. For vancomycin, the efficacy of the combination seemed to be slightly decreased by constant rate infusion, especially on planktonic bacteria, but there were not enough replicates to draw a definitive conclusion. Contrary to the planktonic population, the addition of vancomycin (as a bolus or constant infusion) to amikacin did not result in an additional bacterial reduction on *S. aureus* biofilm, and no synergy between the two drugs was observed. The distinct activity of the combination on planktonic bacteria and BEB confirmed the different phenotypes of these two populations of bacteria and that the drugs were less active on BEB. Indeed, biofilms are supposed to contain more persister

bacteria which have lower growth rates and are therefore less affected by antibiotic drugs (Singh et al., 2009; Conlon et al., 2015). Moreover, no dosing regimen tested in this study, even if it exceeded the recommended PK/PD index values, was able to fully eradicate the planktonic bacteria co-existing with a biofilm, which could suggest that some planktonic bacteria were continuously released from the biofilm. As our study is the first one focusing on the biofilm in the HF, microscopy imaging will be further needed to investigate the distribution of the biofilm in the HF cartridge, which could be influenced, among others, by the shear forces in the extracapillary space. It should also be kept in mind that our system was characterized by an absence of the immune system and the presence of a rich medium – more favorable to bacterial growth -, that both limit the efficacy of antibiotic treatments compared to the *in vivo* situation. However, our *in vitro* results are in agreement with the reported lack of efficacy of systemic antibiotic treatments in patients for whom additional treatments, such as mechanical removal of biofilms or very high local antibiotic concentrations, are advised whenever possible (McConoughey et al., 2014; Wu et al., 2015).

In addition to efficacy, we assessed the ability of the combination to reduce the selection of resistant bacteria in planktonic and biofilm populations. The absence of resistance to vancomycin in this study was in accordance with other experiments conducted on *S. aureus* (LaPlante and Rybak, 2004). Conversely, bacteria (approximately 10^{-6}) able to grow on agar supplemented with 6 μg/mL (sixfold MIC) of amikacin were systematically present in the planktonic and biofilm populations before drug exposure, implying that small proportions of such bacteria are spontaneously present in large populations, as previously reported (Ferro et al., 2015). Since similar proportions were also found at the end of the control experiments, it suggests that the growth and survival rates of less-susceptible and fully susceptible bacteria were similar in the absence of drugs. After 5 days of antibiotic exposure, the MIC of amikacin for these bacteria able to grow on agar supplemented with amikacin and termed "less-susceptible," never exceeded the resistance breakpoint (>16 μg/mL). These bacteria showed an intermediate amikacin-susceptibility with regard to the EUCAST breakpoints, implying that the administration of amikacin to patients infected by these bacteria would have an uncertain therapeutic effect (Rodloff et al., 2008), but it should also be stressed that the initial MIC of the tested strain was low (1 μg/mL). This suggests that the same selection phenomenon occurring on a strain with a two or four-fold higher MIC would lead to the selection of "true" resistant bacteria. The selection of less-susceptible bacteria, which represented the main population of planktonic bacteria and BEB after exposure for 5 days to amikacin in monotherapy, could be explained by an inducible mechanism of resistance, known as adaptive resistance, in which thickening of the cell wall results in less penetration of amikacin into the bacterial cell (Yuan et al., 2013). Interestingly, the addition of vancomycin to amikacin considerably reduced the proportions of these less-susceptible bacteria in both planktonic bacteria and BEB compared to amikacin alone, especially when vancomycin was administered in boluses. These results suggest that vancomycin was able to limit the growth of these bacteria less-susceptible to amikacin and prevent their selection. The vancomycin administered by CRI associated with amikacin seemed to limit the selection of less-susceptible bacteria to a lesser extent, but these differences require more thorough investigation.

CONCLUSION

By studying planktonic bacteria and BEB in parallel and by mimicking the fluctuations in antibiotic concentrations over 5 days, as can occur *in vivo* after daily administrations, we demonstrated the increased efficacy of a combination of amikacin and vancomycin on planktonic bacteria but not on BEB. However, even though vancomycin did not increase the killing activity of amikacin on BEB, it reduced the selection of bacteria less-susceptible to amikacin, which could help to maintain the efficacy of this drug during treatments. Even if these results need to be further confirmed with clinically relevant strains of MSSA and MRSA, they highlight the importance of selecting combination therapies not only based on efficacy but also on resistance selection endpoints by taking into account the 2 co-existing populations of planktonic bacteria and BEB.

Equations:

$$\text{Concentration HF} = \frac{\begin{array}{c}(\text{Concentration CR} * \text{Volume CR}) + \\ (\text{Concentration ECS} * \text{Volume ECS})\end{array}}{\text{Volume CR} + \text{Volume ECS}} \quad (1)$$

With HF being the Hollow-Fiber, CR the Central Reservoir and ECS the Extra-Capillary Space.

AUTHOR CONTRIBUTIONS

DB, AF, FW, FE, P-LT, and AB-M: substantial contributions to the conception or design of the work. DB, ML, AF, P-LT, and AB-M: acquisition, analysis, or interpretation of data for the work. DB, ML, FW, FE, P-LT, AB-M, and AF drafting the work or revising it critically for important intellectual content. Final approval of the version to be published. Agreement to be accountable for all aspects of the work in ensuring that questions related to the accuracy or integrity of any part of the work are appropriately investigated and resolved.

REFERENCES

Adamis, G., Papaioannou, M. G., Giamarellos-Bourboulis, E. J., Gargalianos, P., Kosmidis, J., and Giamarellou, H. (2004). Pharmacokinetic interactions of ceftazidime, imipenem and aztreonam with amikacin in healthy volunteers. *Int. J. Antimicrob. Agents* 23, 144–149. doi: 10.1016/j.ijantimicag.2003.07.001

Aeschlimann, J. R., Allen, G. P., Hershberger, E., and Rybak, M. J. (2000). Activities of LY333328 and vancomycin administered alone or in combination with

gentamicin against three strains of vancomycin-intermediate *Staphylococcus aureus* in an in vitro pharmacodynamic infection model. *Antimicrob. Agents Chemother.* 44, 2991–2998. doi: 10.1128/AAC.44.11.2991-2998.2000

Álvarez, R., López Cortés, L. E., Molina, J., Cisneros, J. M., and Pachón, J. (2016). Optimizing the clinical use of vancomycin. *Antimicrob. Agents Chemother.* 60, 2601–2609. doi: 10.1128/AAC.03147-14

Backo, M., Gaenger, E., Burkart, A., Chai, Y. L., and Bayer, A. S. (1999). Treatment of experimental staphylococcal endocarditis due to a strain with reduced susceptibility in vitro to vancomycin: efficacy of ampicillin-sulbactam. *Antimicrob. Agents Chemother.* 43, 2565–2568.

Brown, M. R., Allison, D. G., and Gilbert, P. (1988). Resistance of bacterial biofilms to antibiotics: a growth-rate related effect? *J. Antimicrob. Chemother.* 22, 777–780. doi: 10.1093/jac/22.6.777

Butterfield, J. M., Patel, N., Pai, M. P., Rosano, T. G., Drusano, G. L., and Lodise, T. P. (2011). Refining vancomycin protein binding estimates: identification of clinical factors that influence protein binding. *Antimicrob. Agents Chemother.* 55, 4277–4282. doi: 10.1128/AAC.01674-10

Cadwell, J. (2015). The hollow fiber infection model: principles and practice. *Adv. Antibiotics Antibodies* 1:101. doi: 10.4172/aaa.1000101

Cargill, J. S., and Upton, M. (2009). Low concentrations of vancomycin stimulate biofilm formation in some clinical isolates of *Staphylococcus epidermidis*. *J. Clin. Pathol.* 62, 1112–1116. doi: 10.1136/jcp.2009.069021

Clinical and Laboratory Standards Institute [CLSI] (2012). *CLSI. Methods for Dilution Antimicrobial Susceptibility Tests f or Bacteria That Grow Aerobically; CLSI Document M07-A9*, 9th Edn. Wayne, PA: *CLSI*.

Cokça, F., Arman, D., and Altay, G. (1998). In vitro activity of vancomycin combined with rifampin, amikacin, ciprofloxacin or imipenem against methicillin-resistant and methicillin-susceptible *Staphylococcus aureus*. *Clin. Microbiol. Infect.* 4, 657–659. doi: 10.1111/j.1469-0691.1998.tb00349.x

Conlon, B. P., Rowe, S. E., and Lewis, K. (2015). Persister cells in biofilm associated infections. *Adv. Exp. Med. Biol.* 831, 1–9. doi: 10.1007/978-3-319-09782-4_1

Davies, D. (2003). Understanding biofilm resistance to antibacterial agents. *Nat. Rev. Drug Discov.* 2, 114–122. doi: 10.1038/nrd1008

Deresinski, S. (2009). Vancomycin in combination with other antibiotics for the treatment of serious methicillin-resistant *Staphylococcus aureus* infections. *Clin. Infect. Dis.* 49, 1072–1079. doi: 10.1086/605572

Donlan, R. M., and Costerton, J. W. (2002). Biofilms: survival mechanisms of clinically relevant microorganisms. *Clin. Microbiol. Rev.* 15, 167–193. doi: 10.1128/CMR.15.2.167-193.2002

Doroshenko, N., Tseng, B. S., Howlin, R. P., Deacon, J., Wharton, J. A., Thurner, P. J., et al. (2014). Extracellular DNA impedes the transport of vancomycin in *Staphylococcus epidermidis* biofilms preexposed to subinhibitory concentrations of vancomycin. *Antimicrob. Agents Chemother.* 58, 7273–7282. doi: 10.1128/AAC.03132-14

Drusano, G. L. (2017). Pre-clinical in vitro infection models. *Curr. Opin. Pharmacol.* 36, 100–106. doi: 10.1016/j.coph.2017.09.011

Ekdahl, C., Hanberger, H., Hällgren, A., Nilsson, M., Svensson, E., and Nilsson, L. E. (2005). Rapid decrease of free vancomycin in dense staphylococcal cultures. *Eur. J. Clin. Microbiol. Infect. Dis.* 24, 596–602. doi: 10.1007/s10096-005-0011-0

European Medicines Agency (2015). *Qualification Opinion, In Vitro Hollow Fiber System Model of Tuberculosis (HFS-TB)*. Canary Wharf: European Medicines Agency.

Ferro, B. E., Srivastava, S., Deshpande, D., Sherman, C. M., Pasipanodya, J. G., van Soolingen, D., et al. (2015). Amikacin pharmacokinetics/pharmacodynamics in a novel hollow-fiber *Mycobacterium abscessus* disease model. *Antimicrob. Agents Chemother.* 60, 1242–1248. doi: 10.1128/AAC.02282-15

Frimodt-Møller, N. (2002). How predictive is PK/PD for antibacterial agents? *Int. J. Antimicrob. Agents* 19, 333–339. doi: 10.1016/S0924-8579(02)00029-8

Gálvez, R., Luengo, C., Cornejo, R., Kosche, J., Romero, C., Tobar, E., et al. (2011). Higher than recommended amikacin loading doses achieve pharmacokinetic targets without associated toxicity. *Int. J. Antimicrob. Agents* 38, 146–151. doi: 10.1016/j.ijantimicag.2011.03.022

Gumbo, T., Pasipanodya, J. G., Nuermberger, E., Romero, K., and Hanna, D. (2015). Correlations between the hollow fiber model of tuberculosis and therapeutic events in tuberculosis patients: learn and confirm. *Clin. Infect. Dis.* 61, S18–S24. doi: 10.1093/cid/civ426

Hanrahan, T., Whitehouse, T., Lipman, J., and Roberts, J. A. (2015). Vancomycin-associated nephrotoxicity: a meta-analysis of administration by continuous versus intermittent infusion. *Int. J. Antimicrob. Agents* 46, 249–253. doi: 10.1016/j.ijantimicag.2015.04.013

Hogan, S., Zapotoczna, M., Stevens, N. T., Humphreys, H., O'Gara, J. P., and O'Neill, E. (2016). In vitro approach for identification of the most effective agents for antimicrobial lock therapy in the treatment of intravascular catheter-related infections caused by *Staphylococcus aureus*. *Antimicrob. Agents Chemother.* 60, 2923–2931. doi: 10.1128/AAC.02885-15

Ivanova, K., Ramon, E., Hoyo, J., and Tzanov, T. (2017). Innovative approaches for controlling clinically relevant biofilms: current trends and future prospects. *Curr. Top. Med. Chem.* [Epub ahead of print] doi: 10.2174/1568026617666170105143315

Jung, Y., Song, K.-H., Cho, J., Kim, H. S., Kim, N.-H., Kim, T. S., et al. (2014). Area under the concentration-time curve to minimum inhibitory concentration ratio as a predictor of vancomycin treatment outcome in methicillin-resistant *Staphylococcus aureus* bacteraemia. *Int. J. Antimicrob. Agents* 43, 179–183. doi: 10.1016/j.ijantimicag.2013.10.017

Kato, H., Hagihara, M., Hirai, J., Sakanashi, D., Suematsu, H., Nishiyama, N., et al. (2017). Evaluation of amikacin pharmacokinetics and pharmacodynamics for optimal initial dosing regimen. *Drugs R D* 17, 177–187. doi: 10.1007/s40268-016-0165-5

Knudsen, J. D., Fuursted, K., Raber, S., Espersen, F., and Frimodt-Møller, N. (2000). Pharmacodynamics of glycopeptides in the mouse peritonitis model of *Streptococcus pneumoniae* or *Staphylococcus aureus* infection. *Antimicrob. Agents Chemother.* 44, 1247–1254. doi: 10.1128/AAC.44.5.1247-1254.2000

Lamp, K. C., Rybak, M. J., Bailey, E. M., and Kaatz, G. W. (1992). In vitro pharmacodynamic effects of concentration, pH, and growth phase on serum bactericidal activities of daptomycin and vancomycin. *Antimicrob. Agents Chemother.* 36, 2709–2714. doi: 10.1128/AAC.36.12.2709

LaPlante, K. L., and Rybak, M. J. (2004). Impact of high-inoculum *Staphylococcus aureus* on the activities of nafcillin, vancomycin, linezolid, and daptomycin, alone and in combination with gentamicin, in an in vitro pharmacodynamic model. *Antimicrob. Agents Chemother.* 48, 4665–4672. doi: 10.1128/AAC.48.12.4665-4672.2004

LaPlante, K. L., and Woodmansee, S. (2009). Activities of daptomycin and vancomycin alone and in combination with rifampin and gentamicin against biofilm-forming methicillin-resistant *Staphylococcus aureus* isolates in an experimental model of endocarditis. *Antimicrob. Agents Chemother.* 53, 3880–3886. doi: 10.1128/AAC.00134-09

Lebeaux, D., Ghigo, J.-M., and Beloin, C. (2014). Biofilm-related infections: bridging the gap between clinical management and fundamental aspects of recalcitrance toward antibiotics. *Microbiol. Mol. Biol. Rev.* 78, 510–543. doi: 10.1128/MMBR.00013-14

Lebeaux, D., Leflon-Guibout, V., Ghigo, J.-M., and Beloin, C. (2015). In vitro activity of gentamicin, vancomycin or amikacin combined with EDTA or l-arginine as lock therapy against a wide spectrum of biofilm-forming clinical strains isolated from catheter-related infections. *J. Antimicrob. Chemother.* 70, 1704–1712. doi: 10.1093/jac/dkv044

Lenhard, J. R., Brown, T., Rybak, M. J., Meaney, C. J., Norgard, N. B., Bulman, Z. P., et al. (2016). Sequential evolution of vancomycin-intermediate resistance alters virulence in *Staphylococcus aureus*: pharmacokinetic/pharmacodynamic targets for vancomycin exposure. *Antimicrob. Agents Chemother.* 60, 1584–1591. doi: 10.1128/AAC.02657-15

Lewis, K. (2008). Multidrug tolerance of biofilms and persister cells. *Curr. Top. Microbiol. Immunol.* 322, 107–131. doi: 10.1007/978-3-540-75418-3_6

Liu, P., Müller, M., and Derendorf, H. (2002). Rational dosing of antibiotics: the use of plasma concentrations versus tissue concentrations. *Int. J. Antimicrob. Agents* 19, 285–290. doi: 10.1016/S0924-8579(02)00024-9

Mandell, L. A., Wunderink, R. G., Anzueto, A., Bartlett, J. G., Campbell, G. D., Dean, N. C., et al. (2007). Infectious Diseases Society of America/American Thoracic Society consensus guidelines on the management of community-acquired pneumonia in adults. *Clin. Infect. Dis.* 44(Suppl. 2), S27–S72. doi: 10.1086/511159

Matzke, G. R., Zhanel, G. G., and Guay, D. R. P. (1986). Clinical pharmacokinetics of vancomycin. *Clin. Pharmacokinet.* 11, 257–282. doi: 10.2165/00003088-198611040-00001

McConoughey, S. J., Howlin, R., Granger, J. F., Manring, M. M., Calhoun, J. H., Shirtlif, M., et al. (2014). Biofilms in periprosthetic orthopedic infections. *Future Microbiol.* 9, 987–1007. doi: 10.2217/fmb.14.64

Moore, R. D., Lietman, P. S., and Smith, C. R. (1987). Clinical response to aminoglycoside therapy: importance of the ratio of peak concentration to minimal inhibitory concentration. *J. Infect. Dis.* 155, 93–99. doi: 10.1093/infdis/155.1.93

Nicasio, A. M., Bulitta, J. B., Lodise, T. P., D'Hondt, R. E., Kulawy, R., Louie, A., et al. (2012). Evaluation of once-daily vancomycin against methicillin-resistant *Staphylococcus aureus* in a hollow-fiber infection model. *Antimicrob. Agents Chemother.* 56, 682–686. doi: 10.1128/AAC.05664-11

Nielsen, E. I., Cars, O., and Friberg, L. E. (2011). Pharmacokinetic/pharmacodynamic (PK/PD) indices of antibiotics predicted by a semimechanistic PKPD model: a step toward model-based dose optimization. *Antimicrob. Agents Chemother.* 55, 4619–4630. doi: 10.1128/AAC.00182-11

Patel, N., Pai, M. P., Rodvold, K. A., Lomaestro, B., Drusano, G. L., and Lodise, T. P. (2011). Vancomycin: we can't get there from here. *Clin. Infect. Dis.* 52, 969–974. doi: 10.1093/cid/cir078

Post, V., Wahl, P., Richards, R. G., and Moriarty, T. F. (2017). Vancomycin displays time-dependent eradication of mature *Staphylococcus aureus* biofilms. *J. Orthop. Res.* 35, 381–388. doi: 10.1002/jor.23291

R Development Core Team (2014). *A Language and Environment for Statistical Computing*. Vienna: R Foundation for Statistical Computing.

Rodloff, A., Bauer, T., Ewig, S., Kujath, P., and Müller, E., (2008). Susceptible, intermediate, and resistant–the intensity of antibiotic action. *Dtsch. Arztebl. Int.* 105, 657–662. doi: 10.3238/arztebl.2008.0657

Rybak, M., Lomaestro, B., Rotschafer, J. C., Moellering, R., Craig, W., Billeter, M., et al. (2009). Therapeutic monitoring of vancomycin in adult patients: a consensus review of the American Society of Health-System Pharmacists, the Infectious Diseases Society of America, and the Society of Infectious Diseases Pharmacists. *Am. J. Health Syst. Pharm.* 66, 82–98. doi: 10.2146/ajhp080434

Singh, R., Ray, P., Das, A., and Sharma, M. (2009). Role of persisters and small-colony variants in antibiotic resistance of planktonic and biofilm-associated *Staphylococcus aureus*: an in vitro study. *J. Med. Microbiol.* 58, 1067–1073. doi: 10.1099/jmm.0.009720-0

Singh, R., Sahore, S., Kaur, P., Rani, A., and Ray, P. (2016). Penetration barrier contributes to bacterial biofilm-associated resistance against only select antibiotics, and exhibits genus-, strain- and antibiotic-specific differences. *Pathog. Dis.* 74:ftw056. doi: 10.1093/femspd/ftw056

Song, K.-H., Kim, H. B., Kim, H., Lee, M. J., Jung, Y., Kim, G., et al. (2015). Impact of area under the concentration-time curve to minimum inhibitory concentration ratio on vancomycin treatment outcomes in methicillin-resistant *Staphylococcus aureus* bacteraemia. *Int. J. Antimicrob. Agents* 46, 689–695. doi: 10.1016/j.ijantimicag.2015.09.010

Srinivasan, A., Dick, J. D., and Perl, T. M. (2002). Vancomycin resistance in Staphylococci. *Clin. Microbiol. Rev.* 15, 430–438. doi: 10.1128/CMR.15.3.430-438.2002

Toutain, P.-L., Bousquet-Mélou, A., and Martinez, M. (2007). AUC/MIC: a PK/PD index for antibiotics with a time dimension or simply a dimensionless scoring factor? *J. Antimicrob. Chemother.* 60, 1185–1188. doi: 10.1093/jac/dkm360

Toutain, P. L., del Castillo, J. R. E., and Bousquet-Mélou, A. (2002). The pharmacokinetic-pharmacodynamic approach to a rational dosage regimen for antibiotics. *Res. Vet. Sci.* 73, 105–114. doi: 10.1016/S0034-5288(02)00039-5

Toutain, P.-L., Ferran, A., and Bousquet-Mélou, A. (2010). "Species differences in pharmacokinetics and pharmacodynamics," in *Comparative and Veterinary Pharmacology*, eds F. Cunningham, J. Elliott, and P. Lees (Berlin: Springer), 19–48. doi: 10.1007/978-3-642-10324-7_2

Waineo, M. F., Kuhn, T. C., and Brown, D. L. (2015). The pharmacokinetic/pharmacodynamic rationale for administering vancomycin via continuous infusion. *J. Clin. Pharm. Ther.* 40, 259–265. doi: 10.1111/jcpt.12270

Watanakunakorn, C., and Glotzbecker, C. (1974). Enhancement of the effects of anti-staphylococcal antibiotics by aminoglycosides. *Antimicrob. Agents Chemother.* 6, 802–806. doi: 10.1128/AAC.6.6.802

Wu, H., Moser, C., Wang, H.-Z., Høiby, N., and Song, Z.-J. (2015). Strategies for combating bacterial biofilm infections. *Int. J. Oral Sci.* 7, 1–7. doi: 10.1038/ijos.2014.65

Yanagisawa, C., Hanaki, H., Matsui, H., Ikeda, S., Nakae, T., and Sunakawa, K. (2009). Rapid depletion of free vancomycin in medium in the presence of β-lactam antibiotics and growth restoration in *Staphylococcus aureus* strains with β-lactam-induced vancomycin resistance. *Antimicrob. Agents Chemother.* 53, 63–68. doi: 10.1128/AAC.00762-08

Yuan, W., Hu, Q., Cheng, H., Shang, W., Liu, N., Hua, Z., et al. (2013). Cell wall thickening is associated with adaptive resistance to amikacin in methicillin-resistant *Staphylococcus aureus* clinical isolates. *J. Antimicrob. Chemother.* 68, 1089–1096. doi: 10.1093/jac/dks522

Zelenitsky, S., Harding, G., Sun, S., Ubhi, K., and Ariano, R. (2003). Treatment and outcome of *Pseudomonas aeruginosa* bacteraemia: an antibiotic pharmacodynamic analysis. *J. Antimicrob. Chemother.* 52, 668–674. doi: 10.1093/jac/dkg403

Conflict of Interest Statement: The authors declare that the research was conducted in the absence of any commercial or financial relationships that could be construed as a potential conflict of interest.

frontiers in Microbiology

PERSPECTIVE
published: 02 July 2018
doi: 10.3389/fmicb.2018.01438

DNA Damage Repair and Drug Efflux as Potential Targets for Reversing Low or Intermediate Ciprofloxacin Resistance in *E. coli* K-12

*Rasmus N. Klitgaard[1], Bimal Jana[2], Luca Guardabassi[2], Karen L. Nielsen[3] and Anders Løbner-Olesen[1]**

[1] Department of Biology, Section for Functional Genomics, University of Copenhagen, Copenhagen, Denmark, [2] Department of Veterinary and Animal Sciences, Section for Veterinary Clinical Microbiology, University of Copenhagen, Copenhagen, Denmark, [3] Department of Clinical Microbiology, Center for Diagnostics, Rigshospitalet, Copenhagen, Denmark

Ciprofloxacin is a potent antibacterial drug that is widely used in human clinical applications. As a consequence of its extensive use, resistance has emerged in almost all clinically relevant bacterial species. A mean to combat the observed ciprofloxacin resistance is by reversing it via co-administration of a potentiating compound, also known as a helper drug. Here, we report on the current advances in identifying ciprofloxacin helper drugs, and put them into perspective of our own findings. We searched for potential helper drug targets in *Escherichia coli* strains with different levels of ciprofloxacin resistance using transcriptomics i.e., RNAseq and by deletion of genes associated with hyper-susceptibility to ciprofloxacin. Differential gene expression analysis of the highly ciprofloxacin resistant uropathogenic *E. coli* strain, ST131 UR40, treated with a clinically relevant concentration of ciprofloxacin (2 μg/mL), showed that the transcriptome was unaffected. Conversely, genetic screening of 23 single gene deletions in the high-level ciprofloxacin resistant laboratory derived *E. coli* strain, LM693, led to a significant decrease in the minimal inhibitory concentration for several genes, including genes encoding the AcrAB-TolC efflux pump, SOS-response proteins and the global regulator Fis. In addition, deletion of *acrA*, *tolC*, *recA*, or *recC* rendered two *E. coli* strains with intermediate susceptibility to ciprofloxacin fully susceptible according to the CLSI recommended breakpoint. Our results corroborate the AcrAB-TolC efflux pump and the SOS response proteins, RecA and RecC, as potential targets for ciprofloxacin helper drugs in treatment of human bacterial infections caused by *E. coli* strains with intermediate sensitivity to ciprofloxacin.

Keywords: antibiotic resistance, ciprofloxacin, helper drugs, RNA-Seq, transcriptomics

OPEN ACCESS

Edited by:
Sanna Sillankorva, University of Minho, Portugal

Reviewed by:
César de la Fuente, Massachusetts Institute of Technology, United States
Munawar Sultana, University of Dhaka, Bangladesh
Azucena Mora Gutiérrez, Universidade de Santiago de Compostela, Spain
Catherine M. Logue, University of Georgia, United States

***Correspondence:**
Anders Løbner-Olesen
lobner@bio.ku.dk

Specialty section:
This article was submitted to Antimicrobials, Resistance and Chemotherapy, a section of the journal Frontiers in Microbiology

Received: *15 March 2018*
Accepted: *11 June 2018*
Published: *02 July 2018*

Citation:
Klitgaard RN, Jana B, Guardabassi L, Nielsen KL and Løbner-Olesen A (2018) DNA Damage Repair and Drug Efflux as Potential Targets for Reversing Low or Intermediate Ciprofloxacin Resistance in E. coli K-12. Front. Microbiol. 9:1438. doi: 10.3389/fmicb.2018.01438

INTRODUCTION

Fluoroquinolones are some of the most prescribed antibacterial drugs in the world, commonly used for the treatment of urinary tract infections and sinusitis (Emmerson and Jones, 2003; Linder et al., 2005; Mitscher, 2005), but this has not always been the case. For the first two decades after the discovery of nalidixic acid in 1962, and its introduction into the clinic in 1964, the quinolones

Abbreviations: MIC, minimal inhibitory concentration; ST, sequence type.

were only used to treat uncomplicated urinary tract infections. This changed with the release of the second generation quinolones, including ciprofloxacin, which showed significant activity outside the urinary tract and against a broad spectrum of both Gram-negative and Gram-positive bacteria. Ciprofloxacin acts by binding to its targets, DNA gyrase and topoisomerase IV, inhibiting the native ability of these two enzymes to re-ligate double stranded DNA breaks, in turn leading to fragmentation of the chromosome. Due to its mechanism of action it is sometimes referred to as *topoisomerase poison* (Aldred et al., 2014). Inevitably, considering its extensive use and misuse, resistance toward ciprofloxacin has increased in almost all clinically relevant bacteria (Werner et al., 2011; Dalhoff, 2012). One method to overcome antibacterial resistance is by combinatorial treatment with a potentiating compound, also known as a helper drug. A helper drug is by definition non-antibacterial when administered alone, but it enhances the activity of the antibiotic when used in concert. The potentiating effect of a helper drug can be achieved by either direct inhibition of the resistance mechanism or by targeting endogenous cellular components and pathways like, cell membranes, efflux pumps and cellular repair systems. A classic example of targeting the resistance mechanism is the combination of amoxicillin and the β-lactamase inhibitor clavulanic acid (White et al., 2004). High-level ciprofloxacin resistance is primarily associated with multiple target site mutations in *gyrA* and *parC*, encoding subunits of the DNA gyrase and topoisomerase IV, respectively (Aldred et al., 2014). Since 1998 three different plasmid-mediated ciprofloxacin resistance mechanisms have been identified; (i) target protection (Qnr proteins), (ii) efflux pumps (QepA and OqxAB) and (iii) drug modification (AAC(6′)-Ib-cr acetyltransferase) (Rodríguez-Martínez et al., 2016).

Potential Ciprofloxacin Helper Drug Targets

Studies of the endogenous cellular mechanisms involved in ciprofloxacin susceptibility and resistance evolution have revealed more than two dozen gene deletions that lead to increased ciprofloxacin susceptibility in wild-type *Escherichia coli* (Cirz et al., 2005; Tamae et al., 2008; Liu et al., 2010; Yamada et al., 2010). Thus, suggesting the gene products as potential ciprofloxacin helper drug targets. Recently, Tran et al. identified 23 single gene deletions that increased the ciprofloxacin susceptibility of a laboratory derived resistant *E. coli* strain. The most significant increase in ciprofloxacin susceptibility was observed for the deletion of SOS-response genes directly involved in DNA damage repair, and the genes encoding the AcrAB-TolC efflux pump (Tran et al., 2016). Recacha et al. recently showed that deletion of *recA* rendered a laboratory derived *E. coli* strain with intermediate sensitivity to ciprofloxacin clinically susceptible *in vitro*. In addition, the *in vivo* efficacy of ciprofloxacin against the same strain was significantly increased in a peritoneal sepsis murine model (Recacha et al., 2017). Thus, the current evidence suggests that targeting the repair of ciprofloxacin induced DNA damage or the efflux pump AcrAB-TolC are the most promising strategies for ciprofloxacin helper drugs. Here, we used a combined transcriptomic and genetic approach in an attempt to both identify novel helper drug targets, as well as further assess the potential of known helper drug targets in laboratory derived *E. coli* strains with different levels and mechanisms of ciprofloxacin resistance.

MATERIALS AND METHODS

Bacterial Strains and Plasmids

Strains LM693 and LM862 were obtained from Diarmaid Hughes from Uppsala University. LM693 is isogenic to the commonly used laboratory strain, MG1655, besides two *gyrA* mutations, S83L and D87N, and one parC mutation, S80I. LM862 is also isogenic to MG1655, but with one *gyrA* S83L mutation and one *parC* S80I mutation. ST131 UR40 has two *gyrA* mutations, S83L and D87, and two parC mutations, S80I and E84V, and carries *aac-6′-Ib-cr* on a plasmid (Cerquetti et al., 2010). The *aac-6′-Ib-cr* carrying plasmid pRNK1 (was constructed as follows: *aac-6′-Ib-cr* gene was amplified by PCR from ST131 UR40, using the following primers: GATCGGATCCATGAGCAACGCAAAAACAAAGTT AGGC and CATCGAATTCTTAGGCATCACTGCGTGTTCGC, and cloned into pMW119 (Nippon Gene, Toyama, Japan) using *Bam*HI and *Eco*RI. The *qnrS*-carrying plasmid pRNK9 was constructed as follows: *qnrS* was amplified by PCR from the clinical *E. coli* isolate EC38 using the following primers: GATCGGATCCATGGAAACCTACAATCATACATAT CGGC and GATCAAGCTTTTAGTCAGGATAAACAACAAT ACCCAGTGC, and cloned into pMG25 using *Bam*HI and *Hin*dIII (M. Mikkelsen and K. Gerdes, unpublished). pRNK1 (4796 bp) and pRNK9 (4723 bp) was then introduced in LM862 by electroporation. Strain EC38 was isolated from a patient with a urinary tract infection at Hvidovre Hospital, Denmark.

Genetic Screening and MIC Tests

For the genetic screen, P1 phage lysates were prepared from the relevant Keio collection strains (Baba et al., 2006) and used for transduction into LM693 and LM862. All the transduced strains were verified by PCR. The ciprofloxacin MICs for LM693 and derived strains were determined using E-tests (0.002–32 μg/ml, BioMerieux) and according to the manufacturer's guidelines. The MICs for LM862 and derived strains were determined by broth micro-dilution using cation adjusted Mueller Hinton broth II with 1 mM and 10 μM IPTG for pRNK1 and pRNK9, respectively. The two different IPTG concentrations were used to obtain a ciprofloxacin MIC for LM862/pRNK1 and LM862/pRNK9 of 2 μg/mL i.e., within the CLSI intermediate susceptible range. The reference *E. coli* strain ATCC 25922 was used as standard in all MIC tests and the susceptibility was evaluated according to CLSI recommended breakpoints.

Checkerboard Assay

All wells in a micro-titter plate were filled with 100 μl cation adjusted Mueller Hinton broth II (200 μL in the negative control wells). Copper phtalocyanine-3,4′,4″,4‴-tetrasulfonic acid, was added to the first row, followed by serial dilution along the

abscissa, leading to a start concentration of 100 μM. Hereafter ciprofloxacin was serial diluted along the ordinate, giving a start concentration of 2 and 64 μg/ml for LM862 and LM693, respectively. Hundred microliter diluted culture with an OD600 of 0.001 was then inoculated in each well and the plates were incubated at 37°C for 24 h.

RNA-Sequencing

Ciprofloxacin was added to a culture of ST131 UR40, which had been growing exponentially for more than six generations, to a final concentration of 2 μg/ml. Samples for RNA isolation were taken at 0 min (prior to ciprofloxacin addition) and 30 and 90 min after ciprofloxacin addition, which has previously been shown to be long enough to induce fragmentation of the *E. coli* chromosome (Charbon et al., 2014). Total RNA was isolated using a Thermo Scientific GeneJET RNA isolation kit. Dnase treated with TURBO DNA-free kit from Ambion. rRNA was depleted using an Illumina Ribo-zero rRNA removal kit, followed by RNA-Seq library prep using an Illumina TruSeq Stranded mRNA Library Prep Kit. Sequencing was performed on an Illumina Miseq with a Miseq reagent kit v3. (75 bp paired-end) from Illumina. Data analysis was performed in Rockhopper ver.2.03 (McClure et al., 2013). *E. coli* NA114 (ST131) (accession number: NC_017644) was used as reference genome (Avasthi et al., 2011). The percentage of successfully aligned reads varied from 91 to 88% of the total read count. The sequencing data files and the Rockhopper results from the differential gene expression analysis are available from the Gene Expression Omnibus (GEO: GSE89507).

RESULTS

Identification of Helper Drug Targets by Genetic Screening

As mentioned in the introduction several single gene deletions are known to increase the ciprofloxacin susceptibility of *E. coli*. To further assess the helper drug target potential of these genes, 23 single gene deletions were introduced into the high-level ciprofloxacin resistant *E. coli* strain LM693 (MIC of 24–32 μg/ml) (Marcusson et al., 2009) and tested for hyper-susceptibility toward ciprofloxacin (**Table 1**). LM693 is isogenic to the commonly used laboratory strain MG1655 besides two GyrA mutations; S83L and D87, and one ParC mutation; S80I. Even though nine of the mutant strains showed a three to four fold reduction in the MIC, none of them were found to be susceptible according to the CLSI MIC breakpoint for ciprofloxacin (≤1 μg/mL). Our results therefore indicate that none of the tested gene-knockouts identify valid helper drug targets in high-level ciprofloxacin resistant *E. coli* strains. However, they could potentially be used as helper drug targets in bacteria with intermediate susceptibility to ciprofloxacin. To create two strains with intermediate ciprofloxacin susceptibility, we constructed the plasmids pRNK1 and pRNK9 carrying the ciprofloxacin resistance determinants aac-6′-Ib-cr and qnrS, respectively. AAC-6′-Ib-cr inactivates ciprofloxacin by *N*-acetylation of the amino nitrogen of its piperazinyl substituent (Robicsek et al., 2006), while QnrS acts as a DNA mimic, binding to and protecting the gyrase from the action of ciprofloxacin (Rodríguez-Martínez et al., 2016). Introduction of pRNK1 and pRNK9 into strain LM862, which carries GyrA S83L and ParC S80I mutations, increased the MIC from 1 to 2 μg/ml, i.e., into the CLSI intermediate susceptible MIC range. We then evaluated the ability of seven of the most promising gene deletions described above to reduce the ciprofloxacin MIC of LM862/pRNK1 and LM862/pRNK9. Four of the gene deletions (*acrA, tolC, recA*, and *recC*) rendered both strains susceptible to ciprofloxacin (**Table 2**). To assess whether inhibition of RecA was an amenable strategy for potentiation of ciprofloxacin, synergy between ciprofloxacin and a RecA inhibitor, copper phtalocyanine-3,4′,4″,4‴-tetrasulfonic acid (Alam et al., 2016), was tested by a checkerboard assay. However, we did not observe a reduction in the ciprofloxacin MICs for either LM693 or LM862.

Identification of Helper Drug Targets by RNA Sequencing

The *E. coli* clonal group ST131 has become the predominant *E. coli* lineage isolated from human extra-intestinal infections and is currently regarded a global problem in hospitals and clinical practices (Nicolas-Chanoine et al., 2014). Two independent studies have shown that more than 90% of ESBL-producing

TABLE 1 | MIC values for the single gene deletions in LM693.

Strain/single deletions	MIC (μg/ml)
LM693	24–32
tolC	1.5
acrA, acrB and *fis*	2
recC, xseA, xseB, uvrD, and *recA*	4
ruvC and *dksA*	6
recG and *hlpA*	8
pgm, ybgF and ybgC	12
deoR, ydcS, yciT and ybjQ	16
ygcO and *nlpC*	24
rimK	24–32

TABLE 2 | MIC values for the single gene deletions in LM862/pRNK1 and LM862/pRNK9.

Strain	MIC (μg/ml)	
LM862	1	1
LM862/Empty vectors	1	1
	pRNK1	**pRNK9**
LM862	2	2
tolC	0.25	0.5
acrA	0.25	0.5
recA	0.5	0.5
recC	0.5	0.5
uvrD	2	1
xseA	1	1
fis	2	4

ST131 isolates are also resistant to ciprofloxacin (Brisse et al., 2012; López-Cerero et al., 2014). Strain ST131 UR40 is resistant to high levels of ciprofloxacin due to GyrA mutations S83L and D87, and ParC mutations S80I and E84V (Cerquetti et al., 2010). Here we used RNA-Seq to map the transcriptomic changes during treatment of ST131 UR40 with a clinically relevant concentration of ciprofloxacin, 2 μg/ml, which is approximately equal to the maximum serum concentration following oral administration of 500 mg ciprofloxacin according to the FDA. The rationale behind this was to identify potential helper drug target genes that were upregulated upon ciprofloxacin exposure and thereby potentially involved in ciprofloxacin resistance. In contrast to the genetic screen, the RNA-Seq analysis would also reveal targets encoded by essential genes and non-coding RNA. The transcriptomic analysis did not show any non-ribosomal transcripts to be significantly upregulated in the presence of ciprofloxacin, i.e., with a false discovery rate of <1% and more than two-fold expression change.

DISCUSSION

By utilizing a combination of "direct genetic screening" and differential gene expression analysis, we have attempted to identify potential genes suitable as targets for ciprofloxacin potentiating compounds. We did not find any genes to be significantly upregulated by ciprofloxacin, indicating that the transcriptome of ST131 UR40 was relatively unaffected by treatment with a sub-inhibitory and yet clinically relevant concentration of ciprofloxacin. The lack of an upregulation of the SOS response genes in the transcriptomic analysis suggests that the ciprofloxacin exposure did not cause sufficient DNA damage to induce a SOS response; hence it was not necessary for ST131 UR40 to upregulate any specific genes to cope with the presence of ciprofloxacin at a sub-inhibitory concentration.

The screening of selected mutant strains revealed a number of genes, which when deleted, lowered the MIC for ciprofloxacin significantly in LM693. These findings are in accordance with genes reported to contribute to high-level ciprofloxacin resistance by Tran et al. (2016). Treatment of bacteria with ciprofloxacin generates double stranded breaks in the DNA of the organism (Drlica et al., 2008), which in turn activates the SOS response. Seven of the tested gene deletions; *recA, recC, recG, uvrD, xseAB*, and *ruvC,* which all significantly reduced the MIC of LM693, are part of the SOS response and involved in DNA damage repair (Chase and Richardson, 1974; Kuzminov, 1993; Michel, 2005). Thus, deletion of any of these seven genes likely lowers the ability of the bacteria to cope with ciprofloxacin induced DNA damage. Deletion of genes encoding the AcrAB-TolC efflux pump, or the global regulator Fis (Factor for inversion stimulation) showed the largest decreases in MIC values for LM693. The Fis protein has been shown to repress the *gyrA* and *gyrB* promoters, thereby reducing the expression of the DNA gyrase (Schneider et al., 1999). Thus, deletion of *fis* likely increases DNA gyrase expression and the number of ciprofloxacin targets. As ciprofloxacin works as a topoisomerase poison, an increase in ciprofloxacin bound DNA gyrase could potentially lead to an increase in double stranded breaks, explaining the decrease in MIC for the *fis* deletion strain. The *fis* deletion did not have the same effect on the intermediate susceptible strains LM862/pRNK1 and LM862/pRNK9, which may be explained by the relatively higher affinity of ciprofloxacin for its target in LM862, compared to that of LM693. Thus, the increase in expression of the DNA gyrase might lead to an increase in ciprofloxacin-gyrase complexes, but if the ciprofloxacin induced DNA damage is already at a level, where the DNA repair mechanisms cannot keep up, the *fis* deletion does not have a dramatic effect on the MIC.

Individual deletions of *acrA, acrB*, or *tolC* genes encoding the AcrAB-TolC efflux pump had a large effect on the ciprofloxacin susceptibility of both LM693 and LM862 strains. This was not surprising as overexpression of the AcrAB-TolC efflux system has been connected to ciprofloxacin resistance numerous times (Mazzariol et al., 2000). The deletion of *acrA* or *tolC* in the LM862 strains lowered the MIC beneath the CLSI susceptible breakpoint indicating that AcrAB-TolC efflux system is a potential target for ciprofloxacin potentiating compounds in intermediate susceptible *E. coli*. A number of AcrAB-TolC inhibitors have been identified (Chevalier et al., 2004; Bohnert et al., 2013; Aparna et al., 2014; Opperman et al., 2014; Yilmaz et al., 2015), two of which have been shown to decrease the MIC of ciprofloxacin in susceptible *E. coli* strains (Opperman et al., 2014; Yilmaz et al., 2015), but none of them are used in clinical practice so far.

Inhibition of RecA and thereby of the SOS response has been proposed as a strategy to fight antibiotic resistance numerous times (Blázquez et al., 2012; Culyba et al., 2015; Alam et al., 2016). Our finding, that deletion of *recA* render intermediate susceptible strains of *E. coli* fully susceptible to ciprofloxacin is in accordance with recent observations by Recacha et al. (2017). Overall, this indicates that RecA could be a potential ciprofloxacin helper drug target.

Even though AcrAB-TolC or RecA deficiency rendered LM862/pRNK1 and LM862/pRNK9 susceptible to ciprofloxacin, the respective MICs were only two to four-folds lower than the susceptible MIC breakpoint. It therefore seems reasonable to assume that a given inhibitor should completely block the activity of either RecA or AcrAB-TolC in order for it to be an efficient helper drug. This hypothesis is backed by the failure of lowering the ciprofloxacin MIC of LM862 and LM693 with the RecA inhibitor phtalocyanine-3,4′,4″,4‴-tetrasulfonic acid.

CONCLUSION

The findings of this study and the evidence given in the literature, indicates that reversal of ciprofloxacin resistance in high-level resistant *E. coli* strains by the use of helper drugs does not appear to be plausible. Conversely, targeting RecA, RecC or the AcrAB-TolC efflux pump is a likely feasible strategy for reversing ciprofloxacin resistance in *E. coli* strains with intermediate susceptibility to ciprofloxacin. However, it should be noted that there is a discrepancy between the MIC breakpoint

for ciprofloxacin susceptibility proposed by the CLSI (≤1 μg/mL) and the EUCAST (≤0.25 μg/mL). Therefore, further *in vivo* studies are needed to asses if targeting either RecA, RecC, or AcrAB-TolC leads to a significant increase in the efficacy of ciprofloxacin against an intermediate susceptible *E. coli* strain.

AUTHOR CONTRIBUTIONS

RK carried out all experimental work, designed the study, analyzed the data, and prepared the final manuscript. AL-O supervised all aspects of the study and helped prepare the final manuscript. BJ assisted and supervised the experimental part of the RNA-seq. LG supervised and delivered the ST131 UR40 strain. KN performed genomic analyses and delivered the EC38 strain carrying the *qnrS* gene. All authors read and approved the final manuscript.

FUNDING

We acknowledge the financial support from the University of Copenhagen Centre for Control of Antibiotic Resistance (UC-Care) and by the Center for Bacterial Stress Response and Persistence (BASP) funded by a grant from the Danish National Research Foundation (DNRF120).

REFERENCES

Alam, M. K., Alhhazmi, A., Decoteau, J. F., Luo, Y., and Geyer, C. R. (2016). RecA inhibitors potentiate antibiotic activity and block evolution of antibiotic resistance. *Cell Chem. Biol.* 23, 381–391. doi: 10.1016/j.chembiol.2016.02.010

Aldred, K. J., Kerns, R. J., and Osheroff, N. (2014). Mechanism of quinolone action and resistance. *Biochemistry* 53, 1565–1574. doi: 10.1021/bi5000564

Aparna, V., Dineshkumar, K., Mohanalakshmi, N., Velmurugan, D., and Hopper, W. (2014). Identification of natural compound inhibitors for multidrug efflux pumps of *Escherichia coli* and *Pseudomonas aeruginosa* using in silico high-throughput virtual screening and in vitro validation. *PLoS One* 9:e101840. doi: 10.1371/journal.pone.0101840

Avasthi, T. S., Kumar, N., Baddam, R., Hussain, A., Nandanwar, N., Jadhav, S., et al. (2011). Genome of Multidrug-resistant uropathogenic *Escherichia coli* strain NA114 from India. *J. Bacteriol.* 193, 4272–4273. doi: 10.1128/JB.05413-11

Baba, T., Ara, T., Hasegawa, M., Takai, Y., Okumura, Y., Baba, M., et al. (2006). Construction of *Escherichia coli* K-12 in-frame, single-gene knockout mutants: the Keio collection. *Mol. Syst. Biol.* 2:msb4100050. doi: 10.1038/msb4100050

Blázquez, J., Couce, A., Rodríguez-Beltrán, J., and Rodríguez-Rojas, A. (2012). Antimicrobials as promoters of genetic variation. *Curr. Opin. Microbiol.* 15, 561–569. doi: 10.1016/j.mib.2012.07.007

Bohnert, J. A., Schuster, S., and Kern, W. V. (2013). Pimozide inhibits the AcrAB-TolC efflux pump in *Escherichia coli*. *Open Microbiol. J.* 7, 83–86. doi: 10.2174/1874285801307010083

Brisse, S., Diancourt, L., Laouénan, C., Vigan, M., Caro, V., Arlet, G., et al. (2012). Phylogenetic distribution of CTX-M- and non-extended-spectrum-β-lactamase-producing *Escherichia coli* isolates: group B2 isolates, except clone ST131, rarely produce CTX-M enzymes. *J. Clin. Microbiol.* 50, 2974–2981. doi: 10.1128/JCM.00919-12

Cerquetti, M., Giufrè, M., García-Fernández, A., Accogli, M., Fortini, D., Luzzi, I., et al. (2010). Ciprofloxacin-resistant, CTX-M-15-producing *Escherichia coli* ST131 clone in extraintestinal infections in Italy. *Clin. Microbiol. Infect.* 16, 1555–1558. doi: 10.1111/j.1469-0691.2010.03162.x

Charbon, G., Bjørn, L., Mendoza-Chamizo, B., Frimodt-Møller, J., and Løbner-Olesen, A. (2014). Oxidative DNA damage is instrumental in hyperreplication stress-induced inviability of *Escherichia coli*. *Nucleic Acids Res.* 42, 13228–13241. doi: 10.1093/nar/gku1149

Chase, J. W., and Richardson, C. C. (1974). Exonuclease VII of *Escherichia coli*: mechanism of action. *J. Biol. Chem.* 249, 4553–4561.

Chevalier, J., Bredin, J., Mahamoud, A., Malléa, M., Barbe, J., and Pagès, J.-M. (2004). Inhibitors of antibiotic efflux in resistant *Enterobacter aerogenes* and *Klebsiella pneumoniae* strains. *Antimicrob. Agents Chemother.* 48, 1043–1046. doi: 10.1128/AAC.48.3.1043-1046.2004

Cirz, R. T., Chin, J. K., Andes, D. R., De Crécy-Lagard, V., Craig, W. A., and Romesberg, F. E. (2005). Inhibition of mutation and combating the evolution of antibiotic resistance. *PLoS Biol.* 3:e176. doi: 10.1371/journal.pbio.0030176

Culyba, M. J., Mo, C. Y., and Kohli, R. M. (2015). Targets for combating the evolution of acquired antibiotic resistance. *Biochemistry* 54, 3573–3582. doi: 10.1021/acs.biochem.5b00109

Dalhoff, A. (2012). Global fluoroquinolone resistance epidemiology and implictions for clinical use. *Interdiscip. Perspect. Infect. Dis.* 2012:976273. doi: 10.1155/2012/976273

Drlica, K., Malik, M., Kerns, R. J., and Zhao, X. (2008). Quinolone-mediated bacterial death. *Antimicrob. Agents Chemother.* 52, 385–392. doi: 10.1128/AAC.01617-06

Emmerson, A. M., and Jones, A. M. (2003). The quinolones: decades of development and use. *J. Antimicrob. Chemother.* 51(Suppl. 1), 13–20. doi: 10.1093/jac/dkg208

Kuzminov, A. (1993). RuvA, RuvB and RuvC proteins: cleaning-up after recombinational repairs in *E. coli*. *Bioessays* 15, 355–358. doi: 10.1002/bies.950150511

Linder, J. A., Huang, E. S., Steinman, M. A., Gonzales, R., and Stafford, R. S. (2005). Fluoroquinolone prescribing in the United States: 1995 to 2002. *Am. J. Med.* 118, 259–268. doi: 10.1016/j.amjmed.2004.09.015

Liu, A., Tran, L., Becket, E., Lee, K., Chinn, L., Park, E., et al. (2010). Antibiotic sensitivity profiles determined with an *Escherichia coli* gene knockout collection: generating an antibiotic bar code. *Antimicrob. Agents Chemother.* 54, 1393–1403. doi: 10.1128/AAC.00906-09

López-Cerero, L., Navarro, M. D., Bellido, M., Martín-Peña, A., Viñas, L., Cisneros, J. M., et al. (2014). *Escherichia coli* belonging to the worldwide emerging epidemic clonal group O25b/ST131: risk factors and clinical implications. *J. Antimicrob. Chemother.* 69, 809–814. doi: 10.1093/jac/dkt405

Marcusson, L. L., Frimodt-Møller, N., and Hughes, D. (2009). Interplay in the selection of fluoroquinolone resistance and bacterial fitness. *PLoS Pathog.* 5:e1000541. doi: 10.1371/journal.ppat.1000541

Mazzariol, A., Tokue, Y., Kanegawa, T. M., Cornaglia, G., and Nikaido, H. (2000). High-level fluoroquinolone-resistant clinical isolates of *Escherichia coli* overproduce multidrug efflux protein AcrA. *Antimicrob. Agents Chemother.* 44, 3441–3443. doi: 10.1128/AAC.44.12.3441-3443.2000

McClure, R., Balasubramanian, D., Sun, Y., Bobrovskyy, M., Sumby, P., Genco, C. A., et al. (2013). Computational analysis of bacterial RNA-Seq data. *Nucleic Acids Res.* 41:e140. doi: 10.1093/nar/gkt444

Michel, B. (2005). After 30 years of study, the bacterial SOS response still surprises us. *PLoS Biol.* 3:e255. doi: 10.1371/journal.pbio.0030255

Mitscher, L. A. (2005). Bacterial topoisomerase inhibitors: quinolone and pyridone antibacterial agents. *Chem. Rev.* 105, 559–592. doi: 10.1021/cr030101q

Nicolas-Chanoine, M.-H., Bertrand, X., and Madec, J.-Y. (2014). *Escherichia coli* ST131, an intriguing clonal group. *Clin. Microbiol. Rev.* 27, 543–574. doi: 10.1128/CMR.00125-13

Opperman, T. J., Kwasny, S. M., Kim, H. S., Nguyen, S. T., Houseweart, C., D'souza, S., et al. (2014). Characterization of a novel pyranopyridine inhibitor of the AcrAB efflux pump of *Escherichia coli*. *Antimicrob. Agents Chemother.* 58, 722–733. doi: 10.1128/AAC.01866-13

Recacha, E., Machuca, J., Díaz De Alba, P., Ramos-Güelfo, M., Docobo-Pérez, F., Rodriguez-Beltrán, J., et al. (2017). Quinolone resistance reversion by targeting the SOS response. *mBio* 8, e00971–17. doi: 10.1128/mBio.00971-17

Robicsek, A., Strahilevitz, J., Jacoby, G. A., Macielag, M., Abbanat, D., Park, C. H., et al. (2006). Fluoroquinolone-modifying enzyme: a new adaptation of

a common aminoglycoside acetyltransferase. *Nat. Med.* 12, 83–88. doi: 10.1038/nm1347

Rodríguez-Martínez, J. M., Machuca, J., Cano, M. E., Calvo, J., Martínez-Martínez, L., and Pascual, A. (2016). Plasmid-mediated quinolone resistance: two decades on. *Drug Resist. Updat.* 29, 13–29. doi: 10.1016/j.drup.2016.09.001

Schneider, R., Travers, A., Kutateladze, T., and Muskhelishvili, G. (1999). A DNA architectural protein couples cellular physiology and DNA topology in *Escherichia coli*. *Mol. Microbiol.* 34, 953–964. doi: 10.1046/j.1365-2958.1999.01656.x

Tamae, C., Liu, A., Kim, K., Sitz, D., Hong, J., Becket, E., et al. (2008). Determination of antibiotic hypersensitivity among 4,000 single-gene-knockout mutants of *Escherichia coli*. *J. Bacteriol.* 190, 5981–5988. doi: 10.1128/JB.01982-07

Tran, T., Ran, Q., Ostrer, L., and Khodursky, A. (2016). De novo characterization of genes that contribute to high-level ciprofloxacin resistance in *Escherichia coli*. *Antimicrob. Agents Chemother.* 60, 6353–6355. doi: 10.1128/AAC.00889-16

Werner, N. L., Hecker, M. T., Sethi, A. K., and Donskey, C. J. (2011). Unnecessary use of fluoroquinolone antibiotics in hospitalized patients. *BMC Infect. Dis.* 11:187. doi: 10.1186/1471-2334-11-187

White, A. R., Kaye, C., Poupard, J., Pypstra, R., Woodnutt, G., and Wynne, B. (2004). Augmentin (amoxicillin/clavulanate) in the treatment of community-acquired respiratory tract infection: a review of the continuing development of an innovative antimicrobial agent. *J. Antimicrob. Chemother.* 53(Suppl. 1), i3–i20. doi: 10.1093/jac/dkh050

Yamada, J., Yamasaki, S., Hirakawa, H., Hayashi-Nishino, M., Yamaguchi, A., and Nishino, K. (2010). Impact of the RNA chaperone Hfq on multidrug resistance in *Escherichia coli*. *J. Antimicrob. Chemother.* 65, 853–858. doi: 10.1093/jac/dkq067

Yilmaz, S., Altinkanat-Gelmez, G., Bolelli, K., Guneser-Merdan, D., Ufuk over-Hasdemir, M., Aki-Yalcin, E., et al. (2015). Binding site feature description of 2-substituted benzothiazoles as potential AcrAB-TolC efflux pump inhibitors in *E. coli*. *SAR QSAR Environ. Res.* 26, 853–871. doi: 10.1080/1062936X.2015.1106581

Conflict of Interest Statement: The authors declare that the research was conducted in the absence of any commercial or financial relationships that could be construed as a potential conflict of interest.

frontiers in Microbiology

ORIGINAL RESEARCH
published: 11 July 2018
doi: 10.3389/fmicb.2018.01535

In Vitro Antibacterial Activity of Teixobactin Derivatives on Clinically Relevant Bacterial Isolates

*Estelle J. Ramchuran[1], Anou M. Somboro[1], Shimaa A. H. Abdel Monaim[2], Daniel G. Amoako[1], Raveen Parboosing[3], Hezekiel M. Kumalo[4], Nikhil Agrawal[5], Fernando Albericio[2,6], Beatriz G. de La Torre[5] and Linda A. Bester[1]**

[1] Biomedical Resource Unit, School of Laboratory Medicine and Medical Sciences, College of Health Sciences, University of KwaZulu-Natal, Durban, South Africa, [2] Peptide Research Group, School of Chemistry and Physics, University of KwaZulu-Natal, Durban, South Africa, [3] Department of Virology, National Health Laboratory Service, University of KwaZulu-Natal, Durban, South Africa, [4] Discipline of Medical Biochemistry, School of Laboratory Medicine and Medical Science, University of KwaZulu-Natal, Durban, South Africa, [5] KRISP, College of Health Sciences, University of KwaZulu-Natal, Durban, South Africa, [6] CIBER-BBN, Networking Centre on Bioengineering, Biomaterials and Nanomedicine, and Department of Organic Chemistry, University of Barcelona, Barcelona, Spain

OPEN ACCESS

Edited by:
Sanna Sillankorva, University of Minho, Portugal

Reviewed by:
Nagendran Tharmalingam, Alpert Medical School, United States
Santi M. Mandal, Indian Institute of Technology Kharagpur, India

***Correspondence:**
Linda A. Bester
besterl@ukzn.ac.za

Specialty section:
This article was submitted to Antimicrobials, Resistance and Chemotherapy, a section of the journal Frontiers in Microbiology

Received: *13 December 2017*
Accepted: *20 June 2018*
Published: *11 July 2018*

Citation:
Ramchuran EJ, Somboro AM, Abdel Monaim SAH, Amoako DG, Parboosing R, Kumalo HM, Agrawal N, Albericio F, de La Torre BG and Bester LA (2018) In Vitro Antibacterial Activity of Teixobactin Derivatives on Clinically Relevant Bacterial Isolates. Front. Microbiol. 9:1535. doi: 10.3389/fmicb.2018.01535

Methicillin-resistant *Staphylococcus aureus* (MRSA) and vancomycin-resistant enterococcus (VRE) are included on the WHO high priority list of pathogens that require urgent intervention. Hence emphasis needs to be placed on developing novel class of molecules to tackle these pathogens. Teixobactin is a new class of antibiotic that has demonstrated antimicrobial activity against common bacteria. Here we examined the antimicrobial properties of three Teixobactin derivatives against clinically relevant bacterial isolates taken from South African patients. The minimum inhibitory concentration (MIC), the minimal bactericidal concentration (MBC), the effect of serum on MICs and the time-kill kinetics studies of our synthesized Teixobactin derivatives (3, 4, and 5) were ascertained following the CLSI 2017 guidelines and using the broth microdilution method. Haemolysis on red blood cells (RBCs) and cytotoxicity on peripheral blood mononuclear cells (PBMCs) were performed to determine the safety of these compounds. The MICs of 3, 4, and 5 against reference strains were 4–64 μg/ml, 2–64 μg/ml, and 0.5–64 μg/ml, respectively. The MICs observed for MRSA were (3) 32 μg/ml, (4) 2–4 μg/ml and (5) 2–4 μg/ml whilst those for VRE were (3) 8–16 μg/ml, (4) 4 μg/ml and (5) 2–16 μg/ml, respectively. In the presence of 50% human serum, there was no significant effect on the MICs. The compounds did not exhibit any effect on cell viability at their effective concentrations. Teixobactin derivatives (3, 4, and 5) inhibited bacterial growth in drug-resistant bacteria and hence emerge as potential antimicrobial agents. Molecular dynamic simulations suggested that the most dominant binding mode of Lys10-teixobactin (4) to lipid II is through the amide protons of the cycle, which is identical to data described in the literature for the natural teixobactin hence predicting the possibility of a similar mechanism of action.

Keywords: teixobactin derivatives, biological activity, antimicrobial agents, resistant bacteria, antimicrobial peptides, *in silico* analysis

INTRODUCTION

The rate of antibiotic resistance is increasing faster than the development of new compounds for clinical practice. In an extremely short period, resistance to antibiotics has become a significant cause of disease and death globally (Penesyan et al., 2015; Brown and Wright, 2016; Hamilton and Wenlock, 2016). Limited success in collective research efforts to synthesize novel and efficient compounds has contributed to the drug-resistance scenario we are now facing and to the lack of new and efficient treatment options.

The first antibiotics were produced through screening soil microorganisms. However, by the 1960s, this limited resource of cultivable bacteria had been overexploited (Lewis, 2012). Synthetic approaches to produce antibiotics have been unable to replace this platform. Uncultured bacteria, which make up 99% of all species in external environments, emerge as a potent source of new antibiotics (Kaeberlein et al., 2002; Nichols et al., 2010; Fang et al., 2012).

Teixobactin (1, **Figure 1**) is a new class of antibiotic that was discovered through the screening of uncultured bacteria using i-Chip (isolation chip), a revolutionary method for bacterial culture (Ling et al., 2015; Piddock, 2015; von Nussbaum and Süssmuth, 2015). Teixobactin was identified as an effective agent against Gram-positive bacteria. It inhibits cell wall synthesis by binding to two lipid cell wall precursors, namely lipid II (peptidoglycan precursor) and lipid III (teichoic acid precursor) (Ling et al., 2015; Homma et al., 2016). Vancomycin also targets lipid II. However, taking into account that Teixobactin has been demonstrated to be active against vancomycin-resistant enterococcus (VRE), its binding is through a different region compared to that of the Vancomycin. In this regard, biochemical assays have demonstrated that teixobactin binds the pyrophosphate and the first sugar moiety present in both, lipid II and lipid III (Ling et al., 2015).

Although much attention has shifted towards combating Gram-negative bacteria, there is still a need for compounds with novel mechanisms and low resistance profiles against Gram-positive strains. In this regard, Texiobactin can satisfy this need and contribute to the treatment of resistant Gram-positive bacteria such as VRE and MRSA. In this study we sought to evaluate three novel derivatives of Teixobactin (3, 4, and 5) and determine their activity against clinically relevant Gram-positive resistant bacteria as well as against Gram-negative species.

MATERIALS AND METHODS

Antibiotics and Reagents

All the derivatives were dissolved in 5% DMSO. GIBCO RPMI-1640 cell culture media (with HEPES, L-glutamine and sodium pyruvate) was obtained from Life Technolgies (Carlsbad, CA, United States). Hyclone fetal bovine serum was purchased from GE Healthcare Life Sciences (Chicago, IL, United States). Phosphate Buffered Saline (PBS) was obtained from Lonza (Basel, Switzerland). Nunclon Delta Surface sterile microtiter plates (including the Edge 2.0 plate) were bought from Thermo Fisher Scientific (Waltham, MA, United States). Human serum from male AB plasma (sterile and filtered), antibiotics, antimycotic solution and all other reagents were obtained from Sigma (St. Louis, MO, United States).

Bacterial Strains

Clinical isolates of MRSA and VRE were obtained from Lancet Laboratories, Durban, South Africa, with ethical approval BE394/15 from the Biomedical Research Ethical Committee of the University of KwaZulu-Natal. Four reference strains of bacteria, namely *Escherichia coli* ATCC 25922, *Pseudomonas aeruginosa* ATCC 27853, *Bacillus subtilis* ATCC 6051 and *Staphylococcus aureus* ATCC 29213 were obtained from the American Type Culture Collection (ATCC).

Synthesis, Purification, and Characterization of Teixobactin Derivatives

Our group previously synthesized the Teixobactin derivatives (3, 4, and 5) (**Figure 1**) used in this study. Furthermore, they were chemically characterized by HPLC and MS and subjected to preliminary biological testing against two Gram-positive and two Gram-negative ATCC strains (Abdel Monaim et al., 2017).

Minimum Inhibition Concentration (MIC) and Minimum Bactericidal Concentration (MBC) Determination

The MICs of the Teixobactin derivatives were determined using the broth microdilution method following the Clinical and Laboratory Standards Institute [CLSI], 2017 guidelines. Two-fold dilutions of each compound solution were prepared using cation adjusted Mueller–Hinton Broth (CAMHB) in a microtiter plate. A 0.5 McFarland-standardized bacterial inoculum was used to prepare a total volume of 200 µl in each microtiter well. The plates were incubated at 37°C for between 18 and 20 h. The MIC was determined as the lowest concentration at which no visible bacterial growth was observed. Control wells for bacteria and media were also included. Meropenem, vancomycin and ampicillin were used as standard control drugs. The plates containing VRE were incubated at 35°C under aerobic conditions. The MBC was determined as the lowest concentration of the test compound that was able to produce a 99.9% decrease in viable bacterial cells on the agar plates. Control wells included the same amount of solvent used in dissolving the drug candidates, medium and bacteria.

Effect of Human Serum on the MICs

The effect of serum on the MICs was determined in a similar way to the MIC method described above, but in this case 50% human serum: Mueller-Hinton broth was prepared.

Time-Kill Kinetic Assays

Time-kill assays were performed following CLSI guidelines and previously described methods (Wang et al., 2015; Clinical Laboratory Standard Institute [CLSI], 2017; Zheng et al., 2017).

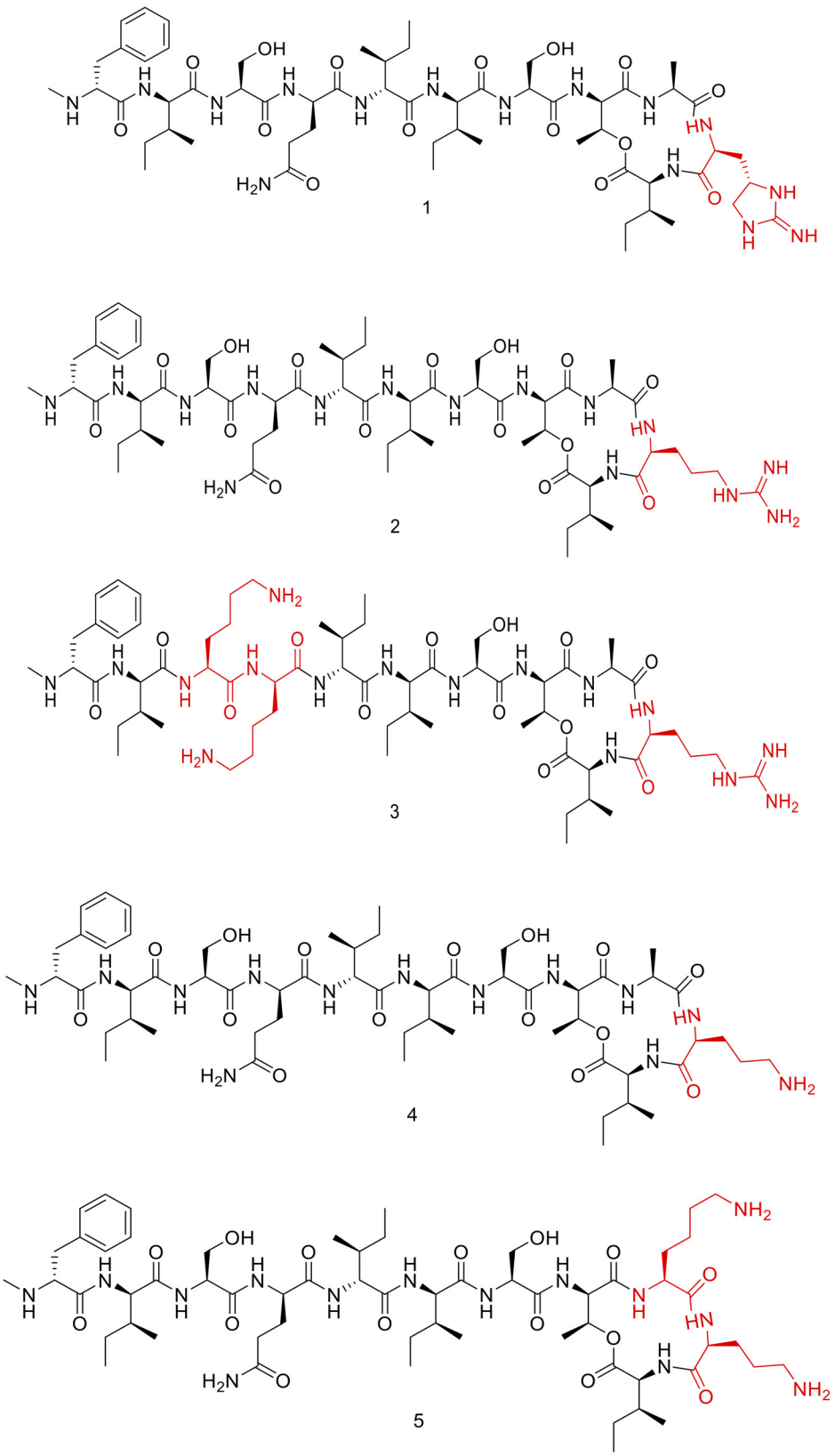

FIGURE 1 | Chemical structure of Teixobactin and derivatives (1, 2, 3, 4, and 5).

Overnight bacterial cell cultures were suspended in CAMHB and adjusted to an absorbance of approximately 10^6 CFU/ml. Varying concentrations of the test compounds were added to the inoculum suspensions, with final concentrations corresponding to 1x MIC, 2x MIC, and/or 4x MIC, and incubated at 37°C. Aliquots were removed from the inoculum cultures after 0, 1, 2, 4, 6, 8, and 24 h of incubation. They were then serially diluted, plated on MH agar and incubated for 24 h at 37°C. Bacterial cell viability was determined by colony count. The assays were performed in triplicate. Data was presented as mean and standard deviation of three independent replicates, analyzed with one-way ANOVA followed by Dunnett's test to determine the significance relative to the untreated bacteria ($P < 0.05$).

Cell Culture

The Buffy coat used in this study was obtained from the South African National Blood Service (SANBS). The anonymised product is provided by the SANBS for research purposes, upon approval from their Ethics Committee (National Health Laboratory Service Clearance Certificate approval no: 2013/18). Aseptic techniques and appropriate biosafety precautions were observed.

Haemolysis Assay on Red Blood Cells (RBCs)

The haemolysis assay was performed as previously described (Tramer et al., 2012; Jayamani et al., 2017), with modifications to allow for a 96-well microtiter plate format. Briefly, washed red blood cell pellet was re-suspended in PBS (to obtain a hematocrit of approximately 20%). Next, 10 μL of the cells was aliquoted into a 96-well microtiter plate containing 170 μL of PBS and lysed by addition of 20 μL of 1% Triton™ X-100 solution. After 30 min, the samples were spun at 3000 *g* for 5 min in an Orto Alresa Digicen 21R plate centrifuge. Absorbance was read at 405 nm in a Tecan Sunrise™ plate reader.

Seven serial 5-fold dilutions of the compounds were then prepared in triplicate by adding 25 μL of the compound to 100 μL of PBS. Controls (i.e., 0% and 100% hemolysis samples) were included. Appropriately diluted RBCs (10 μL RBCs and 90 μL PBS per well) were added to the microtiter plate and incubated at 37°C for 30 min and then spun at 3000 *g* for 5 min. The supernatants were then transferred to a fresh microtiter plate, and absorbance was read at 405 nm. The viability of the RBCs at each concentration of the compound was calculated as follows: % viability = $100 \times [1 - [A_t/(A_{100} - A_0)]]$ where A_t = mean absorbance of the test compound at a given concentration, A_0 = mean absorbance of the untreated control, and A_{100} = mean absorbance of the sample lysed with Triton™ X-100. The results were represented graphically. The experiment was performed in triplicate ($n = 3$). The error bars indicate the standard deviation. One-way ANOVA followed by Dunnett's test was performed to determine the significance relative to the untreated RBC ($P < 0.05$; indicated by *).

TABLE 1 | Minimum inhibitory concentration (MIC), minimum bactericidal concentration (MBC) and MIC in presence of 50% human serum of Teixobactin derivatives against susceptible reference strains of bacteria.

Antimicrobial agents	Organism											
	Gram-positive						Gram-negative					
	S. aureus ATCC 29213			*B. subtilis ATCC 6051*			*E. coli ATCC 25922*			*P. aeruginosa ATCC 27853*		
	MIC (μg/ml)	MBC (μg/ml)	50% serum (MIC μg/ml)	MIC (μg/ml)	MBC (μg/ml)	50% serum (MIC μg/ml)	MIC (μg/ml)	MBC (μg/ml)	50% serum (MIC μg/ml)	MIC (μg/ml)	MBC (μg/ml)	50% serum (MIC μg/ml)
3	32	64	64	4	8	2	64	64	>64	64	128	>64
4	4	16	4	2	8	1	64	64	>64	>64	128	>64
5	2	8	4	0.5	1	0.5	32	64	>64	64	128	>64
Meropenem	0.25	ND	ND	0.125	ND	ND	0.125	ND	ND	1	ND	ND

TABLE 2 | Minimum inhibitory concentration of Teixobactin derivatives against methicillin-resistant *Staphylococcus aureus* (MRSA).

Isolates	Origin[a]	Species	3	4	5	Vancomycin	Ampicillin
			MIC (μg/ml)	MIC (μg/ml)	MIC (μg/ml)	MIC (μg/ml)	MIC (μg/ml)
B11970	Blood	*S. aureus*	32	2	2	1	>512
P10781	Nasal	*S. aureus*	32	2	2	1	>512
P10747	CVP	*S. aureus*	32	2	2	1	>512
S37938	–	*S. aureus*	32	2	2	1	>512
S18155	ETT	*S. aureus*	32	2	2	0.5	>512
B13178	Blood	*S. aureus*	32	2	2	1	>512
440260	–	*S. aureus*	32	4	4	1	>512
S18970	–	*S. aureus*	32	2	2	1	>512
P11520	Pus	*S. aureus*	32	4	4	1	512
T5683	Nasal	*S. aureus*	32	2	2	1	>512
	MIC50		32	2	2	1	>512

[a]*ETT, Endotracheal tube; CVP, Central venous catheter, –, Missing data.*

TABLE 3 | Minimum inhibitory concentration of Teixobactin derivatives against vancomycin-resistant enterococci (VRE).

Isolates	Species	3	4	5	Vancomycin
		MIC (μg/ml)	MIC (μg/ml)	MIC (μg/ml)	MIC (μg/ml)
951245262 (A)	*Enterococcus faecium*	8	4	4	>128
951234856 (B)	*Enterococcus faecium*	16	4	4	>128
951208931 (C)	*Enterococcus faecium*	16	4	4	>128
938636470 (D)	*Enterococcus faecium*	16	8	4	>128
938666613 (E)	*Enterococcus faecium*	16	16	4	>128
938600912 (F)	*Enterococcus faecium*	16	2	8	>128
938072607 (G)	*Enterococcus faecium*	16	8	4	>128
944414000 (H)	*Enterococcus faecium*	16	8	4	>128
945530665 (I)	*Enterococcus faecium*	16	4	4	>128
U43821 (J)	*Enterococcus faecium*	16	8	4	>128
	MIC50	16	4	4	>128

Cytotoxicity on Peripheral Blood Mononuclear Cells (PBMCs)

The cytotoxicity assay was performed as previously described with slight modifications (Pannecouque et al., 2008; Pinto et al., 2011; Araújo et al., 2013; Azumah et al., 2016). Briefly, PBMCs (100,000 viable cells/well) were placed into the wells of a Nunclon^{TM} Delta Surface Edge 2.0 microtiter plate containing 100 μl of RPMI-1640 with 10% fetal bovine serum, 1% Antibiotic Antimycotic solution and 3% phytohemagglutinin. The cells were then incubated for 24 h at 37°C and 5% CO_2. Seven serial 5-fold dilutions of test compounds were prepared and transferred to the appropriate wells of the plate containing the cells. The plate was then incubated for 72 h at 37°C and 5% CO_2. Thereafter, 20 μl of MTT salt (7.5 mg/ml) was added to each well, and the plate was incubated for a further 4 h. Then 100 μl of the media was carefully removed from each well (avoiding agitation of the crystals) and replaced with 100 μl of solubilisation solution (containing acidified isopropanol and Triton^{TM} X-100). The plate was then placed on a shaker for 30 min to facilitate dissolution of the crystals. Absorbance was read at 550 nm (background: 690 nm). The results were shown graphically. The experiment was performed in triplicate ($n = 3$). The error bars indicate the standard deviation. One-way ANOVA followed by Dunnett's test was performed to determine the significance relative to the untreated PMBC ($P < 0.05$; indicated by *).

Molecular Dynamics Simulation

Structures of lipid II and teixobactin were downloaded from Automated Topology Builder (ATB) and Repository (Malde et al., 2011). In the teixobactin structure, the residue of enduracididine was replaced by Lys by molefacture program of VMD to get Lys_{10}-teixobactin (4) structure (Humphrey et al., 1996). CHARMM General Force Field (CGenFF) parameters were used for simulation of both molecules (Vanommeslaeghe et al., 2010). The molecular dynamics simulation system contains one lipid II molecule, one Lys10-teixobactin (4) molecule, and 6767 water molecules. The TIP3P water model was used for the water molecules (Mark and Nilsson, 2001). The system was first energy minimized using the steepest descent algorithm (Bixon and Lifson, 1967), after which two sequential equilibrations were performed using canonical ensemble (NVT), followed by an isobaric-isothermic ensemble (NPT) for 100 picoseconds

(ps) each, and production simulation was performed using NPT ensemble for 100 nanoseconds (ns). The simulation was performed at 310 K temperature and 1 atm pressure, for temperature coupling velocity-rescale method and for pressure coupling the Parrinello-Rahman method was used (Parrinello and Rahman, 1981). The Particle Mesh Ewald method was used for long-range electrostatic interactions (Darden et al., 1993), with 10Å cut-off being used to calculate the VdW and short-range coulombic interactions. MD simulation was performed using the GROMACS simulation package (Abraham et al., 2015). To identify the binding region of lipid II with Lys_{10}-teixobactin (4) an *in-house* TCL script was used. Script counts the numbers of frames that each oxygens atoms of lipid II were within 3.5 Å of protons of Lys10-teixobactin (4) throughout the simulation time.

RESULTS

Teixobactin Derivatives

Teixobactin is an 11-amino acid "head to side-chain" cyclodepsipeptide (**Figure 1**) with a D-Thr as a bridge head that forms the ester with the carboxylic group of a L-Ile. L-Ala and the post-translational modified L-*allo*-enduracidine (End), which contains a cyclic guanidine, are also part of the cycle (Abdel Monaim et al., 2016a; Dhara et al., 2016; Giltrap et al., 2016; Jin et al., 2016, 2017; Yang et al., 2016, 2017; Monaim et al., 2017; Parmar et al., 2017a,b; Schumacher et al., 2017; Wu et al., 2017). The tail is formed by two moieties of L-Ser, two moieties of L-Ile, D-*allo*-Ile and D-Gln ending with a *N*-Me-D-Phe. As L-*allo*-End was not commercially available, our group concentrated their efforts on synthesizing Arg_{10}-Teixobactin (2, **Figure 1**), in which the L-*allo*-End is substituted by Arg (Jad et al., 2015; Parmar et al., 2016).

Arg_{10}-Teixobactin (2), which has been converted from the parent Teixobactin analog, has slightly lower activity than Teixobactin. Our group had previously used a Lys-scanning strategy to prepare a small library of Teixobactin analogs containing more than one Lys residue—a residue that is absent in the natural structure (Abdel Monaim et al., 2016b, 2017). From this collection of peptides, three (3, 4, and 5, **Figure 1**) with good MICs against sensitive bacteria (ATCC strains) were selected for further *in vitro* evaluation in this study.

Antimicrobial Activity of Teixobactin Derivatives and the Effects of Human Serum on the MICs

The antimicrobial activity of the three derivatives (3, 4, and 5) was examined by *in vitro* screening against drug-resistant and -sensitive bacteria using the broth micro-dilution method, following CSLI guidelines. The derivatives inhibited sensitive Gram-positive (ATCC strains) and resistant MRSA and VRE isolates (**Tables 1**–**3**). They demonstrated potent antimicrobial activity against Gram-positive bacteria as opposed to Gram-negative bacteria. Three conventional antibiotics (meropenem, vancomycin and ampicillin) were used as controls and exhibited activity against the drug-sensitive ATCC strains. The following

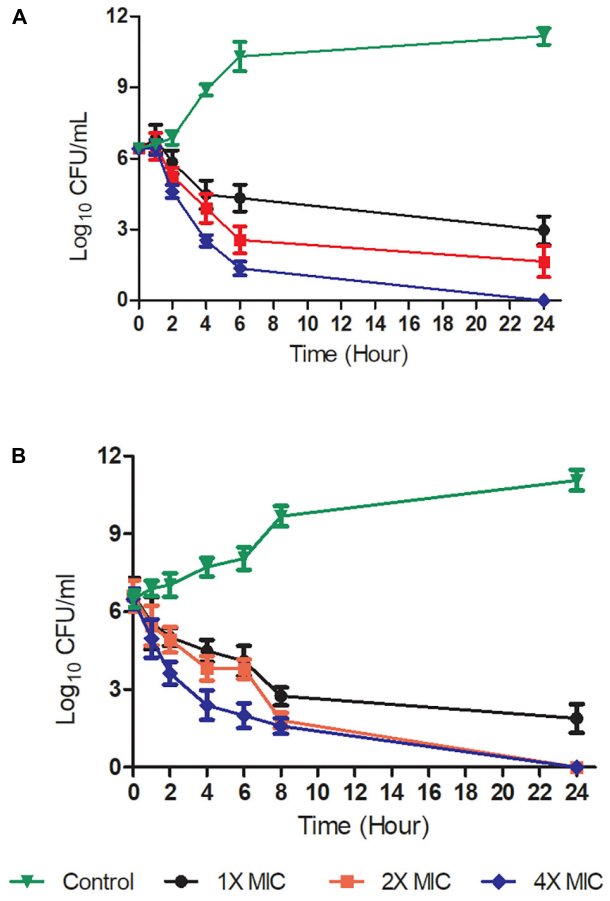

FIGURE 2 | Time-kill kinetics at a range of concentrations of Teixobactin derivative 4. Gram-positive bacteria [*S. aureus* ATCC 29213 **(A)** and *B. subtilis* ATCC 6051 **(B)**] were challenged with compound 4 at 1X, 2X, and 4X MIC levels. The experiment was performed in triplicate ($n = 3$). Data was presented as mean and standard deviation of three independent replicates, analyzed with one-way ANOVA followed by Dunnett's test to determine the significance relative to the untreated bacteria ($P < 0.05$).

MIC_{50} were recorded for the derivatives: (3) 32 μg/ml, (4/5) 2 μg/ml for MRSA, as well as (3) 16 μg/ml and (4/5) 4 μg/ml for VRE. The derivatives yielded MICs as low as 2 μg/ml and 0.5 μg/ml for Gram-positive reference ATCC strains *S. aureus* and *B. subtilis* respectively. The MICs of the experimental compounds against susceptible Gram-negative bacteria were 32 μg/ml for *E. coli* and 64 μg/ml for *P. aeruginosa*. These compounds also inhibited drug-resistant clinical isolates of MRSA at concentrations of 32 μg/ml, 4 μg/ml and 2 μg/ml for 3, 5, and 4 respectively. Vancomycin, the current drug of choice for the treatment of MRSA, had an MIC of 1 μg/ml; while the MIC of ampicillin against MRSA was ≥512 μg/ml. Compounds 3, 4, and 5 showed MICs against VRE of 16 μg/ml, 8 μg/ml, and 4 μg/ml and respectively.

No significant effect of serum on the MICs was observed when the reference bacterial strains were tested with varying concentrations of the derivatives in the presence of 50% human serum; the values varied by only ±1 in fold dilutions. Compounds

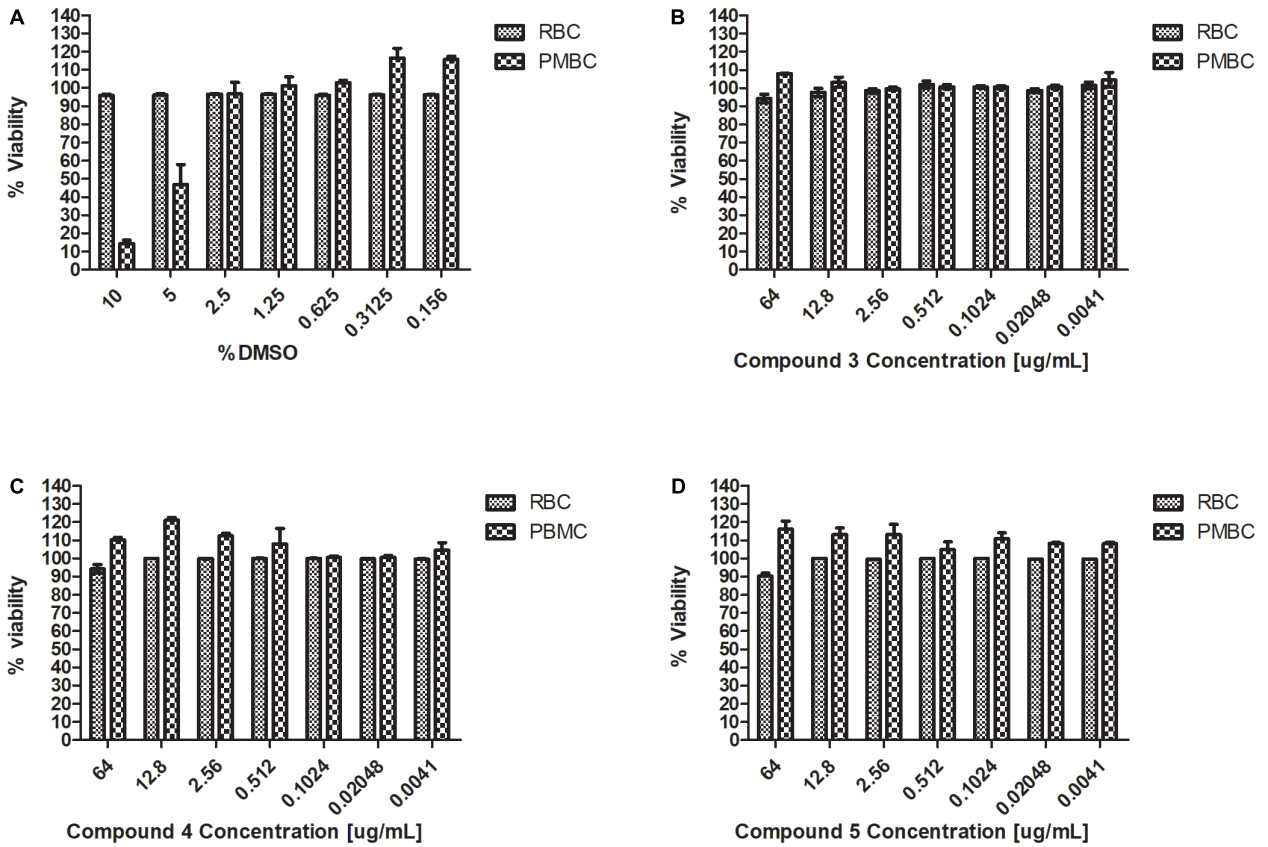

FIGURE 3 | Haemolysis and cytotoxicity effects of Teixobactin derivatives at various concentrations **(A)** Viability (%) of RBCs and PBMCs treated with DMSO; **(B)** Viability (%) of RBCs and PBMCs treated with compound 3; **(C)** Viability (%) of RBCs and PBMCs treated with compound 4; **(D)** Viability (%) of RBCs and PBMCs treated with compound 5. The experiment was performed in triplicate ($n = 3$). The error bars indicate the standard deviation. One-way ANOVA followed by Dunnett's test was performed to determine the significance relative to the RBC and PMBC ($P < 0.05$).

3, 4, and 5 demonstrated bactericidal activities, yielding a 99.9% decrease in viable cells on the agar plates at concentrations $\leq$ 4x MIC values. All the experiments were conducted in triplicate to confirm the outcomes.

Time-Kill Kinetics

Time-kill kinetic assays were performed to determine whether the Teixobactin derivatives showed time-dependent or concentration-dependent properties, as well as whether their effects were bacteriostatic or bactericidal. The time-kill curves of compound 4 against Gram-positive *S. aureus* ATCC 29213 and *B. subtilis* ATCC 6051 are shown in **Figure 2**. The kinetics indicated time- and concentration- dependent bacterial killing for this compound, and the bactericidal effect was observed at a concentration of 2x and 4x MIC levels at 6 h, as well as at 1x MIC at 24 h against *S. aureus* and *B. subtilis*. Exposure of *S. aureus* and *B. subtilis* to 4 at 2x and 4x MIC resulted in a decrease in bacterial cell count greater than 3 $\log_{10}$ relative to the initial density from 6 and 4 h respectively, which was also indicative of a bactericidal effect. At a concentration of 1x MIC, compound 4 caused a significant reduction in $\log_{10}$ CFU 6 h after its addition (**Figure 2**).

TABLE 4 | Number of frames (>1000) that lipid I oxygens was within 3.5 Å of Lys10-teixobactin (4) protons.

Oxygens of lipid II (Atom number)	Number of frames
Pyrophosphate oxygen (O14)[a]	3518
Pyrophosphate oxygen (O15)	2772
Pyrophosphate oxygen (O8)	2676
Pyrophosphate oxygen (O9)	1713
Oxygen acetyl of sugar moiety 1	1447
Ala-6 oxygen carbonyl group	1066
Glu-7 oxygen α-carboxyl group	1050

[a] *The number of the O atoms are shown in the* ***Figure 4B****.*

Haemolysis and Cytotoxicity

Haemolysis and cytotoxicity effects were evaluated by exposing RBCs and PBMCs to varying concentrations of the Teixobactin derivatives. The concentrations tested showed no cytotoxic effect on PBMCs or any hemolytic effect on erythrocytes. RBC and PBMC viability was above 90% at the highest concentration of the derivatives used in this study (64 μg/mL) (**Figure 3**).

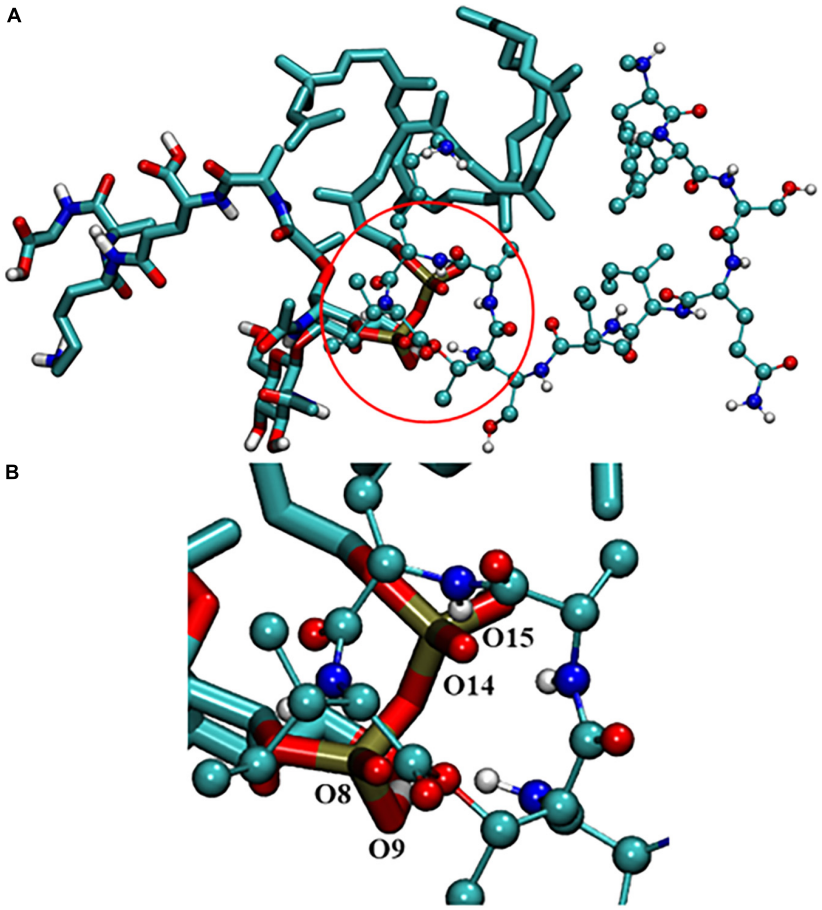

FIGURE 4 | (A) Interaction between lipid II and Lys10-teixobactin (4); **(B)** magnification of the pyrophosphate and the cycle. For clarity purposes, only polar hydrogens were shown.

Molecular Dynamics Simulation: Binding of Lys10-Teixobactin (4) With Lipid II

To understand the binding modes of Lys_{10}-teixobactin (4) with lipid II, 100 nanoseconds (ns) molecular dynamics simulations were performed. The data revealed different binding modes of Lipid II with Lys10-teixobactin (4) out of which pyrophosphate interaction with amide group proton of the cycle was the most dominant. To identify the interacting region of lipid II with Lys10-teixobactin (4), the number of frames that oxygens of lipid II is within 3.5 Å (hydrogen bonding distance) of proton atoms of Lys10-teixobactin (4) for whole simulations was calculated (**Table 4** indicates > 1000). As there are 10000 frames (10ps each), it was observed that four oxygens of pyrophosphate groups were formed the most interaction with Lys10-teixobactin (4) cycle amide group protons (**Figure 4**).

DISCUSSION

Although antibiotic resistance in Gram-positive bacteria is increasing worldwide, as indicated by the WHO list of high-priority pathogens (i.e., VRE and MRSA), much attention has shifted to combating Gram-negative bacteria. Teixobactin has been demonstrated as effective against Gram-positive bacteria and no detectable resistance has been reported yet. The capacity of Teixobactin is attributed to it being structurally distinct from glycopeptides and it being the first member of a new class of lipid II binding antibiotics.

The MICs of compounds 4 and 5 for reference strains *S. aureus* and *B. subtilis* were between 0.5 and 4 μg/ml (**Table 1**) while for the MRSA isolates they were between 2 and 4 μg/ml. Compound 3 had an MIC of 32 μg/ml, a value that was much higher than that reported for the control antibiotic vancomycin (0.5–1 μg/ml). Other groups reported compound 3 to have a MIC of 4 μg/ml against MRSA (Jin et al., 2016; Parmar et al., 2017a; Schumacher et al., 2017). These results were echoed in the present study, as the MIC observed against MRSA for this compound was between 2 and 4 μg/ml.

The MBC reported by Ling et al. (2015) was 2x the MIC of Teixobactin. The bactericidal activity of Teixobactin and its derivatives against Gram-positive bacteria is superior to that of vancomycin, and these compounds retain excellent bactericidal activity against VRE (Ling et al., 2015). The strong bactericidal activity of Teixobactin and its derivatives is attributed to not

only inhibition of peptidoglycan synthesis but also the synergistic inhibition of cell wall teichoic acid synthesis. These derivatives show the same bactericidal activity as that observed for Teixobactin and the MIC/MBC ratios were ≤4 for all the three derivatives.

Time-kill kinetic assays were carried out with compound 4 as it showed the best MICs against *S. aureus* and *B. subtilis*. Complete bactericidal activity was observed at concentrations of 16 and 8 μg/ml at 4 h. Similar to observations of other Teixobactin derivatives, compounds 3, 4, and 5 had no cytotoxic or hemolytic effect *in vitro*. In the presence of 50% serum, there was no drastic change in the MICs (**Table 1**).

On the basis of our observations, we can conclude that human serum has no effect on the antibacterial activity of compounds 3, 4, and 5. These results are similar to those observed by Parmar et al. (2017a). The serum effect is essential as it aids in speculating the probable *in vivo* activity of the drug. These derivatives will possibly have low protein binding properties because they bind to multiple target sites, none of which are proteins. The present study confirms that Teixobactin derivatives 3, 4, and 5 are safe and can thus be considered potential treatment options against resistant bacterial infections (VRE and MRSA).

Interestingly, we observed that, at higher concentrations, 3, 4, and 5 were also active against Gram-negative bacteria (**Table 1**). This is a relevant observation given the low toxicity of these compounds. These derivatives may exert their activity against Gram-negative bacteria by disrupting the outer membrane layer. In conclusion, we have demonstrated the highly potent antimicrobial activity of three Teixobactin derivatives against clinically significant isolates of bacteria. Unlike vancomycin, these derivatives showed early stage killing kinetics.

Due to the lack of crystallography or NMR data of the complex lipid II-teixobactin, until now it has not been possible to establish the interaction of teixobactin residues with lipid II experimentally. However, Lewis and co-workers (Ling et al., 2015) have hypothesized that lipid II pyrophosphate group and *N*-acetylmuramic acid are essential for the binding to teixobactin. This was further supported by recent MD simulation study of Liu et al. (2017) that showed the importance of the participation of the oxygens of pyrophosphate group of lipid II with amide protons of the teixobactin cycle. In the MD simulation study carried out herein, similar interactions were also observed with Lys10-teixobactin (4) and pyrophosphate of lipid II (**Table 4** and **Figure 4**). These data suggest that the most dominant binding mode of Lys10-teixobactin (4) to lipid II is through the amide protons of the cycle, which is identical to data described in the literature for the natural teixobactin hence predicting the possibility of a similar mechanism of action.

Given these promising results, further research should address the mechanism/s of action exerted by these compounds. The findings of this study will contribute to the development of other Teixobactin derivatives with high potent antimicrobial activity against resistant bacterial strains and to the development of novel peptide-based antimicrobial agents to tackle the global threat of drug resistance.

AUTHOR CONTRIBUTIONS

ER, AS, SM, DA, BT, and FA conceived and designed the experiments. ER, AS, SM, DA, HK, and NA performed the experiments. ER, AS, DA, RP, HK, and NA analyzed the data. RP, BT, FA, and LB contributed to reagents, materials, and analysis tools. ER wrote the paper. All authors did a critical revision of the manuscript.

FUNDING

This study was supported by College of Health Sciences, University of KwaZulu-Natal, Durban, South Africa, and the South African National Research Foundation (NRF) (Grant number: 103107).

ACKNOWLEDGMENTS

We would like to thank the Center for High-Performance Computing (CHPC), Cape Town for supercomputing resources.

REFERENCES

Abdel Monaim, S. A., Jad, Y. E., Ramchuran, E. J., El-Faham, A., Acosta, G. A., Naicker, T., et al. (2016a). Re-evaluation of the N-terminal substitution and the D-residues of teixobactin. *RSC Adv.* 6, 73827–73829. doi: 10.1039/C6RA17720D

Abdel Monaim, S. A., Jad, Y. E., Ramchuran, E. J., El-Faham, A., Govender, T., Kruger, H. G., et al. (2016b). Lysine scanning of Arg10–teixobactin: deciphering the role of hydrophobic and hydrophilic residues. *ACS Omega* 1, 1262–1265. doi: 10.1021/acsomega.6b00354

Abdel Monaim, S. A., Ramchuran, E. J., El-Faham, A., Albericio, F., and De La Torre, B. G. (2017). Converting teixobactin into a cationic antimicrobial peptide (AMP). *J. Med.Chem.* 60, 7476–7482. doi: 10.1021/acs.jmedchem.7b00834

Abraham, M. J., Murtola, T., Schulz, R., Páll, S., Smith, J. C., Hess, B., et al. (2015). GROMACS: high performance molecular simulations through multi-level parallelism from laptops to supercomputers. *SoftwareX* 1, 19–25. doi: 10.1016/j.softx.2015.06.001

Araújo, L. C. C., Aguiar, J. S., Napoleão, T. H., Mota, F. V. B., Barros, A. L. S., Moura, M. C., et al. (2013). Evaluation of cytotoxic and anti-inflammatory activities of extracts and lectins from *Moringa oleifera* seeds. *PLoS One* 8:e81973. doi: 10.1371/journal.pone.0081973

Azumah, R., Dutta, J., Somboro, A., Ramtahal, M., Chonco, L., Parboosing, R., et al. (2016). In vitro evaluation of metal chelators as potential metallo-β-lactamase inhibitors. *J. Appl. Microbiol.* 120, 860–867. doi: 10.1111/jam.13085

Bixon, M., and Lifson, S. (1967). Potential functions and conformations in cycloalkanes. *Tetrahedron* 23, 769–784. doi: 10.1016/0040-4020(67)85023-3

Brown, E. D., and Wright, G. D. (2016). Antibacterial drug discovery in the resistance era. *Nature* 529, 336–343. doi: 10.1038/nature17042

Clinical and Laboratory Standards Institute (2017). *Performance Standards for Antimicrobial Susceptibility Testing: 27th edition Informational Supplement M100–S27*. Wayne, PA: CLSI.

Darden, T., York, D., and Pedersen, L. (1993). Particle mesh Ewald: an N log (N) method for Ewald sums in large systems. *J. Chem. Phys.* 98, 10089–10092. doi: 10.1063/1.464397

Dhara, S., Gunjal, V. B., Handore, K. L., and Srinivasa Reddy, D. (2016). Solution-phase synthesis of the macrocyclic core of teixobactin. *Eur. J. Org. Chem.* 2016, 4289–4293. doi: 10.1002/ejoc.201600778

Fang, X., Chen, H., Xu, L., Jiang, X., Wu, W., and Kong, J. (2012). A portable and integrated nucleic acid amplification microfluidic chip for identifying bacteria. *Lab Chip* 12, 1495–1499. doi: 10.1039/c2lc40055c

Giltrap, A. M., Dowman, L. J., Nagalingam, G., Ochoa, J. L., Linington, R. G., Britton, W. J., et al. (2016). Total synthesis of teixobactin. *Org. Lett.* 18, 2788–2791. doi: 10.1021/acs.orglett.6b01324

Hamilton, W. L., and Wenlock, R. (2016). Antimicrobial resistance: a major threat to public health. *Cambridge Med. J.* doi: 10.7244/cmj.2016.01.001

Homma, T., Nuxoll, A., Gandt, A. B., Ebner, P., Engels, I., Schneider, T., et al. (2016). Dual targeting of cell wall precursors by teixobactin leads to cell lysis. *Antimicrob. Agents Chemother.* 60, 6510–6517. doi: 10.1128/AAC.01050-16

Humphrey, W., Dalke, A., and Schulten, K. (1996). VMD: visual molecular dynamics. *J. Mol. Graph.* 14, 33–38. doi: 10.1016/0263-7855(96)00018-5

Jad, Y. E., Acosta, G. A., Naicker, T., Ramtahal, M., El-Faham, A., Govender, T., et al. (2015). Synthesis and biological evaluation of a teixobactin analogue. *Org. Lett.* 17, 6182–6185. doi: 10.1021/acs.orglett.5b03176

Jayamani, E., Tharmalingam, N., Rajamuthiah, R., Coleman, J. J., Kim, W., Okoli, I., et al. (2017). Characterization of a *Francisella tularensis-Caenorhabditis elegans* pathosystem for the evaluation of therapeutic compounds. *Antimicrob. Agents Chemother.* 61, e310-17. doi: 10.1128/AAC.00310-17

Jin, K., Po, K. H. L., Wang, S., Reuven, J. A., Wai, C. N., Lau, H. T., et al. (2017). Synthesis and structure-activity relationship of teixobactin analogues via convergent Ser ligation. *Bioorg. Med. Chem.* 25, 4990–4995. doi: 10.1016/j.bmc.2017.04.039

Jin, K., Sam, I. H., Po, K. H. L., Lin, D. A., Ghazvini Zadeh, E. H., Chen, S., et al. (2016). Total synthesis of teixobactin. *Nat. Commun.* 7:12394. doi: 10.1038/ncomms12394

Kaeberlein, T., Lewis, K., and Epstein, S. S. (2002). Isolating" uncultivable" microorganisms in pure culture in a simulated natural environment. *Science* 296, 1127–1129. doi: 10.1126/science.1070633

Lewis, K. (2012). Antibiotics: recover the lost art of drug discovery. *Nature* 485, 439–440. doi: 10.1038/485439a

Ling, L. L., Schneider, T., Peoples, A. J., Spoering, A. L., Engels, I., Conlon, B. P., et al. (2015). A new antibiotic kills pathogens without detectable resistance. *Nature* 517, 455–459. doi: 10.1038/nature14098

Liu, Y., Liu, Y., Chan-Park, M. B., and Mu, Y. (2017). Binding modes of teixobactin to lipid II: molecular dynamics study. *Sci. Rep.* 7:17197. doi: 10.1038/s41598-017-17606-5

Malde, A. K., Zuo, L., Breeze, M., Stroet, M., Poger, D., Nair, P. C., et al. (2011). An automated force field topology builder (ATB) and repository: version 1.0. *J. Chem. Theory Comput.* 7, 4026–4037. doi: 10.1021/ct200196m

Mark, P., and Nilsson, L. (2001). Structure and dynamics of the TIP3P, SPC, and SPC/E water models at 298 K. *J. Phys. Chem. A* 105, 9954–9960. doi: 10.1021/jp003020w

Monaim, S. A., Noki, S., Ramchuran, E. J., El-Faham, A., Albericio, F., and Torre, B. G. (2017). Investigation of the N-terminus amino function of Arg10-teixobactin. *Molecules* 22:E1632. doi: 10.3390/molecules22101632

Nichols, D., Cahoon, N., Trakhtenberg, E., Pham, L., Mehta, A., Belanger, A., et al. (2010). Use of ichip for high-throughput in situ cultivation of "uncultivable" microbial species. *Appl. Environ. Microbiol.* 76, 2445–2450. doi: 10.1128/AEM.01754-09

Pannecouque, C., Daelemans, D., and De Clercq, E. (2008). Tetrazolium-based colorimetric assay for the detection of HIV replication inhibitors: revisited 20 years later. *Nat. Protoc.* 3, 427–434. doi: 10.1038/nprot.2007.517

Parmar, A., Iyer, A., Lloyd, D. G., Vincent, C. S., Prior, S. H., Madder, A., et al. (2017a). Syntheses of potent teixobactin analogues against methicillin-resistant *Staphylococcus aureus* (MRSA) through the replacement of l-allo-enduracididine with its isosteres. *Chem. Commun.* 53, 7788–7791. doi: 10.1039/c7cc04021k

Parmar, A., Prior, S. H., Iyer, A., Vincent, C. S., Van Lysebetten, D., Breukink, E., et al. (2017b). Defining the molecular structure of teixobactin analogues and understanding their role in antibacterial activities. *Chem. Commun.* 53, 2016–2019. doi: 10.1039/c6cc09490b

Parmar, A., Iyer, A., Vincent, C. S., Van Lysebetten, D., Prior, S. H., Madder, A., et al. (2016). Efficient total syntheses and biological activities of two teixobactin analogues. *Chem. Commun.* 52, 6060–6063. doi: 10.1039/c5cc10249a

Parrinello, M., and Rahman, A. (1981). Polymorphic transitions in single crystals: a new molecular dynamics method. *J. Appl. Phys.* 52, 7182–7190. doi: 10.1063/1.328693

Penesyan, A., Gillings, M., and Paulsen, I. T. (2015). Antibiotic discovery: combatting bacterial resistance in cells and in biofilm communities. *Molecules* 20, 5286–5298. doi: 10.3390/molecules20045286

Piddock, L. J. (2015). Teixobactin, the first of a new class of antibiotics discovered by iChip technology? *J. Antimicrob. Chemother.* 70, 2679–2680. doi: 10.1093/jac/dkv175

Pinto, M. C., Dias, D. F., Del Puerto, H. L., Martins, A. S., Teixeira-Carvalho, A., Martins-Filho, O. A., et al. (2011). Discovery of cytotoxic and pro-apoptotic compounds against leukemia cells: tert-butyl-4-[(3-nitrophenoxy) methyl]-2, 2-dimethyloxazolidine-3-carboxylate. *Life Sci.* 89, 786–794. doi: 10.1016/j.lfs.2011.09.012

Schumacher, C. E., Harris, P. W., Ding, X.-B., Krause, B., Wright, T. H., Cook, G. M., et al. (2017). Synthesis and biological evaluation of novel teixobactin analogues. *Org. Biomol. Chem.* 15, 8755–8760. doi: 10.1039/c7ob02169k

Tramer, F., Da Ros, T., and Passamonti, S. (2012). Screening of fullerene toxicity by hemolysis assay. *Methods Mol. Biol.* 926, 203–217. doi: 10.1007/978-1-62703-002-1_15

Vanommeslaeghe, K., Hatcher, E., Acharya, C., Kundu, S., Zhong, S., Shim, J., et al. (2010). CHARMM general force field: a force field for drug like molecules compatible with the CHARMM all atom additive biological force fields. *J. Comput. Chem.* 31, 671–690. doi: 10.1002/jcc.21367

von Nussbaum, F., and Süssmuth, R. D. (2015). Multiple attack on bacteria by the new antibiotic teixobactin. *Angew. Chem. Int. Ed. Engl.* 54, 6684–6686. doi: 10.1002/anie.201501440

Wang, D., Zhang, W., Wang, T., Li, N., Mu, H., Zhang, J., et al. (2015). Unveiling the mode of action of two antibacterial tanshinone derivatives. *Int. J. Mol. Sci.* 16, 17668–17681. doi: 10.3390/ijms160817668

Wu, C., Pan, Z., Yao, G., Wang, W., Fang, L., and Su, W. (2017). Synthesis and structure–activity relationship studies of teixobactin analogues. *RSC Adv.* 7, 1923–1926. doi: 10.1039/C6RA26567G

Yang, H., Chen, K. H., and Nowick, J. S. (2016). Elucidation of the teixobactin pharmacophore. *ACS Chem. Biol.* 11, 1823–1826. doi: 10.1021/acschembio.6b00295

Yang, H., Du Bois, D., Ziller, J., and Nowick, J. (2017). X-ray crystallographic structure of a teixobactin analogue reveals key interactions of the teixobactin pharmacophore. *Chem. Commun.* 53, 2772–2775. doi: 10.1039/c7cc00783c

Zheng, Z., Tharmalingam, N., Liu, Q., Jayamani, E., Kim, W., Fuchs, B. B., et al. (2017). Synergistic efficacy of *Aedes aegypti* antimicrobial peptide cecropin A2 and tetracycline against *Pseudomonas aeruginosa*. *Antimicrob. Agents Chemother.* 61, e686-17. doi: 10.1128/AAC.00686-17

Conflict of Interest Statement: The authors declare that the research was conducted in the absence of any commercial or financial relationships that could be construed as a potential conflict of interest.

frontiers in Microbiology

ORIGINAL RESEARCH
published: 12 April 2018
doi: 10.3389/fmicb.2018.00721

Novel Polymyxin Combination With Antineoplastic Mitotane Improved the Bacterial Killing Against Polymyxin-Resistant Multidrug-Resistant Gram-Negative Pathogens

*Thien B. Tran[1,2], Jiping Wang[1,2], Yohei Doi[3], Tony Velkov[2,4], Phillip J. Bergen[2,5] and Jian Li[1]**

[1] Monash Biomedicine Discovery Institute, Department of Microbiology, School of Biomedical Sciences, Faculty of Medicine, Nursing and Health Sciences, Monash University, Melbourne, VIC, Australia, [2] Drug Delivery, Disposition and Dynamics, Monash Institute of Pharmaceutical Sciences, Monash University, Melbourne, VIC, Australia, [3] Division of Infectious Diseases, Department of Medicine, University of Pittsburgh Medical Center, Pittsburgh, PA, United States, [4] Department of Pharmacology and Therapeutics, School of Biomedical Sciences, Faculty of Medicine, Dentistry and Health Sciences, The University of Melbourne, Melbourne, VIC, Australia, [5] Centre for Medicine Use and Safety, Monash Institute of Pharmaceutical Sciences, Monash University, Melbourne, VIC, Australia

OPEN ACCESS

Edited by:
Maria Olivia Pereira,
University of Minho, Portugal

Reviewed by:
Vishvanath Tiwari,
Central University of Rajasthan, India
Govindan Rajamohan,
Institute of Microbial Technology (CSIR), India

***Correspondence:**
Jian Li
jian.li@monash.edu

Specialty section:
This article was submitted to Antimicrobials, Resistance and Chemotherapy, a section of the journal Frontiers in Microbiology

Received: 26 October 2017
Accepted: 27 March 2018
Published: 12 April 2018

Citation:
Tran TB, Wang J, Doi Y, Velkov T, Bergen PJ and Li J (2018) Novel Polymyxin Combination With Antineoplastic Mitotane Improved the Bacterial Killing Against Polymyxin-Resistant Multidrug-Resistant Gram-Negative Pathogens. Front. Microbiol. 9:721. doi: 10.3389/fmicb.2018.00721

Due to limited new antibiotics, polymyxins are increasingly used to treat multidrug-resistant (MDR) Gram-negative bacteria, in particular carbapenem-resistant *Acinetobacter baumannii*, *Pseudomonas aeruginosa*, and *Klebsiella pneumoniae*. Unfortunately, polymyxin monotherapy has led to the emergence of resistance. Polymyxin combination therapy has been demonstrated to improve bacterial killing and prevent the emergence of resistance. From a preliminary screening of an FDA drug library, we identified antineoplastic mitotane as a potential candidate for combination therapy with polymyxin B against polymyxin-resistant Gram-negative bacteria. Here, we demonstrated that the combination of polymyxin B with mitotane enhances the *in vitro* antimicrobial activity of polymyxin B against 10 strains of *A. baumannii*, *P. aeruginosa*, and *K. pneumoniae*, including polymyxin-resistant MDR clinical isolates. Time-kill studies showed that the combination of polymyxin B (2 mg/L) and mitotane (4 mg/L) provided superior bacterial killing against all strains during the first 6 h of treatment, compared to monotherapies, and prevented regrowth and emergence of polymyxin resistance in the polymyxin-susceptible isolates. Electron microscopy imaging revealed that the combination potentially affected cell division in *A. baumannii*. The enhanced antimicrobial activity of the combination was confirmed in a mouse burn infection model against a polymyxin-resistant *A. baumannii* isolate. As mitotane is hydrophobic, it was very likely that the synergistic killing of the combination resulted from that polymyxin B permeabilized the outer membrane of the Gram-negative bacteria and allowed mitotane

to enter bacterial cells and exert its antimicrobial effect. These results have important implications for repositioning non-antibiotic drugs for antimicrobial purposes, which may expedite the discovery of novel therapies to combat the rapid emergence of antibiotic resistance.

Keywords: polymyxin, mitotane, repurposing, combination therapy, multidrug-resistance

INTRODUCTION

The emergence of Gram-negative bacteria with resistance to multiple classes of antibiotics is causing serious problems for health care centers worldwide (Boucher et al., 2013). Infections caused by multidrug-resistant (MDR) Gram-negative bacteria not only have higher mortality rates (Harris et al., 2015) but also lead to more economic burden than infections caused by susceptible Gram-negative bacteria (Gandra et al., 2014). Among these MDR Gram-negative bacteria, carbapenem-resistant *Acinetobacter baumannii* has been identified as one of the most difficult-to-treat pathogens and is becoming increasingly problematic for critically ill patients and war-wounded soldiers (Davis et al., 2005; Gupta et al., 2006; Peleg et al., 2008; Centers for Disease Control and Prevention [CDC], 2013). *A. baumannii* possesses numerous mechanisms of carbapenem resistance (Tiwari et al., 2012a,b; Tiwari and Moganty, 2014; Roy et al., 2017; Verma et al., 2017), and can cause a wide range of infections including pneumonia, urinary tract and wound infections, bacteremia, and meningitis (Gupta et al., 2006; Maragakis and Perl, 2008; Tiwari et al., 2012a). More recently, the World Health Organization (WHO) has classified carbapenem-resistant *A. baumannii*, *Pseudomonas aeruginosa*, and Enterobacteriaceae as the top priorities for research and development of new antibiotics (Tacconelli and Magrini, 2017).

Due to the current lack of effective antibiotics against MDR Gram-negative bacteria, the polymyxins (colistin and polymyxin B) have been revived as antibiotics of last resort (Li et al., 2006; Nation et al., 2015). However, resistance to polymyxins is on the rise (Marchaim et al., 2011; Kim et al., 2014; Goli et al., 2016) and a growing body of evidence suggests that resistance to polymyxins can emerge with monotherapy (Tam et al., 2005; Tan et al., 2007; Bergen et al., 2011; Meletis et al., 2011; Deris et al., 2012; Hermes et al., 2013; Lee et al., 2013; Ly et al., 2015; Lenhard et al., 2017; Zhao et al., 2017). *In vitro* studies have revealed that polymyxin resistance may occur within 24 h after colistin or polymyxin B monotherapy (Bergen et al., 2011; Deris et al., 2012; Tran et al., 2016). The two main mechanisms of polymyxin resistance identified in Gram-negative bacteria are lipid A modifications and loss of LPS (Moffatt et al., 2010; Arroyo et al., 2011).

Unfortunately, the *de novo* drug discovery and development process is lengthy (usually 10–17 years) and has a low success rate (<10%; Ashburn and Thor, 2004). With limited new antibiotics in the pipeline, an approach to expedite the discovery process is through the repositioning of non-antibiotic FDA-approved drugs. This process can be as short as 3 years as these drugs have already passed the FDA safety requirements and have well-defined pharmacokinetics (Ashburn and Thor, 2004). In light of the dire resistance problem, we screened an FDA drugs' library to identify potential synergistic candidates with polymyxins for the treatment of MDR Gram-negative bacteria. Our screening identified FDA-approved antineoplactic mitotane as a highly potential non-antibiotic candidate for combination therapy with polymyxin B. In this study, we evaluated the *in vitro* antimicrobial activity of the combination of polymyxin B and mitotane against highly resistant clinical isolates of Gram-negative bacteria including carbapenem-resistant *A. baumannii*, carbapenem-resistant *P. aeruginosa*, and New Delhi metallo-β-lactamase (NDM)-producing *Klebsiella pneumoniae*. Our findings highlight the potential of this novel polymyxin/non-antibiotic combination for treatment of these problematic Gram-negative "superbugs".

MATERIALS AND METHODS

Bacterial Isolates

Ten bacterial strains which included multidrug- and polymyxin-resistant isolates were examined in this study (**Table 1**). *A. baumannii* ATCC 17978, *A. baumannii* ATCC 19606, *K. pneumoniae* ATCC 13883, and *P. aeruginosa* ATCC 27853 were obtained from the American Type Culture Collection (Rockville, MD, United States). *A. baumannii* FADDI-AB225 (formally designated ATCC 17978-R2) is a polymyxin-resistant *pmrB* mutant (due to phosphoethanolamine-modified lipid A) derived from ATCC 17978 (Arroyo et al., 2011). *A. baumannii* FADDI-AB065 (formally designated ATCC 19606R) is a polymyxin-resistant, LPS-deficient, *lpxA* mutant derived from ATCC 19606 (Moffatt et al., 2010). Polymyxin-susceptible *A. baumannii* FADDI-AB180 (formally designated 2949) and lipid A modified (with phosphoethanolamine and galactosamine) polymyxin-resistant *A. baumannii* FADDI-AB181 (formally designated 2949A) are carbapenem-resistant MDR clinical isolates from the bronchoalveolar lavage fluid of a patient before and after colistin therapy (Pelletier et al., 2013). *P. aeruginosa* FADDI-PA070 is a non-mucoid, MDR (including carbapenem- and polymyxin-resistant) clinical isolate from the sputum of a patient with cystic fibrosis (formally designated 19147 n/m; Bergen et al., 2011). *K. pneumoniae* FADDI-KP027 is a polymyxin-resistant, NDM-producing clinical isolate from the sputum of a patient with respiratory tract infection. Isolates were stored in tryptone soy broth (Oxoid) with 20% glycerol (Ajax Finechem, Seven Hills, NSW, Australia) in cryovials at −80°C and subcultured onto nutrient agar plates (Media Preparation Unit, University of Melbourne, Melbourne, VIC, Australia) before use.

TABLE 1 | Minimum inhibitory concentrations (MICs) for polymyxin B and mitotane against bacterial isolates examined in this study.

Bacterial isolate (former nomenclature)	MIC (mg/L)			
	Polymyxin B	Mitotane	Mitotane in the presence of 2 mg/L polymyxin B	Polymyxin susceptibility and mechanism of resistance
A. baumannii ATCC 17978	0.25	>128	–	Susceptible
A. baumannii FADDI-AB225 (ATCC 17978-R2)^{PR}	16	>128	4	Lipid A modification
A. baumannii ATCC 19606	0.5	>128	–	Susceptible
A. baumannii FADDI-AB065 (ATCC 19606R)^{PR}	64	4	4	LPS loss
A. baumannii FADDI-AB180 (2949)^{MDR}	1	>128	–	Susceptible
A. baumannii FADDI-AB181 (2949A)^{MDR,PR}	64	>128	4	Lipid A modification
P. aeruginosa ATCC 27853	0.5	>128	–	Susceptible
P. aeruginosa FADDI-PA070 (19147 n/m)^{MDR,PR}	64	>128	4	Uncharacterized
K. pneumoniae ATCC 13883	0.5	>128	–	Susceptible
K. pneumoniae FADDI-KP027^{MDR,PR}	256	>128	4	Uncharacterized

^{MDR}, multidrug-resistant: defined as non-susceptible to ≥1 treating agent in ≥3 antimicrobial categories (Magiorakos et al., 2012). ^{PR}, polymyxin resistant: defined as an MIC of ≥4 mg/L for Acinetobacter spp. and ≥8 mg/L for P. aeruginosa as per CLSI guideline (Clinical and Laboratory Standards Institute [CLSI], 2016); and >2 mg/L for Enterobacteriaceae as per EUCAST guidelines (The European Committee on Antimicrobial Susceptibility Testing [EUCAST], 2017); and mitotane breakpoints are not available. –, Not performed.

Antimicrobial Agents and Susceptibility Testing

Polymyxin B (Beta Pharma, China; batch number 20120204) solutions were prepared in Milli-Q water (Millipore, North Ryde, NSW, Australia) and sterilized using a 0.20-μm cellulose acetate syringe filter (Millipore, Bedford, MA, United States). Mitotane (Sigma-Aldrich, Australia; lot number BCBG9480V) solutions were prepared in dimethyl sulfoxide (DMSO; Sigma-Aldrich, Australia). Stock solutions were stored at −20°C for no longer than 1 month. The minimum inhibitory concentrations (MICs) to polymyxin B and mitotane were determined for all isolates in three replicates on separate days using broth microdilution with cation-adjusted Mueller–Hinton broth (CAMHB; Oxoid, England; 20–25 mg/L Ca^{2+} and 10–12.5 mg/L Mg^{2+}) according to the Clinical and Laboratory Standards Institute guidelines (Clinical and Laboratory Standards Institute [CLSI], 2016). Stock solutions of polymyxin B were diluted to the desired concentrations in CAMHB, while mitotane was initially prepared in DMSO and subsequently in CAMHB to obtain the desired drug concentrations with 10% DMSO (v/v). The procedure to measure the MICs of polymyxin B and mitotane was adapted from our previous method (Tran et al., 2016). Briefly, 100 μL of the bacterial suspension (10^6 cfu/mL) was combined with 100 μL of the prepared polymyxin B solutions or 50 μL of CAMHB plus 50 μL of the prepared mitotane solutions in 96-well microtiter plates (Techno Plas, St Marys, SA, Australia). For mitotane MICs, the final concentration of 2.5% DMSO (v/v) was employed, as preliminary studies demonstrated that 2.5% DMSO (v/v) had no effect on the bacterial growth. The plates were incubated standing at 37°C for 20 h and MICs were determined as the lowest drug concentrations that inhibited the visible growth of the bacteria. For polymyxin-resistant isolates, MICs of mitotane in the presence of 2 mg/L of polymyxin B were also determined. According to the CLSI guidelines, polymyxin B MIC is ≤2 mg/L for polymyxin-susceptible *A. baumannii* and *P. aeruginosa*, ≥4 mg/L for polymyxin-resistant *A. baumannii*, and ≥8 mg/L for polymyxin-resistant *P. aeruginosa* (Clinical and Laboratory Standards Institute [CLSI], 2016). For *K. pneumoniae*, breakpoints have not yet been established by the CLSI. Consequently, susceptibility to polymyxin B was extrapolated from the European Committee on Antimicrobial Susceptibility Testing (EUCAST) colistin breakpoints where susceptibility is defined as an MIC ≤2 mg/L and resistance an MIC of >2 mg/L (The European Committee on Antimicrobial Susceptibility Testing [EUCAST], 2017).

Time-Kill Studies

Time-kill studies were conducted for all isolates based on our previously described method (Tran et al., 2016). Briefly, bacteria were grown overnight in 20 mL CAMHB. The overnight broth cultures were transferred to 20 mL of fresh CAMHB at ∼50–100-fold dilutions and incubated for an additional 3–4 h to generate log-phase culture at ∼0.55 McFarland standard. The log-phase cultures were transferred to 20 mL of fresh CAMHB at ∼100-fold dilution in borosilicate glass tubes for treatment to minimize loss of drug due to non-specific binding to the plastic. For the drug-containing tubes, polymyxin B, mitotane, or both compounds were added to achieve final concentrations of 2 mg/L for polymyxin B and 4 mg/L for mitotane (the minimum concentration of mitotane identified by broth microdilution assay to inhibit to growth of polymyxin-resistant isolates in the presence of 2 mg/L polymyxin B). The final concentration of 0.4% DMSO (v/v) was achieved for all treatments; 2.5% DMSO (v/v) had no effect on bacterial growth with 2 mg/L of polymyxin B (Tran et al., 2016). Samples (1 mL) were aseptically removed at 0, 0.5, 1, 2, 4, 6, and 24 h and inoculated onto nutrient agar plates for viable-cell counting. Colonies were counted after 24 h incubation at 37°C using a ProtoCOL colony counter (Synbiosis, Cambridge, United Kingdom). The combination of polymyxin B and mitotane was considered synergistic if the bacterial killing was ≥2 $\log_{10}$ compared to the most active

monotherapy (Pillai et al., 2005). Changes to polymyxin B MICs were determined for all cultures that showed regrowth after 24 h to evaluate the emergence of polymyxin resistance.

Phase Contrast, Scanning Electron, and Transmission Electron Microscopy

Phase contrast microscopy, scanning electron microscopy (SEM), and transmission electron microscopy (TEM) were employed to examine the effect of the polymyxin B/mitotane combination on the cellular morphology of polymyxin-susceptible *A. baumannii* ATCC 17978 and polymyxin-resistant *A. baumannii* FADDI-AB225. Bacteria were subcultured and treated with 2 mg/L polymyxin B, 4 mg/L mitotane, or both antibiotics for 2 h in CAMHB as per the time-kill studies. For phase contrast microscopy, 20 μL of each culture was used to prepare wet samples for instant observation on a phase contrast microscope. For the SEM and TEM studies, samples were transferred to 50-mL polypropylene tubes (Greiner Bio-One, Frickenhausen, Germany) and centrifuged at 3220 × *g* for 10 min three times. Between centrifugation steps, supernatants were discarded and bacterial pellets resuspended and washed in 1 mL phosphate buffered saline (PBS). Following the final centrifugation step, the supernatants were removed and bacterial pellets resuspended and fixed in 0.5 mL 2.5% glutaraldehyde in PBS. The tubes were left in a rocker shaker for 20 min at room temperature. Once fixed, tubes were centrifuged at 3220 × *g* for 10 min, the fixatives removed, and bacterial pellets washed twice in 1 mL PBS as above. Pellets were finally resuspended in 1 mL PBS, and SEM and TEM were conducted at the Department of Botany, University of Melbourne, Australia.

Mouse Burn Wound Infection Model

A mouse burn wound infection model was employed to assess the *in vivo* antimicrobial activity of the polymyxin B/mitotane combination against polymyxin-resistant *A. baumannii* FADDI-AB225. Bacterial inoculums were prepared with early log-phase culture. After centrifugation at 3220 × *g* for 10 min, the supernatant was removed and bacterial cell pellets were suspended in 0.9% saline to approximately 10^9 cfu/mL. Bacterial samples (100 μL) were then loaded into 29-G 0.3-mL insulin syringes for inoculation of burn wounds. Drug solutions were prepared by initially dissolving mitotane in polyethylene glycol (PEG) 200 to ∼4,096 mg/L and polymyxin B in 0.9% saline to ∼1,536 mg/L. An equal amount of the two drug solutions was later combined to produce the combination solution with ∼2,048 mg/L mitotane and 768 mg/L polymyxin B. For mitotane monotherapy, mitotane solution was combined with an equal volume of 0.9% saline. For polymyxin B monotherapy, polymyxin B was combined with an equal volume of PEG 200. For solvent controls, equal volumes of blank PEG 200 and 0.9% saline were combined. Prior to infection, female NIH Swiss mice (6–10 weeks old, ∼30 g body weight) were sedated with isoflurane and anesthesia was maintained throughout the entire procedure. Hair from the mouse dorsal skin was removed and the local skin area was injected with 100 μL of Bupivacaine (Marcaine 0.5%). A burn wound was established with a hot iron bolt from boiling water and bacteria injected into the burn eschar. After 2 h, different treatments were applied topically by evenly spreading 200 μL of the drug solutions across the wounds of groups of four mice. This study included five groups of four mice comprising blank control (no treatment), solvent control, polymyxin B monotherapy, mitotane monotherapy, and the combination (polymyxin B and mitotane). Each wound of the treated groups received 154 μg of polymyxin B (0.5%, w/w), 410 μg of mitotane (1.4%, w/w), or both. Four hours after treatment, mice were sacrificed and the burn wound skin tissues and the muscle tissue (∼0.3 g) under the burn wounds were aseptically removed and placed separately into 8 mL of sterile saline in 50-mL Falcon tubes. Burn wound skin tissues were homogenized under sterile conditions and filtered using a filter bag (Bag Stomacher Filter Sterile, Pore Size 280 micrometer, 0.5 cm × 16 cm, Labtek Pty Ltd.). Filtrate (1 mL) was then transferred into a sterile test tube for serial dilution and 100 μL was cultured onto nutrient agar for viable counting. Viable counts were performed on the next day following overnight incubation at 37°C. Statistical significance for the bacterial killing of different treatment groups was calculated with one-way ANOVA and Tukey's multiple comparisons (Tukey's HSD).

RESULTS

MICs of Polymyxin B and Mitotane Against Polymyxin-Susceptible and -Resistant Isolates of *A. baumannii*, *P. aeruginosa*, and *K. pneumoniae*

The polymyxin B and mitotane MICs against all 10 Gram-negative isolates are shown in **Table 1**. Additionally, **Table 1** shows the MICs of mitotane in the presence of 2 mg/L polymyxin B against the polymyxin-resistant isolates. Apart from *A. baumannii* FADDI-AB065, mitotane monotherapy had no antimicrobial activity at concentrations up to 128 mg/L. However, in the presence of 2 mg/L polymyxin B, 4 mg/L of mitotane was effective at inhibiting growth of five polymyxin-resistant isolates (**Table 1**).

The changes to the polymyxin B MICs of 10 examined isolates after overnight treatment with either polymyxin B monotherapy, mitotane monotherapy, or polymyxin B/mitotane combination are shown in **Table 2**. In the control group (overnight incubation in drug-free CAMHB), polymyxin B MICs of all isolates at 24 h were not affected as all values remained within two folds of the baseline MICs (European Committee for Antimicrobial Susceptibility Testing (EUCAST) of the European Society of Clinical Microbiology and Infectious Diseases (ESCMID), 2003). After treatment with polymyxin B monotherapy at 2 mg/L, polymyxin B MICs of the polymyxin-resistant isolates at 24 h remained unchanged. However, with the three polymyxin-susceptible isolates that showed regrowth at 24 h, polymyxin B MICs of the 24-h samples increased significantly (≥32 times). Following mitotane monotherapy at 4 mg/L, polymyxin B MICs remained unchanged for all polymyxin-susceptible isolates and

TABLE 2 | Changes in baseline polymyxin B MICs following overnight treatment with polymyxin B (PMB) monotherapy, mitotane (MIT) monotherapy, and polymyxin B/mitotane combination.

Bacterial isolate	Polymyxin B MICs relative to their baseline values			
	Control	PMB 2 mg/L	MIT 4 mg/L	PMB 2 mg/L + MIT 4 mg/L
A. baumannii ATCC 17978	2 × MIC	NG	2 × MIC	NG
A. baumannii FADDI-AB225	2 × MIC	2 × MIC	1/32 × MIC	1 × MIC
A. baumannii ATCC 19606	1 × MIC	32 × MIC	1 × MIC	NG
A. baumannii FADDI-AB065	1 × MIC	1 × MIC	NG	NG
A. baumannii FADDI-AB180	1 × MIC	32 × MIC	1 × MIC	NG
A. baumannii FADDI-AB181	1 × MIC	1 × MIC	2 × MIC	1 × MIC
P. aeruginosa ATCC 27853	2 × MIC	NG	1 × MIC	NG
P. aeruginosa FADDI-PA070	1 × MIC	1 × MIC	1 × MIC	1 × MIC
K. pneumoniae ATCC 13883	1/2 × MIC	64 × MIC	1/2 × MIC	NG
K. pneumoniae FADDI-KP027	1 × MIC	1 × MIC	1 × MIC	1 × MIC

NG, no growth at 24 h.

three polymyxin-resistant isolates; the polymyxin B MIC of polymyxin-resistant *A. baumannii* FADDI-AB065 at 24 h could not be determined, as it was highly susceptible to mitotane and showed no regrowth after 24 h. Interestingly, the polymyxin B MIC of polymyxin-resistant *A. baumannii* FADDI-AB225 was reduced significantly (32-fold lower than the baseline) after 24-h exposure to mitotane. In the combination treatment group, the polymyxin B MICs did not change for all four polymyxin-resistant isolates that showed regrowth after 24 h.

Time-Kill Results for Polymyxin B and Mitotane Against Polymyxin-Susceptible and -Resistant Isolates of *A. baumannii*, *P. aeruginosa*, and *K. pneumoniae*

Time-kill profiles for polymyxin B and mitotane mono- and combination therapy are shown in **Figure 1**. Against the five polymyxin-susceptible isolates, polymyxin B monotherapy (2 mg/L) showed effective bacterial killing within 6 h with a minimum of ∼3 $\log_{10}$ cfu/mL killing (FADDI-AB180) and ∼6 $\log_{10}$ cfu/mL killing for the remaining susceptible isolates; however, regrowth to control values occurred by 24 h with three isolates (**Figure 1A**). There was no bacterial killing of polymyxin-susceptible isolates with mitotane monotherapy (4 mg/L), with growth comparable to that of controls (**Figure 1A**). With the combination, bacterial counts for all five polymyxin-susceptible isolates were reduced to below the limit of detection within 0.5–1 h, with no viable colonies detected thereafter (**Figure 1A**). Against the five polymyxin-resistant isolates, 2 mg/L polymyxin B monotherapy was ineffective with growth paralleling that of the controls (**Figure 1B**). Similarly, mitotane monotherapy displayed no antimicrobial activity against four of the five isolates (**Figure 1B**). However, against *A. baumannii* FADDI-AB065 mitotane monotherapy reduced bacterial counts to below the level of detection within the first 0.5 h and prevented regrowth over 24 h. Combination treatment showed synergistic bacterial killing (i.e., >2 $\log_{10}$ reduction compared to the most active monotherapy) between 0.5 and 6 h with the remaining four isolates; interestingly, regrowth occurred at 24 h in all four cases and was close to control values in three cases (**Figure 1B**).

Impact of Polymyxin B and Mitotane Treatment on the Cellular Morphology of Polymyxin-Susceptible and -Resistant *A. baumannii*

Figure 2 shows phase contrast microscopy, SEM and TEM images of polymyxin-susceptible *A. baumannii* ATCC 17978 following treatment with polymyxin B (2 mg/L), mitotane (4 mg/L), or both. Phase contrast microscopy images showed that polymyxin B (**Figure 2B**) or mitotane (**Figure 2C**) monotherapy had minimal impacts on the overall morphology of the bacterial cells compared to the control group (**Figure 2A**); the average cell length remained approximately 2 μm in all cases. However, more clumps of cells were observed with polymyxin B monotherapy (**Figure 2B**). In combination (**Figure 2D**), polymyxin B and mitotane resulted in significantly shorter cells compared to the other groups with the average cell length reduced to approximately 1 μm. From SEM, polymyxin B monotherapy (**Figure 2F**) affected the integrity of the cell surface in polymyxin-susceptible *A. baumannii*. Without treatment (**Figure 2E**), the bacterial surface appeared even and smooth, while the surface became uneven and rough following treatment with polymyxin B (**Figure 2F**). Mitotane monotherapy (**Figure 2G**) and polymyxin B/mitotane combination therapy (**Figure 2H**) had minimal impacts on the bacterial surface, although the cell length was confirmed to be much shorter. TEM results reveal that polymyxin B monotherapy (**Figure 2J**) caused membrane blebbing. Compared to the control group (**Figure 2I**), treatment with mitotane monotherapy (**Figure 2K**) had little impact on the bacterial surface. Similar to polymyxin B monotherapy, membrane blebbing was also observed for the treatment with polymyxin B/mitotane combination (**Figure 2L**). Additionally, TEM images showed that bacterial cells treated with the polymyxin B/mitotane combination were much shorter in length and most appeared to be undergoing a cell division cycle, with evident chromosomal segregation.

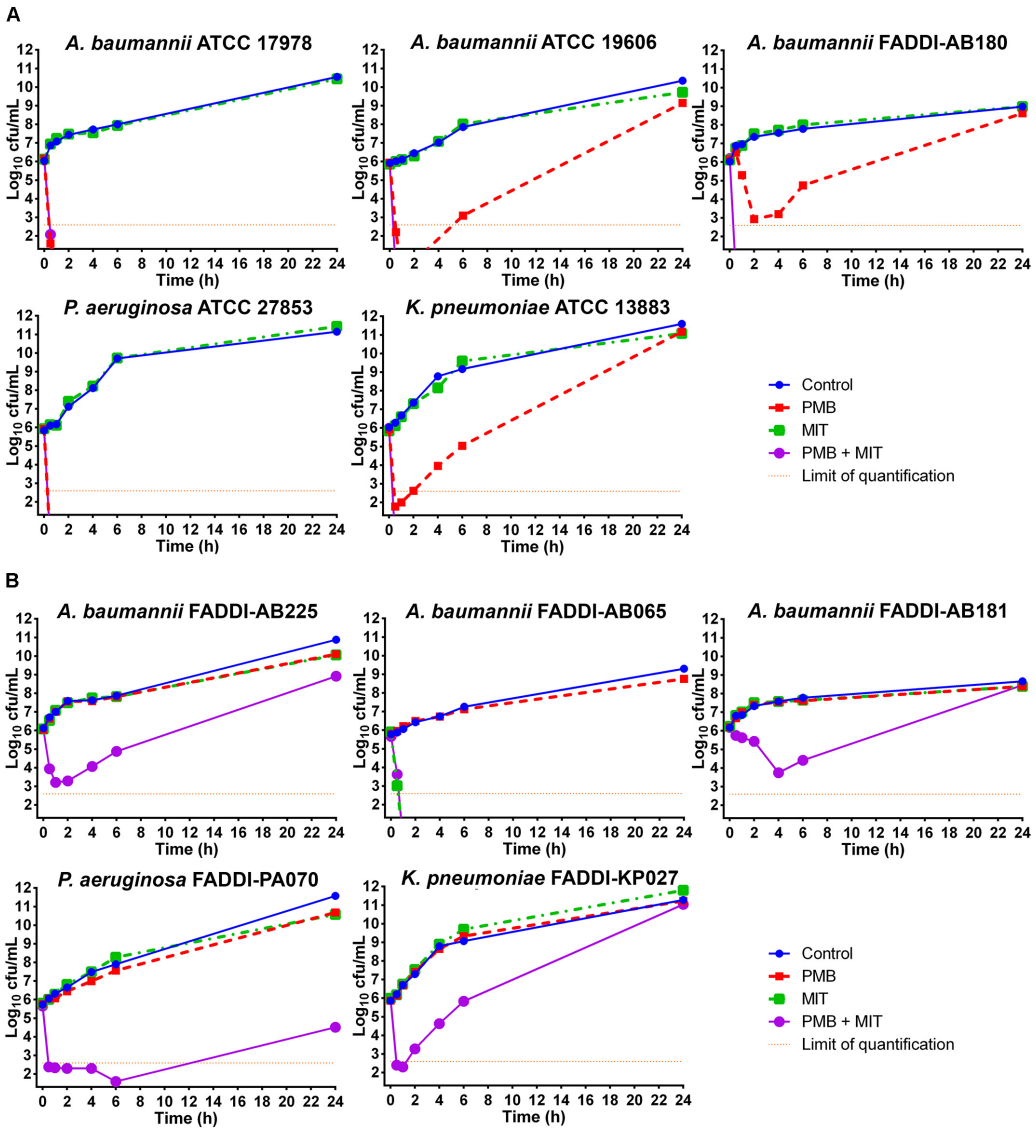

FIGURE 1 | Time-kill kinetics of polymyxin B (PMB; 2 mg/L) and mitotane (MIT; 4 mg/L) monotherapy and combination therapy against five polymyxin-susceptible Gram-negative isolates **(A)** and five polymyxin-resistant Gram-negative isolates **(B)**. The *y*-axis starts from the limit of detection and the limit of quantification is indicated by the orange dotted line.

Phase contrast microscopy, SEM, and TEM images for polymyxin-resistant *A. baumannii* FADDI-AB225 treated with polymyxin B (2 mg/L), mitotane (4 mg/L), or both are shown in **Figure 3**. Similar to the results for polymyxin-susceptible *A. baumannii* ATCC 17978, phase contrast microscopy results showed no changes in bacterial size compared to the control group (**Figure 3A**) following treatment with polymyxin B (**Figure 3B**) and mitotane (**Figure 3C**) monotherapy, while the polymyxin B/mitotane combination (**Figure 3D**) led to a significant reduction in the cell length. For SEM, treatment with polymyxin B monotherapy (**Figure 3F**) did not affect the bacterial cell surface; however, the overall structure appeared distorted. Treatment with mitotane monotherapy (**Figure 3G**) affected the cell surface of polymyxin-resistant *A. baumannii* FADDI-AB225, as the surface was more uneven and rough compared to the control group (**Figure 3E**). Combination therapy (**Figure 3H**) did not affect the membrane surface, although it led to substantial shortening of the cells. For TEM, similar results to polymyxin-susceptible isolates were once again observed. Membrane blebbing was evident in bacteria treated only with polymyxin B (**Figure 3J**), but not in those treated only with mitotane (**Figure 3K**). With the polymyxin B/mitotane combination (**Figure 3L**), most cells were substantially shorter compared to the control group (**Figure 3I**) and appeared to be going through cell division. Unlike the polymyxin-susceptible isolate, no membrane blebbing was observed with the combination in the polymyxin-resistant isolate.

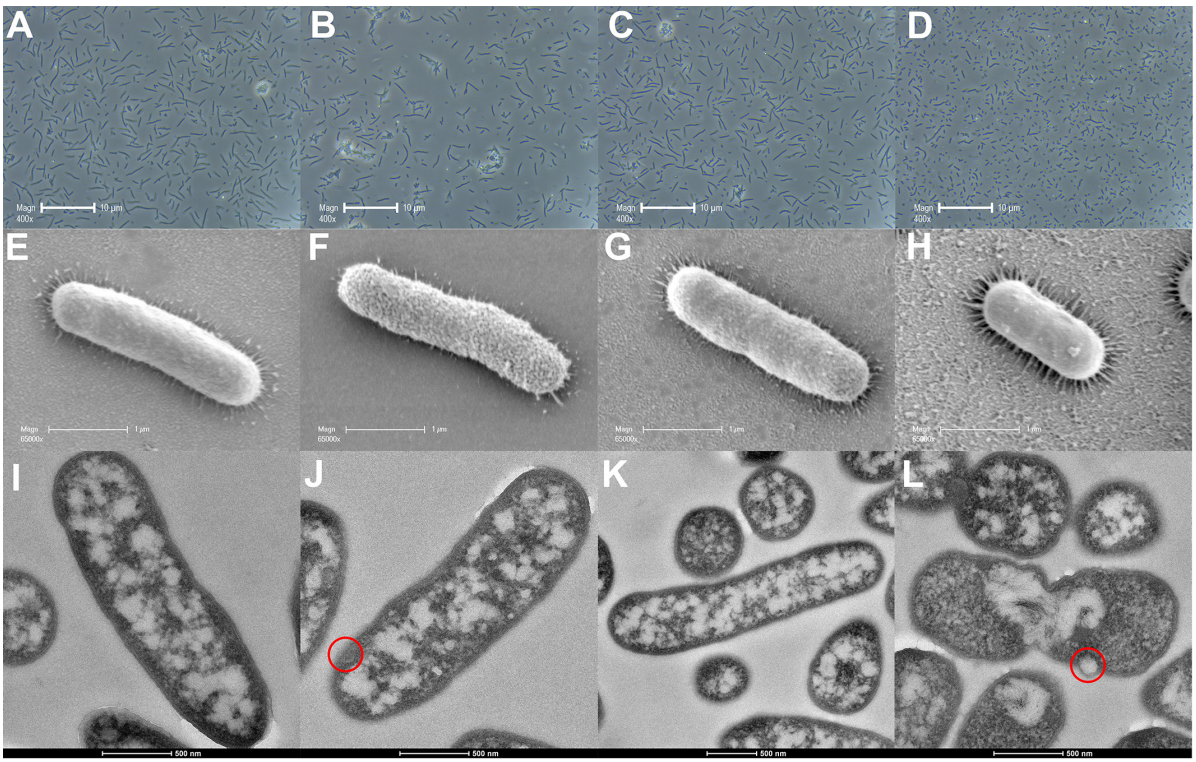

FIGURE 2 | Images from phase contrast microscopy **(A–D)**, scanning electron microscopy **(E–H)**, and transmission electron microscopy **(I–L)** for polymyxin-susceptible *A. baumannii* ATCC 17978 treated with 2 mg/L polymyxin B **(B,F,J)**, 4 mg/L mitotane **(C,G,K)**, or both **(D,H,L)**. **A**, **E**, and **I** represent the control condition. Membrane blebs are indicated by red circles.

In Vivo Antimicrobial Activity of Polymyxin B and Mitotane Against Polymyxin-Resistant *A. baumannii* FADDI-AB225 in a Mouse Burn Wound Infection Model

Figure 4 shows the bacterial killing of polymyxin B (0.5%, w/w), mitotane (1.4%, w/w), and the polymyxin B/mitotane combination against polymyxin-resistant *A. baumannii* FADDI-AB225. One-way ANOVA showed significant difference between the means of all groups ($p < 0.0001$). There was no significant difference in the bacterial load between the blank control (i.e., no treatment) and solvent control groups (mean $\log_{10}$ cfu/wound difference, −0.33; Tukey's HSD, $p > 0.05$), indicating that the solvent possessed no major antimicrobial activity. Although this isolate was polymyxin-resistant, topical polymyxin B (0.5%, w/w) monotherapy significantly reduced the bacterial load (mean $\log_{10}$ cfu/wound difference, −1.44 vs. blank control; Tukey's HSD, $p \leq 0.0001$). However, there was no significant reduction in the bacterial load (mean $\log_{10}$ cfu/wound difference, −0.11 vs. blank control; Tukey's HSD, $p > 0.5$) with topical mitotane (1.4%, w/w) alone (**Figure 4**). Importantly, both agents used in combination produced a further significant reduction in the bacterial load compared to polymyxin B monotherapy (mean $\log_{10}$ cfu/wound difference, −0.74; Tukey's HSD, $p \leq 0.01$). Compared to the blank control group, the polymyxin B/mitotane combination resulted in a mean $\log_{10}$ cfu/wound difference of −2.19 (Tukey's HSD, $p \leq 0.0001$).

DISCUSSION

Given the rapid emergence of multidrug-resistance and the limited new effective antibiotics developed over the last two decades (Boucher et al., 2009, 2013), novel approaches for the treatment of MDR Gram-negative bacteria infections are urgently needed. This is the first study to investigate the potential utility of polymyxin B in combination with the FDA-approved antineoplastic mitotane to treat infections caused by polymyxin-resistant MDR Gram-negative pathogens. Mitotane is a derivative of the insecticide dichlorodiphenyl-trichloroethane and is currently used for the treatment of adrenocortical carcinoma (ACC) (Lalli, 2015). The precise mechanism of action of mitotane in ACC is not well understood, but it has been shown to inhibit the activity of sterol-*O*-acyl-transferase and induce endoplasmic reticulum (ER) stress in ACC cells (Sbiera et al., 2015). Our study is the first to demonstrate its potential application for the treatment of Gram-negative infections when combined with polymyxin B.

To ensure the applicability of the combination of polymyxin B and mitotane to a diverse population of problematic Gram-negative bacteria, three Gram-negative bacterial species

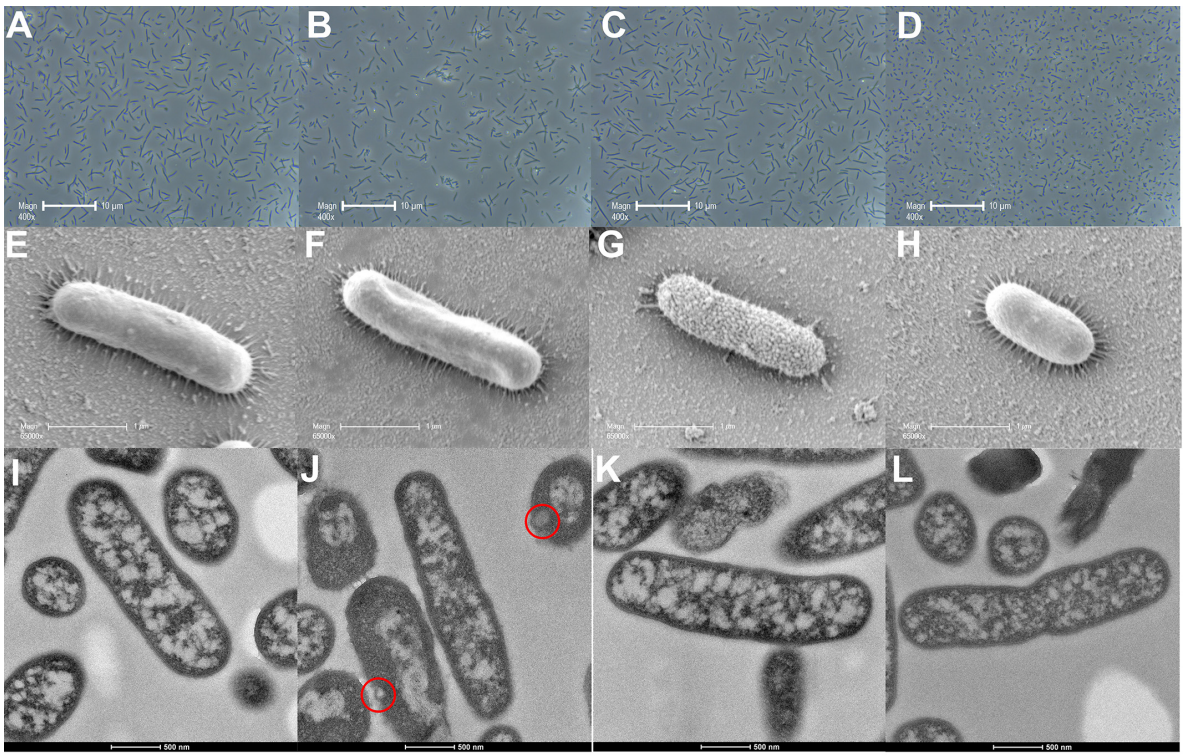

FIGURE 3 | Images from phase contrast microscopy **(A–D)**, scanning electron microscopy **(E–H)**, and transmission electron microscopy **(I–L)** for polymyxin-resistant *A. baumannii* FADDI-AB225 treated with 2 mg/L polymyxin B **(B,F,J)**, 4 mg/L mitotane **(C,G,K)**, or both **(D,H,L)**. **A**, **E**, and **I** represent the control condition. Membrane blebs are indicated by red circles.

(*A. baumannii*, *P. aeruginosa*, and *K. pneumoniae*) were selected for the initial *in vitro* antimicrobial activity evaluation. Isolates selected included MDR, carbapenem-resistant, and polymyxin-resistant strains with known different mechanisms of polymyxin resistance. *A. baumannii* and *P. aeruginosa* were selected as they are frequently resistant to multiple classes of antibiotics and are currently considered by the WHO as two of the top bacterial "superbugs" requiring urgent antibiotic development (Tacconelli and Magrini, 2017). *K. pneumoniae* was also examined as it is also identified as a top bacterial "superbug" by the WHO due to the rapid emergence of carbapenem resistance (including NDM production) (Yong et al., 2009; Kumarasamy et al., 2010; Farzana et al., 2013). Concentrations of 2 mg/L for polymyxin B and 4 m/L for mitotane were examined as they were achievable in patients (Hermsen et al., 2011; Sandri et al., 2013).

One of the major concerns surrounding the intravenous use of polymyxin B or colistin monotherapy for the treatment of infections caused by Gram-negative bacteria is the development of resistance *via* amplification of polymyxin-resistant subpopulations (Tam et al., 2005; Tan et al., 2007; Bergen et al., 2011; Meletis et al., 2011; Deris et al., 2012; Hermes et al., 2013; Lee et al., 2013; Ly et al., 2015; Lenhard et al., 2017; Zhao et al., 2017). Consequently, the use of antibiotic combination therapy represents a potential option to increase bacterial killing and prevent the emergence of polymyxin resistance as the combination may result in subpopulation or mechanistic synergy (Landersdorfer et al., 2013). Despite extensive bacterial killing by polymyxin B monotherapy against five polymyxin-susceptible isolates, regrowth with associated polymyxin resistance (the latter evident by significantly increased polymyxin B MICs compared to baseline values) subsequently occurred with three isolates (*A. baumannii* ATCC 19606, *A. baumannii* FADDI-AB180, and *K. pneumoniae* ATCC 13883; **Figure 1A**). When used as monotherapy, mitotane showed antimicrobial activity against only one isolate (**Figure 1B**). However, the combination of polymyxin B and mitotane significantly improved bacterial killing against the less susceptible isolates (i.e., those that were resistant to polymyxin B or mitotane monotherapy, or showed regrowth at 24 h; **Figures 1A,B**). The enhanced antimicrobial killing was indicated by the complete prevention of regrowth in all polymyxin-susceptible isolates after 24 h (**Figure 1A**) and >2 $\log_{10}$ cfu/mL reduction within the first 6-h treatment against the four polymyxin-resistant isolates compared to the more active monotherapy (**Figure 1B**). Although regrowth occurred in four of the five polymyxin-resistant isolates, the combination still enhanced initial bacterial killing which may assist with the bacterial clearance from the body. Since polymyxins are well known for their ability to permeabilize the outer membrane of Gram-negative bacteria (Salmelin et al., 2000; Tsubery et al., 2000; Sahalan and Dixon, 2008), a possible mechanism for the enhanced killing observed with the combination is

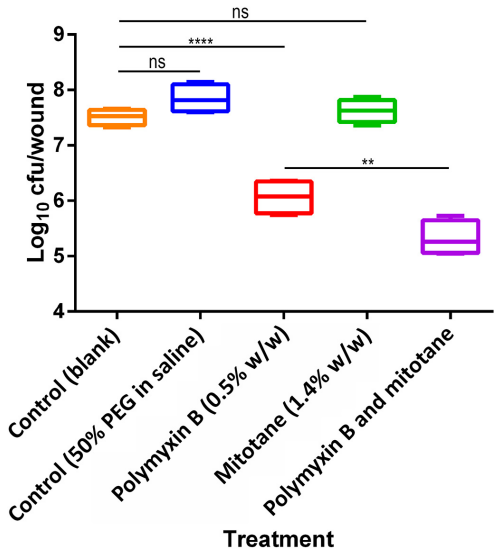

FIGURE 4 | Efficacy of polymyxin B alone, mitotane alone, and the combination against polymyxin-resistant *A. baumannii* FADDI-AB225 in a mouse wound infection model. Statistical significance was calculated with one-way ANOVA and Tukey's multiple comparisons (ns = $p > 0.5$, ** = $p \leq 0.01$, and **** = $p \leq 0.0001$). Box plots indicate upper and lower quartiles (top and bottom of box); median (line within box); and the spread of data (whiskers).

permeabilization of the outer membrane by polymyxin B leading to the entry of mitotane into the bacterial cell. Indeed, polymyxin B and its derivative polymyxin B nonapeptide had previously been shown to enhance the antimicrobial activity of hydrophobic antibiotics against Gram-negative bacteria and yeasts (Ofek et al., 1994; Pietschmann et al., 2009). Interestingly, mitotane monotherapy displayed substantial antimicrobial activity against LPS-deficient, polymyxin-resistant *A. baumannii* FADDI-AB065 (**Figure 1B**). LPS in the outer membrane of Gram-negative bacteria acts as a highly selective permeability barrier that protects bacteria from harmful substances (Nikaido, 2003). Consequently, it is possible that in the absence of LPS, mitotane was able to enter bacterial cells and exert its antimicrobial activity. Another notable finding is that mitotane monotherapy also lowered the polymyxin B MIC of polymyxin-resistant *A. baumannii* FADDI-AB225 (**Table 2**); however, it did not affect the polymyxin B MICs of the other polymyxin-resistant isolates. The mechanism for this phenomenon is currently unclear, although it may result from the expression of LPS variants by the different isolates. Coincidently, it has been reported that *Moraxella catarrhalis* and *Salmonella typhimurium* with deep rough-type LPS displayed higher susceptibility to hydrophobic antimicrobial agents (Tsujimoto et al., 1999). Further mechanistic studies are warranted.

According to the SEM imaging results, it is possible that the polymyxin resistance in *A. baumannii* FADDI-AB225 altered their surface interaction with mitotane, as the outer membrane appeared disrupted (uneven and rough) following mitotane monotherapy in *A. baumannii* FADDI-AB225 (**Figure 3G**), but not *A. baumannii* ATCC 17978 (**Figure 2G**). Both the SEM and TEM images showed disruptive changes to the outer membrane of polymyxin-susceptible *A. baumannii* ATCC 17978 following polymyxin B monotherapy (**Figures 2F,J**), which confirmed the known impact of polymyxin B on the outer membrane of Gram-negative bacteria. For the lipid A modified polymyxin-resistant *A. baumannii* FADDI-AB225, no disruptive effect on the surface membrane by polymyxin B monotherapy was observed with SEM (**Figure 3F**), most likely due to the modification of lipid A which resulted in minimal polymyxin B affinity. Membrane blebs, however, were still observed by TEM in polymyxin-resistant *A. baumannii* FADDI-AB225 treated with 2 mg/L polymyxin B alone (**Figure 3J**), indicating that blebbing might not necessarily result in cell death, but was enough to allow the mitotane to enter and exert antibacterial effect. Although monotherapy with mitotane or polymyxin B appeared to impact the outer membrane of polymyxin-resistant and -susceptible *A. baumannii*, the combination impacted the overall structure of both strains leading to an extensive shortening in the length of the bacteria (**Figures 2**, **3**). SEM images showed a smooth membrane surface on the shortened bacterial cells, suggesting that the combination prevented the formation of the rough surface, which could be an adaptive response to polymyxin B or mitotane monotherapy. Numerous incompletely separated cells revealed by TEM images (**Figures 2L**, **3L**) suggest a possible impact on the bacterial DNA replication.

In our mouse burn wound infection study, the combination displayed effective antimicrobial activity against polymyxin-resistant *A. baumannii*. The doses of 5 mg/kg for polymyxin B (subcutaneous median lethal dose in mice [LD_{50}] 59 mg/kg) and 14 mg/kg for mitotane (oral LD_{50} > 4,000 mg/kg in mice, dermal LD_{50} not available) were selected, as they are safe in animals according to their material safety data sheets. Based on the available LD_{50} limits of polymyxin B and mitotane, it is likely that much higher doses of both drugs can be used for topical combination therapy. Given the lack of an optimized topical formulation, it is possible that the *in vivo* efficacy of the combination in the current study was underestimated. Nevertheless, the combination treatment was able to significantly reduce the number of polymyxin-resistant *A. baumannii*, compared to polymyxin B or mitotane monotherapy.

CONCLUSION

Our study is the first to reveal the synergistic activity of mitotane, an FDA-approved non-antibiotic drug, in combination with polymyxin B against problematic Gram-negative bacteria. Importantly, the combination also prevented the emergence of polymyxin resistance. As mitotane is currently used in humans, its repositioning for antimicrobial purposes may be easier than discovering novel antibacterial compounds against Gram-negative "superbugs". The synergistic antibacterial killing of polymyxin B with mitotane in animals raises hopes for the potential repositioning of mitotane against MDR Gram-negative bacteria and further clinical investigations are warranted.

ETHICS STATEMENT

This study was carried out in accordance with the recommendations of "Australian Code of Practice for the Care and Use of Animals for Scientific Purposes" and Monash Institute of Pharmaceutical Sciences Animal Ethics Committee. The protocol was approved by the Monash Institute of Pharmaceutical Sciences Animal Ethics Committee before the study started.

AUTHOR CONTRIBUTIONS

TT carried out the main experiments, data analysis, and wrote the manuscript draft. JW participated in the animal study. PB participated in *in vitro* studies' design. YD and TV participated in data analysis. JL designed the project and guided all experimental designs and data analysis. All authors participated in manuscript revision and read and approved the final manuscript.

FUNDING

This study was supported by a research grant from the National Institute of Allergy and Infectious Diseases of the National Institutes of Health (R01AI111965) awarded to JL and TV. YD was supported in part by R01AI10 4895.

REFERENCES

Arroyo, L. A., Herrera, C. M., Fernandez, L., Hankins, J. V., Trent, M. S., and Hancock, R. E. (2011). The pmrCAB operon mediates polymyxin resistance in *Acinetobacter baumannii* ATCC 17978 and clinical isolates through phosphoethanolamine modification of lipid A. *Antimicrob. Agents Chemother.* 55, 3743–3751. doi: 10.1128/AAC.00256-11

Ashburn, T. T., and Thor, K. B. (2004). Drug repositioning: identifying and developing new uses for existing drugs. *Nat. Rev. Drug Discov.* 3, 673–683. doi: 10.1038/nrd1468

Bergen, P. J., Tsuji, B. T., Bulitta, J. B., Forrest, A., Jacob, J., Sidjabat, H. E., et al. (2011). Synergistic killing of multidrug-resistant *Pseudomonas aeruginosa* at multiple inocula by colistin combined with doripenem in an in vitro pharmacokinetic/pharmacodynamic model. *Antimicrob. Agents Chemother.* 55, 5685–5695. doi: 10.1128/AAC.05298-11

Boucher, H. W., Talbot, G. H., Benjamin, D. K. Jr., Bradley, J., Guidos, R. J., Jones, R. N., et al. (2013). 10 x ′20 Progress–development of new drugs active against gram-negative bacilli: an update from the Infectious Diseases Society of America. *Clin. Infect. Dis.* 56, 1685–1694. doi: 10.1093/cid/cit152

Boucher, H. W., Talbot, G. H., Bradley, J. S., Edwards, J. E., Gilbert, D., Rice, L. B., et al. (2009). Bad bugs, no drugs: no ESKAPE! An update from the Infectious Diseases Society of America. *Clin. Infect. Dis.* 48, 1–12. doi: 10.1086/595011

Centers for Disease Control and Prevention [CDC] (2013). *Antibiotic/Antimicrobial Resistance: Antibiotic Resistance Threats in the United States*. Atlanta: National Center for Emerging and Zoonotic Infectious Diseases.

Clinical and Laboratory Standards Institute [CLSI] (2016). *Performance Standards for Antimicrobial Susceptibility Testing*. Wayne, PA: CLSI.

Davis, K. A., Moran, K. A., Mcallister, C. K., and Gray, P. J. (2005). Multidrug-resistant Acinetobacter extremity infections in soldiers. *Emerg. Infect. Dis.* 11, 1218–1224. doi: 10.3201/1108.050103

Deris, Z. Z., Yu, H. H., Davis, K., Soon, R. L., Jacob, J., Ku, C. K., et al. (2012). The combination of colistin and doripenem is synergistic against *Klebsiella pneumoniae* at multiple inocula and suppresses colistin resistance in an in vitro pharmacokinetic/pharmacodynamic model. *Antimicrob. Agents Chemother.* 56, 5103–5112. doi: 10.1128/AAC.01064-12

European Committee for Antimicrobial Susceptibility Testing (EUCAST) of the European Society of Clinical Microbiology and Infectious Diseases (ESCMID) (2003). Determination of minimum inhibitory concentrations (MICs) of antibacterial agents by broth dilution. *Clin. Microbiol. Infect.* 9:ix-xv. doi: 10.1046/j.1469-0691.2003.00790.x

Farzana, R., Shamsuzzaman, S., and Mamun, K. Z. (2013). Isolation and molecular characterization of New Delhi metallo-beta-lactamase-1 producing superbug in Bangladesh. *J. Infect. Dev. Ctries.* 7, 161–168. doi: 10.3855/jidc.2493

Gandra, S., Barter, D. M., and Laxminarayan, R. (2014). Economic burden of antibiotic resistance: how much do we really know? *Clin. Microbiol. Infect.* 20, 973–980. doi: 10.1111/1469-0691.12798

Goli, H. R., Nahaei, M. R., Ahangarzadeh Rezaee, M., Hasani, A., Samadi Kafil, H., and Aghazadeh, M. (2016). Emergence of colistin resistant *Pseudomonas aeruginosa* at Tabriz hospitals, Iran. *Iran. J. Microbiol.* 8, 62–69.

Gupta, E., Mohanty, S., Sood, S., Dhawan, B., Das, B. K., and Kapil, A. (2006). Emerging resistance to carbapenems in a tertiary care hospital in north India. *Indian J. Med. Res.* 124, 95–98.

Harris, P., Paterson, D., and Rogers, B. (2015). Facing the challenge of multidrug-resistant gram-negative bacilli in Australia. *Med. J. Aust.* 202, 243–247. doi: 10.5694/mja14.01257

Hermes, D. M., Pormann Pitt, C., Lutz, L., Teixeira, A. B., Ribeiro, V. B., Netto, B., et al. (2013). Evaluation of heteroresistance to polymyxin B among carbapenem-susceptible and -resistant *Pseudomonas aeruginosa*. *J. Med. Microbiol.* 62, 1184–1189. doi: 10.1099/jmm.0.059220-0

Hermsen, I. G., Fassnacht, M., Terzolo, M., Houterman, S., Den Hartigh, J., Leboulleux, S., et al. (2011). Plasma concentrations of o,p′DDD, o,p′DDA, and o,p′DDE as predictors of tumor response to mitotane in adrenocortical carcinoma: results of a retrospective ENS@T multicenter study. *J. Clin. Endocrinol. Metab.* 96, 1844–1851. doi: 10.1210/jc.2010-2676

Kim, Y., Bae, I. K., Lee, H., Jeong, S. H., Yong, D., and Lee, K. (2014). In vivo emergence of colistin resistance in *Acinetobacter baumannii* clinical isolates of sequence type 357 during colistin treatment. *Diagn. Microbiol. Infect. Dis.* 79, 362–366. doi: 10.1016/j.diagmicrobio.2014.03.027

Kumarasamy, K. K., Toleman, M. A., Walsh, T. R., Bagaria, J., Butt, F., Balakrishnan, R., et al. (2010). Emergence of a new antibiotic resistance mechanism in India, Pakistan, and the UK: a molecular, biological, and epidemiological study. *Lancet Infect. Dis.* 10, 597–602. doi: 10.1016/S1473-3099(10)70143-2

Lalli, E. (2015). Mitotane revisited: a new target for an old drug. *Endocrinology* 156, 3873–3875. doi: 10.1210/en.2015-1796

Landersdorfer, C. B., Ly, N. S., Xu, H., Tsuji, B. T., and Bulitta, J. B. (2013). Quantifying subpopulation synergy for antibiotic combinations via mechanism-based modeling and a sequential dosing design. *Antimicrob. Agents Chemother.* 57, 2343–2351. doi: 10.1128/AAC.00092-13

Lee, H. J., Bergen, P. J., Bulitta, J. B., Tsuji, B., Forrest, A., Nation, R. L., et al. (2013). Synergistic activity of colistin and rifampin combination against multidrug-resistant *Acinetobacter baumannii* in an in vitro pharmacokinetic/pharmacodynamic model. *Antimicrob. Agents Chemother.* 57, 3738–3745. doi: 10.1128/AAC.00703-13

Lenhard, J. R., Thamlikitkul, V., Silveira, F. P., Garonzik, S. M., Tao, X., Forrest, A., et al. (2017). Polymyxin-resistant, carbapenem-resistant *Acinetobacter baumannii* is eradicated by a triple combination of agents that lack individual activity. *J. Antimicrob. Chemother.* 72, 1415–1420. doi: 10.1093/jac/dkx002

Li, J., Nation, R. L., Turnidge, J. D., Milne, R. W., Coulthard, K., Rayner, C. R., et al. (2006). Colistin: the re-emerging antibiotic for multidrug-resistant Gram-negative bacterial infections. *Lancet Infect. Dis.* 6, 589–601. doi: 10.1016/S1473-3099(06)70580-1

Ly, N. S., Bulitta, J. B., Rao, G. G., Landersdorfer, C. B., Holden, P. N., Forrest, A., et al. (2015). Colistin and doripenem combinations against *Pseudomonas*

aeruginosa: profiling the time course of synergistic killing and prevention of resistance. *J. Antimicrob. Chemother.* 70, 1434–1442. doi: 10.1093/jac/dku567

Magiorakos, A. P., Srinivasan, A., Carey, R. B., Carmeli, Y., Falagas, M. E., Giske, C. G., et al. (2012). Multidrug-resistant, extensively drug-resistant and pandrug-resistant bacteria: an international expert proposal for interim standard definitions for acquired resistance. *Clin. Microbiol. Infect.* 18, 268–281. doi: 10.1111/j.1469-0691.2011.03570.x

Maragakis, L. L., and Perl, T. M. (2008). *Acinetobacter baumannii*: epidemiology, antimicrobial resistance, and treatment options. *Clin. Infect. Dis.* 46, 1254–1263. doi: 10.1086/529198

Marchaim, D., Chopra, T., Pogue, J. M., Perez, F., Hujer, A. M., Rudin, S., et al. (2011). Outbreak of colistin-resistant, carbapenem-resistant *Klebsiella pneumoniae* in metropolitan Detroit. *Michigan. Antimicrob. Agents Chemother.* 55, 593–599. doi: 10.1128/AAC.01020-10

Meletis, G., Tzampaz, E., Sianou, E., Tzavaras, I., and Sofianou, D. (2011). Colistin heteroresistance in carbapenemase-producing *Klebsiella pneumoniae*. *J. Antimicrob. Chemother.* 66, 946–947. doi: 10.1093/jac/dkr007

Moffatt, J. H., Harper, M., Harrison, P., Hale, J. D., Vinogradov, E., Seemann, T., et al. (2010). Colistin resistance in *Acinetobacter baumannii* is mediated by complete loss of lipopolysaccharide production. *Antimicrob. Agents Chemother.* 54, 4971–4977. doi: 10.1128/AAC.00834-10

Nation, R. L., Li, J., Cars, O., Couet, W., Dudley, M. N., Kaye, K. S., et al. (2015). Framework for optimisation of the clinical use of colistin and polymyxin B: the Prato polymyxin consensus. *Lancet Infect. Dis.* 15, 225–234. doi: 10.1016/S1473-3099(14)70850-3

Nikaido, H. (2003). Molecular basis of bacterial outer membrane permeability revisited. *Microbiol. Mol. Biol. Rev.* 67, 593–656. doi: 10.1128/MMBR.67.4.593-656.2003

Ofek, I., Cohen, S., Rahmani, R., Kabha, K., Tamarkin, D., Herzig, Y., et al. (1994). Antibacterial synergism of polymyxin B nonapeptide and hydrophobic antibiotics in experimental gram-negative infections in mice. *Antimicrob. Agents Chemother.* 38, 374–377. doi: 10.1128/AAC.38.2.374

Peleg, A. Y., Seifert, H., and Paterson, D. L. (2008). *Acinetobacter baumannii*: emergence of a successful pathogen. *Clin. Microbiol. Rev.* 21, 538–582. doi: 10.1128/CMR.00058-07

Pelletier, M. R., Casella, L. G., Jones, J. W., Adams, M. D., Zurawski, D. V., Hazlett, K. R., et al. (2013). Unique structural modifications are present in the lipopolysaccharide from colistin-resistant strains of *Acinetobacter baumannii*. *Antimicrob. Agents Chemother.* 57, 4831–4840. doi: 10.1128/AAC.00865-13

Pietschmann, S., Hoffmann, K., Voget, M., and Pison, U. (2009). Synergistic effects of miconazole and polymyxin B on microbial pathogens. *Vet. Res. Commun.* 33, 489–505. doi: 10.1007/s11259-008-9194-z

Pillai, S. K., Moellering, R. C., and Eliopoulos, G. M. (2005). "Antimicrobial combinations," in *Antibiotics in Laboratory Medicine*, 5th Edn, ed. V. Lorian (Philadelphia, PA: Lippincott Williams & Wilkins).

Roy, R., Tiwari, M., Donelli, G., and Tiwari, V. (2017). Strategies for combating bacterial biofilms: a focus on anti-biofilm agents and their mechanisms of action. *Virulence* 9, 522–554. doi: 10.1080/21505594.2017.1313372

Sahalan, A. Z., and Dixon, R. A. (2008). Role of the cell envelope in the antibacterial activities of polymyxin B and polymyxin B nonapeptide against *Escherichia coli*. *Int. J. Antimicrob. Agents* 31, 224–227. doi: 10.1016/j.ijantimicag.2007.10.005

Salmelin, C., Hovinen, J., and Vilpo, J. (2000). Polymyxin permeabilization as a tool to investigate cytotoxicity of therapeutic aromatic alkylators in DNA repair-deficient *Escherichia coli* strains. *Mutat. Res.* 467, 129–138. doi: 10.1016/S1383-5718(00)00026-7

Sandri, A. M., Landersdorfer, C. B., Jacob, J., Boniatti, M. M., Dalarosa, M. G., Falci, D. R., et al. (2013). Population pharmacokinetics of intravenous polymyxin B in critically-ill patients: implications for selection of dosage regimens. *Clin. Infect. Dis.* 57, 524–531. doi: 10.1093/cid/cit334

Sbiera, S., Leich, E., Liebisch, G., Sbiera, I., Schirbel, A., Wiemer, L., et al. (2015). Mitotane inhibits sterol-O-acyl transferase 1 triggering lipid-mediated endoplasmic reticulum stress and apoptosis in adrenocortical carcinoma cells. *Endocrinology* 156, 3895–3908. doi: 10.1210/en.2015-1367

Tacconelli, E., and Magrini, N. (2017). *Global Priority List of Antibiotic-Resistant Bacteria to Guide Research, Discovery, and Development of New Antibiotics*. Geneva: World Health Organization.

Tam, V. H., Schilling, A. N., Vo, G., Kabbara, S., Kwa, A. L., Wiederhold, N. P., et al. (2005). Pharmacodynamics of polymyxin B against *Pseudomonas aeruginosa*. *Antimicrob. Agents Chemother.* 49, 3624–3630. doi: 10.1128/AAC.49.9.3624-3630.2005

Tan, C. H., Li, J., and Nation, R. L. (2007). Activity of colistin against heteroresistant *Acinetobacter baumannii* and emergence of resistance in an in vitro pharmacokinetic/pharmacodynamic model. *Antimicrob. Agents Chemother.* 51, 3413–3415. doi: 10.1128/AAC.01571-06

The European Committee on Antimicrobial Susceptibility Testing [EUCAST] (2017). *Breakpoint Tables for Interpretation of MICs and Zone Diameters. Version 7.1, 2017*. Available at: http://www.eucast.org

Tiwari, V., Kapil, A., and Moganty, R. R. (2012a). Carbapenem-hydrolyzing oxacillinase in high resistant strains of *Acinetobacter baumannii* isolated from India. *Microb. Pathog.* 53, 81–86. doi: 10.1016/j.micpath.2012.05.004

Tiwari, V., and Moganty, R. R. (2014). Conformational stability of OXA-51 beta-lactamase explains its role in carbapenem resistance of *Acinetobacter baumannii*. *J. Biomol. Struct. Dyn.* 32, 1406–1420. doi: 10.1080/07391102.2013.819789

Tiwari, V., Vashistt, J., Kapil, A., and Moganty, R. R. (2012b). Comparative proteomics of inner membrane fraction from carbapenem-resistant *Acinetobacter baumannii* with a reference strain. *PLoS One* 7:e0039451. doi: 10.1371/journal.pone.0039451

Tran, T. B., Cheah, S. E., Yu, H. H., Bergen, P. J., Nation, R. L., Creek, D. J., et al. (2016). Anthelmintic closantel enhances bacterial killing of polymyxin B against multidrug-resistant *Acinetobacter baumannii*. *J. Antibiot.* 69, 415-421. doi: 10.1038/ja.2015.127

Tsubery, H., Ofek, I., Cohen, S., and Fridkin, M. (2000). Structure-function studies of polymyxin B nonapeptide: implications to sensitization of gram-negative bacteria. *J. Med. Chem.* 43, 3085–3092. doi: 10.1021/jm0000057

Tsujimoto, H., Gotoh, N., and Nishino, T. (1999). Diffusion of macrolide antibiotics through the outer membrane of *Moraxella* catarrhalis. *J. Infect. Chemother.* 5, 196–200. doi: 10.1007/s101560050034

Verma, P., Tiwari, M., and Tiwari, V. (2017). In silico high-throughput virtual screening and molecular dynamics simulation study to identify inhibitor for AdeABC efflux pump of *Acinetobacter baumannii*. *J. Biomol. Struct. Dyn.* 36, 1182–1194. doi: 10.1080/07391102.2017.1317025

Yong, D., Toleman, M. A., Giske, C. G., Cho, H. S., Sundman, K., Lee, K., et al. (2009). Characterization of a new metallo-beta-lactamase gene, bla(NDM-1), and a novel erythromycin esterase gene carried on a unique genetic structure in *Klebsiella pneumoniae* sequence type 14 from India. *Antimicrob. Agents Chemother.* 53, 5046–5054. doi: 10.1128/AAC.00774-09

Zhao, M., Bulman, Z. P., Lenhard, J. R., Satlin, M. J., Kreiswirth, B. N., Walsh, T. J., et al. (2017). Pharmacodynamics of colistin and fosfomycin: a 'treasure trove' combination combats KPC-producing *Klebsiella pneumoniae*. *J. Antimicrob. Chemother.* 72, 1985–1990. doi: 10.1093/jac/dkx070

Conflict of Interest Statement: The content is solely the responsibility of the authors and does not necessarily represent the official views of the National Institute of Allergy and Infectious Diseases or the National Institutes of Health. JL is an Australian National Health and Medical Research Council (NHMRC) Senior Research Fellow. TV is an Australian NHMRC Industry Career Development Research Fellow.

The other authors declare that the research was conducted in the absence of any commercial or financial relationships that could be construed as a potential conflict of interest.

frontiers in Microbiology

ORIGINAL RESEARCH
published: 22 December 2017
doi: 10.3389/fmicb.2017.02599

Low Concentrations of Vitamin C Reduce the Synthesis of Extracellular Polymers and Destabilize Bacterial Biofilms

*Santosh Pandit[1], Vaishnavi Ravikumar[1], Alyaa M. Abdel-Haleem[2,3], Abderahmane Derouiche[1], V. R. S. S. Mokkapati[1], Carina Sihlbom[4], Katsuhiko Mineta[2], Takashi Gojobori[2], Xin Gao[2], Fredrik Westerlund[1] and Ivan Mijakovic[1,5]**

[1] Systems and Synthetic Biology Division, Department of Biology and Biological Engineering, Chalmers University of Technology, Gothenburg, Sweden, [2] Computational Bioscience Research Center, King Abdullah University of Science and Technology, Thuwal, Saudi Arabia, [3] Biological and Environmental Sciences and Engineering Division, King Abdullah University of Science and Technology, Thuwal, Saudi Arabia, [4] Proteomics Core Facility, Sahlgrenska Academy, University of Gothenburg, Gothenburg, Sweden, [5] Novo Nordisk Foundation Center for Biosustainability, Technical University of Denmark, Kongens Lyngby, Denmark

Extracellular polymeric substances (EPS) produced by bacteria form a matrix supporting the complex three-dimensional architecture of biofilms. This EPS matrix is primarily composed of polysaccharides, proteins and extracellular DNA. In addition to supporting the community structure, the EPS matrix protects bacterial biofilms from the environment. Specifically, it shields the bacterial cells inside the biofilm, by preventing antimicrobial agents from getting in contact with them, thereby reducing their killing effect. New strategies for disrupting the formation of the EPS matrix can therefore lead to a more efficient use of existing antimicrobials. Here we examined the mechanism of the known effect of vitamin C (sodium ascorbate) on enhancing the activity of various antibacterial agents. Our quantitative proteomics analysis shows that non-lethal concentrations of vitamin C inhibit bacterial quorum sensing and other regulatory mechanisms underpinning biofilm development. As a result, the EPS biosynthesis in reduced, and especially the polysaccharide component of the matrix is depleted. Once the EPS content is reduced beyond a critical point, bacterial cells get fully exposed to the medium. At this stage, the cells are more susceptible to killing, either by vitamin C-induced oxidative stress as reported here, or by other antimicrobials or treatments.

Keywords: biofilms, exopolymeric matrix, quantitative proteomics, *Bacillus subtilis*, vitamin C

OPEN ACCESS

Edited by:
Mariana Henriques, University of Minho, Portugal

Reviewed by:
Vishvanath Tiwari, Central University of Rajasthan, India
Ana Isabel Pelaez, Universidad de Oviedo Mieres, Spain

***Correspondence:**
Ivan Mijakovic
ivan.mijakovic@chalmers.se;
ivmi@biosustain.dtu.dk

Specialty section:
This article was submitted to Antimicrobials, Resistance and Chemotherapy, a section of the journal Frontiers in Microbiology

Received: *15 October 2017*
Accepted: *13 December 2017*
Published: *22 December 2017*

Citation:
Pandit S, Ravikumar V, Abdel-Haleem AM, Derouiche A, Mokkapati VRSS, Sihlbom C, Mineta K, Gojobori T, Gao X, Westerlund F and Mijakovic I (2017) Low Concentrations of Vitamin C Reduce the Synthesis of Extracellular Polymers and Destabilize Bacterial Biofilms. Front. Microbiol. 8:2599. doi: 10.3389/fmicb.2017.02599

INTRODUCTION

Bacterial biofilms are culprits of various human infectious diseases, industrial corrosion and food contamination (Flemming et al., 2016). Bacteria within the biofilms synthesize a dense protective matrix composed of extracellular polymeric substances (EPS) (Branda et al., 2005). This matrix is mainly composed of polysaccharides, proteins and extracellular DNA (eDNA), whose continuous release leads to the establishment of a complex "mushroom-shaped" biofilm architecture (Branda et al., 2006; Barnes et al., 2012). Exopolysaccharides and proteins are the most abundant component of the biofilm matrix, defining its physico-chemical properties and morphology (Marvasi et al., 2010; Roy et al., 2017). Furthermore, the EPS serve as a food storage, which gets mobilized during extended nutrient depletion (Xiao et al., 2012). The structure of the EPS matrix varies considerably

among bacterial strains, and its composition is influenced by the local environment and nutrient availability.

Antibiotics are widely used to eradicate bacterial biofilms when treating infections. However, their prolonged use increases the risk of developing multi-resistant strains, and disrupts the ecology of the residential microflora (Cegelski et al., 2008). Hence an increasing interest for chemo-prophylactic agents, which can affect biofilm formation, and thereby reduce the time and dose of antibiotics treatments (Xavier et al., 2005; Cegelski et al., 2008). Vitamin C, a major dietary micronutrient, has been shown to exhibit bactericidal activity against mycobacteria (Vilcheze et al., 2013). However, this killing effect seems to be confined to mycobacteria, since vitamin C did not kill other opportunistic bacterial pathogens, such as *Staphylococcus epidermidis, Staphylococcus aureus, Escherichia coli,* and *Pseudomonas aeruginosa* (Khameneh et al., 2016). Interestingly, vitamin C has been reported to enhance the effect of antibiotics vs. a broad spectrum of bacteria via a synergistic effect, but the mechanism of this synergy remains unclear (Kallio et al., 2012; Khameneh et al., 2016). Similarly, vitamin C has been shown to enhance the killing effect of a physical bactericidal agent, cold atmospheric plasma, against biofilms of *S. epidermidis*, *E. coli,* and *P. aeruginosa* (Helgadóttir et al., 2017). In this study we set out to characterize the mechanism of this non-lethal synergistic effect of vitamin C, which enhances the effect of antibiotics and physical killing agents.

We performed an initial characterization with several bacterial strains, and different doses of vitamin C. Our conclusion was that while the low doses of vitamin C are harmless to the planktonic bacteria, they effectively destabilizes biofilms. We then focused on an in-depth quantitative analysis with *Bacillus subtilis*, a model organism for biofilm development (Vlamakis et al., 2013). Our findings, based on quantification of the biofilm EPS content and cell viability, quantitative proteome analyses and genome-scale metabolic modeling point to a vitamin C-dependent inhibition of the synthesis of polysaccharides that form the biofilm matrix. This proceeds via inhibition of the quorum sensing and other regulatory mechanisms, leading to repression of specific biosynthetic operons. Once the EPS content is reduced beyond a critical point, bacterial cells become exposed, and more susceptible to killing by any external factors.

MATERIALS AND METHODS

Bacterial Strains, Culture Media, and Reagents

Bacillus subtilis NCIB 3610, *E. coli* UTI89 and *P. aeruginosa* PAO1 were used in this study. LB (10 g of tryptone, 5 g of yeast extract and 5 g of NaCl per liter) or solid LB medium supplemented with 1.5% agar were used for the routine growth of all bacteria. Sodium ascorbate was purchased from Sigma–Aldrich.

Bacterial Growth and Biofilm Formation

For growth analysis, an overnight bacterial culture was diluted 1:100 (1×10^7 CFU) in LB medium with 1% glycerol for *B. subtilis*, plain LB medium for *P. aeruginosa* and *E. coli*, with varying concentrations of sodium ascorbate (neutral pH form). The diluted cultures were incubated at 37°C with continuous agitation (200 rpm) and the absorbance of the culture was measured periodically at 600 nm for 9 h with intervals of 1 h. *B. subtilis* biofilms were formed in LBGM medium (LB medium containing 1% glycerol; 1 mM $MnSO_4$). 2–5 $\times$ 10^6 CFU/mL of bacterial culture was inoculated into 5 mL of LBGM medium and incubated at 37°C for 24 h without agitation. *E. coli* and *P. aeruginosa* biofilms were formed on 24 well plates. 2–5 $\times$ 10^6 CFU/mL of an overnight bacterial culture was inoculated into a 24 well plate containing 2 mL of LB broth and incubated for 24 h without agitation.

B. subtilis Biofilm Analysis

For the biofilm analysis, 24 h old biofilms, grown in the presence of various concentrations of sodium ascorbate, were removed and sonicated at 10 W for 30 s to homogenize the biofilm. The homogenized suspension (5 mL) was used to determine the biomass, colony forming units (CFU), polysaccharides, protein and eDNA. Briefly, for the determination of biomass, the homogenized suspension was washed three times (5000 *g* for 20 min) with sterile water, lyophilized and weighed. For the determination of viability, an aliquot (100 μL) from the homogenized suspension was diluted serially and plated on LB agar plates to count colonies. Water insoluble polysaccharide was extracted from the lyophilized sample by using 1 N sodium hydroxide (300 μL/mg biomass for three times) and quantified by using a phenol-sulfuric acid assay as described previously (Pandit et al., 2011). For protein quantification, biofilms were collected and homogenized in 1 N NaOH (300 μL/mg biomass for three times). The supernatant from the homogenized suspensions were collected after centrifugation (5000 *g*, 20 min) and protein content was quantified by using the Bradford assay. For quantification of eDNA in the EPS matrix, the filtered supernatant from the homogenized suspension was used. eDNA was extracted by using a DNA extraction kit (Thermo Fisher Scientific) and the quantity was measured using a nanodrop UV-Vis spectrophotometer (NanoDrop 2000, Thermo Scientific).

Fluorescence Microscopy Analysis

The effect of sodium ascorbate on *B. subtilis* biofilms was analyzed by simultaneous labeling of the bacterial cells and the polysaccharides in the biofilm. Briefly, 10 μg/mL of Alexa flour® 633-labeled wheat germ agglutinin conjugate (absorbance/fluorescence emission maxima 632/647 nm; Molecular Probes Inc., Eugene, OR, United States) and 50 μg/mL of Concanavalin A, Tetramethylrhodamine conjugate (555/580 nm; Molecular Probes) was added to the culture medium during biofilm formation. The toxicity of these fluorescence probe toward the bacterial cells in biofilms was evaluated by comparison of viability and biomass with control samples. After 24 h, the biofilms were exposed to 2.5 μm of SYTO® 9 green-fluorescent nucleic acid stain (480/500 nm; Molecular Probes) for 30 min. The stained biofilms were transferred to a glass slide and laser scanning confocal microscope imaging of the biofilms was performed using an LSM 710 NLO (Carl Zeiss) equipped with argon-ion and helium

neon lasers. Three independent experiments were performed and image stacks from five sites per experiment were collected (n = 15). EPS biovolume was quantified from confocal stacks by COMSTAT (Heydorn et al., 2000). Biovolume is defined as the volume of the biomass (μm^3) divided by substratum area (μm^2). For the detection of reactive oxygen species (ROS) in biofilm cells, 24 h old *B. subtilis* biofilms grown with or without presence of vitamin C were stained with DAPI and CellRox deep ROS sensor (Life Technologies) as described previously (Durmus et al., 2013). Briefly, biofilms were stained with 5 μM of CellRox deep red stain for 30 min, washed with sterile water and counter- stained with DAPI for 20 min. The stained biofilms were visualized by fluorescence microscopy. To visualize the live/dead cells in *B. subtilis* biofilms grown with and without presence of vitamin C, biofilms were stained with 6.0 μM SYTO 9 and 30 μM propidium iodide (LIVE/DEAD BacLight bacterial viability kit L13152, Invitrogen, Molecular Probes, Inc., Eugene, OR, United States). Imaging was performed with a fluorescence microscope (Axio Imager 2. Carl Zeiss, Zena, Germany).

Assay for Biofilm Formation of *E. coli* and *P. aeruginosa*

For the biofilm formation assay, 24 h old biofilms of *E. coli* and *P. aeruginosa* were rinsed three times with sterile water to remove the loosely adherent bacteria and dried for 30 min at room temperature. Dried biofilms were then stained with 1% crystal violet for 5 min without agitation. All the biofilms were washed at least five times with sterile water to remove the excess stain and dried for 1 h at room temperature. Absolute ethanol (1 mL) was added to the dried stained biofilm and agitated vigorously for 15 min to dissolve the stain. Optical density was measured at 600 nm.

Proteome Analysis

All experiments for MS analysis were carried out in biological triplicates. 24 h biofilms of *B. subtilis* were collected and centrifuged to obtain a cell pellet. Cell lysis was performed by re-suspending the cell pellets in an SDS lysis buffer containing 4% SDS in 100 mM triethylammonium bicarbonate pH 8.5, 5 mM β-glycerophosphate, 5 mM sodium fluoride, 5 mM sodium orthovanadate and 10 mM ethylenediaminetetraacetic acid, along with a protease inhibitor cocktail (Roche). The cell extracts were boiled at 90°C for 10 min followed by sonication. The cell debris was removed by centrifugation at 13400 rpm for 30 min and the crude protein extracts were cleaned up by chloroform/methanol precipitation. Dried protein pellets were dissolved in denaturation buffer containing 8 M urea in 10 mM Tris-HCl pH 8.0. The protein lysate was reduced with 1 mM dithiothreitol and alkylated with 5.5 mM iodoacetamide in the dark, for 1 h each at room temperature. Proteins were then subjected to overnight digestion with an endoproteinase Trypsin (1:100, w/w; Pierce™). The reaction was stopped by acidification with 10% trifluoroacetic acid and stage-tipped before injecting the samples into the mass spectrometer (Ishihama et al., 2006). Samples were analyzed on an Q Exactive mass spectrometer coupled to an Easy-nLC 1200 (both Thermo Fisher Scientific, Inc., Waltham, MA, United States). Chromatographic separation was performed using an in-house constructed pre-column (45 mm × 0.075 mm I.D) and analytical (200 mm × 0.075 mm I.D.) column set up packed with 3 μm Reprosil-Pur C18-AQ particles (Dr. Maisch GmbH, Ammerbuch, Germany). Peptides were injected onto the column with solvent A (0.2% formic acid in water) at a flow rate of 300 nL/min and 500 bars. Peptides were then eluted using a segmented gradient of 7–27% B-solvent (80% acetonitrile with 0.2% formic acid) over 45 min, 27–40% B over 5 min, 40–100% B over 5 min with a final hold at 100% B for 10 min. The mass spectrometer was operated on a data-dependent mode. Survey full-scans for the MS spectra were recorded between 400 and 1600 Thompson at a resolution of 70,000 with a target value of 1e6 charges in the Orbitrap mass analyzer. The top 10 most intense peaks from the survey scans of doubly or multiply charged precursor ions were selected for fragmentation with higher-energy collisional dissociation (HCD) with a target value of 1e5 in the Orbitrap mass analyzer in each scan cycle. Dynamic exclusion was set for 30 s. Triplicate injections (technical replicates) were carried out for each of the samples for label free quantitation (LFQ).

Data Processing and Analysis

Acquired MS spectra were processed with the MaxQuant software suite (version 1.5.3.30) (Cox et al., 2009), integrated with an Andromeda search engine. Database search was performed against a target-decoy database of *B. subtilis* 168 downloaded from UniProt (taxonomy ID 1423), containing 4,195 protein entries, and additionally including also 248 commonly observed laboratory contaminant proteins. Endoprotease Trypsin/P was set as the protease with a maximum missed cleavage of two. Carbamidomethylation (Cys) was set as a fixed modification. Label free quantification was enabled with a minimum ratio count of two. A false discovery rate of 1% was applied at the peptide and protein level individually for filtering identifications. Initial mass tolerance was set to 20 ppm. In case of the main search, the peptide mass tolerance of precursor and the fragment ions were set to 4.5 and 20 ppm, respectively. Downstream bioinformatics analysis was performed using Perseus version 1.5.3.2 (Tyanova et al., 2016). Grouping of proteins with similar expression profiles was achieved by hierarchical clustering analysis. Log10 transformation of mean LFQ intensities of proteins was performed for all the tested conditions. Missing values were replaced from the normal distribution via imputation. Hierarchical clustering was performed on Z-score transformed values using Euclidean as a distance measure and Average linkage cluster analysis. Significance B ($p \leq 0.05$) was calculated to identify significantly regulated proteins in each of the ascorbate treatment conditions relative to the control.

Reconstruction of Context-Specific Models Using Proteomics Data

Log10 LFQ protein intensities were used to generate sodium ascorbate concentration specific models by mapping the protein intensities to the genome-scale metabolic model of *B. subtilis*

(Bs-iYO844) (Oh et al., 2007). Log10 LFQ protein intensities from biological replicates (three replicates for each sodium ascorbate concentration and 2 for the control) were averaged and used to constrain the fluxes in the associated reaction using Gene Inactivity Moderated by Metabolism and Expression (GIMME) (Becker and Palsson, 2008). GIMME was run using 90% of the objective function threshold and 50th percentile of proteins expression level. Since properly constrained reactions do not demonstrate uniform distributions of feasible steady-state fluxes, the range and distribution of feasible metabolic flux for each reaction were determined by using *Markov Chain Monte Carlo* (MCMC) sampling (Lewis et al., 2012). To do this, a large number of feasible sets of metabolic fluxes were randomly moved within the solution space until they were well mixed, thereby sampling the entire solution space (Lewis et al., 2012). This sampling process yielded a distribution of feasible steady-state fluxes for each reaction. Sampling was done using *gpSampler* with default settings from the COBRA toolbox (Schellenberger et al., 2011) using Gurobi (Gurobi Optimization, Inc., Houston, TX, United States) and MATLAB® (The MathWorks Inc., Natick, MA, United States). Averaged sampled predicted flux distributions for each reaction at each sodium ascorbate concentration were compared to those from the control model in order to identify reactions (and their associated genes) that have significantly altered flux rates upon adding sodium ascorbate to *B. subtilis*.

Statistical Analysis

The data are presented as the mean ± standard deviation. Intergroup differences were estimated by one-way analysis of variance (ANOVA), followed by a *post hoc* multiple comparison (Tukey) test to compare the multiple means. Differences between values were considered to be statistically significant when the P-value was <0.05.

RESULTS

Vitamin C Does Not Affect Bacterial Growth in a Liquid Medium, but Inhibits Biofilm Formation

Five–ten millimeter doses of vitamin C were previously reported to completely exterminate mycobacteria (Vilcheze et al., 2013). By contrast, it has been reported that vitamin C is not bactericidal toward opportunistic pathogens such as *E. coli* and *P. aeruginosa*, but it renders them more susceptible to antibiotics and some physical treatments (Kallio et al., 2012; Khameneh et al., 2016; Helgadóttir et al., 2017). To clarify this effect of vitamin C on non-mycobacterial species, we used the opportunistic pathogens *E. coli* and *P. aeruginosa*. Since we previously hypothesized that the synergistic effects of vitamin C may be related to biofilms (Helgadóttir et al., 2017), we included also *B. subtilis*, the model organism for biofilm development (Vlamakis et al., 2013). We exposed these bacterial strains to a concentration range of vitamin C from 10 to 40 mM (sodium ascorbate, neutral pH form), assessing both the survival and growth in liquid media and biofilms. Up to 40 mM vitamin C did not significantly inhibit the planktonic growth of *B. subtilis*, *E. coli,* or *P. aeruginosa* (**Supplementary Figure S1**). However, in the same concentration range, biofilm formation was impaired for all three species (**Figure 1** and **Supplementary Figure S2**). Since the vitamin C effect was most pronounced on biofilms, we focused on *B. subtilis* for an in-depth study of the mechanism behind this effect. *B. subtilis* biofilm is the most robust and easiest to analyze in terms of structure and composition, and the mechanisms leading to its formation are well characterized (Vlamakis et al., 2013). The normal *B. subtilis* pellicle (control, 0 mM) exhibits wrinkled and folded architecture (**Figure 1C**). Vitamin C treatment abolished this wrinkled architecture and visibly attenuated the pellicle in a concentration-dependent manner (**Figure 1C**). This effect was accompanied by a linear decrease in biofilm biomass (**Figure 1A**). However, the viability of *B. subtilis* in the pellicle was not significantly affected, suggesting that the reduced biofilm biomass could be due to loss of EPS and not the loss of cells.

Low Concentrations of Vitamin C Do Not Kill *B. subtilis* but Deplete the EPS Matrix

Next, we examined in details the content of various biofilm components in response to the same concentration range of vitamin C. All three major components of the biofilm matrix, polysaccharides, proteins and eDNA, were reduced in the presence of vitamin C (**Figures 2A–C**). The reduction in protein content vs. vitamin C concentration showed a linear regression coefficient of only 0.88, but the trend of exopolysaccharide and DNA reduction was more closely correlated to increasing concentration of vitamin C and the loss of pellicle biomass (**Supplementary Figure S3**). The polysaccharide content and bacterial bio-volume in the *B. subtilis* biofilm were examined by laser scanning confocal microscopy, in the same concentration range of vitamin C (**Figures 2E–G**). EPS account for over 40% of the mass of the *B. subtilis* biofilm, but their identification and characterization is not complete. Roux et al. (2015) identified that poly *n*-acetylglucosamine is the major polysaccharide component of the *B. subtilis* biofilm matrix (Roux et al., 2015). We therefore used fluorescence probes to visualize EPS components: Alexa flour, WGA conjugate, for *n*-acetylglucosamine and ConA, Tetramethylrhodamine conjugate, as an unspecific EPS binder for proteins and other polysaccharides. We first established that these probes had no effect on biofilm formation and exhibited no toxicity to *B. subtilis* cells (**Supplementary Figure S4**). The n-acetylglucosamine (stained in red) occupied a significant part of the bio-volume in the untreated sample (**Figure 2G**). With increasing concentrations of vitamin C, the overall thickness of the biofilm decreased, and the content of the poly *n*-acetylglucosamine (red) and the unspecific EPS matrix (blue) decreased as well (**Figure 2G**). The decreasing pattern of NAG with vitamin C treatment was consistent with the total polysaccharides content observed by colorimetric assay, where significant inhibition was observed with $\geq$20 mM of concentration. Meanwhile, the bacterial bio-volume remained constant up to 30 mM vitamin C. The decreasing pattern of bacterial bio-volume was

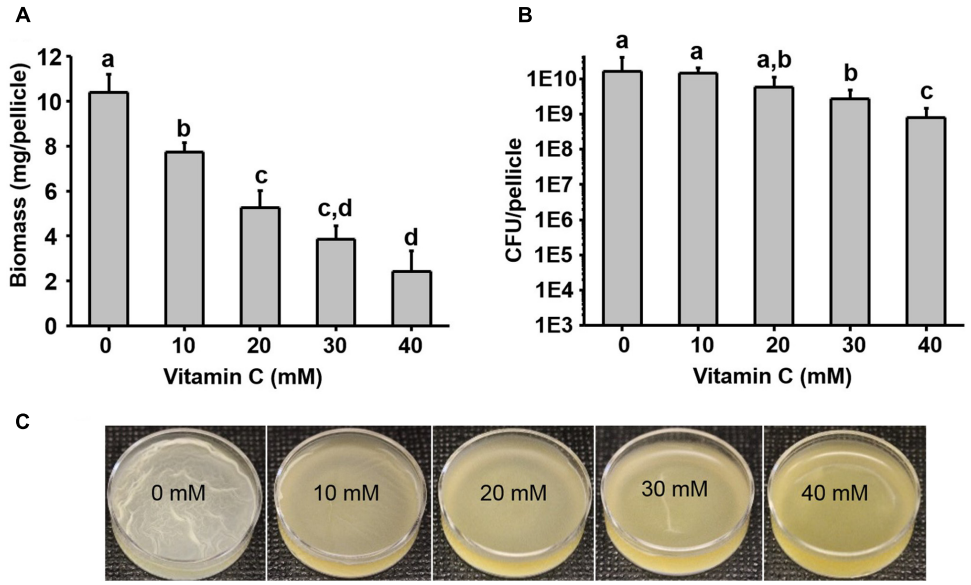

FIGURE 1 | Effect of vitamin C on biomass and bacterial viability of *Bacillus subtilis* biofilm. **(A)** Biomass of a 24 h old *B. subtilis* biofilm in the presence of increasing concentrations of vitamin C. **(B)** Viability of bacteria in a 24 h old biofilm grown in the presence of increasing concentrations of vitamin C. **(C)** Representative images of a 24 h old *B. subtilis* biofilm grown with different concentrations of vitamin C. All data in **(A,B)** are mean values ± standard deviation from three biological replicates. Values labeled by the same superscript are not significantly different from each other ($P > 0.05$).

not consistent with other results because vitamin C treatment is mainly affecting the ECM production but not the growth and viability of bacteria at lower concentrations as shown in **Figure 1**. Viability of cells was examined by live/dead staining (**Figure 3A**) where it was observed that, at low concentration of vitamin C (10 mM) the cell survival rate was similar to that of untreated control biofilms. By contrast, a significant number of cells were dead in biofilms treated with a higher concentration of vitamin C (40 mM). The killing of cells at the higher concentration of vitamin C coincided with higher levels of detectable oxidative stress (**Figure 3B**). This confirmed that vitamin C effect on biofilms takes place in two stages: at concentrations of up to 30 mM the cell viability is preserved, but there is a loss of the EPS, primarily exopolysaccharides. Above 30 mM vitamin C, the bacterial cells start dying.

Stage 1: Low Concentrations of Vitamin C Inhibit Exopolysaccharide Synthesis, Stage 2: High Concentrations of Vitamin C Induce Lethal Oxidative Stress

Since vitamin C seemed to inhibit *B. subtilis* biofilm formation in two stages: reduction of EPS components at up to 30 mM (**Figure 2**), and killing of cells at 30 mM and higher by inducing the oxidative stress (**Figures 1B**, **3**), we performed an in-depth label-free quantitative proteome analysis of vitamin-C treated biofilms in this critical concentration range. A total of 2056 *B. subtilis* proteins were identified, of which 1373 were quantified (**Supplementary Table S1**). Three biological replicates showed a high degree of correlation (Pearson correlation coefficient $\geq$ 0.9) (**Supplementary Figure S5**). Hierarchical clustering analysis was employed for grouping similar expression profiles of proteins (**Figures 4A–C**). Differentially regulated proteins grouped in four clusters (**Figure 4B**). The majority grouped in clusters 1 (expression reduced upon the addition of vitamin C) and 4 (expression enhanced upon the addition of vitamin C). Clusters 2 and 3 showed variation across the range of vitamin C concentrations. All proteins falling in the four different clusters are listed in the **Supplementary Table S1**. Proteins for which the expression levels were most strongly affected by vitamin C treatment ($p \leq 0.05$) were identified by plotting log2 transformed label-free quantification (LFQ) ratios against log10 transformed LFQ intensities (**Figure 4C**). Around 100 proteins were found in this category. Among these, at lower vitamin C concentrations, many proteins directly involved in exopolysaccharides synthesis, export and biofilm formation were depleted: notably PtkA, SlrR, SpeA, EpsC, EpsD, EpsE, EpsH, EpsI, EpsO, TuaD, Ugd (Kobayashi, 2008; Gerwig et al., 2014; Mijakovic and Deutscher, 2015). This correlated with disrupted expression of the key regulators controlling synthesis or activity of these proteins, such as ComA, RepC, Spo0A, YmdB, KinC, FloT, and PtkA (Lazazzera et al., 1999; Diethmaier et al., 2011; Yepes et al., 2012). By contrast, at higher vitamin C concentrations, oxidative stress associated proteins (Antelmann et al., 2000; Grimaud et al., 2001; Towe et al., 2007) were strongly overexpressed: MsrA, MsrB, MhqA, MhqD, AzoR2, and RocA. Individual roles of these proteins in biofilm production and oxidative stress response are reviewed in detail in the discussion section. It was evident from this dataset that vitamin C treatment provoked a two-stage global

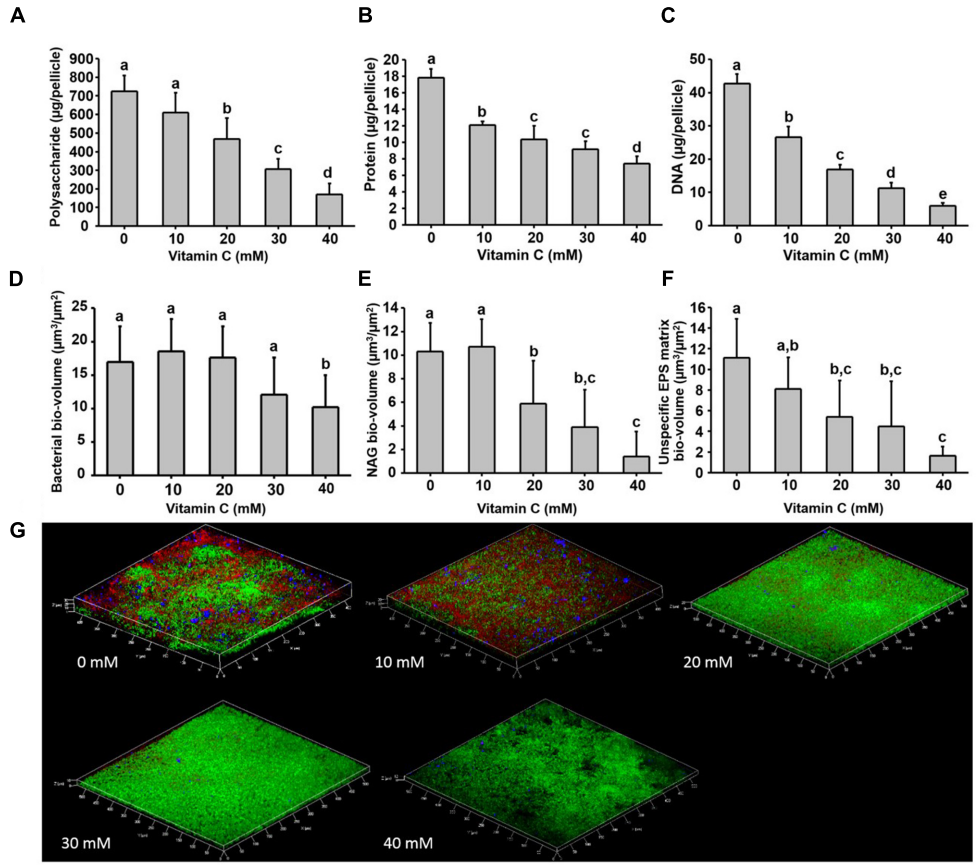

FIGURE 2 | Biochemical and confocal laser scanning microscopy analysis of *B. subtilis* biofilm grown in the presence of vitamin C. **(A)** Content of polysaccharide, **(B)** content of protein and **(C)** eDNA concentration in a 24 h old biofilm. **(D)** Bacterial biovolume, **(E)** biovolume of poly *n*-acetylglucosamine and **(F)** biovolume of unspecific EPS matrix (proteins and polysaccharides) in a 24 h biofilm. **(G)** Representative 3-D architecture of a 24 h old *B. subtilis* biofilm grown in the presence of vitamin C (green: bacteria; red: *n*-acetylglucosamine; blue: unspecific EPS matrix). All data **(A–F)** are mean values ± standard deviation from three biological replicates. Values marked by the same superscripts in panels **(A–F)** are not significantly different from each other ($P > 0.05$).

rearrangement of the cellular proteome, which correlated well to our previous observations on EPS content and cell viability. At low concentrations of vitamin C, biosynthetic pathways leading to exopolysaccharide synthesis and export were down-regulated, explaining the observed depletion of biofilm EPS. At higher vitamin C concentrations, the cell started expressing proteins to cope with excessive oxidative stress, which correlates to cell death and loss of the bacterial bio-volume in the biofilm. To assess the specific impact of this global proteome adaptation on redistribution of metabolic fluxes, we used the quantitative proteomics data to generate vitamin C concentration-specific genome-scale metabolic models, by mapping the protein intensities to the available *B. subtilis* model Bs-iYO844 (Oh et al., 2007) (**Supplementary Figure S6**). This enabled us to identify several metabolic pathways with flux redistribution provoked by vitamin C, which corroborate our findings (**Figure 5**). Notably, the model guided analysis showed that pyrroline-5-carboxylate dehydrogenase (P5CDH)/RocA had a significantly upregulated flux in the presence of vitamin C (**Figure 5**), which indicates that the cells are trying to neutralize ROS.

DISCUSSION

The interest toward bacterial biofilms is driven by the protection that their complex architecture offers toward antimicrobial agents (Donlan, 2002; Peterson et al., 2015). The key element of this architecture are the EPS (Romero et al., 2010; Xiao et al., 2012). Although different ratios of polysaccharides, proteins and eDNA components were reported in biofilms of different species, they collectively act as a backbone for the structural integrity and protection of the bacterial communities (Jennings et al., 2015; Klein et al., 2015; Voberkova et al., 2016). Polysaccharides and proteins of the biofilm matrix form a hydrophobic coating, which retards the penetration of antimicrobial agents and confers biofilm resistance (Epstein et al., 2011; Tiwari et al., 2017). Inhibiting EPS production is a viable strategy for fighting bacterial pathogens. Our results indicate that vitamin C, at concentrations up to 20 mM can be used to effectively disrupt bacterial biofilm formation by inhibiting EPS production.

At sub-lethal doses of vitamin C, i.e., below 30 mM, our proteomics data suggested that quorum sensing of *B. subtilis*

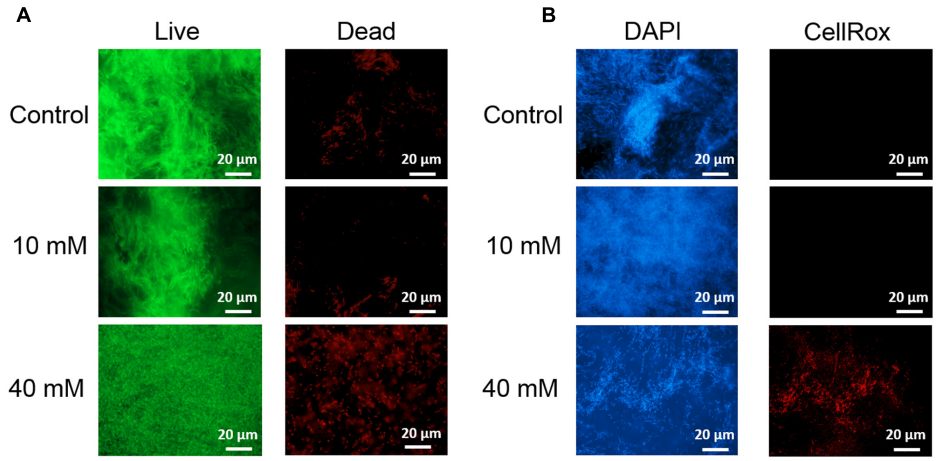

FIGURE 3 | Live/dead staining of *B. subtilis* biofilm grown with or without presence of vitamin C (concentration indicated besides each image) **(A)**. Live bacteria are stained green and red bacteria are dead. Effect of vitamin C on the ROS generation in *B. subtilis* biofilm cells **(B)**. Blue color represents the bacterial cells (DAPI, nucleic acid stain), and the red color (CellRox) intensity corresponds to the amount of ROS induced in bacterial cells.

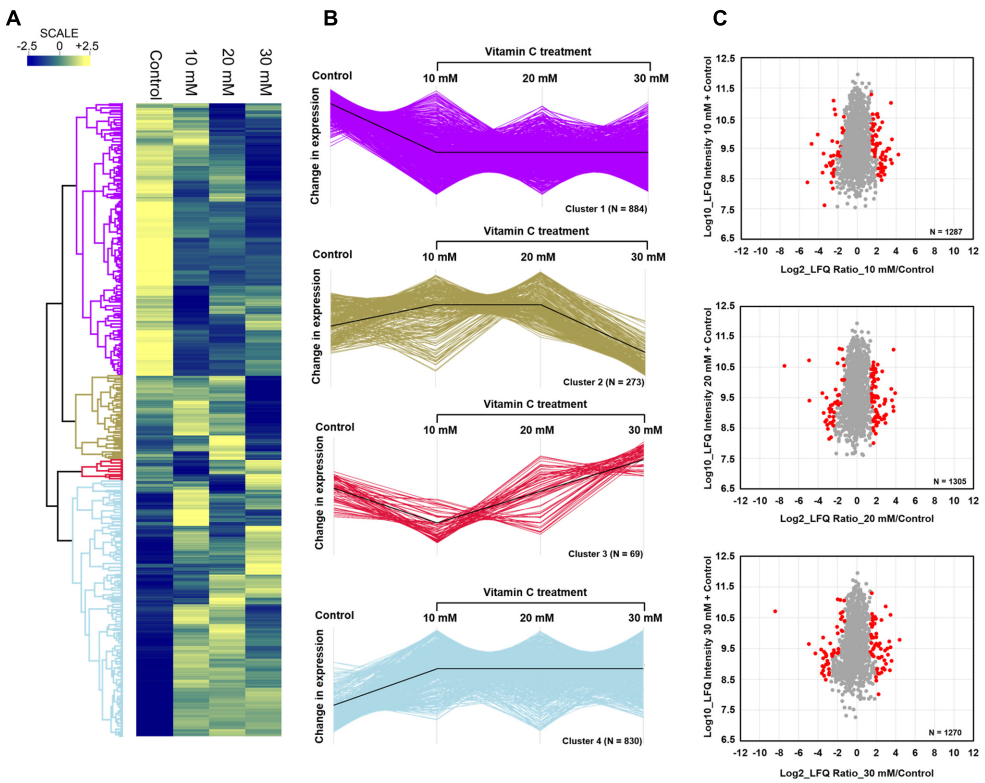

FIGURE 4 | Quantitative proteome analysis of the *B. subtilis* response to vitamin C. **(A)** Hierarchical clustering analysis depicting protein clusters showing differential fluctuations. Mean LFQ intensities of the three biological replicates for each condition were calculated for the clustering analysis. **(B)** All proteins with expression change due to vitamin C grouped into four clusters with different response profiles. The black line indicates the overall trend of the protein expression profile in each of the individual clusters. **(C)** Scatter plot depicting significantly ($p \leq 0.05$) upregulated or downregulated proteins (in red) in each of the vitamin C treatment conditions relative to the control. Log2 calculated LFQ ratios are plotted against log10 LFQ intensities.

was impaired, which is in accord with previous observations in *P. aeruginosa* (El-Mowafy et al., 2014). The major *B. subtilis* quorum sensing associated protein, the response regulator ComA, became less abundant upon vitamin C treatment. ComA affects the transcription of more than 10% of the *B. subtilis* genome, and it activates the transcription of genes for biofilm

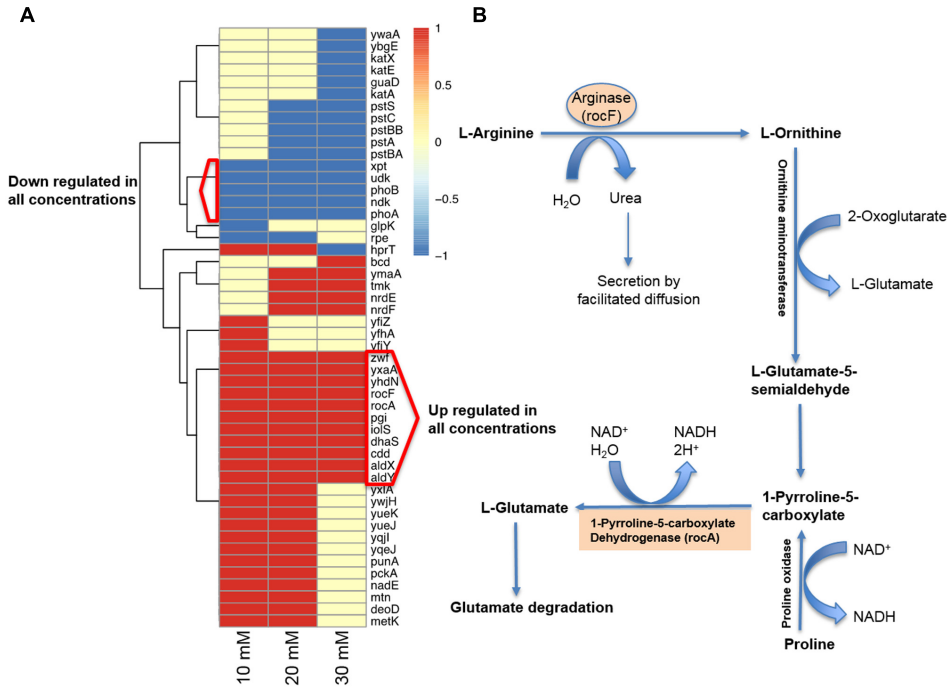

FIGURE 5 | Model-guided contextualization of proteomics data. **(A)** Proteins that are associated to reactions that are significantly altered when adding increasing concentrations of sodium ascorbate to *B. subtilis*. **(B)** Degradative pathway of arginine generating P5CDH/RocA and ARGN/RocF are significantly upregulated at all concentrations of vitamin C, producing glutamate and NADH, and contributing to protection against oxidative stress.

formation (Mielich-Süss and Lopez, 2015). In addition to ComA depletion, vitamin C provoked overexpression of RapC, a negative regulator of ComA activity (Lazazzera et al., 1999). Consequently, vitamin C provoked a drop in expression levels of a number of ComA-RapC-dependent proteins essential for biofilm formation, such as Spo0A, SlrR, YmdB, KinC, FloT, and SpeA. Inactivation of Spo0A, a major early sporulation transcriptional factor, causes a defect in biofilm formation due to its role in negatively regulating AbrB (Hamon and Lazazzera, 2001) and controlling the expression of an operon responsible for the synthesis of the exopolysaccharide matrix (McLoon et al., 2011). Cells with defective FloT are known to reduce the level of FtsH protease which indirectly regulates the phosphorylation and activity of Spo0A via phosphatase degradation (Yepes et al., 2012). SlrR acts in concert with SinR, and induces the *eps* and *yqxM* operons required for biofilm formation, by consequence, a mutation of *slrR* leads to a defect in biofilm formation (Kobayashi, 2008). Inactivating *ymdB* has been demonstrated to suppress SinR-dependent biofilm gene expression (*slrR*, *tapA*, *epsA*) and to induce the expression of SigD dependent motility genes (*hag*, *cheV*, and *motA*) (Diethmaier et al., 2011). SpeA, an arginine decarboxylase, is essential for the production of polyamines which are required for *B. subtilis* biofilm formation (Burrell et al., 2010). Finally, low concentrations of vitamin C inhibited the expression of a number of proteins involved directly in synthesis and export of extracellular polysaccharides (Cluster 1), namely the operon *epsA-O* (Barnes et al., 2012; Pozsgai et al., 2012). Among the *eps* genes, *epsH-K* encodes proteins responsible for the production of poly-n-acetyl glucosamine (Roux et al., 2015), *epsH-J* encodes glycosyltransferases, while *epsK* is an exporter of poly-*N*-acetylglucosamine. EpsE has been demonstrated to have a dual function: production of exopolysaccharides and functional control of the flagellum (Guttenplan et al., 2010). In our dataset, proteins EpsC, EpsD, EpsE, EpsH, EpsI, and EpsO were no longer detectable in the presence of vitamin C. Similarly, UDP-glucose dehydrogenases TuaD and Ugd, which synthesize glucuronic acid, a precursor for exopolysaccharide production (Mijakovic and Deutscher, 2015), were also less abundant in vitamin C-treated samples. The activity of several key proteins in the exopolysaccharide production and export cluster are known to be positively regulated by tyrosine-phosphorylation, catalyzed by BY-kinases (Mijakovic et al., 2003; Whitfield and Larue, 2008). In our dataset, the expression BY-kinase PtkA, a control protein for exopolysaccharide production and biofilm formation, was also strongly repressed in the presence of vitamin C. While we clearly observe the consequences of disruption of specific regulatory networks that control the EPS synthesis on the proteome level, it is still unclear how vitamin C targets these regulators. Further studies will be needed to elucidate the exact molecular mechanism behind this effect.

The killing effect of vitamin C against *B. subtilis* biofilm cells occurred at concentrations of 30 mM and above (**Figures 1A**, **2D**). It has been previously demonstrated that the bactericidal effect of vitamin C against mycobacteria was mainly associated with oxidative stress (Roux et al., 2015). Accordingly, in our dataset several proteins known to provide

protection against oxidative stress (Towe et al., 2007) were overexpressed at high vitamin C concentrations: MsrA, MsrB, MhqA, MhqD, and AzoR2 (**Figure 4B**, cluster 5). MsrA and MsrB belong to the methionine sulfoxide reductase (Msrs) family and are known to protect cells from oxidative stress by reducing methionine sulfoxide to methionine (Grimaud et al., 2001). Both MsrA and MsrB mutants of *E. coli* were shown to have more sensitivity toward oxidative stress generated by H_2O_2 (Towe et al., 2007). It has been reported that genes belonging to the MhqR regulon: *mhqA*, *mhqD,* and *azoR2* are overexpressed under the electrophile and oxidative stress (Antelmann et al., 2000). The glyoxalases (MhqA, MhqE, and MhqN) were also demonstrated as critical for the detoxification of cytotoxic methylglyoxal in bacteria and eukaryal cells (Antelmann et al., 2000). Azoreductases (AzoR1/2) are enzymes which catalyze the NADH dependent two-electron of substrates to protect the cells from toxic effects of free radicals and ROS arising from one-electron reduction (Antelmann et al., 2000). In addition, pyrroline-5-carboxylate dehydrogenase (P5CDH)/RocA was overexpressed, leading to a significantly higher predicted flux rate in vitamin C-treated genome-scale metabolic models (**Figure 5B**). P5CDH converts Δ^1-pyrroline-5-carboxylate (P5C) to glutamate. Proline oxidase (YcgM), which degrades proline into P5C, was not upregulated in the presence of vitamin C. By contrast, arginase (ARGN/RocF) had a significantly higher flux in all vitamin C models, as well as the secretion of urea, a byproduct of the arginase reaction. Accumulation of P5C was found to induce cell death by producing reactive oxygen species (Nishimura et al., 2012), and the activation of P5CDH counters that effect (Miller et al., 2009). Therefore, it is plausible that vitamin C-induced oxidative stress provokes the overexpression of RocA, as a protective effect. We propose that this oxidative stress, clearly evidenced by the proteome rearrangement, is the most probable cause of death for cells that become exposed once the protective EPS matrix is lost, i.e., at elevated concentrations of vitamin C, above 30 mM.

Based on these findings, we propose that the inhibitory effect of vitamin C on biofilm formation proceeds by inhibition of quorum sensing and other stationary phase regulatory mechanisms underpinning biofilm development, which specifically leads to inhibition of polysaccharide biosynthesis. Once the EPS content is reduced, at vitamin C concentrations of 30 mM and above in the case of *B. subtilis*, bacterial cells get fully exposed to the medium. Thereby they become more susceptible to killing by vitamin C-induced oxidative stress reported here, and other antibacterial compounds or treatments (Khameneh et al., 2016; Helgadóttir et al., 2017). In situations where the risk of developing resistance by administering excessive doses of antibiotics is too high, we would argue that low concentrations of vitamin C can be effectively used as a pre-treatment or a combined treatment to destabilize bacterial biofilms.

AUTHOR CONTRIBUTIONS

SP, VR, AA-H, AD, and CS performed the experiments. SP, VR, AD, AA-H, VM, KM, TG, XG, FW, and IM analyzed the data. SP, VR, AA-H, and IM wrote the manuscript with support from all authors.

FUNDING

This work was funded by grants from the Chalmers University of Technology and VINNOVA to IM and FW, and ÅForsk to IM.

ACKNOWLEDGMENT

The authors would like to thank the Centre for Cellular Imaging at the Sahlgrenska Academy, University of Gothenburg.

SUPPLEMENTARY MATERIAL

The mass spectrometry proteomics data have been deposited to the ProteomeXchange Consortium via the PRIDE (Vizcaíno et al., 2013) partner repository with the dataset identifier PXD007533.

The Supplementary Material for this article can be found online at: https://www.frontiersin.org/articles/10.3389/fmicb.2017.02599/full#supplementary-material

FIGURE S1 | Effect of vitamin C on bacterial growth. Growth of **(A)** *Bacillus subtilis*, **(B)** *Escherichia Coli,* and **(C)** *Pseudomonas aeruginosa*, in the presence of different concentrations of vitamin C, as indicated in the color-coded legend. The experiment was performed with biological triplicates, and the error bar shows the standard deviation.

FIGURE S2 | Effect of vitamin C treatment on biofilm formation by *E. coli* and *P. aeruginosa*. The biofilms were stained with crystal violet and optical density was measured. All data represent mean ± standard deviation. Values followed by the same superscripts are not significantly different from each other ($P > 0.05$).

FIGURE S3 | Relationship between concentration of sodium ascorbate and biomass and constituents of EPS matrix. Linear fitting of biomass, polysaccharide, DNA and protein of biofilm vs. increasing concentration of vitamin C.

FIGURE S4 | Effect of polysaccharide fluorescence stain on biofilms. Biomass **(A)** and viability **(B)** of *B. subtilis* biofilm grown in the presence of two different polysaccharide stains alone or in combination: Concanavalin A Tetramethylrhodamine conjugate (ConA; 50 μg/ml) and Alexa flour® 633-labeled wheat germ agglutinin conjugate (WGA; 10 μg/ml).

FIGURE S5 | Correlation between biological replicates of the proteomics analysis. Correlation plots depicting correlation of proteins between biological replicates in the control and in 10, 20, and 30 mM vitamin C treatment conditions. The figure shows Log10 intensities of individual replicates plotted against each other.

FIGURE S6 | Workflow for model-guided analysis of proteomics data. **(A)** Log10 LFQ protein intensities from the biological replicates were averaged and mapped using GIMME (Becker and Palsson, 2008) to Bs-iYO844, the *B. subtilis* genome-scale metabolic model (Oh et al., 2007) to constrain the fluxes in the associated reactions. **(B)** The range and distribution of feasible metabolic flux for each reaction were determined by using Markov Chain Monte Carlo (MCMC) sampling (Lewis et al., 2012). Averaged sampled predicted flux distributions for each reaction at each sodium ascorbate concentration were compared to those from the control model (ascorbic acid concentration = 0 mM) in order to identify differentially active reactions which are later decomposed into their corresponding genes through the gene-protein reaction associations embedded in the model.

TABLE S1 | List of all identified proteins, proteins belonging to cluster 1, 2, 3, 4 from **Figure 3**, and regulated proteins.

REFERENCES

Antelmann, H., Scharf, C., and Hecker, M. (2000). Phosphate starvation-inducuble proteins of *Bacillus subtilis*: proteomics and transcriptional analysis. *J. Bacteriol.* 182, 4478–4490. doi: 10.1128/JB.182.16.4478-4490.2000

Barnes, A. M., Ballering, K. S., Leibman, R. S., Wells, C. L., and Dunny, G. M. (2012). Enterococcus faecalis produces abundant extracellular structures containing DNA in the absence of cell lysis during early biofilm formation. *mBio* 3:e00193-12. doi: 10.1128/mBio.00193-12

Becker, S. A., and Palsson, B. O. (2008). Context-specific metabolic networks are consistent with experiments. *PLOS Comput. Biol.* 4:e1000082. doi: 10.1371/journal.pcbi.1000082

Branda, S. S., Chu, F., Kearns, D. B., Losick, R., and Kolter, R. A. (2006). major protein component of the *Bacillus subtilis* biofilm matrix. *Mol. Microbiol.* 59, 1229–1238. doi: 10.1111/j.1365-2958.2005.05020.x

Branda, S. S., Vik, S., Friedman, L., and Kolter, R. (2005). Biofilms: the matrix revisited. *Trends Microbiol.* 13, 20–26. doi: 10.1016/j.tim.2004.11.006

Burrell, M., Hanfrey, C. C., Murray, E. J., Stanley-Wall, N. R., and Michael, A. J. (2010). Evolution and multiplicity of arginine decarboxylases in polyamine biosynthesis and essential role in *Bacillus subtilis* biofilm formation. *J. Biol. Chem.* 285, 39224–39238. doi: 10.1074/jbc.M110.163154

Cegelski, L., Marshall, G. R., Eldridge, G. R., and Hultgren, S. J. (2008). The biology and future prospects of antivirulence therapies. *Nat. Rev. Microbiol.* 6, 17–27. doi: 10.1038/nrmicro1818

Cox, J., Matic, I., Hilger, M., Nagaraj, N., Selbach, M., Olsen, J. V., et al. (2009). A practical guide to the MaxQuant computational platform for SILAC-based quantitative proteomics. *Nat. Protocols* 4, 698–705. doi: 10.1038/nprot.2009.36

Diethmaier, C., Pietack, N., Gunka, K., Wrede, C., Lehnik-Habrink, M., Herzberg, C., et al. (2011). A novel factor controlling bistability in *Bacillus subtilis*: the YmdB Protein affects flagellin expression and biofilm formation. *J. Bacteriol.* 193, 5997–6007. doi: 10.1128/JB.05360-11

Donlan, R. M. (2002). Biofilms: microbial life on surfaces. *Emerg. Infect. Dis.* 8, 881–890. doi: 10.3201/eid0809.020063

Durmus, N. G., Taylor, E. N., Kummer, K. M., and Webster, T. J. (2013). Enhanced efficacy of super paramagnetic iron oxide nanoparticles against antibiotic-resistant biofilms in the presence of metabolites. *Adv. Mater.* 25, 5706–5713. doi: 10.1002/adma.201302627

El-Mowafy, S. A., Shaaban, M. I., and Abd El Galil, K. H. (2014). Sodium ascorbate as a quorum sensing inhibitor of *Pseudomonas aeruginosa*. *J. Appl. Microbiol.* 117, 1388–1399. doi: 10.1111/jam.12631

Epstein, A. K., Pokroy, B., Seminara, A., and Aizenberg, J. (2011). Bacterial biofilm shows persistent resistance to liquid wetting and gas penetration. *Proc. Natl. Acad. Sci. U.S.A.* 108, 995–1000. doi: 10.1073/pnas.1011033108

Flemming, H. C., Wingender, J., Szewzyk, U., Steinberg, P., Rice, S. A., and Kjelleberg, S. (2016). Biofilms: an emergent form of bacterial life. *Nat. Rev. Microbiol.* 14, 563–575. doi: 10.1038/nrmicro.2016.94

Gerwig, J., Kiley, T. B., Gunka, K., Stanley-Wall, N., and Stülke, J. (2014). The protein tyrosine kinases EpsB and PtkA differentially affect biofilm formation in *Bacillus subtilis*. *Microbiology* 160, 682–691. doi: 10.1099/mic.0.074971-0

Grimaud, R., Ezraty, B., Mitchell, J. K., Lafitte, D., Briand, C., Derrick, P. J., et al. (2001). Repair of oxidized proteins. Identification of a new methionine sulfoxide reductase. *J. Biol. Chem.* 276, 48915–48920. doi: 10.1099/mic.0.074971-0

Guttenplan, S. B., Blair, K. M., and Kearns, D. B. (2010). The EpsE flagellar clutch is bifunctional and synergizes with EPS biosynthesis to promote *Bacillus subtilis* biofilm formation. *PLOS Genet.* 6:e1001243. doi: 10.1371/journal.pgen.1001243

Hamon, M. A., and Lazazzera, B. A. (2001). The sporulation transcription factor Spo0A is required for biofilm development in *Bacillus subtilis*. *Mol. Microbiol.* 42, 1199–1209. doi: 10.1046/j.1365-2958.2001.02709.x

Helgadóttir, S., Pandit, S., Mokkapati, V. R. S. S., Westerlund, F., Apell, P., and Mijakovic, I. (2017). Vitamin C pretreatment enhances the antibacterial effect of cold atmospheric plasma. *Front. Cell. Infect. Microbiol.* 7:43. doi: 10.3389/fcimb.2017.00043

Heydorn, A., Nielsen, A. T., Hentzer, M., Sternberg, C., Givskov, M., Ersbøll, B. K., et al. (2000). Quantification of biofilm structures by the novel computer program comstat. *Microbiology* 146, 2395–2407. doi: 10.1099/00221287-146-10-2395

Ishihama, Y., Rappsilber, J., and Mann, M. (2006). Modular stop and go extraction tips with stacked disks for parallel and multidimensional peptide fractionation in proteomics. *J. Proteome Res.* 5, 988–994. doi: 10.1021/pr050385q

Jennings, L. K., Storek, K. M., Ledvina, H. E., Coulon, C., Marmont, L. S., Sadovskaya, I., et al. (2015). Pelis a cationic exopolysaccharide that cross-links extracellular DNA in the *Pseudomonas aeruginosa* biofilm matrix. *Proc. Natl. Acad. Sci. U.S.A.* 112, 11353–11358. doi: 10.1073/pnas.1503058112

Kallio, J., Jaakkola, M., Maki, M., Kilpelainen, P., and Virtanen, V. (2012). Vitamin C inhibits *Staphylococcus aureus* growth and enhances the inhibitory effect of quercetin on growth of *Escherichia coli* in vitro. *Planta Med.* 78, 1824–1830. doi: 10.1055/s-0032-1315388

Khameneh, B., Fazly Bazzaz, B. S., Amani, A., Rostami, J., and Vahdati-Mashhadian, N. (2016). Combination of anti-tuberculosis drugs with vitamin C or NAC against different Staphylococcus aureus and *Mycobacterium tuberculosis* strains. *Microb. Pathog.* 93, 83–87. doi: 10.1016/j.micpath.2015.11.006

Klein, M. I., Hwang, G., Santos, P. H., Campanella, O. H., and Koo, H. (2015). *Streptococcus mutans*- derived extracellular matrix in cariogenic oral biofilms. *Front. Cell. Infect. Microbiol.* 5:10. doi: 10.3389/fcimb.2015.00010

Kobayashi, K. (2008). SlrR/SlrA controls the initiation of biofilm formation in *Bacillus subtilis*. *Mol. Microbiol.* 69, 1399–1410. doi: 10.1111/j.1365-2958.2008.06369.x

Lazazzera, B. A., Kurtser, I. G., McQuade, R. S., and Grossman, A. D. (1999). An autoregulatory circuit affecting peptide signaling in *Bacillus subtilis*. *J. Bacteriol.* 181, 5193–5200.

Lewis, N. E., Nagarajan, H., and Palsson, B. O. (2012). Constraining the metabolic genotype–phenotype relationship using a phylogeny of in silico methods. *Nat. Rev. Microbiol.* 10, 291–305. doi: 10.1038/nrmicro2737

Marvasi, M., Visscher, P. T., and Casillas Martinez, L. (2010). Exopolymeric substances (EPS) from *Bacillus subtilis*: polymers and genes encoding their synthesis. *FEMS Microbiol. Lett.* 313, 1–9. doi: 10.1111/j.1574-6968.2010.02085.x

McLoon, A. L., Kolodkin-Gal, I., Rubinstein, S. M., Kolter, R., and Losick, R. (2011). Spatial regulation of histidine kinases governing biofilm formation in *Bacillus subtilis*. *J. Bacteriol.* 193, 679–685. doi: 10.1128/JB.01186-10

Mielich-Süss, B., and Lopez, D. (2015). Molecular mechanisms involved in *Bacillus subtilis* biofilm formation. *Environ. Microbiol.* 17, 555–565. doi: 10.1111/1462-2920.12527

Mijakovic, I., and Deutscher, J. (2015). Protein-tyrosine phosphorylation in *Bacillus subtilis*: a 10-year retrospective. *Front. Microbiol.* 6:18. doi: 10.3389/fmicb.2015.00018

Mijakovic, I., Poncet, S., Boël, G., Mazé, A., Gillet, S., Jamet, E., et al. (2003). Transmembrane modulator-dependent bacterial tyrosine kinase activates UDP-glucose dehydrogenases. *EMBO J.* 22, 4709–4718. doi: 10.1093/emboj/cdg458

Miller, G., Honig, A., Stein, H., Suzuki, N., Mittler, R., and Zilberstein, A. (2009). Unraveling Δ1- pyrroline-5- carboxylate-proline cycle in plants by uncoupled expression of proline oxidation enzymes. *J. Biol. Chem.* 284, 26482–26492. doi: 10.1074/jbc.M109.009340

Nishimura, A., Nasuno, R., and Takagi, H. (2012). The proline metabolism intermediate Δ1-pyrroline-5- carboxylate directly inhibits the mitochondrial respiration in budding yeast. *FEBS Lett.* 586, 2411–2416. doi: 10.1016/j.febslet.2012.05.056

Oh, Y.-K., Palsson, B. O., Park, S. M., Schilling, C. H., and Mahadevan, R. (2007). Genome-scale reconstruction of metabolic network in *Bacillus subtilis* based on high-throughput phenotyping and gene essentiality data. *J. Biol. Chem.* 282, 28791–28799. doi: 10.1074/jbc.M703759200

Pandit, S., Kim, J. E., Jung, K. H., Chang, K. W., and Jeon, J. G. (2011). Effect of sodium fluoride on the virulence factors and composition of *Streptococcus mutans* biofilms. *Arch. Oral. Biol.* 56, 643–649. doi: 10.1016/j.archoralbio.2010.12.012

Peterson, B. W., He, Y., Ren, Y., Zerdoum, A., Libera, M. R., Sharma, P. K., et al. (2015). Viscoelasticity of biofilms and their recalcitrance to mechanical and chemical challenges. *FEMS Microbiol. Rev.* 39, 234–245. doi: 10.1093/femsre/fuu008

Pozsgai, E. R., Blair, K. M., and Kearns, D. B. (2012). Modified mariner transposons for random inducible-expression insertions and transcriptional reporter fusion insertions in *Bacillus subtilis*. *Appl. Environ. Microbiol.* 78, 778–785. doi: 10.1128/AEM.07098-11

Romero, D., Aguilar, C., Losick, R., and Kolter, R. (2010). Amyloid fibers provide structural integrity to *Bacillus subtilis* biofilms. *Proc. Natl. Acad. Sci. U.S.A.* 107, 2230–2234. doi: 10.1073/pnas.0910560107

Roux, D., Cywes-Bentley, C., Zhang, Y. F., Pons, S., Konkol, M., Kearns, D. B., et al. (2015). Identification of poly-n-acetylglucosamine as a major polysaccharide component of the *Bacillus subtilis* biofilm matrix. *J. Biol. Chem.* 290, 19261–19272. doi: 10.1074/jbc.M115.648709

Roy, R., Tiwari, M., Donelli, G., and Tiwari, V. (2017). Strategies for combating bacterial biofilms: A focus on anti-biofilm agents and their mechanisms of action. *Virulence* doi: 10.1080/21505594.2017.1313372 [Epub ahead of print].

Schellenberger, J., Que, R., Fleming, R. M. T., Thiele, I., Orth, J. D., Feist, A. M., et al. (2011). Quantitative prediction of cellular metabolism with constraint-based models: the COBRA Toolbox v2.0. *Nat. Protoc.* 6, 1290–1307. doi: 10.1038/nprot.2011.308

Tiwari, V., Tiwari, D., Patel, V., and Tiwari, M. (2017). Effect of secondary metabolite of Actinidia deliciosa on the biofilm and extra-cellular matrix components of *Acinetobacter baumannii*. *Microb. Pathog.* 110, 345–351. doi: 10.1016/j.micpath.2017.07.013

Towe, S., Leelakriangsak, M., Kobayashi, K., Van Duy, N., Hecker, M., Zuber, P., et al. (2007). The MarR-type repressor MhqR (YkvE) regulates multiple dioxygenases/glyoxalases and an azoreductase which confer resistance to 2-methylhydroquinone and catechol in *Bacillus subtilis*. *Mol. Microbiol.* 66, 40–54. doi: 10.1111/j.1365-2958.2007.05891.x

Tyanova, S., Temu, T., Sinitcyn, P., Carlson, A., Hein, M. Y., Geiger, T., et al. (2016). The Perseus computational platform for comprehensive analysis of (prote)omics data. *Nat. Methods* 13, 731–740. doi: 10.1038/nmeth.3901

Vilcheze, C., Hartman, T., Weinrick, B., and Jacobs, W. R. Jr. (2013). *Mycobacterium* tuberculosis is extraordinarily sensitive to killing by a vitamin C-induced Fenton reaction. *Nat. Commun.* 4:1881. doi: 10.1038/ncomms2898

Vizcaíno, J. A., Côté, R. G., Csordas, A., Dianes, J. A., Fabregat, A., Foster, J. M., et al. (2013). The Proteomics Identifications (PRIDE) database and associated tools: status in 2013. *Nucleic Acids Res.* 41, D1063–D1069. doi: 10.1093/nar/gks1262

Vlamakis, H., Chai, Y., Beauregard, P., Losick, R., and Kolter, R. (2013). Sticking together: building a biofilm the *Bacillus subtilis* way. *Nat. Rev. Microbiol.* 11, 157–168. doi: 10.1038/nrmicro2960

Voberkova, S., Hermanova, S., Hrubanova, K., and Krzyzanek, V. (2016). Biofilm formation and extracellular polymeric substances (EPS) production by *Bacillus subtilis* depending on nutritional conditions in the presence of polyester film. *Folia Microbiol.* 61, 91–100. doi: 10.1007/s12223-015-0406-y

Whitfield, C., and Larue, K. (2008). Stop and go: regulation of chain length in the biosynthesis of bacterial polysaccharides. *Nat. Struct. Mol. Biol.* 15, 121–123. doi: 10.1038/nsmb0208-121

Xavier, J. B., Picioreanu, C., Rani, S. A., van Loosdrecht, M. C., and Stewart, P. S. (2005). Biofilm- control strategies based on enzymic disruption of the extracellular polymeric substance matrix–a modelling study. *Microbiology* 151(Pt 12), 3817–3832. doi: 10.1099/mic.0.28165-0

Xiao, J., Klein, M. I., Falsetta, M. L., Lu, B., Delahunty, C. M., Yates, J. R., et al. (2012). The exopolysaccharide matrix modulates the interaction between 3D architecture and virulence of a mixed-species oral biofilm. *PLOS Pathog.* 8:e1002623. doi: 10.1371/journal.ppat.1002623

Yepes, A., Schneider, J., Mielich, B., Koch, G., García-Betancur, J.-C., Ramamurthi, K. S., et al. (2012). The biofilm formation defect of a *Bacillus subtilis* flotillin-defective mutant involves the protease FtsH. *Mol. Microbiol.* 86, 457–471. doi: 10.1111/j.1365-2958.2012.08205.x

Conflict of Interest Statement: The authors declare that the research was conducted in the absence of any commercial or financial relationships that could be construed as a potential conflict of interest.

frontiers in Microbiology

ORIGINAL RESEARCH
published: 24 July 2018
doi: 10.3389/fmicb.2018.01661

Lactobacillus rhamnosus GR-1 Ameliorates *Escherichia coli*-Induced Activation of NLRP3 and NLRC4 Inflammasomes With Differential Requirement for ASC

*Qiong Wu†, Yao-Hong Zhu†, Jin Xu, Xiao Liu, Cong Duan, Mei-Jun Wang and Jiu-Feng Wang**

Department of Veterinary Clinical Sciences, College of Veterinary Medicine, China Agricultural University, Beijing, China

Escherichia coli is a common cause of mastitis in dairy cows. The adaptor protein apoptosis-associated speck-like protein containing a caspase recruitment domain (ASC) synergizes with caspase-1 to regulate inflammasome activation during pathogen infection. Here, the *ASC* gene was knocked out in bovine mammary epithelial (MAC-T) cells using clustered, regularly interspaced, short palindromic repeat (CRISPR)/CRISPR-associated (Cas)-9 technology. MAC-T cells were pre-incubated with and without *Lactobacillus rhamnosus* GR-1 and then exposed to *E. coli*. Western blot analysis demonstrated increased expression of NLRP3 and NLRC4 following *E. coli* infection, but this increase was attenuated by pre-incubation with *L. rhamnosus* GR-1, regardless of *ASC* knockout. Western blot and immunofluorescence analyses revealed that pre-incubation with *L. rhamnosus* GR-1 decreased *E. coli*-induced caspase-1 activation at 6 h after *E. coli* infection, as also observed in *ASC*-knockout MAC-T cells. The *E. coli*-induced increase in *caspase-4* mRNA expression was inhibited by pre-incubation with *L. rhamnosus* GR-1. *ASC* knockout diminished, but did not completely prevent, increased production of IL-1β and IL-18 and cell pyroptosis associated with *E. coli* infection, whereas pre-incubation with *L. rhamnosus* GR-1 inhibited this increase. Our data indicate that *L. rhamnosus* GR-1 suppresses activation of ASC-dependent NLRP3 and NLRC4 inflammasomes and production of downstream IL-lβ and IL-18 during *E. coli* infection. *L. rhamnosus* GR-1 also inhibited *E. coli*-induced cell pyroptosis, in part through attenuation of NLRC4 and non-canonical caspase-4 activation independently of ASC.

Keywords: bovine mammary epithelial cell, *Lactobacillus rhamnosus*, *Escherichia coli*, inflammasome, ASC

OPEN ACCESS

Edited by:
Sanna Sillankorva, University of Minho, Portugal

Reviewed by:
Atte Von Wright, University of Eastern Finland, Finland
Rebecca Leigh Schmidt, Upper Iowa University, United States

***Correspondence:**
Jiu-Feng Wang
jiufeng_wang@hotmail.com

† These authors have contributed equally to this work.

Specialty section:
This article was submitted to Antimicrobials, Resistance and Chemotherapy, a section of the journal Frontiers in Microbiology

Received: *27 February 2018*
Accepted: *04 July 2018*
Published: *24 July 2018*

Citation:
Wu Q, Zhu Y-H, Xu J, Liu X, Duan C, Wang M-J and Wang J-F (2018) Lactobacillus rhamnosus GR-1 Ameliorates Escherichia coli-Induced Activation of NLRP3 and NLRC4 Inflammasomes With Differential Requirement for ASC. Front. Microbiol. 9:1661. doi: 10.3389/fmicb.2018.01661

INTRODUCTION

Escherichia coli is a frequent cause of bovine mastitis and a leading cause of clinical mastitis in bovine (Shaheen et al., 2015). The NLR family member pyrin domain-containing protein 3 (NLRP3) inflammasome is considered a suitable target for new alternatives to antibiotics to treat bovine mastitis (Thacker et al., 2012). Our previous study showed that probiotic *Lactobacillus rhamnosus* GR-1 ameliorates *E. coli*-induced inflammatory damage via

attenuation of apoptosis-associated speck-like protein containing a caspase recruitment domain (ASC)-independent NLRP3 inflammasome activation in primary bovine mammary epithelial cells (PBMCs) (Wu et al., 2016). Therefore, *L. rhamnosus* GR-1 represents a potentially promising therapeutic agent targeting inflammasome activity in *E. coli*-associated bovine mastitis.

Binding of lipopolysaccharide (LPS) from gram-negative bacteria to toll-like receptor (TLR) 4 increases cellular expression of NLRP3 protein through nuclear factor-κB (NF-κB) signaling, leading to rapidly NLRP3 activation (Afonina et al., 2017). Upon activation, NLRP3 nucleates the adaptor protein ASC through interaction with the pyrin domain (PYD). Pro-caspase-1 is subsequently autoproteolytically processed through CARD–CARD (caspase recruitment domain) interactions in the NLRP3/ASC complex scaffold and cleaves precursors of the proinflammatory interleukin (IL)-1 family into their bioactive forms, IL-1β and IL-18. We found that *L. rhamnosus* GR-1 reduces *E. coli*-induced caspase-1 activation and production of IL-1β and IL-18. However, in contrast to increases in the expression of NLRP3 and caspase-1, expression of the adaptor protein ASC is decreased in PBMCs infected with *E. coli*, even in cells pretreated with *L. rhamnosus* GR-1 (Wu et al., 2016).

In contrast to the multiple stimuli that activate NLRP3, NLRC4 is activated by flagellin and the rod protein EscI of the *E. coli* type III secretion system (T3SS) apparatus (Miao et al., 2010). NLRC4 contains a CARD motif, through which it directly oligomerizes with caspase-1 independent of ASC; this complex activates caspase-1 without autoproteolysis, triggering pyroptosis, an inflammatory form of cell death (Broz et al., 2010b). However, ASC greatly enhances the efficiency of NLRC4-mediated maturation of IL-1β and IL-18 by inducing caspase-1 autoproteolysis (Lamkanfi and Dixit, 2014). NLRC4-dependent production of IL-1β is induced by pathogenic *Salmonella* or *Pseudomonas* but not commensal *Lactobacillus plantarum*, indicating that the NLRC4 inflammasome specifically discriminates pathogens and probiotic bacteria (Franchi et al., 2012). However, the contributions of the NLRC4 inflammasome to inflammatory responses that control *E. coli* infections are less clear in relation to *L. rhamnosus* GR-1.

NLRP3 and NLRC4 inflammasomes play a crucial role in potentiating the host antimicrobial response (Guo et al., 2015). Studies using ASC-deficient cells from $ASC^{-/-}$ mice demonstrated the dual role of ASC in bridging NLRP3 and NLRC4 inflammasomes and caspase-1 via PYD and CARD and regulating the result of inflammasome activation (Broz et al., 2010a; Gueya et al., 2014). ASC-dependent inflammasome activation results in the production of proinflammatory IL-1 family cytokines, whereas ASC-independent inflammasome activation induces cell pyroptosis. Given the significant potential of IL-1 family cytokines to cause detrimental inflammation and pyroptosis to control the spread of intracellular pathogens (Jorgensen et al., 2016; Lannitti et al., 2016), the role of ASC in regulating inflammasome activity during *E. coli* infection must be examined in detail to determine and how *L. rhamnosus* GR-1 regulates the immune response to prevent *E. coli*-associated bovine mastitis.

In the present study, we knocked out the *ASC* gene in bovine mammary epithelial (MAC-T) cells using the RNA-guided clustered regularly interspaced short palindrome repeats (CRISPR)-CRISPR-associated nuclease 9 (Cas9) system. We hypothesized that during *E. coli* infection, the activity of NLRP3 and NLRC4 inflammasomes is differentially regulated by *L. rhamnosus* GR-1, inducing maturation of IL-1β and IL-18 or cell pyroptosis, depending on ASC. We provide evidence that *L. rhamnosus* GR-1 suppresses *E. coli*-induced ASC-dependent activation of NLRP3 and NLRC4 inflammasomes and thus decreases production of IL-lβ and IL-18 during *E. coli* infection. In addition, *L. rhamnosus* GR-1 suppresses *E. coli*-induced cell pyroptosis, in part through attenuation of NLRC4 inflammasome and non-canonical caspase-4 activation, independent of ASC.

MATERIALS AND METHODS

Biosecurity Statement

All bacterial strains were treated in strict accordance with the *Regulations on Biological Safety Management of Pathogen Microbiology Laboratory* (000014349/2004-00195) from the State Council of the People's Republic of China. The *E. coli* CVCC1450 was subjected to all necessary safety procedures to avoid pathogen transmission and infection.

Construction of CRISPR/Cas9 System Expression Vector

Three guide RNAs (ASC-sgRNA1, ASC-sgRNA 2, and ASC-sgRNA 3) were designed to target the exon 1 regions of the bovine ASC gene (**Table 1**). A pair of oligos for each targeting site was annealed and ligated into the *Bbs*I site of pCRISPR-sg5, which was kindly provided by Professor Sen Wu (China Agricultural University, Beijing, China), to generate pCRISPR-sg5-ASC-sgRNA1, pCRISPR-sg5-ASC-sgRNA2, and pCRISPR-sg5-ASC-sgRNA3 plasmids. All plasmids were confirmed by sequencing (Sangon Biotech, Shanghai, China).

Cell Culture and Transfection

MAC-T cells transferred with the SV40 T antigen (Huynh et al., 1991) was a gift from Dr. Ying Yu (China Agricultural University). MAC-T cells were cultured in Dulbecco's Modified Eagle medium/Ham's F-12 medium (1:1) supplemented with 10% heat-inactivated fetal calf serum, 100 U/mL of penicillin, and 1 g/mL of streptomycin (Invitrogen, Carlsbad, CA, United States) at 37°C in an atmosphere of 5% CO_2 and 95% air at 95% relative humidity.

Plasmid DNA for cell transfection was prepared using an Omega Endo-free Plasmid Mini Kit II (Omega Bio-Tek Inc., Doraville, GA, United States). MAC-T cells (1×10^6) were electroporated with 1.5 μg of pCRISPR-W9 plasmid, 1.5 μg of pCRISPR-sg5-ASC-sgRNA plasmid, and 1 μg of pCAG-PBase plasmid using the T-020 program of an Amaxa electroporator (Lonza, Allendale, NJ, United States), in which pCRISPR-W9 encoded Cas9 nuclease and pCRISPR-sg5-ASC-sgRNA encoded ASC-sgRNA. After electroporation, 300 cells

TABLE 1 | Sequences of three guide RNAs designed to target the exon 1 region of the bovine *ASC* gene and primers for PCR amplification.

Gene product[a]	Primer		Accession number
	Direction[b]	Sequence (5′–3′)	
ASC-sgRNA1	F	CACCGCGATGCCATC CTGGATGCGC	NM_174730.2
	R	AAACGCGCATCCAGGAT GGCATCGC	
ASC-sgRNA2	F	CACCGCTTTCAGTGCC GCTGCGGGA	NM_174730.2
	R	AAACTCCCGCAGCG GCACTGAAAGC	
ASC-sgRNA3	F	CACCGCAAGCTCGT CAGCTACTATC	NM_174730.2
	R	AAACGATAGTAGCTG ACGAGCTTGC	
ASC	F	CCAGGTTCCTGATTTG GCTAGCTA	NM_174730.2
	R	GAAGTCTCGGTCCGGAG GCCAAGG	

[a]*ASC, apoptosis-associated speck-like protein containing a caspase-recruitment domain; sgRNA = Cas9/single guide RNA (sgRNA).* [b]*F, forward; R, reverse.*

were plated in a 10-cm dish using growth medium containing 350 μg/ml of selectable marker G418 (Sigma-Aldrich, St. Louis, MO, United States). After 10 days, individual clones were picked, and clonal cell populations were expanded. Before experiments, MAC-T cells were electroporated with pmaxGFP™ (Lonza) encoding green fluorescent protein to determine transfection efficiency using the T-020 and W-001 programs. MAC-T cells were chosen for CRISPR-Cas9 inactivation experiments due to their good transfection efficiency.

Sequencing and Protein Analysis of the Gene Target Site

Genomic DNA samples were extracted using a TIANamp Genomic DNA Kit (Tiangen, Beijing, China) according to the manufacturer's instructions, and 50 ng of DNA template was used to amplify the 630-bp fragment encompassing the gene inactivation locus in 25 μl of PCR buffer (Takara, Shiga, Japan) using primer pairs listed in **Table 1**. The resulting PCR products were purified and subsequently sequenced to identify deletions. In addition, clonal cell population whole-cell extracts were analyzed by Western blotting.

Immunocytochemistry

The epithelial origin of MAC-T cells was tested by staining for cytokeratin 18. MAC-T cells (6×10^4 cells/well) were seeded into a 24-well culture plate with glass coverslips. After 24 h, cells were washed three times with phosphate-buffered saline (PBS) and fixed with 4% paraformaldehyde for 15 min on ice. The cells were then permeabilized with 0.2% (v/v) Triton X-100 (Sigma-Aldrich) and blocked with 1% bovine serum albumin. Subsequently, cells were incubated with mouse anti-cytokeratin-18 primary monoclonal antibody at a dilution of 1:200 (Ab668; Abcam, Cambridge, United Kingdom) for 45 min at 4°C, following by incubation with secondary antibody, goat anti-mouse fluorescein isothiocyanate (FITC)-conjugated IgG (F4143; Sigma-Aldrich). Cell nuclei were stained using 4′,6′-diamidino-2-phenylindole (DAPI; Sigma-Aldrich). Coverslips were imaged on an FV1000 confocal laser scanning biological microscope (Olympus, Tokyo, Japan).

Bacterial Strains and Growth Conditions

Lactobacillus rhamnosus GR-1 ATCC 55826 was purchased from the American Type Culture Collection (Manassas, VA, United States) and grown in De Man, Rogosa, and Sharpe (MRS) broth (Oxoid, Hampshire, United Kingdom) for 24 h at 37°C under microaerophilic conditions. After overnight incubation, *L. rhamnosus* GR-1 was subcultured at a dilution of 1:100 in fresh MRS broth for approximately 8 h until reaching mid-log phase [optical density (OD) at 600 nm (OD_{600}) of 0.5] for all experiments.

Escherichia coli CVCC1450 (serotype O111:K58) was purchased from the China Institute of Veterinary Drug Center (Beijing, China) and grown in Luria–Bertani (LB) broth (Oxoid). After overnight incubation at 37°C with vigorous shaking, bacteria were diluted 1:100 in fresh LB and grown for approximately 3 h until reaching mid-log phase (OD_{600} of 0.5).

Adhesion Assay

Wild-type (WT) and $ASC^{-/-}$ MAC-T cells (3×10^5 cells/well) were seeded onto a six-well transwell collagen-coated polytetrafluoroethylene (PTFE) filter. Confluent cell monolayers were pretreated with *L. rhamnosus* GR-1 (3×10^7 CFU) for 3 h, and then were washed three times with PBS and exposed to *E. coli* (3×10^7 CFU). At 1.5, 3, and 6 h after *E. coli* challenge, the cell monolayers were washed four times with PBS to remove non-adherent bacteria and treated with 0.05% trypsin for 10 min at 37°C. Cells were harvested by centrifugation for 10 min at 4000 *g* and lysed using 100 μl of 0.2% Triton X-100 (Sigma-Aldrich) in sterile water. The populations of *E. coli* and *L. rhamnosus* GR-1 were determined on LB and MRS agar plates, respectively. The adhesion rate of *E. coli* was defined as the adhered *E. coli* population on the cells pretreated with *L. rhamnosus* GR-1 relative to the adhered *E. coli* population in the adhesion assay of *E. coli* infection alone.

Immunofluorescence

Confluent monolayers of WT and $ASC^{-/-}$ MAC-T cells (6×10^4 cells/well) grown on glass coverslips in a 24-well flat-bottom culture plate were treated under four different conditions, as follows: (i) medium alone (CONT); (ii) *E. coli* alone (6×10^6 CFU) at a multiplicity of infection (MOI) of 100:1 (ECOL); (iii) incubation with *L. rhamnosus* GR-1 (6×10^6 CFU) at a MOI of 100:1 for 3 h (LRGR); or (iv) pre-incubation with *L. rhamnosus* GR-1 (6×10^6 CFU) for 3 h prior to addition of *E. coli* (LRGR + ECOL). At 6 h after *E. coli* infection, the cells were washed, fixed with 4% paraformaldehyde for 15 min on ice, permeabilized with 0.2%

(v/v) Triton X-100 (Sigma-Aldrich), and blocked with 1% bovine serum albumin. Subsequently, the following primary monoclonal antibodies were used: mouse anti-cytokeratin-18 (Ab668, 1:200 dilution; Abcam), rabbit anti-ASC (10500-1-AP, 1:500 dilution; Proteintech Group, Chicago, IL, United States), and mouse anti-caspase-1 (22915-1-AP, 1:500 dilution; Proteintech Group). The cells were incubated with the primary antibody for 45 min at 4°C, followed by incubation with goat anti-rabbit Cy-3 (AP307F, 1:200 dilution; Sigma-Aldrich) or FITC-conjugated IgG (F-0382, 1:40 dilution; Sigma-Aldrich) as the secondary antibody. Cell nuclei were stained with DAPI. The coverslips and slides were visualized and photographed under an FV1000 confocal laser scanning biological microscope (Olympus).

Western Blotting

WT and $ASC^{-/-}$ MAC-T cells (6×10^4 cells/well) were seeded onto a six-well transwell collagen-coated PTFE filter and treated with *E. coli* or *L. rhamnosus* GR-1 at a MOI of 100:1, as described above. Cells were also simultaneously treated with lactate at a concentration of 0.6 g/L (equivalent to 7 mM) and *E. coli* at a MOI of 100:1. At 1.5, 3, and 6 h after *E. coli* infection, cells were extracted using Radio-Immunoprecipitation Assay buffer (Sigma-Aldrich), as previously described (Wu et al., 2016). The primary antibodies were as follows: rabbit anti-NLRP3 (19771-1-AP, 1:200 dilution; Proteintech Group), rabbit anti-NLRC4 (12421, 1:1,000 dilution; Cell Signaling Technologies Inc., Danvers, MA, United States), mouse anti-caspase-1 (sc56036) (14F468, 1:500 dilution; Santa Cruz Biotechnology, Dallas, TX, United States), rabbit anti-cleaved caspase-4 (Gln81) (GTX86890, 1:250 dilution; GeneTex, Inc., San Antonio, TX, United States), and mouse anti-glyceraldehyde-3-phosphate dehydrogenase (GAPDH, 60004-1-Ig, 1:500 dilution; Proteintech Group). Horseradish peroxidase-conjugated AffiniPure goat anti-mouse IgG (SA00001-1, 1:5,000 dilution; Proteintech Group) or goat anti-rabbit IgG (SA00001-2, 1:5,000 dilution; Proteintech Group) were used as secondary antibodies. The detection of NLRP3 and caspase-1 proteins was performed in the same gel. After NLRP3 and caspase-1 proteins were visualized, blots were then stripped using Restore Western Blot Stripping Buffer (Solarbio, Beijing, China), and re-probed with the desired antibodies for GAPDH. The OD of each band was quantified by densitometric analysis using Quantity One software (Bio-Rad Laboratories, Richmond, CA, United States). Results are presented as the ratio of the NLRP3, NLRC4, caspase p10 subunit or cleaved caspase-4 band intensity to the GAPDH band intensity.

Lactate Dehydrogenase (LDH) Assay

The death of WT or $ASC^{-/-}$ MAC-T cells under the different conditions was assessed using the CytoTox 96 Non-Radioactive Cytotoxicity Assay (Promega, Madison, WI, United States) according to the manufacturer's instructions. The assay measures the release of LDH into the supernatant, calculated as the percentage of total LDH content as determined from cell lysates (100%). LDH released by uninfected cells was used as a maximum-lysis control. The percentage of LDH released was calculated using the following equation: [(LDH infected–LDH uninfected)/(LDH total lysis–LDH uninfected)] × 100.

Enzyme-Linked Immunosorbent Assay (ELISA)

The concentrations of IL-1β and IL-18 in cell-free supernatants of WT or $ASC^{-/-}$ cells were determined at 1.5, 3, and 6 h after *E. coli* infection using commercially available ELISA kits specific for bovine IL-1β (DG90995Q) and bovine IL-18 (DG91524Q; Beijing Dongge Biotechnology Co., Beijing, China).

Quantification of Lactate Content

Cell culture supernatants were collected. Lactate content in the supernatants were quantified using the enzymatic kit K-DLATE (Megazyme, Bray, Ireland) that allows the measurement of both D-lactate and L-lactate.

Statistical Analysis

Statistical analysis was performed using the SAS statistical software package, version 9.1 (SAS Institute Inc., Cary, NC, United States). With regard to small sample sizes, normal distribution and homogeneity of variance were assumed using the UNIVARIATE (Shapiro–Wilk test) and HOVTEST procedures. Natural logarithm transformation was performed prior to analysis for IL-1β and IL-18 data to yield a normal distribution. Statistical significance of differences was tested using ANOVA procedures, following Tukey's honestly significant difference *post hoc* test. Data of adhesion assay were compared by an unpaired two-tailed Student's *t*-test. Data were visualized using GraphPad Prism5 software (GraphPad Software Inc., San Diego, CA, United States). Data from adhesion assay are presented as the mean ± standard deviation (SD) and data from Western blotting, LDH, ELISA and lactate quantification assays are presented as the mean ± standard error of the mean (SEM). Results are representative of three independent experiments, each performed in triplicate. *P*-values: $^*P < 0.05$; $^{**}P < 0.01$; $^{***}P < 0.001$.

RESULTS

CRISPR/Cas9 Mediates Knockout of ASC in MAC-T Cells

To demonstrate the role of ASC in *L. rhamnosus* GR-1 modulation of inflammasome activation during *E. coli* infection, we attempted knockout of the *ASC* gene in MAC-T cells using the CRISPR/Cas9 system. Upon immunocytochemistry analysis, MAC-T cells showed intense positive staining for epithelial cell-specific cytokeratin-18 in the cytoplasmic meshwork of cytokeratin fibrils (**Supplementary Figure S1**). Compared with program W-001, after electroporation with program T-020, MAC-T cells exhibited higher transfection efficiency (**Figure 1A**). Thus, the *ASC* gene knockout experiment was subsequently performed in MAC-T cells using program

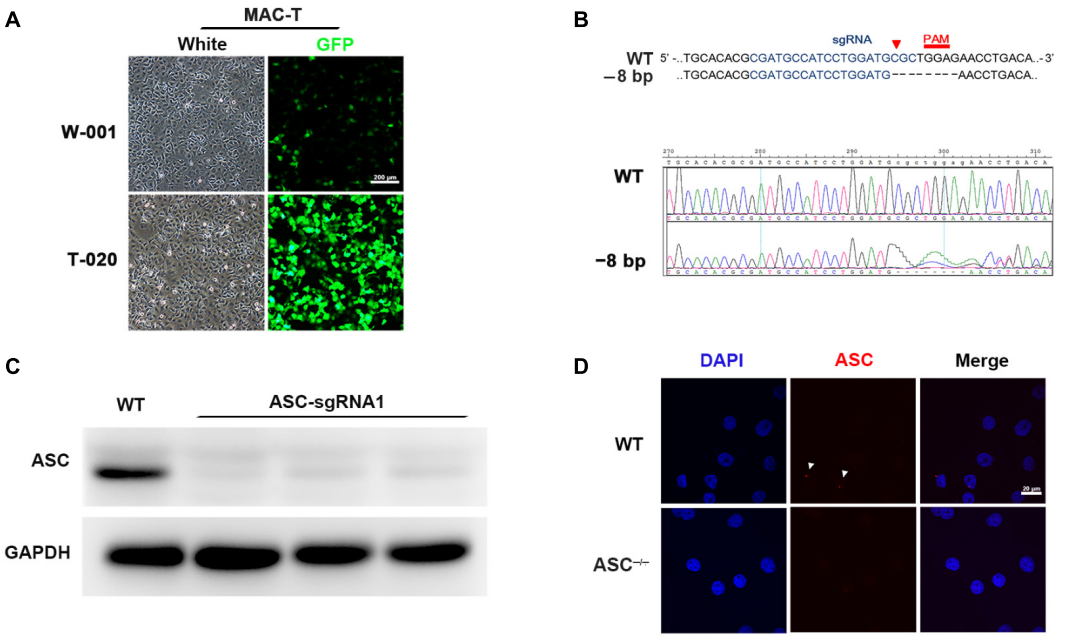

FIGURE 1 | CRISPR/Cas9 system-mediated knockout of the *ASC* gene in MAC-T cells. **(A)** To determine transfection efficiency, MAC-T cells were electroporated with pmaxGFP encoding green fluorescent protein using the programs W-001 and T-020, respectively. **(B)** Schematic illustrating Cas9 inactivation of the bovine *ASC* locus. The 20-bp guide RNA target sequence is shown in blue, and the protospacer-adjacent motif (PAM) is shown in red. An 8-bp deletion was detected (Upper). Representative Sanger sequencing results of target regions of *ASC* (frameshift indels; Lower). **(C)** Analysis of ASC protein in WT and $ASC^{-/-}$ cells transfected with Cas-9 and ASC guide RNA expression vector by Western blotting. **(D)** Immunofluorescence staining of ASC (red) in WT and $ASC^{-/-}$ cells at 6 h after *Escherichia coli* challenge. DAPI was used for nuclear staining (blue). Representative confocal immunofluorescence images show staining of ASC. Scale bar, 20 μm. Data are representative of three independent experiments.

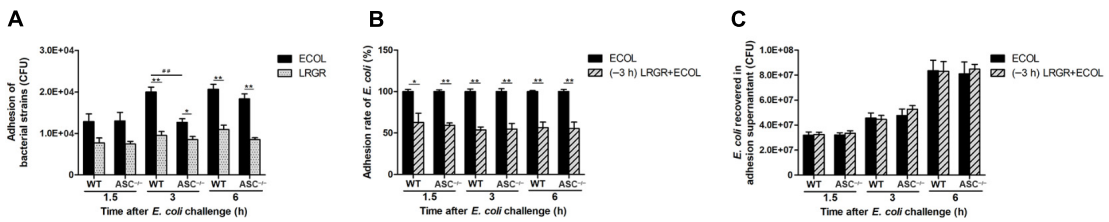

FIGURE 2 | Pre-incubation with *Lactobacillus rhamnosus* GR-1 reduced the adhesion of *E. coli* to MAC-T cell monolayers. An adhesion assay was performed. Cells and supernatants were collected. The number of adherent *E. coli* and *L. rhamnosus* GR-1 was determined **(A)**. The adhesion rate of *E. coli* was defined as the adhered *E. coli* population on the cells pretreated with *L. rhamnosus* GR-1 relative to the adhered *E. coli* population in the adhesion assay of *E. coli* infection alone **(B)**. The number of *E. coli* recovered was determined in adhesion assay supernatants **(C)**. Data are presented as the mean ± SD of three independent experiments. Asterisks indicate the significances among different treatments in the same cell type. Pound signs indicate the significance among WT and $ASC^{-/-}$ MAC-T cells infected with *E. coli* alone at 3 h. $^{*}P < 0.05$, $^{**}P < 0.01$, $^{\#\#}P < 0.01$.

T-020. Among the three designed sgRNA sequences, the specific 20-nucleotide sgRNA1 sequence targeted the exon 1 regions of the *ASC* gene and directed Cas9 nuclease to precisely introduce a DNA double-strand break in front of a protospacer adjacent motif (PAM). After cloning and sequencing of the DNA fragment, an 8-bp deletion was observed (**Figure 1B**). Western blot analysis did not show expression of ASC protein in sgRNA1 sequence-targeted MAC-T cells (**Figure 1C**). Furthermore, *E. coli* infection triggered assembly of ASC specks in WT cells, whereas pre-incubation with *L. rhamnosus* GR-1 attenuated *E. coli*-induced ASC speck assembly. No ASC specks were observed in $ASC^{-/-}$ cells, regardless of *E. coli* infection (**Figure 1D**). These results demonstrated that knockout of the *ASC* gene in MAC-T cells was successful.

Pre-incubation With *L. rhamnosus* GR-1 Reduces the Adhesion of *E. coli* to MAC-T Cell Monolayers

Escherichia coli or *L. rhamnosus* GR-1 exhibited similar adhesion capacity in WT and $ASC^{-/-}$ MAC-T cells. The number of adherent *E. coli* was about $1.29 \times 10^4 \pm 0.67 \times 10^2$ CFU (means ± standard deviation) at 1.5 h after *E. coli* infection,

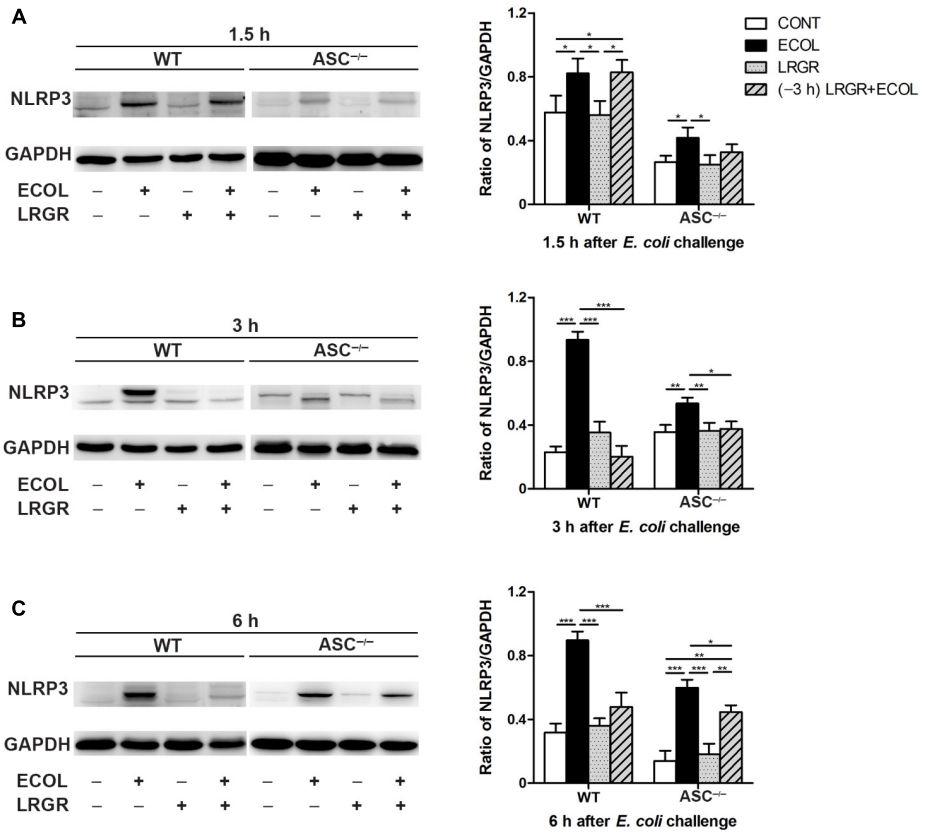

FIGURE 3 | Pre-incubation with *L. rhamnosus* GR-1 attenuated *E. coli*-induced NLRP3 expression. Western blot detection of NLRP3 in WT and $ASC^{-/-}$ cells collected from the indicated cell cultures at 1.5 h **(A)**, 3 h **(B)**, and 6 h **(C)** after *E. coli* challenge. Representative panels showing expression of NLRP3 protein (Left). Results are presented as the ratio of NLRP3 band intensity to that of GAPDH (Right). Data are presented as the mean ± SEM of three independent experiments. $^{*}P < 0.05$, $^{**}P < 0.01$, $^{***}P < 0.001$.

and increased to $1.95 \times 10^4 \pm 1.17 \times 10^3$ CFU at 6 h. At 3 h after *E. coli* challenge, the number of adherent *E. coli* in $ASC^{-/-}$ cells was lower ($P = 0.007$) than in WT MAC-T cells (**Figure 2A**). *L. rhamnosus* GR-1 had a lower adhesion capacity and the number of adherent *L. rhamnosus* GR-1 was about $8.75 \times 10^3 \pm 1.56 \times 10^3$ CFU, regardless of infection time. Pre-incubation with *L. rhamnosus* GR-1 resulted in a reduction in the *E. coli* adhesion rate to 57% of that observed in MAC-T cells infected with *E. coli* alone (**Figure 2B**). No differences were observed in the number of *E. coli* recovered from the supernatant fraction among two groups (**Figure 2C**).

Pre-incubation With *L. rhamnosus* GR-1 Attenuates *E. coli*-Induced NLRP3 Expression and Increases Lactate Content in the Supernatants

Compared with untreated control WT cells, Western blot analysis showed an increase in NLRP3 protein expression at 1.5, 3, and 6 h after *E. coli* challenge in cells only infected with *E. coli*, but not in cells incubated with *L. rhamnosus* GR-1 alone ($P = 0.046$, $P < 0.001$, and $P < 0.001$, respectively; **Figures 3A–C**). In contrast, WT cells pre-incubated with *L. rhamnosus* GR-1 had a lower expression of NLRP3 protein than did WT cells only infected with *E. coli* at 3 and 6 h ($P < 0.001$ for both).

Compared with WT cells, $ASC^{-/-}$ MAC-T cells exhibited a similar differential response to *E. coli* challenge and *L. rhamnosus* GR-1 incubation. Compared with untreated control $ASC^{-/-}$ cells, at 1.5, 3, and 6 h after *E. coli* challenge, NLRP3 protein expression was elevated in $ASC^{-/-}$ cells only infected with *E. coli* ($P = 0.036$, $P = 0.005$, and $P < 0.001$, respectively; **Figures 3A–C**) but not in $ASC^{-/-}$ cells pre-incubated with *L. rhamnosus* GR-1.

The lactate content (D-lactate plus L-lactate) in the supernatants was quantified. Compared with untreated control cells, the lactate content was increased in the supernatants from both WT and $ASC^{-/-}$ cells incubated with *L. rhamnosus* GR-1 alone or pre-incubated with *L. rhamnosus* GR-1, but not the cells only infected with *E. coli* at 1.5, 3, and 6 h after infection, regardless of *ASC* knockout ($P < 0.05$; **Supplementary Figure S2A**). Western blot analysis showed that compared with untreated control cells, at 6 h after *E. coli* challenge, NLRP3 protein expression was elevated in WT or $ASC^{-/-}$ cells infected with *E. coli*, but not in cells only treated with lactate alone ($P < 0.05$; **Supplementary Figure S2B**). Lactate addition did not attenuate *E. coli*-induced increase in NLRP3 protein expression in either WT or $ASC^{-/-}$ cells.

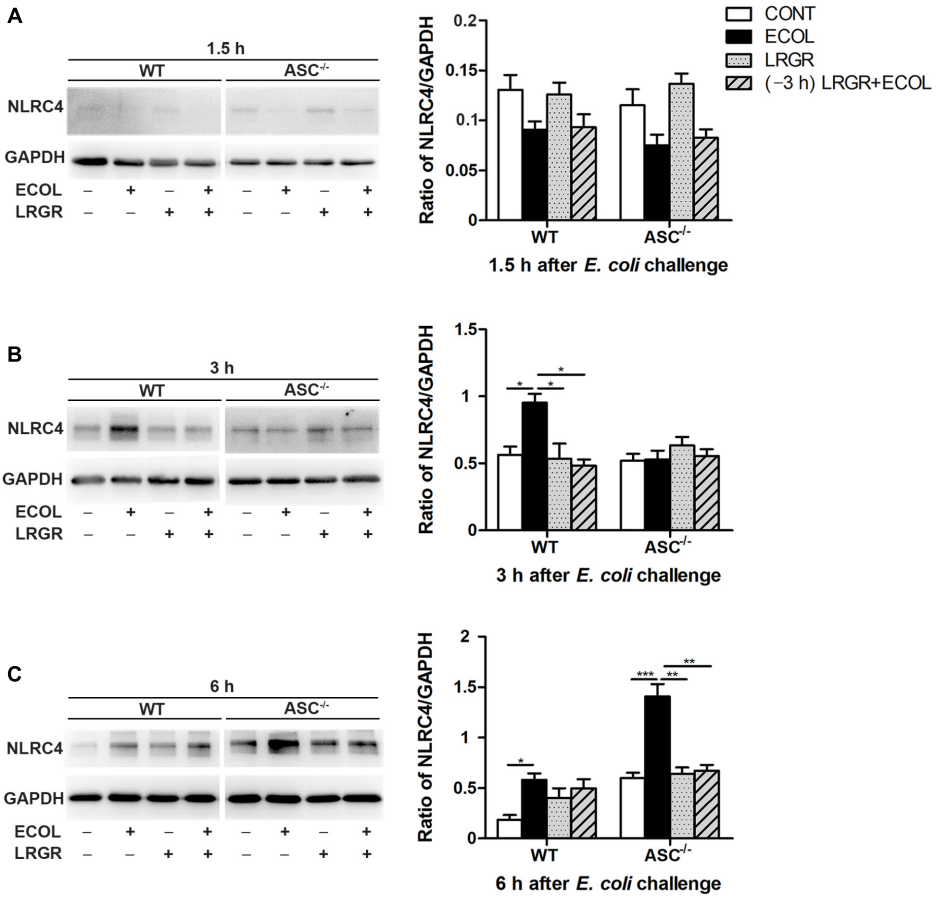

FIGURE 4 | Western blot detection of NLRC4 protein. Representative panels showing expression of NLRP4 protein in WT and $ASC^{-/-}$ cells collected from the indicated cultures at 1.5 h **(A)**, 3 h **(B)**, and 6 h **(C)** after *E. coli* challenge (Left). Results are presented as the ratio of NLRC4 band intensity to that of GAPDH (Right). Data are presented as the mean ± SEM of three independent experiments. $^{*}P < 0.05$, $^{**}P < 0.01$, $^{***}P < 0.001$.

Effect of *L. rhamnosus* GR-1 on NLRC4 Activation During *E. coli* Infection

Compared with untreated control cells, expression of NLRC4 protein was elevated at 3 h after *E. coli* infection in WT cells only infected with *E. coli* ($P = 0.027$; **Figure 4B**) but not in WT cells incubated with *L. rhamnosus* GR-1 alone or pre-incubated with *L. rhamnosus* GR-1. Compared with WT cells only infected with *E. coli*, expression of NLRC4 protein at 3 h was decreased in WT cells incubated with *L. rhamnosus* GR-1 alone and pre-incubated with *L. rhamnosus* GR-1 ($P = 0.019$ and $P = 0.001$, respectively). No differences were observed at 3 h in $ASC^{-/-}$ cells, regardless of treatment.

Compared with untreated control cells, *E. coli* challenge led to increased expression of NLRC4 protein at 6 h after *E. coli* challenge in WT cells ($P = 0.019$) and $ASC^{-/-}$ cells ($P < 0.001$; **Figure 4C**). Expression of NLRC4 protein was lower in $ASC^{-/-}$ cells incubated with *L. rhamnosus* GR-1 alone and pre-incubated with *L. rhamnosus* GR-1 ($P = 0.001$ for both) than in $ASC^{-/-}$ cells only infected with *E. coli*. No changes were observed at 1.5 h after *E. coli* infection in WT cells or $ASC^{-/-}$ cells, regardless of treatment (**Figure 4A**).

Pre-incubation With *L. rhamnosus* GR-1 Attenuates *E. coli*-Induced Caspase-1 Maturation

Immunofluorescence staining showed that compared with untreated control cells, *E. coli* challenge triggered assembly of ASC specks in WT cells at 6 h after *E. coli* challenge, and this was attenuated in WT cells pre-incubated with *L. rhamnosus* GR-1 (**Figure 5A**). No ASC specks were observed in $ASC^{-/-}$ cells, regardless of treatment. Compared with untreated control cells, bright foci indicative of increased caspase-1 expression was observed in WT cells only infected with *E. coli* at 6 h after challenge; this increase was attenuated by incubation with *L. rhamnosus* GR-1 (**Figure 5B**). Compared with WT cells, ASC deletion attenuated, but did not abolish, caspase-1 staining in response to *E. coli* infection and pre-incubation with *L. rhamnosus* GR-1. A punctate staining pattern for caspase-1 was observed in $ASC^{-/-}$ cells only infected with *E. coli*, and pre-incubation with *L. rhamnosus* GR-1 inhibited the *E. coli*-induced punctate caspase-1 staining pattern. Compared with untreated control cells, incubation with *L. rhamnosus* GR-1 only did not result in

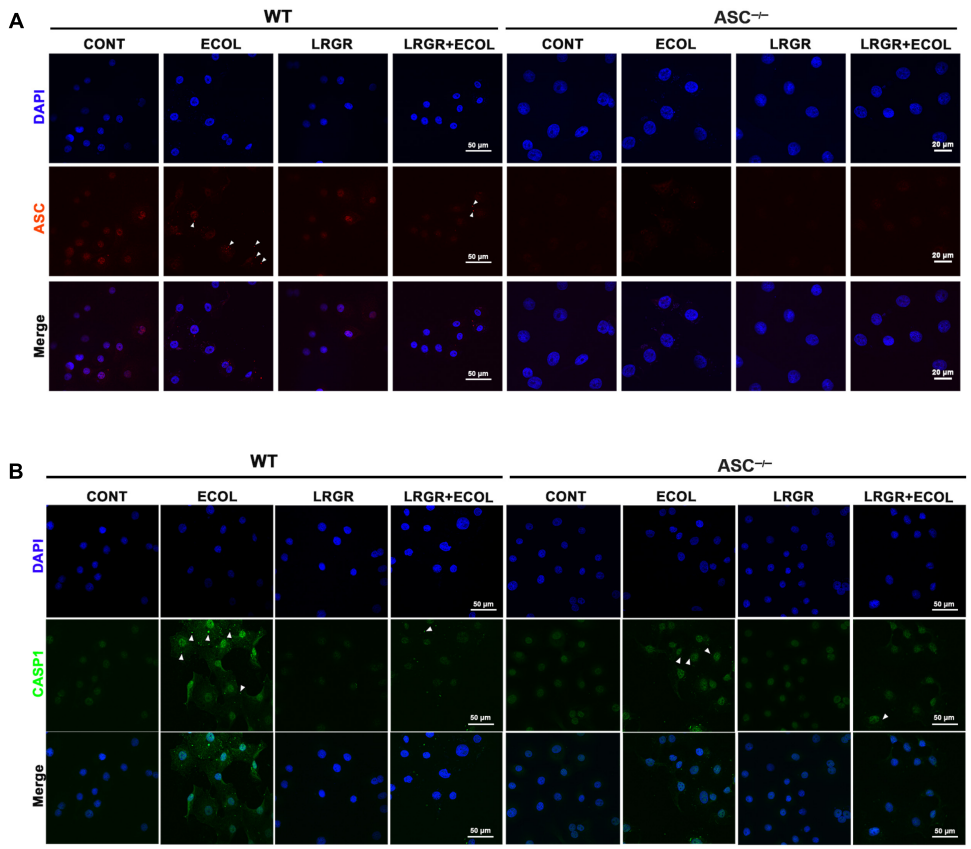

FIGURE 5 | Immunofluorescence staining for ASC and caspase-1. Immunofluorescence staining for ASC **(A)** and caspase-1 **(B)** in WT and *ASC*$^{-/-}$ cells collected from the indicated cell cultures at 6 h after *E. coli* challenge. Cells were immunostained for ASC (red) and caspase-1 (green). DAPI (blue) was used to localize nuclei. Arrows mark specks. Scale bars, immunofluorescence staining for ASC in WT cells and for caspase-1 in WT and *ASC*$^{-/-}$ cells: 50 μm, and immunofluorescence staining for ASC in *ASC*$^{-/-}$ cells: 20 μm. Data are representative of three independent experiments.

increase in caspase-1 activation either in WT or *ASC*$^{-/-}$ cells (**Figure 5B**).

Compared with untreated control cells, increased maturation of procaspase-1 into its catalytic 10-kDa subunit was observed at 6 h after *E. coli* challenge in WT and *ASC*$^{-/-}$ cells only infected with *E. coli* ($P < 0.001$ for both; **Figure 6C**). However, maturation of caspase-1 declined in WT and *ASC*$^{-/-}$ cells pre-incubated with *L. rhamnosus* GR-1 ($P = 0.014$ and $P = 0.006$, respectively) or incubated with *L. rhamnosus* GR-1 alone ($P < 0.001$ for both), compared with WT cells infected with *E. coli* only. No differences were observed in caspase-1 maturation at 1.5 and 3 h after *E. coli* infection in WT cells or *ASC*$^{-/-}$ cells, regardless of treatment (**Figures 6A,B**).

Pre-incubation With *L. rhamnosus* GR-1 Attenuates *E. coli*-Induced Caspase-4 Activation

At 3 h after *E. coli* infection, expression of cleaved caspase-4 (26 kDa) in WT and *ASC*$^{-/-}$ cells pre-incubated with *L. rhamnosus* GR-1 was lower than in untreated control cells and cells only infected with *E. coli* (**Figure 7B**). Infection with *E. coli* resulted in increased expression of cleaved caspase-4 in WT and *ASC*$^{-/-}$ cells ($P = 0.001$ and $P = 0.004$, respectively; **Figure 7C**) at 6 h. However, expression of caspase-4 decreased in WT and *ASC*$^{-/-}$ cells pre-incubated with *L. rhamnosus* GR-1, compared with cells only infected with *E. coli* ($P < 0.001$ and $P = 0.001$, respectively). No differences were observed in the expression of cleaved caspase-4 at 1.5 h after *E. coli* infection in WT or *ASC*$^{-/-}$ cells, regardless of treatment (**Figure 7A**).

Pre-incubation With *L. rhamnosus* GR-1 Attenuates *E. coli*-Induced Production of IL-1β and IL-18 and Cell Pyroptosis

Compared with untreated control cells, IL-1β production was increased at 3 and 6 h after *E. coli* infection in WT cells only infected with *E. coli* ($P < 0.001$ for both; **Figure 8A**). IL-1β production was lower at 3 and 6 h both in WT cells incubated with *L. rhamnosus* GR-1 alone ($P = 0.002$ and $P = 0.004$, respectively) and cells pre-incubated with *L. rhamnosus* GR-1 ($P = 0.013$ and $P = 0.011$, respectively) than in WT cells only infected with *E. coli*. Compared with WT cells, *ASC* deletion led to a decrease in production of IL-1β in *ASC*$^{-/-}$ cells in response to different treatments. Challenge with *E. coli* resulted in elevated production of IL-1β at 1.5, 3, and 6 h after *E. coli*

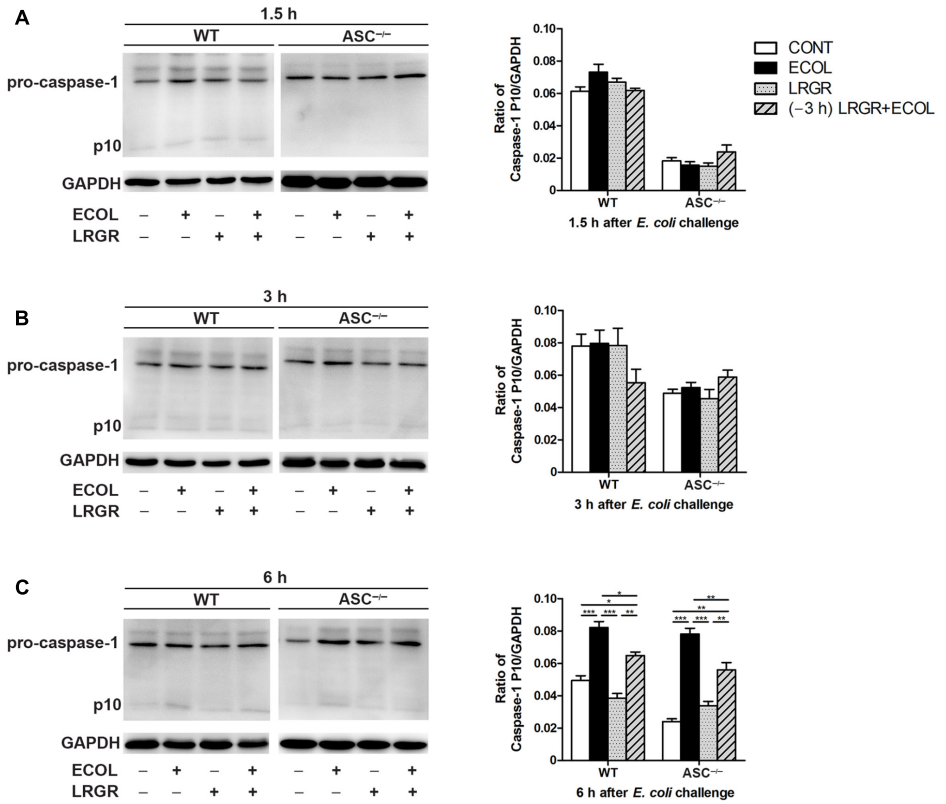

FIGURE 6 | Pre-incubation with *L. rhamnosus* GR-1 attenuated *E. coli*-induced activation of caspase-1. Western blot detection of caspase-1 in WT and $ASC^{-/-}$ cells collected from the indicated cell cultures at 1.5 h **(A)**, 3 h **(B)**, and 6 h **(C)** after *E. coli* challenge. Representative panels showing expression of caspase-1 (Left). Results are presented as the ratio of caspase-1 p10 subunit band intensity to that of GAPDH (Right). The detection of NLRP3 and caspase-1 proteins was performed in the same gel. Caspase-1 blots shared the same GAPDH blots with NLRP3 protein. Data are presented as the mean ± SEM of three independent experiments. $^{*}P < 0.05$, $^{**}P < 0.01$, $^{***}P < 0.001$.

infection in $ASC^{-/-}$ cells only infected with *E. coli* ($P = 0.009$, $P = 0.021$, and $P = 0.001$, respectively; **Figure 8A**) compared with untreated control cells; however, the *E. coli*-induced increase in IL-1β production was attenuated at 3 and 6 h by incubation with *L. rhamnosus* GR-1 alone ($P = 0.014$ and $P = 0.007$, respectively) and pre-incubation with *L. rhamnosus* GR-1 ($P = 0.009$ and $P = 0.003$, respectively).

IL-18 exhibited similar differential production as IL-1β. Compared with untreated control cells, production of IL-18 was increased at 3 and 6 h after *E. coli* challenge both in WT ($P = 0.001$ for both) and $ASC^{-/-}$ ($P < 0.001$ for both) cells only infected with *E. coli* (**Figure 8A**). However, incubation with *L. rhamnosus* GR-1 alone and pre-incubation with *L. rhamnosus* GR-1 attenuated the *E. coli*-induced elevation in the concentration of IL-18 at 3 and 6 h after *E. coli* challenge both in WT and $ASC^{-/-}$ cells. Compared with untreated control $ASC^{-/-}$ cells, the concentration of IL-18 was elevated at 3 and 6 h in $ASC^{-/-}$ cells pre-incubated with *L. rhamnosus* GR-1 ($P = 0.008$ and $P = 0.002$, respectively).

Cell pyroptosis was quantified by monitoring the release of LDH into the supernatants after *E. coli* challenge. Compared with untreated control cells, the percentage of pyroptotic cells at 3 and 6 h was increased in WT cells only infected with *E. coli* ($P < 0.001$ for both; **Figure 8B**) but not in WT cells incubated with *L. rhamnosus* GR-1 alone and pre-incubated with *L. rhamnosus* GR-1. Compared with WT cells, *ASC* deletion let to a similarly differential but attenuated cell pyroptosis. Compared with untreated control cells, the percentage of pyroptotic cells was increased at 3 and 6 h in $ASC^{-/-}$ cells only infected with *E. coli* ($P = 0.020$ and $P < 0.001$, respectively), whereas incubation with *L. rhamnosus* GR-1 alone and pre-incubation with *L. rhamnosus* GR-1 ameliorated the *E. coli*-induced increase in pyroptotic cell death at 6 h ($P < 0.001$ and $P = 0.002$, respectively). No changes were observed in WT and $ASC^{-/-}$ cells, regardless of treatment.

DISCUSSION

Bacterial adhesion to host epithelial cells is an essential step in the initiation of infection. *Lactobacillus* can reduce pathogen adhesion to epithelial cells and exert direct antimicrobial activity due to accumulation of antimicrobial substances (Gudina et al., 2015). We found that *L. rhamnosus* GR-1 did not directly kill *E. coli*, but did decrease the level of *E. coli* adhesion to 57% of that observed in MAC-T cells infected with

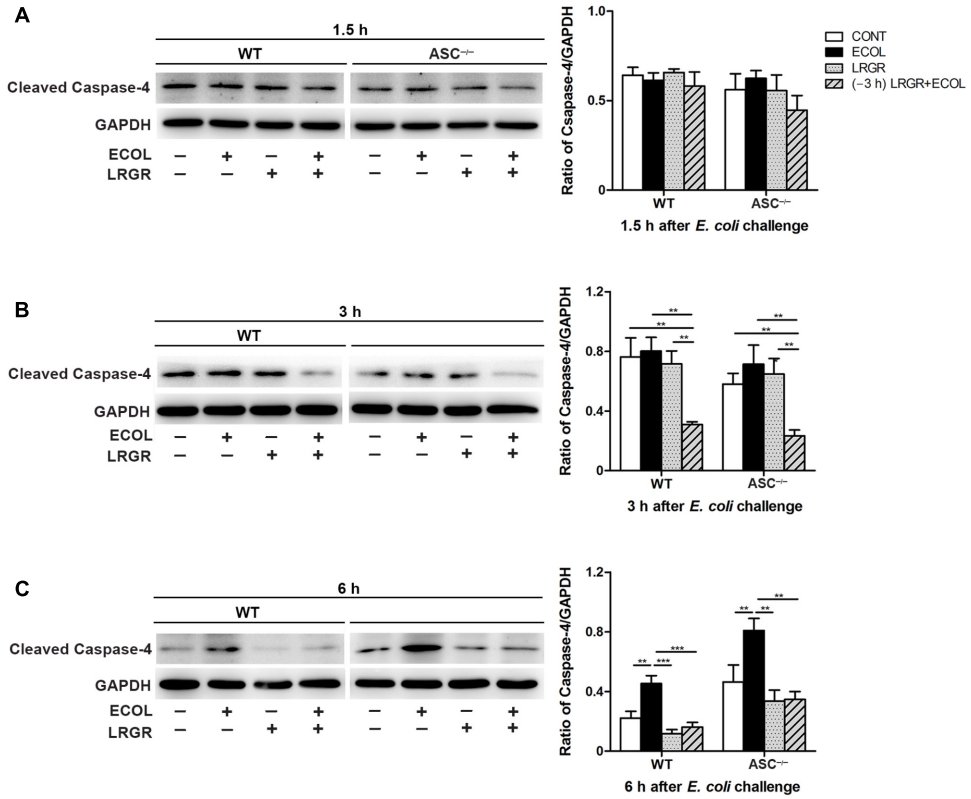

FIGURE 7 | Pre-incubation with *L. rhamnosus* GR-1 attenuated *E. coli*-induced activation of caspase-4. Western blot detection of cleaved caspase-4 in WT and *ASC*$^{-/-}$ cells collected from the indicated cell cultures at 1.5 h **(A)**, 3 h **(B)**, and 6 h **(C)** after *E. coli* challenge. Representative panels showing expression of cleaved caspase-4 (Left). Results are presented as the ratio of cleaved caspase-4 band intensity to that of GAPDH (Right). Data are presented as the mean ± SEM of three independent experiments. $^{**}P < 0.01$, $^{***}P < 0.001$.

E. coli alone. We previously revealed that live and ultraviolet-irradiated *L. rhamnosus* GR-1 rather than culture supernatant of *L. rhamnosus* GR-1 and medium acidified with lactate lead to a decrease in the *E. coli* adhesion rate in bovine mammary epithelial cells (Wu et al., 2016). The reduced *E. coli* adhesion level mediated by *L. rhamnosus* GR-1 may be attributed to steric hindrance due to competition for attachment sites (Ardita et al., 2014; Tytgat et al., 2016).

NLRP3 is activated by a wide variety of stimuli, including pore-forming toxins, extracellular adenosine triphosphate, RNA-DNA hybrid molecules, and pathogens (Jo et al., 2016). We found that *E. coli* infection also increased the expression of NLRP3 protein from 1.5 to 6 h, but *L. rhamnosus* GR-1 pretreatment inhibited this increase. NLRP3 must be primed before activation. *Escherichia coli* LPS binds to TLR4 to induce expression of NLRP3 protein via NF-κB signaling. Bacterial mRNA from viable *E. coli* cells that have been phagocytosed enters the cytosolic compartment, resulting in assembly of the NLRP3 inflammasome (Sander et al., 2011). Intake of *L. plantarum* CECT 7315/7316 downregulates expression of *Nlrp3* in the ileum of rats (Vilahur et al., 2015). However, the NLRP3 inflammasome is also activated by *L. rhamnosus* GG and LC705 originating from dairy sources (Miettinen et al., 2012).

In a mouse immune hepatitis model, lactate treatment was shown to attenuate hepatic and pancreatic injury by negatively regulating TLR4-mediated activation of the NLRP3 inflammasome and production of IL-1β through arrestin β2 and G-protein-coupled receptor 81 (Hoque et al., 2014). In the present study, there was a higher lactate content in the supernatants of cells incubated with *L. rhamnosus* GR-1. However, additional lactate treatment did not attenuate the *E. coli*-induced increase in expression of NLRP3. This indicates that the elevated lactate content in the supernatant is a secondary effect of *L. rhamnosus* GR-1 treatment and cannot account for attenuation of *E. coli*-induced activation of NLRP3. Previously, we have shown that *L. rhamnosus* GR-1 attenuates *E. coli*-induced TLR4 expression in bovine mammary epithelial cells (Wu et al., 2016). This may contribute to attenuating the priming step and subsequent activation of NLRP3 through TLR4-mediated NF-κB signaling (Bauernfeind et al., 2009). The mitogen-activated protein kinase (MAPK) subfamilies, c-Jun N-terminal kinase (JNK) and extracellular regulated protein kinase (ERK) are essential for NLRP3 inflammasome activation and addition of JNK1/2 inhibitor SP600125 or upstream MAPK/ERK kinase inhibitor PD98059 of ERK inhibits the LPS-induced increase in NLRP3 protein expression (Liao et al., 2013). Culture medium of *L. rhamnosus* GR-1 inhibits LPS-induced JNK

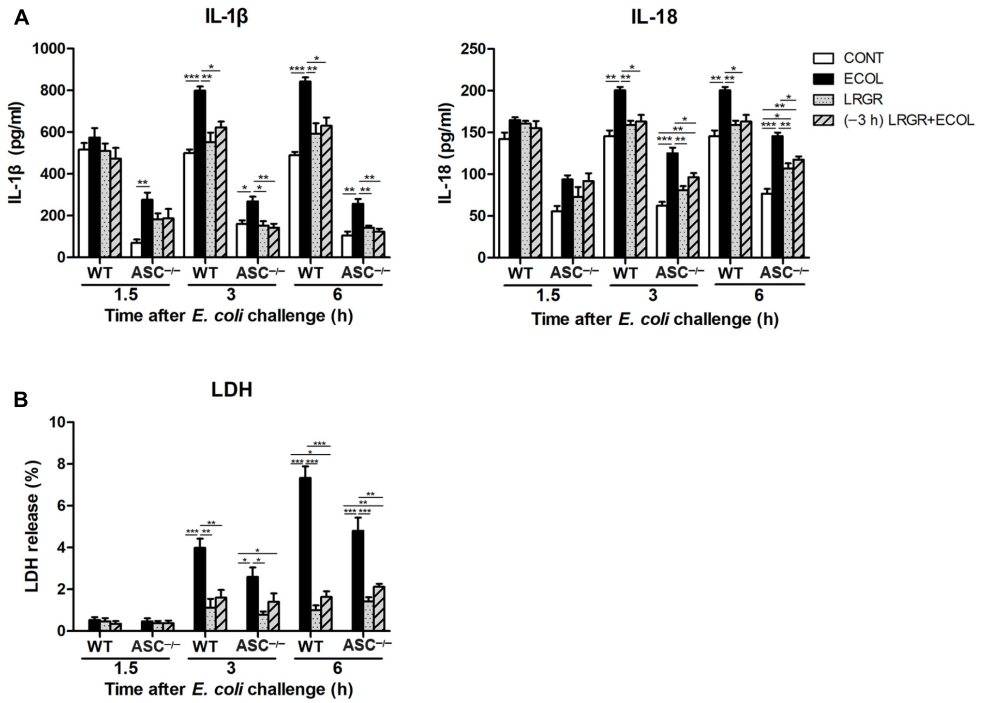

FIGURE 8 | Pre-incubation with *L. rhamnosus* GR-1 attenuated *E. coli*-induced production of IL-1β and IL-18 and cell pyroptosis. Secretion of IL-1β and IL-18 **(A)** into the indicated cell culture supernatants at 1.5, 3, and 6 h after *E. coli* challenge as determined by ELISA. Cell pyroptosis was determined by measurement of LDH release **(B)**. Data are presented as the mean ± SEM of three independent experiments. $^{*}P < 0.05$, $^{**}P < 0.01$, $^{***}P < 0.001$.

activation in macrophages or monocytic THP-1 cells (Kim et al., 2006). Histamine derived from *Lactobacillus reuteri* 6475 inhibits activation of ERK in THP-1 cells (Thomas et al., 2012). It is possible that *L. rhamnosus* GR-1 attenuates *E. coli*-induced NLRP3 activation through reducing the adhesion of *E. coli* to MAC-T cells and subsequently negatively regulating the functional synergy between NF-κB and JNK/ERK MAPK pathways mediated by some uncertain soluble factors. Further studies are required to determine active components derived from *L. rhamnosus* GR-1 and elucidate possible mechanisms underlying the antagonistic effects of *L. rhamnosus* GR-1 on NLRP3 activation during *E. coli* infection.

NLRP3 contains only a PYD, which engages the PYD of ASC, leaving the CARD of ASC to interact with the CARD-containing region of pro-caspase-1. Caspase-1 is thought to be activated by a proximity-induced dimerization and autoproteolytic process in the NLRP3/ASC complex platform (Shi, 2004). Active caspase-1 cleaves pro-IL-lβ and pro-IL-18 into mature IL-lβ and IL-18, which are essential for coordination of immune responses to pathogen infection through allograft neutrophil sequestration, mononuclear phagocyte recruitment, and T-cell activation (Samuel Weigt et al., 2017). In the present study, *L. rhamnosus* GR-1 attenuated *E. coli*-induced caspase-1 autoproteolysis and elevated production of mature IL-lβ and IL-18 at 6 h after challenge. Another study also showed that the NLRP3 inflammasome pathway plays a critical role in the host immune response to pathogen infection (Dikshit et al., 2018). However, inappropriate activation of the NLRP3 inflammasome is linked not only to local inflammation but also several autoimmune inflammatory disorders in humans (Seo et al., 2015). Indeed, activation of the NLRP3 inflammasome amplifies inflammation and promotes pathogen infection via a process involving triggering of T helper 2-biased adaptive immune responses (Gurung et al., 2015) or secretion of secondary danger-associated molecular pattern molecules (Bui et al., 2016). Our data suggest that *L. rhamnosus* GR-1 prevents *E. coli*-induced inflammation by suppressing activation of ASC-dependent NLRP3 inflammasomes.

In mice, non-canonical caspase-11 was identified as a key regulator of NLRP3 inflammasome-associated caspase-1 activation in response to *E. coli* infection. Caspase-11 is activated via NLRP3-independent mechanisms, but it is essential for NLRP3-dependent and ASC-dependent caspase-1 processing and IL-1β maturation in response to *E. coli* infection (Kayagaki et al., 2011). In addition, binding of LPS to human caspase-4 or murine caspase-11 via the CARD directly induces cell pyroptosis, independently of NLRP3 and ASC (Shi et al., 2014). A recent study revealed that outer-membrane-vesicle-mediated cytoplasmic delivery of extracellular *E. coli* LPS activates murine caspase-11 to induce pyroptosis and IL-1β maturation (Vanaja et al., 2016). Bovine caspase-4 is a homolog of human caspase-4 and mouse caspase-11 and plays a role in the processing of IL-1β and IL-18 precursors (Koenig et al., 2001; Martinon and Tschopp, 2004). In the present study, caspase-4 was activated by *E. coli* at 6 h; however, *L. rhamnosus* GR-1 pretreatment attenuated this activation.

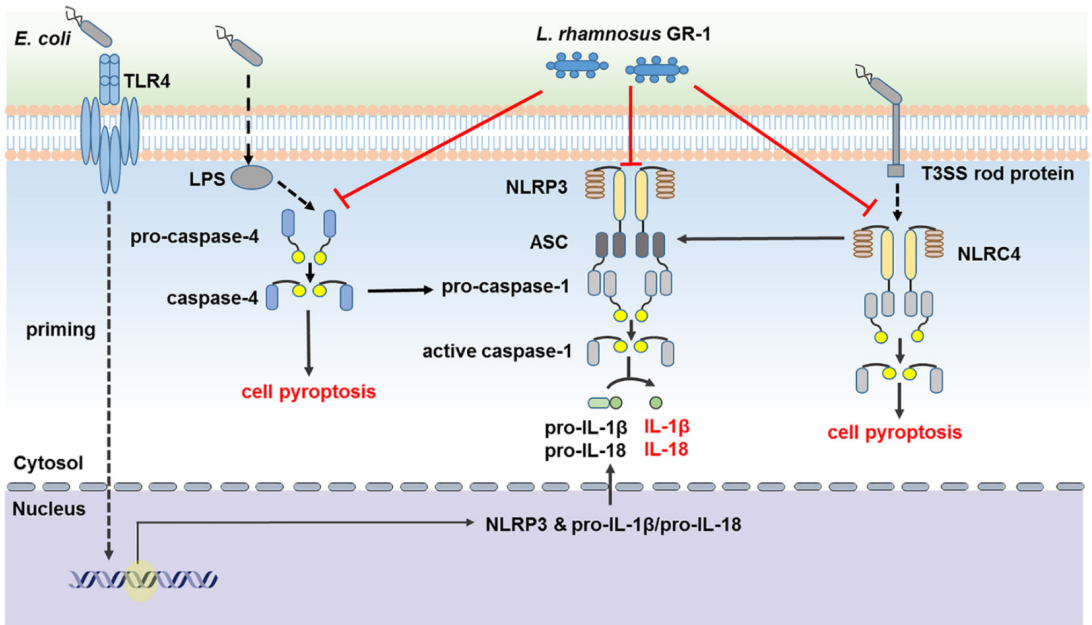

FIGURE 9 | *Lactobacillus rhamnosus* GR-1 attenuated activation of ASC-dependent and ASC-independent inflammasomes during *E. coli* infection. *L. rhamnosus* GR-1 ameliorates *E. coli*-induced inflammatory damage via attenuation of both ASC-dependent and ASC-independent inflammasome activation in MAC-T cells. *L. rhamnosus* GR-1 inhibits activation of ASC-dependent NLRP3 and NLRC4 inflammasomes and production of the downstream proinflammatory cytokines IL-lβ and IL-18 during *E. coli* infection. *L. rhamnosus* GR-1 suppresses *E. coli*-induced cell pyroptosis, in part through attenuation of NLRC4 inflammasome activation, independently of ASC. In addition, *L. rhamnosus* GR-1 inhibits non-canonical caspase-4 activation, which subsequently synergizes with the NLRP3 inflammasome to attenuate caspase-1 activation and potentially inhibit caspase-1-independent cell pyroptosis and IL-lβ and IL-18 production. Full lines represent the results of the present study, and dashed lines represent the conclusions drawn in other studies.

Interestingly, there was a lower number of adherent *E. coli* in $ASC^{-/-}$ MAC-T cells at 3 h after *E. coli* challenge compared with WT MAC-T cells. It must be noted that ASC deficiency reduced, but did not abolish, caspase-1 processing, IL-1β and IL-18 maturation, and cell pyroptosis during *E. coli* infection. Decreased *E. coli* adhesion may delay the expression of NLRC4 receptor and the downstream activation of caspase-1, maturation of proinflammatory cytokines and cell pyroptosis in $ASC^{-/-}$ MAC-T cells. Caspase-1 activation by *E. coli* requires NLRP3 and ASC, but caspase-11 processing and cell pyroptosis do not (Kayagaki et al., 2011). A previous study reported weaker oligomerization of both ASC and caspase-1 in macrophages infected with *E. coli* compared with the canonical NLRP3 inflammasome activator nigericin, but with comparable production of IL-1β (Rathinam et al., 2012). Caspase-11 interacts with caspase-1 in infected cells, forming a heterodimeric complex (Kayagaki et al., 2011). These data suggest that caspase-4/-11 amplify caspase-1 activation independently of ASC by enabling caspase-1 autoprocessing through heterodimerization. Indeed, in the present study, caspase-4 activation was enhanced in $ASC^{-/-}$ cells compared with WT cells, which could have compensated for the loss of caspase-1 activation due to ASC-dependent NLRP3 inflammasome activation. Our findings indicate that *E. coli* infection activates caspase-4, subsequently resulting in cell pyroptosis and maturation of IL-1β and IL-18 via an NLRP3 inflammasome-dependent and ASC-independent pathway. *Lactobacillus rhamnosus* GR-1 suppresses ASC-dependent NLRP3 inflammasome activation and ASC-independent caspase-1 processing by inhibiting caspase-4 activation, thereby attenuating cell pyroptosis and cytokine production and thus preventing establishment of *E. coli* infection.

In contrast to NLRP3 activation in response to diverse stimuli, upon *E. coli* infection, NLRC4 responds to bacterial rod protein of the T3SS apparatus and flagellin (Zhao et al., 2011). We found that *L. rhamnosus* GR-1 inhibited *E. coli*-induced NLRC4 expression, as was also observed in $ASC^{-/-}$ cells. NLRC4 contains a CARD motif through which it directly interacts with caspase-1 to induce pyroptosis, independently of ASC. This NLRC4-dependent/ASC-independent cell death pathway proceeds in the absence of caspase-1 autoproteolysis. Interestingly, we observed weaker staining for caspase-1 in $ASC^{-/-}$ cells. Caspase-1 autoproteolysis is often used as an indicator of caspase-1 activation. However, it was also reported that uncleaved caspase-1 is enzymatically active in $ASC^{-/-}$ cells and can induce pyroptosis. In contrast to the formation of a single large ASC/caspase-1 focus for efficient IL-lβ and IL-18 processing, pro-caspase-1 could be recruited to NLRC4, with which it forms a smaller complex that induces pyroptosis (Broz et al., 2010b). Although NLRC4 contains a CARD, ASC amplifies NLRC4 inflammasome activity because ASC is essential for NLRC4-induced caspase-1 autoprocessing and maturation of IL-lβ and IL-18 (Brubaker et al., 2015). Our data suggest that *L. rhamnosus* GR-1 inhibits *E. coli*-induced cell pyroptosis via suppression of ASC-independent NLRC4 inflammasome

activation. During *E. coli* infection in the present study, *L. rhamnosus* GR-1 decreased the secretion of IL-lβ and IL-18, in part due to suppression of ASC-dependent NLRC4 inflammasome activation.

This MAC-T cell model of *E. coli* and *L. rhamnosus* GR-1 co-incubation presents an *in vitro* framework for assessing bovine mammary immune response to pathogen infection, and evaluating the efficiency of *Lactobacillus*-based intervention in preventing bovine mastitis. The results require further confirmation in other cell lines and *in vivo* studies. However, several concerns need to be addressed before the clinical application of *Lactobacillus* in bovine mastitis. Oral ingestion of probiotics promotes mucosal immune response to pathogen infection in the gut. The mechanism underlying how the immunomodulatory effect extends to the mammary glands remains unclear. The means of probiotic supplementation (e.g., mixed into the feed, oral capsules or intra-mammary infection) and dose effect also needs to be studied in more details. The molecular mechanism underlying regulation of inflammasome activity by *Lactobacillus* requires further investigation. Our findings identify NLRP3 and NLRC4 inflammasomes as potential targets for bovine mastitis therapy and could strengthen the development for other inflammasome-targeted therapies in *E. coli*-associated mastitis.

CONCLUSION

In conclusion, our findings suggest that *L. rhamnosus* GR-1 ameliorates *E. coli*-induced inflammatory damage by attenuating both ASC-dependent and ASC-independent inflammasome activation in MAC-T cells (**Figure 9**). *L. rhamnosus* GR-1 inhibits activation of ASC-dependent NLRP3 and NLRC4 inflammasome activation and production of the downstream proinflammatory cytokines IL-lβ and IL-18 during *E. coli* infection. In addition, *L. rhamnosus* GR-1 suppresses *E. coli*-induced cell pyroptosis, in part through attenuation of NLRC4 inflammasome activation, independently of ASC. Furthermore, *L. rhamnosus* GR-1 inhibits non-canonical caspase-4 activation, which subsequently synergizes with NLRP3-/ASC-dependent caspase-1 activation to potentially inhibit ASC-independent caspase-1 activation, thus suppressing cell pyroptosis and IL-lβ and IL-18 production.

AUTHOR CONTRIBUTIONS

QW, Y-HZ, and J-FW conceived and designed the experiments, analyzed the data, and wrote the manuscript. QW, JX, XL, CD, and M-JW performed the experiments.

FUNDING

This work was supported by the National Key R&D Program of China (Project No. 2017YFD0502200), the National Natural Science Foundation of China (Project Nos. 31472242 and 31672613), and J-FW received funding from the program for the Beijing Dairy Industry Innovation Team.

ACKNOWLEDGMENTS

We would like to thank Professor Sen Wu for the pCRISPR-sg5 plasmid and Dr. Ying Yu for providing MAC-T cells.

SUPPLEMENTARY MATERIAL

The Supplementary Material for this article can be found online at: https://www.frontiersin.org/articles/10.3389/fmicb.2018.01661/full#supplementary-material

FIGURE S1 | Immunodetection of cytokeratin-18 in MAC-T cells. Representative confocal immunocytochemistry images showing typical morphology of MAC-T cells. MAC-T cells were immunostained for cytokeratin-18 (red). DAPI (blue) was used to localize nuclei. Scale bar, 20 μm. Data are representative of three independent experiments.

FIGURE S2 | The lactate content in the cell supernatants and the effect of lactate on NLRP3 expression during *E. coli* infection. Lactate content in the supernatants was determined **(A)**. Cells were also simultaneously treated with lactate (LACT) at a concentration of 0.6 g/L (equivalent to 7 mM) and *E. coli* at a MOI of 100:1. Western blot detection of NLRP3 in WT and $ASC^{-/-}$ cells collected from the indicated cell cultures at 6 h after *E. coli* challenge **(B)**. Representative panels showing expression of NLRP3 protein (Left). NLRP3 band intensity was determined using Quantity One software. Results are presented as the ratio of NLRP3 band intensity to that of GAPDH (Right). Data are presented as the mean ± SEM of three independent experiments. $^{*}P < 0.05$, $^{**}P < 0.01$, $^{***}P < 0.001$.

REFERENCES

Afonina, I. S., Zhong, Z., Karin, M., and Beyaert, R. (2017). Limiting inflammation-the negative regulation of NF-kappaB and the NLRP3 inflammasome. *Nat. Immunol.* 18, 861–869. doi: 10.1038/ni.3772

Ardita, C. S., Mercante, J. W., Kwon, Y. M., Luo, L., Crawford, M. E., Powell, D. N., et al. (2014). Epithelial adhesion mediated by pilin SpaC is required for *Lactobacillus rhamnosus* GG-induced cellular responses. *Appl. Environ. Microbiol.* 80, 5068–5077. doi: 10.1128/AEM.01039-14

Bauernfeind, F. G., Horvath, G., Stutz, A., Alnemri, E. S., MacDonald, K., Speert, D., et al. (2009). NF-kB activating pattern recognition and cytokine receptors license NLRP3 inflammasome activation by regulating NLRP3 expression. *J. Immunol.* 183, 787–791. doi: 10.4049/jimmunol.0901363

Broz, P., Newton, K., Lamkanfi, M., Mariathasan, S., Dixit, V. M., and Monack, D. M. (2010a). Redundant roles for inflammasome receptors NLRP3 and NLRC4 in host defense against *Salmonella*. *J. Exp. Med.* 207, 1745–1755. doi: 10.1084/jem.20100257

Broz, P., von Moltke, J., Jones, J. W., Vance, R. E., and Monack, D. M. (2010b). Differential requirement for caspase-1 autoproteolysis in pathogen-induced cell death and cytokine processing. *Cell Host Microbe* 8, 471–483. doi: 10.1016/j.chom.2010.11.007

Brubaker, S. W., Bonham, K. S., Zanoni, I., and Kagan, J. C. (2015). Innate immune pattern recognition: a cell biological perspective. *Annu. Rev. Immunol.* 33, 257–290. doi: 10.1146/annurev-immunol-032414-112240

Bui, F. Q., Johnson, L., Roberts, J., Hung, S. C., Lee, J., Atanasova, K. R., et al. (2016). *Fusobacterium nucleatum* infection of gingival epithelial cells leads to NLRP3 inflammasome-dependent secretion of IL-1beta and the danger signals ASC and HMGB1. *Cell Microbiol.* 18, 970–981. doi: 10.1111/cmi.12560

Dikshit, N., Kale, S. D., Khameneh, H. J., Balamuralidhar, V., Tang, C. Y., Kumar, P., et al. (2018). NLRP3 inflammasome pathway has a critical role in the

host immunity against clinically relevant *Acinetobacter baumannii* pulmonary infection. *Mucosal Immunol.* 11, 257–272. doi: 10.1038/mi.2017.50

Franchi, L., Kamada, N., Nakamura, Y., Burberry, A., Kuffa, P., Suzuki, S., et al. (2012). NLRC4-driven production of IL-1beta discriminates between pathogenic and commensal bacteria and promotes host intestinal defense. *Nat. Immunol.* 13, 449–456. doi: 10.1038/ni.2263

Gudina, E. J., Fernandes, E. C., Teixeira, J. A., and Rodrigues, L. R. (2015). Antimicrobial and anti-adhesive activities of cell-bound biosurfactant from *Lactobacillus agilis* CCUG31450. *RSC Adv.* 5, 90960–90968. doi: 10.1039/C5RA11659G

Gueya, B., Bodnara, M., Maniéa, S. N., Tardivele, A., and Petrilli, V. (2014). Caspase-1 autoproteolysis is differentially required for NLRP1b and NLRP3 inflammasome function. *Proc. Natl. Acad. Sci. U.S.A.* 111, 17254–17259. doi: 10.1073/pnas.1415756111

Guo, H., Callaway, J. B., and Ting, J. P. (2015). Inflammasomes: mechanism of action, role in disease, and therapeutics. *Nat. Med.* 21, 677–687. doi: 10.1038/nm.3893

Gurung, P., Karki, R., Vogel, P., Watanabe, M., Bix, M., Lamkanfi, M., et al. (2015). An NLRP3 inflammasome-triggered Th2-biased adaptive immune response promotes leishmaniasis. *J. Clin. Invest.* 125, 1329–1338. doi: 10.1172/JCI79526

Hoque, R., Farooq, A., Ghani, A., Gorelick, F., and Mehal, W. Z. (2014). Lactate reduces liver and pancreatic injury in Toll-like receptor- and inflammasome-mediated inflammation via GPR81-mediated suppression of innate immunity. *Gastroenterology* 146, 1763–1774. doi: 10.1053/j.gastro.2014.03.014

Huynh, H. T., Robitaille, G., and Turner, J. D. (1991). Establishment of bovine mammary epithelial cells (MAC-T): an in vitro model for bovine lactation. *Exp. Cell Res.* 197, 191–199. doi: 10.1016/0014-4827(91)90422-Q

Jo, E. K., Kim, J. K., Shin, D. M., and Sasakawa, C. (2016). Molecular mechanisms regulating NLRP3 inflammasome activation. *Cell. Mol. Immunol.* 13, 148–159. doi: 10.1038/cmi.2015.95

Jorgensen, I., Lopez, J. P., Laufer, S. A., and Miao, E. A. (2016). IL-1beta, IL-18, and eicosanoids promote neutrophil recruitment to pore-induced intracellular traps following pyroptosis. *Eur. J. Immunol.* 46, 2761–2766. doi: 10.1002/eji.201646647

Kayagaki, N., Warming, S., Lamkanfi, M., Vande Walle, L., Louie, S., Dong, J., et al. (2011). Non-canonical inflammasome activation targets caspase-11. *Nature* 479, 117–121. doi: 10.1038/nature10558

Kim, S. O., Sheikh, H. I., Ha, S., Martins, A., and Reid, G. (2006). G-CSF-mediated inhibition of JNK is a key mechanism for *Lactobacillus rhamnosus*-induced suppression of TNF production in macrophages. *Cell. Microbiol.* 8, 1958–1971. doi: 10.1111/j.1462-5822.2006.00763.x

Koenig, U., Eckhart, L., and Tschachler, E. (2001). Evidence that caspase-13 is not a human but a bovine gene. *Biochem. Biophys. Res. Commun.* 285, 1150–1154. doi: 10.1006/bbrc.2001.5315

Lamkanfi, M., and Dixit, V. M. (2014). Mechanisms and functions of inflammasomes. *Cell* 157, 1013–1022. doi: 10.1016/j.cell.2014.04.007

Lannitti, R. G., Napolioni, V., Oikonomou, V., De Luca, A., Galosi, C., Pariano, M., et al. (2016). IL-1 receptor antagonist ameliorates inflammasome-dependent inflammation in murine and human cystic fibrosis. *Nat. Commun.* 7:10791. doi: 10.1038/ncomms10791

Liao, P. C., Chao, L. K., Chou, J. C., Dong, W. C., Lin, C. N., Lin, C. Y., et al. (2013). Lipopolysaccharide/adenosine triphosphate-mediated signal transduction in the regulation of NLRP3 protein expression and caspase-1-mediated interleukin-1β secretion. *Inflamm. Res.* 62, 89–96. doi: 10.1007/s00011-012-0555-2

Martinon, F., and Tschopp, J. (2004). Inflammatory caspases: linking an intracellular innate immune system to autoinflammatory diseases. *Cell* 117, 561–574. doi: 10.1016/j.cell.2004.05.004

Miao, E. A., Mao, D. P., Yudkovsky, N., Bonneau, R., Lorang, C. G., Warren, S. E., et al. (2010). Innate immune detection of the type III secretion apparatus through the NLRC4 inflammasome. *Proc. Natl. Acad. Sci. U.S.A.* 107, 3076–3080. doi: 10.1073/pnas.0913087107

Miettinen, M., Pietila, T. E., Kekkonen, R. A., Kankainen, M., Latvala, S., Pirhonen, J., et al. (2012). Nonpathogenic *Lactobacillus rhamnosus* activates the inflammasome and antiviral responses in human macrophages. *Gut Microbes* 3, 510–522. doi: 10.4161/gmic.21736

Rathinam, V. A., Vanaja, S. K., Waggoner, L., Sokolovska, A., Becker, C., Stuart, L. M., et al. (2012). TRIF licenses caspase-11-dependent NLRP3 inflammasome activation by gram-negative bacteria. *Cell* 150, 606–619. doi: 10.1016/j.cell.2012.07.007

Samuel Weigt, S., Palchevskiy, V., and Belperio, J. A. (2017). Inflammasomes and IL-1 biology in the pathogenesis of allograft dysfunction. *J. Clin. Invest.* 127, 2022–2029. doi: 10.1172/JCI93537

Sander, L. E., Davis, M. J., Boekschoten, M. V., Amsen, D., Dascher, C. C., Ryffel, B., et al. (2011). Detection of prokaryotic mRNA signifies microbial viability and promotes immunity. *Nature* 474, 385–389. doi: 10.1038/nature10072

Seo, S. U., Kamada, N., Munoz-Planillo, R., Kim, Y. G., Kim, D., Koizumi, Y., et al. (2015). Distinct commensals induce interleukin-1beta via NLRP3 inflammasome in inflammatory monocytes to promote intestinal inflammation in response to injury. *Immunity* 42, 744–755. doi: 10.1016/j.immuni.2015.03.004

Shaheen, M., Tantary, H. A., and Nabi, S. U. (2015). A treatise on bovine mastitis: disease and disease economics, etiological basis, risk factors, impact on human health, therapeutic management, prevention and control strategy. *Adv. Dairy Res.* 4:150.

Shi, J., Zhao, Y., Wang, Y., Gao, W., Ding, J., Li, P., et al. (2014). Inflammatory caspases are innate immune receptors for intracellular LPS. *Nature* 514, 187–192. doi: 10.1038/nature13683

Shi, Y. (2004). Caspase activation: revisiting the induced proximity model. *Cell* 117, 855–858. doi: 10.1016/j.cell.2004.06.007

Thacker, J. D., Balin, B. J., Appelt, D. M., Sassi-Gaha, S., Purohit, M., Rest, R. F., et al. (2012). NLRP3 inflammasome is a target for development of broad-spectrum anti-infective drugs. *Antimicrob. Agents Chemother.* 56, 1921–1930. doi: 10.1128/AAC.06372-11

Thomas, C. M., Hong, T., Peter van Pijkeren, J., Hemarajata, P., Trinh, D. V., Hu, W., et al. (2012). Histamine derived from probiotic *Lactobacillus reuteri* suppresses TNF via modulation of PKA and ERK signaling. *PLoS One* 7:e31951. doi: 10.1371/journal.pone.0031951

Tytgat, H. L. P., Douillard, F. P., Reunanen, J., Rasinkangas, P., Hendrickx, A. P., Laine, P. K., et al. (2016). *Lactobacillus rhamnosus* GG outcompetes *Enterococcus faecium* via mucus-binding pili: evidence for a novel and heterospecific probiotic mechanism. *Appl. Environ. Microbiol.* 82, 5756–5762. doi: 10.1128/AEM.01243-16

Vanaja, S. K., Russo, A. J., Behl, B., Banerjee, I., Yankova, M., Deshmukh, S. D., et al. (2016). Bacterial outer membrane vesicles mediate cytosolic localization of LPS and caspase-11 activation. *Cell* 165, 1106–1119. doi: 10.1016/j.cell.2016.04.015

Vilahur, G., Lopez-Bernal, S., Camino, S., Mendieta, G., Padro, T., and Badimon, L. (2015). *Lactobacillus plantarum* CECT 7315/7316 intake modulates the acute and chronic innate inflammatory response. *Eur. J. Nutr.* 54, 1161–1171. doi: 10.1007/s00394-014-0794-9

Wu, Q., Liu, M. C., Yang, J., Wang, J. F., and Zhu, Y. H. (2016). *Lactobacillus rhamnosus* GR-1 ameliorates *Escherichia coli*-induced inflammation and cell damage via attenuation of ASC-independent NLRP3 inflammasome activation. *Appl. Environ. Microbiol.* 82, 1173–1182. doi: 10.1128/AEM.03044-15

Zhao, Y., Yang, J., Shi, J., Gong, Y., Lu, Q., Xu, H., et al. (2011). The NLRC4 inflammasome receptors for bacterial flagellin and type III secretion apparatus. *Nature* 477, 596–600. doi: 10.1038/nature10510

Conflict of Interest Statement: The authors declare that the research was conducted in the absence of any commercial or financial relationships that could be construed as a potential conflict of interest.

frontiers in Microbiology

ORIGINAL RESEARCH
published: 24 August 2018
doi: 10.3389/fmicb.2018.01953

Probiotic *Lactobacillus plantarum* Promotes Intestinal Barrier Function by Strengthening the Epithelium and Modulating Gut Microbiota

Jing Wang, Haifeng Ji, Sixin Wang, Hui Liu, Wei Zhang, Dongyan Zhang and Yamin Wang*

Institute of Animal Husbandry and Veterinary Medicine, Beijing Academy of Agriculture and Forestry Sciences, Beijing, China

Weaning disturbs the intestinal barrier function and increases the risk of infection in piglets. Probiotics exert beneficial health effects, mainly by reinforcing the intestinal epithelium and modulating the gut microbiota. However, the mechanisms of action, and especially, the specific regulatory effects of modulated microbiota by probiotics on the intestinal epithelium have not yet been elucidated. The present study aimed to decipher the protective effects of the probiotic *Lactobacillus plantarum* strain ZLP001 on the intestinal epithelium and microbiota as well as the effects of modulated microbiota on epithelial function. Paracellular permeability was measured with fluorescein isothiocyanate-dextran (FD-4). Gene and protein expression levels of tight junction (TJ) proteins, proinflammatory cytokines, and host defense peptides were determined by RT-qPCR, ELISA, and western blot analysis. Short-chain fatty acid (SCFA) concentrations were measured by ion chromatography. Fecal microbiota composition was assessed by high-throughput sequencing. The results showed that pretreatment with 10^8 colony forming units (CFU) mL^{-1} of *L. plantarum* ZLP001 significantly counteracted the increase in gut permeability to FD-4 induced by 10^6 CFU mL^{-1} enterotoxigenic *Escherichia coli* (ETEC). In addition, *L. plantarum* ZLP001 pretreatment alleviated the reduction in TJ proteins (claudin-1, occludin, and ZO-1) and downregulated proinflammatory cytokines IL-6 and IL-8, and TNFα expression and secretion caused by ETEC. *L. plantarum* ZLP001 also significantly increased the expression of the host defense peptides *pBD2* and *PG1-5* and pBD2 secretion relative to the control. Furthermore, *L. plantarum* ZLP001 treatment affected piglet fecal microbiota. The abundance of butyrate-producing bacteria *Anaerotruncus* and *Faecalibacterium* was significantly increased in *L. plantarum* ZLP001-treated piglets, and showed a positive correlation with fecal butyric and acetic acid concentrations. In addition, the cell density of *Clostridium sensu stricto* 1, which may cause epithelial inflammation, was decreased after *L. plantarum* ZLP001 administration, while the beneficial *Lactobacillus* was significantly increased. Our findings suggest that *L. plantarum* ZLP001 fortifies the intestinal barrier by strengthening epithelial defense functions and modulating gut microbiota.

Keywords: *Lactobacillus plantarum*, permeability, tight junction, immune response, host defense, microbiota

OPEN ACCESS

Edited by:
Maria Olivia Pereira, University of Minho, Portugal

Reviewed by:
M. Andrea Azcarate-Peril, University of North Carolina at Chapel Hill, United States
Maryam Dadar, Razi Vaccine and Serum Research Institute, Iran

****Correspondence:***
Haifeng Ji
jhf207@126.com

Specialty section:
This article was submitted to Antimicrobials, Resistance and Chemotherapy, a section of the journal Frontiers in Microbiology

Received: *09 April 2018*
Accepted: *02 August 2018*
Published: *24 August 2018*

Citation:
Wang J, Ji H, Wang S, Liu H, Zhang W, Zhang D and Wang Y (2018) Probiotic Lactobacillus plantarum Promotes Intestinal Barrier Function by Strengthening the Epithelium and Modulating Gut Microbiota. Front. Microbiol. 9:1953. doi: 10.3389/fmicb.2018.01953

INTRODUCTION

The sudden changes in diet and the physical and social environment associated with weaning are significant piglet stressors. Elevated plasma cortisol and corticotropin-releasing factor levels are indices of weaning stress (Van der Meulen et al., 2010). The feed intake of most piglets after weaning is relatively low because of the dietary change from liquid milk to solid feed. Decreased feed and water intake cause small intestinal villous atrophy (Lallès et al., 2004), which in turn results in diminished digestive and absorptive capacities and reduced growth rate. Maternal separation and changes in environment are social and environmental stresses that cause tension in piglets and weaken their immune system. Furthermore, the dietary and environmental changes associated with weaning are associated with a substantial modification of the intestinal microbiota and may cause post-weaning diarrhea and enteric infection (Lallès et al., 2007). Perturbations of the intestinal epithelium, weakened immune system, and modified intestinal microbiota induced by weaning stress can profoundly impact piglet health and growth performance and may, in some cases, lead to mortality (Campbell et al., 2013).

The intestine plays a critical role in the defense against harmful external factors. Poor intestinal defense renders piglets more susceptible to weaning stress, leading to infection and disease. In post-weaning piglets, transepithelial electrical resistance (TER) significantly decreases while paracellular permeability increases (Hu et al., 2013). The expression of the tight junction (TJ) proteins occludin, claudin-1, and ZO-1 decreases during weaning, and as a result, barrier integrity is impaired. This facilitates pathogen penetration and permits bacteriotoxins to enter the body. Weaned piglets also exhibit elevated expression of the proinflammatory cytokines TNF-α and IL-6 (Hu et al., 2013), which is associated with weak epithelium and inflammatory disease. Furthermore, weaning lowers intestinal microbial diversity and alters the microbiota composition in that the abundance of obligate anaerobic bacteria decreases and that of facultative anaerobic bacteria increases (Winter et al., 2013), which weakens intestinal function. For instance, *Lactobacillus* spp. and other beneficial bacteria play an important role in protecting against intestinal pathogens, and the reduction in their abundance after weaning enhances disease risk (Konstantinov et al., 2006). *S. enterica* and *E. coli* are two major pathogens infecting piglets. An increased abundance of these pathogens in the intestine often results in severe infection.

Evidence indicates that the consumption of probiotic bacteria contributes to intestinal function by maintaining paracellular permeability, enhancing the physical mucous layer, stimulating the immune system, and modulating resident microbiota composition and activity (Boirivant and Strober, 2007). The regulatory effects of probiotics on human, pig, and chicken intestinal homeostasis have been studied extensively (Van Baarlen et al., 2013; Cisek and Binek, 2014; Gresse et al., 2017), and interactions between probiotic and commensal bacteria and the epithelial barrier are thought to be the main underlying mechanism. *Lactobacillus* is a predominant indigenous bacterial genus found in the human and animal gastrointestinal tract, and species of this genus are commonly used as probiotics. *In vitro* and *in vivo* studies in various cell lines and animal models have demonstrated that *L. plantarum* MB452, *L. casei*, *L. rhamnosus* GG, and *L. reuteri* I5007 affect TER and epithelial permeability and modulate TJ protein expression and distribution (Anderson et al., 2010; Eun et al., 2011; Patel et al., 2012; Yang et al., 2015). *Lactobacillus spp.* boost the immune system by promoting the expression of anti-inflammatory cytokines, such as IL-10 and IFN-γ (*Lactobacillus* GG, Kopp et al., 2008; *L. rhamnosus* CRL1505, Villena et al., 2014), or by inhibiting that of pro-inflammatory cytokines, such as IL-6, IL-8, and TNF-α (*L. reuteri* LR1, Wang et al., 2016; *L. plantarum* 2142, Farkas et al., 2014). *L. reuteri* I5007 and *L. plantarum* DSMZ 12028 can modulate the synthesis of antimicrobials by the intestinal epithelium (Paolillo et al., 2009; Liu et al., 2017). Multiple studies have confirmed that *Lactobacillus* spp., such as *L. salivarius* UCC118 and *L. acidophilus*, significantly modulate resident intestinal microbiota composition and activity (Riboulet-Bisson et al., 2012; Li et al., 2017). Thus, through enhancing intestinal epithelial function, probiotics improve host health. However, the effects of probiotics on intestinal barrier function are strain-dependent and not ubiquitous. The unique effects of specific strains on the intestinal epithelium and microbiota, and whether the modulated microbiota affect intestinal epithelial function remain unclear.

The results of our previous studies indicated that dietary supplementation with *Lactobacillus plantarum* ZLP001 isolated from healthy piglet intestinal tract (Wang et al., 2011) improves growth performance and antioxidant status in post-weaning piglets (Wang et al., 2012). However, its impact on intestinal barrier function and microbiota, and the interaction between barrier function and microbiota after *L. plantarum* ZLP001 treatment remained to be investigated. In this study, the impact of *L. plantarum* ZLP001 on intestinal epithelial function was evaluated by measuring gut permeability and the expression of TJ proteins, inflammatory cytokines, and host defense peptides (HDP). Further, we evaluated the ability of this strain to regulate microbiota composition and community structure. The regulatory effects of the microbiota modulated by the probiotic strain on intestinal epithelium function were also analyzed.

MATERIALS AND METHODS

Bacteria and Culture Conditions

L. plantarum ZLP001 was isolated in our laboratory from the intestine of a healthy piglet. It was identified by the China Center of Industrial Culture Collection (Beijing, China) and preserved in the China General Microbiological Culture Collection Center (CGMCC No. 7370). It was grown in improved De Man, Rogosa, and Sharpe liquid medium (10 g peptone, 5 g yeast powder, 20 g glucose, 10 g beef extract, 5 g sodium acetate, 2 g ammonium citrate dibasic, 2 g dipotassium phosphate, 0.58 g magnesium sulfate, 0.19 g manganese sulfate, 1 mL of Tween 80, and water to 1,000 mL; pH 6.5) at 37°C under anaerobic conditions.

Enteropathic *E. coli* strain expressing F4 (F4+ ETEC), serotype O149:K91, K88ac, was obtained from the China Veterinary Culture Collection Center. It was grown in Luria-Bertani medium (Oxoid, Basingstoke, United Kingdom) at 37°C.

Cell Line and Culture Conditions

The porcine intestinal epithelial cell line (IPEC-J2) used in this study was purchased from JENNIO Biological Technology (Guangzhou, China). It was originally derived from the jejuna of neonatal piglets. The cells were cultured in DMEM/F12 (Dulbecco's modified Eagle's medium/nutrient mixture F-12, a 1:1 mixture of DMEM and Ham's F-12; Invitrogen, Carlsbad, CA, United States) supplemented with 10% fetal bovine serum (FBS; Invitrogen, Carlsbad, CA, United States), streptomycin (100 μg mL^{-1}), and amphotericin B (0.5 μg mL^{-1}). IPEC-J2 cells were cultured at 37°C in a 5% CO_2/95% air atmosphere and 90% relative humidity. Cells were separated at each passage with 0.25% w/v trypsin (Invitrogen, Carlsbad, CA, United States) and replenished with fresh media every 2–3 days.

Paracellular Permeability Determination

Changes in paracellular permeability after *L. plantarum* ZLP001 treatment were determined with fluorescein isothiocyanate-dextrans (FD-4; average molecular mass, 4.4 kDa; Sigma-Aldrich Corp., St. Louis, MO, United States) according to the method reported by Wang et al. (2016) with some modifications. IPEC-2 cells were seeded into 6-well Transwell insert chambers (0.4 μm pore size; Corning, Inc., Corning, NY, United States) at a density of 2.5×10^5 cells per well and were cultured to form differentiated monolayers. The cells were pretreated or not with *L. plantarum* ZLP001 (LP, 10^8 CFU mL^{-1}) for 6 h and then challenged or not with 10^6 CFU mL^{-1} ETEC for 3 h. FD-4 was added to the apical sides of the IPEC-J2 cell monolayers at a final concentration of 1 mg mL^{-1}. After incubation, medium (100 μL) was sampled from the basolateral chambers, and the FD-4 concentration was quantified using a fluorescence microplate reader (FLx800; BioTek, Winooski, VT, United States). Calibration curves were plotted with an FD-4 gradient series. All experiments were carried out in triplicate.

IPEC-J2 Cells Treatment With *L. plantarum* ZLP001 and ETEC

IPEC-J2 cells were seeded into 6-well plates (Corning, Inc., Corning, NY, United States) at a density of 2.5×10^5 cells per well. At 80% confluence, the cells were pretreated or not with *L. plantarum* ZLP001 (LP, 10^8 CFU mL^{-1}) at 37°C for 6 h. Then, the cells were washed three times with PBS and the supernatant was removed. The cells were challenged or not with 10^6 CFU mL^{-1} ETEC at 37°C for 3 h. Fresh medium containing bacteria was prepared by resuspending and diluting collected bacteria in DMEM/F12 without FBS or streptomycin/penicillin. After incubation, the cells were rinsed with PBS three times and collected for subsequent assays. Culture medium supernatants were collected simultaneously. All experiments were carried out in triplicate.

Determination of mRNA Expression

The mRNA expression levels of TJ proteins, cytokines, and HDPs were determined by quantitative real-time PCR (RT-qPCR). IPEC-J2 cells collected after incubation were lysed with RNAzol (MRC, Cincinnati, OH, United States). Total RNA was extracted following the manufacturer's instructions. RNA concentrations were determined with a NanoDrop spectrophotometer (Thermo Fisher Scientific, Waltham, MA, United States) and purity was verified by A260:A280 and A260:A230 absorbance ratios. The RNA was reverse transcribed with an iScript cDNA Synthesis Kit (Bio-Rad Laboratories Ltd., Hercules, CA, United States) according to the manufacturer's instructions. qPCR was performed using iTaq Universal SYBR Green Supermix (Bio-Rad Laboratories Ltd., Hercules, CA, United States) on a QuantStudio 3 real-time PCR system (Thermo Fisher Scientific, Waltham, MA, United States). Porcine-specific primers are listed in **Supplementary Table S1**. The expression of each gene was normalized to that of glyceraldehyde-3-phosphate dehydrogenase (*GAPDH*) to yield a relative transcript level. PCR conditions were 95°C for 10 min followed by 40 amplification cycles (95°C for 30 s, 60°C for 30 s, and 72°C for 20 s). Relative gene expression was calculated by the $2^{-\Delta\Delta C_T}$ method.

Protein Extraction and Immunoblotting

Total protein from IPEC-J2 cells was extracted after the various treatments using a lysis buffer containing 150 mM NaCl, 1% Triton X-100, 0.5% sodium deoxycholate, 0.1% SDS, and 50 mM Tris–HCl adjusted to pH 7.4 and supplemented with a protease inhibitor cocktail (Applygene, Beijing, China). The IPEC-J2 cells were collected into precooled lysis buffer and kept on ice for 30 min. The lysed samples were centrifuged at 4°C and 12,000 $\times$ *g* for 5 min to collect the supernatants. Protein concentrations were determined with a Bicinchoninic Acid Protein Assay Kit (Thermo Fisher Scientific, Waltham, MA, United States). After separation on 10% SDS polyacrylamide gel, proteins were electrophoretically transferred to polyvinylidene difluoride membranes (EMD Millipore, Billerica, MA, United States). The membranes were blocked with 5% skim milk and then incubated with primary antibodies overnight (∼12–16 h) at 4°C. They were then incubated with horseradish peroxidase-conjugated secondary antibodies for 1 h at 20–25°C. The antibodies used are listed in **Supplementary Table S2**. Immunoreactive proteins were detected on a ChemiDoc XRS imaging system (Bio-Rad Laboratories Ltd., Hercules, CA, United States) using Western Blotting Luminol Reagent (Santa Cruz Biotechnology, Dallas, TX, United States). Band densities were analyzed with ImageJ (National Institutes of Health, Bethesda, MD, United States). Results were calculated and recorded as the protein abundance relative to β-actin.

Proinflammatory Cytokine and Porcine β-Defensin 2 (pBD2) Measurement

Proinflammatory cytokines and porcine β-defensin 2 were measured by an enzyme linked immunosorbent assay (ELISA). Cell culture medium supernatant (500 μL) was centrifuged

at 4,000 × *g* for 10 min and then passed through a 0.25-μm pore diameter filter (Corning Inc., Corning, NY, United States). The concentrations of interleukin 6 (IL-6), interleukin 8 (IL-8), tumor necrosis factor α (TNF-α), and pBD2 were determined with porcine-specific ELISA Kits (Abcam, Cambridge, United Kingdom), according to the manufacturer's instructions.

Animal Groups and Diets

The experimental protocol was reviewed and approved by the Ethics Committee of the Institute of Animal Husbandry and Veterinary Medicine, Beijing Academy of Agriculture and Forestry Sciences, Beijing, PRC. Humane animal care was practiced throughout the trial.

Ten post-weaning piglets (siblings; Large White × Landrace; 8.54 ± 0.58 kg) were assigned to *L. plantarum* ZLP001 treatment or placebo control groups. Each group consisted of two males and three females. Animals were raised at the Beijing Xiqingminfeng Farm (Beijing, China) in a separate room decontaminated prior to the study and were housed at 25–28°C. Each piglet was kept in an individual 1.28-m^2 pen with a mesh floor. Each pen contained a feeder and a water nipple. Free access to feed and water was provided throughout the 30-day trial. Piglets received a complete feed specially formulated according to the NRC (2012) and the Feeding Standard of Swine (2004). Detailed information about the diet is shown in **Supplementary Table S3**. The control group received a basal diet supplemented with placebo (2 g kg^{-1} feed). The treatment group was administered the basal diet supplemented with freeze-dried *L. plantarum* ZLP001 (5.0×10^9 CFU g^{-1}, 2 g kg^{-1} feed).

Fecal Sample Collection and Microbiota Analysis

Fresh fecal samples were individually collected from piglet recta at the end of the feeding experiment. The samples were immediately transferred to the laboratory and processed for genomic DNA extraction with an E.Z.N.A. Stool DNA Kit (Omega Bio-Tek, Norcross, GA, United States) according to the manufacturer's instructions. V3+V4 hypervariable sequences of 16S rDNA were amplified by PCR with TransStart FastPfu DNA Polymerase (TransGen Biotech Ltd., Beijing, China) with barcode-modified universal primers (forward: 338F, 5′-ACTCCTACGGGAGGCAGCA-3′; reverse: 806R, 5′-GGACTACHVGGGTWTCTAAT-3′). Amplified products were separated on 2% agarose gels and extracted and purified with an AxyPrep DNA Gel Extraction Kit (Axygen Biosciences, Union City, CA, United States). Barcoded V3+V4 amplicons were sequenced by the paired-end method with Illumina MiSeq at Shanghai Majorbio Bio-pharm Technology Co. (Shanghai, China). Raw sequences were denoised using Trimmomatic and FLASH software and filtered according to their barcodes and primer sequences with QIIME v. 1.5.0. Chimeras were identified and excluded using the UCHIME algorithm v. 4.2.40. Optimized, high-quality sequences were clustered into operational taxonomic units (OTUs) at 97% sequence identity against a subset of the Silva 16S sequence database (Release 119[1]). Taxon-dependent analysis was carried out using the Ribosomal Database Project (RDP) naive Bayesian classifier, with an 80% bootstrap cutoff. Alpha diversity (Shannon and Simpson indices), abundance (Chao1 and ACE indices), and Good's coverage and rarefaction were analyzed with mothur v. 1.31.2. Principle coordinates analysis (PCoA) was conducted to visualize differences in fecal community composition. PCoA plots were generated on the basis of Bray–Curtis indices. The linear discriminant analysis effect size (LEfSe) algorithm was used to identify the taxa responsible for the differences between the treatment and control groups. The biomarkers used in the present study had an effect-size threshold of two.

Determination of Fecal Short-Chain Fatty Acid (SCFA) Concentrations

Fecal SCFA concentrations were determined following modified procedures of Qiu and Jin (2002). Half-gram fecal samples were homogenized in 10 mL of double-distilled water. After centrifugation at 12,000 × *g* for 10 min, the supernatants were removed and filtered through 0.25-μm-pore filters (Corning Inc., Corning, NY, United States). Acetic, propionic, and butyric acids were measured with an ion chromatography system (Dionex Corp., Sunnyvale, CA, United States).

Statistical Analysis

SPSS v. 22.0 (IBM Corp., Armonk, NY, United States) was used for statistical analysis. The FD-4 concentration and mRNA expression levels were analyzed by one-way ANOVA. Fecal SCFA concentrations were analyzed with unpaired Student's two-tailed *t*-tests. The results are expressed as the mean ± standard error of the mean (SEM). The significance level was $P < 0.05$. Correlations between fecal SCFA concentration and intestinal-associated microbiota were examined with Spearman's rank-order correlation test in R v. 3.2.1.

RESULTS

Effects of *L. plantarum* ZLP001 on Epithelial Permeability

FD-4 diffusion is a good indicator of paracellular permeability. Therefore, FD-4 transport was measured in this study to evaluate the protective effect of *L. plantarum* ZLP001 on epithelial integrity (**Figure 1**). FD-4 concentrations in the *L. plantarum* ZLP001-treated group were not significantly different from those in the untreated control. When IPEC-J2 cells were exposed to 10^6 CFU mL^{-1} ETEC alone, FD-4 permeation was significantly increased relative to that of the control group ($P < 0.05$). Pretreatment with *L. plantarum* ZLP001 (10^8 CFU mL^{-1}) significantly counteracted this permeation.

Effects of *L. plantarum* ZLP001 on TJ Expression

Abundances of *claudin-1* (**Figure 2A**), *occludin* (**Figure 2B**), and *ZO-1* (**Figure 2C**) transcripts in IPEC-J2 cells after bacterial

[1]http://www.arb-silva.de

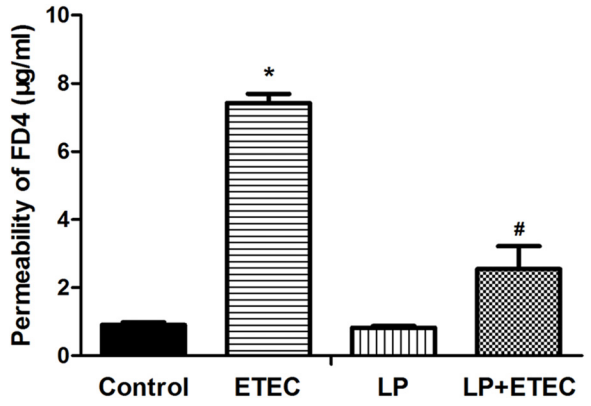

FIGURE 1 | FD-4 diffusion in *L. plantarum* ZLP001-treated IPEC-J2 cells. Cells were left untreated or pretreated with *L. plantarum* ZLP001 (LP, 10^8 CFU mL^{-1}) for 6 h on the apical sides of the cell monolayers and then challenged or not with 10^6 CFU mL^{-1} ETEC for 3 h. FD-4 concentrations in the basal compartments were measured. Values are shown as the means ± SE of three independent experiments. $^*P < 0.05$ vs. non-treated controls; $^{\#}P < 0.05$ vs. ETEC alone.

treatments were examined by RT-qPCR (**Figure 2**). After IPEC-J2 cells were incubated with ETEC alone, the mRNA expression levels of these genes were significantly decreased ($P < 0.05$) relative to those in the untreated control. *L. plantarum* ZLP001 treatment alone had no significant influence on TJ mRNA expression as compared to the untreated control. *L. plantarum* ZLP001 pretreatment significantly ($P < 0.05$) abrogated the decreases in TJ-related mRNA expression caused by ETEC infection.

Differences in TJ protein expression after the bacterial treatments were examined by western blotting. Expression levels of claudin-1 (**Figure 2D**), occludin (**Figure 2E**), and ZO-1 (**Figure 2F**) were significantly lower ($P < 0.05$) in cells exposed to ETEC than in the untreated controls. These results were consistent with those for mRNA expression. *L. plantarum* ZLP001 treatment alone did not significantly affect protein expression relative to the untreated control. *L. plantarum* ZLP001 pretreatment negated the reduction in claudin-1 (**Figure 2D**) and ZO-1 (**Figure 2F**) abundance caused by ETEC treatment.

Effects of *L. plantarum* ZLP001 on the Epithelial Immunological Barrier

Proinflammatory cytokines in IPEC-J2 cells were quantified after the treatments (**Figures 3A–C**). Incubation with ETEC alone significantly upregulated *IL-6*, *IL-8*, and *TNFα* transcripts. Treatment with *L. plantarum* ZLP001 alone had no significant effect on cytokine expression. However, pretreatment with *L. plantarum* ZLP001 prior to the ETEC challenge reduced cytokine expression in the IPEC-J2 cells to levels lower than those observed after ETEC treatment alone ($P < 0.05$). Therefore, *L. plantarum* ZLP001 reduced the ETEC-induced upregulation of proinflammatory cytokines.

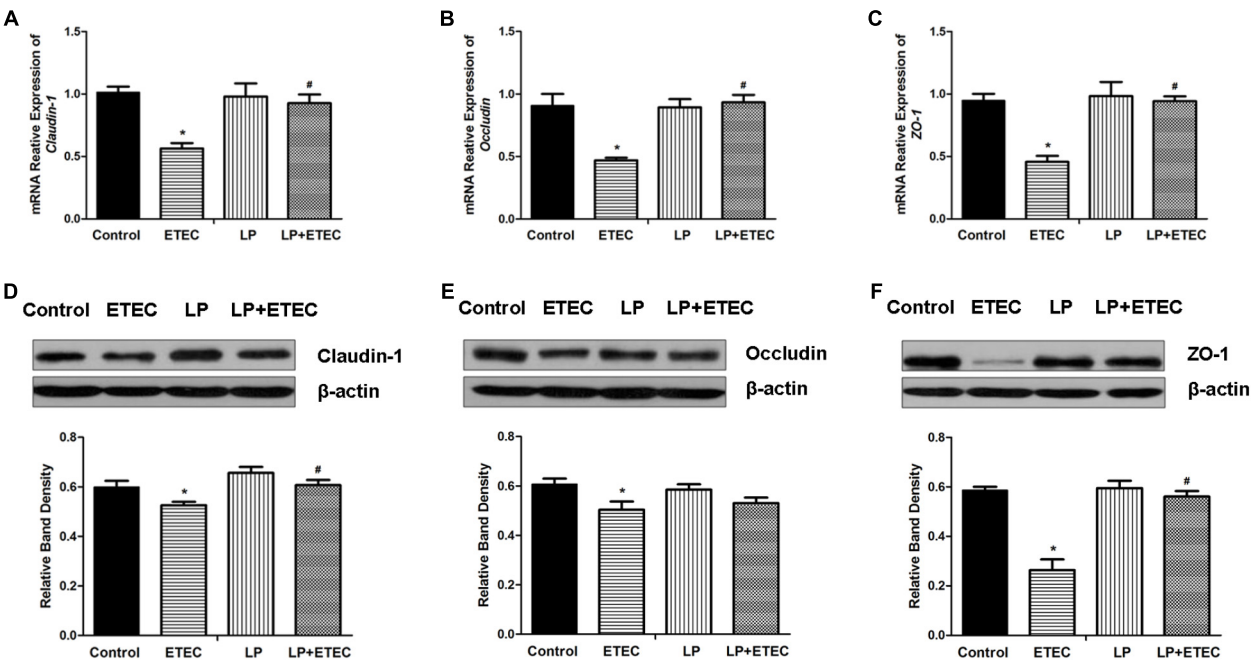

FIGURE 2 | Relative mRNA transcript and protein levels of TJ proteins in IPEC-J2 cells left untreated or pretreated with *L. plantarum* ZLP001 (LP, 10^8 CFU mL^{-1}) for 6 h, and then challenged or not with 10^6 CFU mL^{-1} ETEC for 3 h. mRNA levels of *claudin-1* **(A)**, *occludin* **(B)**, and *ZO-1* **(C)** were standardized to that of *GAPDH*. Expression levels relative to non-treated controls were calculated by the $2^{-\Delta\Delta C_T}$ method. TJ protein levels were assessed by immunoblotting. Data are western blotting results and gradation analysis of claudin-1 **(D)**, occludin **(E)**, ZO-1 **(F)**. Values are shown as the means ± SE of three independent experiments. $^*P < 0.05$ vs. non-treated controls; $^{\#}P < 0.05$ vs. ETEC alone.

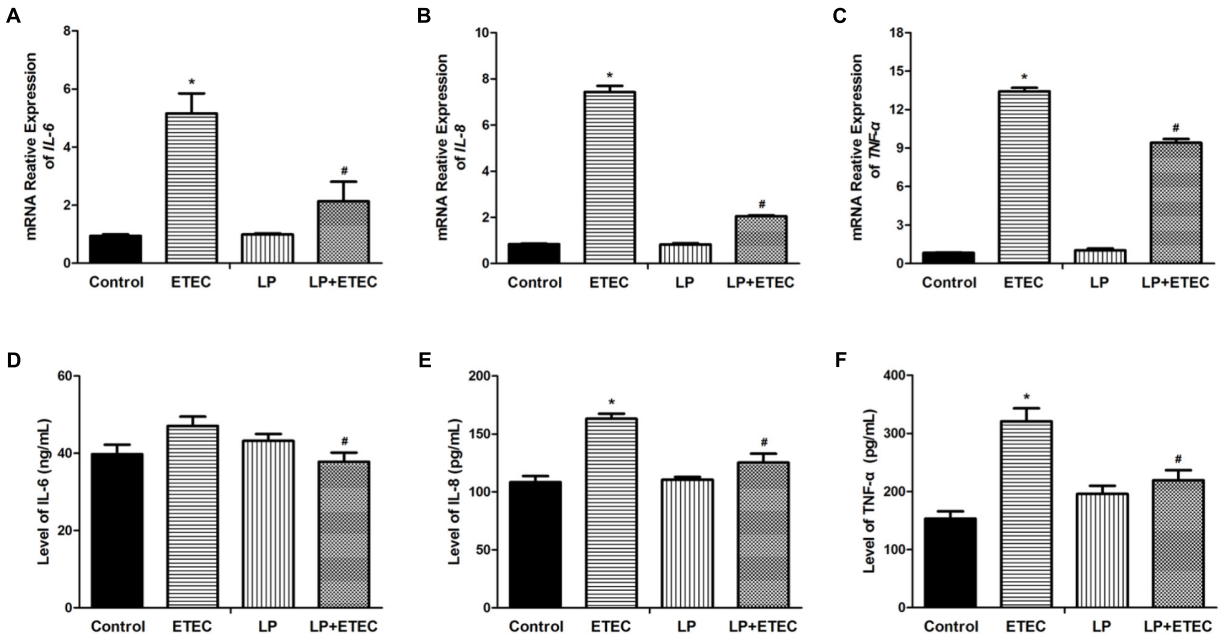

FIGURE 3 | Relative mRNA transcript levels and concentrations of proinflammatory cytokines in the culture supernatant of IPEC-J2 cells left untreated or pretreated with *L. plantarum* ZLP001 (LP, 10^8 CFU mL^{-1}) for 6 h then either unchallenged or challenged with 10^6 CFU mL^{-1} ETEC for 3 h. mRNA levels of *IL-6* **(A)**, *IL-8* **(B)**, and *TNF-α* **(C)** were standardized to that of *GAPDH*. Expression levels relative to non-treated controls were calculated by the $2^{-\Delta\Delta C_T}$ method. Protein expression of IL-6 **(D)**, IL-8 **(E)**, and TNF-α **(F)** was assessed by ELISA. Values are shown as the means ± SE of three independent experiments. $^*P < 0.05$ vs. non-treated controls; $^{\#}P < 0.05$ vs. ETEC alone.

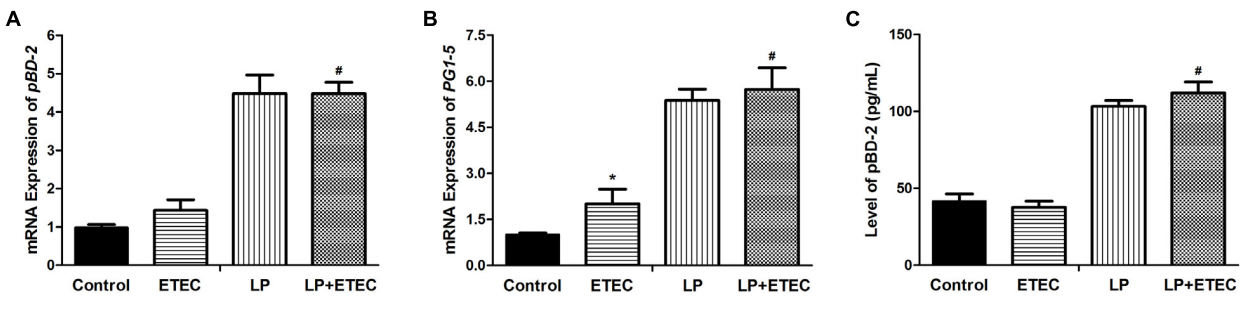

FIGURE 4 | Relative mRNA transcript levels of *pBD2* **(A)** and *PG1-5* **(B)** and concentrations of pBD2 **(C)** in the culture supernatant of IPEC-J2 cells left untreated or pretreated with *L. plantarum* ZLP001 (LP, 10^8 CFU mL^{-1}) for 6 h and then challenged or not with 10^6 CFU mL^{-1} ETEC for 3 h. mRNA expression levels were standardized to that of *GAPDH*. Expression levels relative to non-treated controls were calculated by the $2^{-\Delta\Delta C_T}$ method. The pBD2 concentration was assessed by ELISA. Values are shown as the means ± SE of three independent experiments. $^*P < 0.05$ vs. non-treated controls; $^{\#}P < 0.05$ vs. ETEC alone.

ELISA was used to verify the protective effect of *L. plantarum* ZLP001 on epithelial immunological function at the protein level after ETEC challenge (**Figures 3D–F**). The results confirmed that, while ETEC did not significantly induced IL-6, *L. plantarum* ZLP001 pretreatment suppressed the increases in IL-6, IL-8, and TNFα secretion in IPEC-J2 cells challenged with ETEC relative to the levels observed in cells incubated with ETEC alone.

Effects of *L. plantarum* ZLP001 on HDP Production

The modulatory effect of *L. plantarum* ZLP001 on the innate immune response was evaluated by measuring porcine HDP mRNA expression (**Figures 4A,B**). Cathelicidins and β-defensins are the two main mammalian HDP families. We selected *pBD2* (a β-defensin, **Figure 4A**) and *PG1-5* (a cathelicidin, **Figure 4B**) as target genes in this study. The results showed that treatment with *L. plantarum* ZLP001 significantly induced mRNA expression of both HDPs in IPEC-J2 cells ($P < 0.05$). ETEC exposure had no significant effect on *pBD2* expression, but significantly induced *PG1-5* expression. Challenge with ETEC 3 h after *L. plantarum* ZLP001 pretreatment had no significant effect on the HDP expression levels observed after incubation with *L. plantarum* ZLP001 alone.

Effects of bacterial treatment on pBD2 secretion were evaluated by ELISA (**Figure 4C**). The result was consistent with

pBD2 mRNA expression. Exposure to *L. plantarum* ZLP001 significantly induced pBD2 secretion in IPEC-J2 cells. In contrast, ETEC treatment had no significant effect on pBD2 secretion. Challenge with ETEC 3 h after *L. plantarum* ZLP001 pretreatment had no significant influence on pBD2 secretion by *L. plantarum* ZLP001 treatment alone.

Sequencing Results

Sequencing of the amplified 16S rRNA genes produced 373,846 reads after quality checks. An average of 37,385 ± 4,742 reads were obtained for each sample. Among the high-quality sequences, >99% were >400 bp. The average read length for each sample was 435 bp. Reads were clustered into 3,746 OTUs using a 97% similarity cut-off. We obtained 329–404 OTUs per sample. Based on rarefaction analysis, the sequencing depth adequately reflected species richness, suggested that the Illumina MiSeq sequencing system detected most of the fecal bacterial diversity in our study.

Effects of *L. plantarum* ZLP001 on Alpha Diversity of Fecal Microbiota

We used the Chao1, ACE, Shannon, and Simpson indices to estimate fecal microbiome taxon abundance and diversity (**Table 1**). *L. plantarum* ZLP001-treated groups exhibited higher diversity than the control group according to the Shannon and Simpson indices. Nevertheless, the difference was not significant ($P > 0.05$). *L. plantarum* ZLP001 treatment had no significant effect on fecal microbiota abundance according to the Chao1 and ACE indices. Good's coverage was >99.6% for all samples. Thus, the dominant bacterial phylotypes present in the feces were captured by this analysis.

Effects of *L. plantarum* ZLP001 on Fecal Microbiota Composition

Taxon-dependent analysis was used to compare microbiota compositions of the feces from piglets treated with *L. plantarum* ZLP001 and those receiving the placebo (**Figure 5**). Firmicutes and Bacteroidetes were the most abundant phyla in both groups and accounted for >97% of the total sequences on average. Firmicutes was the dominant phylum and constituted 58.1% in all treatments. Bacteroidetes accounted for 39.6%. Other phyla were present at lower frequencies. **Figure 5B** shows a hierarchically clustered heatmap of the fecal microbiota composition at the genus level. *Prevotella* was the most abundant; it accounted for an average of 21.5% of the sequences in all treatments by the end of the experiment. *Clostridium sensu stricto 1* (14.2%) was identified in the control piglets. *Lactobacillus* (12.8%) was detected in the *L. plantarum* ZLP001-treated piglets. LEfSe analysis indicated no significant differences between the placebo- and *L. plantarum*-treated piglets at the phylum level in terms of relative OTU abundance. Significant differences were observed between groups at several other taxa (**Figure 6**). The probiotic-treated group was enriched in Bacilli at the class level, Lactobacillales at the order level, Lactobacillaceae and Ruminococcaceae at the family level, and *Alloprevotella*, *Anaerotruncus*, *Faecalibacterium*, *Lactobacillus*, *Subdoligranulum*, unclassified *Lachnospiraceae*, and no-rank *Ruminococcaceae* at the genus level. However, it was depleted in Clostridiaceae_1 and Peptostreptococcaceae at the family level and *Clostridium sensu stricto 1*, *Terrisporobacter*, *Ruminococcaceae_UCG_007*, *Ruminococcaceae_UCG_004*, and *Ruminococcaceae_UCG_009* at the genus level. Fecal microbiota composition PCoA revealed that *L. plantarum* ZLP001 treatment significantly affected overall fecal microbiota composition. The microbiota communities in the piglets treated with *L. plantarum* ZLP001 were clustered together and were distinctly separated from those of the control pigs (**Supplementary Figure S1**).

TABLE 1 | Effects of *L. plantarum* ZLP001 treatment on average richness and diversity of bacterial community in piglet feces.

Treatment	Abundance		Coverage	Diversity	
	ACE	Chao1		Shannon	Simpson
Control	559.3	569.8	0.9968	4.31	0.0394
L. plantarum ZLP001	556.5	565.7	0.9971	4.47	0.0313
SEM	14.15	16.21		0.730	0.00355
P-value	0.929	0.908		0.311	0.282

Effects of *L. plantarum* ZLP001 on Fecal SCFA Concentrations

Table 2 shows the SCFA concentrations in piglet feces. *L. plantarum* ZLP001 treatment increased butyric acid concentrations relative to those in the controls ($P = 0.068$). Acetic and propionic acid concentrations did not significantly differ between the placebo and *L. plantarum* ZLP001 treatments ($P > 0.05$).

Correlation Between SCFA Concentrations and Fecal Microbiota

Correlations between SCFA concentration and fecal bacterial abundance (relative abundance of the top 30 genera) are shown in **Figure 7**. The results demonstrated positive associations between butyric acid concentration and *Anaerotruncus* ($r = 0.721$, $P = 0.019$) and unclassified_f_*Lachnospiraceae* ($r = 0.758$, $P = 0.011$) abundance. Acetic acid concentration was positively correlated with *Faecalibacterium* ($r = 0.879$, $P = 0.001$), *Subdoligranulum* ($r = 0.721$, $P = 0.019$), and *Prevotellaceae*_NK3B31_group ($r = 0.648$, $P = 0.043$) abundance. It was negatively correlated with *Clostridium sensu stricto 1* abundance ($r = -0.661$, $P = 0.038$). Propionic acid concentration was negatively correlated with *Phascolarctobacterium* abundance ($r = -0.697$, $P = 0.025$).

DISCUSSION

Using porcine IPEC-2 cells as a model, we demonstrated that *L. plantarum* ZLP001 plays multiple protective roles in epithelial barrier regulation. The present study showed that ETEC treatment significantly increased gut permeability to FD-4, whereas treatment with probiotic *L. plantarum* ZLP001 alone had no significant effect on gut permeability. These findings corroborate those of a previous study, in which probiotic

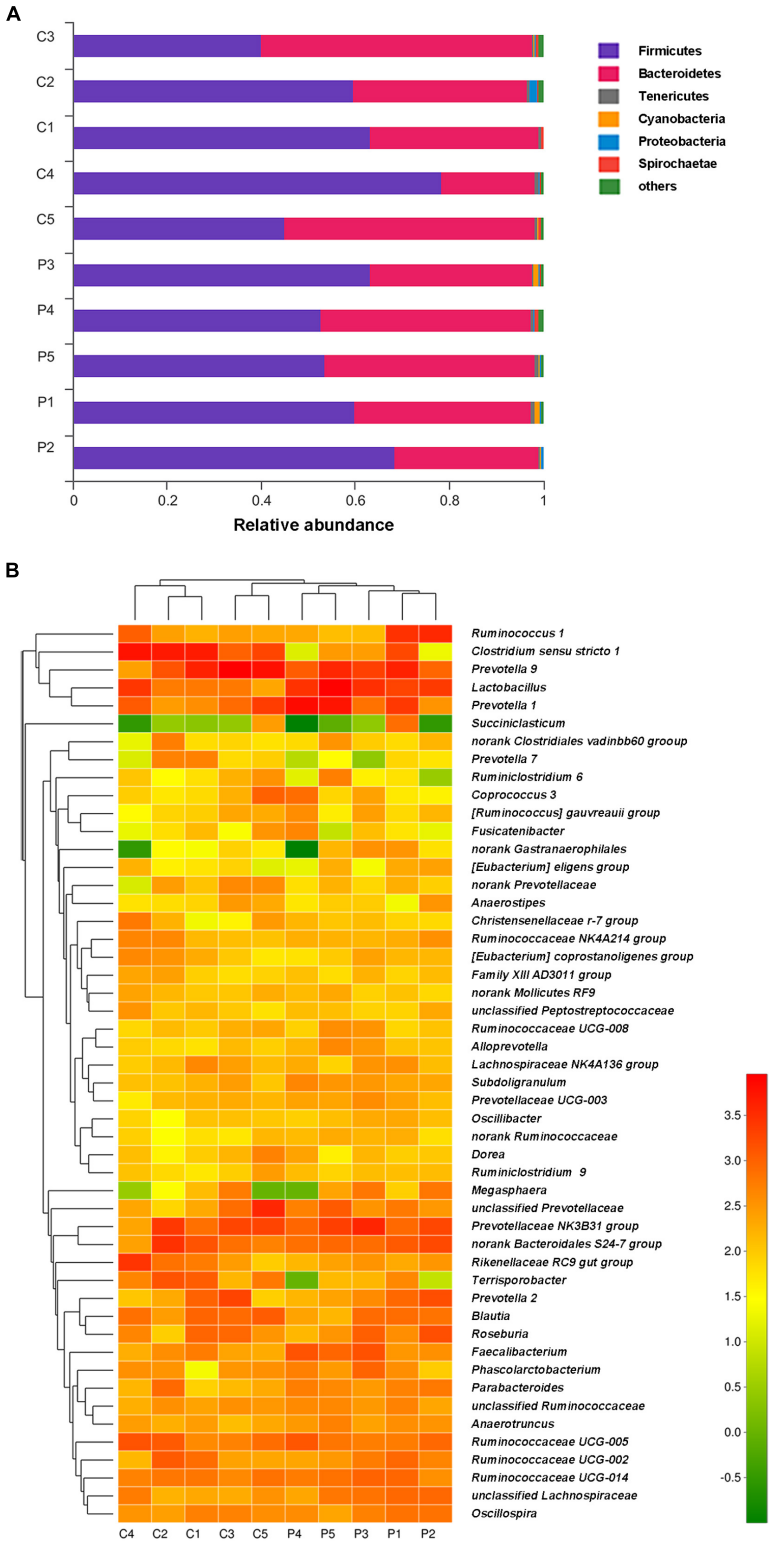

FIGURE 5 | Phylum-level microbiota profile of *L. plantarum* ZLP001-treated piglets as compared to that of placebo-treated control piglets **(A)**. Stacked column chart showing the relative phylum-level bacterial abundance per fecal sample. Genus-level microbiota profile of *L. plantarum* ZLP001-treated piglets as compared to that of placebo-treated control piglets **(B)**. The heatmap shows genera whose relative abundance was >0.1%. Relative abundance is indicated by a color gradient from green to red, with green representing low abundance and red representing high abundance. C and P represent the control and the probiotic-treated group, respectively. Numbers represent individual animals.

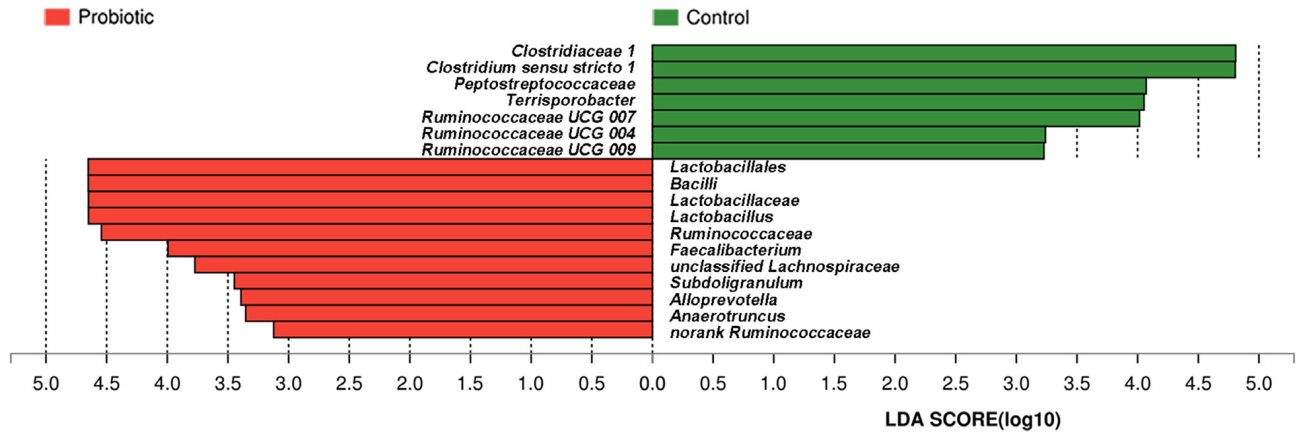

FIGURE 6 | Differences between bacterial taxa in *L. plantarum* ZLP001-treated piglets and placebo-treated control piglets. The histogram shows differentially abundant bacteria in the treatment and control groups ranked by linear discriminant analysis (LDA) scores. Red bars (negative LDA scores) represent bacteria that are more abundant in probiotic-treated fecal samples than in controls. Green bars (positive LDA scores) represent bacteria that are more abundant in placebo-treated fecal samples than in probiotic-treated fecal samples.

TABLE 2 | Effects of *L. plantarum* ZLP001 on SCFA concentration (mmol kg^{-1}) in piglet feces.

Short chain fatty acid	Acetic acid (AA)	Propionic acid (PA)	Butyric acid (BA)
Control	28.3	14.7	8.2
L. plantarum ZLP001	30.3	13.8	9.3
SEM	1.26	0.52	0.48
P-value	0.276	0.117	0.068

L. reuteri did not significantly change FD-4 fluorescence intensity in IPEC-J1 cells (Wang et al., 2016). On the other hand, *L. plantarum* ZLP001 pretreatment significantly suppressed the increase in gut permeability caused by ETEC infection, suggesting that *L. plantarum* ZLP001 can alleviate epithelial damage caused by ETEC. This result was consistent with that of a previous study in which permeability to FD-4 indicated that *L. reuteri* treatment maintains the barrier integrity of IPEC-J1 cells exposed to ETEC (Wang et al., 2016).

TJ proteins play crucial roles in maintaining barrier integrity and function. They include transmembrane proteins such as claudins and occludins, and cytoplasmic scaffolding proteins, such as the ZO family, which have linking and sealing effects (Suzuki, 2013). In this study, relative TJ transcript and protein abundances were significantly reduced after ETEC infection. However, these reductions were abrogated by pretreatment with *L. plantarum* ZLP001. Previous studies using various probiotic strains reported similar results *in vivo* and in *vitro* (Yang et al., 2014; Wu et al., 2016). Therefore, probiotic *L. plantarum* ZLP001 may fortify intestinal epithelial resistance to pathogens by maintaining TJ protein abundance.

Cytokines play significant regulatory roles in the intestinal inflammatory response. Several studies have demonstrated the effects of probiotics on cytokine expression. Nevertheless, this regulatory action varies with strain. *L. reuteri* ACTT 6475 shows immunosuppressive action by inhibiting *TNF*α overexpression in LPS-activated human monocytoid THP1 cells (Lin et al., 2008). However, *L. reuteri* ACTT 55730 significantly stimulates TNF-α production as an immunostimulatory action (Jones and Versalovic, 2009). In the present study, *L. plantarum* ZLP001 *per se* did not influence the expression of proinflammatory cytokines, but inhibited their ETEC-induced overexpression, thus exerting an immunosuppressive action. Certain pro-inflammatory cytokines reportedly are associated with pathogen-induced TJ protein changes (Otte and Podolsky, 2004). ETEC K88 substantially increases IL-8 and disrupts the membrane barrier; however, this disruption can be alleviated by *L. plantarum* pretreatment (Wu et al., 2016). We obtained similar results in the present study. ETEC-induced increases in IL-6-, IL-8-, and TNF-α expression were effectively counteracted by *L. plantarum* ZLP001 pretreatment. This observation was consistent with the FD-4 assay results and TJ protein expression levels. Similar findings indicated that *L. reuteri* inhibits *TNF*-α expression and may protect TJ proteins (Yang et al., 2015). High-throughput sequencing analysis of post-weaning piglet feces after *L. plantarum* ZLP001 or control treatment revealed relatively low abundances of certain bacterial genera in the probiotic-treated group. Some of these are associated with various pathological conditions, e.g., *Peptostreptococcaceae incertae sedi*, which is dominant in viral diarrhea (Ma et al., 2011). Wang et al. (2017) reported that *IL-1*β and *TNF*-α transcript levels were positively correlated with *Clostridium sensu stricto 1* enrichment in the sheep colon. In the present study, *Clostridium sensu stricto 1* was significantly less abundant in the probiotic-treated than in the control group. Certain *Clostridium* spp. are harmful to host health. Epithelial inflammation observed in weaned piglets may be correlated with *Clostridium sensu stricto 1* enrichment in their intestinal mucosa (Wang et al., 2017). The protective effect of probiotics in terms of epithelial immunity may be partially explained by microbiota modulation. One limitation of

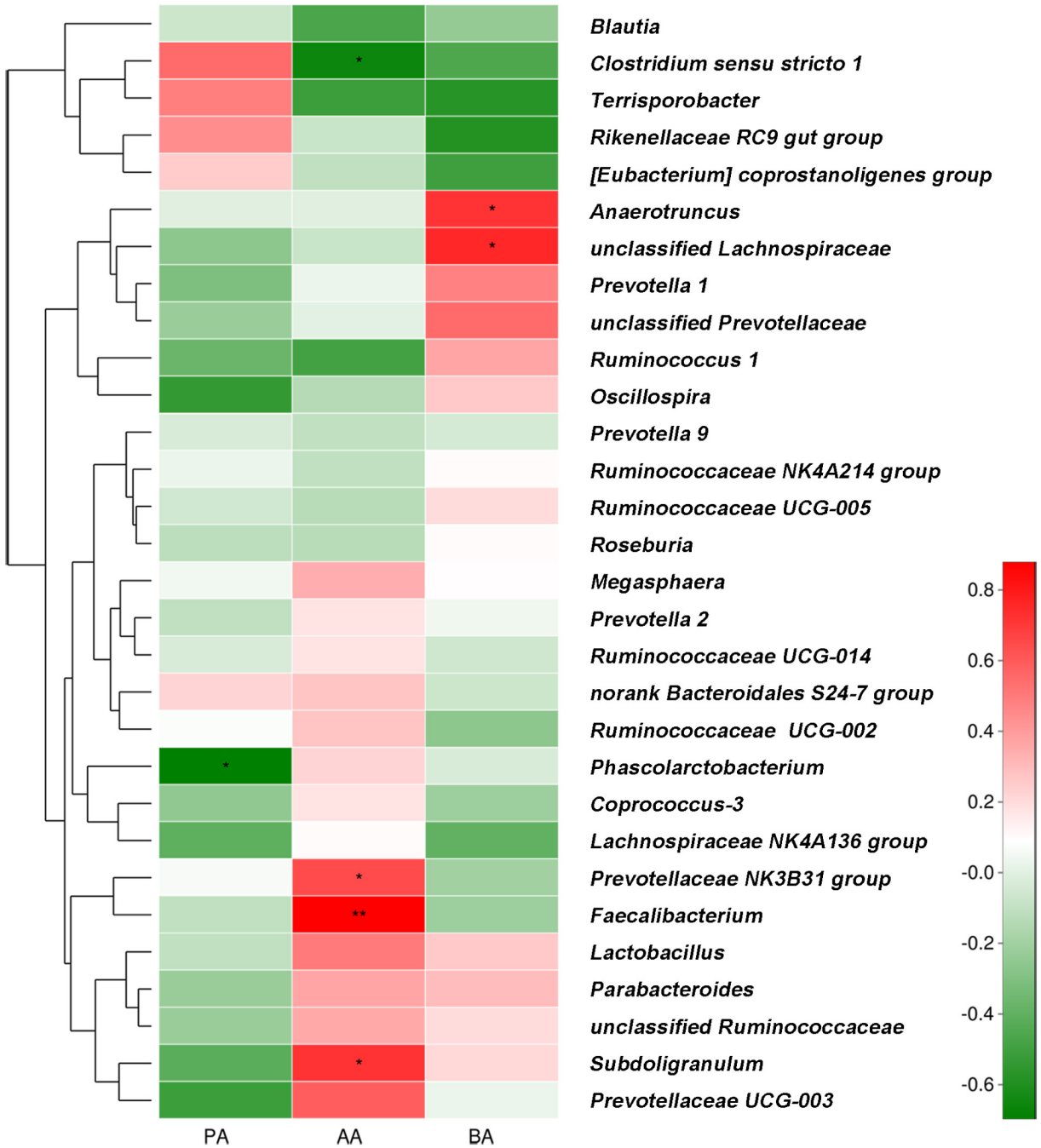

FIGURE 7 | Correlations between relative generic abundance and SCFA concentrations in feces obtained from post-weaning piglets. Only the relative abundances of the top 30 bacterial genera are shown. Correlation is indicated by a color gradient from green to red based on Spearman's correlation coefficients. Asterisks in red cells represent significant positive correlations (*$P < 0.05$; **$P < 0.01$). Asterisks in green cells represent significant negative correlations ($P < 0.05$). AA, acetic acid; PA, propionic acid; BA, butyric acid.

the present study was that we did not evaluate proinflammatory cytokines in the piglet intestinal tissue and thus, we could not analyze the correlation with microbiota abundance. Such relationships merit further investigation.

The secretion of HDPs, which exert both antimicrobial and immunomodulatory activities, is an epithelial innate immunity mechanism (Bevins et al., 1999; Zhang et al., 2000). Enhancing endogenous HDP synthesis improves the early response to bacterial infection and inflammation (Veldhuizen et al., 2008). Nutrients, such as VD_3, butyrate, and zinc induce HDP secretion (Talukder et al., 2011; Zeng et al., 2013; Merriman et al., 2015). Probiotics can also stimulate HDP expression (Schlee et al., 2008;

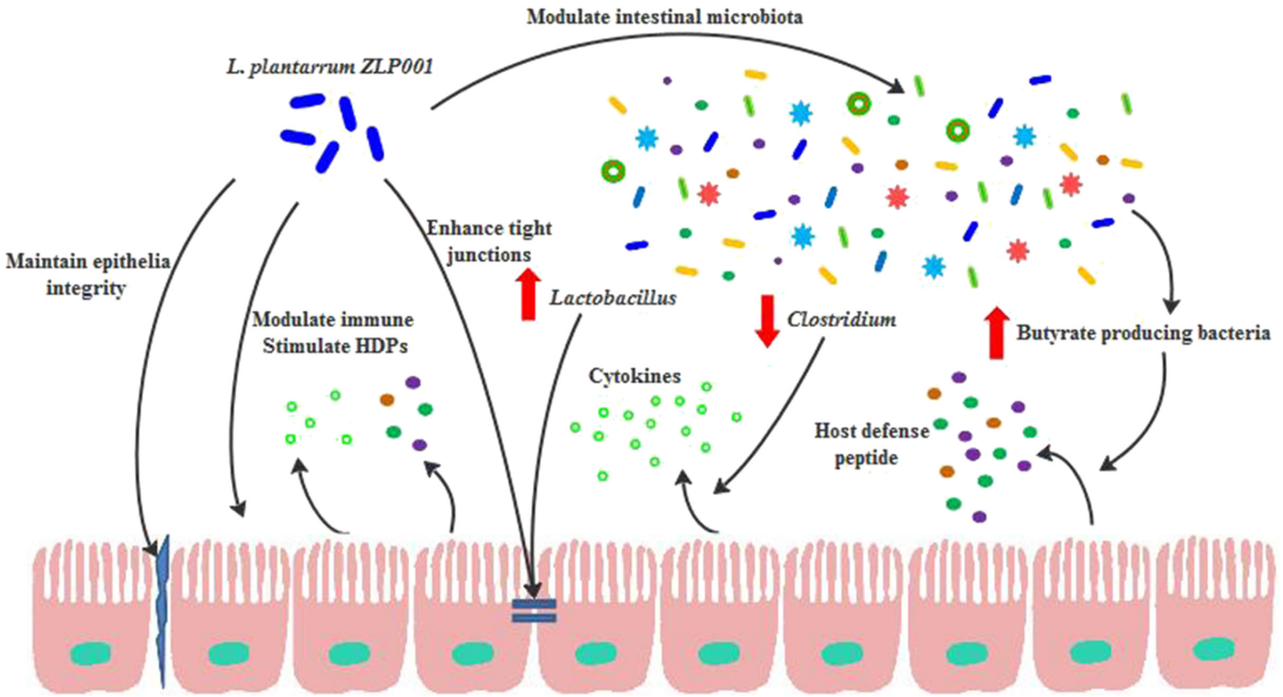

FIGURE 8 | Suggested mechanism by which *L. plantarum ZLP001* protects intestinal barrier function from weaning stress. *L. plantarum ZLP001* functions not only through maintaining epithelial integrity, improving TJs, regulating the immune response, and stimulating HDPs, but also via modulating the intestinal indigenous microbiota. Modulated microbiota and alterations in certain bacterial taxa in turn enhance epithelial function.

Liu et al., 2017). In the present study, increased *pBD2* and *PG1-5* expression and pBD2 secretion were observed after *L. plantarum* ZLP001 treatment, suggesting that this strain can induce HDPs, to protect against bacterial infection. Similar results have been reported for the probiotic strain *L. reuteri* I5007 (Liu et al., 2017). The administration of synthetic HDPs reportedly can improve weaned piglet growth performance, nutrient digestion and assimilation, intestinal health, and antioxidant capacity (Xiao et al., 2013; Yoon et al., 2013; Yu et al., 2017). Therefore, the induction of HDP expression by *L. plantarum* ZLP001 may be correlated with the improved growth and reduced risk of diarrhea reported in our previous studies. SCFAs, especially butyrate, induce HDPs (Zeng et al., 2013). Butyrate production by enteric microbiota is the only microbial stimulus capable of inducing HDP expression (Schauber et al., 2003). Most butyrate-producing bacteria belong to *Clostridium* clusters IV and XIVa. Butyrate metabolism has been observed in species of *Faecalibacterium* and *Anaerotruncus*, e.g., *Faecalibacterium prausnitzii* and *Anaerotruncus colihominis* are butyrate producers (El Aidy et al., 2013; Wrzosek et al., 2013). *A. colihominis* has been shown to specifically colonize the lumen whereas *F. prausnitzii* is enriched in the mucus (Van den Abbeele et al., 2013). In the present study, *Faecalibacterium* spp. and *Anaerotruncus* spp. were significantly abundant in *L. plantarum* ZLP001-treated piglets. Therefore, increasing the abundances of these genera may elevate butyrate levels and epithelial HDP expression. The present study confirmed a positive correlation between fecal butyric acid and *Anaerotruncus* spp. abundance after *L. plantarum* ZLP001 treatment. In addition, *Faecalibacterium* spp. abundance showed a positive correlation with acetic acid concentration. Acetic acid can be converted to butyrate by *Eubacterium rectale* (Duncan and Flint, 2008), which may enhance HDP expression. The modulation of butyrate producers with probiotics to generate butyrate to stimulate HDP levels in the epithelium may thus be a meaningful approach for future interventions that aim to improve intestinal balance. Few studies have focused on the association between HDP production and probiotic function. Future studies involving probiotical and the non-pathogenic enteric bacterial regulation of antimicrobial peptides may elucidate the beneficial effects of probiotics against pathogen infection.

The piglet intestinal microbiota undergoes substantial dynamic changes after weaning, and this alteration can be associated with severe disorders and bowel disease. In the present study, fecal bacterial communities were dominated by Firmicutes and Bacteroidetes, regardless of treatment. This result was expected because the colon is a strictly anaerobic environment and most of the species within these phyla are anaerobic. Similar results were reported in previous pig studies (Konstantinov et al., 2004; Kim and Isaacson, 2015). *Prevotella*, which is associated with hemicelluloses degradation, reportedly is the predominant genus in piglets at nursery stage (Konstantinov et al., 2004). A high *Prevotella* spp. abundance may be essential for post-weaning piglets to be able to digest plant-based diets. Post-weaning increases in the proportions of *Lactobacillus* spp. are desirable and beneficial. Previous studies have shown that

oral administration of lactic acid bacteria enhances the relative abundance of intestinal *Lactobacillus* spp. in weaned piglets (Hu et al., 2015; Zhang et al., 2016). In the present study, dietary *L. plantarum* ZLP001 supplementation significantly increased *Lactobacillus* spp. abundance in the post-weaning piglet intestine. *L. plantarum* ZLP001 may produce molecules that stimulate *Lactobacillus* spp. growth in the piglet intestine (Ohashi et al., 2001). Alternatively, the observed increase in *Lactobacillus* abundance may have resulted from the proliferation of the administered probiotic strain (Takahashi et al., 2007). Certain lactobacilli, such as *L. rhamnosus*, *L. reuteri*, and *L. plantarum*, protect TJ proteins after stress and infection and may, therefore, contribute to TJ integrity and intestinal barrier function (Yang et al., 2015; Blackwood et al., 2017). Further studies are needed to investigate specific species and their effects on piglet epithelial TJ proteins. The effects on gut microbiota composition and community observed after *L. plantarum* ZLP001 treatment in this study suggest that the modulation of the intestinal flora by *L. plantarum* ZLP001 helps to maintain a well-balanced gut microbiota, thereby improving the health and growth of pigs.

CONCLUSION

Our IPEC-J2 model demonstrated that *L. plantarum* ZLP001 enhances intestinal barrier function by (1) maintaining epithelial integrity and preventing ETEC-induced gut permeability, (2) forming TJs and reducing ETEC-induced TJ damage, (3) modulating immune function and repressing the ETEC-induced immune response, and (4) inducing the secretion of antimicrobial peptides to protect against pathogens. Our study also indicated that *L. plantarum* ZLP001 supplementation improved gut bacterial ecology and barrier function in weaned piglets by (1) reducing the abundance of certain bacterial species correlated with proinflammatory cytokine expression, (2) modulating butyrate-producing enteric microbiota to induce epithelial HDP expression, and (3) enhancing intestinal *Lactobacillus* abundance to improve the gut microbiota composition and reinforce TJs (**Figure 8**). Elucidation of the mechanisms by which probiotics act on the intestinal barrier will promote their use in livestock production. In addition, further animal studies are required to determine how *L. plantarum* ZLP001 protects the piglet intestinal barrier both before and after pathogenesis.

AUTHOR CONTRIBUTIONS

JW and HJ conceived and designed the experiments. JW, SW, HL, and DZ performed the experiments. JW and WZ analyzed the data. YW contributed reagents and materials. JW and HJ helped to draft the manuscript. All authors read and approved the final manuscript.

FUNDING

This study was financially supported by the Youth Fund of the Beijing Academy of Agriculture and Forestry Sciences (Grant No. QNJJ201607), the Beijing Innovation Consortium of Agriculture Research System (Grant No. BAIC02-2017), the Special Program on Science and Technology Innovation Capacity Building of BAAFS (Grant Nos. KJCX20180109 and KJCX20161503), and the International Scientific and Technological Cooperation Funding (Grant No. GJHZ2018-06).

SUPPLEMENTARY MATERIAL

The Supplementary Material for this article can be found online at: https://www.frontiersin.org/articles/10.3389/fmicb.2018.01953/full#supplementary-material

FIGURE S1 | Effects of *L. plantarum* ZLP001 on microbial community structure in piglet feces based on principal coordinate analysis (PCoA). PCoA plot showing microbiota clustering in various treatments. Each dot represents an individual sample. Red and green indicate control and probiotic-treated samples, respectively. C and P represent control and probiotic-treated groups, respectively. Numbers represent individual animals.

TABLE S1 | Primers used in this study.

TABLE S2 | Antibodies used in this study.

TABLE S3 | Ingredients and chemical composition of the basal diet.

REFERENCES

Anderson, R. C., Cookson, A., McNabb, W., Park, Z., McCann, M., Kelly, W., et al. (2010). *Lactobacillus plantarum* MB452 enhances the function of the intestinal barrier by increasing the expression levels of genes involved in tight junction formation. *BMC Microbiol.* 10:316. doi: 10.1186/1471-2180-10-316

Bevins, C. L., Martin-Porter, E., and Ganz, T. (1999). Defensins and innate host defence of the gastrointestinal tract. *Gut* 45, 911–915. doi: 10.1136/gut.45.6.911

Blackwood, B. P., Yuan, C. Y., Wood, D. R., Nicolas, J. D., Grothaus, J. S., and Hunter, C. J. (2017). Probiotic *Lactobacillus* species strengthen intestinal barrier function and tight junction integrity in experimental necrotizing enterocolitis. *J. Probiotics Health* 5:159. doi: 10.4172/2329-8901.1000159

Boirivant, M., and Strober, W. (2007). The mechanism of action of probiotics. *Curr. Opin. Gastroenterol.* 23, 679–692. doi: 10.1097/MOG.0b013e3282f0cffc

Campbell, J. M., Crenshaw, J. D., and Polo, J. (2013). The biological stress of early weaned piglets. *J. Anim. Sci. Biotechnol.* 4:19. doi: 10.1186/2049-1891-4-19

Cisek, A. A., and Binek, M. (2014). Chicken intestinal microbiota function with a special emphasis on the role of probiotic bacteria. *Pol. J. Vet. Sci.* 17, 385–394. doi: 10.2478/pjvs-2014-0057

Duncan, S. H., and Flint, H. J. (2008). Proposal of a neotype strain (A1–86) for Eubacterium rectale. Request for an opinion. *Int. J. Syst. Evol. Microbiol.* 58, 1735–1736. doi: 10.1099/ijs.0.2008/004580-0

El Aidy, S., Van den Abbeele, P., Van de Wiele, T., Louis, P., and Kleerebezem, M. (2013). Intestinal colonization: how key microbial players become established in this dynamic process. *Bioessays* 35, 913–923. doi: 10.1002/bies.201300073

Eun, C. S., Kim, Y. S., Han, D. S., Choi, J. H., Lee, A. R., and Park, Y. K. (2011). Lactobacillus casei prevents impaired barrier function in intestinal epithelial cells. *APMIS* 119, 49–56. doi: 10.1111/j.1600-0463.2010.02691.x

Farkas, O., Mátis, G., Pászti-Gere, E., Palócz, O., Kulcsár, A., Petrilla, J., et al. (2014). Effects of *Lactobacillus plantarum* 2142 and sodium n-butyrate in lipopolysaccharide-triggered inflammation: comparison of a porcine intestinal epithelial cell line and primary hepatocyte monocultures with a porcine enterohepatic co-culture system. *J. Anim. Sci.* 92, 3835–3845. doi: 10.2527/jas.2013-7453

Feeding Standard of Swine (2004). *Feeding Standard of Swine*. Beijing: China Agriculture Press.

Gresse, R., Chaucheyras-Durand, F., Fleury, M. A., Van de Wiele, T., Forano, E., and Blanquet-Diot, S. (2017). Gut microbiota dysbiosis in postweaning piglets: understanding the keys to health. *Trends Microbiol.* 25, 851–873. doi: 10.1016/j.tim.2017.05.004

Hu, C. H., Xiao, K., Luan, Z. S., and Song, J. (2013). Early weaning increases intestinal permeability, alters expression of cytokine and tight junction proteins, and activates mitogen-activated protein kinases in pigs. *Anim. Sci.* 91, 1094–1101. doi: 10.2527/jas2012-5796

Hu, Y., Dun, Y., Li, S., Zhang, D., Peng, N., Zhao, S., et al. (2015). Dietary *Enterococcus faecalis* LAB 31 improves growth performance, reduces diarrhea, and increases fecal Lactobacillus number of weaned piglets. *PLoS One* 10:e0116635. doi: 10.1371/journal.pone.0116635

Jones, S. E., and Versalovic, J. (2009). Probiotic *Lactobacillus reuteri* biofilms produce antimicrobial and anti-inflammatory factors. *BMC Microbiol.* 9:35. doi: 10.1186/1471-2180-9-35

Kim, H. B., and Isaacson, R. E. (2015). The pig gut microbial diversity: understanding the pig gut microbial ecology through the next generation high throughput sequencing. *Vet. Microbiol.* 177, 242–251. doi: 10.1016/j.vetmic.2015.03.014

Konstantinov, S. R., Awati, A. A., Williams, B. A., Miller, B. G., Jones, P., Stokes, C. R., et al. (2006). Post-natal development of the porcine microbiota composition and activities. *Environ. Microbiol.* 8, 1191–1199. doi: 10.1111/j.1462-2920.2006.01009.x

Konstantinov, S. R., Favier, C. F., Zhu, W. Y., Williams, B. A., Klüß, J., Souffrant, W. B., et al. (2004). Microbial diversity studies of the porcine gastrointestinal ecosystem during weaning transition. *Anim. Res.* 53, 317–324. doi: 10.1051/animres:2004019

Kopp, M. V., Goldstein, M., Dietschek, A., Sofke, J., Heinzmann, A., and Urbanek, R. (2008). Lactobacillus GG has in vitro effects on enhanced interleukin- 10 and interferon-g release of mononuclear cells but no in vivo effects in supplemented mothers and their neonates. *Clin. Exp. Allergy* 38, 602–610. doi: 10.1111/j.1365-2222.2007.02911.x

Lallès, J. P., Bosi, P., Smidt, H., and Stokes, C. R. (2007). Weaning – A challenge to gut physiologists. *Livest. Sci.* 108, 82–93. doi: 10.1016/j.livsci.2007.01.091

Lallès, J. P., Boudry, G., Favier, C., Floc'h, N. L., Luron, I., Montagne, L., et al. (2004). Gut function and dysfunction in young pigs: physiology. *Anim. Res.* 53, 301–316. doi: 10.1051/animres:2004018

Li, Z., Wang, W., Liu, D., and Guo, Y. (2017). Effects of *Lactobacillus acidophilus* on gut microbiota composition in broilers challenged with Clostridium perfringens. *PLoS One* 12:e0188634. doi: 10.1371/journal.pone.0188634

Lin, Y. P., Thibodeaux, C. H., Pena, J. A., Ferry, G. D., and Versalovic, J. (2008). Probiotic Lactobacillus reuteri suppress proinflammatory cytokines via c-Jun. *Inflamm. Bowel Dis.* 14, 1068–1083. doi: 10.1002/ibd.20448

Liu, H., Hou, C., Wang, G., Jia, H., Yu, H., Zeng, X., et al. (2017). Lactobacillus reuteri I5007 modulates intestinal host defense peptide expression in the model of IPEC-J2 cells and neonatal piglets. *Nutrients* 9:559. doi: 10.3390/nu9060559

Ma, C., Wu, X., Nawaz, M., Li, J., Yu, P., Moore, J. E., et al. (2011). Molecular characterization of fecal microbiota in patients with viral diarrhea. *Curr. Microbiol.* 63, 259–266. doi: 10.1007/s00284-011-9972-7

Merriman, K. E., Kweh, M. F., Powell, J. L., Lippolis, J. D., and Nelson, C. D. (2015). Multiple beta defensin genes are upregulated by the vitamin D pathway in cattle. *J. Steroid. Biochem. Mol. Biol.* 154, 120–129. doi: 10.1016/j.jsbmb.2015.08.002

NRC (2012). *Nutrient Requirements of Swine*, 11th revised Edn. Washington, DC: National Academy Press.

Ohashi, Y., Inoue, R., Tanaka, K., Matsuki, T., Umesaki, Y., and Ushida, K. (2001). Lactobacillus casei strain Shirota-fermented milk stimulates indigenous lactobacilli in the pig intestine. *J. Nutr Sci. Vitaminol.* 47, 172–176. doi: 10.3177/jnsv.47.172

Otte, J. M., and Podolsky, D. K. (2004). Functional modulation of enterocytes by gram-positive and gram-negative microorganisms. *Am. J. Physiol. Gastrointest. Liver Physiol.* 286, G613–G626. doi: 10.1152/ajpgi.00341.2003

Paolillo, R., Romano Carratelli, C., Sorrentino, S., Mazzola, N., and Rizzo, A. (2009). Immunomodulatory effects of *Lactobacillus plantarum* on human colon cancer cells. *Int. Immunopharmacol.* 9, 1265–1271. doi: 10.1016/j.intimp.2009.07.008

Patel, R. M., Myers, L. S., Kurundkar, A. R., Maheshwari, A., Nusrat, A., and Lin, P. W. (2012). Probiotic bacteria induce maturation of intestinal claudin 3 expression and barrier function. *Am. J. Pathol.* 180, 626–635. doi: 10.1016/j.ajpath.2011.10.025

Qiu, J., and Jin, X. (2002). Development and optimization of organic acid analysis in tobacco with ion chromatography and suppressed conductivity detection. *J. Chromatogr. A* 950, 81–88. doi: 10.1016/S0021-9673(02)00034-1

Riboulet-Bisson, E., Sturme, M. H. J., Jeffery, I. B., O'Donnell, M. M., Neville, B. A., Forde, B. M., et al. (2012). Effect of Lactobacillus salivarius Bacteriocin Abp118 on the mouse and pig intestinal microbiota. *PLoS One* 7:e31113. doi: 10.1371/journal.pone.0031113

Schauber, J., Svanholm, C., Termén, S., Iffland, K., Menzel, T., Scheppach, W., et al. (2003). Expression of the cathelicidin LL-37 is modulated by short chain fatty acids in colonocytes: relevance of signalling pathways. *Gut* 52, 735–741. doi: 10.1136/gut.52.5.735

Schlee, M., Harder, J., Koten, B., Stange, E. F., Wehkamp, J., and Fellermann, K. (2008). Probiotic lactobacilli and VSL#3 induce enterocyte β-defensin 2. *Clin. Exp. Immunol.* 151, 528–535. doi: 10.1111/j.1365-2249.2007.03587.x

Suzuki, T. (2013). Regulation of intestinal epithelial permeability by tight junctions. *Cell. Mol. Life Sci.* 70, 631–659. doi: 10.1007/s00018-012-1070-x

Takahashi, S., Egawa, Y., Simojo, N., Tsukahara, T., and Ushida, K. (2007). Oral administration of *Lactobacillus plantarum* strain Lq80 to weaning piglets stimulates the growth of indigenous lactobacilli to modify the lactobacillal population. *J. Gen. Appl. Microbiol.* 53, 325–332. doi: 10.2323/jgam.53.325

Talukder, P., Satho, T., Irie, K., Sharmin, T., Hamady, D., Nakashima, Y., et al. (2011). Trace metal zinc stimulates secretion of antimicrobial peptide LL-37 from Caco-2 cells through ERK and p38 MAP kinase. *Int. Immunopharmacol.* 11, 141–144. doi: 10.1016/j.intimp.2010.10.010

Van Baarlen, P., Wells, J. M., and Kleerebezem, M. (2013). Regulation of intestinal homeostasis and immunity with probiotic lactobacilli. *Trends Immunol.* 34, 208–215. doi: 10.1016/j.it.2013.01.005

Van den Abbeele, P., Belzer, C., Goossens, M., Kleerebezem, M., De Vos, W. M., Thas, O., et al. (2013). Butyrate-producing Clostridium cluster XIVa species specifically colonize mucins in an in vitro gut model. *ISME J.* 7, 949–961. doi: 10.1038/ismej.2012.158

Van der Meulen, J., Koopmans, S. J., Dekker, R. A., and Hoogendoorn, A. (2010). Increasing weaning age of piglets from 4 to 7 weeks reduces stress, increases post-weaning feed intake but does not improve intestinal functionality. *Animal* 4, 1653–1661. doi: 10.1017/S1751731110001011

Veldhuizen, E. J., Rijnders, M., Claassen, E. A., Van Dijk, A., and Haagsman, H. P. (2008). Porcine beta-defensin 2 displays broad antimicrobial activity against pathogenic intestinal bacteria. *Mol. Immunol.* 45, 386–394. doi: 10.1016/j.molimm.2007.06.001

Villena, J., Chiba, E., Vizoso-Pinto, M. G., Tomosada, Y., Takahashi, T., Ishizuka, T., et al. (2014). Immunobiotic Lactobacillus rhamnosus strains differentially modulate antiviral immune response in porcine intestinal epithelial and antigen presenting cells. *BMC Microbiol.* 14:126. doi: 10.1186/1471-2180-14-126

Wang, J., Ji, H., Wang, S., Zhang, D., Liu, H., Shan, D., et al. (2012). *Lactobacillus plantarum* ZLP001: in vitro assessment of antioxidant capacity and effect on growth performance and antioxidant status in weaning piglets. *Asian Austral. J. Anim. Sci.* 25, 1153–1158. doi: 10.5713/ajas.2012.12079

Wang, J., Ji, H., Zhang, D., Liu, H., Wang, S., Shan, D., et al. (2011). Assessment of probiotic properties of *Lactobacillus plantarum* ZLP001 isolated from gastrointestinal tract of weaning pigs. *Afr. J. Biotechnol.* 10, 11303–11308. doi: 10.5897/AJB11.255

Wang, Y., Xu, L., Liu, J., Zhu, W., and Mao, S. (2017). A high grain diet dynamically shifted the composition of mucosa-associated microbiota and induced mucosal

injuries in the colon of sheep. *Front. Microbiol.* 8:2080. doi: 10.3389/fmicb.2017.02080

Wang, Z., Wang, L., Chen, Z., Ma, X., Yang, X., Zhang, J., et al. (2016). In Vitro evaluation of swine-derived Lactobacillus reuteri: probiotic properties and effects on intestinal porcine epithelial cells challenged with enterotoxigenic *Escherichia coli* K88. *J. Microbiol. Biotechnol.* 26, 1018–1025. doi: 10.4014/jmb.1510.10089

Winter, S. E., Winter, M. G., Xavier, M. N., Thiennimitr, P., Poon, V., Keestra, A. M., et al. (2013). Host-derived nitrate boosts growth of *E. coli* in the inflamed gut. *Science* 339, 708–711. doi: 10.1126/science.1232467

Wrzosek, L., Miquel, S., Noordine, M. L., Bouet, S., Joncquel Chevalier-Curt, M., Robert, V., et al. (2013). *Bacteroides thetaiotaomicron* and *Faecalibacterium prausnitzii* influence the production of mucus glycans and the development of goblet cells in the colonic epithelium of a gnotobiotic model rodent. *BMC Biol.* 11:61. doi: 10.1186/1741-7007-11-61

Wu, Y., Zhu, C., Chen, Z., Chen, Z., Zhang, W., Ma, X., et al. (2016). Protective effects of *Lactobacillus plantarum* on epithelial barrier disruption caused by enterotoxigenic *Escherichia coli* in intestinal porcine epithelial cells. *Vet. Immunol. Immunopathol.* 172, 55–63. doi: 10.1016/j.vetimm.2016.03.005

Xiao, H., Wu, M. M., Tan, B. E., Yin, Y. L., Li, T. J., Xiao, D. F., et al. (2013). Effects of composite antimicrobial peptides in weanling piglets challenged with deoxynivalenol: I. Growth performance, immune function, and antioxidation capacity. *J. Anim. Sci.* 91, 4772–4780. doi: 10.2527/jas.2013-6426

Yang, F., Wang, A., Zeng, X., Hou, C., Liu, H., and Qiao, S. (2015). Lactobacillus reuteri I5007 modulates tight junction protein expression in IPEC-J2 cells with LPS stimulation and in newborn piglets under normal conditions. *BMC Microbiol.* 15:32. doi: 10.1186/s12866-015-0372-1

Yang, K. M., Jiang, Z. Y., Zheng, C. T., Wang, L., and Yang, X. F. (2014). Effect of *Lactobacillus plantarum* on diarrhea and intestinal barrier function of young piglets challenged with enterotoxigenic *Escherichia coli* K88. *J. Anim. Sci.* 92, 1496–1503. doi: 10.2527/jas.2013-6619

Yoon, J. H., Ingale, S. L., Kim, J. S., Kim, K. H., Lohakare, J., Park, Y. K., et al. (2013). Effects of dietary supplementation with antimicrobial peptide-P5 on growth performance, apparent total tract digestibility, faecal and intestinal microflora and intestinal morphology of weanling pigs. *J. Sci. Food Agric.* 93, 587–592. doi: 10.1002/jsfa.5840

Yu, H. T., Ding, X. L., Li, N., Zhang, X. Y., Zeng, X. F., Wang, S., et al. (2017). Dietary supplemented antimicrobial peptide microcin J25 improves the growth performance, apparent total tract digestibility, fecal microbiota, and intestinal barrier function of weaned pigs. *J. Anim. Sci.* 95, 5064–5076. doi: 10.2527/jas2017.1494

Zeng, X., Sunkara, L. T., Jiang, W., Bible, M., Carter, S., Ma, X., et al. (2013). Induction of porcine host defense peptide gene expression by short-chain fatty acids and their analogs. *PLoS One* 8:e72922. doi: 10.1371/journal.pone.0072922

Zhang, G., Ross, C. R., and Blecha, F. (2000). Porcine antimicrobial peptides: new prospects for ancient molecules of host defense. *Vet. Res.* 31, 277–296. doi: 10.1051/vetres:2000121

Zhang, W., Zhu, Y. H., Zhou, D., Wu, Q., Song, D., Dicksved, J., et al. (2016). Oral administration of a select mixture of Bacillus probiotics affects the gut microbiota and goblet cell function following *Escherichia coli* challenge in newly weaned pigs of genotype MUC4 that are supposed to be enterotoxigenic E. *coli* F4ab/ac receptor negative. *Appl. Environ. Microbiol.* 83:e02747-16. doi: 10.1128/AEM.02747-16

Conflict of Interest Statement: The authors declare that the research was conducted in the absence of any commercial or financial relationships that could be construed as a potential conflict of interest.

frontiers in Microbiology

ORIGINAL RESEARCH
published: 26 June 2018
doi: 10.3389/fmicb.2018.01364

Swine-Derived Probiotic *Lactobacillus plantarum* Inhibits Growth and Adhesion of Enterotoxigenic *Escherichia coli* and Mediates Host Defense

*Jing Wang, Yanxia Zeng, Sixin Wang, Hui Liu, Dongyan Zhang, Wei Zhang, Yamin Wang and Haifeng Ji**

Institute of Animal Husbandry and Veterinary Medicine, Beijing Academy of Agriculture and Forestry Sciences, Beijing, China

OPEN ACCESS

Edited by:
Mariana Henriques, University of Minho, Portugal

Reviewed by:
Jason Sahl, Northern Arizona University, United States
Sunil D. Saroj, Symbiosis International University, India
Philip R. Hardwidge, Kansas State University, United States

***Correspondence:**
Haifeng Ji
jhf207@126.com

Specialty section:
This article was submitted to Antimicrobials, Resistance and Chemotherapy, a section of the journal Frontiers in Microbiology

Received: *01 February 2018*
Accepted: *05 June 2018*
Published: *26 June 2018*

Citation:
Wang J, Zeng Y, Wang S, Liu H, Zhang D, Zhang W, Wang Y and Ji H (2018) Swine-Derived Probiotic Lactobacillus plantarum Inhibits Growth and Adhesion of Enterotoxigenic Escherichia coli and Mediates Host Defense. Front. Microbiol. 9:1364. doi: 10.3389/fmicb.2018.01364

Weaning stress renders piglets susceptible to pathogen infection, which leads to post-weaning diarrhea, a severe condition characterized by heavy diarrhea and mortality in piglets. Enterotoxigenic *Escherichia coli* (ETEC) is one of typical strains associated with post-weaning diarrhea. Thus, prevention and inhibition of ETEC infection are of great concern. Probiotics possess anti-pathogenic activity and can counteract ETEC infection; however, their underlying mechanisms and modes of action have not yet been clarified. In the present study, the direct and indirect protective effects of *Lactobacillus plantarum* ZLP001 against ETEC infection were investigated by different methods. We found that bacterial culture and culture supernatant of *L. plantarum* ZLP001 prevented ETEC growth by the Oxford cup method, and ETEC growth inhibition was observed in a co-culture assay as well. This effect was suggested to be caused mainly by antimicrobial metabolites produced by *L. plantarum* ZLP001. In addition, adhesion capacity of *L. plantarum* ZLP001 to IPEC-J2 cells were observed using microscopy and counting. *L. plantarum* ZLP001 also exhibited a concentration-dependent ability to inhibit ETEC adhesion to IPEC-J2 cells, which mainly occurred via exclusion and competition mode. Furthermore, quantitative real time polymerase chain reaction (qPCR) analysis showed that *L. plantarum* ZLP001 upregulated the expression of host defense peptides (HDPs) but did not trigger an inflammatory response. In addition, *L. plantarum* ZLP001 induced HDP secretion, which enhanced the potential antimicrobial activity of IPEC-J2 cell-culture supernatant after incubation with *L. plantarum* ZLP001. Our findings demonstrate that *L. plantarum* ZLP001, an intestinal *Lactobacillus* species associated with piglet health, possesses anti-ETEC activity. *L. plantarum* ZLP001 might prevent ETEC growth, inhibit ETEC adhesion to the intestinal mucosa, and activate the innate immune response to secret antimicrobial peptides. *L. plantarum* ZLP001 is worth investigation as a potential probiotics.

Keywords: *Lactobacillus plantarum*, ETEC, growth prevention, adhesion inhibition, host defense peptides

INTRODUCTION

Piglets are exposed to various stresses after weaning and are vulnerable to infections caused by enteric pathogens that cause post-weaning diarrhea. Intestinal infection severely affects piglet health and growth performance (Campbell et al., 2013) and sometimes results in mortality, thus causing considerable economic loss. Therefore, the inhibition of pathogens, especially certain strains of *Escherichia coli* (*E. coli*), responsible for significant infections in piglets, with disease forms ranging from mild to bloody diarrhea, is of special interest in the swine industry (Fairbrother et al., 2005). Enterotoxigenic *E. coli* (ETEC) is one of the main pathogens associated with post-weaning diarrhea in piglets, and ETEC infection can be fatal for piglets and leads to death in more than 50% of piglets (Gyles, 1994; Bailey, 2009).

Probiotics have been studied extensively as a main potential antibiotic alternative in animal husbandry and have been demonstrated to benefit animal health in multiple ways. Moreover, they are considered to be the only efficient feed additive against pathogen infection in piglets (Gresse et al., 2017). Probiotics have been shown to counteract ETEC-induced injury and inflammation (Guerra-Ordaz et al., 2014; Yang et al., 2015; Trevisi et al., 2017). However, not all probiotic species exert anti-infection activity in the intestines, and their underlying mechanisms are still insufficiently characterized. Their protective effect against pathogenic infections was recently shown to involve inhibition of pathogen growth, prevention of adhesion of pathogens to the intestinal mucosa, and modulation of the inflammatory responses of intestinal epithelial cells (Gresse et al., 2017).

Growth inhibition of pathogens is one of the most direct and important ways in which probiotics act against pathogens, and is considered the most essential characteristic of probiotic strains. Growth inhibition by probiotics is thought to occur mainly via a lowering of the pH to a level not suitable for most pathogens (Sreekumar and Hosono, 2000; Lin et al., 2009). Probiotics also combat pathogens by producing a variety of microbicidal substances, such as bacteriocins and microcins, which exert bactericidal or bacteriostatic actions (Dubreuil, 2017). Multiple probiotics have been demonstrated to inhibit pathogen growth by one or both of these mechanisms. Probiotics may also have the ability to reduce or prevent pathogen colonization of the animal intestine by inhibiting pathogen adhesion in a strain-specific and concentration-dependent manner (Walsham et al., 2016; Wang et al., 2016). Moreover, different probiotics employ different adhesion inhibition mechanisms, such as steric hindrance, competitive exclusion, or regulation of the immune system (Roselli et al., 2006). In addition, host defense peptides (HDPs), produced mainly by intestinal epithelial cells and phagocytes in the gastrointestinal tract, are important components of the innate immune system that play critical roles in pathogen elimination. These HDPs can be stimulated by nutritional compounds, including vitamin D_3, butyrate, and zinc, in addition to infection and inflammation (Talukder et al., 2011; Zeng et al., 2013; Merriman et al., 2015). Recent studies have revealed that probiotics can stimulate HDP expression without modulating inflammatory responses (Schlee et al., 2008; Liu et al., 2017). However, different probiotic strains show varying HDP-inducing abilities, and the HDP secretion induction and antibacterial activity of secreted HDP have not yet been studied.

Lactobacillus is among the predominant indigenous genera in human and animal gastrointestinal tracts and is commonly used in probiotics. Our previous studies revealed that dietary supplementation with *L. plantarum* ZLP001, originally isolated from the intestinal tract of a healthy weaned piglet (Wang et al., 2011), exerted beneficial effects on growth performance and antioxidant status in weaning piglets (Wang et al., 2012). However, the potential inhibitory impact on pathogenic bacterial growth and adhesion, and the induction of antimicrobial peptides by this strain are still under investigation. In this study, *L. plantarum* ZLP001 was evaluated for its ETEC growth and adhesion inhibitory abilities as well as for its ability to stimulate the expression and secretion of HDPs and thus enhance the antimicrobial activity of epithelial cell culture supernatant after incubation with *L. plantarum* ZLP001.

MATERIALS AND METHODS

Bacterial Culture

Lactobacillus plantarum ZLP001 was isolated from a healthy piglet in our laboratory, identified by the China Center of Industrial Culture Collection (Beijing, China), and preserved in the China General Microbiological Culture Collection Center (CGMCC No. 7370). *L. plantarum* ZLP001 were grown in improved De Man Rogosa Sharpe (MRS) medium at 37°C under anaerobic condition.

The *E. coli* used in our study was an F4-expressing ETEC strain (serotype O149:K91, K88ac) obtained from the China Veterinary Culture Collection Center. $F4^+$ ETEC were grown in Luria-Bertani (LB) medium (Oxoid, Basingstoke, United Kingdom) at 37°C.

Antimicrobial Activity Assay

The pathogen growth inhibition by *L. plantarum* ZLP001 were investigated according to the method of Benavides et al. (2016) with some modifications. After overnight culture, *L. plantarum* ZLP001 was inoculated at 1:100 (v/v) in improved MRS liquid medium and cultured for 18 h at 37°C under anaerobic condition. The supernatant and bacterial cells were collected by centrifugation at 4000 × *g* for 10 min at 4°C. The supernatant was sterilized using a 0.25-μm filter (Corning Inc., Corning, NY, United States). Bacterial cells of *L. plantarum* ZLP001 were washed with phosphate-buffered saline (PBS) and then resuspended to original concentration. To determine the antimicrobial activity of ZLP001, the indicator ETEC strain was grown using LB broth and adjusted to a concentration of 10^7 colony-forming units (CFU)/mL with LB broth. This prepared culture was poured on pre-prepared nutrient agar plates containing several Oxford cups, which were removed when the agar was solidified. The *L. plantarum* ZLP001 culture solution, supernatant, and resuspended bacterial cells (100 μL) were spotted onto the wells and incubated at 37°C.

After 12-h incubation, the inhibition zones were determined. Three independent experiments were carried out. The mean diameters of inhibition zones were estimated, and inhibition halos >15 mm indicated high inhibitory activity (Benavides et al., 2016).

Coculture of *L. plantarum* ZLP001 and ETEC

After overnight culture, *L. plantarum* ZLP001 and ETEC were diluted to 10^7 CFU/mL in sterile MRS medium, which equally supports the growth of *L. plantarum* and ETEC. Then, 10^7 CFU *L. plantarum* ZLP001 and ETEC were inoculated together in fresh MRS medium to a final volume of 50 mL. One milliliter of pure culture samples and 1 mL of co-culture samples were collected after 6, 12, and 24 h of incubation to evaluate bacterial growth. Samples were spread in dilutions of 10^{-1}–10^{-6}, and *L. plantarum* ZLP001 and ETEC on MRS and LB agar plates, respectively, and incubated at 37°C for colony enumeration. The pH of the samples was measured at different intervals.

Cell Line and Culture Conditions

The porcine intestinal epithelial cell line IPEC-J2 was originally derived from jejunums of neonatal piglets (Schierack et al., 2006) and is considered a valuable *in vitro* model system for investigating the interaction of bacteria (commensal or transient) with the small intestinal epithelium. The IPEC-J2 cells used in the present study were purchased from JENNIE-O Biological Technology (Guangzhou, China). IPEC-J2 cells were cultured in a 1:1 mixture of Dulbecco's modified Eagle's medium/Ham's Nutrient Mixture F-12 (DMEM/F12) supplemented with 10% fetal bovine serum (FBS), streptomycin (100 μg/mL), and amphotericin B (0.5 μg/mL) under 5% CO_2 in a 95% air atmosphere with 90% humidity at 37°C. The cells were maintained by replacing the medium with fresh medium every 2–3 days and were split with 0.25% w/v trypsin (Gibco-Invitrogen, Carlsbad, CA, United States) at each passage.

Adhesion and Adhesion Inhibition Assays

Adhesion of *L. plantarum* ZLP001 to IPEC-J2 cells was evaluated by microscopy and agar plate counting. IPEC-J2 cells were seeded into 6-well plates at a density of 2.5×10^5 cells/well (Costar, Corning Inc., Corning, NY, United States). When the cells had grown to ∼80% confluence (approximately overnight), they were exposed to *L. plantarum* ZLP001 at different concentrations (10^7, 10^8, and 10^9 CFU/mL). *L. plantarum* ZLP001 bacteria were resuspended and diluted in DMEM/F12 without FBS or antibiotics. The plates were incubated for 2 h at 37°C. All assays were replicated in duplicate wells. Treated IPEC-J2 cells were washed three times with PBS, fixed with methanol, followed by gram staining, and then sealed with resin (Sigma-Aldrich, St. Louis, MO, United States). Adhered *L. plantarum* ZLP001 were observed by microscopy at a magnification of 1,000×. The number of bacteria adhered per 100 IPEC-J2 cells was counted and is reported as the adhesion index. Agar plate counting was performed according to the method described by Kaushik et al. (2009). After incubation, the supernatant was discarded and the cells were washed with PBS. After the cells were lysed with 100 μL of 0.2% Triton™ X-100 (Sigma-Aldrich, St. Louis, MO, United States), viable counts of *L. plantarum* ZLP001 were determined by serial dilution and plating on MRS agar. Adhesion was expressed as bacteria adhering to IPEC-J2 cells per well.

To evaluate the inhibitory effect of *L. plantarum* ZLP001 on ETEC adhesion to IPEC-J2 cells, *L. plantarum* ZLP001 was added at 10^7, 10^8, and 10^9 CFU/mL 1 h before (pre-addition), at the same time (co-addition), or 1 h after (post-addition) the indicator ETEC strain was added. Cells treated with only ETEC were used as a control. After 2 h of incubation, the IPEC-J2 cells were washed to remove unbound bacteria. The cells were lysed with 100 μL of 0.2% Triton™ X-100, and viable ETEC counts were determined by serial dilution and plating on LB agar. Adhesion was calculated as the percentage of adhering ETEC normalized to the control.

Detection of HDP and Proinflammatory Cytokine Expression by Real-Time PCR

To evaluate the stimulatory effects of *L. plantarum* ZLP001 on HDP and proinflammatory cytokine expression in IPEC-J2 cells, the cells were incubated with or without *L. plantarum* ZLP001 at different concentrations. The concentrations for concentration-dependent experiments were 10^5, 10^6, 10^7, 10^8, and 10^9 CFU/mL *L. plantarum* ZLP001. DMEM/F12 containing different concentrations of *L. plantarum* ZLP001 was obtained as described above. The incubation time was set at 6 h after a time-dependent (3, 6, 9, and 12 h) preliminary experiment (data not shown).

After treatment, the cells were lysed directly in RNAzol (Molecular Research Center, Cincinnati, OH, United States) to extract total RNA, according to the manufacturer's instructions. RNA concentration and purity were determined using a NanoDrop Spectrophotometer (NanoDrop Technologies, Inc., Wilmington, DE, United States). First-strand cDNA was synthesized by reverse transcription of 1 μg of total RNA using an iScript™ cDNA Synthesis Kit (Bio-Rad Laboratories, Inc., Hercules, CA, United States), according to the manufacturer's instructions. Real-time PCR was carried out on a QuantStudio 3 Real-Time PCR System (Applied Biosystems, Foster City, CA, United States) with iTaq™ Universal SYBR® Green Supermix (Bio-Rad Laboratories, Inc., Hercules, CA, United States). The porcine-specific primers used in this study were designed using the Primer Express software (Applied Biosystems, Foster City, CA, United States). The expression level of each gene was normalized to that of the housekeeping gene glyceraldehyde-3-phosphate dehydrogenase (*GAPDH*). All primers used in this study are listed in **Table 1**. The ΔΔCt method as described by Livak and Schmittgen (2001) was used to calculate relative gene expression.

TABLE 1 | Primer sequences used for quantitative real-time PCR.

Gene	Forward primer	Reverse primer	Product size (bp)	Accession number
GAPDH	GCTACACTGAGGACCAGGTTG	CCTGTTGCTGTAGCCAAATTC	146	XM_021091114.1
pBD-1	TTCCTCCTCATGGTCCTGTT	AGGTGCCGATCTGTTTCATC	130	NM_213838.1
pBD-2	TGTCTGCCTCCTCTCTTCC	AACAGGTCCCTTCAATCCTG	149	NM_214442.2
pBD-3	CCTTCTCTTTGCCTTGCTCTT	GCCACTCACAGAACAGCTACC	163	XM_021074698.1
PG1-5	ACGGTGAAGGAGACTGTG	CGCAGAACCTACGCCTACAA	196	XM_021070622.1
pEP2C	ACTGCTTGTTCTCCAGAGCC	TGGCACAGATGACAAAGCCT	92	XM_003362076.4
IL-6	AAATGCTCTTCACCTCTC	TCACACTTCTCATACTTCTC	106	NM_001252429.1
IL-8	TTCGATGCCAGTGCATAAATA	CTGTACACCTTCTGCACCCA	176	NM_213867.1
TNF-α	CCCCTCTGAAAAAGACACCA	TCGAAGTGCAGTAGGCAGAA	180	NM_214022.1

Enzyme-Linked Immunosorbent Assay (ELISA) of Porcine β-Defensin 1 (pBD-1) and pBD-2

From each treatment described as above, 500 μL of cell culture supernatant was collected, centrifuged at 4,000 × *g* for 10 min at 4°C, and passed through a 0.25-μm filter. Secreted pBD-1 and pBD-2 were quantified using commercial ELISA kits (Cloud-Clone Corp. USCN Life Science, Inc., Wuhan, China), according to the manufacturer's protocols.

Antibacterial Activity of the Cell Culture Supernatant

Antibacterial activity of the cell culture supernatant was determined refer to the method by Wan M.L. et al. (2016). Prepared IPEC-J2 cells were treated with *L. plantarum* ZLP001 at different concentrations (10^5, 10^6, 10^7, 10^8, and 10^9 CFU/mL) in triplicate. DMEM-F12 containing different concentrations of *L. plantarum* ZLP001 was prepared as described above. Non-treated IPEC-J2 cells were used as a negative control. Wells containing only *L. plantarum* ZLP001 at different concentrations resuspended in DMEM/F12 were used as positive controls to subtract any influence of *L. plantarum* ZLP001 metabolites on antimicrobial activity. After 6 h of incubation, the cell culture supernatant was collected and passed through a 0.25-μm filter. The indicator ETEC strain was used to evaluate the antibacterial activity of the supernatant. Overnight-grown ETEC was harvested by centrifugation, washed three times in PBS, and resuspended to a final concentration of 10^7 CFU/mL. Ten microliters of ETEC suspension was incubated with 500 μL of cell culture supernatant. After 2 h of incubation at 37°C with shaking at 200 rpm, the number of viable ETEC bacteria was quantified by serial dilution and plating on LB agar.

Statistical Analysis

Statistical analysis was performed using one-way analysis of variance (ANOVA) and Student's *t*-test in the SAS statistical software package version 9.3 (SAS Institute Inc., Cary, NC, United States). Duncan's multiple range test was performed to compare the differences between means (Harter, 1960). GraphPad Prism version 5 (GraphPad Software, Inc., San Diego, CA, United States) was used to visualize the data. The level of confidence at which experimental results were considered significant was $P < 0.05$.

RESULTS

L. plantarum ZLP001 Exhibits Antimicrobial Activity

Lactobacillus plantarum ZLP001 bacterial culture solution and supernatant exhibited antimicrobial activity against 10^7 CFU/mL ETEC, with mean inhibition-zone diameters of 21.8 and 20.7 mm, respectively (**Figure 1**). No inhibition zone was observed with *L. plantarum* ZLP001 resuspended in PBS (the inhibition zone diameter was approximately 0–1 mm). **Supplementary Figure S1** visualizes an inhibition zone formed by *L. plantarum* ZLP001 on 10^7 CFU/mL ETEC.

L. plantarum ZLP001 Inhibits ETEC Growth

Figure 2 shows the growth patterns of *L. plantarum* ZLP001 and ETEC in pure culture and in co-culture. The viable count of each species and medium pH were measured. *L. plantarum* ZLP001

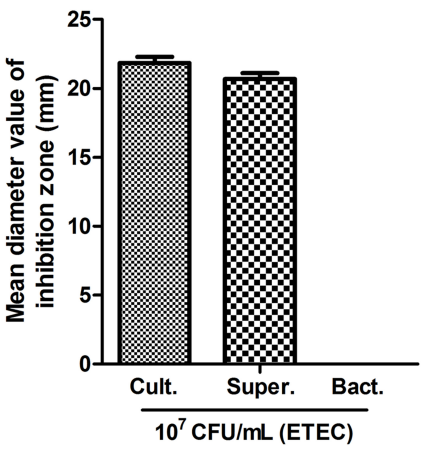

FIGURE 1 | Antimicrobial activity of *L. plantarum* ZLP001. Mean inhibition zone diameter in mm recorded after 12 h of incubation. Bars represent means ± standard errors (SEs) of three independent experiments.

showed similar growth patterns in pure culture and co-culture (**Figure 2A**). The number of viable cells was slightly higher in co-culture than in pure culture. ETEC grew in MRS medium and reached a concentration of 10^8 CFU/mL at the end of culture (24 h) (**Figure 2B**). ETEC growth was inhibited in co-culture with *L. plantarum* ZLP001, and the viable counts were constant until 12 h and then rapidly declined. After 24 h, no viable ETEC bacteria were detected. Acid production by *L. plantarum* ZLP001, as indicated by a decrease in medium pH (**Figure 2C**), was the same under each of the culture conditions. The decline in pH in pure ETEC culture was slower than that in pure *L. plantarum* ZLP001 culture and co-culture, with the pH dropping to 5.32 at the end of the culture (24 h).

L. plantarum ZLP001 Adheres to Porcine Intestinal Cells and Inhibits ETEC Adhesion

Adhesion of *L. plantarum* ZLP001 to IPEC-J2 cells was observed by light microscopy after methanol fixation and Gram staining (**Figure 3A**). The adhesion index showed an obvious concentration-dependent effect ($P < 0.01$); the number of *L. plantarum* ZLP001 cells adhered to 100 IPEC-J2 cells sharply increased with inoculated bacterial concentration (**Figure 3B**). The adhesion capacity as assessed by the agar-plate counting method was also concentration-dependent ($P < 0.01$). The adhered *L. plantarum* ZLP001 increased from 4.72 log CFU at 10^7 inoculated bacteria to 7.68 log CFU at 10^9 inoculated bacteria (**Figure 3C**).

To investigate the inhibitory effects of *L. plantarum* ZLP001 on ETEC adhesion, a high (10^9 CFU/mL), intermediate (10^8 CFU/mL), and low concentration (10^7 CFU/mL) of *L. plantarum* ZLP001 were tested. *L. plantarum* ZLP001 inhibited ETEC adhesion at all concentrations (**Figure 4**, $P < 0.01$) in a concentration-dependent manner, and the inhibition ratio increased considerably with inoculated bacterial concentration. To compare different inhibition assays, *L. plantarum* ZLP001 was added to IPEC-J2 cells 1 h before (pre-addition, **Figure 4A**), simultaneously with (co-addition, **Figure 4B**), or 1 h after (post-addition, **Figure 4C**) addition of ETEC. The results showed that *L. plantarum* ZLP001 inhibited ETEC adhesion regardless of the time of administration. Post-addition had a lesser inhibitory effect than pre- and co-addition. When data obtained for the three concentrations were pooled, ETEC adhesion was 47.4% for the pre-addition assay, 52.3% for the co-addition assay, and 70.0% for the post-addition assay.

L. plantarum ZLP001 Induces HDP mRNA Expression in Porcine Intestinal Cells

The mRNA expression of porcine HDPs was measured in IPEC-J2 cells to assess the effects of *L. plantarum* ZLP001 on HDP modulation. We detected most of the porcine HDP genes, including the two main families in mammals (cathelicidins and β-defensins), by real-time PCR (**Figure 5**). HDP genes with significantly induced expression in IPEC-J2 cells upon exposure to *L. plantarum* ZLP001 included *pBD1*, *pBD2*, *pBD3*, protegrins 1–5 (*PG1–5*), and epididymis protein 2 splicing variant C (*pEP2C*). Genes showing undetectable expression levels before or after treatment, undetectable expression levels in unstimulated cells, or no significant difference in expression levels after incubation were excluded from further analysis. Most genes with significant induction following exposure of IPEC-J2 cells to *L. plantarum* ZLP001 showed concentration-dependence. The expression levels of *pBD2* (**Figure 5B**) and *pBD3* (**Figure 5C**) obviously increased along with *L. plantarum* ZLP001 concentration, with the highest fold inductions at 10^9 CFU/mL ($P < 0.05$). For *pBD1* (**Figure 5A**) and *PG1-5* (**Figure 5D**), the expression levels first increased and then tended to decrease, with mRNA expression of *pBD1* peaking at 10^8 CFU/mL and that of *PG1-5* at 10^6 CFU/mL. Additionally, *pEP2C* (**Figure 5E**) mRNA expression was maximal at 10^8 CFU/mL, while other concentrations did not induce an obvious increase ($P > 0.05$). The magnitude of induction also varied among several genes; *pB*D2 showed the highest maximum fold change, whereas *pEP2C* showed the lowest maximum fold change.

L. plantarum ZLP001 Does Not Induce Proinflammatory Cytokine mRNA Expression in Porcine Intestinal Cells

Relative mRNA expression of interleukin 6 (*IL-6*), *IL-8*, and tumor necrosis factor α (*TNF*α) induced by *L. plantarum* ZLP001 in porcine IPEC-J2 cells was determined (**Supplementary Figures S2A–C**). The results showed that none of the detected proinflammatory cytokines were induced by *L. plantarum* ZLP001 inoculation, regardless of concentration ($P > 0.05$), which suggested that *L. plantarum* ZLP001 did not provoke an inflammatory response in the intestine.

L. plantarum ZLP001 Induces HDP Secretion by Porcine Intestinal Cells

The antibacterial effect of *L. plantarum* ZLP001 on IPEC-J2 cells against ETEC may be associated with the HDP expression and secretion. We investigated the levels of pBD1 and pBD2 (commercial ELISA kits with antibodies for other HDPs were not available) in the cell-culture supernatant using ELISA after treatment of cells with *L. plantarum* ZLP001 at different concentrations (**Figure 6**). *L. plantarum* ZLP001 showed different abilities to promote pBD1 and pBD2 secretions compared to that of the control at different concentrations. For pBD1 (**Figure 6A**), high concentrations of inoculated *L. plantarum* ZLP001 induced significantly increased defensin secretion (10^7–10^9 CFU/mL, $P < 0.05$), whereas for pBD2 (**Figure 6B**), only the highest inoculated concentration showed a significant induction of secretion ($P < 0.05$).

Antibacterial Activity of Cell-Culture Supernatant

To further evaluate the antibacterial effects of *L. plantarum* ZLP001 after stimulation of IPEC-J2 cells, the antibacterial activity of cell-culture supernatant was measured using the indicator ETEC strain (**Figure 7**). IPEC-J2 cells were incubated

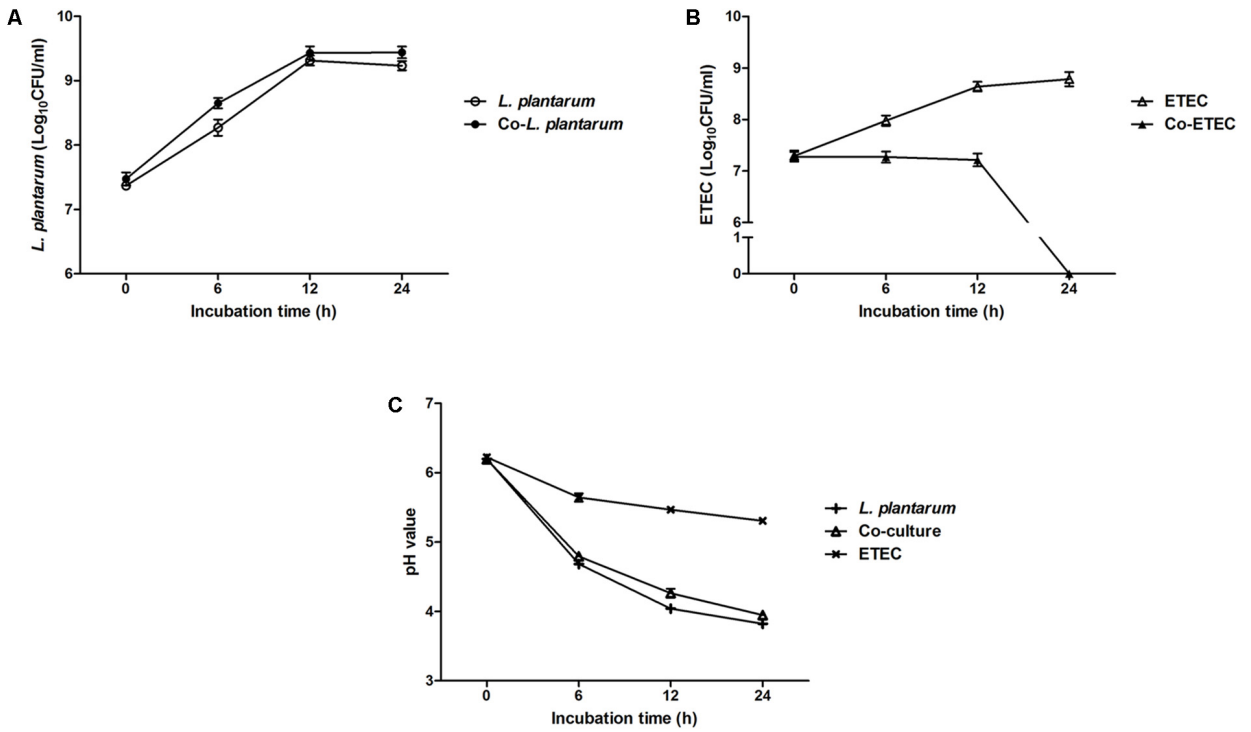

FIGURE 2 | Growth of *L. plantarum* ZLP001 **(A)** and ETEC **(B)** in pure culture and co-culture in MRS medium, and pH of *L. plantarum* ZLP001 and ETEC **(C)** pure culture and co-culture medium. Data are presented as means ± SEs of three independent experiments.

in the absence or presence of *L. plantarum* ZLP001 at different concentrations. Considering the proliferation and antibacterial activity of *L. plantarum* ZLP001 itself, we inoculated *L. plantarum* ZLP001 alone in DMEM/F12 as a positive control. Supernatant collected from *L. plantarum* ZLP001-treated IPEC-J2 cells reduced ETEC counts compared to the negative control (without *L. plantarum* ZLP001) at all concentrations of ZLP001, and further reduced the counts as compared to supernatant collected from *L. plantarum* ZLP001 alone, at the concentration of 10^8 CFU/mL($P < 0.05$).

DISCUSSION

Many *L. plantarum* have been studied extensively and shown to possess broad-spectrum antimicrobial properties in different hosts (Guerra-Ordaz et al., 2014; El Halfawy et al., 2017). However, the mechanisms underlying pathogen inhibition and interaction with the host are still not thoroughly understood. In order to explain the mode of action of this species, antimicrobial properties were evaluated from different perspectives.

Growth inhibition of harmful bacteria is a major property of probiotics. The present study indicated that *L. plantarum* ZLP001 inhibited the growth of the common intestinal pathogen ETEC based on inhibition zone and co-culture assays. *Lactobacillus* spp. have the ability to upregulate host antimicrobial factors (Kirjavainen et al., 2008), which is possibly related to the lactic acid they produce, low pH, and antimicrobial compounds (Longdet et al., 2011; Benavides et al., 2016). Acidic environment and stress induction in the outer membrane are all factors that potentially affect ETEC survival (Delley et al., 2015). In the present study, the *L. plantarum* ZLP001 bacterial culture as well as the supernatant showed antagonistic activity against ETEC, while no antagonistic activity (no inhibition zone) was observed with bacterial cells. This result suggested that the antimicrobial activity of *L. plantarum* ZLP001 is mainly related to its metabolism or the low pH condition rather than the bacteria *per se*. In our co-culture assay, the decreasing trend of pH under co-culture of *L. plantarum* ZLP001 and ETEC was similar to that observed for *L. plantarum* ZLP001 cultured alone. However, the negative effects of *L. plantarum* ZLP001 on viable ETEC count were not as pronounced when the co-culture period was less than 12 h. This suggested that the inhibitory effects of *L. plantarum* ZLP001 on ETEC viability occurred mainly via antibacterial metabolism. This observation is supported the finding that acidic conditions mediated by lactic acid are not the predominant mechanism by which *Lactobacilli* probiotics act (Fayol-Messaoudi et al., 2005). *Lactobacillus* can produce broad-spectrum antimicrobial substances, such as extracellular organic acids, hydrogen peroxide, and bacteriocin-like compounds, which act against gram-positive and gram-negative pathogens (Azizi et al., 2017; Wang et al., 2017). We previously assessed the production of lactic acid by *L. plantarum* ZLP001 after 24 h of fermentation, which was in the range of 50–60 mmol/L (data not published). In addition, we demonstrated that *L. plantarum* ZLP001 has the ability to produce hydrogen peroxide based on

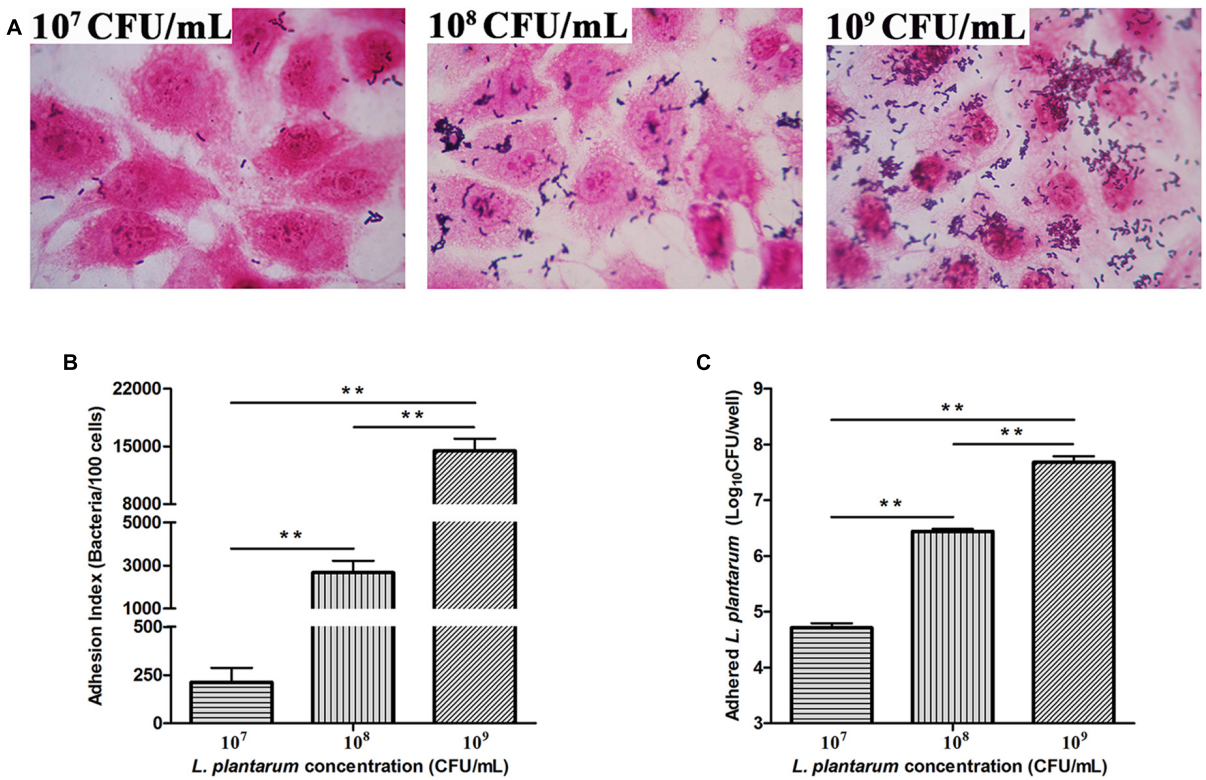

FIGURE 3 | Adhesion of *L. plantarum* ZLP001 to porcine small intestinal epithelial cells (IPEC-J2) **(A)**. Adhesion of *L. plantarum* ZLP001 to IPEC-J2 cells as indicated by adhesion index, which represents the number of adhered *L. plantarum* ZLP001 to 100 cells **(B)** and count of adhered viable *L. plantarum* ZLP001 **(C)**. Cells were incubated with *L. plantarum* ZLP001 at different concentrations (10^7,10^8, and 10^9 CFU/mL) for 2 h. The magnification was 1,000×. Values are presented as means ± SEs of three independent experiments. $^{**}P < 0.01$ compared to each concentration.

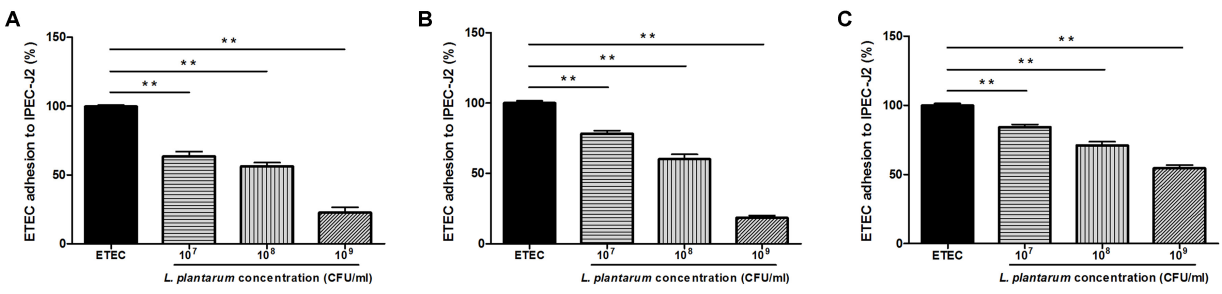

FIGURE 4 | Inhibitory effect of *L plantarum* ZLP001 on ETEC adhesion to IPEC-J2 cells. ETEC adhesion inhibition was determined upon incubation in medium containing ~10^7, ~10^8, and ~10^9 CFU/mL of *L. plantarum* ZLP001 added 1 h before (pre-addition, **A**), at the same time (co-addition, **B**), or 1 h after (post-addition, **C**) addition of ETEC. Values are presented as means ± SEs of three independent experiments. $^{**}P < 0.01$ compared to ETEC treatment.

DAB staining intensity. With respect to bacteriocin, the presence of structural genes encoding for plantacirin in this strain as well as the antimicrobial agents secreted by *L. plantarum* ZLP001 remain to be confirmed.

Adhesion property is considered one of the most essential factors for a probiotic to fulfill its beneficial function. This study demonstrated that *L. plantarum* ZLP001 can effectively adhere to IPEC-J2 cells, which is consistent with the findings of a previous study using other *Lactobacillus* strains on IPEC-1 cells (Wang et al., 2016). The concentration of inoculated *L. plantarum* ZLP001 and the number of adhered viable bacteria or the adhesion index showed a clear concentration-dependent relationship. However, pathogen adhesion is a prerequisite for the initiation of the infection, which is associated with the destruction of the intestinal epithelial structure and is crucial for targeted delivery of secreted enterotoxins. Besides producing enterotoxin, F4-fimbriated ETEC specifically attach to receptors on the brush border of the mucosa by expressing F4 fimbrial adhesins, which initiate infection (González-Ortiz et al., 2013). Several studies have demonstrated that probiotics have the

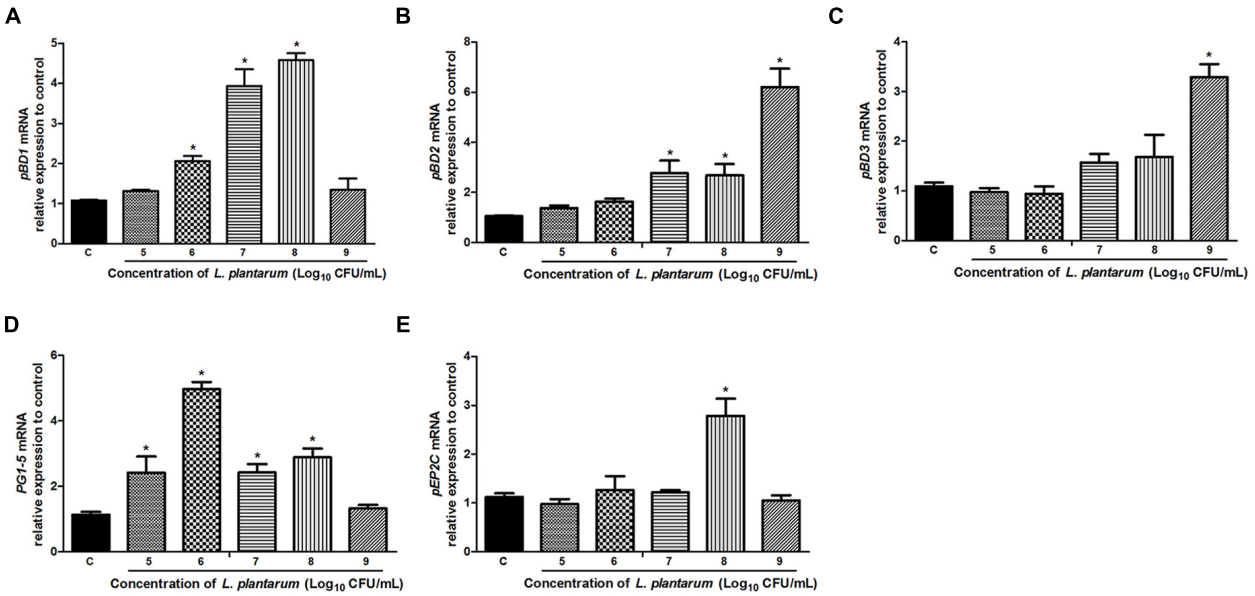

FIGURE 5 | Relative gene expression of *pBD1* **(A)**, *pBD2* **(B)**, *pBD3* **(C)**, *PG1-5* **(D)**, and *pEP2C* **(E)** induced by *L. plantarum* ZLP001 in IPEC-J2 cells. Cells were incubated with *L. plantarum* ZLP001 at different concentrations (10^5,10^6,10^7,10^8, and 10^9 CFU/mL) for 6 h. mRNA expression was standardized to *GAPDH* expression. The relative fold changes versus the unstimulated control were calculated by the $\Delta\Delta$Ct method. Values are presented as means ± SEs of three independent experiments. $^*P < 0.05$ compared to non-stimulated control. C, non-stimulated control.

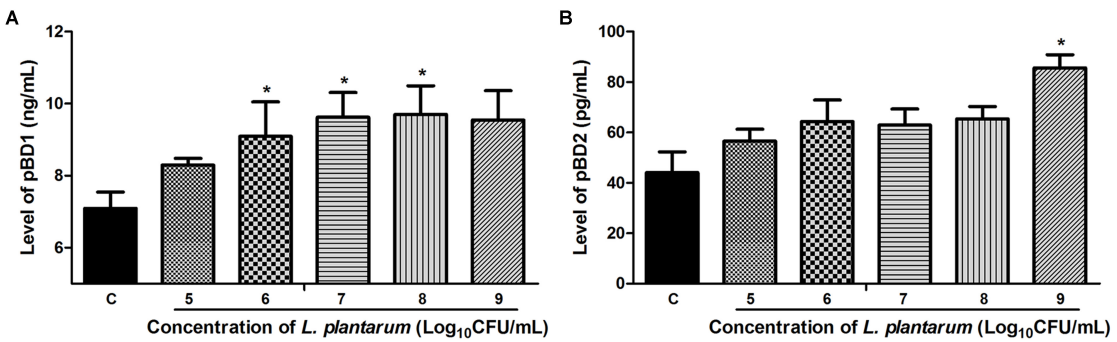

FIGURE 6 | Levels of pBD1 **(A)** and pBD2 **(B)** protein in IPEC-J2 cell-culture supernatant following treatment of the cells with *L. plantarum* ZLP001 (10^5, 10^6, 10^7, 10^8, and 10^9 CFU/mL) for 6 h. Protein levels in the supernatant were determined by ELISA. Data are presented as means ± SEs of three independent experiments. $^*P < 0.05$ compared to non-stimulated control. C, non-stimulated control.

potential to prevent infection by inhibiting pathogen adhesion and penetration (Zareie et al., 2006; Fukuda et al., 2011). Our present results suggested that *L. plantarum* ZLP001 has the ability to inhibit ETEC adhesion to IPEC-J2 cells. This inhibition was more effective when *L. plantarum* ZLP001 was added at higher concentrations. Similar results have been reported by Jin et al. (2000), who showed that *Enterococcus faecium* 18C23 effectively inhibited the adhesion of *E. coli* F4ac to piglet intestinal immobilized mucus, especially at 10^9 CFU or more. Probiotics can pre-occupy or compete for pathogen-binding sites, thus interfering with pathogen adhesion and colonization (Tuomola et al., 1999). Our results were similar to those from other reports demonstrating that inhibition by probiotic added to epithelial cells prior to pathogens is more effective than attempting to disrupt established pathogen colonization (Dunne et al., 2014; Manning et al., 2016). This suggested that *L. plantarum* ZLP001 can prevent ETEC adherence mechanistically through steric hindrance or binding-site competition (Wong et al., 2013). The binding sites are composed of different types of molecules, like fibronectin and collagen. *Lactobacillus* species have the ability to bind these molecules (Lorca et al., 2002; de Leeuw et al., 2006). In addition, bacterial co-aggregation may inhibit adhesion. Further, secretion of bacteriocin and other antimicrobial substances may be involved (Lebeer et al., 2010).

Host defense peptides exert both antimicrobial and immunomodulatory activities, and contribute to epithelial innate immune defense (Bevins et al., 1999; Zhang et al., 2000). The antimicrobial activity of HDPs is associated

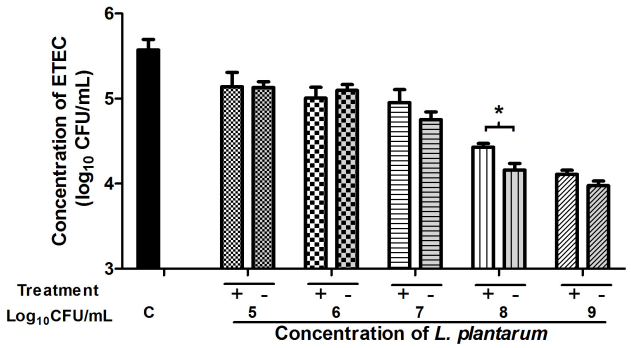

FIGURE 7 | Antibacterial activity of IPEC-J2 cell-culture supernatants collected after incubation with *L. plantarum* ZLP001 at different concentrations (10^5, 10^6, 10^7, 10^8, and 10^9 CFU/mL) for 6 h or supernatants of *L. plantarum* alone incubated in DMEM)/F12. Values are expressed as the number of viable enterotoxigenic ETEC present after 2 h incubation in the supernatant in three independent experiments. C, non-stimulated cell control (negative control); Treatment +, supernatant of *L. plantarum* ZLP001 culture in DMEM/F12 (positive control); Treatment –, cell-culture supernatant after *L. plantarum* ZLP001 incubation. $^*P < 0.05$.

with the intestine microbiota and protects the host against pathogens, including bacteria, fungi, and viruses (Smet and Contreras, 2005; Veldhuizen et al., 2008). Enhancing the synthesis of endogenous HDPs is beneficial to the early response to infection and inflammation (Veldhuizen et al., 2008). Probiotic microbes are able to induce HDP production, including in pigs (Borchers et al., 2009; Wan L.Y. et al., 2016; Liu et al., 2017). We observed that *pBD1* mRNA expression was significantly upregulated after exposure to *L. plantarum* ZLP001, which is inconsistent with the results of Liu et al. (2017), who showed that *pBD1* mRNA expression was not significantly increased in IPEC-J2 cells or piglets exposed to *Lactobacillus reuteri* I5007. The potency of probiotics to modulate HDP production varies among strains (Schlee et al., 2008), which may result in different efficacies of different strains. Upregulation of *pBD2* in response to *L. plantarum* ZLP001 likely inhibited pathogenic bacteria in our study, as reported previously that pBD2 protects against a wide range of pathogenic bacteria *in vitro* (Veldhuizen et al., 2007; Zhang et al., 2011; Deng et al., 2013). pBD3 exhibits not only profound antimicrobial properties, but also strong immunoregulatory ability by regulating the expression of the proinflammatory cytokine IL-8 (Dou et al., 2017). In the present study, *pBD3* mRNA expression was considerably increased only at the highest concentration of *L. plantarum* ZLP001, which was inconsistent with another report of high *pBD3* expression at 10^7 and 10^8 CFU/mL (Liu et al., 2017). Furthermore, increases in the expression of other antimicrobial peptides (*PG1-5* and *pEP2C*) were observed in the present study, accounting for the *L. plantarum* ZLP001-mediated protective effects against pathogen infection. In addition to defense-response modification, HDPs are also correlated with nutrient digestibility, intestinal morphology, and growth performance in weaning pigs (Yoon et al., 2013). This implies that *L. plantarum* ZLP001-induced HDP gene expression may be beneficial not only to the innate immune response, but also to body health and production performance.

Our results suggested that *L. plantarum* ZLP001 enhances the intestinal defense response via induction of HDP secretion. To our knowledge, this is the first study to illustrate that *Lactobacillus* can stimulate porcine HDP secretion in intestinal epithelial cells. Only one previous study using human intestinal epithelial cells (Caco-2) showed induction of defensin secretion by the probiotic *Lactobacillus fermentum* and *E. coli* (strain Nissle 1917) (Schlee et al., 2008). Similarly, this is the first study to show ETEC-antimicrobial activity of cell-culture supernatant post-*Lactobacillus* treatment. The results obtained in our study were not as pronounced as those reported by Wan M.L. et al. (2016) who used cell-culture supernatant from epigallocatechin-3-gallate (EGCG)-treated cells and observed 32% lower *E. coli* counts than those in the control. EGCG has no antibacterial effects on *E. coli*. In contrast, the stimulator strain used in our study possesses strong antibacterial activity *per se*. Thus, maybe the effective positive control to evaluate the antimicrobial effect of the cell culture supernatant after *L. plantarum* ZLP001 treatment was insufficient. However, based on our results, it can be concluded that the antibacterial activity of *L. plantarum* ZLP001-stimulated IPEC-J2 cell-culture supernatant was not due to *L. plantarum* ZLP001 *per se*, but rather was a result of antimicrobial substances being secreted into the supernatant by IPEC-J2 cells induced by *L. plantarum* ZLP001. Certainly, further studies are required to verify the antimicrobial activities of the HDPs secreted by probiotic-induced epithelial cells. The effectiveness of probiotics in innate immune defense is an important starting point for future deeper studies of the benefits of probiotics to intestinal health and against infection.

CONCLUSION

In conclusion, we demonstrated that *L. plantarum* ZLP001 possesses antimicrobial activity. It can prevent ETEC growth by producing certain antimicrobial substances in combination with generating a relatively acidic environment. *L. plantarum* ZLP001 adhered to IPEC-J2 cells and inhibited ETEC adhesion mainly through exclusion and competition. *L. plantarum* ZLP001 also induced the expression and secretion of HDPs in intestinal epithelial cells, thus enhancing the antimicrobial activity of cell-culture supernatant after *L. plantarum* ZLP001 incubation. These functions of *L. plantarum* ZLP001 may account for its protective effects against pathogenic infection. Thus, *L. plantarum* ZLP001 may prove useful as a probiotic strain in piglet production. However, the lack of *in vivo* experiments was a limitation of the present study and thus, further studies *in vivo* are essential to verify the protective effect of *L. plantarum* ZLP001 and to delineate the exact underlying mechanism.

AUTHOR CONTRIBUTIONS

JW and HJ conceived and designed the study. JW was responsible for the bacterial and cell assays, data

analysis, and writing. HJ conceived and designed the experiments. YZ participated in the adhesion inhibition assay. SW participated in the ETEC growth inhibition assay. HL participated in the real-time PCR test. WZ participated in the bacterial adhesion assay. DZ and YW participated in the ELISA.

FUNDING

This study was financially supported by the Special Program on Science, Technology, and Innovation Capacity Building of BAAFS (KJCX20180109), International Scientific and Technological Cooperation funding (GJHZ2018-06), the Youth Fund of Beijing Academy of Agriculture and Forestry Sciences (QNJJ201607), and Beijing Innovation Consortium of Agriculture Research System (BAIC02-2017).

SUPPLEMENTARY MATERIAL

The Supplementary Material for this article can be found online at: https://www.frontiersin.org/articles/10.3389/fmicb.2018.01364/full#supplementary-material

FIGURE S1 | Visualization of the inhibition zone produced by *L. plantarum* ZLP001 toward enterotoxigenic *Escherichia coli* (ETEC). Cult., culture solution; Super., supernatant; Bact., bacteria; CFU, colony-forming unit.

FIGURE S2 | Relative gene expression of interleukin 6 (*IL-6*, **A**), *IL-8* **(B)**, and tumor necrosis factor α (*TNFα*, **C**) induced by *Lactobacillus plantarum* ZLP001 in porcine small intestinal epithelial cells (IPEC-J2). Cells were incubated with *L. plantarum* ZLP001 at different concentrations (10^5,10^6,10^7,10^8, and 10^9 CFU/mL) for 6 h. mRNA expression was standardized to glyceraldehyde-3-phosphate dehydrogenase (*GAPDH*) expression. The relative fold changes versus the unstimulated control were calculated with the ΔΔCt method. Values are presented as means ± standard errors of three independent experiments. C, unstimulated control; CFU, colony-forming unit.

REFERENCES

Azizi, F., Habibi Najafi, M. B., and Edalatian Dovom, M. R. (2017). The biodiversity of *Lactobacillus* spp. from Iranian raw milk Motal cheese and antibacterial evaluation based on bacteriocin-encoding genes. *AMB Express* 7:176. doi: 10.1186/s13568-017-0474-2

Bailey, M. (2009). The mucosal immune system: recent developments and future directions in the pig. *Dev. Comp. Immunol.* 33, 375–383. doi: 10.1016/j.dci.2008.07.003

Benavides, A. B., Ulcuango, M., Yépez, L., and Tenea, G. N. (2016). Assessment of the *in vitro* bioactive properties of lactic acid bacteria isolated from native ecological niches of Ecuador. *Rev. Argent. Microbiol.* 48, 236–244. doi: 10.1016/j.ram.2016.05.003

Bevins, C., Martin-Porter, E., and Ganz, T. (1999). Defensins and innate host defence of the gastrointestinal tract. *Gut* 45, 911–915. doi: 10.1136/gut.45.6.911

Borchers, A. T., Selmi, C., Meyers, F. J., Keen, C. L., and Gershwin, M. E. (2009). Probiotics and immunity. *J. Gastroenterol.* 44, 26–46. doi: 10.1007/s00535-008-2296-0

Campbell, J. M., Crenshaw, J. D., and Polo, J. (2013). The biological stress of early weaned piglets. *J. Anim. Sci. Biotechnol.* 4:19. doi: 10.1186/2049-1891-4-19

de Leeuw, E., Li, X., and Lu, W. (2006). Binding characteristics of the Lactobacillus brevis ATCC 8287 surface layer to extracellular matrix proteins. *FEMS Microbiol. Lett.* 260, 210–215. doi: 10.1111/j.1574-6968.2006.00313.x

Delley, M., Bruttin, A., Richard, M., Affolter, M., Rezzonico, E., and Brück, W. M. (2015). *In vitro* activity of commercial probiotic *Lactobacillus* strains against uropathogenic *Escherichia coli*. *FEMS Microbiol. Lett.* 362:fnv096. doi: 10.1093/femsle/fnv096

Deng, J., Li, Y., Zhang, J., and Yang, Q. (2013). Co-administration of *Bacillus subtilis* RJGP16 and *Lactobacillus salivarius* B1 strongly enhances the intestinal mucosal immunity of piglets. *Res. Vet. Sci.* 94, 62–68. doi: 10.1016/j.rvsc.2012.07.025

Dou, X., Han, J., Song, W., Dong, N., Xu, X., Zhang, W., et al. (2017). Sodium butyrate improves porcine host defense peptide expression and relieves the inflammatory response upon Toll-like receptor 2 activation and histone deacetylase inhibition in porcine kidney cells. *Oncotarget* 8, 26532–26551. doi: 10.18632/oncotarget.15714

Dubreuil, J. D. (2017). Enterotoxigenic *Escherichia coli* and probiotics in swine: what the bleep do we know? *Biosci. Microbiota Food Health* 36, 75–90. doi: 10.12938/bmfh.16-030

Dunne, E. M., Toh, Z. Q., John, M., Manning, J., Satzke, C., and Licciardi, P. (2014). Investigating the effects of probiotics on pneumococcal colonization using an *in vitro* adherence assay. *J. Vis. Exp.* 86:e51069. doi: 10.3791/51069

El Halfawy, N. M., El-Naggar, M. Y., and Andrews, S. C. (2017). Complete genome sequence of *Lactobacillus plantarum* 10CH, a potential probiotic lactic acid bacterium with potent antimicrobial activity. *Genome Announc.* 5:e1398-17. doi: 10.1128/genomeA.01398-17

Fairbrother, J. M., Nadeau, E., and Gyles, C. L. (2005). *Escherichia coli* in postweaning diarrhea in pigs: an update on bacterial types, pathogenesis, and prevention strategies. *Anim. Health Res. Rev.* 6, 17–39. doi: 10.1079/AHR2005105

Fayol-Messaoudi, D., Berger, C. N., Coconnier-Polter, M. H., Lievin-Le Moal, V., and Servin, A. L. (2005). pH-, lactic acid-, and non-lactic acid-dependent activities of probiotic Lactobacilli against *Salmonella enterica* serovar Typhimurium. *Appl. Environ. Microbiol.* 71, 6008–6013. doi: 10.1128/AEM.71.10.6008-6013.2005

Fukuda, S., Toh, H., Hase, K., Oshima, K., Nakanishi, Y., Yoshimura, K., et al. (2011). Bifidobacteria can protect from enteropathogenic infection through production of acetate. *Nature* 469, 543–547. doi: 10.1038/nature09646

González-Ortiz, G., Hermes, R. G., Jiménez-Díaz, R., Pérez, J. F., and Martín-Orúe, S. M. (2013). Screening of extracts from natural feed ingredients for their ability to reduce enterotoxigenic *Escherichia coli* (ETEC) K88 adhesion to porcine intestinal epithelial cell-line IPEC-J2. *Vet. Microbiol.* 167, 494–499. doi: 10.1016/j.vetmic.2013.07.035

Gresse, R., Chaucheyras-Durand, F., Fleury, M. A., Van de Wiele, T., Forano, E., and Blanquet-Diot, S. (2017). Gut microbiota dysbiosis in postweaning piglets: understanding the keys to health. *Trends Microbiol.* 25, 851–873. doi: 10.1016/j.tim.2017.05.004

Guerra-Ordaz, A. A., González-Ortiz, G., La Ragione, R. M., Woodward, M. J., Collins, J. W., Pérez, J. F., et al. (2014). Lactulose and *Lactobacillus plantarum*, a potential complementary synbiotic to control post-weaning colibacillosis in piglets. *Appl. Environ. Microbiol.* 80, 4879–4886. doi: 10.1128/AEM.00770-14

Gyles, C. L. (1994). "*Escherichia coli* verotoxin and other cytotoxins," in *Escherichia coli in Domestic Animals and Humans*, ed. C. L. Gyles (Wallingford: CAB International), 151–170.

Harter, H. L. (1960). Critical values for Duncan's new multiple range test. *Biometrics* 16, 671–685. doi: 10.2307/2527770

Jin, L. Z., Marquardt, R. R., and Zhao, X. (2000). A strain of *Enterococcus faecium* (18C23) inhibits adhesion of enterotoxigenic *Escherichia coli* K88 to porcine small intestine mucus. *Appl. Environ. Microbiol.* 66, 4200–4204. doi: 10.1128/AEM.66.10.4200-4204.2000

Kaushik, J. K., Kumar, A., Duary, R. K., Mohanty, A. K., Grover, S., and Batish, V. K. (2009). Functional and probiotic attributes of an indigenous isolate of *Lactobacillus plantarum*. *PLoS One* 4:e8099. doi: 10.1371/journal.pone.0008099

Kirjavainen, P. V., Laine, R. M., Carter, D. E., Hammond, J., and Reid, G. (2008). Expression of antimicrobial defense factors in vaginal mucosa following exposure to *Lactobacillus rhamnosus* GR-1. *Int. J. Probiotics Prebiotics* 3, 99–106.

Lebeer, S., Vanderleyden, J., and de Keersmaecker, S. C. (2010). Host interactions of probiotic bacterial surface molecules: comparison with commensals and pathogens. *Nat. Rev. Microbiol.* 8, 171–184. doi: 10.1038/nrmicro2297

Lin, P. P., Hsieh, Y. M., and Tsai, C. C. (2009). Antagonistic activity of *Lactobacillus acidophilus* RY2 isolated from healthy infancy feces on the growth and adhesion characteristics of enteroaggregative *Escherichia coli*. *Anaerobe* 15, 122–126. doi: 10.1016/j.anaerobe.2009.01.009

Liu, H., Hou, C., Wang, G., Jia, H., Yu, H., Zeng, X., et al. (2017). *Lactobacillus reuteri* I5007 modulates intestinal host defense peptide expression in the model of IPEC-J2 cells and neonatal piglets. *Nutrients* 9:559. doi: 10.3390/nu9060559

Livak, K. J., and Schmittgen, T. D. (2001). Analysis of relative gene expression data using real-time quantitative PCR and the 2-((CT method. *Methods* 25, 402–408. doi: 10.1006/meth.2001.1262

Longdet, I. Y., Kutdhik, R. J., and Nwoyeocha, I. G. (2011). The probiotic efficacy of *Lactobacillus casei* from human breast milk against Shigellosis in albino rats. *Adv. Biotechnol. Chem. Proc.* 1, 12–16.

Lorca, G., Torino, M. I., Font de Valdez, G., and Ljungh, A. A. (2002). Lactobacilli express cell surface proteins which mediate binding of immobilized collagen and fibronectin. *FEMS Microbiol. Lett.* 206, 31–37. doi: 10.1111/j.1574-6968.2002.tb10982.x

Manning, J., Dunne, E. M., Wescombe, P. A., Hale, J. D. F., Mulholland, E. K., Tagg, J. R., et al. (2016). Investigation of *Streptococcus salivarius* mediated inhibition of pneumococcal adherence to pharyngeal epithelial cells. *BMC Microbiol.* 16:225. doi: 10.1186/s12866-016-0843-z

Merriman, K. E., Kweh, M. F., Powell, J. L., Lippolis, J. D., and Nelson, C. D. (2015). Multiple β-defensin genes are upregulated by the vitamin D pathway in cattle. *J. Steroid Biochem. Mol. Biol.* 154, 120–129. doi: 10.1016/j.jsbmb.2015.08.002

Roselli, M., Finamore, A., Britti, M. S., and Mengheri, E. (2006). Probiotic bacteria *Bifidobacterium animalis* MB5 and *Lactobacillus rhamnosus* GG protect intestinal Caco-2 cells from the inflammation-associated response induced by enterotoxigenic *Escherichia coli* K88. *Br. J. Nutr.* 95, 1177–1184. doi: 10.1079/BJN20051681

Schierack, P., Nordhoff, M., Pollmann, M., Weyrauch, K. D., Amasheh, S., Lodemann, U., et al. (2006). Characterization of a porcine intestinal epithelial cell line for *in vitro* studies of microbial pathogenesis in swine. *Histochem. Cell Biol.* 125, 293–305. doi: 10.1007/s00418-005-0067-z

Schlee, M., Harder, J., Koten, B., Stange, E. F., Wehkamp, J., and Fellermann, K. (2008). Probiotic lactobacilli and VSL#3 induce enterocyte β-defensin 2. *Clin. Exp. Immunol.* 151, 528–535. doi: 10.1111/j.1365-2249.2007.03587.x

Smet, K. D., and Contreras, R. (2005). Human antimicrobial peptides: defensins, cathelicidins and histatins. *Biotechnol. Lett.* 27, 1337–1347. doi: 10.1007/s10529-005-0936-5

Sreekumar, O., and Hosono, A. (2000). Immediate effect of *Lactobacillus acidophilus* on the intestinal flora and fecal enzymes of rats and the *in vitro* inhibition of *Escherichia coli* in coculture. *J. Dairy Sci.* 83, 931–939. doi: 10.3168/jds.S0022-0302(00)74956-3

Talukder, P., Satho, T., Irie, K., Sharmin, T., Hamady, D., Nakashima, Y., et al. (2011). Trace metal zinc stimulates secretion of antimicrobial peptide LL-37 from Caco-2 cells through ERK and p38 MAP kinase. *Int. Immunopharmacol.* 11, 141–144. doi: 10.1016/j.intimp.2010.10.010

Trevisi, P., Latorre, R., Priori, D., Luise, D., Archetti, I., Mazzoni, M., et al. (2017). Effect of feed supplementation with live yeast on the intestinal transcriptome profile of weaning pigs orally challenged with *Escherichia coli* F4. *Animal* 11, 33–44. doi: 10.1017/S1751731116001178

Tuomola, E. M., Ouwehand, A. C., and Salminen, S. J. (1999). The effect of probiotic bacteria on the adhesion of pathogens to human intestinal mucus. *FEMS Immunol. Med. Microbiol.* 26, 137–142. doi: 10.1111/j.1574-695X.1999.tb01381.x

Veldhuizen, E. J., Rijnders, M., Claassen, E. A., van Dijk, A., and Haagsman, H. P. (2008). Porcine beta-defensin 2 displays broad antimicrobial activity against pathogenic intestinal bacteria. *Mol. Immunol.* 45, 386–394. doi: 10.1016/j.molimm.2007.06.001

Veldhuizen, E. J., van Dijk, A., Tersteeg, M. H., Kalkhove, S. I., van der Meulen, J., Niewold, T. A., et al. (2007). Expression of beta-defensins pBD-1 and pBD-2 along the small intestinal tract of the pig: lack of upregulation in vivo upon *Salmonella* typhimurium infection. *Mol. Immunol.* 44, 276–283. doi: 10.1016/j.molimm.2006.03.005

Walsham, A. D., MacKenzie, D. A., Cook, V., Wemyss-Holden, S., Hews, C. L., Juge, N., et al. (2016). *Lactobacillus reuteri* inhibition of enteropathogenic *Escherichia coli* adherence to human intestinal epithelium. *Front. Microbiol.* 7:244. doi: 10.3389/fmicb.2016.00244

Wan, L. Y., Chen, Z. J., Shah, N. P., and El-Nezami, H. (2016). Modulation of intestinal epithelial defense responses by probiotic bacteria. *Crit. Rev. Food Sci. Nutr.* 56, 2628–2641. doi: 10.1080/10408398.2014.905450

Wan, M. L., Ling, K. H., Wang, M. F., and El-Nezami, H. (2016). Green tea polyphenol epigallocatechin-3-gallate improves epithelial barrier function by inducing the production of antimicrobial peptide pBD-1 and pBD-2 in monolayers of porcine intestinal epithelial IPEC-J2 cells. *Mol. Nutr. Food Res.* 60, 1048–1058. doi: 10.1002/mnfr.201500992

Wang, J., Ji, H., Wang, S., Zhang, D., Liu, H., Shan, D., et al. (2012). *Lactobacillus plantarum* ZLP001: in vitro assessment of antioxidant capacity and effect on growth performance and antioxidant status in weaning piglets. *Asian Australas. J. Anim. Sci.* 25, 1153–1158. doi: 10.5713/ajas.2012.12079

Wang, J., Ji, H., Zhang, D., Liu, H., Wang, S., Shan, D., et al. (2011). Assessment of probiotic properties of *Lactobacillus plantarum* ZLP001 isolated from gastrointestinal tract of weaning pigs. *Afr. J. Biotechnol.* 10, 11303–11308. doi: 10.5897/AJB11.255

Wang, S., Wang, Q., Yang, E., Yan, L., Li, T., and Zhuang, H. (2017). Antimicrobial compounds produced by vaginal *Lactobacillus crispatus* are able to strongly inhibit *Candida albicans* growth, hyphal formation and regulate virulence-related gene expressions. *Front. Microbiol.* 8:564. doi: 10.3389/fmicb.2017.00564

Wang, Z., Wang, L., Chen, Z., Ma, X., Yang, X., Zhang, J., et al. (2016). *In vitro* evaluation of swine-derived *Lactobacillus reuteri*: probiotic properties and effects on intestinal porcine epithelial cells challenged with enterotoxigenic *Escherichia coli* K88. *J. Microbiol. Biotechnol.* 26, 1018–1025. doi: 10.4014/jmb.1510.10089

Wong, S. S., Quan Toh, Z., Dunne, E. M., Mulholland, E. K., Tang, M. L., Robins-Browne, R. M., et al. (2013). Inhibition of *Streptococcus pneumoniae* adherence to human epithelial cells *in vitro* by the probiotic *Lactobacillus rhamnosus* GG. *BMC Res. Notes* 6:135. doi: 10.1186/1756-0500-6-135

Yang, G. Y., Zhu, Y. H., Zhang, W., Zhou, D., Zhai, C. C., and Wang, J. F. (2015). Influence of orally fed a select mixture of *Bacillus* probiotics on intestinal T-cell migration in weaned MUC4 resistant pigs following *Escherichia coli* challenge. *Vet. Res.* 47, 71–89. doi: 10.1186/s13567-016-0355-8

Yoon, J. H., Ingale, S. L., Kim, J. S., Kim, K. H., Lohakare, J., Park, Y. K., et al. (2013). Effects of dietary supplementation with antimicrobial peptide-P5 on growth performance, apparent total tract digestibility, faecal and intestinal microflora and intestinal morphology of weanling pigs. *J. Sci. Food Agric.* 93, 587–592. doi: 10.1002/jsfa.5840

Zareie, M., Johnson-Henry, K., Jury, J., Yang, P. C., Ngan, B. Y., Mckay, D. M., et al. (2006). Probiotics prevent bacterial translocation and improve intestinal barrier function in rats following chronic psychological stress. *Gut* 55, 1553–1560. doi: 10.1136/gut.2005.080739

Zeng, X., Sunkara, L. T., Jiang, W., Bible, M., Carter, S., Ma, X., et al. (2013). Induction of porcine host defense peptide gene expression by short-chain fatty acids and their analogs. *PLoS One* 8:e72922. doi: 10.1371/journal.pone.0072922

Zhang, G., Ross, C. R., and Blecha, F. (2000). Porcine antimicrobial peptides: new prospects for ancient molecules of host defense. *Vet. Res.* 31, 277–296. doi: 10.1051/vetres:2000121

Zhang, J., Deng, J., Li, Y., and Yang, Q. (2011). The effect of *Lactobacillus* on the expression of porcine-defensin-2 in the digestive tract of piglets. *Livest. Sci.* 138, 259–265. doi: 10.1016/j.livsci.2011.01.001

Conflict of Interest Statement: The authors declare that the research was conducted in the absence of any commercial or financial relationships that could be construed as a potential conflict of interest.

frontiers in Microbiology

ORIGINAL RESEARCH
published: 04 July 2018
doi: 10.3389/fmicb.2018.01493

Synergistic Anti-MRSA Activity of Cationic Nanostructured Lipid Carriers in Combination With Oxacillin for Cutaneous Application

Ahmed Alalaiwe[1], Pei-Wen Wang[2], Po-Liang Lu[3,4], Ya-Ping Chen[5], Jia-You Fang[5,6,7,8] and Shih-Chun Yang[9]**

[1] Department of Pharmaceutics, College of Pharmacy, Prince Sattam Bin Abdulaziz University, Al Kharj, Saudi Arabia, [2] Department of Medical Research, China Medical University Hospital, China Medical University, Taichung, Taiwan, [3] Department of Internal Medicine, Kaohsiung Medical University Hospital, Kaohsiung, Taiwan, [4] College of Medicine, Kaohsiung Medical University, Kaohsiung, Taiwan, [5] Pharmaceutics Laboratory, Graduate Institute of Natural Products, Chang Gung University, Taoyuan, Taiwan, [6] Chinese Herbal Medicine Research Team, Healthy Aging Research Center, Chang Gung University, Taoyuan, Taiwan, [7] Research Center for Industry of Human Ecology and Research Center for Chinese Herbal Medicine, Chang Gung University of Science and Technology, Taoyuan, Taiwan, [8] Department of Anesthesiology, Chang Gung Memorial Hospital at Linkou, Taoyuan, Taiwan, [9] Department of Cosmetic Science, Providence University, Taichung, Taiwan

OPEN ACCESS

Edited by:
Sanna Sillankorva, University of Minho, Portugal

Reviewed by:
Sebastian Cerdan, Consejo Superior de Investigaciones Científicas (CSIC), Spain
Caterina Guiot, Università degli Studi di Torino, Italy

***Correspondence:**
Jia-You Fang
fajy@mail.cgu.edu.tw
Shih-Chun Yang
yangsc@pu.edu.tw

Specialty section:
This article was submitted to Antimicrobials, Resistance and Chemotherapy, a section of the journal Frontiers in Microbiology

Received: *17 April 2018*
Accepted: *18 June 2018*
Published: *04 July 2018*

Citation:
Alalaiwe A, Wang P-W, Lu P-L, Chen Y-P, Fang J-Y and Yang S-C (2018) Synergistic Anti-MRSA Activity of Cationic Nanostructured Lipid Carriers in Combination With Oxacillin for Cutaneous Application. Front. Microbiol. 9:1493. doi: 10.3389/fmicb.2018.01493

Nanoparticles have become a focus of interest due to their ability as antibacterial agents. The aim of this study was to evaluate the anti-methicillin-resistant *Staphylococcus aureus* (MRSA) activity of cationic nanostructured lipid carriers (NLC) combined with oxacillin against ATCC 33591 and clinical isolate. The cationic resource on the NLC surface was soyaethyl morpholinium ethosulfate (SME). NLC loaded with oxacillin was produced to assess the antibacterial activity and the effectiveness of topical application for treating cutaneous infection. The hydrodynamic diameter and zeta potential of oxacillin-loaded NLC were 177 nm and 19 mV, respectively. When combined with NLC, oxacillin exhibited synergistic MRSA eradication. After NLC encapsulation, the minimum bactericidal concentration (MBC) of oxacillin decreased from 250 to 62.5 μg/ml. The combined NLC and oxacillin reduced the MRSA biofilm thickness from 31.2 to 13.0 μm, which was lower than the effect of NLC (18.2 μm) and antibiotic (25.2 μm) alone. The oxacillin-loaded NLC showed significant reduction in the burden of intracellular MRSA in differentiated THP-1 cells. This reduction was greater than that achieved with individual treatment. The mechanistic study demonstrated the ability of cationic NLC to disrupt the bacterial membrane, leading to protein leakage. The cell surface disintegration also increased oxacillin delivery into the cytoplasm, activating the bactericidal process. Topical NLC treatment of MRSA abscess in the skin decreased the bacterial load by log 4 and improved the skin's architecture and barrier function. Our results demonstrated that a combination of nanocarriers and an antibiotic could synergistically inhibit MRSA growth.

Keywords: nanostructured lipid carriers, cationic surfactant, oxacillin, methicillin-resistant *Staphylococcus aureus*, skin

INTRODUCTION

The growing amount of drug-resistant strains has become a serious health threat, especially the methicillin-resistant *Staphylococcus aureus* (MRSA) (Tong et al., 2015). Some MRSA strains are even resistant to second-line treatment such as vancomycin and doxycycline (Cihalova et al., 2015). The skin is the major organ infected by MRSA (Dréno et al., 2016). Topical application can be an efficient route to administer antibiotics for direct MRSA eradication. Only 6 antibacterial agents have been approved by the USFDA for MRSA management. Since none of these drugs is used for topical treatment (Rodvold and McConeghy, 2014), the development of new anti-MRSA agents for cutaneous use is urgently needed.

In the past 10 years, nanomedicine has become an innovative approach for combating drug-resistant pathogens. The large surface-to-volume ratio, the possibility of surface functionalization, and the capacity for drug entrapment contribute to the efficient antibacterial activity of nanoparticles (Zazo et al., 2016). Among these nanosystems, lipid-based nanoparticles such as liposomes, nanoemulsions, and nanostructured lipid carriers (NLC) are usually employed for carrying antibacterial drugs. In addition to their role as carriers for antibiotics, some cationic surfactants exhibiting antimicrobial impact can be intercalated in the surface of lipid-based nanoparticles; these include amino acid–based surfactants and quaternary ammonium salts (Colomer et al., 2013; Hwang et al., 2013; Tavano et al., 2014). The combination therapy of more than one antibacterial agent can reveal the synergistic activity against MRSA; thus the dose can be reduced to minimize the adverse effects (Henson et al., 2017). Some investigations involve combining nanoparticles and antibacterial agents for the synergistic inhibition of MRSA infection. For instance, Banche et al. (2015) developed chitosan nanodroplets loaded with oxygen for efficiently eradicating MRSA and *Candida albicans* without resultant cytotoxicity on keratinocytes. Argenziano et al. (2017) demonstrated that ultrasound-mediated vancomycin-loaded nanobubbles were more effective than free vancomycin for killing MRSA. In this study, we aimed to investigate the applicability of synergistic MRSA inhibition by cationic nanocarriers in combination with antibiotic for topical delivery. NLC consisting of mixed liquid and crystalline lipids in the nanoparticulate cores were utilized to load cationic surfactant for enhanced anti-MRSA potency. Soyaethyl morpholinium ethosulfate (SME) was chosen as the cationic surfactant because of the low cytotoxicity against mammalian cells such as neutrophils and keratinocytes (Hwang et al., 2015; Yang et al., 2016).

Oxacillin is a β-lactam commonly used to treat complicated skin infections, but it is ineffective against MRSA invasion (Thomsen et al., 2006). We used oxacillin entrapped in NLC for increased effectiveness against MRSA. A panel comprising *S. aureus*, MRSA, and drug-resistant clinical isolate was used as the pathogens to assess the antibacterial activity of the nanosystems. MRSA in the planktonic, biofilm, and intracellular forms was tested in the present study. The encapsulation of oxacillin in lipid nanoparticles may enhance the delivery ability into the biofilm and host cells. To estimate the *in vivo* efficiency of combined NLC and oxacillin, the transepidermal water loss (TEWL), MRSA burden, and histology were evaluated using a BALB/c mouse model with MRSA skin infection.

MATERIALS AND METHODS

Preparation of NLC

The lipid and water phases of NLC were prepared separately. The lipid phase consisted of 2% squalene, 2% hexadecyl palmitate, 1.5% soy phosphatidylcholine (Phospholipon 80H®), 1% deoxycholic acid, and 0.4% SME. The water phase consisted of 1.5% Pluronic F68 and double-distilled water. Both phases were heated to 85°C for 15 min. The water phase was added to the lipid phase in the presence of high-shear homogenization (Pro250, Pro Scientific) at 12,000 rpm for 20 min. The mixture was subsequently treated using a probe-type sonicator (VCX600, Sonics and Materials) for 15 min at 35 W. Oxacillin (0.1%) was included in the lipid phase as needed.

Size and Surface Charge of NLC

The average diameter and zeta potential of NLC with and without oxacillin were determined using dynamic light scattering (Nano ZS90, Malvern). The nanocarriers were diluted by double-distilled water 100-fold before measurement.

Oxacillin Encapsulation in NLC

The entrapment percentage of oxacillin was determined by utilizing the ultracentrifugation method to separate the incorporated compound from the free form. The NLC was centrifuged at 48,000 × *g* and 4°C for 40 min. The free antibiotic in the supernatant and the encapsulated antibiotic in the precipitate were analyzed by high-performance liquid chromatography to measure the entrapment efficiency.

Bacterial Strains and the Culture Conditions

Staphylococcus aureus (ATCC 6538) and MRSA (ATCC 33591) were obtained from American Type Culture Collection. KM1 was a clinical isolate of MRSA purchased from Kaohsiung Medical University Hospital. The strains were grown in tryptic soy broth (TSB) medium at 37°C and 150 rpm.

Minimum Bactericidal Concentration (MBC)

A broth with twofold serial dilution method was utilized to measure the MBC. An overnight culture of bacteria was diluted in TSB to achieve OD_{600} of 0.01 (about 5×10^6 CFU/ml). The bacteria population was exposed to several dilutions of oxacillin and/or NLC with TSB and incubated at 37°C for 18 h. Subsequently, the CFU was counted. The MBC was defined as the lowest concentration that killed ≥ 99.9% of the bacteria.

MRSA Viability Detection by Fluorescence Microscopy

The viability and death of MRSA after oxacillin and/or NLC treatment were monitored using a Live/Dead BacLight® kit (Molecular Probes). The bacterial pellet was obtained by centrifugation at 12,000 rpm for 3 min. The pellet was resuspended in culture medium (1 ml) with oxacillin (125 μg/ml) and/or NLC (equivalent to 500 μg/ml SME). After incubation at 37°C for 2 h, the resulting suspension was stained with the kit for 15 min. The stained sample was analyzed two-dimensionally by fluorescence microscopy (IX81, Olympus).

Biofilm Detection

The MRSA biofilm was grown in a Cellview® dish by incubating the bacteria ($OD_{600} = 0.1$) in TSB containing 1% glucose at 37°C for 24 h. The biofilm was treated with 125 μg/ml cetylpyridium chloride (CPC, the positive control), 125 μg/ml oxacillin, NLC (equivalent to 500 μg/ml SME), or NLC + oxacillin for 24 h. The biofilm was then stained using a Live/Dead BacLight® kit for 15 min. The biofilm was gently rinsed with PBS. The three-dimensional structure was visualized by Leica TSC SP2 confocal microscopy. The SYTO9 green color intensity and biofilm thickness in the confocal images were estimated.

MRSA Morphology Visualization by Transmission Electron Microscopy (TEM)

MRSA was incubated overnight at 37°C in TSB broth. The bacterial suspension was diluted to achieve an OD_{600} of 0.3. The microbes were then fixed in 3% glutaraldehyde in 0.1 M cacodylate buffer for 2 h. After fixation in 1% osmium teroxide for 2 h, followed by dehydration in an ascending series of ethanol concentrations, the samples were embedded in Spurr's resin. Sections of 70 nm were stained with 4% uranyl acetate and 0.4% lead citrate prior to observation under Hitachi H-7500 TEM.

Intracellular MRSA Eradication

Differentiated THP-1 were employed as the host cells to examine the activity of oxacillin and NLC in relation to intracellular MRSA. The differentiation of THP-1 into macrophages was carried out at a phorbol 12-myristate 13-acetate concentration of 100 μg/ml. The cell line was infected by MRSA at an MOI of 50 for 20 min. After being washed with PBS, the cells were incubated in the fresh medium supplemented with 125 μg/ml oxacillin and/or NLC (equivalent to 500 μg/ml SME). Triton X-100 (1%) was pipetted into the medium for cell lysis. The lysate of the cell medium was cultured on the agar dish for 18 h to count the CFU. For the confocal imaging of MRSA killing in THP-1, 4′-6-diamidino-2-phenylindole and anti-*S. aureus* antibody/Alexa Fluor® 488 goat anti-mouse IgG were used to stain the THP-1 nucleus and MRSA, respectively. We also stained the THP-1 actin using an anti-α tubulin antibody/microtubule marker (Alexa Fluor® 594) for visualizing the cytoskeleton under confocal microscopy.

Proteomic Identification

The MRSA was treated using oxacillin and/or NLC for 3 h. After centrifugation, the bacterial pellet was suspended with 0.5 ml double-distilled water. The MRSA was then centrifuged at 10,000 rpm and 4°C for 15 min after 20-min sonication. The total protein content of MRSA was measured using a Bio-Rad protein assay kit with ELISA at 595 nm. The SDS-PAGE analysis was conducted with a 5% stacking gel and a 10% separating gel followed by silver staining. The bands in the protein gel staining were digested by trypsin at 37°C for 24 h. The digested proteins were acidified with 0.5% trichloroacetic acid and then loaded into an AnchorChip® 600/384. A Bruker Ultraflex® spectrometer was employed for MALDI/TOF/TOF identification. The procedure for this analysis was shown in a previous report (Pan et al., 2010).

Genomic DNA Analysis

MRSA genomic DNA was extracted using a Presto® Mini bacteria kit according to the manufacturer's instruction. The aliquot of purified genomic DNA (100 ng) was analyzed by electrophoresis on a 0.8% agarose gel.

Animal

An 8-week-old female BALB/c mouse was purchased from the National Laboratory Animal Center (Taipei, Taiwan). The animal experiment was done in strict accordance with the recommendations in the Guidelines for the Care and Use of Laboratory Animals of Chang Gung University. The protocol was approved by the Committee of Care and Use of Laboratory Animals.

In Vivo MRSA Infection

The mouse's back hair was shaved. The back was subcutaneously injected with 1×10^6 CFU MRSA in PBS (150 μl). Subsequently, oxacillin and/or NLC with a volume of 0.2 ml was topically administered on the injection area every 24 h for 3 days. The gross and microscopic appearance of the skin surface was monitored each day. A handheld digital magnifier (Mini Scope-V, M&T Optics) was used to visualize the microscopic skin appearance. TEWL was estimated by Tewameter® TM300 (Courage and Khazaka) from 0 to 3 days post-injection of MRSA. At the end of the experiment, the skin was excised for homogenization by NagNA Lyser (Roche) to count the CFU of MRSA in the skin. The treated skin sample was fixed in 10% formalin, buffered in the phosphate saline, and processed for hematoxylin and eosin (H&E) staining. The unstained slices of formalin-fixed paraffin-embedded skin samples were prepared for immunohistochemical (IHC) staining of lymphocyte antigen 6 complex locus G6D (Ly6G), which is the indicator of neutrophil infiltration. The skin section was incubated with anti-mouse Ly6G antibody for 1 h at room temperature and observed under optical microscopy (DMi8, Leica).

In Vivo Cutaneous Irritation

Oxacillin (625 μg/ml) and/or NLC at a volume of 150 μl were immersed in a non-woven cloth (1.5×1.5 cm^2). This cloth was

applied to the dorsal skin of the mouse. Tegaderm® film was used to fix the cloth onto the mouse's back. The bacterial agent was applied daily for 5 consecutive days. After the treatment, the skin area was monitored by a handheld digital magnifier and TEWL.

Statistical Measurement

The statistical measurement was conducted using GraphPad Prism 5 software. Dual comparisons were made with unpaired Student's *t*-test. Groups of three or more were analyzed by ANOVA with Tukey or Dunnett posttests. The significance was indicated as * for $p < 0.05$, ** for $p < 0.01$, and *** for $p < 0.001$ in the figures.

RESULTS

Size and Surface Charge of NLC

The molecular structure of oxacillin-loaded NLC is illustrated in **Figure 1A**. We proposed that oxacillin was entrapped in the inner core of NLC, whereas SME was intercalated in the emulsifier layer (oil-water interface). The two antibacterial agents were resided in the different phases of nanoparticulate system. **Table 1** summarizes the diameter, polydispersity index (PDI), and surface charge of the lipid nanocarriers. The average particle size of NLC without the antibiotic was 117 nm, and that of NLC containing oxacillin was 177 nm. Both nanosystems revealed stable unimodal size distribution with PDI of ≤0.3, demonstrating a narrow

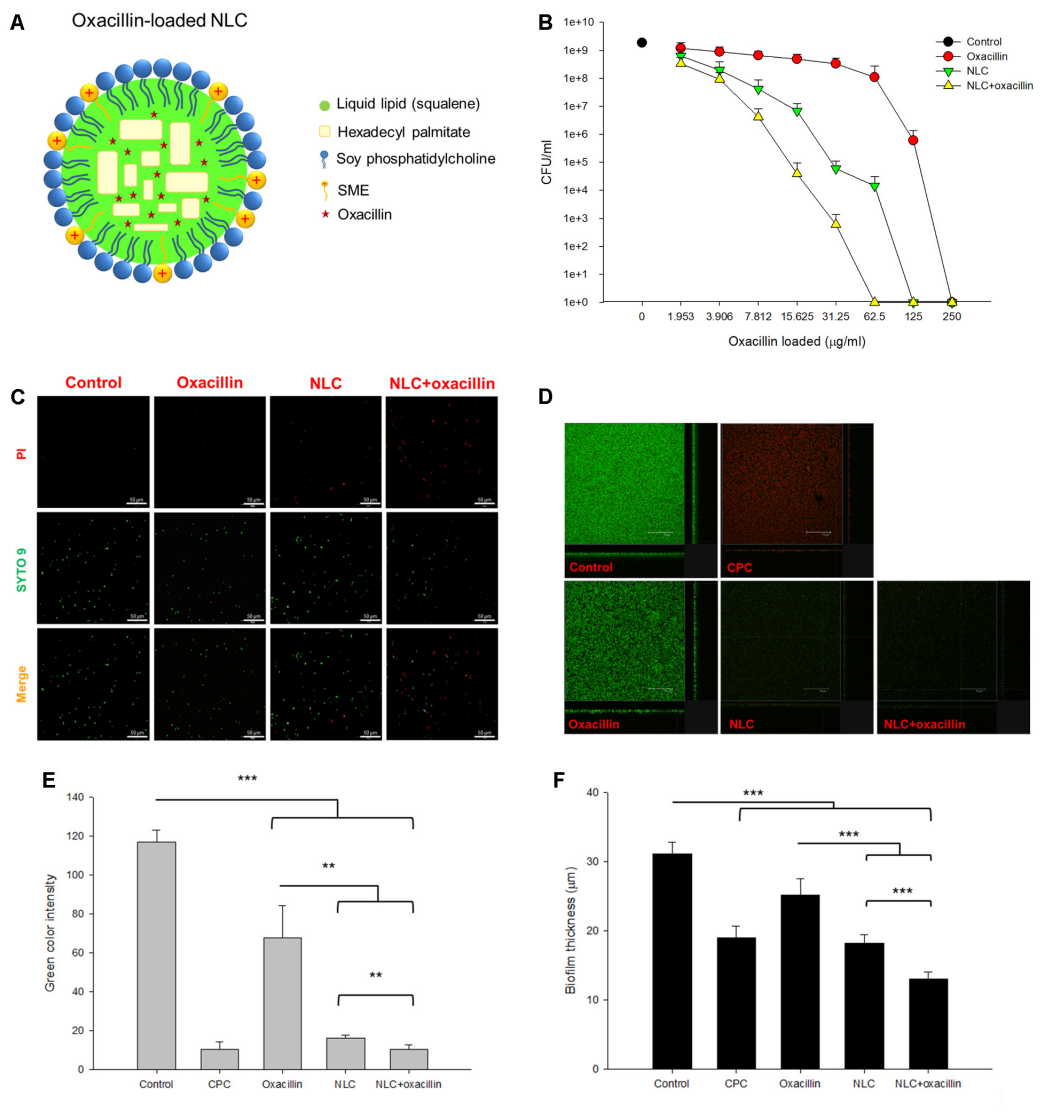

FIGURE 1 | Determination of the anti-MRSA activity of oxacillin and/or NLC. **(A)** The proposed structure of oxacillin-loaded NLC: oxacillin is included in the lipid matrix, whereas SME is intercalated in the emulsifier layers. **(B)** Dose-dependent MRSA killing measured by CFU. **(C)** The planktonic live/dead MRSA strain viewed under fluorescence microscopy. **(D)** The three-dimensional images viewed under confocal microscopy. **(E)** Quantification of fluorescence intensity of MRSA biofilm. **(F)** The corresponding biofilm thickness analyzed by confocal microscopy. Each value represents the mean ± SD ($n = 3$). **$p < 0.01$ and ***$p < 0.001$.

TABLE 1 | The physicochemical properties of NLC and NLC + oxacillin.

Formulation	Size (nm)	PDI	Zeta potential (mV)
NLC	116.92 ± 23.21	0.30 ± 0.02	12.82 ± 2.34
NLC + oxacillin	177.00 ± 9.55	0.29 ± 0.03	18.70 ± 0.82

Each value represents the mean ± SD (n = 3). PDI, polydispersity index.

distribution. Positively charged nanoparticles were achieved (13 mV) for NLC without oxacillin because of the existence of SME on the particulate surface. The oxacillin addition generated greater zeta potential than did the nanoparticles without the drug. The result revealed that the entrapment percentage of oxacillin in NLC was 76.8 ± 7.0%. The encapsulation could be reduced to 59.1 ± 5.5% after 24 h of fresh preparation, indicating a drug release during the experiment.

Synergistic Antibacterial Activity of NLC in Combination With Oxacillin

Table 2 shows the MBC value of oxacillin alone, NLC alone, and the NLC-oxacillin combination. The MBC of oxacillin alone against non-resistant *S. aureus* was 0.488∼0.976 μg/ml, whereas the MBC for SME in NLC was 62.5 μg/ml. The oxacillin MBC was not reduced after NLC incorporation. The combined NLC and oxacillin reduced SME MBC by 16-fold. MRSA was found to be more resistant to NLC and oxacillin as compared to drug-sensitive bacteria. Oxacillin synergized with NLC to inhibit MRSA growth. The oxacillin MBC of treatment alone and in combination with NLC was 250 and 62.5 μg/ml, respectively. The SME MBC of NLC for MRSA decreased twofold after oxacillin entrapment. The clinical MRSA strain (KM1) was more strongly inhibited by NLC and oxacillin than ATCC 33591. The anti-KM1 activity of oxacillin increased in the presence of cationic NLC. The MBC profile clearly indicates an enhancement in antibacterial potency of NLC and oxacillin upon the combination of both agents.

Figure 1B represents the concentration-dependent microbicidal action of NLC and oxacillin on MRSA ATCC 33591. The counting of CFU was log-transformed in this figure. No significant decrease of CFU was detected in the oxacillin concentrations of ≤31.25 μg/ml. The oxacillin concentrations of >31.25 μg/ml showed a dose-dependent decrease in viability. With respect to NLC, the inhibitory effect increased with the increased concentration against MRSA. The combination of NLC with oxacillin reduced CFU/ml counts by at least log 5, leading to a killing of >99.9% MRSA at the oxacillin concentration of 62.5 μg/ml. The viability of MRSA was observed with fluorescence microscopy with the staining of dead and live bacteria by propidium iodide (PI) and SYTO9, respectively (**Figure 1C**). The untreated control MRSA was mainly composed of live cells, which were green-stained. Fluorescence analysis revealed that some bacteria co-localized with PI after incubation with NLC and/or oxacillin. Combining nanocarriers and antibiotic proved superior for killing microorganisms as compared to individual treatment because of the increased PI staining.

Figure 1D shows the anti-biofilm activity of NLC and/or oxacillin against MRSA under confocal microscopy. The bacteria were able to create a dense biofilm with a large amount of live MRSA after 24 h, which is shown as the negative control. CPC is a cationic surfactant affecting the antibacterial effect via cell wall destruction, with a strong potency. As a positive control, CPC markedly reduced the green signal and enhanced the red signal in the biofilm. Oxacillin exhibited a limited activity against biofilm due to the significant green signal after treatment. The image of biofilm from MRSA treated with NLC alone showed that the biofilm had disintegrated, with an obvious reduction in the number of live bacteria. A similar result was observed in the case of combined NLC and oxacillin. The quantification of green fluorescence in biofilm showed a negligible signal of live cells after CPC treatment (**Figure 1E**). Incubation of oxacillin and NLC alone decreased the green color intensity by about 2- and 6-fold, respectively. The combination permitted a synergistic effect on intensity reduction with statistical significance. Oxacillin-loaded NLC exhibited greater biofilm thickness reduction (13.0 μm) compared to that of drug or NLC alone (**Figure 1F**).

TABLE 2 | The MBC of *S. aureus*, MRSA, and KM1 clinical strain after treatment of oxacillin, NLC, and NLC + oxacillin.

Strain	Treatment	Oxacillin (μg/ml)	SME in NLC (μg/ml)
S. aureus	Oxacillin	0.488∼0.976	N
	NLC	N	62.5
	NLC + oxacillin	0.976	3.906
MRSA	Oxacillin	250	N
	NLC	N	250∼500
	NLC + oxacillin	62.5	125
KM1	Oxacillin	62.5∼125	N
	NLC	N	62.5
	NLC + oxacillin	7.812	31.25

N, no data. Each value represents the mean ± SD (n = 3).

Intracellular MRSA Killing by NLC and/or Oxacillin

Figure 2A presents the TEM images of the MRSA morphology. The intact bacteria (control) reveal an integrated cell surface with homogenous cytosol distribution. Oxacillin caused cell membrane deformation with a rough surface (arrow in **Figure 2A**). The MRSA membrane was disrupted after NLC treatment. Some cytoplasmic materials were released from the cytosol (arrow in **Figure 2A**). The observation of fewer dark zones in the cells treated by NLC than in the control can be attributed to cytoplasm dissolution. The cell wall tended to separate from the cytoplasmic membrane since vacuoles formed between them. More cell wall damage and cytoplasmic leakage are seen after combined treatment (arrow in **Figure 2A**). The antibacterial efficacy of oxacillin and NLC was examined using macrophages as the host cells for MRSA infection. Time-dependent intracellular MRSA killing was detected, and is depicted in **Figure 2B**. The MRSA burden in the mammalian cells gradually increased following the increase of time in the untreated control group. Although treatment with NLC and/or

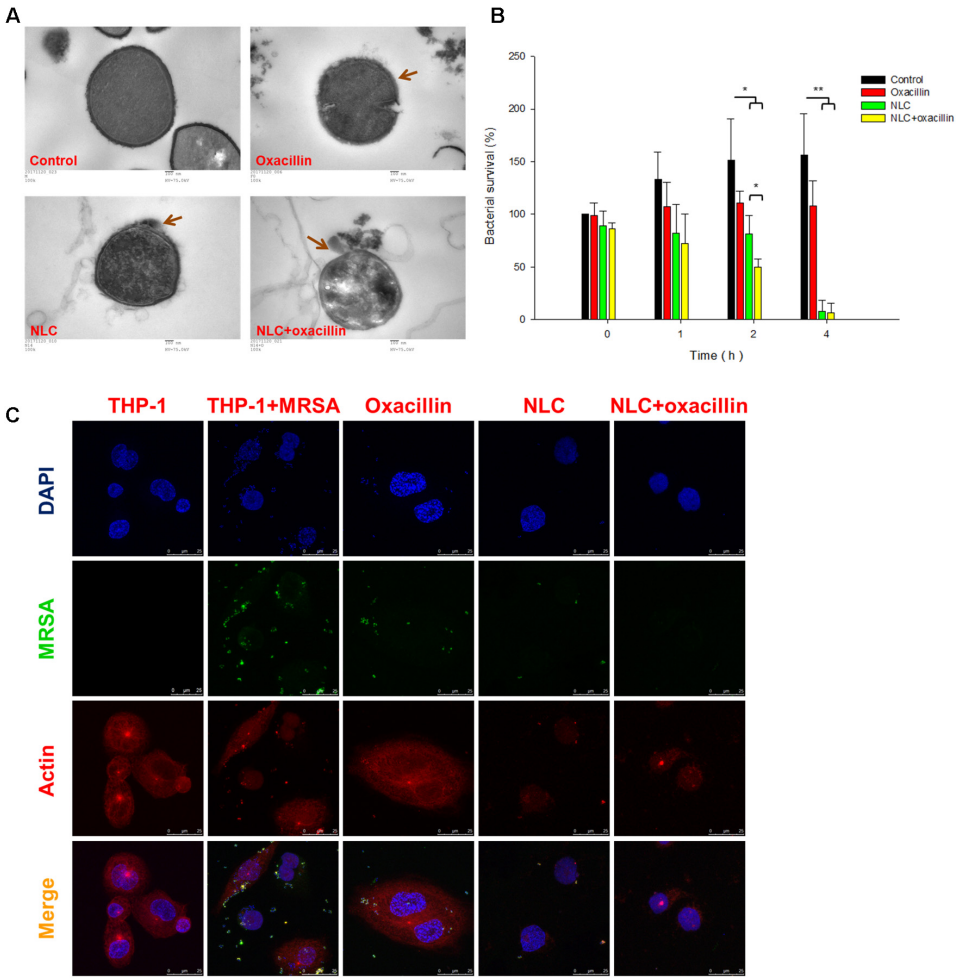

FIGURE 2 | Bacterial morphology change and intracellular MRSA killing by treatment of oxacillin and/or NLC. **(A)** Morphological changes of MRSA viewed under TEM. **(B)** Measurement of MRSA survival in macrophages (THP-1). **(C)** Intracellular MRSA distribution in macrophages (THP-1) viewed under confocal microscopy. Each value represents the mean ± SD (n = 3). $^{**}p < 0.01$; $^{*}p < 0.05$.

oxacillin reduced MRSA production at 1 h, no significant difference was shown after a comparison with the control group. At 2 h, NLC with and without antibiotic resulted in a marked reduction in intracellular MRSA survival. On the other hand, oxacillin alone had no effect on the intracellular viability of bacteria for all the time points tested. Synergy was demonstrated by the combination of NLC and the drug after 2-h incubation. There was a threefold decrease of MRSA survival for the combined treatment as compared with the untreated control. A complete inhibition of MRSA growth occurred consistently after 4 h of contact with NLC alone or NLC + oxacillin.

Figure 2C shows the confocal microscopic images of MRSA-infected THP-1 cells. In the images of THP-1 without any treatment, the cytosol is full of red signals, indicating the presence of cytoskeleton stained by actin. Some punctuated green signals in the MRSA-infected THP-1 cytoplasm indicate the invasion of bacteria inside the macrophages. After 4-h incubation of oxacillin or cationic NLC alone, less green fluorescence was visualized in the cytosol. The oxacillin-entrapped NLC resulted in negligible MRSA residence in the cytosol, demonstrating a synergistic effect. We hypothesize that NLC can be utilized as Trojan horses to promote the antibiotic delivery into host cells for killing bacterial.

Anti-MRSA Mechanisms of NLC and/or Oxacillin

We next explored the anti-MRSA mechanisms of NLC in the presence or absence of oxacillin intervention. **Figure 3A** illustrates the profiles of SDS-PAGE. The bands of NLC- and/or oxacillin-treated MRSA are quite different from those of the untreated microbes. There were 12 protein bands differentially expressed after treatment. The quantification of the protein level was conducted in mass as shown in **Table 3**. All 12 proteins exerted comparable or slightly higher expression by treatment with oxacillin alone, in comparison to the untreated group. No protein exhibited upregulation greater than 2-fold after oxacillin application. The 3 proteins with the highest molecular weights: DNA-directed RNA polymerase subunit β,

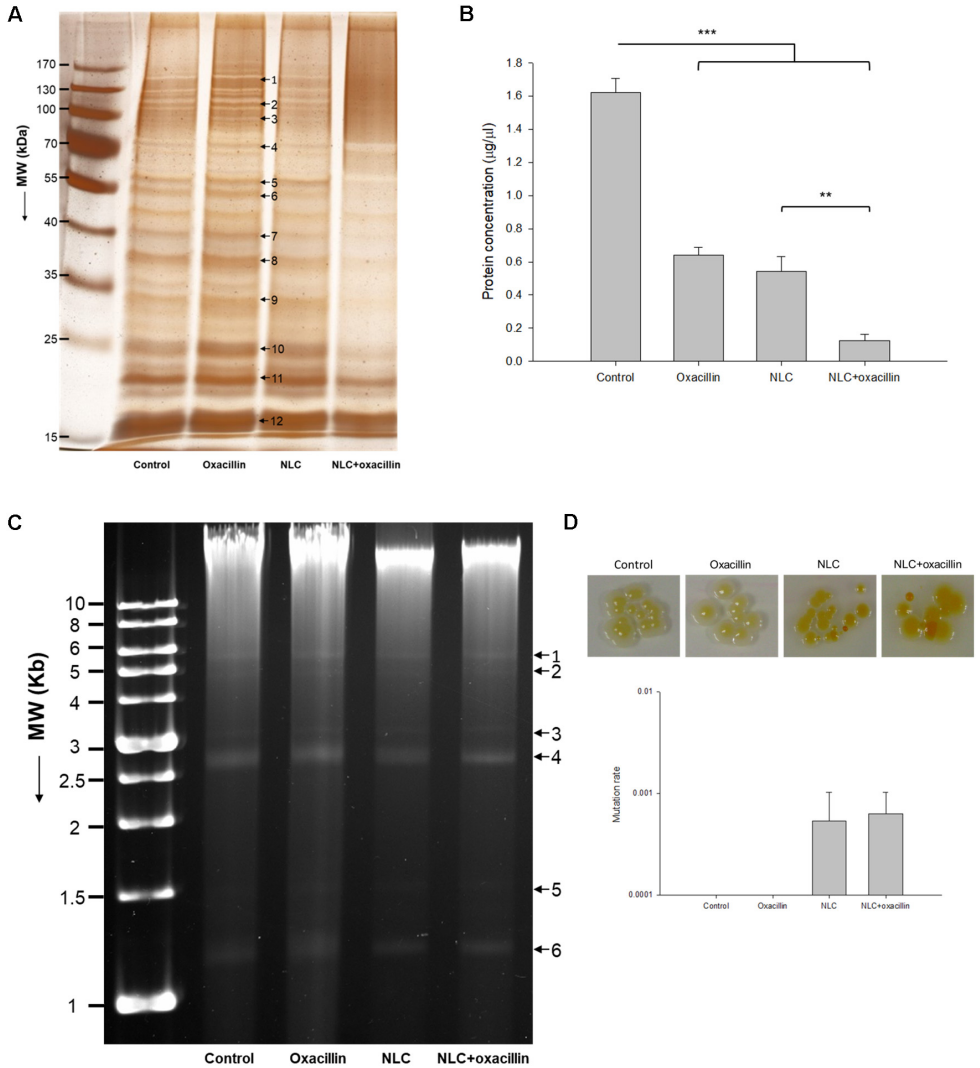

FIGURE 3 | Anti-MRSA mechanisms of oxacillin and/or NLC. **(A)** The protein change of MRSA analyzed by SDS-PAGE and MALDI-TOF/TOF mass. **(B)** Protein concentration in MRSA. **(C)** Analysis of the quality of MRSA genomic DNA by 0.8% agarose gel electrophoresis. **(D)** Mutation rate of MRSA analyzed by colony color change. Each value represents the mean ± SD ($n = 3$). $^{**}p < 0.01$ and $^{***}p < 0.001$.

chaperone ClpB, and elongation factor G, were downregulated by the NLC treatment. Increased expression was detected for the other 9 proteins. However, the expression increment of these 9 proteins was insignificant (<1.25-fold). The NLC and oxacillin combination produced a notable decrease in protein expression, as shown in the SDS-PAGE profiles, especially in the case of ornithine carbamoyltransferase and 30S ribosomal protein S4. Both proteins were decreased by >5-fold in the MRSA with NLC+oxacillin. The total MRSA protein amount was measured after the application of NLC and/or oxacillin as shown in **Figure 3B**. Oxacillin and NLC alone caused a 60 and 66% loss of total protein content compared to the control, respectively. A further reduction was observed with the use of antibiotic-loaded NLC, resulting in a 13-fold decrease.

We studied the anti-MRSA mechanisms of oxacillin and NLC by genomic DNA detection, as shown in **Figure 3C**. We differentiated 6 plasmid bands in the agarose gel image. DNA obtained from MRSA treated with NLC and/or the drug exhibited a pattern similar to that found in the control. No significant elimination of DNA was observed by oxacillin or NLC treatment. This result suggests that the extensive damage to the integrity of DNA might not occur when MRSA is treated with both agents; however, small region deletions/insertions or inactivating point mutations of DNA might be occurred. We also examined the possible genomic mutation of the MRSA. The mutation rate assay was performed by spotting a 10-fold dilution of overnight culture onto the agar supplemented with 62.5 μg/ml SME in NLC or NLC + oxacillin. The plate was incubated at 37°C overnight and imaged. As shown in the upper panel of **Figure 3D**, the treatment of NLC alone or the combined strategy was able to modify the color of some colonies from yellow to orange or white, indicating of bacterial mutation. Oxacillin alone did not

TABLE 3 | Differentially expressed proteins follow the treatment of oxacillin, NLC, and NLC + oxacillin.

Band No.	Protein	Accession No.	MW (Da)	Matched-peptides	Sequence Coverage % (SCORE)	Ratios to control[a,b]			Biological function
						Oxacillin	NLC	NLC + oxacillin	
1	DNA-directed RNA polymerase subunit beta	Q6GBV4	134,735	29	30% (152)	1.82	−0.72	1.32	Initiation factors that promote the attachment of RNA polymerase to specific initiation sites and are then released.
2	Chaperone ClpB	Q6GAV1	87,165	23	41% (167)	1.99	−0.64	1.54	Part of a stress-induced multi- chaperone system, it is involved in the recovery of the cell from heat-induced damage, in cooperation with DnaK, DnaJ and GrpE.
3	Elongation factor G	P68791	76,877	13	22% (113)	1.59	−0.65	1.24	Catalyzes the GTP-dependent ribosomal translocation step during translation elongation.
4	Molecular Chpaerone DnaK	P64408	66,321	21	39% (143)	1.23	0.52	−1.33	Acts as a chaperone.
5	Catalase	Q8NWV5	58,516	17	41% (93)	1.42	1.13	−2.44	Decomposes hydrogen peroxide into water and oxygen; serves to protect cells from the toxic effects of hydrogen peroxide.
6	Enolase	P64079	46,277	17	48% (120)	1.27	0.94	−3.33	Catalyzes the reversible conversion of 2-phosphoglycerate into phosphoenolpyruvate. It is essential for the degradation of carbohydrates via glycolysis.
6	Elongation factor Tu	P64029	43,148	16	58% (109)	1.27	0.94	−2.78	This protein promotes the GTP-dependent binding of aminoacyl-tRNA to the A-site of ribosomes during protein biosynthesis.
7	Arginine deiminase (ARCA)	Q8NUK7	47,139	17	35% (120)	1.33	0.52	−3.85	L-arginine + H_2O = L-citrulline + NH_3.
8	Ornithine carbamoyltransferase	Q6GDG8	37,792	14	52% (113)	1.06	0.55	−5.28	Reversibly catalyzes the transfer of the carbamoyl group from carbamoyl phosphate (CP) to the N(epsilon) atom of ornithine (ORN) to produce L-citrulline.
9	Fructose-bisphosphate aldolase class 1	Q6GDJ7	32,875	11	44% (100)	0.96	1	−2.56	D-fructose 1,6-bisphosphate = glycerone phosphate + D-glyceraldehyde 3-phosphate.
10	30S ribosomal protein S4 (RS4)	P66564	23,027	17	61% (159)	1.31	1.25	−6.25	One of the primary rRNA binding proteins, it binds directly to 16S rRNA where it nucleates assembly of the body of the 30S subunit.
11	50S ribosomal protein L6	Q7A084	19,802	10	62% (96)	0.75	0.81	−1.63	This protein binds to the 23S rRNA, and is important in its secondary structure. It is located near the subunit interface in the base of the L7/L12 stalk, and near the tRNA binding site of the peptidyltransferase center.
12	Alkaline shock protein 23 (ASP23)	P0A0P7	19,210	11	68% (124)	0.75	0.80	−0.43	May play a key role in alkaline pH tolerance.

[a]*Ratios to control indicated the fold changes in protein volume among Oxacillin, NLC, NLC + oxacillin treated samples versus MRSA samples, respectively. The higher ratios (>1.0) mean the proteins whose expression levels were increased upon treatments of compounds, while lower ratios (<−1.0) indicate the proteins were downregulated under the exposure to compounds.* [b]*Analyzing the gel images using GeneTools software.*

change the colony color. The mutation rate was calculated based on the MRSA numbers of orange or white colonies normalized to the numbers of total colonies. As shown in the bottom panel of **Figure 3D**, NLC and NLC + oxacillin caused a mutation rate of about 6×10^{-4}. No colony color phenotype mutation was detected for oxacillin alone.

In Vivo MRSA Infection

Nanostructured lipid carriers and/or oxacillin were topically applied onto the region of subcutaneous abscess generated in a mouse model by local MRSA infection. **Figure 4A** shows the demonstrative gross appearance of the mouse back after 3-day treatment. The abscess caused by MRSA is indicated by the arrow in this figure. A significant lesion is seen in the group of MRSA infection without treatment. The improvement in lesion healing was limited in the mouse receiving oxacillin alone. The lesion was reduced with no open wound by topical application of NLC and antibiotic-containing NLC. A nearly complete abscess resolution was detected for the combined NLC and oxacillin. The handheld digital magnifier offered visualization of the changes caused by the MRSA on the demonstrative mouse skin surface, as demonstrated in **Figure 4B**. The end face view of the skin exhibited that the wound was worse following the increase of time in the MRSA and MRSA + oxacillin groups. The treatment with NLC and drug-loaded NLC significantly cleared the abscess with skin texture comparable to healthy skin. The open wound formed by MRSA infection disturbed the cutaneous barrier function. The TEWL-time curves are plotted in **Figure 4C**. The baseline of TEWL (non-treatment) was maintained at 4∼6 g/m^2/h during 3 days. MRSA inoculation resulted in an immediate and large increase of TEWL, indicating the barrier function deficiency. Oxacillin alone was ineffective in reducing TEWL, while NLC and NLC + oxacillin demonstrated a significant inhibition of water loss in the infected area.

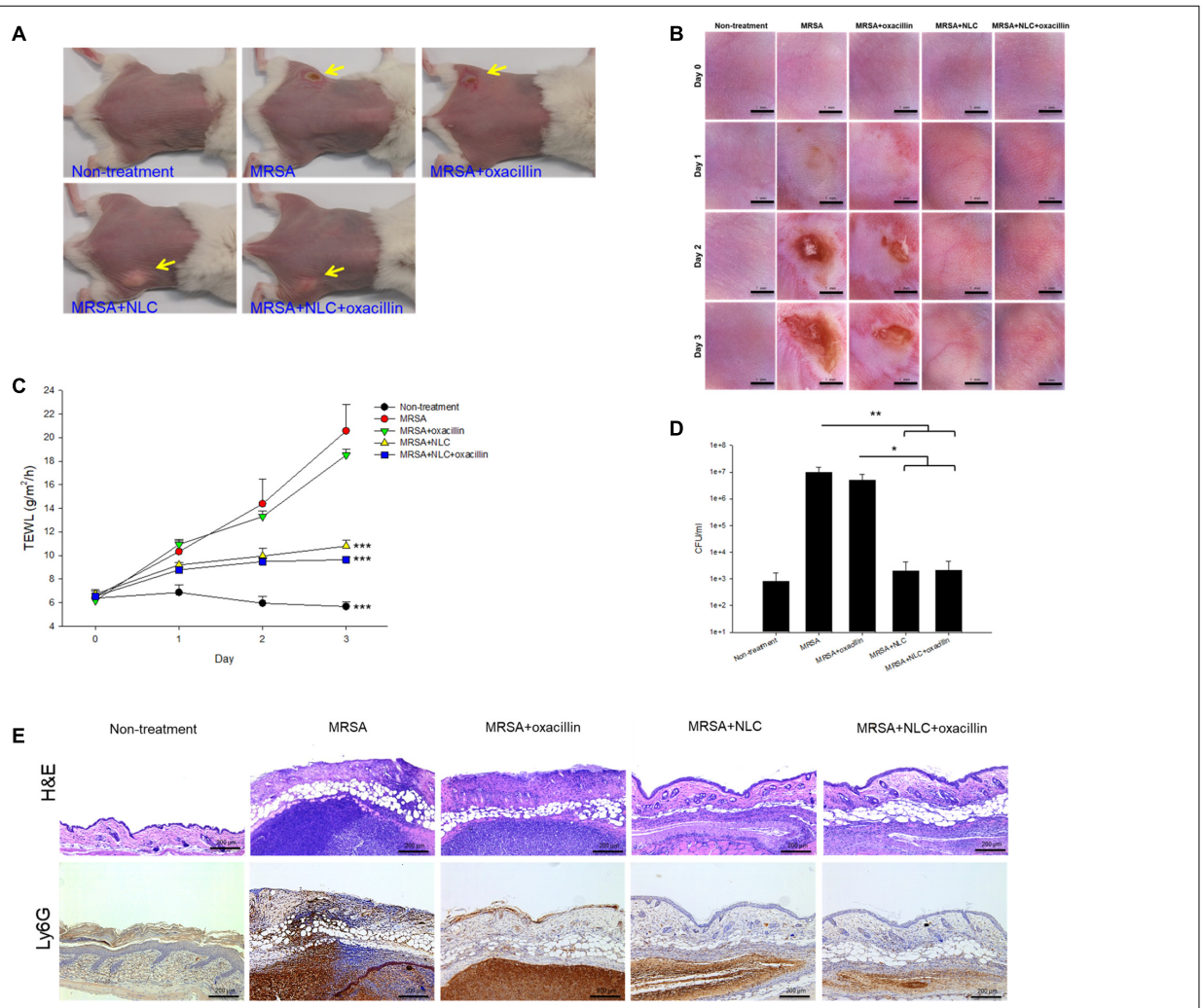

FIGURE 4 | *In vivo* topical application of oxacillin and/or NLC against MRSA. **(A)** The representative macroscopic skin surface observation of mouse after a 3-day treatment MRSA injection. **(B)** The representative skin surface of mouse after treatment of MRSA at day 0, 1, 2, and 3 viewed under handheld digital magnifier. **(C)** TEWL of mice skin after treatment of MRSA at day 0, 1, 2, and 3. **(D)** Survival of MRSA in mice skin treated with MRSA. **(E)** Histological observation of mice skin biopsy stained by H&E and Ly6G antibody after treatment of MRSA. Each value represents the mean ± SD (n = 6). *$p < 0.05$, **$p < 0.01$, and ***$p < 0.001$.

The bacterial count in the skin was estimated 3 days post-injection, as shown in **Figure 4D**. MRSA injection produced a 4-log enhancement in CFU/ml as compared to normal skin. No significant reduction in the MRSA count of oxacillin treatment alone was observed when compared to bacterial infection without intervention. In the mouse infected with MRSA, both NLC and drug-loaded NLC resulted in a 10^4 reduction of CFU/ml compared with the placebo control. **Figure 4E** shows the qualitative evaluation of skin histopathology of the infection of MRSA with and without intervention. As compared to healthy skin, MRSA injection created a significant disorganization in the epidermis, degenerated dermis, and immune cell infiltration. A large MRSA burden was seen under the subcutis. The generation of the abscess led to thickened tissue. The epidermal damage confirmed the deficiency of barrier integrity as measured by the enhanced TEWL. The wound treated with either NLC or oxacillin-loaded NLC showed a minor inflammation. The distribution of the infiltrated neutrophils in the skin was visualized using Ly6G IHC, as shown in the bottom panel of **Figure 4E**. The large neutrophil infiltration overlapped the MRSA distribution in the subcutaneous region, suggesting deep inflammation. We could also observe the neutrophil diffusion to viable skin. Topical oxacillin suppressed the neutrophil migration in viable skin but not in the subcutaneous area. We found attenuation of neutrophil accumulation after nanoparticle treatment, with the oxacillin-loaded NLC displaying greater amelioration.

In Vivo Cutaneous Irritation

The formulations tested in this study were topically applied on healthy mouse skin each day for 5 days. **Figure 5A** illustrates the representative skin surface images visualized by a handheld magnifier. Slight erythema and scaling occurred when the mouse skin was administered with the vehicle (double-distilled water). In contrast, no visible erythema or edema was observed in the oxacillin-treated skin. The severity of erythema and excoriation was worsened by NLC alone. It was surprising that the addition of oxacillin in NLC could lessen the cutaneous abnormalities caused by NLC. The results of TEWL after 5-day treatment reflected the condition of the skin surface. As shown in **Figure 5B**, the increased TEWL induced by vehicle control was reversed to the non-treatment baseline by oxacillin administration. Application of NLC alone revealed an approximately 4-fold higher TEWL compared to healthy skin. Oxacillin incorporation significantly decreased TEWL from 26 to 18 g/m^2/h, demonstrating that oxacillin as a protector possesses the capability to reduce possible cutaneous irritation raised by the vehicle or NLC.

DISCUSSION

Oxacillin is effective in inhibiting non-resistant *S. aureus*, whereas MRSA is known to resist antibiotics such as methicillin and oxacillin (Cihalova et al., 2015). Our results confirm that oxacillin has limited anti-MRSA activity. Oxacillin incorporation in cationic NLC increased the killing efficacy against MRSA. The assembling ability of SME on the nanoparticulate shell was responsible for the antibacterial activity of cationic NLC. The synergistic effect on the antibacterial effect can be described as the combination of two different approaches producing greater activity than either approach alone (Basri and Sandra, 2016). Qin et al. (2013) also define the synergism of two drugs combined causing bacterial killing by a 4-fold lower dose than that of either agent used separately. We achieved the synergism of anti-MRSA activity by combining NLC and antibiotic according to the MBC profile of oxacillin.

Bacterial wall integrity is vital for their survival because it is the outermost and most accessible layer encountering the surrounding environment. It is an important area of action for many antibiotics (Radovic-Moreno et al., 2012). Oxacillin presents cell wall biosynthesis inhibition. The cationic quaternary ammonium surfactants demonstrate antimicrobial activity by targeting and disrupting the cell wall via electrostatic and lipophilic interactions (Zhou et al., 2017). The cell wall of MRSA carries negative charges due to the presence of lipopolysaccharides and teichoic acid (Hemeg, 2017). SME on the NLC surface can bind to the negatively charged cell membrane, permeabilizing it to induce lysis and cellular content leakage. The long alkyl chains in the SME structure might assist the interaction in the cell wall because of the facile intercalation into the lipid bilayers in the membrane. The destabilization of the

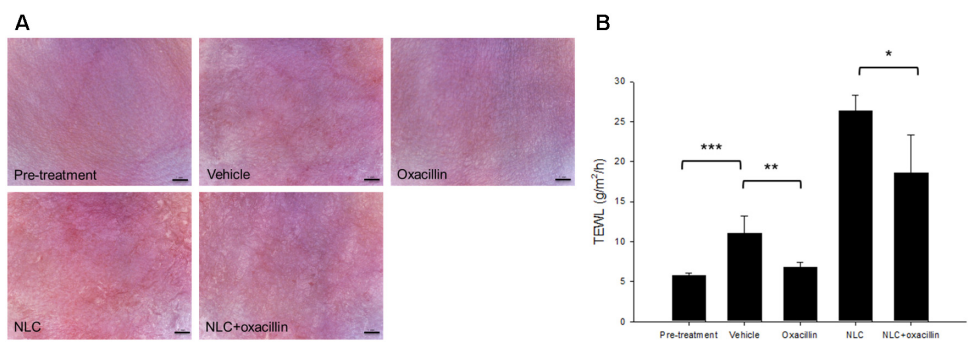

FIGURE 5 | Skin tolerance examination of mouse skin by a 5-day treatment of topically applied oxacillin and/or NLC. **(A)** The representative skin surface of mice viewed under handheld digital magnifier. **(B)** TEWL of mice skin at day 5. Each value represents the mean ± SD ($n = 6$). *$p < 0.05$, **$p < 0.01$, and ***$p < 0.001$.

bacterial wall involves the creation of pores on the cell surface to release ions and molecules as confirmed by our TEM results, after which bacterial death occurs. The demonstration of synergistic antibacterial activity by the combined treatment herein suggests the different mechanisms of action for both antibacterial agents (Bassolé and Juliani, 2012). The oxacillin-loaded NLC interacted strongly with the MRSA surface to damage the membrane. A considerable amount of oxacillin was released from the nanocarriers to generate high local drug concentration near the bacterial surface or inside the bacteria. The sustained bactericidal concentration of combined SME and oxacillin exhibit an anti-MRSA effect superior to that of separate treatment. Oxacillin entrapment increased the positive zeta potential of cationic NLC. The more-positive charges of antibiotic-loaded nanocarriers improved the electrostatic targeting to exert greater MRSA eradication.

Different from the case with planktonic bacteria, conventional antibiotics are less effective in treating biofilm bacteria due to the resistance to antibiotic delivery and avoidance of innate immune intervention (Abee et al., 2011). Using biofilm, we demonstrated that oxacillin-loaded nanoparticles penetrated into the extracellular polymer substance (EPS) and eradicated biofilm MRSA more effectively than individual treatment did. Extracellular DNA plays a key role in biofilm production, acting as a chelator of cationic molecules (Baelo et al., 2015). The interaction between EPS and the nanoparticles featuring lipids can cause a strong affinity and biofilm disintegration (Cheow et al., 2011). The cationic NLC designed in this study fit these criteria. The extremely non-wetting property of biofilm led to the restricted diffusion of antimicrobial liquid formulations (Lin et al., 2017). The low surface tension of cationic NLC caused by the presence of emulsifier systems might assist the penetration into non-wetting biofilm. NLC can hide the physicochemical characteristics of oxacillin to diminish the unfavorable interaction with biofilm.

The killing of intracellular MRSA is a complicated procedure. The pathogens in the host cells favor intracellular replication and the extensive spread of infection. Most of the antibiotics poorly penetrate into the host cells and therefore do not display satisfactory intracellular infection inhibition (Xie et al., 2014). Our results showed that the nanocarriers were preferentially taken up by macrophages, revealing greater activity against intracellular MRSA compared to free oxacillin. The change in the cytoskeleton morphology by the nanoparticles is evidence of phagocytosis (May and Machesky, 2001). The cationic NLC can modify the actin distribution in THP-1 cells; however, it must be noted that NLC might produce some toxicity on macrophages. It is generally recognized that the lipophilic nanoparticles are more facilely phagocytosed into macrophages than are hydrophilic nanoparticles, by the hydrophobic interaction with the cellular membrane (Hsu et al., 2017). The cationic nanoparticles ensure better uptake to macrophages with negatively charged membrane as compared to neutral and anionic ones (Zazo et al., 2016).

Soyaethyl morpholinium ethosulfate on the NLC shell can directly interfere with the bacterial cell wall and damage the membrane. The cationic nanocarriers altered the membrane to release cytoplasmic materials, as shown in the TEM images. The significant loss of proteins in the MRSA co-treated with NLC and oxacillin verified the cell wall leakage; however, the leakage can be acknowledged as mild according to the TEM. The anti-MRSA activity of oxacillin-loaded NLC may also rely on other mechanisms of action. The nanoparticles possibly interact with DNA and the proteins of microbes to disturb the replication, translation, and transcription of the cellular pathways (Hemeg, 2017; Richter et al., 2017). Our previous study (Yang et al., 2016) suggested the antibacterial mechanisms of SME to evoke the Fenton reaction and reactive oxygen species (ROS). The preliminary genome analysis showed no significant alteration of the DNA level after NLC and/or oxacillin management. The greater molecular size of bacterial DNA compared to proteins retarded the leakage to the extracellular space. It is hypothesized that, besides membrane leakage by direct targeting, the nanosystems predominantly acted on proteins, thereby constraining MRSA growth.

The three proteins with the highest molecular weights revealed no significant change under combined NLC and oxacillin. On the other hand, all proteins with the molecular weight of $<$75 kDa exhibited loss after co-treatment. The mild leakage in the bacterial membrane created by antibiotic-entrapped nanoparticles might allow the liberation of proteins of $<$75 kDa. Among the detected proteins of $>$75 kDa, chaperone is central to survival in stress and antibiotic resistance (Frees et al., 2014). It is also a protein predominating in the resistance of MRSA to oxacillin (Jousselin et al., 2012). Treatment of oxacillin and NLC alone moderately increased and decreased chaperone expression, respectively. The combined NLC and oxacillin exhibited an offset effect on chaperone expression. A similar trend was shown in the other two proteins with high molecular weights (DNA-directed RNA polymerase and elongation factor G).

Ribosomes, a primary target for some antibiotics, such as macrolides and tetracyclines, are a critical catalyst for substrate stabilization of *S. aureus* protein synthesis (Wall et al., 2015). Oxacillin-loaded nanocarriers might interact and deactivate ribosomal subunits in the same way that some metal nanoparticles do (Hemeg, 2017), which can lead to the obstruction of protein translation. Elongation factor Tu is responsible for the protein synthesis through translation in the ribosomes (Pereira et al., 2015). NLC in combination with the drug showed significant downregulation of both ribosomes and elongation factor Tu. The attachment of invasive phenotype *S. aureus* to the biological surface is a requirement for eliciting virulence infection. Enolase and ornithine carbamoyltransferase are the proteins on the bacterial surface for binding with extracellular matrix proteins such as fibronectin, elastin, and collagen (Hussain et al., 1999; Carneiro et al., 2004). Both surface proteins were largely decreased by NLC and oxacillin co-treatment, thus impeding the pathogenesis of MRSA in the biological system. A similar case was the significant reduction of arginine deiminase after combined treatment. Arginine deiminase is a virulence factor of bacteria in biofilm growth and intracellular survival (Lindgren et al., 2014). The presence of NLC can produce some bacterial mutation. The change of colony color on the agar plate could be due to a response to oxidative stress (Strand et al., 2003), and also indicates of the

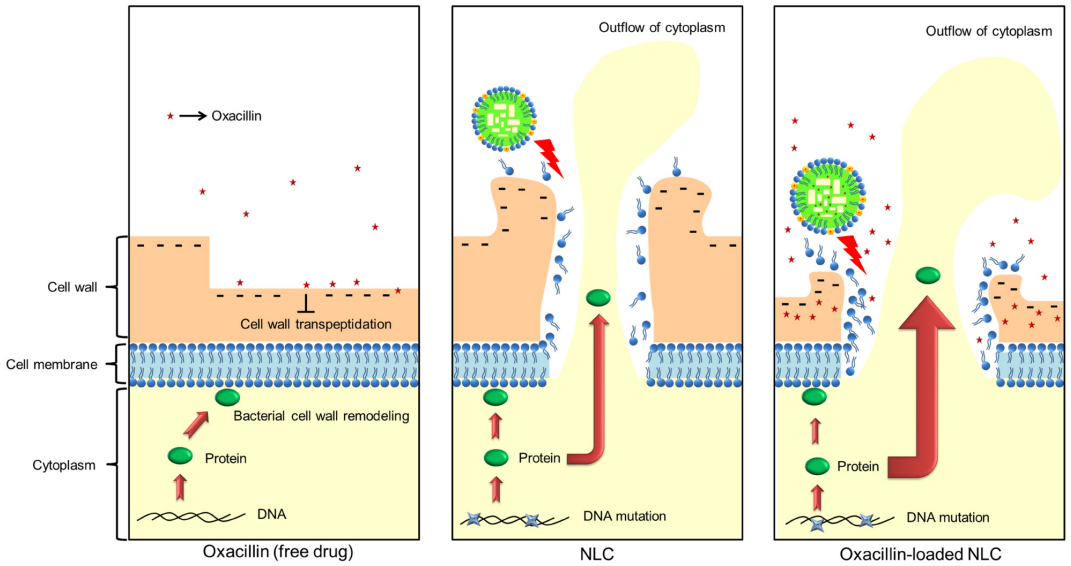

FIGURE 6 | The possible mechanisms of oxacillin and/or NLC for MRSA killing.

loss of infectious force. However, it should be noted with caution that the bacterial resistance against the antibiotics may increase after mutation. The oxacillin encapsulation was slightly reduced 24 h post-preparation. Since most of the *in vitro* and *in vivo* experiments were performed within 24 h, we believed that the structure of oxacillin-NLC complex generally remained intact during the experiments. Of course some oxacillin molecules were released from NLC nanoparticles in the nanosystem. It is our opinion that the unencapsulated oxacillin still could synergize with cationic NLC to eradicate MRSA because of the different antibacterial mechanisms of both agents. The possible mechanisms of oxacillin-loaded NLC for killing MRSA are illustrated in **Figure 6**.

The biofilm-like property of bacterial abscess in the skin weakens conventional antibiotic therapy (Han et al., 2009). MRSA contributes to cutaneous inflammation and barrier deterioration. NLC was able to diffuse into the nidus to decrease the MRSA burden and repair the barrier capacity, especially the drug-loaded NLC, which showed smaller abscess size and neutrophil infiltration compared to the NLC without the drug in the *in vivo* experiment. According to the previous studies (Hung et al., 2015), NLC would remain intact because of the soft and deformable characteristics for facile transport into the skin. The fusion of NLC in SC lipids is another possibility (Gelfuso et al., 2016). MRSA infection would damage the skin barrier function because of the formation of wound (Soong et al., 2012; Lin et al., 2017). It was possible that NLC could penetrate into the skin in the intact form. Although NLC can be a potential therapy for MRSA eradication, it is important to examine whether nanotoxicity is induced by the lipid nanocarriers. Our *in vivo* cutaneous tolerance study suggests the symptoms of erythema and excoriation on the skin surface treated by NLC. The TEWL increased 4-fold after 5 consecutive days of topical NLC administration, suggesting barrier disruption. The cutaneous irritation could be classified as mild. A previous study (Shimada et al., 2008) suggests about a 5-fold TEWL increase in dog skin after stratum corneum stripping. Another study (Yan et al., 2010) reports a 10∼25-fold increase of TEWL in rat skin receiving microneedle puncture, which is a permeation-enhancing approach. Both tape stripping and microneedles demonstrate a greater barrier loss as compared to cationic NLC.

It is well-known that quaternary ammonium-based surfactants are typical skin irritants producing some toxicity, including CPC, cetyltrimethylammonium bromide, tri(dodecyldimethylammonioacetoxyl)diethyltriamine trichloride, and benzalkonium chloride (BKC) (Kano and Sugibayashi, 2006; Zhou et al., 2016, 2017). Toxicity is usually a concern in developing antibacterial nanoparticles such as cationic surfactant-coated, zinc oxide, and silver nanoparticles (Pati et al., 2014; Pérez-Díaz et al., 2016). It is critical to improve the safety of cationic nanocarriers while maintaining the antibacterial effect. We had screened a series of cationic surfactants for the cytotoxicity and found that SME demonstrated a wider therapeutic window than the others such as CPC and BKC (Yang et al., 2016). Our previous result approved a safe use of SME. It is the reason why we employed SME in the study.

CONCLUSION

We assembled cationic NLC to load oxacillin as a drug-delivery nanosystem for MRSA infection therapy. Since oxacillin encapsulation in NLC achieved > 70%, the free oxacillin was also present in the nanosystems. However, the high loading efficiency of NLC for oxacillin led to the elucidation that the synergistic anti-MRSA effect was mainly attributed to the oxacillin-NLC complex but not free drug or NLC alone. The combined NLC and oxacillin showed lower MBC against MRSA compared to

individual treatment. NLC and oxacillin co-treatment increased the efficacy against MRSA residing both extracellularly and intracellularly. The combination was superior in eradicating biofilm compared to mono treatment. Topical administration of oxacillin-loaded nanoparticles significantly reduced cutaneous infection and improved skin barrier function and architecture. NLC has potential for use in combination with antibiotic against MRSA, especially with the currently increasing drug resistance among microbial species. The dose and dosage interval can be reduced with this association. The reduced dose, easy scale-up fabrication, and inexpensiveness of the SME-coated NLC may lessen the expenditure needed for antibacterial therapy. Our nanocarriers can be potential candidates for topical treatment of MRSA infection.

AUTHOR CONTRIBUTIONS

AA and J-YF conceived and designed the experiments. P-WW, Y-PC, and S-CY performed the experiments. AA, Y-PC, and S-CY analyzed the data. P-WW and P-LL contributed reagents, materials, and analysis tools. AA, J-YF, and S-CY wrote the paper.

FUNDING

The authors are grateful to the financial support by Chang Gung Memorial Hospital (CMRPD1F0231-3 and CMRPG2 G0661-3).

REFERENCES

Abee, T., Kovacs, A. T., Kuipers, O. P., and van der Veen, S. (2011). Biofilm formation and dispersal in Gram-positive bacteria. *Curr. Opin. Biotechnol.* 22, 172–179. doi: 10.1016/j.copbio.2010.10.016

Argenziano, M., Banche, G., Luganini, A., Finesso, N., Allizond, V., Gulino, G. R., et al. (2017). Vancomycin-loaded nanobubbles: a new platform for controlled antibiotic delivery against methicillin-resistant *Staphylococcus aureus* infections. *Int. J. Pharm.* 523, 176–188. doi: 10.1016/j.ijpharm.2017.03.033

Baelo, A., Levato, R., Julián, E., Crespo, A., Astola, J., Gavaldà, J., et al. (2015). Disassembling bacterial extracellular matrix with DNase-coated nanoparticles to enhance antibiotic delivery in biofilm infections. *J. Control. Release* 209, 150–158. doi: 10.1016/j.jconrel.2015.04.028

Banche, G., Prato, M., Magnetto, C., Allizond, V., Giribaldi, G., Argenziano, M., et al. (2015). Antimicrobial chitosan nanodroplets: new insights for ultrasound-mediated adjuvant treatment of skin infection. *Future Microbiol.* 10, 929–939. doi: 10.2217/fmb.15.27

Basri, D. F., and Sandra, V. (2016). Synergistic interaction of methanol extract from *Canarium odontophyllum* Miq. Leaf in combination with oxacillin against methicillin-resistant *Staphylococcus aureus* (MRSA) ATCC 33591. *Int. J. Microbiol.* 2016:5249534. doi: 10.1155/2016/5249534

Bassolé, I. H. N., and Juliani, H. R. (2012). Essential oils in combination and their antimicrobial properties. *Molecules* 17, 3989–4006. doi: 10.3390/molecules17043989

Carneiro, C. R. W., Postol, E., Nomizo, R., Reis, L. F. L., and Brentani, R. R. (2004). Identification of enolase as a laminin-binding protein on the surface of *Staphylococcus aureus*. *Microbes Infect.* 6, 604–608. doi: 10.1016/j.micinf.2004.02.003

Cheow, W. S., Chang, M. W., and Hadinoto, K. (2011). The roles of lipid in anti-biofilm efficacy of lipid-polymer hybrid nanoparticles encapsulating antibiotics. *Colloids Surf. A* 389, 158–165. doi: 10.1016/j.colsurfa.2011.08.035

Cihalova, K., Chudobova, D., Michalek, P., Moulick, A., Guran, R., Kopel, P., et al. (2015). *Staphylococcus aureus* and MRSA growth and biofilm formation after treatment with antibiotics and SeNPs. *Int. J. Mol. Sci.* 16, 24656–24672. doi: 10.3390/ijms161024656

Colomer, A., Perez, L., Pons, R., Infante, M. R., Perez-Clos, D., Manresa, A., et al. (2013). Mixed monolayer of DPPC and lysine-based cationic surfactants: an investigation into the antimicrobial activity. *Langmuir* 29, 7912–7921. doi: 10.1021/la401092j

Dréno, B., Araviiskaia, E., Berardesca, E., Gontijo, G., Sanchez Viera, M., Xiang, L. F., et al. (2016). Microbiome in healthy skin, update for dermatologists. *J. Eur. Acad. Dermatol. Venereol.* 30, 2038–2047. doi: 10.1111/jdv.13965

Frees, D., Gerth, U., and Ingmer, H. (2014). Clp chaperones and proteases are central in stress survival, virulence and antibiotic resistance of *Staphylococcus aureus*. *Int. J. Med. Microbiol.* 304, 142–149. doi: 10.1016/j.ijmm.2013.11.009

Gelfuso, G. M., Cunha-Filho, M. S., and Gratieri, T. (2016). Nanostructured lipid carriers for targeting drug delivery to the epidermal layer. *Ther. Deliv.* 7, 735–737. doi: 10.4155/tde-2016-0059

Han, G., Martinez, L. R., Mihu, M. R., Friedman, A. J., Friedman, J. M., and Nosanchuk, J. D. (2009). Nitric oxide releasing nanoparticles are therapeutic for *Staphylococcus aureus* abscesses in a murine model of infection. *PLoS One* 4:e7804. doi: 10.1371/journal.pone.0007804

Hemeg, H. A. (2017). Nanomaterials for alternative antibacterial therapy. *Int. J. Nanomed.* 12, 8211–8225. doi: 10.2147/IJN.S132163

Henson, K. E. R., Yim, J., Smith, J. R., Sakoulas, G., and Rybak, M. J. (2017). β-lactamase inhibitors enhance the synergy between β-lactam antibiotics and daptomycin against methicillin-resistant *Staphylococcus aureus*. *Antimicrob. Agents Chemother.* 61:e1564-16. doi: 10.1128/AAC.01564-16

Hsu, C. Y., Yang, S. C., Sung, C. T., Weng, Y. H., and Fang, J. Y. (2017). Anti-MRSA malleable liposomes carrying chloramphenicol for ameliorating hair follicle targeting. *Int. J. Nanomed.* 12, 8227–8238. doi: 10.2147/IJN.S147226

Hung, C. F., Chen, W. Y., Hsu, C. Y., Aljuffali, I. A., Shih, H. C., and Fang, J. Y. (2015). Cutaneous penetration of soft nanoparticles via photodamaged skin: lipid-based and polymer-based nanocarriers for drug delivery. *Eur. J. Pharm. Biopharm.* 94, 94–105. doi: 10.1016/j.ejpb.2015.05.005

Hussain, M., Peters, G., Chhatwal, G. S., and Herrmann, M. (1999). A lithium chloride-extracted, broad-spectrum-adhesive 42-kilodalton protein of *Staphylococcus epidermidis* is ornithine carbamoyltransferase. *Infect. Immun.* 67, 6688–6690.

Hwang, T. L., Hsu, C. Y., Aljuffali, I. A., Chen, C. H., Chang, Y. T., and Fang, J. Y. (2015). Cationic liposomes evoke inflammatory responses and neutrophil extracellular traps (NETs) toward human neutrophils. *Colloids Surf. B* 128, 119–126. doi: 10.1016/j.colsurfb.2015.02.022

Hwang, Y. Y., Ramalingam, K., Bienek, D. R., Lee, V., You, T., and Alvarez, R. (2013). Antimicrobial activity of nanoemulsion in combination with cetylpyridinium chloride in multidrug-resistant *Acinetobacter baumannii*. *Antimicrob. Agents Chemother.* 57, 3568–3575. doi: 10.1128/AAC.02109-12

Jousselin, A., Renzoni, A., Andrey, D. O., Monod, A., Lew, D. P., and Kelly, W. L. (2012). The posttranslocational chaperone lipoprotein Prs A is involved in both glycopeptides and oxacillin resistance in *Staphylococcus aureus*. *Antimicrob. Agents Chemother.* 56, 3629–3640. doi: 10.1128/AAC.06264-11

Kano, S., and Sugibayashi, K. (2006). Kinetic analysis on the skin disposition of cytotoxicity as an index of skin irritation produced by cetylpyridinium chloride: comparison of in vitro data using a three-dimensional cultured human skin model with in vivo results in hairless mice. *Pharm. Res.* 23, 329–335. doi: 10.1007/s11095-006-9141-z

Lin, M. H., Hung, C. F., Aljuffali, I. A., Sung, C. T., Huang, C. T., and Fang, J. Y. (2017). Cationic amphiphile in phospholipid bilayer or oil-water interface of nanocarriers affects planktonic and biofilm bacteria killing. *Nanomedicine* 13, 353–361. doi: 10.1016/j.nano.2016.08.011

Lindgren, J. K., Thomas, V. C., Olson, M. E., Chaudhari, S. S., Nuxoll, A. S., Schaeffer, C. R., et al. (2014). Arginine deiminase in *Staphylococcus epidermidis* functions to augment biofilm maturation through pH homeostasis. *J. Bacteriol.* 196, 2277–2289. doi: 10.1128/JB.00051-14

May, R. C., and Machesky, L. M. (2001). Phagocytosis and the actin cytoskeleton. *J. Cell Sci.* 114, 1061–1077.

Pan, T. L., Wang, P. W., Al-Suwayeh, S. A., Chen, C. C., and Fang, J. Y. (2010). Skin toxicology of lead species evaluated by their permeability and proteomic profiles: a comparison of organic and inorganic lead. *Toxicol. Lett.* 197, 19–28. doi: 10.1016/j.toxlet.2010.04.019

Pati, R., Mehta, R. K., Mohanty, S., Padhi, A., Sengupta, M., Vaseeharan, B., et al. (2014). Topical application of zinc oxide nanoparticles reduces bacterial skin infection in mice and exhibits antibacterial activity by inducing oxidative stress response and cell membrane disintegration in macrophages. *Nanomedicine* 10, 1195–1208. doi: 10.1016/j.nano.2014.02.012

Pereira, S. F. F., Gonzalez, R. L., and Dworkin, J. (2015). Protein synthesis during cellular quiescence is inhibited by phosphorylation of a translational elongation factor. *Proc. Natl. Acad. Sci. U.S.A.* 112, E3274–E3281. doi: 10.1073/pnas.1505297112

Pérez-Díaz, M., Alvarado-Gomez, E., Magaña-Aquino, M., Sánchez-Sánchez, R., Velasquillo, C., Gonzalez, C., et al. (2016). Anti-biofilm activity of chitosan gels formulated with silver nanoparticles and their cytotoxic effect on human fibroblasts. *Mater. Sci. Eng. C* 60, 317–323. doi: 10.1016/j.msec.2015.11.036

Qin, R., Xiao, K., Li, B., Jiang, W., Peng, W., Zheng, J., et al. (2013). The combination of catechin and epicatechin gallate from *Fructus crataegi* potentiates β-lactam antibiotics against methicillin-resistant *Staphylococcus aureus* (MRSA) in vitro and in vivo. *Int. J. Mol. Sci.* 14, 1802–1821. doi: 10.3390/ijms14011802

Radovic-Moreno, A. F., Lu, T. K., Puscasu, V. A., Yoon, C. J., Langer, R., and Farokhad, O. C. (2012). Surface charge-switching polymeric nanoparticles for bacterial cell wall-targeted delivery of antibiotics. *ACS Nano* 6, 4279–4287. doi: 10.1021/nn3008383

Richter, K., Facal, P., Thomas, N., Vandecandelaere, I., Ramezanpour, M., Cooksley, C., et al. (2017). Taking the silver bullet colloidal silver particles for the topical treatment of biofilm-related infections. *ACS Appl. Mater. Interfaces* 9, 21631–21638. doi: 10.1021/acsami.7b03672

Rodvold, K. A., and McConeghy, K. W. (2014). Methicillin-resistant *Staphylococcus aureus* therapy: past, present, and future. *Clin. Infect. Dis.* 58(Suppl. 1), S20–S27. doi: 10.1093/cid/cit614

Shimada, K., Yoshihara, T., Yamamoto, M., Konno, K., Momoi, Y., Nishifuji, K., et al. (2008). Transepidermal water loss (TEWL) reflects skin barrier function of dog. *J. Vet. Med. Sci.* 70, 841–843. doi: 10.1292/jvms.70.841

Soong, G., Chun, J., Parker, D., and Prince, A. (2012). *Staphylococcus aureus* activation of caspase 1/calpain signaling mediates invasion through human keratinocytes. *J. Infect. Dis.* 205, 1571–1579. doi: 10.1093/infdis/jis244

Strand, M. K., Stuart, G. R., Longley, M. J., Graziewicz, M. A., Dominick, O. C., and Copeland, W. C. (2003). *POS5* gene of *Saccharomyces cerevisiae* encodes a mitochondrial NADH kinase required for stability of mitochondrial DNA. *Eukaryot. Cell* 2, 809–820. doi: 10.1128/EC.2.4.809-820.2003

Tavano, L., Pinazo, A., Abo-Riya, M., Infante, M. R., Manresa, M. A., Muzzalupo, R., et al. (2014). Cationic vesicles based on biocompatible diacyl glycerol-arginine surfactants: physicochemical properties, antimicrobial activity, encapsulation efficiency and drug release. *Colloids Surf. B* 120, 160–167. doi: 10.1016/j.colsurfb.2014.04.009

Thomsen, M. K., Rasmussen, M., Fuursted, K., Westh, H., Pedersen, L. N., Deleuran, M., et al. (2006). Clonal spread of *Staphylococcus aureus* with reduced susceptibility to oxacillin in a dermatological hospital unit. *Acta Derm. Venereol.* 86, 230–234. doi: 10.2340/00015555-0072

Tong, S. Y. C., Davis, J. S., Eichenberger, E., Holland, T. L., and Fowler, V. G. (2015). *Staphylococcus aureus* infections: epidemiology, pathophysiology, clinical manifestations, and management. *Clin. Microbiol. Rev.* 28, 603–661. doi: 10.1128/CMR.00134-14

Wall, E. A., Caufield, J. H., Lyons, C. E., Manning, K. A., Dokland, T., and Christie, G. E. (2015). Specific N-terminal cleavage of ribosomal protein L27 in *Staphylococcus aureus* and related bacteria. *Mol. Microbiol.* 95, 258–269. doi: 10.1111/mmi.12862

Xie, S., Tao, Y., Pan, Y., Qu, W., Cheng, G., Huang, L., et al. (2014). Biodegradable nanoparticles for intracellular delivery of antimicrobial agents. *J. Control. Release* 187, 101–117. doi: 10.1016/j.jconrel.2014.05.034

Yan, G., Warner, K. S., Zhang, J., Sharma, S., and Gale, B. K. (2010). Evaluation needle length and density of microneedle arrays in the pretreatment of skin for transdermal drug delivery. *Int. J. Pharm.* 391, 7–12. doi: 10.1016/j.ijpharm.2010.02.007

Yang, S. C., Aljuffali, I. A., Sung, C. T., Lin, C. F., and Fang, J. Y. (2016). Antimicrobial activity of topically-applied soyaethyl morpholinium ethosulfate micelles against *Staphylococcus* species. *Nanomedicine* 11, 657–671. doi: 10.2217/nnm.15.217

Zazo, H., Colino, C. I., and Lanao, J. M. (2016). Current applications of nanoparticles in infectious disease. *J. Control. Release* 224, 86–102. doi: 10.1016/j.jconrel.2016.01.008

Zhou, C., Wang, D., Cao, M., Chen, Y., Liu, Z., Wu, C., et al. (2016). Self-aggregation, antibacterial activity, and mildness of cyclodextrin/cationic trimeric surfactant complexes. *ACS Appl. Mater. Interfaces* 8, 30811–30823. doi: 10.1021/acsami.6b11667

Zhou, C., Wang, H., Bai, H., Zhang, P., Liu, L., Wang, S., et al. (2017). Tuning antibacterial activity of cyclodextrin-attached cationic ammonium surfactants by a supramolecular approach. *ACS Appl. Mater. Interfaces* 9, 31657–31666. doi: 10.1021/acsami.7b11528

Conflict of Interest Statement: The authors declare that the research was conducted in the absence of any commercial or financial relationships that could be construed as a potential conflict of interest.

frontiers in Microbiology

ORIGINAL RESEARCH
published: 11 May 2018
doi: 10.3389/fmicb.2018.00917

Safety and Efficacy of Topical Chitogel- Deferiprone-Gallium Protoporphyrin in Sheep Model

*Mian L. Ooi[1], Katharina Richter[1,2], Amanda J. Drilling[1], Nicky Thomas[2,3], Clive A. Prestidge[3], Craig James[4], Stephen Moratti[5], Sarah Vreugde[1], Alkis J. Psaltis[1] and Peter-John Wormald[1]**

[1] Department of Surgery- Otolaryngology, Head and Neck Surgery, Basil Hetzel Institute for Translational Health Research, The University of Adelaide, Adelaide, SA, Australia, [2] Adelaide Biofilm Test Facility, Sansom Institute for Health Research, University of South Australia, Adelaide, SA, Australia, [3] School of Pharmacy and Medical Sciences, University of South Australia, Adelaide, SA, Australia, [4] Clinpath Laboratories, Adelaide, SA, Australia, [5] Department of Chemistry, Otago University, Dunedin, New Zealand

OPEN ACCESS

Edited by:
Mariana Henriques, University of Minho, Portugal

Reviewed by:
Airat R. Kayumov, Kazan Federal University, Russia
Nagendran Tharmalingam, Alpert Medical School, United States

***Correspondence:**
Peter-John Wormald
peterj.wormald@adelaide.edu.au

Specialty section:
This article was submitted to Antimicrobials, Resistance and Chemotherapy, a section of the journal Frontiers in Microbiology

Received: *25 January 2018*
Accepted: *20 April 2018*
Published: *11 May 2018*

Citation:
Ooi ML, Richter K, Drilling AJ, Thomas N, Prestidge CA, James C, Moratti S, Vreugde S, Psaltis AJ and Wormald P-J (2018) Safety and Efficacy of Topical Chitogel-Deferiprone-Gallium Protoporphyrin in Sheep Model. Front. Microbiol. 9:917. doi: 10.3389/fmicb.2018.00917

Objectives: Increasing antimicrobial resistance has presented new challenges to the treatment of recalcitrant chronic rhinosinusitis fuelling a continuous search for novel antibiofilm agents. This study aimed to assess the safety and efficacy of Chitogel (Chitogel®, Wellington New Zealand) combined with novel antibiofilm agents Deferiprone and Gallium Protoporphyrin (CG-DG) as a topical treatment against *S. aureus* biofilms *in vivo*.

Methods: To assess safety, 8 sheep were divided into two groups of 7 day treatments (n = 8 sinuses per treatment); (1) Chitogel (CG) with twice daily saline flush, and (2) CG-DG gel with twice daily saline flush. Tissue morphology was analyzed using histology and scanning electron microscopy (SEM). To assess efficacy we used a *S. aureus* sheep sinusitis model. Fifteen sheep were divided into three groups of 7 day treatments (n = 10 sinuses per treatment); (1) twice daily saline flush (NT), (2) Chitogel (CG) with twice daily saline flush, and (3) CG-DG gel with twice daily saline flush. Biofilm biomass across all groups was compared using LIVE/DEAD BacLight stain and confocal scanning laser microscopy.

Results: Safety study showed no cilia denudation on scanning electron microscopy and no change in sinus mucosa histopathology when comparing CG-DG to CG treated sheep. COMSTAT2 assessment of biofilm biomass showed a significant reduction in CG-DG treated sheep compared to NT controls.

Conclusion: Results indicate that CG-DG is safe and effective against *S. aureus* biofilms in a sheep sinusitis model and could represent a viable treatment option in the clinical setting.

Keywords: chronic rhinosinusitis, *Staphylococcus aureus*, biofilm, Chitogel, Deferiprone, Gallium Protoporphyrin, topical agents, antimicrobial therapy

INTRODUCTION

Recalcitrant chronic rhinosinusitis is a difficult clinical entity to manage. Bacterial biofilms contribute to disease recalcitrance and have been shown to be associated with more severe disease (Bendouah et al., 2006; Psaltis et al., 2008; Singhal et al., 2010, 2011). Although oral antibiotics are frequently ineffective against biofilms (Costerton, 1995), it remains the only option available to achieve symptom control for many recalcitrant patients. However, with the growing prevalence of resistance to first-line antibiotics (World Health Organization, 2016) and the lack of research and development of new antibiotics (Conly and Johnston, 2005; World Health Organization, 2017), novel topical anti-biofilm agents are needed to help improve the outcomes in these patients.

Richter et al. first described the potent synergistic antimicrobial properties of Deferiprone and Gallium Protoporphyrin (DG) (Richter et al., 2016, 2017a,b). This agent targets the iron metabolism that is crucial for bacterial growth and survival (Braun, 2001; Weinberg, 2009). Deferiprone is an iron chelator approved by the U.S. Food and Drug Administration to treat thalassaemia major. Gallium Protoporphyrin IX is a heme analog with strong antibacterial activity against gram-positive bacteria, gram-negative bacteria and mycobacteria (Stojiljkovic et al., 1999; Hijazi et al., 2017). Gallium Protoporphyrin IX has been shown to kill *S. aureus* and Methicillin Resistant *S. aureus* (MRSA) in planktonic, biofilm and small colony variant form and has been shown to enhance the antimicrobial properties of commonly used antibiotics (Richter et al., 2017c). Deferiprone is thought to chelate iron from the bacteria's surrounding environment, forcing the bacteria to upregulate their iron transporter proteins. Deferiprone-dependent increased expression of iron transporter proteins are thought to enhance Gallium Protoporphyrin IX uptake into bacterial cells, thereby augmenting bacterial killing efficacy (Richter et al., 2016, 2017b). Consequently, the synergistic antimicrobial effects are observed mainly when Deferiprone and Gallium Protoporphyrin IX are given consecutively (Richter et al., 2016).

In this study, DG is incorporated within Chitogel (chitosan and dextran), a surgical hydrogel FDA approved for the use after sinus surgery, which acts as a drug carrier, that can be applied topically to fill the sinus cavities. The gel has been shown to allow the immediate and complete release of Deferiprone whilst Gallium Protoporphyrin IX is released more slowly (Richter et al., 2017b). This topical application allows higher concentration of drugs to be used for a localized action with less systemic side effects. The mucoadhesive properties of the hydrogel also increases contact time of these topical agents with the sinus mucosa and biofilms (Illum et al., 1994; Nakamura et al., 1999) augmenting its anti-biofilm effects.

The aims of this study were to assess the safety of CG-DG on healthy sinus mucosa and evaluate its efficacy as an anti-biofilm agent in a previously validated *S. aureus* biofilm-induced sheep sinusitis model.

Abbreviations: CG, Chitogel; CG-DG, Chitogel- Deferiprone-Gallium Protoporphyrin; GaPP, Gallium Protoporphyrin; SEM, scanning electron microscopy; CRS, chronic rhinosinusitis.

MATERIALS AND METHODS

This study was approved by the Animal Ethics Committee of both The University of Adelaide and the South Australian Health and Medical Research Institute (SAHMRI).

Animals

Twenty three male merino sheep between 2 and 4 dental age (1–2 years of age) were used. All animals were drenched to eradicate the parasite *Oestrus Ovis*. Fifteen sheep were allocated to the efficacy arm and 8 to the safety arm. For the efficacy arm 5 sheep were randomized to each efficacy group (i) Twice daily saline flush (NT), (ii) Chitogel (CG) and (iii) Chitogel- Deferiprone-Gallium Protoporphyrin (CG-DG). For the safety arm, 4 sheep were randomized to each safety group (i) Chitogel (CG) and (ii) Chitogel- Deferiprone-Gallium Protoporphyrin (CG-DG).

Bacterial Inoculum

A known biofilm-forming reference strain of S. *aureus*, American Type Culture Collection (ATCC) 25923, was supplied by the Department of Microbiology, TQEH. A frozen glycerol stock was defrosted and subcultured overnight in 3 mL of nutrient broth (Oxoid, Adelaide, Australia) on a shaker at 37°C for 24 h before being transferred to a 1% nutrient agar plate (Oxoid). The plate was incubated at 37°C for 16–18 h, at which point a single colony forming unit (CFU) was diluted in 0.45% sterile saline to 0.5 McFarland standard and transferred on ice for instillation into sheep sinuses.

Chitogel

The Chitogel is made up of a combination of three components; 5% succinyl-chitosan, 0.3% phosphate buffer and 3% dextran aldehyde (Chitogel®, Wellington, NZ). The components are manufactured and sterilized by Chitogel®. All stocks were stored at room temperature.

Deferiprone and Gallium Protoporphyrin

Deferiprone (3-hydroxy-1,2-dimethylpyridin-4(1*H*)-one) (Sigma-Aldrich, St Louis, USA) and Gallium Protoporphyrin IX (Ga-PP IX) (Frontier Scientific, Logan, USA) were stored at room temperature.

Preparation of Chitogel

Dextran aldehyde (0.3 g) was dissolved in 10 mL of phosphate buffer then mixed with succinyl chitosan solution (0.5 g in 10 mL buffer) using sterile technique.

Preparation of Chitogel-Deferiprone-Gallium Protoporphyrin

Deferiprone (20 mM) and Gallium Protoporphyrin (250 μg/mL) were diluted in 10 mL of phosphate buffer under sterile conditions the day before use. This prepared solution was then used to dissolve dextran aldehyde prior to mixing with 10 mL of succinyl chitosan using sterile techniques.

Anaesthetic Protocol

For every surgical procedure, all sheep underwent general anesthesia given by an experienced animal handler. Intravenous phenobarbitone was given at induction (19 mg/kg) and sheep were intubated and placed onto 1.5–2% inhalation isoflurane to maintain anesthesia. Each sheep was placed in a supine position on a wooden cradle and supported on a head ring with neck slightly flexed. Each nasal cavity was sprayed twice with Cophenylcaine Forte (ENT Technologies Pty Ltd., Australia) 10 min prior to any procedures.

Surgical Protocol

As per protocol all sheep underwent middle turbinectomy and anterior ethmoid complex resection, which is then followed by a 3–4 week convalescence period. Frontal trephination was later performed by placing mini trephines bilaterally on the sheep's forehead, 1cm lateral from the midline and along a line connecting the superior aspect of the orbital rims. The placement of trephines was confirmed when fluorescein flushed via trephines (0.1 mL diluted in 100 mL of physiological saline) was visualized to be draining from the frontal sinus ostium.

Safety Arm

In the safety arm, following frontal trephination, the gels were instilled into each sinus cavity via mini trephines until gel extrusion from the frontal sinus ostium was visualized under direct endoscopic view. The mini trephines were then capped. Gel instilled was left undisturbed within the sinus cavities for 24 h before beginning sinus irrigation via mini trephines with 15 mL of sterile physiological saline twice a day. On day 8, all safety sheep were euthanized and sinus mucosa harvested for histopathological and SEM analysis.

Efficacy Arm

In the efficacy arm, following frontal trephination the frontal ostia were packed with petroleum gauze (Vaseline, Kendall, Mansfield, MA). 1 mL of 0.5 McFarland Units of *S. aureus* was then instilled into each sinus cavity via mini trephines and capped. Bacterial biofilms were allowed to form over the next 7 days. On day 8, the petroleum gauze was removed and each sheep was randomly assigned into one of three efficacy groups (i) Twice daily saline flush (NT), (ii) Chitogel (CG) and (iii) Chitogel- Deferiprone-Gallium Protoporphyrin (CG-DG). For sheep assigned to gel groups (ii) and (iii), the gels were instilled into each sinus cavity via mini trephines until gel extrusion from the frontal sinus ostium was visualized under direct endoscopic view. The mini trephines were then capped. For all groups, sinuses were irrigated 24 h later with 15 mL of sterile physiological saline twice a day for the remaining 6 days of treatment. On day 8, all sheep were euthanized and sinus mucosa harvested for histopathological analysis and biofilm biomass imaging.

Safety Analysis

Histopathology Evaluation

One 1 × 1 cm mucosal section from each sinus was fixed in 2% formalin solution and sent for histopathology preparation (Adelaide Pathology and Partners, Adelaide, Australia). Samples were embedded in paraffin and stained with hematoxylin & eosin. Microscopic evaluation of tissue damage and inflammation was performed by a pathologist blinded to all clinical data using light microscopy (Eclipse 90i, Nikon instruments Inc, Melville, NY).

Scanning Electron Microscopy Evaluation

From each sinus, a sample of 5 × 5 mm tissue was obtained, sonicated in saline, then submerged in SEM fixative (4% paraformaldehyde/1.25% glutaraldehyde in PBS + 4% sucrose, pH 7.2) for at least 24 h. Tissues were washed in a washing buffer (PBS + 4% sucrose) for 5 min then post fixed in 2% OsO_4 in water for 1 h. All samples underwent a graded dehydration of 70, 90, and 100% ethanol, then dried using hexamethyldisilazane (HMDS). Following that, all tissues were mounted on stubs and carbon coated. Images were taken using an XL30 Field Emission Gun Scanning Electron Microscope (Phillips, Eindhoven, Netherlands).

Quantification of Plasma Deferiprone and Gallium Protoporphyrin Levels

Plasma samples were analyzed for Deferiprone and GaPP using high performance liquid chromatography (HPLC) on a Shimadzu UFLC XR (Shimadzu Cooperation, Kyoto, Japan). For the quantification of Deferiprone, 250 μl plasma was mixed with 750 μl methanol (HPLC grade, Merck, Darmstadt, Germany). The samples were vortexed for 1 min and centrifuged for 4 min at 14,800 rpm at room temperature (Eppendorf 5804R, Eppendorf, Hamburg, Germany). The clear supernatant (50 μl) was quantified on a Phenomenex Synergi 4 μm Fusion-RP LC column coupled to a security guard cartridge (Phenomenex, Lane Cove, NSW, Australia) using methanol/0.1 M orthophosphate buffer pH 7.2 (15%: 85%) as mobile phase at a flow rate of 2.0 ml/min. The Deferiprone concentration was detected at 280 nm and calculated against a standard curve ranging from 1.0 to 10.0 μg/ml Deferiprone ($R^2 > 0.992$). For the quantification of GaPP, solid phase extraction (SPE) was performed using Oasis PRiME HLB cartridges 1 cc/30 mg (Waters, Dundas, NSW, Australia). Samples were prepared according to the manufacturer's protocol. Briefly, 250 μl plasma was mixed with 250 μl orthophosphoric acid (4%) and placed in a SPE cartridge. After washing with 5% methanol in Milli-Q water, 500 μl methanol was used to elute GaPP. The clear eluate (50 μl) was quantified using methanol/0.1 M orthophosphate buffer pH 7.2 (70%: 30%) as mobile phase at a flow rate of 1.0 ml/min. The GaPP concentration was detected at 405 nm and calculated against a standard curve ranging from 0.02 to 10.0 μg/ml GaPP ($R^2 > 0.995$).

Efficacy Analysis

Biofilm Biomass

Method of biofilm analysis were as described in previous studies (Ha et al., 2007; Singhal et al., 2012; Drilling et al., 2014; Paramasivan et al., 2014b; Rajiv et al., 2015). Two random 1 × 1 cm mucosal sections from each sinus were sampled. Each

sample was briefly immersed in phosphate buffered solution to wash off planktonic cells and stained with LIVE/DEAD BacLight stain (Life Technology, Mulgrave, VIC, Australia) as per manufacturer's instructions. Biofilm biomass was assessed using confocal scanning laser microscope (LSM 710, Zeiss, Germany). Within each sample 3 of the areas with highest biofilm presence had axial Z stacks recorded to construct a 3D virtual image of the overlying tissue mucosa and biofilm, making a total of 6 Z-stack images per sinus. Eighty individual images of each representative area were taken as one Z stack image (Image properties: line average 4, 512 × 512 pixels, Z-stack 80 steps). The COMSTAT2 computer software (Lyngby, Denmark) was utilized to quantify biofilm biomass in each Z-stack (Heydorn et al., 2000; Klinger-Strobel et al., 2016).

Histopathology Grading

One 1 × 1 cm mucosal section from each sinus was fixed in 2% formalin solution and sent for histopathology preparation (Adelaide Pathology and Partners). Samples were embedded in paraffin and stained with hematoxylin & eosin. Microscopic evaluation and tissue grading was performed by a pathologist blinded to all clinical data using light microscopy (Eclipse 90i, Nikon instruments Inc, Melville, NY). Degree of inflammation (lymphocytes, plasma cells, histiocytes and mast cells), acute inflammation (neutrophils), oedema, fibrosis and cilia were graded using an arbitrary scale (Boase et al., 2013; Drilling et al., 2014; Rajiv et al., 2015). Degree of inflammation, oedema and fibrosis were each graded from 0 to 3; 0 = none, 1 = mild, 2 = moderate, 3 = severe. Acute inflammation was graded from 0 to 2; 0 = none, 1 = mild, 2 = severe. Cilia were graded as minimal loss, focal loss, moderate loss, severe loss.

Statistical Analysis

Comparison of mucosal biofilms between treatment groups were analyzed using Kruskal Wallis One-way analysis of variance (ANOVA) with Dunn's multiple comparison test. Comparison of histopathology grading between treatment groups in the efficacy arm were analyzed using Two-way analysis of variance (ANOVA) with Dunnett's multiple comparison test. Statistical significance was considered at $p < 0.05$. All statistical tests were done using GraphPad Prism 7.0b software (San Diego, CA).

RESULTS

Safety Arm

Histopathological Analysis

Similar mucosal architecture was noted in all sinus samples obtained from CG and CG-DG treated groups, showing a pseudostratified columnar epithelial layer intersected with goblet cells. No squamous metaplasia of epithelium was identified in any samples (**Figure 1**). These images reflect that the test treatments are safe to apply topically to sinus mucosa.

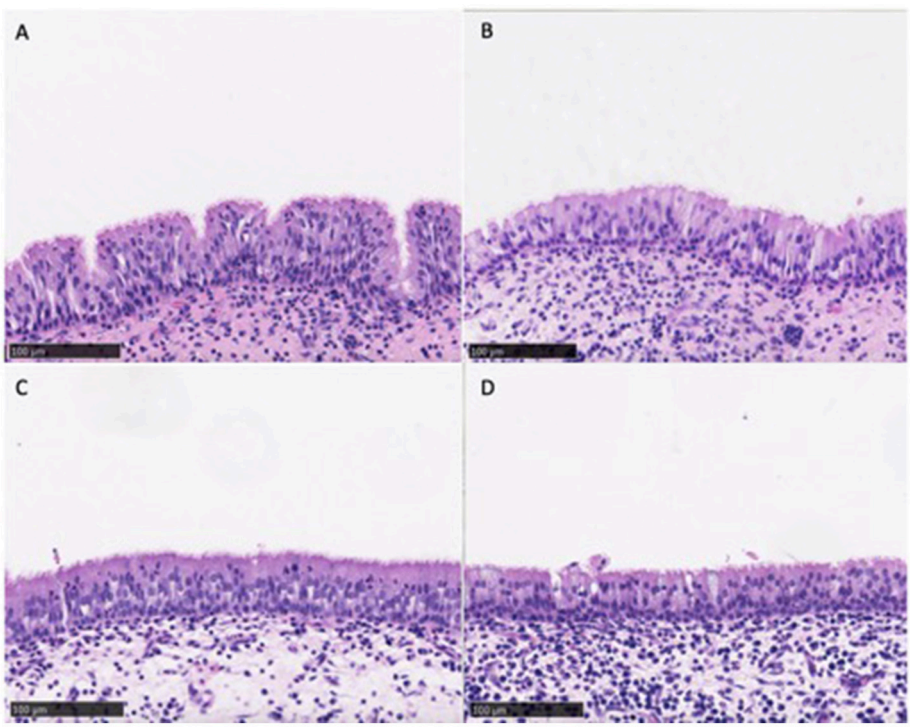

FIGURE 1 | Representative images of sinus mucosa histology harvested from sheep in the safety arm treated with CD **(A,B)** and CD-DG **(C,D)**. All sinus mucosa showed pseudostratified columnar epithelial layer with no metaplasia, indicating that test treatments were safe for sinus topical application. CG, Chitogel; CG-DG, Chitogel- Deferiprone-Gallium Protoporphyrin.

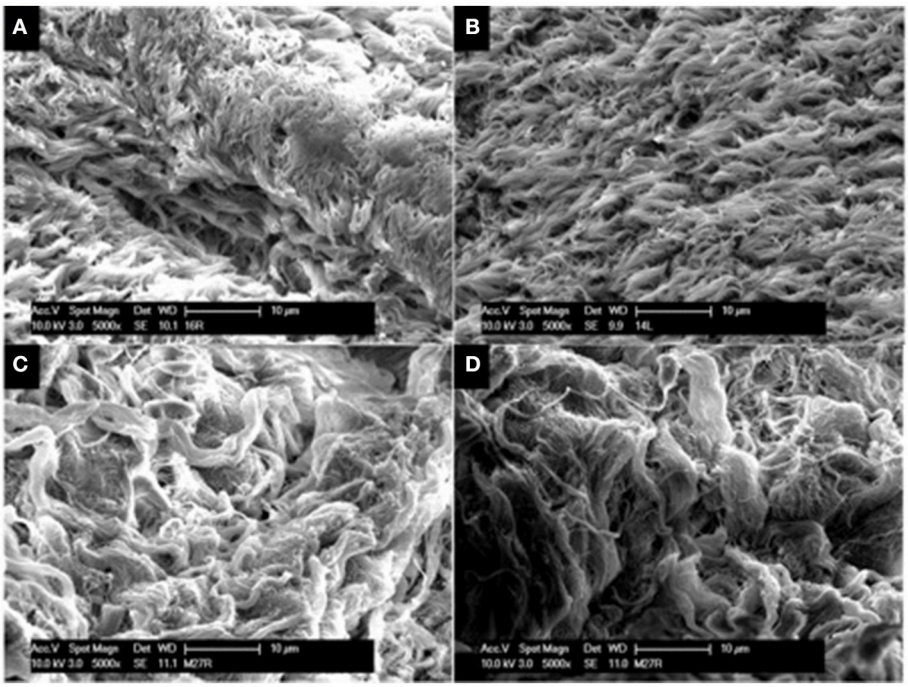

FIGURE 2 | Representative SEM images of sinus mucosa harvested from sheep in the safety arm treated with CG gel **(A,B)** and CG-DG gel **(C,D)**. SEM allowed assessment for ciliary presence and morphology on sinus mucosa. No ciliary denudation were observed in both treated groups, indicating that test treatments were not ciliotoxic. CG, Chitogel; CG-DG, Chitogel- Deferiprone-Gallium Protoporphyrin.

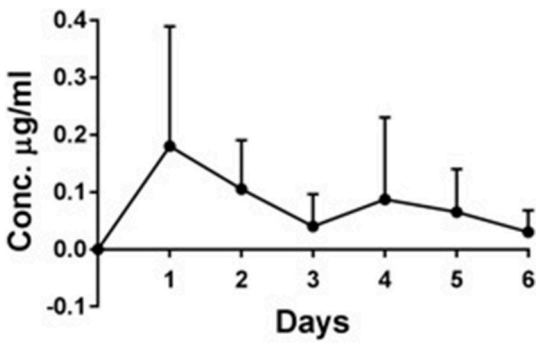

FIGURE 3 | *In vivo* plasma concentration (µg/ml) ± standard deviation of deferiprone over 6 days, $n = 4$. Maximum Deferiprone plasma level of 0.18 µg/ml was detected at day 1 of topical application to sinuses, which is 110 times less than one oral dose of Deferiprone. No GaPP was detected in the plasma of all 4 sheep treated with CG-DG (data not shown). This indicates that CG-DG has negligible systemic effect from topical sinus application. GaPP, Gallium Protoporphyrin, CG, Chitogel; CG-DG, Chitogel- Deferiprone-Gallium Protoporphyrin.

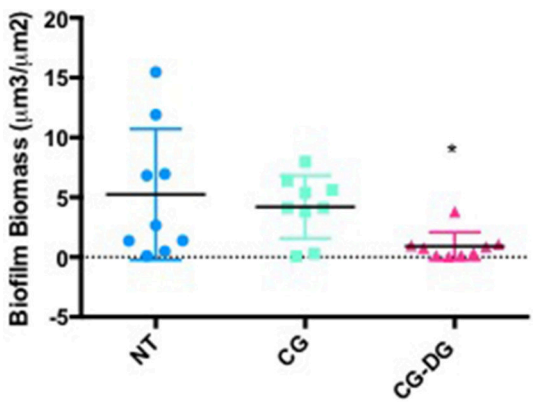

FIGURE 4 | Scatter plots showing COMSTAT computation of *Staphylococcus aureus* biofilm biomass between **(A)** Twice daily saline flush (NT), **(B)** CG gel with twice-daily saline flush, and **(C)** CG-DG gel with twice-daily saline flush. Significant reduction of biofilm biomass seen in CG-DG treated group compared to NT and CG gel. *$P < 0.05$, Kruskal Wallis 1-way analysis of variance (ANOVA) with Dunn's multiple comparison test. NT, No treatment; CG, Chitogel; CG-DG, Chitogel- Deferiprone-Gallium Protoporphyrin.

SEM Tissue Analysis

SEM was employed to assess the presence and integrity of cilia present on sinus mucosal samples. In all sinus mucosal samples collected, there were no signs of ciliary denudation in both CG and CG-DG treated groups (**Figure 2**). These images reflect that the test treatments were not ciliotoxic on ciliated human respiratory cells.

Plasma Deferiprone and Gallium Protoporphyrin Levels

The maximum Deferiprone concentration was reached after 1 day (0.18 µg/ml Deferiprone) in the 4 sheep treated with CG-DG (**Figure 3**). After 6 days the Deferiprone plasma concentration decreased to 0.03 µg/ml.

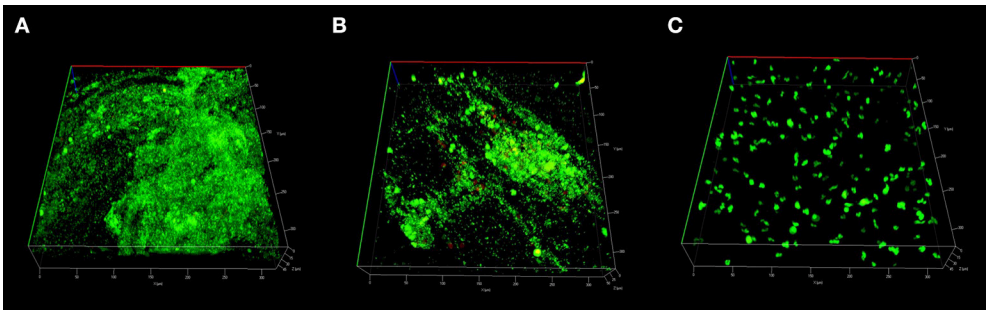

FIGURE 5 | Representative CLSM images of *S. aureus* biofilms stained with LIVE/DEAD Baclight reconstructed into 3D virtual image. Small light green stains represents live bacteria, large dark green stains represents mammalian cells and large red stains represents dead mammalian cells. Sinus mucosa treated with **(A)** Twice daily saline flush (NT) showing dense population of live bacterial biofilms; **(B)** CG gel with twice-daily saline flush showing moderate population of live bacterial biofilms; **(C)** CG-DG gel with twice-daily saline flush showing no bacterial biofilms. CLSM, Confocal laser scanning microscopy; *S. aureus*, *Staphylococcus aureus*; NT, No treatment; CG, Chitogel; CG-DG, Chitogel- Deferiprone-Gallium Protoporphyrin.

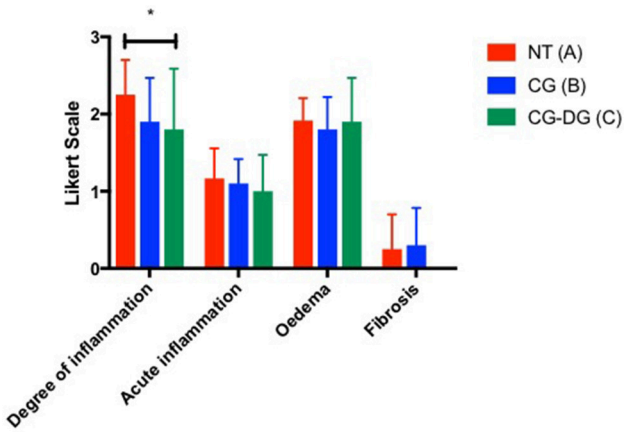

FIGURE 6 | Bar graph showing degree of inflammation, acute inflammation, oedema and fibrosis grading between (A) Twice daily saline flush (NT), (B) CG gel with twice-daily saline flush, and (C) CG-DG gel with twice-daily saline flush. Significant reduction is seen in degree of inflammation of sinus mucosa between CG-DG and NT. *$P < 0.05$, 2-way analysis of variance (ANOVA) with Dunnett's multiple comparison test. NT, No treatment; CG, Chitogel; CG-DG, Chitogel- Deferiprone-Gallium Protoporphyrin.

GaPP was not detected in the plasma of any of the 4 sheep treated with CG-DG (data not shown). According to the quantification level ranging from 0.02 to 10 μg/ml, this indicates a GaPP plasma concentration was below 0.02 μg/ml.

Efficacy Arm

Biofilm Biomass Analysis

COMSTAT2 assessment showed a significant reduction of biofilm biomass in CG-DG treated sheep compared to NT controls ($p = 0.03$, One-way ANOVA, Kruskal-Wallis test), but not between NT and CG treated sheep. Compared to no-treatment controls, CG-DG gel and CG reduced *S. aureus* biofilms by 82 and 20% respectively (**Figure 4**). Representative CLSM images showing LIVE/DEAD BacLight staining of *S. aureus* biofilms seen in **Figure 5**.

Histopathology Analysis of Sinus Mucosa Harvested From Sheep in Efficacy Arm

There was a significant reduction in the degree of inflammation of sheep sinus mucosa between CG-DG treated group and no treatment ($p = 0.0476$, CI 95% 0.004116 to 0.8959). No significant differences were observed in degree of inflammation between CG only group and no treatment controls. Looking at acute inflammation, oedema, fibrosis and cilia, there were no significant differences in sheep sinus mucosa across all groups (**Figure 6**).

DISCUSSION

In this study we were able to show that CG-DG is safe and effective in killing *S. aureus* biofilms *in vivo* using a sheep sinusitis model described previously. The anti-inflammatory effects seen in the sinus mucosa of CG-DG group might be due to the effective eradication of biofilms.

The FDA approved oral dose of Deferiprone that is safe to use in humans is up to 75–99 mg/kg/day. Spino et al reported that following an oral dose of 1,500 mg Deferiprone (20 mg/kg) the mean maximum serum deferiprone concentration (Cmax) of non-iron-loaded healthy subjects was 20 μg/mL (Spino et al., 2015). Following one topical CG-DG application the highest plasma Deferiprone concentration measured in this study was 0.18 μg/ml, which is 110 times less than one oral dose of Deferiprone. In addition, GaPP was not detected in the plasma of any of the sheep treated with CG-DG gel. In an *in vivo* model we have to also account for some accidental oral ingestion of the sinus flushes which may reflect that the true plasma level of deferiprone might be even lower in human application as patients are instructed to apply sinus rinses head down and allow the rinses to wash out. Therefore, negligible Deferiprone plasma concentrations and the absence of GaPP in plasma, together with no observed adverse effects (e.g., no sinus mucosa damage, no ciliary denudation) indicate safety of CG-DG gel *in vivo*.

Iron is an essential element for bacterial growth, survival and replication. Deferiprone is an iron-chelator, capable

of chelating free iron at the ratio 3:1 and approved by the Food and Drug Administration (FDA) for the treatment of Thalassemia Major (Olivieri et al., 1998). Deferiprone has slight anti-microbial properties by capturing iron from the environment around bacteria, causing a depletion of iron as a nutrient source (de Léséleuc et al., 2012). Deferiprone also has been shown to accelerate wound healing with enhanced skin closure after topical application *in vivo* (Mohammadpour et al., 2013). Gallium Protoporphyrin IX belongs to the family of non-iron metalloporphyrins and has antibacterial properties. The compound shows structural similarity to haem, therefore, it can mimic haem as a preferred iron source of bacteria (Stojiljkovic et al., 1999). Once inside the bacterial cell however, non-iron metalloporphyrins such as Gallium Protoporphyrin IX preserve their structure and show antibacterial effects by interfering with essential cellular pathways in the cytoplasm and in the plasma membrane causing bacterial cell death (Reniere et al., 2007). Combining Deferiprone and Gallium Protoporphyrin IX has potent synergistic antimicrobial properties against a range of bacteria including Multi Drug Resistant bacteria and Methicillin Resistant *S. aureus* (MRSA) (Richter et al., 2016). The Deferiprone and Gallium Protoporphyrin IX combination is thought to exert its anti-biofilm effects by interfering with the iron metabolism of *S. aureus* which is involved in membrane bound respiration, bacterial growth, protects against reactive oxygen species, and increases bacterial virulence factors (Braun, 2001; Weinberg, 2009).

In this study, CG gel showed the capacity to act as a drug carrier, facilitating the topical delivery of DG to biofilms in the sinonasal cavities. To exert the full anti-biofilm potential of DG it is imperative that Deferiprone is first applied followed by Gallium Protoporphyrin IX (Richter et al., 2016). Richter et al. described the quick release of hydrophilic Deferiprone from the CG gel within the first 48–72 h followed by a sustained release of hydrophobic Gallium Protoporphyrin IX reaching 20–25% over 20 days (Richter et al., 2017b) which reinforces the anti-biofilm effects of DG.

In the last decade, Chitogel has been largely used in ENT surgery to improve patient outcomes post endoscopic sinus surgery (Athanasiadis et al., 2008; Valentine et al., 2010; Ngoc Ha et al., 2013; Chung et al., 2016) due to its effective hemostatic (Klokkevold et al., 1991, 1992; Rao and Sharma, 1997; Chou et al., 2003; Pusateri et al., 2003; Valentine et al., 2009, 2010, 2011; Chung et al., 2016), wound healing (Biagini et al., 1991; Stone et al., 2000; Azad et al., 2004), anti-adhesion (Kennedy et al., 1996; Costain et al., 1997; Vlahos et al., 2001; Diamond et al., 2003; Zhou et al., 2004, 2010; Athanasiadis et al., 2008; Medina et al., 2012; Medina and Das, 2013; Cabral et al., 2015) and antimicrobial (Rhoades and Roller, 2000; No et al., 2002; Paramasivan et al., 2014a) properties and was recently FDA approved for use after sinus surgery. CG gel comprises succinyl-chitosan which is a chitosan polymer produced by the hydrolysis of chitin, found in the exoskeletons of crustaceans. Incorporating DG into CG gel strengthens the gel's anti-biofilm effects which might help improve the outcome of recalcitrant and post endoscopic sinus surgery patients.

CG-DG has been shown to have significant anti-biofilm activity not only against *S. aureus* but also MRSA, *S. epidermidis* and *P. aeruginosa* biofilms (Richter et al., 2017b). The anti-biofilm activity of DG against multiple pathogens has the added potential of treating polymicrobial infections. This broad activity makes topical CG-DG a valuable treatment alternative that can be applied within the same outpatient setting while waiting for sensitivity result to become available.

In February 2017, the World Health Organization (WHO) released a global priority list of pathogens to guide research and development of new antibiotics. Amongst the list, MRSA has been classified as a high priority pathogen and *P. aeruginosa* as critical. This also suggests that as a novel antimicrobial agent CG-DG gel has great potential for broader applications in various clinical settings.

CONCLUSIONS

Topically applied CG-DG gel effectively reduced *S. aureus* biofilms with no observed topical and systemic adverse effects in a sheep sinusitis model, indicating safety and efficacy of CG-DG gel *in vivo*. The use of Chitogel to enhance the delivery of Deferiprone and Gallium Protoporphyrin IX offers otolaryngologists an alternative method to treat surgically recalcitrant CRS.

Clinical trials are currently underway to investigate the safety and efficacy of CG-DG gel in patients with recalcitrant chronic rhinosinusitis and in the post-operative setting.

AUTHOR CONTRIBUTIONS

MO: project design, data collection and analysis, manuscript preparation. KR: data analysis, manuscript preparation. AD: project design, data collection. NT, CP, CJ: data analysis. SM: product manufacture and quality control. SV, AP, P-JW: project design, manuscript preparation.

FUNDING

The University of Adelaide, School of Medicine, Department of Otolaryngology Head and Neck Surgery, Adelaide, South Australia, Australia.

ACKNOWLEDGMENTS

We thank Loren Matthews, Paul Herde, Kevin Neuman, Robb Muirhead, Dr. Tim Kuchel, Carol Hewitt, for their amazing technical support at the Large Animal Research and Imaging Facility (LARIF); Lyn Waterhouse from Adelaide Microscopy.

This work was supported by The Hospital Research Foundation, Woodville, Australia; the Department of Surgery, Otolaryngology Head and Neck Surgery; the Australian Government Research Training Program Scholarship, University of Adelaide, Adelaide, Australia.

REFERENCES

Athanasiadis, T., Beule, A. G., Robinson, B. H., Robinson, S. R., Shi, Z., and Wormald, P. J. (2008). Effects of a novel chitosan gel on mucosal wound healing following endoscopic sinus surgery in a sheep model of chronic rhinosinusitis. *Laryngoscope* 118, 1088–1094. doi: 10.1097/MLG.0b013e31816ba576

Azad, A. K., Sermsintham, N., Chandrkrachang, S., and Stevens, W. F. (2004). Chitosan membrane as a wound-healing dressing: characterization and clinical application. *J. Biomed. Mater. Res. B Appl. Biomater.* 69, 216–222. doi: 10.1002/jbm.b.30000

Bendouah, Z., Barbeau, J., Hamad, W. A., and Desrosiers, M. (2006). Biofilm formation by *Staphylococcus aureus* and *Pseudomonas aeruginosa* is associated with an unfavorable evolution after surgery for chronic sinusitis and nasal polyposis. *Otolaryngol. Head Neck Surg.* 134, 991–996. doi: 10.1016/j.otohns.2006.03.001

Biagini, G., Bertani, A., Muzzarelli, R., Damadei, A., DiBenedetto, G., Belligolli, A., et al. (1991). Wound management with N-carboxybutyl chitosan. *Biomaterials* 12, 281–286. doi: 10.1016/0142-9612(91)90035-9

Boase, S., Jervis-Bardy, J., Cleland, E., Pant, H., Tan, L., and Wormald, P. J. (2013). Bacterial-induced epithelial damage promotes fungal biofilm formation in a sheep model of sinusitis. *Int. Forum Allergy Rhinol.* 3, 341–348. doi: 10.1002/alr.21138

Braun, V. (2001). Iron uptake mechanisms and their regulation in pathogenic bacteria. *Int. J. Med. Microbiol.* 291, 67–79. doi: 10.1078/1438-4221-00103

Cabral, J. D., McConnell, M. A., Fitzpatrick, C., Mros, S., Williams, G., Wormald, P. J., et al. (2015). Characterization of the *in vivo* host response to a bi-labeled chitosan-dextran based hydrogel for postsurgical adhesion prevention. *J. Biomed. Mater. Res. A* 103, 2611–2620. doi: 10.1002/jbm.a.35395

Chou, T. C., Fu, E., Wu, C. J., and Yeh, J. H. (2003). Chitosan enhances platelet adhesion and aggregation. *Biochem. Biophys. Res. Commun.* 302, 480–483. doi: 10.1016/S0006-291X(03)00173-6

Chung, Y.-J., An, S.-Y., Yeon, J.-Y., Shim, W. S., and Mo, J.-H. (2016). Effect of a chitosan gel on hemostasis and prevention of adhesion after endoscopic sinus surgery. *Clin. Exp. Otorhinolaryngol.* 9, 143–149. doi: 10.21053/ceo.2015.00591

Conly, J., and Johnston, B., (2005). Where are all the new antibiotics? The new antibiotic paradox. *Can. J. Infect. Dis. Med. Microbiol.* 16, 159–160. doi: 10.1155/2005/892058

Costain, D. J., Kennedy, R., Ciona, C., McAlister, V. C., and Lee, T. D. (1997). Prevention of postsurgical adhesions with N,O-carboxymethyl chitosan: examination of the most efficacious preparation and the effect of N,O-carboxymethyl chitosan on postsurgical healing. *Surgery* 121, 314–319. doi: 10.1016/S0039-6060(97)90360-3

Costerton, J. W. (1995). Overview of microbial biofilms. *J. Ind. Microbiol.* 15, 137–140. doi: 10.1007/BF01569816

de Léséleuc, L., Harris, G., KuoLee, R., and Chen, W. (2012). *In vitro* and *in vivo* biological activities of iron chelators and gallium nitrate against *Acinetobacter baumannii*. *Antimicrob. Agents Chemother.* 56, 5397–5400. doi: 10.1128/AAC.00778-12

Diamond, M. P., Luciano, A., Johns, D. A., Dunn, R., Young, P., and Bieber, E. (2003). Reduction of postoperative adhesions by N,O-carboxymethylchitosan: a pilot study. *Fertil. Steril.* 80, 631–636. doi: 10.1016/S0015-0282(03)00759-3

Drilling, A., Morales, S., Boase, S., Jervis-Bardy, J., James, C., Jardeleza, C., et al. (2014). Safety and efficacy of topical bacteriophage and ethylened iaminetetraacetic acid treatment of *Staphylococcus aureus* infection in a sheep model of sinusitis. *Int. Forum Allergy Rhinol.* 4, 176–186. doi: 10.1002/alr.21270

Ha, K. R., Psaltis, A. J., Tan, L., and Wormald, P. J. (2007). A sheep model for the study of biofilms in rhinosinusitis. *Am. J. Rhinol.* 21, 339–345. doi: 10.2500/ajr.2007.21.3032

Heydorn, A., Nielsen, A. T., Hentzer, M., Sternberg, C., Givskov, M., Ersbøll, B. K., et al. (2000). Quantification of biofilm structures by the novel computer program comstat. *Microbiology*146, 2395–2407. doi: 10.1099/00221287-146-10-2395

Hijazi, S., Visca, P., and Frangipani, E. (2017). Gallium-protoporphyrin IX inhibits *Pseudomonas aeruginosa* growth by targeting cytochromes. *Front. Cell. Infect. Microbiol.* 7:12. doi: 10.3389/fcimb.2017.00012

Illum, L., Farraj, N. F., and Davis, S. S. (1994). Chitosan as a novel nasal delivery system for peptide drugs. *Pharm. Res.* 11, 1186–1189. doi: 10.1023/A:1018901302450

Kennedy, R., Costain, D. J., McAlister, V. C., and Lee, T. D. (1996). Prevention of experimental postoperative peritoneal adhesions by N,O-carboxymethyl chitosan. *Surgery* 120, 866–870. doi: 10.1016/S0039-6060(96)80096-1

Klinger-Strobel, M., Suesse, H., Fischer, D., Pletz, M. W., and Makarewicz, O. (2016). A novel computerized cell count algorithm for biofilm analysis. *PLoS ONE* 11:e0154937. doi: 10.1371/journal.pone.0154937

Klokkevold, P. R., Lew, D. S., Ellis, D. G., and Bertolami, C. N. (1991). Effect of chitosan on lingual hemostasis in rabbits. *J. Oral Maxillofac. Surg.* 49, 858–863. doi: 10.1016/0278-2391(91)90017-G

Klokkevold, P. R., Subar, P., Fukayama, H., and Bertolami, C. N. (1992). Effect of chitosan on lingual hemostasis in rabbits with platelet dysfunction induced by epoprostenol. *J. Oral Maxillofac. Surg.* 50, 41–45. doi: 10.1016/0278-2391(92)90194-5

Medina, J. G., and Das, S. (2013). Sprayable chitosan/starch-based sealant reduces adhesion formation in a sheep model for chronic sinusitis. *Laryngoscope* 123, 42–47. doi: 10.1002/lary.23583

Medina, J. G., Steinke, J. W., and Das, S. (2012). A chitosan-based sinus sealant for reduction of adhesion formation in rabbit and sheep models. *Otolaryngol. Head Neck Surg.* 147, 357–363. doi: 10.1177/0194599812443647

Mohammadpour, M., Behjati, M., Sadeghi, A., and Fassihi, A. (2013). Wound healing by topical application of antioxidant iron chelators: kojic acid and deferiprone. *Int. Wound J.* 10, 260–264. doi: 10.1111/j.1742-481X.2012.00971.x

Nakamura, K., Maitani, Y., Lowman, A. M., Takayama, K., Peppas, N. A., and Nagai, T. (1999). Uptake and release of budesonide from mucoadhesive, pH-sensitive copolymers and their application to nasal delivery. *J. Control. Release* 61, 329–335. doi: 10.1016/S0168-3659(99)00150-9

Ngoc Ha, T., Valentine, R., Moratti, S., Robinson, S., Hanton, L., and Wormald, P. J. (2013). A blinded randomized controlled trial evaluating the efficacy of chitosan gel on ostial stenosis following endoscopic sinus surgery. *Int. Forum Allergy Rhinol.* 3, 573–580. doi: 10.1002/alr.21136

No, H. K., Park, N. Y., Lee, S. H., and Meyers, S. P. (2002). Antibacterial activity of chitosans and chitosan oligomers with different molecular weights. *Int. J. Food Microbiol.* 74, 65–72. doi: 10.1016/S0168-1605(01)00717-6

Olivieri, N. F., Brittenham, G. M., McLaren, C. E., Templeton, D. M., Cameron, R. G., McClelland, R. A., et al. (1998). Long-term safety and effectiveness of iron-chelation therapy with deferiprone for thalassemia major. *N. Engl. J. Med.* 339, 417–423. doi: 10.1056/NEJM199808133390701

Paramasivan, S., Drilling, A. J., Jardeleza, C., Jervis-Bardy, J., Vreugde, S., and Wormald, P. J. (2014b). Methylglyoxal-augmented manuka honey as a topical anti-*Staphylococcus aureus* biofilm agent: safety and efficacy in an *in vivo* model. *Int. Forum Allergy Rhinol.* 4, 187–195. doi: 10.1002/alr.21264

Paramasivan, S., Jones, D., Baker, L., Hanton, L., Robinson, S., Wormald, P. J., et al. (2014a). The use of chitosan-dextran gel shows anti-inflammatory, antibiofilm, and antiproliferative properties in fibroblast cell culture. *Am. J. Rhinol. Allergy* 28, 361–365. doi: 10.2500/ajra.2014.28.4069

Psaltis, A. J., Weitzel, E. K., Ha, K. R., and Wormald, P. J. (2008). The effect of bacterial biofilms on post-sinus surgical outcomes. *Am. J. Rhinol.* 22, 1–6. doi: 10.2500/ajr.2008.22.3119

Pusateri, A. E., McCarthy, S. J., Gregory, K. W., Harris, R. A., Cardenas, L., McManus, A. T., et al. (2003). Effect of a chitosan-based hemostatic dressing on blood loss and survival in a model of severe venous hemorrhage and hepatic injury in swine. *J. Trauma* 54, 177–182. doi: 10.1097/00005373-200301000-00023

Rajiv, S., Drilling, A., Bassiouni, A., James, C., Vreugde, S., and Wormald, P. J. (2015). Topical colloidal silver as an anti-biofilm agent in a *Staphylococcus aureus* chronic rhinosinusitis sheep model. *Int. Forum Allergy Rhinol.* 5, 283–288. doi: 10.1002/alr.21459

Rao, S. B., and Sharma, C. P. (1997). Use of chitosan as a biomaterial: studies on its safety and hemostatic potential. *J. Biomed. Mater. Res.* 34, 21–28.

Reniere, M. L., Torres, V. J., and Skaar, E. P. (2007). Intracellular metalloporphyrin metabolism in *Staphylococcus aureus*. *Biometals* 20, 333–345. doi: 10.1007/s10534-006-9032-0

Rhoades, J., and Roller, S. (2000). Antimicrobial actions of degraded and native chitosan against spoilage organisms in laboratory media and foods. *Appl. Environ. Microbiol.* 66, 80–86. doi: 10.1128/AEM.66.1.80-86.2000

Richter, K., Ramezanpour, M., Thomas, N., Prestidge, C. A., Wormald, P. J., and Vreugde, S. (2016). Mind "De GaPP": *in vitro* efficacy of deferiprone and gallium-protoporphyrin against *Staphylococcus aureus* biofilms. *Int. Forum Allergy Rhinol.* 6, 737–743. doi: 10.1002/alr.21735

Richter, K., Thomas, N., Claeys, J., McGuane, J., Prestidge, C. A., Coenye, T., et al. (2017b). A topical hydrogel with deferiprone and gallium-protoporphyrin targets bacterial iron metabolism and has antibiofilm activity. *Antimicrob. Agents Chemother.* 61:e00481-17. doi: 10.1128/AAC.00481-17

Richter, K., Thomas, N., Zhang, G., Prestidge, C. A., Coenye, T., Wormald, P.-J., et al. (2017c). Deferiprone and gallium-protoporphyrin have the capacity to potentiate the activity of antibiotics in *Staphylococcus aureus* small colony variants. *Front. Cell. Infect. Microbiol.* 7:280. doi: 10.3389/fcimb.2017.00280

Richter, K., Van den Driessche, F., and Coenye, T. (2017a). Innovative approaches to treat *Staphylococcus aureus* biofilm-related infections. *Essays Biochem.* 61, 61–70. doi: 10.1042/EBC20160056

Singhal, D., Foreman, A., Jervis-Bardy, J., and Wormald, P. J. (2011). *Staphylococcus aureus* biofilms: nemesis of endoscopic sinus surgery. *Laryngoscope* 121, 1578–1583. doi: 10.1002/lary.21805

Singhal, D., Jekle, A., Debabov, D., Wang, L., Khosrovi, B., Anderson, M., et al. (2012). Efficacy of NVC-422 against *Staphylococcus aureus* biofilms in a sheep biofilm model of sinusitis. *Int. Forum Allergy Rhinol.* 2, 309–315. doi: 10.1002/alr.21038

Singhal, D., Psaltis, A. J., Foreman, A., and Wormald, P. J. (2010). The impact of biofilms on outcomes after endoscopic sinus surgery. *Am. J. Rhinol. Allergy* 24, 169–174. doi: 10.2500/ajra.2010.24.3462

Spino, M., Connelly, J., Tsang, Y.-C., Fradette, C., and Tricta, F. (2015). Deferiprone pharmacokinetics with and without iron overload and in special patient populations. *Blood* 126, 3365–3365.

Stojiljkovic, I., Kumar, V., and Srinivasan, N. (1999). Non-iron metalloporphyrins: potent antibacterial compounds that exploit haem/Hb uptake systems of pathogenic bacteria. *Mol. Microbiol.* 31, 429–442. doi: 10.1046/j.1365-2958.1999.01175.x

Stone, C. A., Wright, H., Clarke, T., Powell, R., and Devaraj, V. S. (2000). Healing at skin graft donor sites dressed with chitosan. *Br. J. Plast. Surg.* 53, 601–606. doi: 10.1054/bjps.2000.3412

Valentine, R., Athanasiadis, T., Moratti, S., Hanton, L., Robinson, S., and Wormald, P. J. (2010). The efficacy of a novel chitosan gel on hemostasis and wound healing after endoscopic sinus surgery. *Am. J. Rhinol. Allergy* 24, 70–75. doi: 10.2500/ajra.2010.24.3422

Valentine, R., Athanasiadis, T., Moratti, S., Robinson, S., and Wormald, P. J. (2009). The efficacy of a novel chitosan gel on hemostasis after endoscopic sinus surgery in a sheep model of chronic rhinosinusitis. *Am. J. Rhinol. Allergy* 23, 71–75. doi: 10.2500/ajra.2009.23.3266

Valentine, R., Boase, S., Jervis-Bardy, J., Dones Cabral, J. D., Robinson, S., and Wormald, P. J. (2011). The efficacy of hemostatic techniques in the sheep model of carotid artery injury. *Int. Forum Allergy Rhinol.* 1, 118–122. doi: 10.1002/alr.20033

Vlahos, A., Yu, P., Lucas, C. E., and Ledgerwood, A. M. (2001). Effect of a composite membrane of chitosan and poloxamer gel on postoperative adhesive interactions. *Am. Surg.* 67, 15–21.

Weinberg, E. D. (2009). Iron availability and infection. *Biochim. Biophys. Acta* 1790, 600–605. doi: 10.1016/j.bbagen.2008.07.002

World Health Organization (2016). *Antibiotic Resistance. Media Centre*. World Health Organization (Fact Sheets).

World Health Organization (2017). "Antibacterial agents in clinical development. an analysis of the antibacterial clinical development pipeline, including tuberculosis," in *Medicines and Health Products Aow, Rational Use of Medicines* (World Health Organization), 48.

Zhou, J., Elson, C., and Lee, T. D. (2004). Reduction in postoperative adhesion formation and re-formation after an abdominal operation with the use of N, O - carboxymethyl chitosan. *Surgery* 135, 307–312. doi: 10.1016/j.surg.2003.07.005

Zhou, J., Lee, J. M., Jiang, P., Henderson, S., and Lee, T. D. (2010). Reduction in postsurgical adhesion formation after cardiac surgery by application of N,O-carboxymethyl chitosan. *J. Thorac. Cardiovasc. Surg.* 140, 801–806. doi: 10.1016/j.jtcvs.2009.11.030

Conflict of Interest Statement: P-JW and SM are part of the consortium that owns the patent for Chitogel and are shareholders in the company. P-JW and SV hold a patent on the treatment combination of Deferiprone and Gallium-Protoporphyrin.

The other authors declare that the research was conducted in the absence of any commercial or financial relationships that could be construed as a potential conflict of interest.

frontiers in Microbiology

ORIGINAL RESEARCH
published: 11 April 2018
doi: 10.3389/fmicb.2018.00720

Topical Colloidal Silver for the Treatment of Recalcitrant Chronic Rhinosinusitis

Mian L. Ooi[1], *Katharina Richter*[1,2], *Catherine Bennett*[1], *Luis Macias-Valle*[1,3], *Sarah Vreugde*[1], *Alkis J. Psaltis*[1] *and Peter-John Wormald*[1]*

[1] *Department of Surgery-Otolaryngology, Head and Neck Surgery, Basil Hetzel Institute for Translational Health Research, The University of Adelaide, Adelaide, SA, Australia,* [2] *Adelaide Biofilm Test Facility, Sansom Institute for Health Research, University of South Australia, Adelaide, SA, Australia,* [3] *Facultad Mexicana de Medicina Universidad La Salle, Department of Otolaryngology Head and Neck Surgery, Spanish Hospital of Mexico, Granada, Mexico*

Background: The management of recalcitrant chronic rhinosinusitis (CRS) is challenged by difficult-to-treat polymicrobial biofilms and multidrug resistant bacteria. This has led to the search for broad-spectrum non-antibiotic antimicrobial therapies. Colloidal silver (CS) has significant antibiofilm activity *in vitro* and *in vivo* against *S. aureus*, *MRSA,* and *P. aeruginosa*. However, due to the lack of scientific efficacy, it is only currently used as an alternative medicine. This is the first study looking at the safety and efficacy of CS in recalcitrant CRS.

Methods: Patients were included when they had previously undergone endoscopic sinus surgery and presented with signs and symptoms of sinus infection with positive bacterial cultures. Twenty-two patients completed the study. Patients were allocated to 10–14 days of culture directed oral antibiotics with twice daily saline rinses ($n = 11$) or 10 days of twice daily 0.015 mg/mL CS rinses ($n = 11$). Safety observations included pre- and post-treatment serum silver levels, University of Pennsylvania Smell Identification Test (UPSIT) and adverse event (AE) reporting. Efficacy was assessed comparing microbiology results, Lund Kennedy Scores (LKS) and symptom scores using Visual Analog Scale (VAS) and Sino-Nasal Outcome Test (SNOT-22).

Results: CS demonstrated good safety profile with no major adverse events, no changes in UPSIT and transient serum silver level changes in 4 patients. CS patients had 1/11 (9.09%) negative cultures, compared to 2/11 (18.18%) in the control group upon completion of the study. Whilst not statistically significant, both groups showed similar improvement in symptoms and endoscopic scores.

Conclusion: This study concludes that twice daily CS (0.015 mg/mL) sinonasal rinses for 10 days is safe but not superior to culture-directed oral antibiotics. Further studies including more patients and looking at longer treatment or improving the tonicity of the solution for better tolerability should be explored.

Keywords: chronic rhinosinusitis, recalcitrant, infection, antimicrobial, topical agent, safety, efficacy

OPEN ACCESS

Edited by:
Maria Olivia Pereira, University of Minho, Portugal

Reviewed by:
Debora Barros Barbosa, São Paulo State University-UNESP, Brazil
Massimo Triggiani, Università degli Studi di Salerno, Italy

***Correspondence:**
Peter-John Wormald
peterj.wormald@adelaide.edu.au

Specialty section:
This article was submitted to Antimicrobials, Resistance and Chemotherapy, a section of the journal Frontiers in Microbiology

Received: *03 December 2017*
Accepted: *27 March 2018*
Published: *11 April 2018*

Citation:
Ooi ML, Richter K, Bennett C, Macias-Valle L, Vreugde S, Psaltis AJ and Wormald P-J (2018) Topical Colloidal Silver for the Treatment of Recalcitrant Chronic Rhinosinusitis. Front. Microbiol. 9:720. doi: 10.3389/fmicb.2018.00720

INTRODUCTION

The management of recalcitrant chronic rhinosinusitis (CRS) is increasingly challenged by difficult-to-treat polymicrobial biofilms and multidrug resistant bacteria which antibiotics often cannot effectively eradicate. For recalcitrant patients, antibiotics often alleviate symptoms in acute exacerbations but fail to eradicate the biofilm nidus which periodically sheds planktonic organisms resulting in a relapsing and remitting course of disease (Foreman et al., 2011). This has fuelled a continuous search for broad-spectrum topical non-antibiotic anti-biofilm therapies. Topical agents allow increased concentration, localized action, less systemic side effects and lessen the risk of antibiotic resistance.

To date, numerous topical agents have been tested and although some have shown anti-biofilm activity (Chiu et al., 2008; Le et al., 2008; Alandejani et al., 2009; Jardeleza et al., 2011; Jervis-Bardy et al., 2012; Paramasivan et al., 2014; Richter et al., 2016, 2017a,b), none have been widely accepted as a treatment option in recalcitrant CRS. Recent evidence suggests that colloidal silver (CS) may be effective against bacterial biofilms. We have previously shown that CS showed significant anti-biofilm activity *in vitro* and *in vivo* against *S. aureus* (Goggin et al., 2014; Rajiv et al., 2015), and against methicillin-resistant *S. aureus* (MRSA) and *P. aeruginosa* biofilms. Spherical nanoparticles were also shown to be non-toxic in human cell culture (THP-1, Nuli-1) (Richter et al., 2017c) and safe in a sheep sinusitis model (Rajiv et al., 2015). Moreover, they were physically stable for over 6 months in storage with no observed loss in anti-biofilm activity (Richter et al., 2017c).

However, due to the lack of evidence for their efficacy, it is only currently used as an alternative medicine. This is the first study investigating the safety and efficacy of CS in recalcitrant CRS patients.

METHODS AND MATERIALS

Participants and Study Design

This was a prospective, open-label, single-blinded, pilot study looking at the safety and efficacy of CS sinonasal rinses in patients with recalcitrant CRS between December 2016 to July 2017. Ethics approval was granted by the Central Northern Adelaide Health Service, Ethics of Human Research Committee (TQEH/LMH/MH HREC) to conduct the trial within its network of teaching hospitals in Adelaide, Australia. All subjects gave written informed consent in accordance with the Declaration of Helsinki.

A total of 22 patients were enrolled in the study (8 females, 14 males, aged 27–86). Patients were allocated to either the colloidal silver arm (CS) ($n = 11$) or control arm (CON) ($n = 11$) depending on availability of silver stock and patient's adverse reaction to culture-sensitive oral antibiotics (**Figure 1**). Full inclusion and exclusion criterias are outlined in **Table 1**. Baseline demographic and clinical characteristic are demonstrated in **Table 2**.

CS patients were provided with 20 sealed bottles of pre-filled 120 mL CS solution in standard nasal irrigation squeeze bottles. Patients were instructed to store these bottles away from light and in the refrigerator. Prior to use, patients were asked to warm the solution to room temperature, fill the rinse bottle to 240 mL with cooled boiled water, then perform the rinses twice daily for 10 days. Patients are to apply gentle pressure onto squeeze bottles which delivers the solution through the inner tube and out of the tip of the bottle into the nostril. CS patients were specifically instructed not to add the usual proprietary buffered salts sachets to avoid chemical interaction with the CS nanoparticles. All squeeze bottles were provided by NeilMed Pharmaceuticals (Santa Rosa, CA). If there were signs of persistent infection on endoscopic examination and a positive culture swab post-treatment, CS patients exited the study and resumed treatment based on clinical grounds.

CON patients received a 10 to 14-day course of culture-directed oral antibiotics and were instructed to perform twice daily saline rinses similar to the delivery of CS. If the patient had persistent infection on endoscopic examination and a positive culture swab at the end of treatment, they received CS.

Those taking INCs on enrolment were instructed to continue throughout the duration of the study.

Synthesis of Silver Nanoparticles

Spherical silver nanoparticles were prepared as previously described (Richter et al., 2017c). Briefly, a mixture of 6.25 mL water, 1.25 mL sodium citrate (1% wt.), 1.25 mL silver nitrate (1% wt.) and 50 μl potassium iodide (300 μM) was prepared under stirring at room temperature and incubated for 5 min. This mixture was added to 237.5 mL of boiling water that included 250 μl ascorbic acid (0.1M). The colorless solution changed to yellow and finally slightly orange, indicating particle formation. The silver nanoparticles were further boiled for 1 h under reflux and stirring at 1,500 rpm. After cooling, the silver nanoparticles were characterized by UV-Vis spectrometry and transmission electron microscopy (quality control). This confirmed a spherical particle shape and size of approximately 40 nm. Silver nanoparticles were stored in amber glass flasks under dark condition at 4°C prior to utilization as a nasal rinse.

Efficacy Assessment

Endoscopic guided sinonasal swabs were taken at every scheduled visit for microbiological evaluation. All patients completed symptoms score questionnaire at every visit, using Sino-Nasal Outcome Test-22 (SNOT-22) (Kennedy et al., 2013) (22 items, each scored from 0 to 5; total score range 0 to 110) and Visual Analog Scale (VAS) (Walker and White, 2000) (average of 6 items and an overall symptom score; each scored from 0 to 100, total score range 0 to 100). At each visit, all patients had entry and exit endoscopic videos recorded and scored by a blinded surgeon using the Lund Kennedy Score (LKS) (Lund and Kennedy, 1995; Kennedy et al., 2013) (score range, 0–20).

Abbreviations: CRS, chronic rhinosinusitis; INC, intranasal corticosteroid; CON, control; CS, Colloidal Silver; VAS, Visual Analog Scale; SNOT-22, Sino-Nasal Outcome Test-22; LKS, Lund Kennedy Scores; UPSIT, University of Pennsylvania Smell Identification Test; AE, Adverse Event.

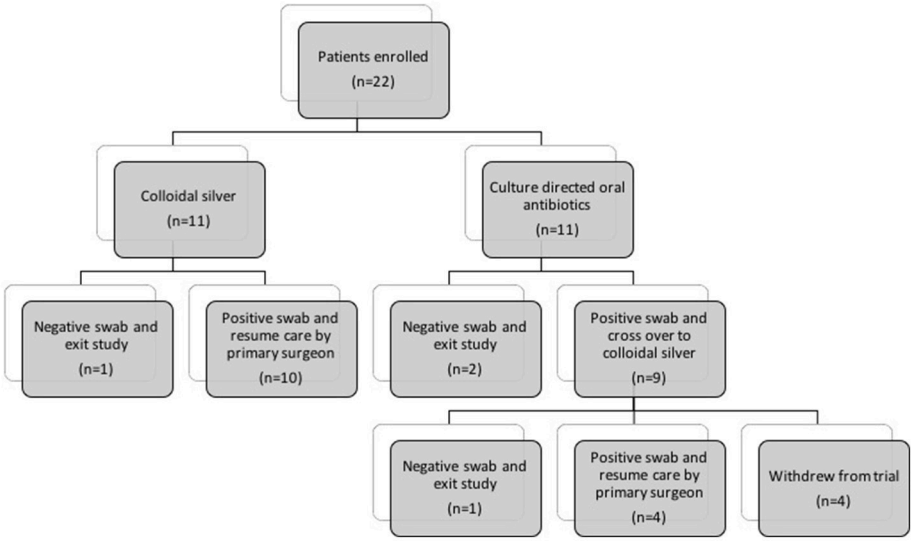

FIGURE 1 | Flow diagram describing patients allocated to (1) Culture-directed oral antibiotics with twice daily saline flush (CON) and (2) Colloidal silver (CS) with twice-daily saline flush. CON, Control; CS, Colloidal silver.

TABLE 1 | Inclusion and exclusion criteria.

Inclusion Criteria	Exclusion criteria
Ongoing symptoms of CRS despite at least one trial of oral antibiotics	Allergy to silver
ESS >12 weeks prior to enrolment	Antibiotics in previous 2 weeks
Positive bacterial microbiology swab	Taking oral corticosteroids
Over 18 years of age AND able to give written informed consent	Pregnant or breastfeeding
Willing to return to this center for postoperative follow-up care	Immunocompromised

ESS, Endoscopic sinus surgery; CRS, Chronic rhinosinusitis.

TABLE 2 | Baseline patient demographics and clinical characteristics.

	CON (n = 11)	CS (n = 11)
Age, year	61 (52–72)	60 (47–73)
Gender, male	7 (63.6%)	7 (63.6%)
History of polyposis	9 (81.82%)	8 (72.73%)
Frontal drillouts	7 (63.64%)	9 (81.82%)
Visual analog scale	38.29 (22.14–51.86)	49.72 (28.75–65)
SNOT-22 score	38.55 (23–59)	58.01 (43–75)
Lund-Kennedy score	6.82 (4–10)	8.57 (6–10)

Data are medians (interquartile range) or numbers (%). CON, Control; CS, Colloidal silver; SNOT-22, Sino-Nasal Outcome Test-22.

Safety Assessment

All patients on CS treatment were required to have pre- and post-treatment serum silver levels and completed the University of Pennsylvania Smell Identification Test (UPSIT). If serum silver level post-treatment was above normal limits, a repeat serum silver level was performed 7 days later to confirm return to baseline. Patients were advised to report any adverse outcomes while on the study.

Data Analysis

Statistical power was calculated for the primary end-point of culture negativity post-treatment. Power analysis estimates determined a sample size of 11 patients per group would be required to achieve statistical significance (80%, $p < 0.05$) based on response rates of 25 and 90% in the control and silver groups, respectively.

All results were statistically analyzed at the completion of the study using 2-way analysis of variance (ANOVA) and student's t-test, with a significance value set at $p < 0.05$.

RESULTS

Efficacy

Microbiology Result

2/11 (18.18%) patients in CON group had negative swabs while 1/11 (9.09%) CS patients had negative swabs upon completion of treatment. List of pathogens treated in both cohorts are described in **Table 3**.

Visual Analog Scale (VAS)

VAS scores in both CON and CS groups showed a similar trend of improvement post-treatment, but both were not statistically significant (CON 1.728 [95% CI −7.785 to 11.24] vs. CS 3.536 [95% CI −5.977 to 13.05]) (**Figure 2**).

Sino-Nasal Outcome Test−22 (SNOT-22)

Patients in the CON group showed no change in SNOT-22 scores post- treatment while CS group showed a trend toward an improvement in SNOT-22 scores, but it was not statistically

TABLE 3 | Standard semi-quantitative analysis of bacterial load reported as scant, light, moderate or heavy (equivalent to 1+, 2+, 3+, or 4+) by laboratory.

Before colloidal silver	After colloidal silver
Heavy *MRSA* + Light *P. aeruginosa*	Heavy *MRSA* + Scant *P. aeroginosa*
Heavy *S. aureus*	Moderate *S. aureus*
Heavy *S. aureus* + Heavy *P. aeruginosa*	Moderate *S. aureus* + Moderate *P. aeroginosa*
Moderate *S. aureus*	Light *S. aureus* + Light *S. pneumoniae*
Scant *K. oxytoca*, Scant *H. influenza*	No growth
Heavy *H. influenza*	Heavy *S. aureus* + Light *E. cloacae* + Light *H. influenzae*
Moderate *K. oxytoca* + Moderate *P. aeruginosa*	Heavy *K. oxytoca* + Moderate *P. aeruginosa*
Light *P. aeruginosa*	Moderate *S. aureus*
Heavy *S. aureus*	Moderate *S. aureus*
Heavy *S. aureus* + Heavy *P. aeruginosa*	Heavy *S. aureus*
Heavy *S. aureus*	Heavy *S. aureus* + Moderate *M. morganii*

Before oral antibiotics	Antibiotics	After oral antibiotics	After colloidal silver
Heavy *S. aureus*	Augmentin DF	Moderate *P. aeruginosa* + Heavy *S. aureus*	Moderate *S. pneumoniae* + Moderate *S. aureus*
Moderate *P. aeruginosa*	Ciprofloxacin	Light *P. stutzeri*	Withdrew due to other commitments
Heavy *H. influenzae*	Bactrim DS	No growth	
Heavy *S. aureus*	Augmentin DF	Heavy *S. maltophilia*	No growth
Moderate *S. aureus*	Augmentin DF	No growth	
Heavy *E. coli*	Augmentin DF	Moderate *E. coli*	Withdrew due to flush discomfort
Heavy *S. aureus*	Cephalexin	Moderate *S. aureus* + Light *H. influenzae*	Withdrew due to lack of efficacy
Moderate *S. aureus*	Augmentin DF	Moderate *S. aureus* + Light *H. influenzae*	Heavy *S. aureus* + Light *E. coli*
Moderate *E. aerogenes*	Ciprofloxacin	Moderate *E. aerogenes* + Scant *S. aureus*	Withdrew due to due to external injury
Moderate *S. pneumoniae* + Scant *S. aureus*	Augmentin DF	Light *S. aureus*	Light *S. aureus*
Moderate *S. pneumoniae* + Scant *S. aureus*	Bactrim DS	Moderate *S. aureus* + Scant *Alternaria* sp.	Light *S. aureus*

P. aeruginosa, Pseudomonas aeruginosa; MRSA, Methicllin resistant staphylococcus aureus; S. aureus, Staphylococcus aureus; H. influenza, Haemophilus Influenzae; E. cloaca, Enteroboacter cloacae; S. pneumonia, Streptococcus pneumonia; K. oxytoca, Klebsiella oxytoca; M. Morganii, Morganella Morganii; P. stutzeri, Pseudomonas stutzeri; S. maltophilia, Stenotrophomonas maltophilia; E. coli, Escherichia coli; E. aerogenes, Enterobacter aerogenes.

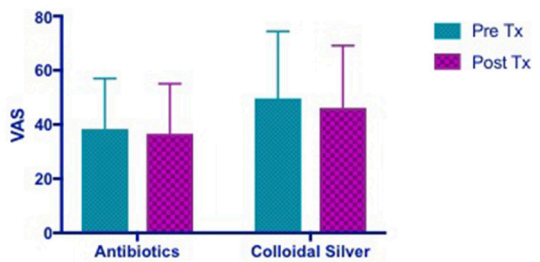

FIGURE 2 | Bar graph showing no significant difference in VAS scores between CON and CS treated groups. VAS, Visual Analog Scale; CON, Control; CS, Colloidal silver.

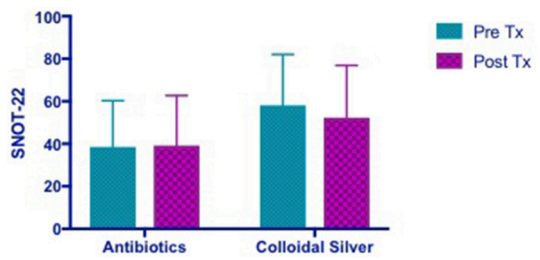

FIGURE 3 | Bar graph showing no change in SNOT-22 scores in CON group, while CS group showed a trend of improved SNOT-22 scores, but not statistically significant. SNOT-22, Sino-Nasal Outcome Test-22; CON, Control; CS, Colloidal silver.

significant (CON −0.6364 [95% CI −6.673 to 5.4] vs. CS 5.818 [95% CI −0.2183 to 11.85]) (**Figure 3**).

Lund Kennedy Score (LKS)

Both CON and CS group showed trends of similar improvements in Lund Kennedy Scores but this was not statistically significant (CON 1.818 [95% CI −1.373 to 5.009] vs. CS 2.167 [95% CI −2.154 to 6.488]) (**Figure 4**).

Subgroup Analyses: Crossover Silver Arm

Five patients completed the crossover CS arm after failing oral antibiotics. Subgroup analyses were performed comparing VAS, SNOT-22, and LKS scores of patients while on either treatment. The mean score difference post antibiotic treatment vs. post CS treatment were compared using Wilcoxon matched-pairs signed rank tests. However, due to the small sample size of our subgroup analyses, data presented is focused on describing observed trends.

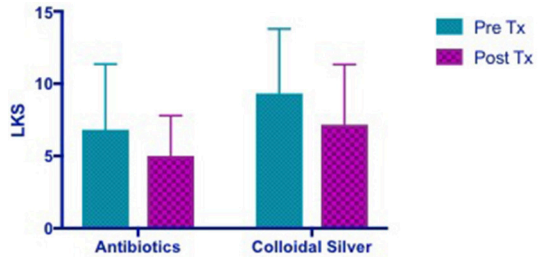

FIGURE 4 | Bar graph showing similar improvements in LKS in both CON and CS groups, but not statistically significant. LKS, Lund Kennedy Scores; CON, Control; CS, Colloidal silver.

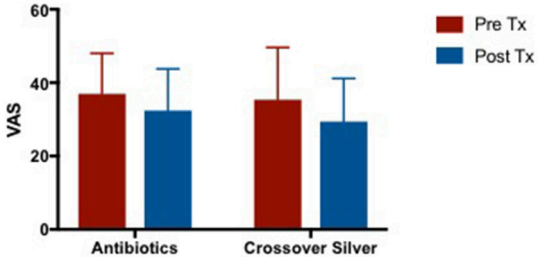

FIGURE 5 | Bar graph comparing VAS scores of patients following failed culture sensitive oral antibiotics and crossed-over to CS treatment. VAS, Visual Analog Scale; CS. Colloidal silver.

Microbiology Result of Crossover arm

1/5 patient had successful infection eradication from CS treatment after failing culture-sensitive oral antibiotics.

Visual Analog Scale (VAS) of Crossover Arm

There were slight improvements in VAS scores after culture sensitive oral antibiotics and CS treatment. There was a trend of greater improvement in VAS while on CS compared to when patients were treated with culture sensitive oral antibiotics. It is also observed that patients' VAS scores appeared to return to baseline after completing course of oral antibiotics and before commencing CS which is consistent with what is observed in clinical practice (**Figure 5**). Mean difference in VAS scores when patients were on culture sensitive oral antibiotics 4.546 [95% CI −8.156 to 17.25] vs. CS treatment 5.94 [95% CI −3.347 to 15.23], $p = 0.4750$.

Sino-Nasal Outcome Test−22 (SNOT-22) of Crossover Arm

There were no changes in SNOT-22 scores after culture sensitive oral antibiotics treatment but showed trends of improvement when patients were crossed over to CS treatment (**Figure 6**). Mean difference in SNOT-22 scores when patients were on culture sensitive oral antibiotics 0.2 [95% CI −2.021 to 2.421] vs. CS treatment −13 [95% CI −22.42 to −3.585], $p = 0.06$.

Lund Kennedy Score (LKS) of Crossover Arm

Patients demonstrated an improvement in LKS post antibiotic treatment and further improvements were observed after completion of CS treatment (**Figure 7**). Mean difference in LKS scores when patients were on culture sensitive oral antibiotics −2.8 [95% CI −7.311 to 1.711] vs. CS treatment −1.4 [95% CI −4.259 to 1.459], $p = 0.50$.

Safety

Serum Silver Levels

Four patients who had received CS had serum silver levels that were above normal limits measured within 24 h after receiving final silver dose. 3 patients had a repeat test 10 days after study exit which saw serum silver levels had returned to normal parameters. One patient had serum silver levels which were above normal ranges pre-treatment and on repeat test had returned to baseline. Our laboratory reference indicates that argyria can be present at serum silver levels of approximately 100 nmol/L, the highest level of serum silver level recorded in our study was 57.3 nmol/L.

Smell Test

There were no significant changes in smell pre- and post-treatment between both groups measured using the University of Pennsylvania Smell Identification Test (UPSIT).

Adverse Events

There were no serious adverse events reported.

DISCUSSION

In this study, looking at the primary end-point of culture negativity post-treatment, CS has not been shown to be superior to culture-directed oral antibiotics. Although interesting to note, CS patients had more severe baseline disease when compared to CON, but demonstrated comparable improvement in subjective symptoms and objective endoscopic scores suggesting it may be more than just a placebo effect. It is possible that CS treatment over 10 days is sufficient to demonstrate symptomatic and endoscopic improvement but insufficient time to achieve bacterial eradication. Indeed, when compared with topical mupirocin rinses which have been one of the more successful topical treatments for recalcitrant patients (Solares et al., 2006; Uren et al., 2008; Jervis-Bardy and Wormald, 2012; Jervis-Bardy et al., 2012; Seiberling et al., 2013), mupirocin has been used as a twice-daily rinse over 3–4 weeks. We believe that this reflects the duration of CS treatment needs to be further optimized. A longer study period including a larger number of study participants would be needed to assess the safety and efficacy of CS topical application in these patients.

The spherical CS nanoparticles used in this study has been shown to have substantial anti-biofilm activity *in vitro* with 96, 97, and 98% biofilm reduction of *S. aureus,* MRSA, and *P. aeruginosa* respectively (Richter et al., 2017c). It has been postulated that CS exerts its antimicrobial properties via multiple mechanisms. It can act on bacterial cell membranes by disrupting phosphate (Schreurs and Rosenberg, 1982) and sodium channels (Semeykina and Skulachev, 1990), inhibits mitochondrial ATPase

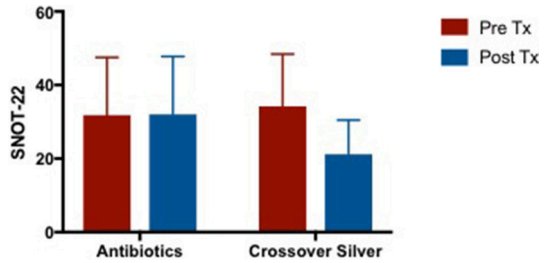

FIGURE 6 | Bar graph comparing SNOT-22 scores of patients following failed culture sensitive oral antibiotics and crossed-over to CS treatment. SNOT-22, Sino-Nasal Outcome Test-22; CS, Colloidal silver.

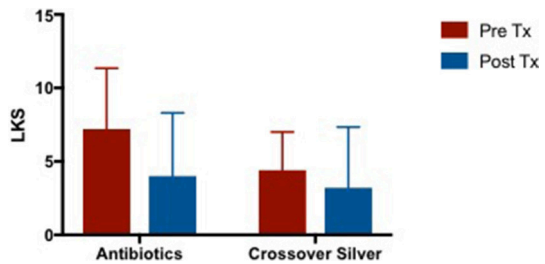

FIGURE 7 | Bar graph comparing LKS scores of patients following failed culture sensitive oral antibiotics and crossed-over to CS treatment. LKS, Lund Kennedy Scores; CS, Colloidal silver.

(Chappell and Greville, 1954) and interacts with bacterial DNA to form dissociable complexes (Rosenkranz and Rosenkranz, 1972; Modak and Fox Jr., 1973).

Some immunomodulatory functions of CS have also been observed in the literature. It has the ability to inhibit matrix metalloproteinases (MMPs) which is pro-inflammatory (Wright et al., 2002) and metallothionein (Wright et al., 2002) (MT) which promotes resistance to immune-mediated apoptosis (Dutsch-Wicherek et al., 2006). Both MTs and MMPs have been found at increased levels in patient with CRS with nasal polyps (CRSwNP) (Wicherek et al., 2007; Eisenberg et al., 2008; Sauter et al., 2008). CS has also been shown to induce inflammatory cells apoptosis by TNF-α and IL-12 suppression (Bhol and Schechter, 2005). An improved host response might be able to account for the efficacy observed in the CS cohort even though there was no eradication of bacteria.

However, one of the limitations of this study is the time-consuming process of manufacturing CS rinses using small scale equipment. Currently, to prepare sufficient CS for a 10-day treatment course a full-time laboratory personnel requires over 10–15 h. If production cannot be upscaled, CS could be evaluated as an adjunct to oral antibiotics.

In the literature, silver has been described to exhibit low toxicity with minimal risks expected from clinical exposure. Silver is absorbed into the systemic circulation as a protein complex and eliminated by the liver and kidneys (Lansdown, 2006). Prolonged silver exposure commonly associated with occupational and/or systemic administration can lead to deposition of silver particles in skin (argyria), eye (argyrosis), and other organs (Tomi et al., 2004). Argyria is a cosmetic concern with irreversible blue-gray skin discoloration in sun-exposed areas, but not life-threatening.

Reported cases of silver toxicity are limited. In the literature, very little data exists correlating serum silver levels with symptomatic presentation of argyria and at present there are no medical guidelines available regarding its use. The World Health Organisation reported that a person can have a total lifetime oral intake of approximately 10 g of silver with no observed adverse effects (World Health Organisation, 1996). The United States Environmental Protection Agency's has reported that a maximum acceptable oral dose of silver to be 0.005 mg/kg/day or about 0.35 mg for a 70 kg person a day, every day during their lifetime (Fung and Bowen, 1996). In this study patients will be exposed to a total of 72 mg of topical CS rinses, which is well under the total lifetime amount of 10 g and to an equivalent of 7.2 mg/day of topical silver treatment for 10 days. Our laboratory reference of serum silver levels indicates argyria could be present when serum silver levels exceed 100 nmol/L. The serum silver levels were well below this concentration and no symptoms of argyria were observed in any patient of this study.

Although this study has shown that CS is safe based on serum silver levels and smell tests, the discomfort of using CS rinses have been noted. This discomfort is likely due to the tonicity and temperature of the rinses and possible stinging properties from silver. To improve the tonicity of the rinse solution for better tolerability, we are currently looking at mixing CS with 5% dextrose isotonic solution.

CONCLUSION

This study concludes that twice daily CS (0.015 mg/mL) sinonasal rinses for 10 days is safe but not superior to culture-directed oral antibiotics. Future studies looking at optimizing the tolerability, duration of treatment and investigating the role of CS as an adjunct treatment to oral antibiotics should be explored and evaluated in a randomized, double-blinded, placebo-controlled trial.

AUTHOR CONTRIBUTIONS

MO: project design, data collection and analysis, manuscript preparation; KR: project design, product manufacture and quality control, manuscript preparation; CB: product manufacture and quality control; LM-V: data analysis; AP project design, manuscript preparation; SV: project design, manuscript preparation; P-JW: project design, manuscript preparation.

FUNDING

The University of Adelaide, School of Medicine, Department of Otolaryngology Head and Neck Surgery, Adelaide, SA, Australia.

REFERENCES

World Health Organisation (1996). *Silver in Drinking Water: Background Document for the Development of WHO Guidelines for Drinking Water Quality*. Geneva: WHO.

Alandejani, T., Marsan, J., Ferris, W., Slinger, R., and Chan, F. (2009). Effectiveness of honey on *Staphylococcus aureus* and *Pseudomonas aeruginosa* biofilms. *Otolaryngol. Head Neck Surg.* 141, 114–118. doi: 10.1016/j.otohns.2009.01.005

Bhol, K. C., and Schechter, P. J. (2005). Topical nanocrystalline silver cream suppresses inflammatory cytokines and induces apoptosis of inflammatory cells in a murine model of allergic contact dermatitis. *Br. J. Dermatol.* 152, 1235–1242. doi: 10.1111/j.1365-2133.2005.06575.x

Chappell, J. B., and Greville, G. D. (1954). Effect of silver ions on mitochondrial adenosine triphosphatase. *Nature* 174, 930–931. doi: 10.1038/174930b0

Chiu, A. G., Palmer, J. N., Woodworth, B. A., Doghramji, L., Cohen, M. B., Prince, A., et al. (2008). Baby shampoo nasal irrigations for the symptomatic post-functional endoscopic sinus surgery patient. *Am. J. Rhinol.* 22, 34–37. doi: 10.2500/ajr.2008.22.3122

Dutsch-Wicherek, M., Tomaszewska, R., Strek, P., Wicherek, L., and Skladzien, J. (2006). The analysis of RCAS1 and DFF-45 expression in nasal polyps with respect to immune cells infiltration. *BMC Immunol.* 7:4. doi: 10.1186/1471-2172-7-4

Eisenberg, G., Pradillo, J., Plaza, G., Lizasoain, I., and Moro, M. A. (2008). [Increased expression and activity of MMP-9 in chronic rhinosinusitis with nasal polyposis]. *Acta Otorrinolaringol. Esp.* 59, 444–447. doi: 10.1016/S0001-6519(08)75116-1

Foreman, A., Jervis-Bardy, J., and Wormald, P.-J. (2011). Do biofilms contribute to the initiation and recalcitrance of chronic rhinosinusitis? *Laryngoscope* 121, 1085–1091. doi: 10.1002/lary.21438

Fung, M. C., and Bowen, D. L. (1996). Silver products for medical indications: risk-benefit assessment. *J. Toxicol. Clin. Toxicol.* 34, 119–126. doi: 10.3109/15563659609020246

Goggin, R., Jardeleza, C., Wormald, P. J., and Vreugde, S. (2014). Colloidal silver: a novel treatment for *Staphylococcus aureus* biofilms? *Int. Forum Allergy Rhinol.* 4, 171–175. doi: 10.1002/alr.21259

Jardeleza, C., Foreman, A., Baker, L., Paramasivan, S., Field, J., Tan, L. W., and Wormald, P. J. (2011). The effects of nitric oxide on *Staphylococcus aureus* biofilm growth and its implications in chronic rhinosinusitis. *Int. Forum Allergy Rhinol.* 1, 438–444. doi: 10.1002/alr.20083

Jervis-Bardy, J., Boase, S., Psaltis, A., Foreman, A., and Wormald, P. J. (2012). A randomized trial of mupirocin sinonasal rinses versus saline in surgically recalcitrant staphylococcal chronic rhinosinusitis. *Laryngoscope* 122, 2148–2153. doi: 10.1002/lary.23486

Jervis-Bardy, J., and Wormald, P. J. (2012). Microbiological outcomes following mupirocin nasal washes for symptomatic, *Staphylococcus aureus*-positive chronic rhinosinusitis following endoscopic sinus surgery. *Int. Forum Allergy Rhinol.* 2, 111–115. doi: 10.1002/alr.20106

Kennedy, J. L., Hubbard, M. A., Huyett, P., Patrie, J. T., Borish, L., and Payne, S. C. (2013). Sino-nasal outcome test (SNOT-22): a predictor of post-surgical improvement in patients with chronic sinusitis. *Ann. Allergy Asthma Immunol.* 111, 246–251.e2. doi: 10.1016/j.anai.2013.06.033

Lansdown, A. B. (2006). Silver in health care: antimicrobial effects and safety in use. *Curr. Probl. Dermatol.* 33, 17–34. doi: 10.1159/000093928

Le, T., Psaltis, A., Tan, L. W., and Wormald, P. J. (2008). The efficacy of topical antibiofilm agents in a sheep model of rhinosinusitis. *Am. J. Rhinol.* 22, 560–567. doi: 10.2500/ajr.2008.22.3232

Lund, V. J., and Kennedy, D. W. (1995). Quantification for staging sinusitis. The Staging and Therapy Group. *Ann. Otol. Rhinol. Laryngol. Suppl.* 167, 17–21.

Modak, S. M., and Fox, C. L., Jr. (1973). Binding of silver sulfadiazine to the cellular components of Pseudomonas aeruginosa. *Biochem. Pharmacol.* 22, 2391–2404. doi: 10.1016/0006-2952(73)90341-9

Paramasivan, S., Drilling, A. J., Jardeleza, C., Jervis-Bardy, J., Vreugde, S., and Wormald, P. J. (2014). Methylglyoxal-augmented manuka honey as a topical anti-*Staphylococcus aureus* biofilm agent: safety and efficacy in an *in vivo* model. *Int. Forum Allergy Rhinol.* 4, 187–195. doi: 10.1002/alr.21264

Rajiv, S., Drilling, A., Bassiouni, A., James, C., Vreugde, S., and Wormald, P. J. (2015). Topical colloidal silver as an anti-biofilm agent in a *Staphylococcus aureus* chronic rhinosinusitis sheep model. *Int. Forum Allergy Rhinol.* 5, 283–288. doi: 10.1002/alr.21459

Richter, K., Facal, P., Thomas, N., Vandecandelaere, I., Ramezanpour, M., Cooksley, C., et al. (2017c). Taking the silver bullet colloidal silver particles for the topical treatment of biofilm-related infections. *ACS Appl. Mater. Interfaces* 9, 21631–21638. doi: 10.1021/acsami.7b03672

Richter, K., Ramezanpour, M., Thomas, N., Prestidge, C. A., Wormald, P. J., and Vreugde, S. (2016). Mind "De GaPP": *in vitro* efficacy of deferiprone and gallium-protoporphyrin against *Staphylococcus aureus* biofilms. *Int. Forum Allergy Rhinol.* 6, 737–743. doi: 10.1002/alr.21735

Richter, K., Thomas, N., Claeys, J., McGuane, J., Prestidge, C. A., Coenye, T., et al. (2017b). A topical hydrogel with deferiprone and gallium-protoporphyrin targets bacterial iron metabolism and has antibiofilm activity. *Antimicrob. Agents Chemother.* 61:e00481-17. doi: 10.1128/AAC.00481-17

Richter, K., Van den Driessche, F., and Coenye, T. (2017a). Innovative approaches to treat *Staphylococcus aureus* biofilm-related infections. *Essays Biochem.* 61, 61–70. doi: 10.1042/EBC20160056

Rosenkranz, H. S., and Rosenkranz, S. (1972). Silver sulfadiazine: interaction with isolated deoxyribonucleic acid. *Antimicrob. Agents Chemother.* 2, 373–383. doi: 10.1128/AAC.2.5.373

Sauter, A., Stern-Straeter, J., Sodha, S., Hormann, K., and Naim, R. (2008). Regulation of matrix metalloproteinases (MMP)-2/-9 expression in eosinophilic chronic rhinosinusitis cell culture by interleukin-5 and−13? *In Vivo* 22, 415–421.

Schreurs, W. J., and Rosenberg, H. (1982). Effect of silver ions on transport and retention of phosphate by *Escherichia coli*. *J. Bacteriol.* 152, 7–13.

Seiberling, K. A., Aruni, W., Kim, S., Scapa, V. I., Fletcher, H., and Church, C. A. (2013). The effect of intraoperative mupirocin irrigation on *Staphylococcus aureus* within the maxillary sinus. *Int. Forum Allergy Rhinol.* 3, 94–98. doi: 10.1002/alr.21076

Semeykina, A. L., and Skulachev, V. P. (1990). Submicromolar Ag^+ increases passive Na+ permeability and inhibits the respiration-supported formation of Na^+ gradient in Bacillus FTU vesicles. *FEBS Lett.* 269, 69–72. doi: 10.1016/0014-5793(90)81120-D

Solares, C. A., Batra, P. S., Hall, G. S., and Citardi, M. J. (2006). Treatment of chronic rhinosinusitis exacerbations due to methicillin-resistant *Staphylococcus aureus* with mupirocin irrigations. *Am. J. Otolaryngol.* 27, 161–165. doi: 10.1016/j.amjoto.2005.09.006

Tomi, N. S., Kränke, B., and Aberer, W. (2004). A silver man. *Lancet* 363:532. doi: 10.1016/S0140-6736(04)15540-2

Uren, B., Psaltis, A., and Wormald, P.-J. (2008). Nasal lavage with mupirocin for the treatment of surgically recalcitrant chronic rhinosinusitis. *Laryngoscope* 118, 1677–1680. doi: 10.1097/MLG.0b013e31817aec47

Walker, F. D., and White, P. S. (2000). Sinus symptom scores: what is the range in healthy individuals? *Clin. Otolaryngol. Allied Sci.* 25, 482–484. doi: 10.1046/j.1365-2273.2000.00349.x

Wicherek, L., Galazka, K., and Lazar, A. (2007). Analysis of metallothionein, RCAS1 immunoreactivity regarding immune cell concentration in the endometrium and tubal mucosa in ectopic pregnancy during the course of tubal rupture. *Gynecol. Obstet. Invest.* 65, 52–61. doi: *10.1159/000107649*

Wright, J. B., Lam, K., Buret, A. G., Olson, M. E., and Burrell, R. E. (2002). Early healing events in a porcine model of contaminated wounds: effects of nanocrystalline silver on matrix metalloproteinases, cell apoptosis, and healing. *Wound Repair Regen.* 10, 141–151. doi: 10.1046/j.1524-475X.2002.10308.x

Conflict of Interest Statement: The authors declare that the research was conducted in the absence of any commercial or financial relationships that could be construed as a potential conflict of interest.

Advantages of publishing in Frontiers

OPEN ACCESS
Articles are free to read for greatest visibility and readership

FAST PUBLICATION
Around 90 days from submission to decision

HIGH QUALITY PEER-REVIEW
Rigorous, collaborative, and constructive peer-review

TRANSPARENT PEER-REVIEW
Editors and reviewers acknowledged by name on published articles

Frontiers
Avenue du Tribunal-Fédéral 34
1005 Lausanne | Switzerland

Visit us: www.frontiersin.org
Contact us: info@frontiersin.org | +41 21 510 17 00

REPRODUCIBILITY OF RESEARCH
Support open data and methods to enhance research reproducibility

DIGITAL PUBLISHING
Articles designed for optimal readership across devices

FOLLOW US
@frontiersin

IMPACT METRICS
Advanced article metrics track visibility across digital media

EXTENSIVE PROMOTION
Marketing and promotion of impactful research

LOOP RESEARCH NETWORK
Our network increases your article's readership